NASA CR 65-332

N66-22353

(ACCESSION NUMBER)

(THRU)

347

(PAGES)

1

(CODE)

CR-65332

(NASA CR OR TMX OR AD NUMBER)

28

(CATEGORY)

FACILITY FORM 602

A Transient Heat Transfer and Thermodynamic Analysis of the Apollo Service Module Propulsion System

CONTRACT NO. NAS 9-3349

Submitted to:

NASA MANNED SPACECRAFT CENTER
PRIMARY PROPULSION BRANCH
Houston, Texas

GPO PRICE $ ______

CFSTI PRICE(S) $ ______

Hard copy (HC) 7.00

Microfiche (MF) 1.75

ff 653 July 65

FOREWORD

This is the final report of a Transient Heat Transfer and Thermodynamic Analysis of the Apollo Service Module Propulsion System conducted for the NASA Manned Spacecraft Center, Houston, Texas. The study was conducted under NASA Contract NAS 9-3349 from 28 July, 1964, to 28 July, 1965, by the Lockheed - California Company. Mr. J. B. Werner was Program Manager; Mr. B. A. Nevelli was the Phase I Project Engineer and Mr. P. S. Starrett was the Phase II Project Engineer. The NASA Technical Monitor was Mr. L. Rhodes.

This report is contained in two volumes: Volume I, Phase I Transient Thermal Analysis, and Volume II, Phase II Thermal Test Program. Appendix D of Volume I, which is classified "Confidential", is bound separately. The remainder of Volume I and all of Volume II are unclassified.

Other reports prepared under this contract are:

LR 18900	A Transient Heat Transfer and Thermodynamic Analysis of the Apollo Service Module Propulsion System - Summary Report
LR 18901	An Introduction to Spacecraft Thermal Control
LR 18902	Thermal Analyzer Computer Program for the Solution of General Heat Transfer Problems
LR 18903	Thermal Analyzer Computer Program for the Solution of Fluid Storage and Pressurization Problems
LR 18904	Computer Program for the Calculation of Incident Orbital Radiant Heat Flux
LR 18905	Computer Program for the Calculation of Three-Dimensional Configuration Factors

This report was prepared by Lockheed's Thermodynamics Department and Rye Canyon Research Laboratory. The principal contributers to Volume I, in addition to Mr. Nevelli, were Messrs. H. R. Holmes, M. A. Kazarian, H. D. Schultz and I. Shuldiner. The discussion of low-gravity fluid mechanics and heat transfer was prepared by Messrs. R. W. Deible and H. M. Satterlee of the Lockheed Missiles and Space Company. The principal

FOREWORD (Cont.)

contributors to Volume II, in addition to Mr. Starrett, were Messrs. K. J. Kahn, M. A. Kazarian, and H. H. Ogimachi. Grateful acknowledgement is made to Mr. R. E. Butler , who was responsible for the test instrumentation, and Mr. R. B. David, who was responsible for computer programming and data processing.

TABLE OF CONTENTS

TABLE OF CONTENTS (cont.)

TABLE OF CONTENTS (cont.)

TABLE OF CONTENTS (cont.)

TABLE OF CONTENTS (cont.)

LIST OF FIGURES

LIST OF FIGURES (Continued)

LIST OF FIGURES (Continued)

LIST OF FIGURES (Continued)

LIST OF FIGURES (Continued)

LIST OF FIGURES (Continued)

LIST OF FIGURES (Continued)

LIST OF FIGURES (Continued)

LIST OF FIGURES (Continued)

LIST OF TABLES

LOCKHEED
CALIFORNIA COMPANY

SUMMARY

This volume presents results of the Phase II Thermal Test Program for the transient heat transfer and thermodynamic analysis of the Apollo Service Module Propulsion System performed for NASA Manned Spacecraft Center. The objective of the Phase II thermal test program is to verify the analytical techniques utilized in the Phase I thermal analysis as described in Volume I of this report.

In this Phase II test program, a series of models related to the Apollo Service Module was tested to thoroughly investigate internal and external heat transfer under a variety of dynamic thermal environments. The test program utilized five series of test models of increasing complexity that led to a 1/3 scale geometric representation of the Apollo Service Module for the Series 5 test. In this model simulation was included of the propellant tanks, pressurization system, a thrust chamber and nozzle extension, and a fuel cell. The first four series of tests were conducted in the Lockheed altitude chamber with infrared lamps, and the Series 5 test was run in the Hughes altitude chamber with solar simulation. A total of 110 hours of space simulation was used during the test program.

For each of the models tested, an equivalent lumped resistance-capacitance thermal analysis network was generated, using the techniques employed in Phase I. The thermal network increased in size with model complexity, ultimately containing 260 nodes, 505 resistors, and 280 radiation resistors for the Series 5 model. The appropriate boundary conditions, either impressed temperatures or solar flux, were used for each test, depending on the mode of heat transfer to be examined. Fifty hours of IBM 7094 computer time were required for the analytical predictions and experimental data reduction.

Analytical predictions of transient temperatures on the models were compared with experimental results to determine the degree of correlation. For the Series 1 model, the initial simplified internal radiation network,

LOCKHEED
CALIFORNIA COMPANY

which did not adequately account for reflections, resulted in systematic discrepancies between predicted and experimental data. Neglect of inter-reflections resulted in low predictions of internal radiant heat transfer. To improve the analysis and yet maintain the program within the computer storage capacity, an approximate method was developed to acount for reflections by modifying the effective emissivity. With this modification, analytical-experimental correlation was markedly improved. For all the models during quasi-steady state test conditions, 85% of the predicted temperatures were within $\pm 20^{o}$ of the measured temperatures.

Correlation during a simulated engine firing (Series 3 and Series 5) showed 60% of the predicted temperatures within ±15° F of experimental and 85% of the predicted temperatures within ± 30° F. Predicted temperatures were generally lower than experimental. This was due to an under-prediction of heat transfer from the simulated thrust chamber. The Fluid Storage and Pressurization Program predicted helium usage within 3% of measured values and oxidizer temperatures within ±2° F of measured values. The results of the insulated model were slightly better than the uninsulated model. For the Series 5 model, predicted shell temperatures on the hot side of the model (250° F) were very good, indicating that external heat transfer was satisfactorily predicted.

The reasonably good overall correlation of the predicted and experimental results, especially during steady state, verified most of the techniques and assumptions employed in the analysis. Internal radiative heat transfer predictions were generally low in areas where reflections were significant. While techniques are available to accurately represent reflected radiant energy (Oppenheim network and Hottel radiation matrix), they are not practical for large, complex models because of computer storage limitations. Although the results of this thermal test program were satisfactory, additional analysis can greatly improve the results of this program as well as provide useful techniques and data for future test programs. Additional effort is recommended in three areas:

1. Develop accurate, simplified techniques to analyze internal radiation for complex models that will not exceed available computer capacity.

2. Conduct further tests to substantiate the Fluid Storage and Pressurization Program under a wider range of conditions than were run in Phase II.

3. Provide a quantitative measure between network complexity and accuracy of analysis.

A final conclusion obtained from this test program is that there exists a definite need for practical techniques to analyze radiation heat transfer for complex geometries. With radiation being a principal mode of heat transfer in spacecraft, research comparable to that done for conduction and convection is highly recommended to improve and to increase the confidence level of the analytical techniques. Until this is done, there is still no substitute for complete thermal testing.

I - INTRODUCTION

TEST OBJECTIVES

The objective of the Phase II thermal test program is to verify the analytical techniques utilized in Phase I thermal analysis of the Apollo Service Module Propulsion System during the lunar mission. The analytical study provides temperature-time histories of all important Service Module components for earth suborbital, earth orbital, and lunar orbit rendezvous missions. In the analysis, thermal networks are formulated with appropriate radiation and conduction resistors connecting nodes representing elements of the vehicle structure. These networks are solved using the Lockheed Thermal Analyzer Program. As with most analytical techniques, a number of simplifying assumptions and compromises with reality are necessary to reduce the complexity of the problem to manageable proportions. In the network formulation, for example, assumptions must be made as to the minimum number of nodes that will acceptably represent a section of the vehicle, the minimum interconnection of radiation and conduction resistors between these nodes, and the degree to which temperature dependence of the thermal properties data needs to be taken into account.

In this Phase II test program, the computer programs as well as the practical techniques and judgements involved in their application are evaluated. With a series of models related to the Apollo Service Module, experimental temperature measurements are compared with analytical predictions. The transient behavior of the models is observed under a variety of dynamic thermal environments and programmed events, such as tank expulsions and solar eclipses. Experimental models are chosen which introduce problems of comparable, and in some cases greater, complexity than those encountered in the Phase I analysis.

GENERAL TECHNICAL APPRCACH

Several fundamental guidelines have been used in planning the test program. The model complexity is increased in steps as the program progresses. Configurations of the models introduce analytical problems of the type encountered in the Phase I analysis. The final model is a 1/3 scale geometric approximation of the Apollo Service Module. Thus, ultimately, scaling effect comparisons are possible when thermal tests are made on the full-scale vehicle.

The test program is separated into a series of tests of increasing complexity. The first series devoted to internal heat transfer, the second series is devoted to external heat transfer, and a final confirmation test demonstrates successful integration of internal and external effects. Thus, a "building block" concept is used with progressive correlation at each level of complexity. Advantages of this approach are:

- Detection of faulty analysis-test correlation on a simple configuration and resolution prior to proceeding to the next level of complexity. Identification of the specific reason for poor correlation becomes evident earlier in this step-wise process.
- Avoidance of "over-simulation", with the attendant expense, by providing adequate simulation for each level of complexity.
- Elimination of need for fabrication and instrumentation of a number of separate models. In most cases, modifications and instrumentation are added to a basic model.

The type of thermal analysis problem encountered is highly dependent on vehicle geometry. The types of radiation shape factor relationships for boom mounted scientific experiments on an unmanned satellite are markedly different from those for enclosed compartments in a vehicle such as the Apollo Service Module. Thus, to preserve validity in the correlation, geometrical configurations similar to the Service Module have been chosen in all cases.

Internal Heat Transfer

Heat transfer within the vehicle is of major importance since it establishes critical equipment temperatures. Since heat transfer within the vehicle is a function only of the vehicle skin temperature distribution, it is possible to perform these tests without solar simulation, using the skin temperatures as boundary value inputs to the computer analysis. A series of tests have been formulated in which the model is heated asymmetrically with radiant lamps on 1/2 the external surface and the other half radiates to liquid-nitrogen cooled chamber walls. In this series, the hot side skin temperatures can be used as boundary inputs to the analysis, and all other temperatures, including the cold side skin temperatures, are computed In these tests, the radiant flux is suddenly applied, driving the hot side temperature to a preselected value in approximately 10 minutes. Thus, typically, this temperature is held for 6 hours and then a cool-down period of about 2 hours follows. The internal heat transfer tests included:

- Series 1 - This model consists of two concentric cylinders with end bulkheads. The model is run at two different hot-side temperature levels, 100°F and 250°F. The purpose of these tests is to establish correlation of analytical predictions with test results for a relatively simple network.

- Series 2 - Six radial beams connecting the inner and outer cylinders are added to the Series 1 model. The Service Module geometry is used in dividing the model into six sectors. Again, two runs are made at two different hot side temperatures. It is the objective of this series to introduce considerable complexity into the conduction network over that of Series 1.

- Series 3 - A major modification is made to the Series 2 model by adding four simulated propellant tanks and plumbing,two high pressure helium bottles with a tank pressurization system, fuel cell, thrust chamber, and nozzle simulation, and an aft-bulkhead heat shield. With this model the following tests are run: (1) tanks empty and all systems passive, (2) with a tank expulsion schedule added, (3) with a tank expulsion schedule, including coordinated nozzle and thrust chamber heating, and (4) the same as the previous run except that all sectors are internally insulated with 10 layers of aluminized mylar. It is the intent of this series of tests to bring the model to a level where it is essentially a 1/3 scale thermal representation of the Service Module. Correlation of analytical predictions and experimental data at this point demonstrates the capability to analyze internal heat exchange under dynamic conditions within a vehicle of the complexity of the Service Module.

External Heat Transfer

The objective of this series is to verify the analysis of an external thermal balance model, particularly with radiant exchange between several elements in a collimated heat flux and shading of one portion of the model by another. The model selected for the test, designated Series 4, is a disk to which a truncated cone is attached in a configuration resembling an engine nozzle protruding from an aft bulkhead. The solar simulator utilized has a 10-in. diameter working beam, and the model is scaled to that dimension. Orientation of the model to the solar flux can be adjusted from outside the chamber. All tests on this model are performed in the Lockheed C-5 Space Simulation Chamber. Again, the "building-block" concept is used. A test consists of precooling the model to a desired temperature. The run is initiated by a step input of solar simulation flux. The flux level is held constant for one hour. The simulator is then turned off, and the model cooled for one hour. Thus, all runs are two hours in length, involving a heating and cooling period. A different pattern of energy exchange takes place during the cooling period, since the solar input to each nodal area goes to zero. Thus, the analytical predictions of transient thermal behavior are checked for both light and dark periods.

Four different orientations relative to the solar flux are run with the basic model. Then the next level of complexity is introduced by adding two small objects to the disk, simulating equipment attachments to an aft bulkhead. Four different orientations relative to the solar flux are run to complete the program on external heat transfer.

Integration

Having investigated the internal and external heat transfer effects independently in Series 1 through 4, a final test, designated Series 5, is performed to integrate these two modes. Where the internal heat transfer studies start with the hot side skin temperatures as boundary conditions, the Series 5 tests utilize the total vehicle environment to establish the boundaries. Working from the solar flux level and the cold wall environment, predictions are made of the quantity of heat absorbed by the vehicle the distribution through the vehicle, and the amount rejected from the vehicle to the wall. Demonstration of ability to predict transient temperatures on the model for this case essentially substantiates the ability to do so for the model (or a full scale vehicle) in the space environment.

For these tests the Series 3 model is adapted for use in the Hughes chamber and redesignated the Series 5 model. The changes permit expulsion of the tanks while the model axis is horizontal. In this position the model can be subjected to the 8' diameter solar simulation beam in the Hughes chamber. In this test, not only is steady and periodic solar flux imposed on the model, but 3 simulated mid-course events are introduced which include nozzle and thrust chamber heating with a coordinated tank expulsion schedule.

SPACE SIMULATION FACILITIES AND DATA ACQUISITION

Lockheed Facilities

All tests at Lockheed were performed in the C-5 space simulation chamber at the Rye Canyon Research Laboratory. The C-5 chamber has a clear working volume of 9-ft-7-in. diameter by 8-ft-1-1/2-in. in height. The chamber is equipped with liquid-nitrogen-cooled walls which can be maintained at -300° F or below. In addition to the roughing pump system, the chamber is equipped with two 32-in. diffusion pumps and an ion-gettering pump. Vacuums in the 10^{-6} range were achievable with the Apollo models during this test series. Heat flux on the model can be achieved with quartz lamps energized through an ignitron-controlled power supply. A 12-in. dia. quartz window permits a 10-in solar simulator, manufactured by Aerospace Controls Corporation, to be used with the C-5 chamber. This simulator blends infrared, xenon, and mercury-xenon lamps to achieve a spectrum match which is within 10% of the Johnson curve.

The Lockheed Mod-Sadic data-acquisition system was used in all tests except the Series 5. This 300-channel system acquires the millivolt signal at 4 channels/second, digitizes the thermocouple or transducer signal, and records it on perforated paper tape. Cards for computer processing are made from the paper tape.

A detailed description of the Lockheed facilities used in the Apollo thermal tests is given in Appendix A.

Hughes Facilities

The Hughes Aircraft Company SERF C-4 chamber with the S-4A solar simulator was used in the Series 5 tests. This chamber is 14-1/2-ft. in diameter and 36-ft. high, with liquid-nitrogen-cooled floor and walls. The chamber pressure can be lowered to 1×10^{-7} torr. An 8-ft. dia. working beam of approximately one solar constant can be provided in this chamber.

A 600-channel data-acquisition system with a scan speed of 1-channel/second is used with this facility to provide a punched card output of all data taken during the test.

Additional details of the Hughes space simulation facilities are given in Appendix A.

THERMAL ANALYSIS TECHNIQUES

The thermal analysis of the laboratory models is based on the utilization of the Thermal Analyzer computer program. In order to use this program the heat transfer situation must be described using a equivalent resistance-capacitance (R-C) network. This is accomplished by dividing the physical system into sections called "lumps" and calculating the resistance and capacitance of these lumps. After network parameters are evaluated and put into the program, the computer solves the network equations using a finite difference method. The computer output consists of the temperatures for all the lumps (nodes) for specified time increments. Thus, the thermal analysis provides predicted temperature histories at various locations on the laboratory model.

Two types of boundary conditions are specified for the Phase II analytical models. For Series 1 to 3 temperatures are specified on the heated side of the outer shell. For Series 4 and 5 solar heat inputs are specified and fuel cell, thrust chamber, and nozzle temperatures are impressed as boundary conditions. In order to have a meaningful comparison of experimental and predicted results, measured initial temperatures are used for the time-zero temperatures in the analytical model.

Constant values were used for thermodynamic properties such as specific heat and thermal conductivity. This was necessary in view of program storage limitations. Although some of the properties vary by as much as 20 percent over the temperature range involved, it is judged that an average value will give good agreement between experimental and predicted results. Thermal contact resistance is assumed negligible everywhere except where the heat shield is attached to the aft bulkhead.

Two computer programs have been specially prepared to aid in comparison and analysis of experimental and predicted data. The first of these converts thermocouple and pressure transducer readings to temperatures and pressures. This program also prepares the experimental data (punched cards) to be inserted directly into the thermal analyzer program as boundary conditions. Another program was written which plots both predicted and experimental node temperature histories on the same graph. This program eliminates the need for manual plotting and facilitates correlation of the results.

Because of the large volume of data generated in the thermal test program, only selected presentations can be made in this report. The selected data are presented in three different ways, depending on the purpose and complexity of the run.

1. Analytical and experimental temperature distributions at a given time and axial station on the model are shown for Series 1 and 2.

2. Analytical and experimental temperature histories of representative nodes for any given region of the model are plotted for Series 1-5.

3. Analytical and experimental correlation plots are used for the Series 3 and 5 models.

In all cases when the results of only a few nodes could be selected, great care was taken to choose the most representative and typical as well as informative and important nodes.

The Phase II analysis was conducted in much the same manner as that for Phase I. Although the Phase II experimental models are not exact scale replicas of the full-size vehicle, the general philosophy of the Phase I analysis has been adhered to as closely as possible to verify the methods and assumptions employed in Phase I.

II - SERIES 1 MODEL

MODEL DESIGN AND FABRICATION

The Series 1 model consists of two 51-in. dia. bulkheads mounted on each end of a 15-in. dia. inner cylinder to form a spool-like figure. The cylindrical side of this figure is enclosed by the six curved cylindrical segments that are attached to the bulkheads. Details of the bulkheads, and of the cylindrical outer segments, are shown in Appendix D. The assembled Series 1 model is shown in Figures 2-1 and 2-2.

Outer Cylinder

The external cylinder was made up of six 3/8-in. thick curved aluminum honeycomb panels. The panels were constructed of .012-in. thick 2024-T42 clad aluminum alloy sheets bonded with Bloomingdale HT424 high-temperature adhesive to a 3/8-in. thick 3/16-.001P perforated 5052 aluminum alloy Hexcel core. The core is ventilated with 14 1/4-in. dia. drilled holes in the .06-in. thick extruded aluminum J-section edging. Each panel was provided with an impression-stamped identification number corresponding to its mating sector. Mating sector numbers were stamped on the outer edge of the bulkheads to facilitate assembly.

After thermocouples were attached to the panels the external surfaces of the panels were coated with CAT-A-LAC black paint (see Appendix B for manufacturer's identification number and emissivity). The internal surface was painted with a non-leafing aluminum acrylic lacquer (see Appendix B for details), which had been previously checked for blistering by heating a test specimen to 250°F in a 10^{-6} torr vacuum.

Inner Cylinder

The 15.0-in. dia by 52.5-in. long inner cylinder was made from a .050-in. thick 5052-0 aluminum alloy sheet. Four 2.5-in. dia. holes were cut in the cylinder wall for access to the instrumentation, and to plumbing bosses on the helium bottles which were to be installed later. Two 0.125-in. thick by 4.0-in. wide by 50.4-in. long doublers were riveted diametrically opposite each other along the length to stiffen the cylinder. With these doublers, the weight of the two helium bottles (about 78 lbs. each) would be distributed to the cylinder walls and the sector webs.

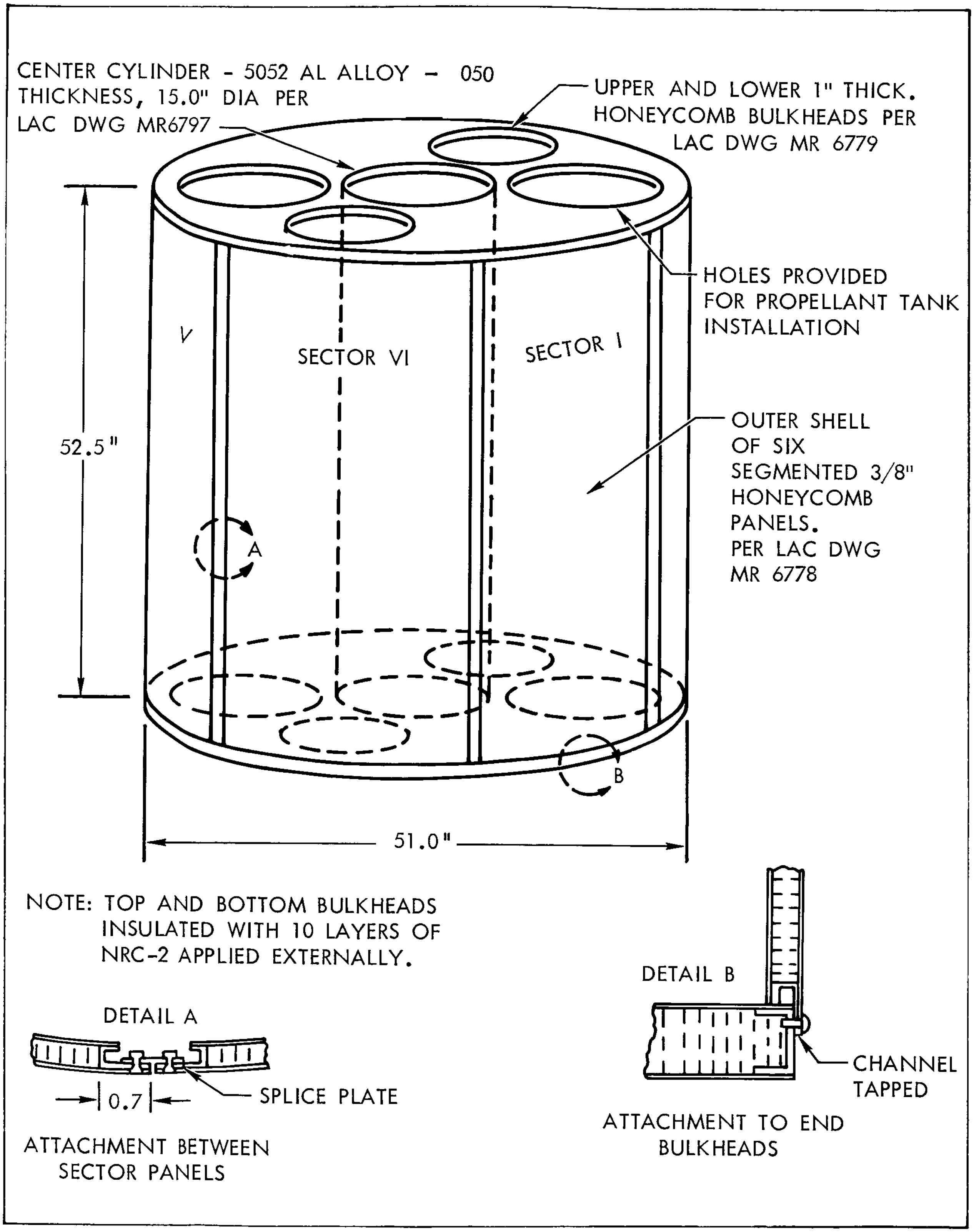

Figure 2-1 Series 1 Model

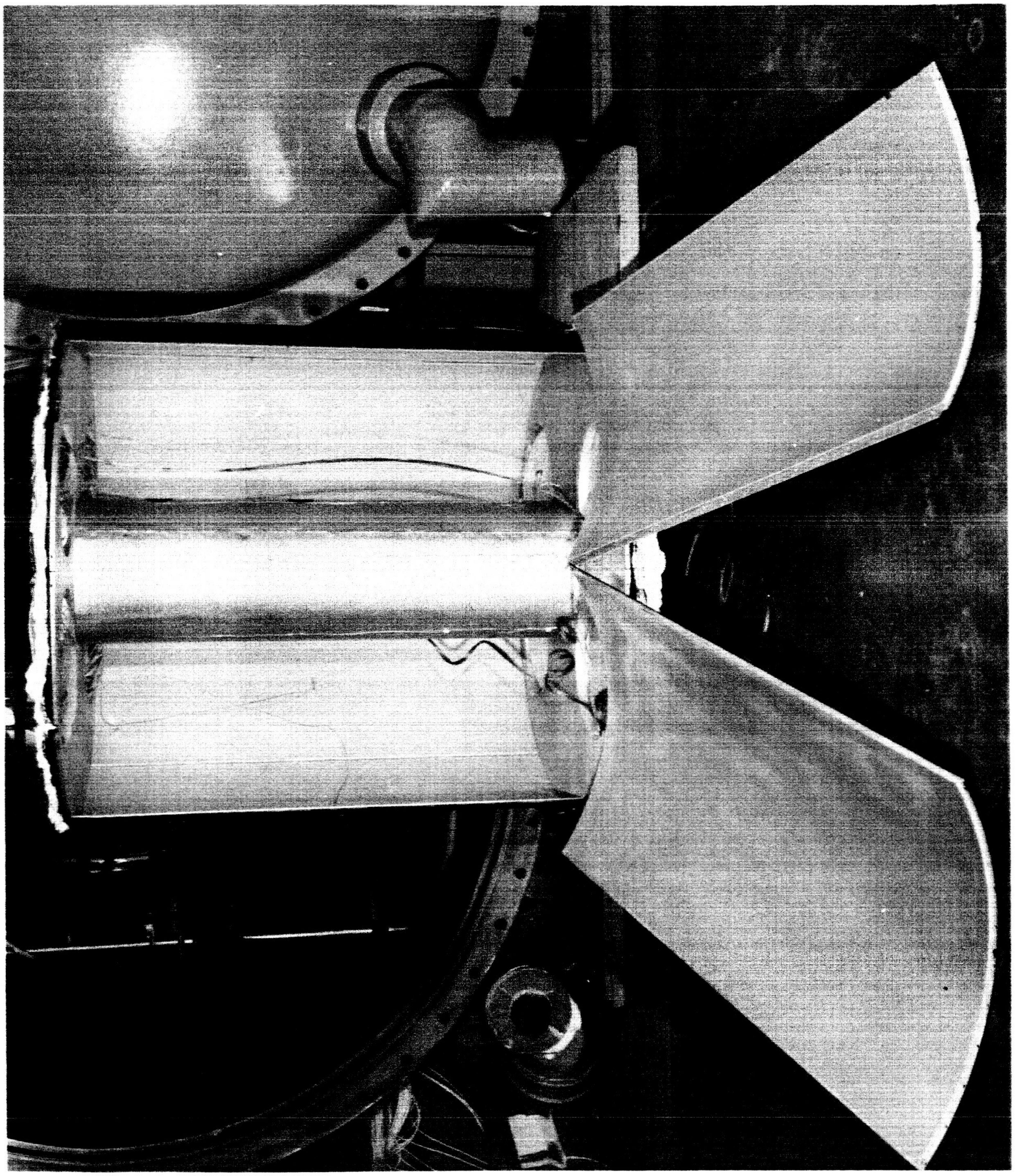

Figure 2-2 Series 1 Model with Two Panels Removed

After the thermocouples were attached, as described in a later section, the inner and outer surfaces of the cylinder were painted with non-leafing aluminum acrylic lacquer (Appendix B).

Bulkheads

The upper and lower bulkheads, 51-in. in dia. and 1.0-in. thick, were fabricated from Hexcel 3/16-.001P core covered with .012-in. thick 2024-T42 clad aluminum alloy sheets on both sides. Circular openings were provided for the inner cylinder and the fuel and oxidizer tanks. The outer periphery of the bulkheads and the circular openings were reinforced by 0.125-in. thick aluminum channel-section extrusions. These extrusions, rolled into closed circles, were welded to each other to form a rigid support before bonding with Bloomingdale HT-424 high-temperature adhesive to the honeycomb core and outer skin. To simplify fabrication and ensure good contact of the honeycomb material inside the flange of the channel-shaped extrusion, this space was filled with the stiffer and heavier Hexcel 1/8-.0015P core material. This heavier 1/8-in. hexagonal cell material is stiffer and more resistant to collapse in the expanded direction. After the adhesives had been cured in the heated presses, holes were drilled in the extruded edging for ventilation, and 4 3/8-in. dia. eyebolts were installed in each bulkhead to serve as support attachments.

Two coats of non-leafing aluminum acrylic lacquer were applied to the bulkheads after the outer edges had been masked. Exposed edges were coated with CAT-A-LAC black paint after assembly with the inner cylinder and external cylindrical segments.

Model Assembly

The ends of the 15.0 in. diameter inner cylinder were slipped into the center hole of the bulkheads and attached with 10-32 screws on about 5-in. centers. Thermocouples were installed on this assembly and the external cylindrical segments as previously described in this section. The external cylindrical segments had to be handled with great care after the thermocouple wires had been installed, since the thermocouples for three separate panels were wired to one common plug. Although this made assembly of the model more difficult, it was necessary to do this to minimize the number of plugs required for the tests. Upon completion of the thermocouple installation, the external segments were attached to the bulkhead with No. 8-32 screws on 3-in. centers. The long edges of the segments were joined with a .050-in. thick by .90-in. wide splice plate (see detail A, Figure 2-1),using No. 8 sheet metal screws on 3-in. centers. The model is shown in the chamber in Figure 2-5 during the checkout phase.

Radiant Lamp Test Fixture

The radiant lamp test fixture (Figure 2-3) for asymmetric heating of the model was fabricated in two welded sections out of 2-in. O.D. aluminum tubing. The circular upper section, rolled on a 40-in. radius, was covered on the inside with .032-in. thick specular-finish reflective aluminum sheets. On the inside of these sheets, 5 3/8-in. by 1 1/4-in. rolled copper bus bars were attached horizontally on 12 3/4-in. centers through 2-in. long ceramic stand-offs. Lamp sockets consisted of shipping-strap banding clips attached to the copper bus bar on 4-in. centers. The lamp extension wires were bolted to the bus bars for positive contact. The end sockets on the General Electric Company 1000T3/CL/HT quartz lamps were inserted into the loose-fitting banding clips for minimum lamp breakage.

The 112 quartz lamps (1,000 watts each) were installed on 4-in. centers on the semi-circular fixture in four parallel rows 11 1/4-in. from the model. These lamps were wired in 56 parallel sets of two lamps, in series such that a 480-volt power supply would impress 240 volts across each lamp. The entire arrangement was powered by a 480-volt, 900-KW ignitron unit (Research Incorporated Controller Model 4080).

While the 112 lamps in the fixture could produce a flux capacity of 4 KW/ft^2 , an input of less than 0.85 KW/ft^2 was actually required to maintain a 250°F skin temperature on the heated side of the model. The number of lamps was governed, in this case, by a flux uniformity requirement rather than flux intensity.

Four-inch-deep aluminum I-beams were added to the top of the lamp-holding fixture for hanging the test model by four 1/8-in. steel cables. These beams, shown in Figure 2-3, in turn are supported by the lamp-holding fixture, but can also be supported by the single eyebolt in the center of

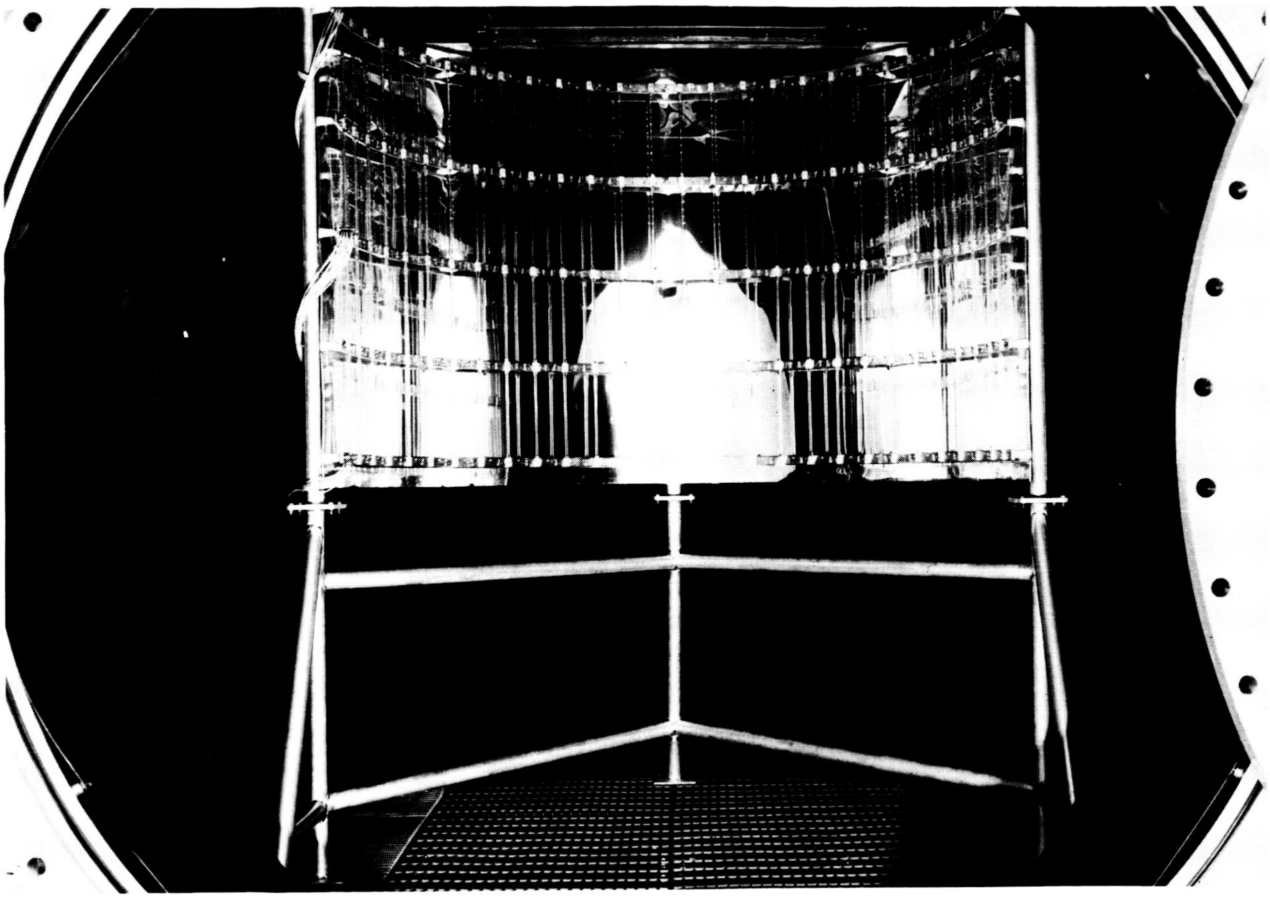

Figure 2-3 Radiant Lamp Test Fixture in the C-5 Chamber

the chamber ceiling. In order to rotate the entire assembly, including the model, the assembly was lifted off the chamber floor by sling cables to a single turnbuckle suspended from this eyebolt. The unheated side of the model was rotated to face away from the door and toward the cold chamber wall.

Instrumentation

Thermocouple Calibration - The thermocouples for the Series 1 and 2 models, complete with chamber feedthroughs, were calibrated through the range from $-320^{\circ}F$ to $+436^{\circ}F$. The couples were Trinity Micro Corp. 30-T-EG premium grade 30-gage Type T (Cu-Cn), with silicone-impregnated fiberglass insulation. The calibration from 50° to 436° was performed using Dow Corning silicone oil No. 550 in a Hallikainen Model 1124 calibration bath. A similar bath was used to hold the reference junctions at $150.0^{\circ}F$. In the range from $+6^{\circ}F$ to $-96^{\circ}F$, a Lexsol 408 (Santa Barbara Chemical Co.) bath, cooled with dry ice, was used. For the $-320^{\circ}F$ point, the couples were immersed in a dewar containing LN_2 (liquid nitrogen). In all cases except the LN_2 points, the standard temperatures were read with precision thermometers with NBS traceability. The LN_2 point was checked with Cryogenics Inc. Model 300-1 thermometer, which read within $0.7^{\circ}F$ of the boiling point of LN_2 ($-320.4^{\circ}F$). The calibration curve for the 126 couples tested is given in Figure 2-4. Standard deviation of individual couples about the average was typically $\pm 0.3^{\circ}F$. Three couples giving erratic readings were discarded. All calibrations were performed with the actual feedthroughs and lead wires to be used during the test.

Thermocouple/Node Location - The copper-constantan thermocouples were then attached to the model with 1/2 in. wide Mystic Tape Co. Type 7455 aluminum-coated silicone adhesive tape at the preselected node locations, except where access presented a problem. In such cases, the thermocouples were installed as close as practical to the selected node location. The tapes were then painted over with a coating having the same emissivity as the local surface. A total of 21 couples were installed on the inner cylinder, 32 on each bulkhead, and 40 on the external cylinder. In addition, a temperature-sensing couple for the temperature controller was installed on

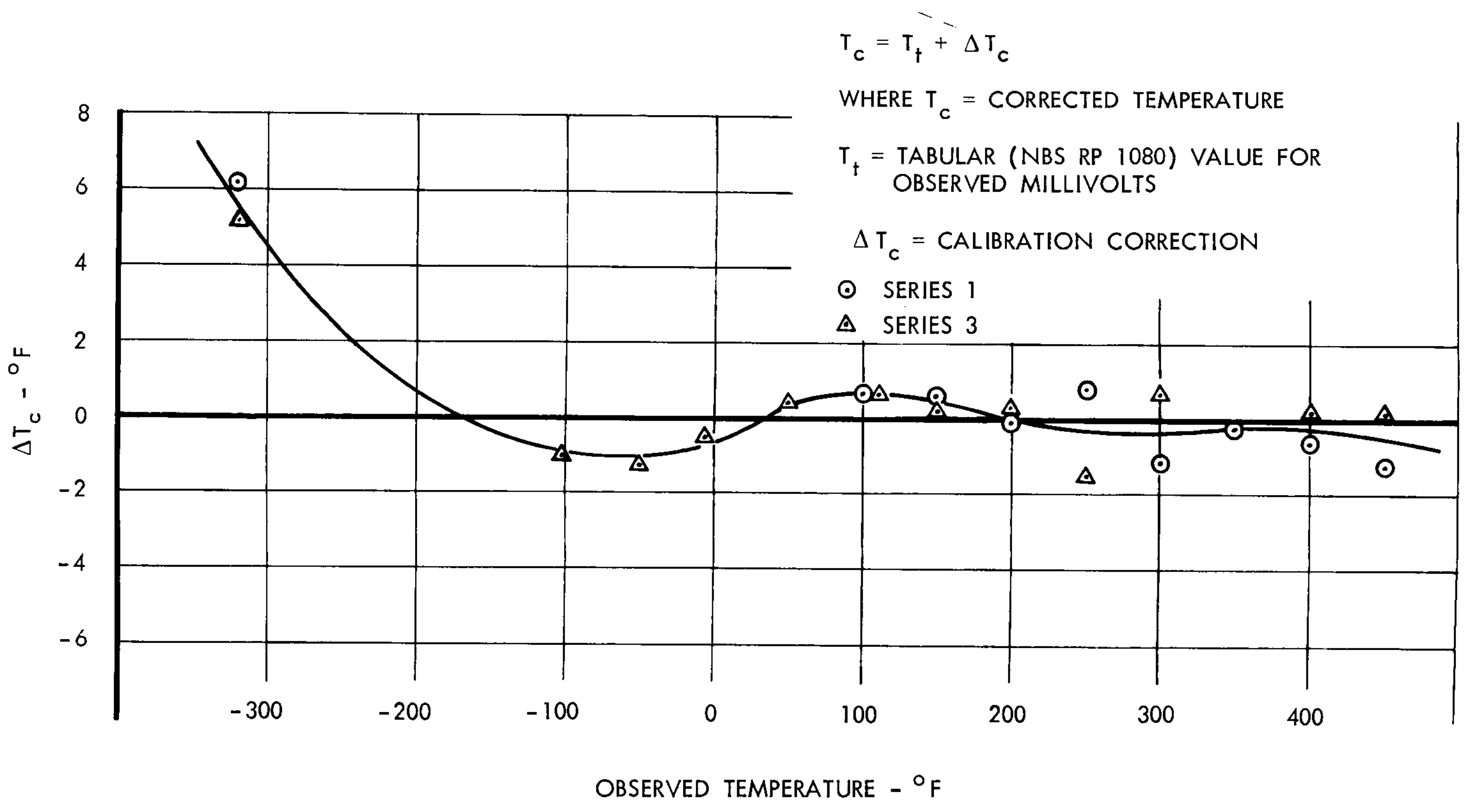

Figure 2-4 Series 1-3 Thermocouple Calibration Copper-Constantan

the cylindrical segment for sector 1. These node locations are shown in figures located in Appendix E. A tabulation of the assigned node number, referenced to the pin and plug number of the thermocouple installed at the particular node location, is also included in Appendix E.

After the model was placed in the vacuum chamber, provision was made for passing the thermocouples through the chamber wall. The copper constantan thermocouples were taken out through Deutsch feedthrough receptacles and the iron-constantan through Conax plugs. These thermocouples were connected to a 150^{o}F reference junction outside of the chamber and then through cables to the data acquisition system. There, the millivolt outputs of the thermocouples were stored on paper tape. The data stored on the tape was then transferred to punched cards and forwarded to a computer for processing.

Test Runs

Run Preparation and Checkout - After the inner and outer cylinders had been assembled to the bulkheads, unpainted edges and screw heads were touched up. The outsides of the upper and lower bulkheads of the model were covered with 10 layers of NRC-2 (National Research Corp. aluminized mylar insulation), 1-in. of fiberglass, and a final cover of one layer of NRC-2. The Series 1 model with two external cylindrical panels removed is shown in Figure 2-2.

The radiant heat test fixture was set up inside the C-5 chamber as shown in Figure 2-3. Then the assembled Series 1 model was moved into the C-5 chamber and suspended from the I-beams on top of the radiant heat fixture. The model is shown in this position in Figure 2-5. After the model was rotated as previously described, the electrical connections to the chamber wall feedthrough were made.

External to the chamber, the thermocouple reference junctions were placed in the 150.0^{o}F constant-temperature bath. From this point, the thermocouple extension wires were routed and connected to the Mod-Sadic Data Acquisition system. A portable heater-blower was used to heat each individual thermocouple, while the Mod-Sadic operator manually monitored the millivolt output of the couple. This checkout procedure was used to ensure node-channel matching, correct polarity, and thermocouple extension-wire continuity.

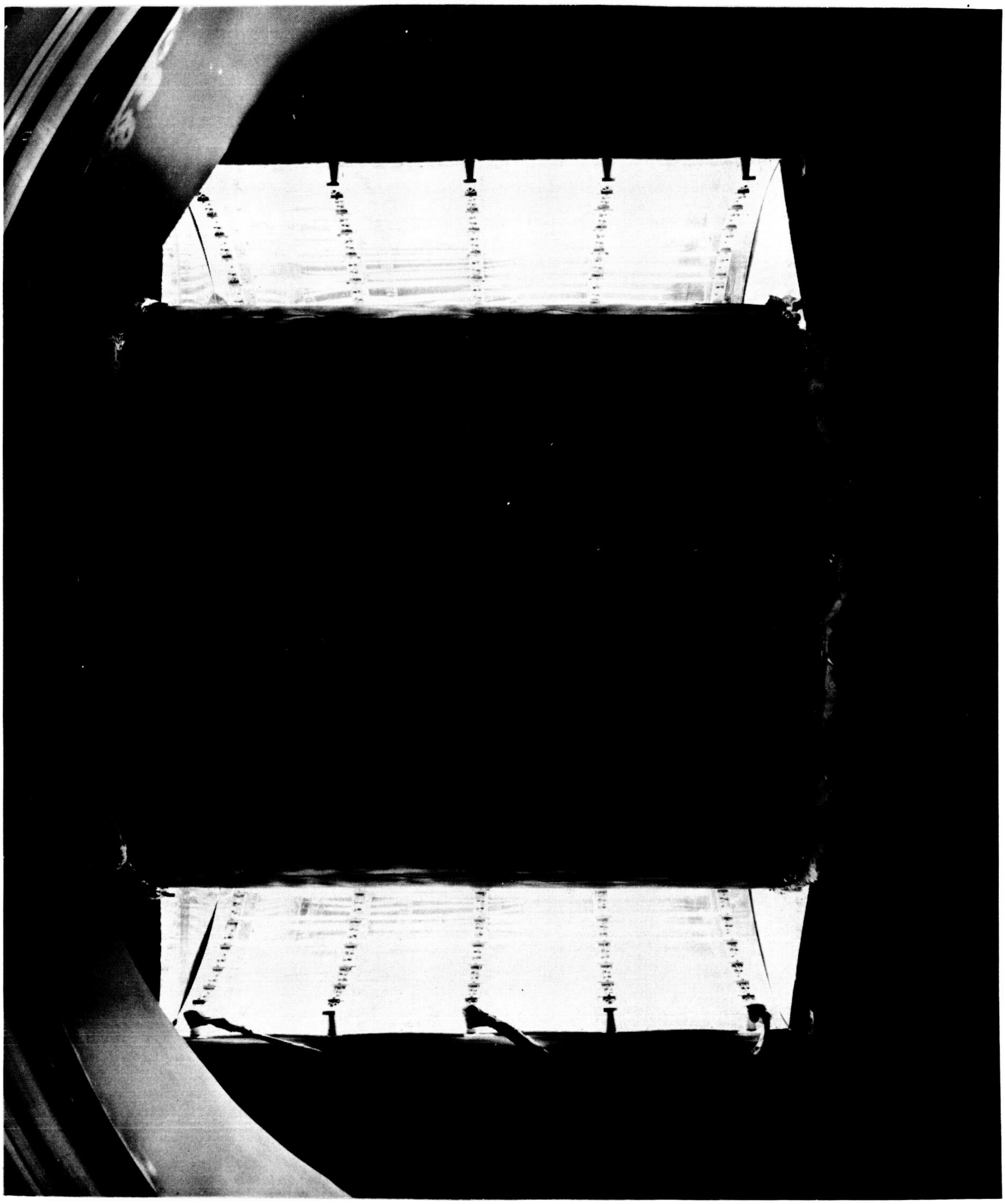

Figure 2-5 Series 1 Model Mounted in the Radiant Heat Fixture

The power leads to the heat lamps were connected and insulated with 1-in. wide Minnesota Mining and Manufacturing Company high-temperature fiberglass electrical tape No. 27. Reduced voltage was applied to the lamps for checkout. After the model had been rotated, reflective shields were positioned around the banks of heat lamps to restrict the radiant flux to approximately 1/2 of the model.

Run Procedure - Two 8-hour runs were made on the Series 1 model. Prior to each run, the model was pre-cooled overnight in a vacuum with the chamber walls cooled by gravity-flowed LN_2 (liquid nitrogen). This produced initial starting skin temperatures on the model in the range from -200°F to -150°F. After the LN_2 pump was turned on, a pre-run data-taking cycle was made to recheck the data system.

The run was then initiated by a very rapid warmup to the control temperature on the heated side of the model. This control temperature was sensed by a thermocouple located near the area center of the heated zone and was recorded on a strip chart on the controller. During this initial heating period, thermocouples located in the heated zone were also monitored on the Mod-Sadic system manually. In this initial heating period the rate of temperature rise was about 47° F/min. for the first run and about 84° F/min. for the second run. After the temperature at the control node had stabilized, data were recorded at 5-minute intervals during the first hour, and 10-minute intervals thereafter.

The control node temperature was held at approximately 100° F for the first run and 260° F for the second run. The time-temperature profiles of the control node and the unheated exterior surface are shown in Figure 2-6 for the two runs. All other model temperatures should lie between these two extremes. The temperatures at the center of the two adjacent cylindrical panels were 9 1/2 to 12° F below the temperature of the center of the middle panel for both runs. This is to be expected since one edge of the adjacent panels is spliced to a panel located in the unheated zone. The two runs were judged satisfactory, and the model was removed from the chamber preparatory to its conversion to the next level of complexity - the Series 2 model.

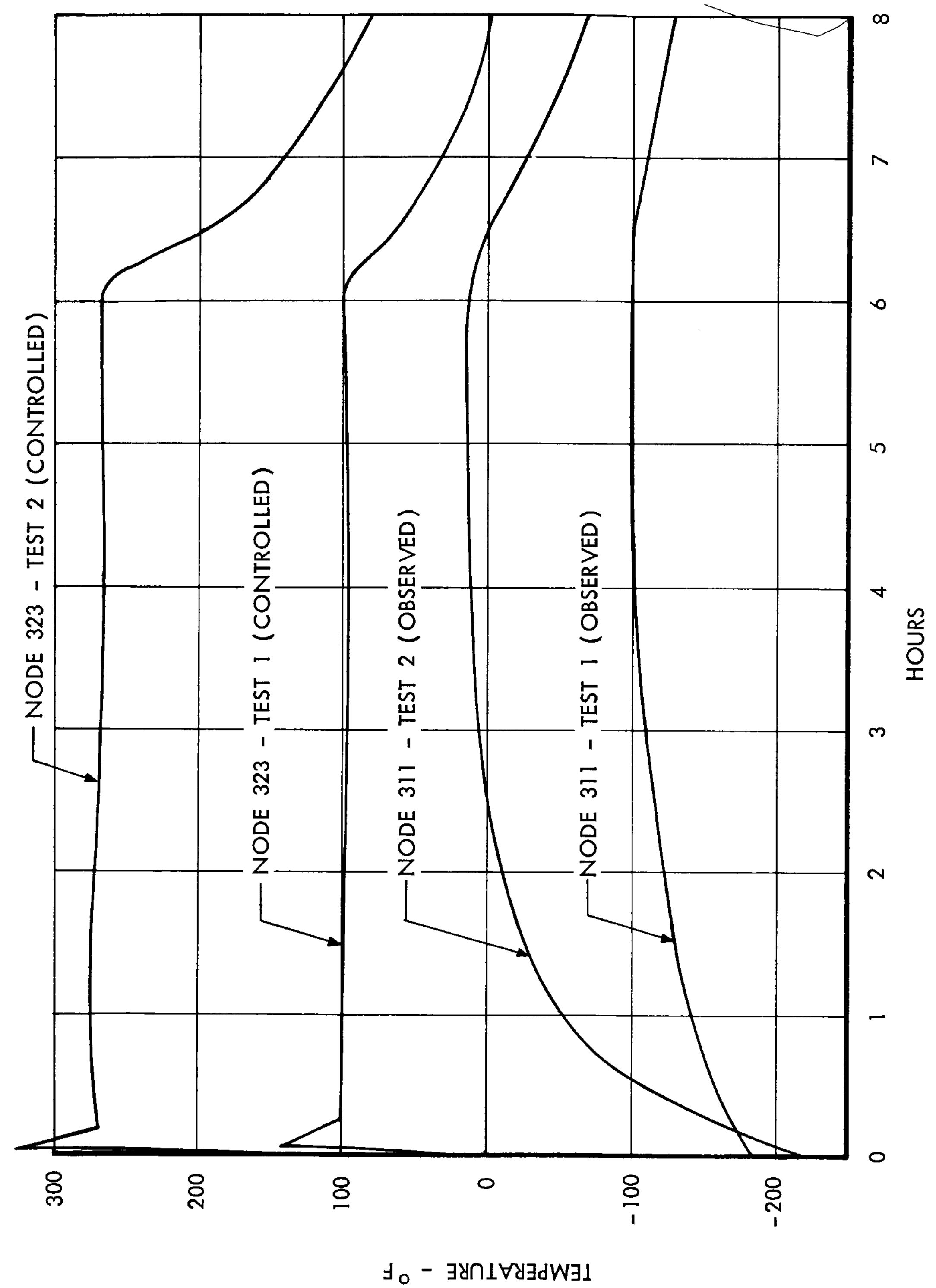

Figure 2-6 Series 1 Control Temperatures

LOCKHEED
CALIFORNIA COMPANY

Analytical Correlation

A general discussion of the analytical techniques used to generate the R-C network for all the models is presented in this section which applies to all the series networks. This discussion includes the choice of lump size, all the calculation of conduction resistors, radiation resistors, and capacitors. Because the radiation resistors are the most difficult to define, a more detailed discussion of these resistors is presented.

Conduction Resistors - In all cases, conduction resistors are computed by the formula

$$R = 3600 \int_0^{\delta} \frac{dx}{kA}, \ \frac{\sec\ ^{\circ}F}{BTU} \qquad (1)$$

where:

k = thermal conductivity, BTU/hr.ft. $^{\circ}$F

A = cross-sectional conductive heat transfer area, ft.^{2}

x = distance along conductive path, ft.

R = resistance, sec- $^{\circ}$F/BTU

δ = limit of x

For a rectangular parallelepiped or a cylinder with vertical sides, or for any configuration with constant cross-section, vertical sides, and parallel faces,

$$R = \frac{3600\ \delta}{kA}, \ \frac{\sec.\ ^{\circ}F}{BTU} \qquad (2)$$

All of the conduction resistors for the Phase II analysis were calculated using equation (2).

In Appendix B, Table 2, are listed the thermal conductivities of the materials used for the models. For the honeycomb material an effective thermal conductivity was computed, based on the conduction paths of the core and facing sheets.

Radiation Resistors - Since the radiation interchange from surface 1 to surface 2 is

$$q_{1-2} = \frac{T_1 - T_2}{R} = \frac{\epsilon_{12} A_1 F_{12} \left(\tau_1^4 - \tau_2^4\right)}{3600} \text{BTU/sec.}, \quad (3)$$

(where τ = absolute temperature, ^oR) the radiation resistor, R, is of the form

$$R = \frac{3600}{\epsilon_{12} A_1 F_{12} \sigma \left(\tau_1^2 + \tau_2^2\right)(\tau_1 + \tau_2)} \quad (4)$$

where:

ϵ_{12} = emissivity factor
A_1 = area of radiating surface, $ft.^2$
F_{12} = shape factor from surface 1 to surface 2
σ = Stefan-Boltzmann constant = 0.1713×10^{-8} BTU/hr.$ft.^2$ $^oR^4$

Because the radiation resistor is temperature dependent, the thermal analyzer program computes these resistors as defined by

$$R = \frac{1.0}{\sigma K_{rad} \left[(T_1 + 460)^2 + (T_2 + 460)^2\right]\left[(T_1 + 460) + (T_2 + 460)\right]} \quad (5)$$

where

$$K_{rad} = \frac{\epsilon_{12} A_1 F_{12}}{3600} \quad \frac{ft.^2 \text{ hr.}}{\text{sec.}} \quad (6)$$

K_{rad} is evaluated by the engineer.

The shape factor, F_{12}, is evaluated by one of three methods, depending on which method is most applicable:

(1) Analytical equations such as developed by Hamilton [1]. These are available in a variety of point-to-surface and surface-to-surface configurations. This method is used extensively in Series 1, 2, 3, and 5.

1. D. Hamilton and W. Morgan, "Radiant Interchange Configuration Factors," NASA TN 2836, Dec. '62.

(2) Optical configuration device. This method allows optical determination of point-to-surface shape factors. A scale model illuminated by a projection lamp representing the differential element casts a shadow onto the surfaces of a marked wall. The configuration factor is obtained directly from the number of sectors of the wall pattern which are shaded by the model. This method is used in Series 3, 4, and 5.

(3) Shape factor program. This method offers a great deal of flexibility in calculating shape factors for almost any geometrically describable situation. It is sometimes by-passed in favor of other methods because it is cumbersome to use. This program is primarily used for surface-to-surface shape factors which cannot be readily determined by other methods. It is used only for Series 4.

When the distance between nodal surfaces is large compared to their areas, the view factors can be computed on a point-to-surface basis. However, when the opposite is true, view factors must be computed using a surface-to-surface method.

The emissivity factor, ϵ_{12}, can be computed by one of two methods, depending on the relative locations of the two surfaces. For two surfaces that have a large view factor, the infinite parallel plate technique is used, which is given by

$$\epsilon_{12} = \frac{1}{1/\epsilon_1 + 1/\epsilon_2 - 1} \tag{7}$$

On the other hand, when view factors are small, the product rule is employed which is given by

$$\epsilon_{12} = \epsilon_1 \epsilon_2 \tag{8}$$

The effective emissivity for these two methods is plotted in Figure 2-7 as a function of surface emissivities. This figure shows that,as surface emissivities decrease, the discrepancies between the two methods increase. For surface emissivities of 0.5, the effective emissivity of the infinite parallel plate method is 0.34, while the product method is 0.25. This 35%

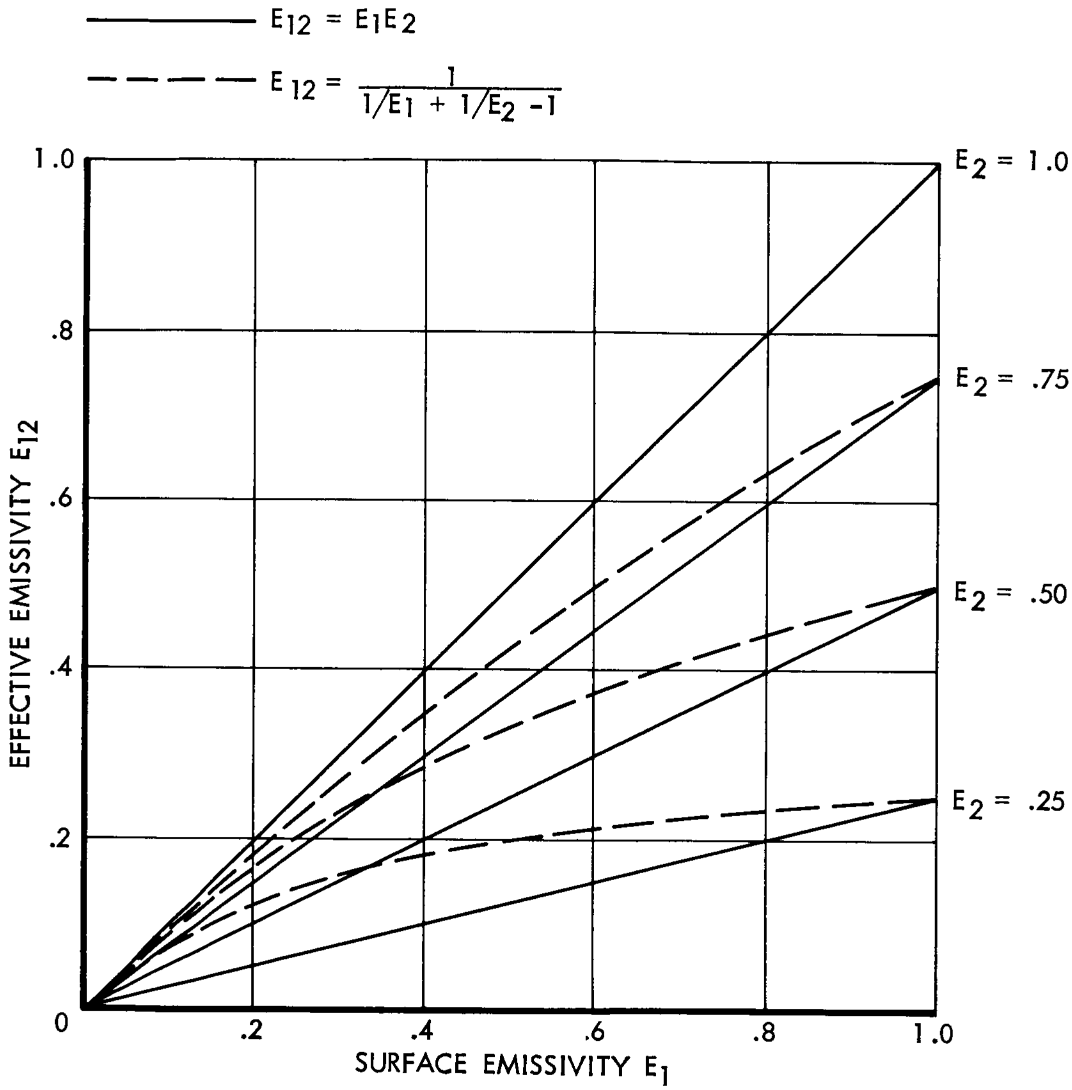

Figure 2-7 Effective Emissivity

discrepancy is minimized by appropriately selecting intermediate values, depending on the geometry of the nodal surfaces.

Surfaces of low emissivity ($\epsilon < 0.7$) introduce the problem of properly representing multiple reflections. The radiation resistors described in this section do not account for reflected energy from a third surface. A more sophisticated network, such as the ones developed by Hottel and Oppenheim, is required to solve reflective-radiation problems in an enclosure. These methods were not directly incorporated in the Phase II or Phase I analysis because their use would cause the Thermal Analyzer program to exceed the capacity of the computer. After the Series 1 test run, it became apparent that, to obtain a good representation of the internal radiation, reflected radiation must be included.

Therefore, an approximate method was developed to modify the effective emissivity to partially account for reflective energy. To ensure applicability to all the models, a two-dimensional configuration of a typical Series 2 bay was analyzed in detail. A simplified radiation network and a Hottel network were set up for this bay as input to the Thermal Analyzer program. With the same boundary conditions for the two methods, the simplified network was solved using several values of effective emissivity. The resultant heat flux across this test model was compared to that obtained by the more rigorous Hottel method, and a value for the effective emissivity was chosen to give the same heat flux as the Hottel method. For this test case, the actual surface emissivity was 0.54, resulting in an original effective emissivity of 0.316. The test case gave a modified effective emissivity of 0.42. Unfortunately, this modified effective emissivity applies only to the configuration and conditions analyzed. For the other configurations encountered in the analysis, modified effective emissivities were estimated from the data of this Hottel test case. In Phase I the problem of accurately representing the internal radiation is much less important because of the internal insulation. The aluminized mylar on the internal surfaces of bays greatly reduces radiant exchange between these surfaces.

<u>Choice of Lump Size</u> - Generally, the choice of lump size will be based upon these factors:

1. Consideration of inaccuracies introduced into the system resulting

from the finite difference method of solution. These inaccuracies decrease (not necessarily linearly) as lump size decreases. About the only definite statement which can be made is that lump size should be as large as possible without causing excessive inaccuracies.

2. Anticipated temperature gradients and relative rates of transient response. Where it is suspected that large temperature gradients will occur, nodes should be placed closer together than those where these gradients are smaller. This is especially true when the thermal diffusivity of a particular section is very small, with the resulting temperature gradients across it being highly nonlinear.
3. Convenience in visualizing the network and making calculations.
4. Program Capacity. The compiled data cannot exceed 15000 storage locations. This fixes the maximum number of resistors, capacitors, and boundary data. Thus, for extremely large and complex problems, program capacity becomes an important consideration.
5. Consideration of machine time, which costs money. Not only do small lumps increase the number of nodes to be computed, but also they result in a smaller computing interval (difference in real time between successive steps), thus greatly increasing machine time.

Capacitor Values - The thermal capacity of a lump is calculated in all cases through the formula

$$C = A\delta \int_{T_1}^{T_2} \frac{\rho c}{T}\, dT + \int_{o}^{\delta} \rho c \; A \; dx \qquad (9)$$

where:

C = thermal capacity, BTU/^{o}F
ρ = density, lb/ft^3
c = specific heat, BTU/lb^{o}F

LOCKHEED
CALIFORNIA COMPANY

For assumed constant properties and nodal lumps that approach parallelepipeds, equation (9) reduces to

$$C = A \delta \rho c$$

where:

A = cross-sectional area of nodal lump, ft^2

δ = thickness, ft

For the materials used in the Phase II models, densities and specific heats are listed in Appendix B, Table I.

Series 1 Network - The general configuration of the Series 1 model is indicated in Figure 2-8, with selected nodes shown. The detailed location of all nodes is given in Appendix E. The nodal numbering system is set up to provide immediate recognition of node location with respect to model elements. There are five axial stations designated 100, 150, 200, 300, and 400. Stations 100 and 150 correspond to the forward and aft bulkhead, respectively. Intersection nodes of the upper bulkhead and inner and outer cylinders are numbered from 101 to 136, while their equivalent counterparts on the aft bulkhead are numbered from 151 to 186. Other nodes on the upper bulkhead are numbered 1 to 50, while the lower bulkhead nodes are 50 to 100. Note that corresponding node numbers on the lower bulkhead are 50 digits higher than those on the upper bulkhead.

At axial station 200, panel nodes are numbered from 201 to 223 while the inner cylinder nodes are numbered from 224 to 236. This scheme is followed for the other two axial stations so that in the axial direction the last two digits of the node numbers are the same. For example, on the hot side of the model on the outer panel numbers in the axial direction are 201, 301, and 401, and radially inward, the inner cylinder node numbers in the axial direction are 225, 325, and 425.

The nodal conduction networks are shown for the upper and lower bulkhead in Figure 2-9, for the external cylinder in Figure 2-9, and for the internal cylinder in Figure 2-10. In regions of the model where there are heavy aluminum channels such as the intersection of the bulkheads and the external and internal cylinders, conduction resistors are based solely

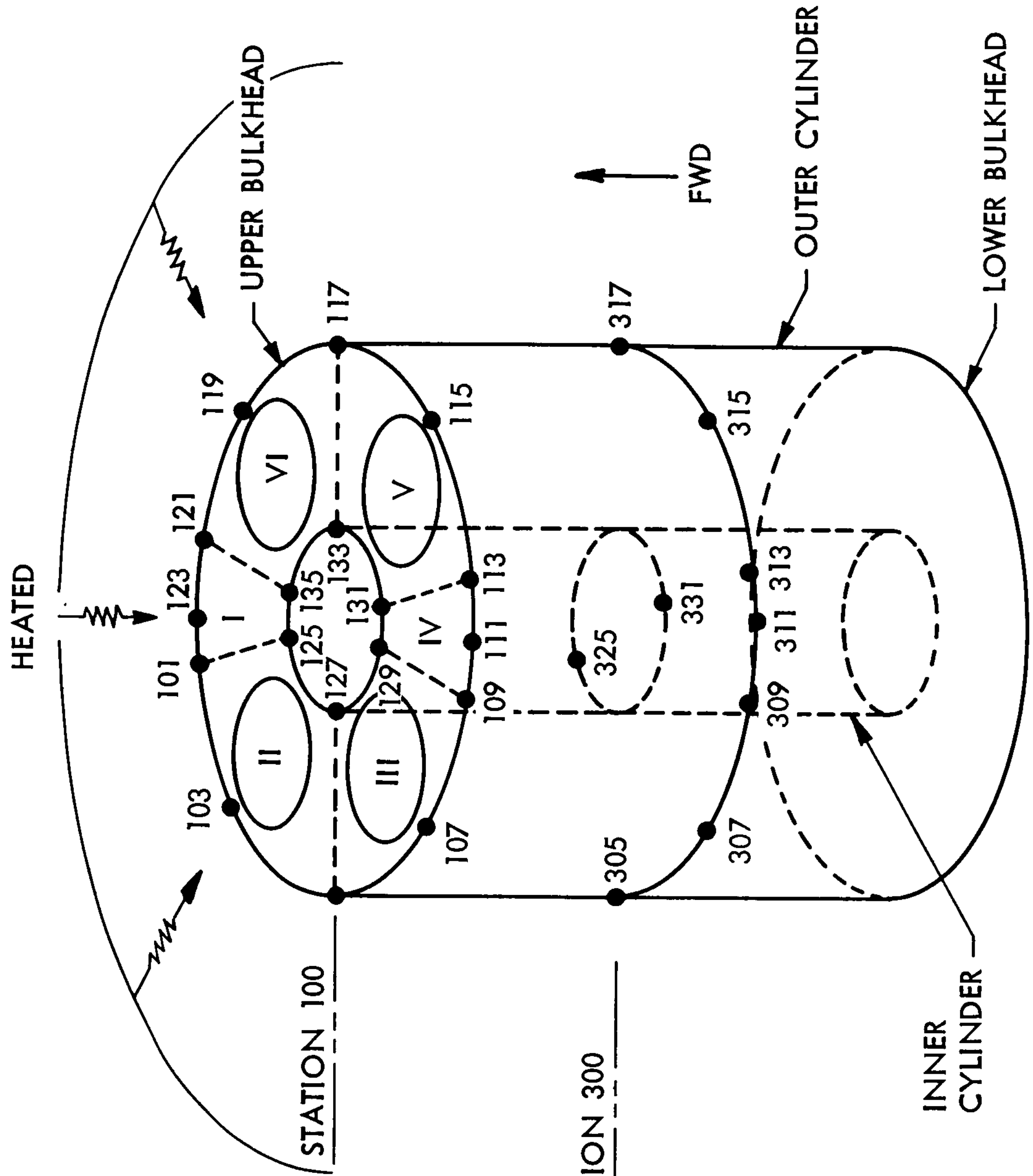

Figure 2-8 Selected Node Locations on Series 1 Model

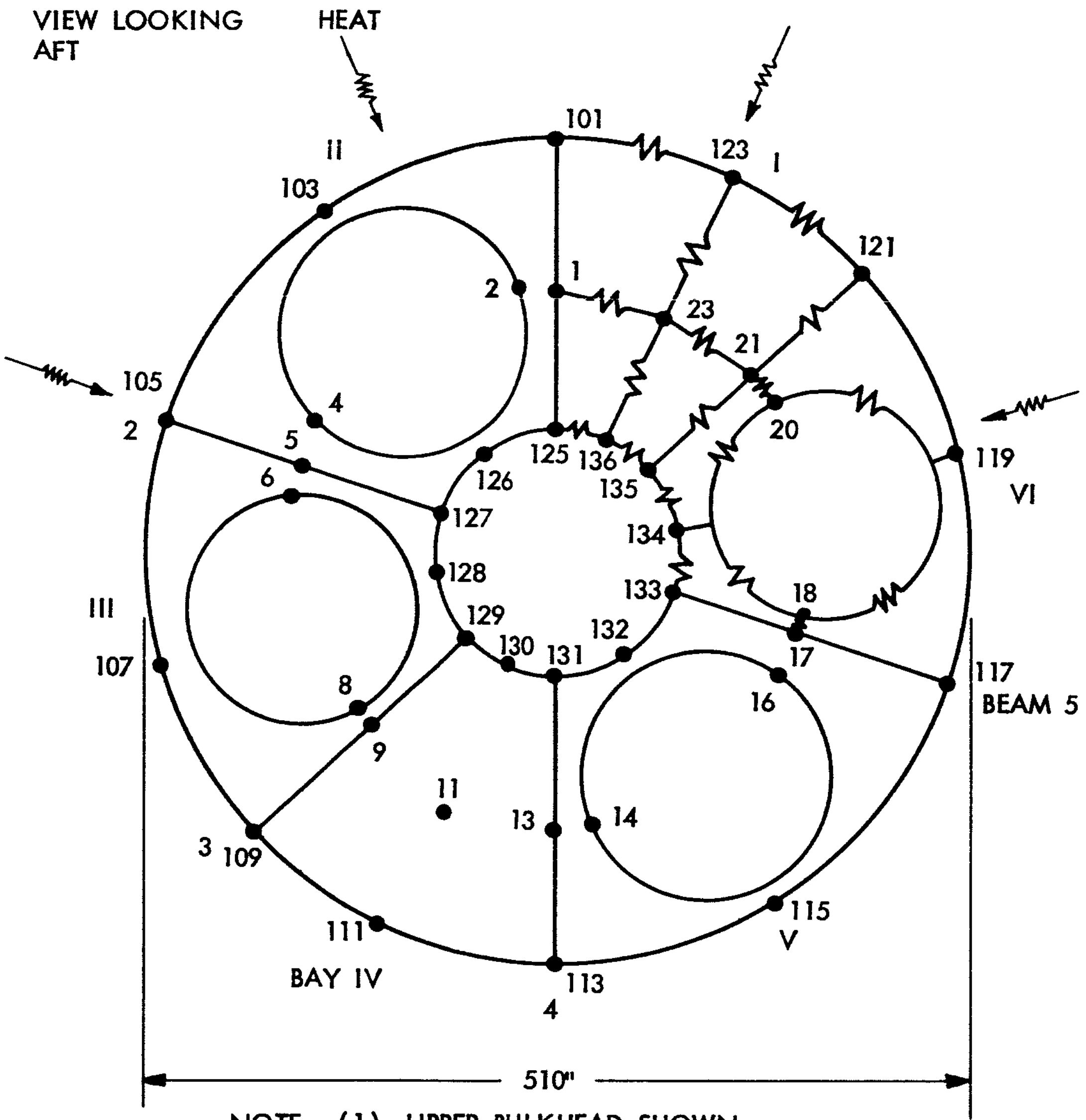

NOTE: (1) UPPER BULKHEAD SHOWN, LOWER BULKHEAD NODE NUMBERS ARE LARGER BY 50.

(2) BAYS AND BEAMS DO NOT APPLY FOR SERIES 1

(3) SEE FIGS E-4, AND E-6 FOR DETAILED THERMOCOUPLE LOCATIONS

Figure 2-9 Conduction Network For Bulkheads

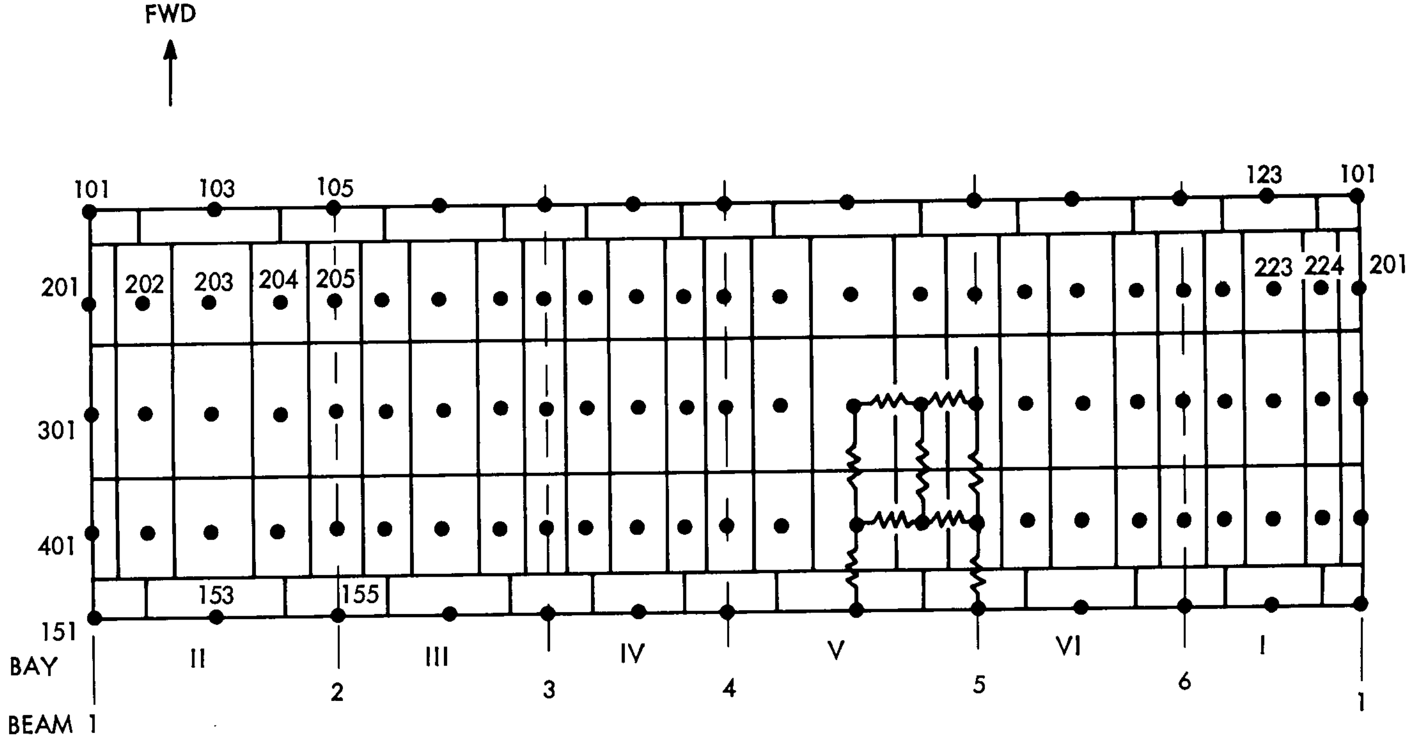

NOTES: (1) BAYS AND BEAMS REFER TO SERIES 2, 3, 5 MODEL
(2) SEE FIG C-1 FOR DETAILED DIMENSIONS AND LOCATIONS OF THERMOCOUPLES

Figure 2-10 Nodel Layout For Outer Cylinder

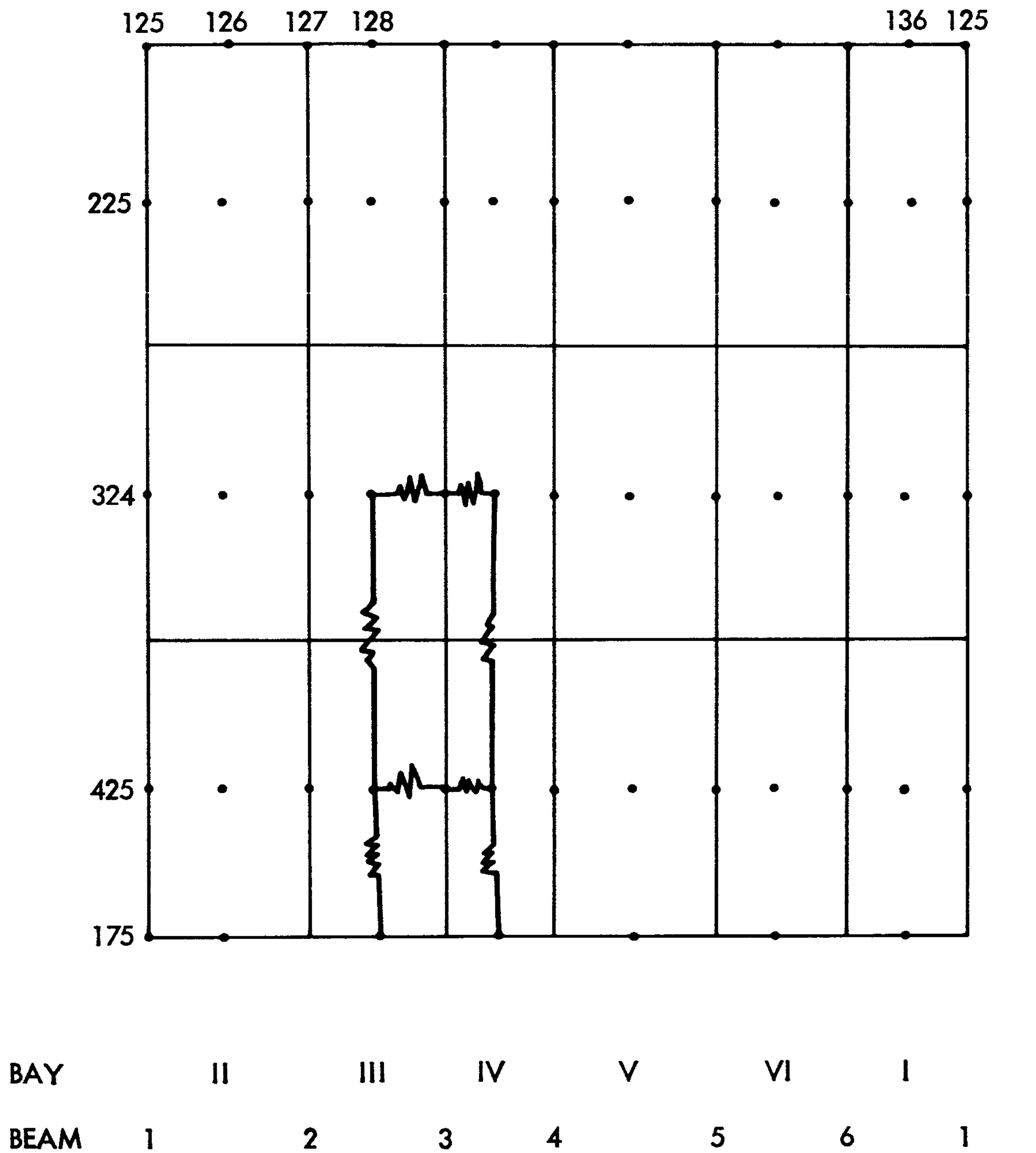

NOTE: (1) BAYS AND BEAMS REFER TO SERIES 2, 3, AND 5 MODEL

(2) SEE FIGURE E-2 FOR DETAILED DEMENSIONS AND LOCATIONS OF THERMOCOUPLES

Figure 2-11 Nodel Layout For Inner Cylinder on these highly conductive channels.

The internal radiation network is shown in Figures 2-12 and 2-13. Figure 2-12 shows the radiation network at axial station 300, which is identical to stations 200 and 400. Radiation resistors across the inner cylinder are included only between nodes that have a significant temperature gradient. In Figure 2-13 are shown the diagonal radiation resistors between the outer shell and inner cylinder. They are located at 6 circumferential stations (X03, X07, X11, X15 and X19). Diagonal radiation resistors from the bulkhead to the shell and inner cylinder were not included because radiation near the corners of the model was assumed negligible compared to the conduction. Moreover, radiation resistors in the axial direction of the model (bulkhead to bulkhead) were not included because the temperature gradient in the axial direction was assumed negligible. Many more radiation resistors could have been added to better represent the physical situation; however, because the internal radiation network is changed with each series model, the added complexity of a finer network could not be justified at the Series 1 level.

There are approximately 200 nodes in the Series 1 network. These nodes are connected by approximately 340 conduction resistors and 230 internal radiation resistors. There are also 43 external radiation resistors from the model outer surface to the chamber walls. Since the external faces of the model bulkheads were well insulated with NRC-2 insulation, these bulkheads were treated as externally adiabatic; i.e., no heat transfer to the chamber.

Run Correlations - Preliminary runs of the Series 1 computer programs indicated systematic discrepancies between experimental and predicted temperatures. This was attributed to the fact that the internal radiant heat transfer across the uninsulated models is significantly underestimated by the use of the simplified network of conventional radiation resistors. This is because energy transmitted from one surface to a second, and then reflected to a third, is unaccounted for. This factor is important only in those situations in which a significant part of the total internal heat transfer is taking place between low-emissivity surfaces having low view factors to each other. This occurs not only

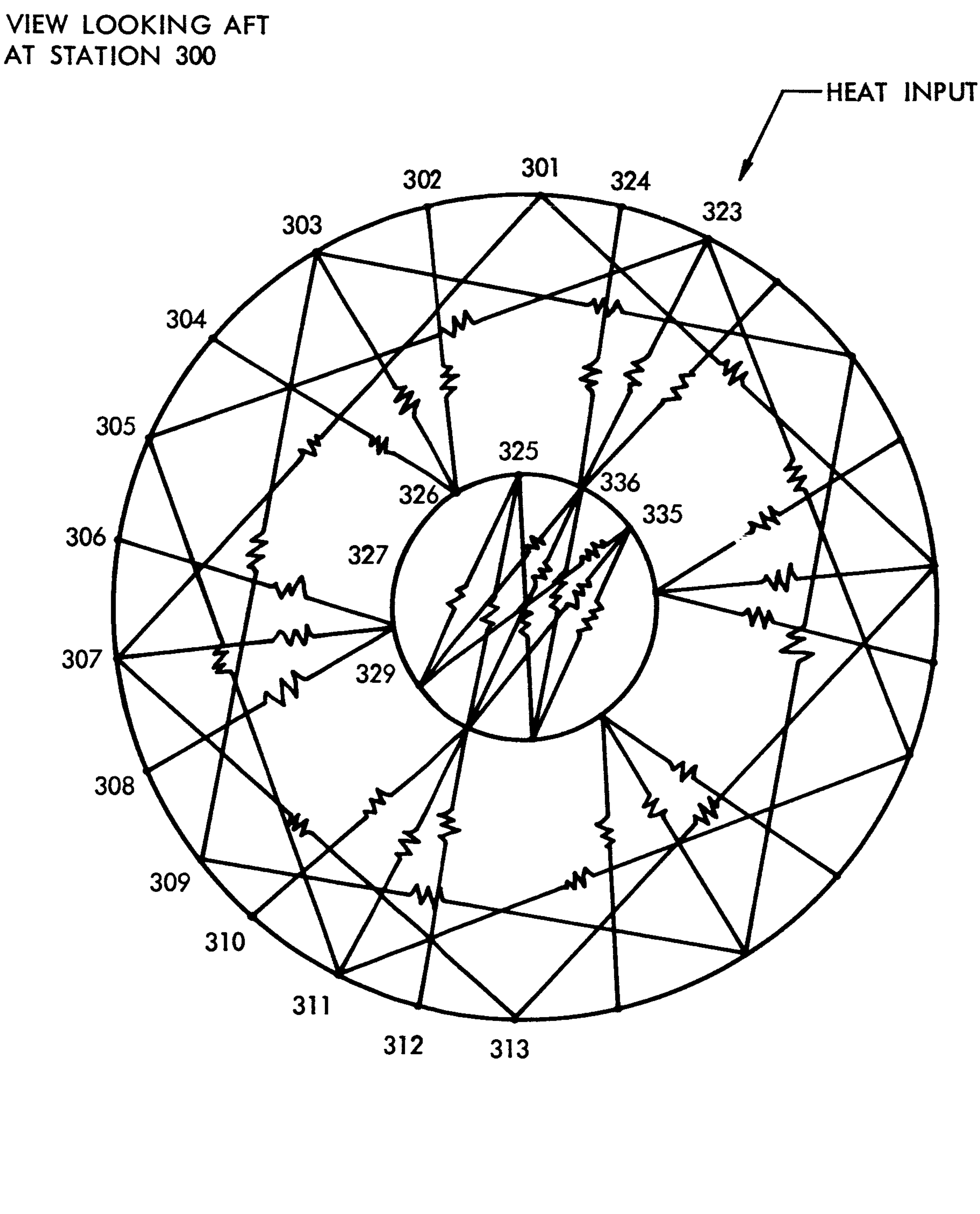

Figure 2-12 Internal Radiation Network at Station 300

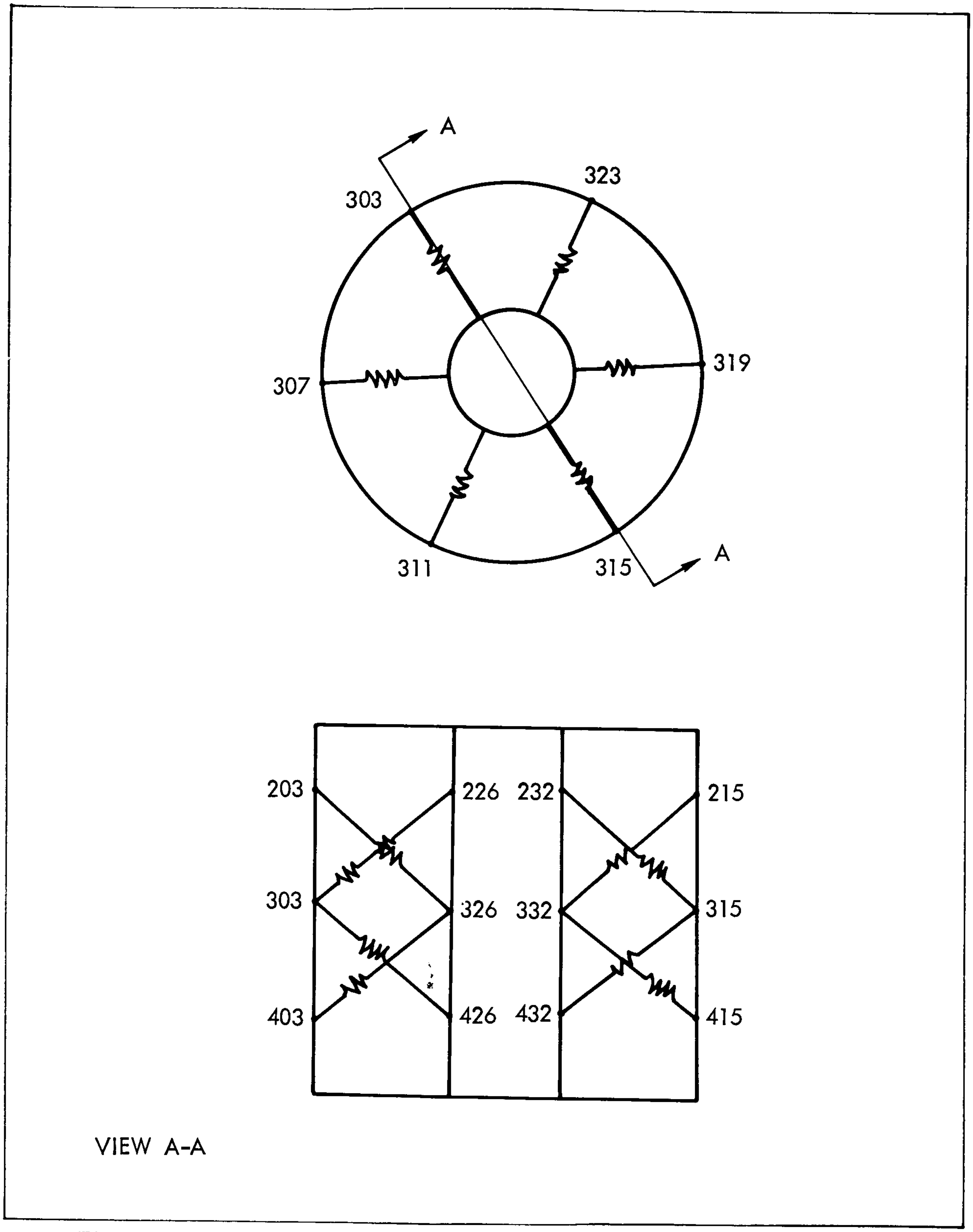

Figure 2-13 Internal Radiation Network for Fore and Aft Sections

in the Series 1 model, but in the Series 2 and uninsulated Series 3 models.

To keep the number of resistors within the storage capacity of the computer, it was judged that a modified effective emissivity could be used with the existing simplified radiation network to account for the reflected energy. The modified effective emissivity was determined by the method outlined in the analytical and techniques section, and was found to be 0.42, while the original value was 0.316. Using the modified effective emissivity, the Series 1 program was re-run. The circumferential temperature distribution on the inner and outer cylinders at 5340 seconds after run start is shown in Figure 2-14 for station 300 (midpoint) and in Figure 2-15 for station 100 (upper bulkhead). These figures indicate the difference between the initial and modified (effective emissivity) analysis. At station 300 the discrepancy between analytical and experimental results was reduced by 40% for the outer cylinder and by 70% for the inner cylinder. The maximum remaining discrepancies were approximately 15^{O}F for the outer cylinder and 10^{O}F for the inner cylinder.

The improvement at station 100 (Figure 2-15) is not as marked. The maximum discrepancy at the intersection of the upper bulkhead and the inner cylinder remains at approximately 10^{O}F. However, considerable discrepancy (as much as 50^{O}F) still exists at the intersection of the bulkheads and the inner and outer cylinders during transient conditions. This is partially due to the incomplete accounting of radiation near the inside corner (see Figure 2-13). Another factor in this discrepancy is the coarseness of the conduction network in this area. One node is used to represent the corner, and the resulting temperature is an average value. The temperature gradient around this corner is very large so that the thermocouple which is mounted on the bulkhead side of the intersection can be expected to read a different temperature than an average value.

Transient behavior of several typical nodes during the first 1.5 hr. of the run are shown in Figures 2-16 and 2-17. Analytical and experimental temperature histories for shell node 313 and bulkhead node 113, on the cold side of the model, are presented in Figure 2-16.

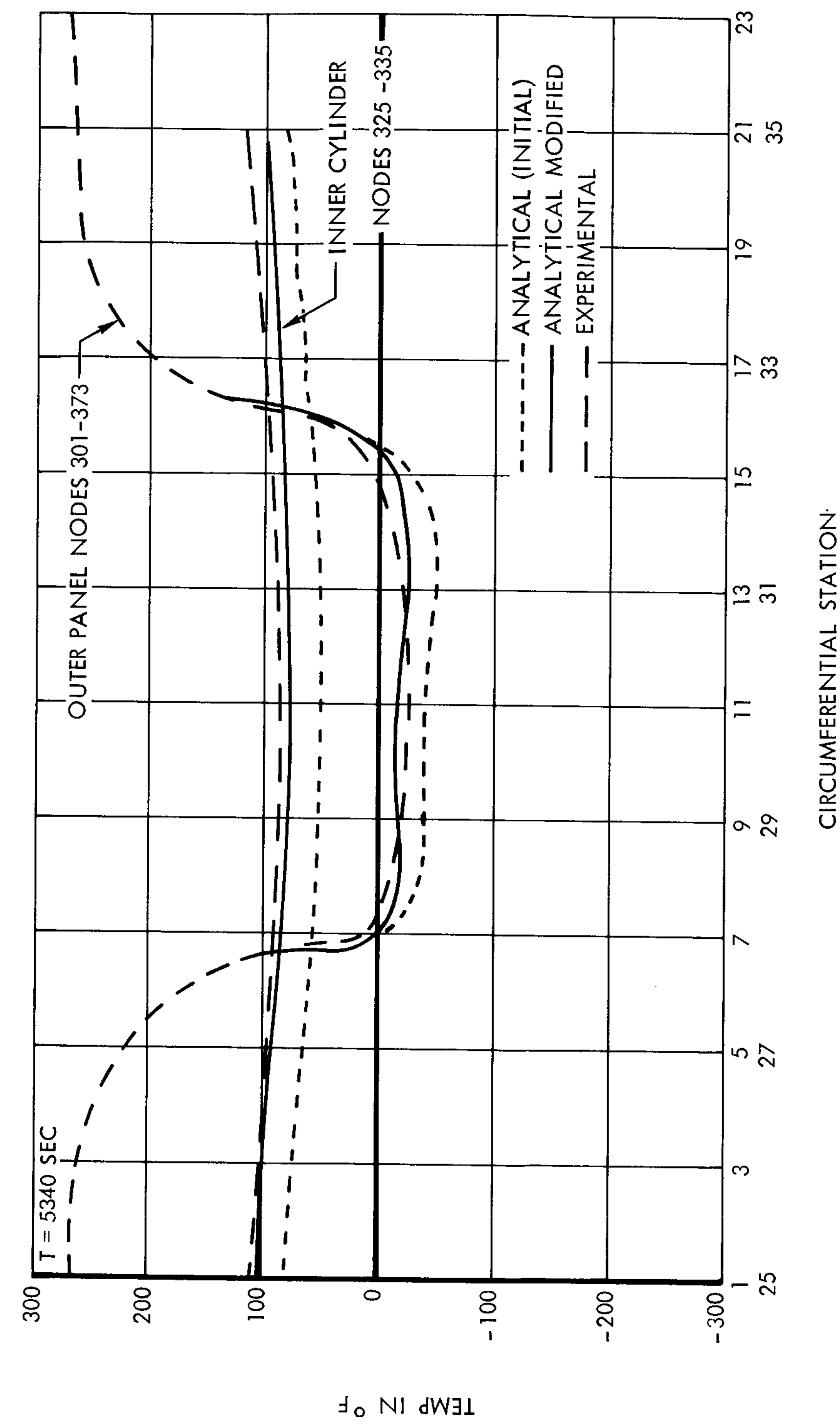

Figure 2-14 Circumferential Temperature Distribution at Station 300

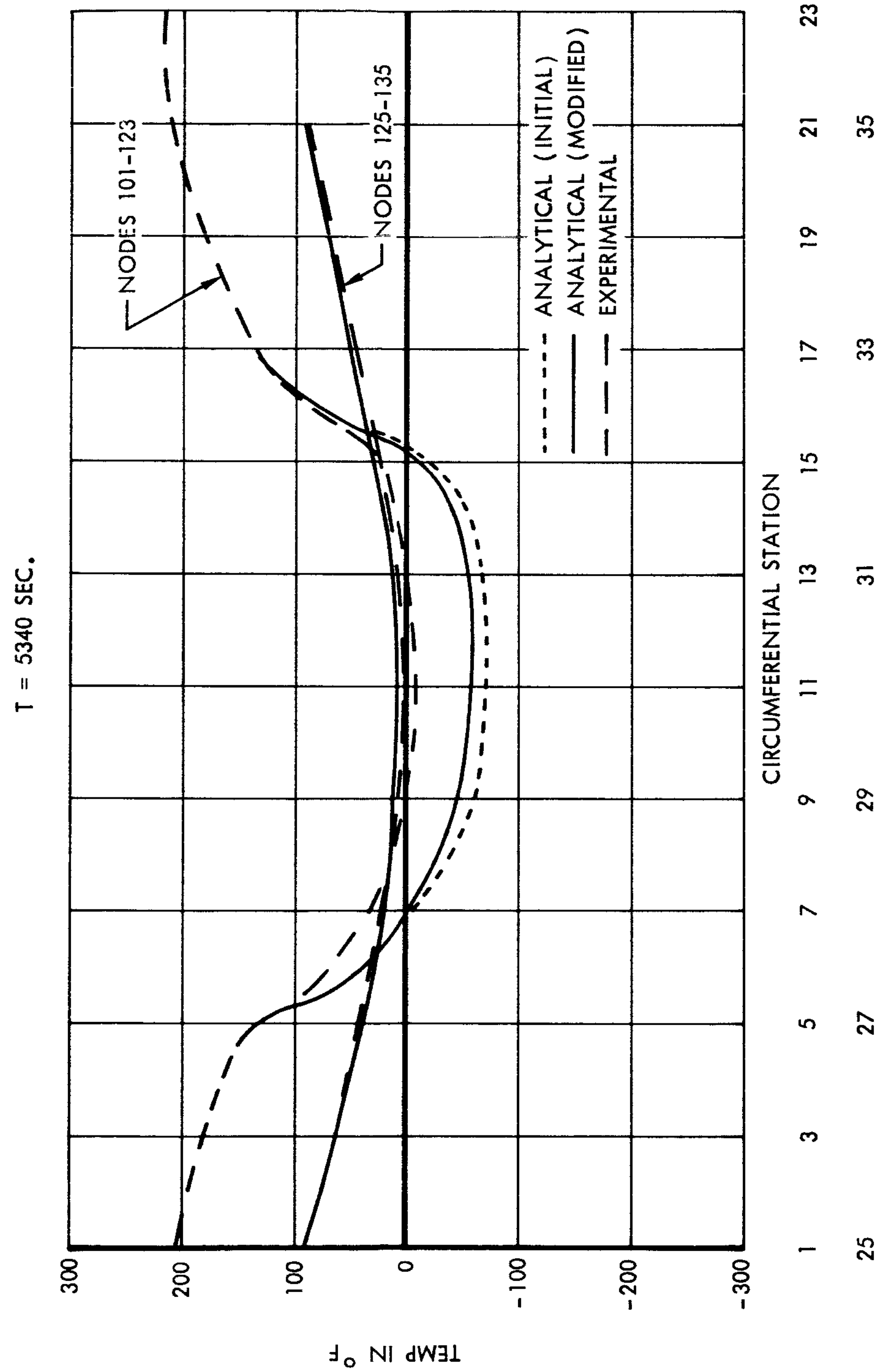

Figure 2-15 Circumferential Temperature Distribution at Station 100

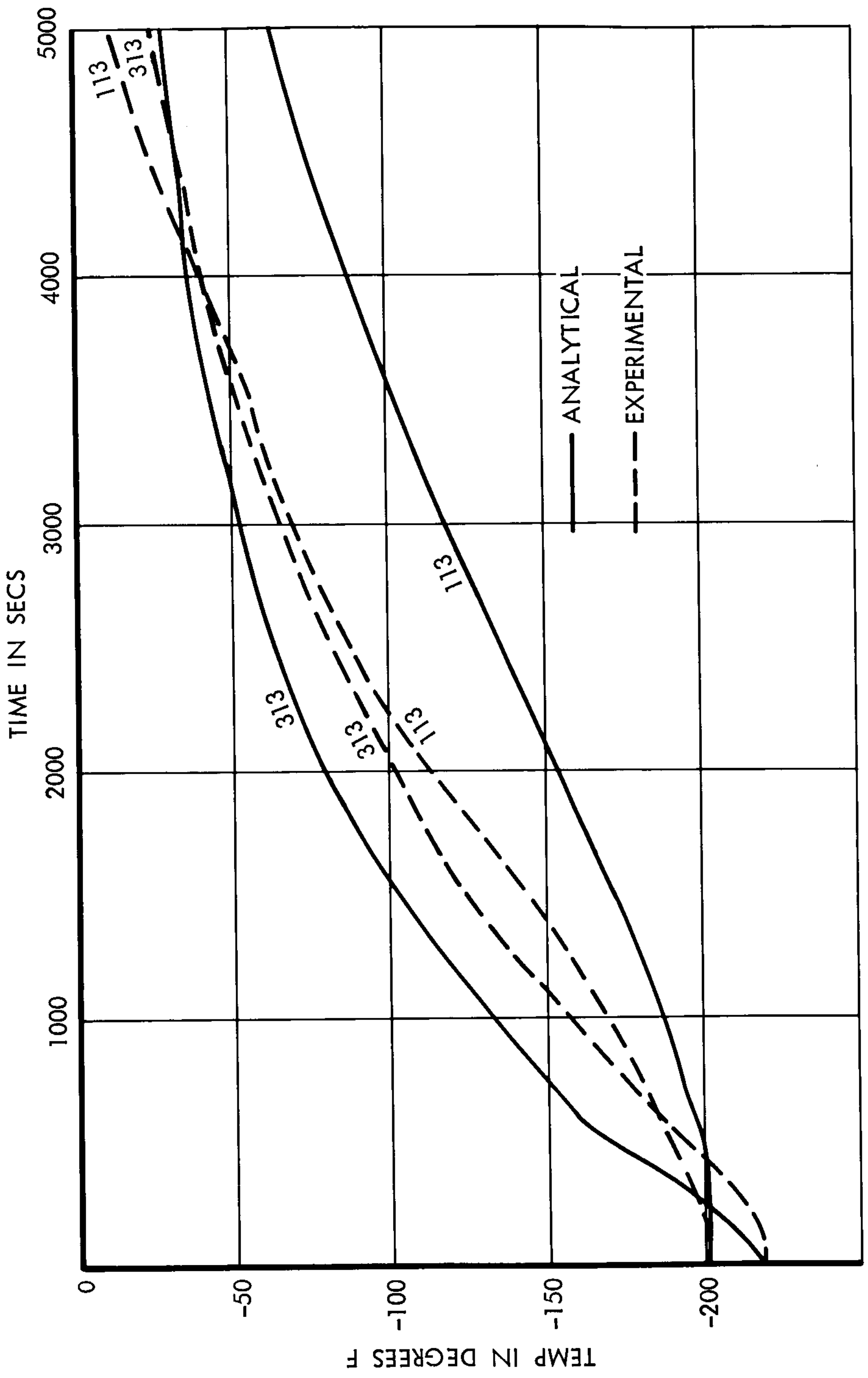

Figure 2-16 Temperature Histories of Nodes 113 and 313

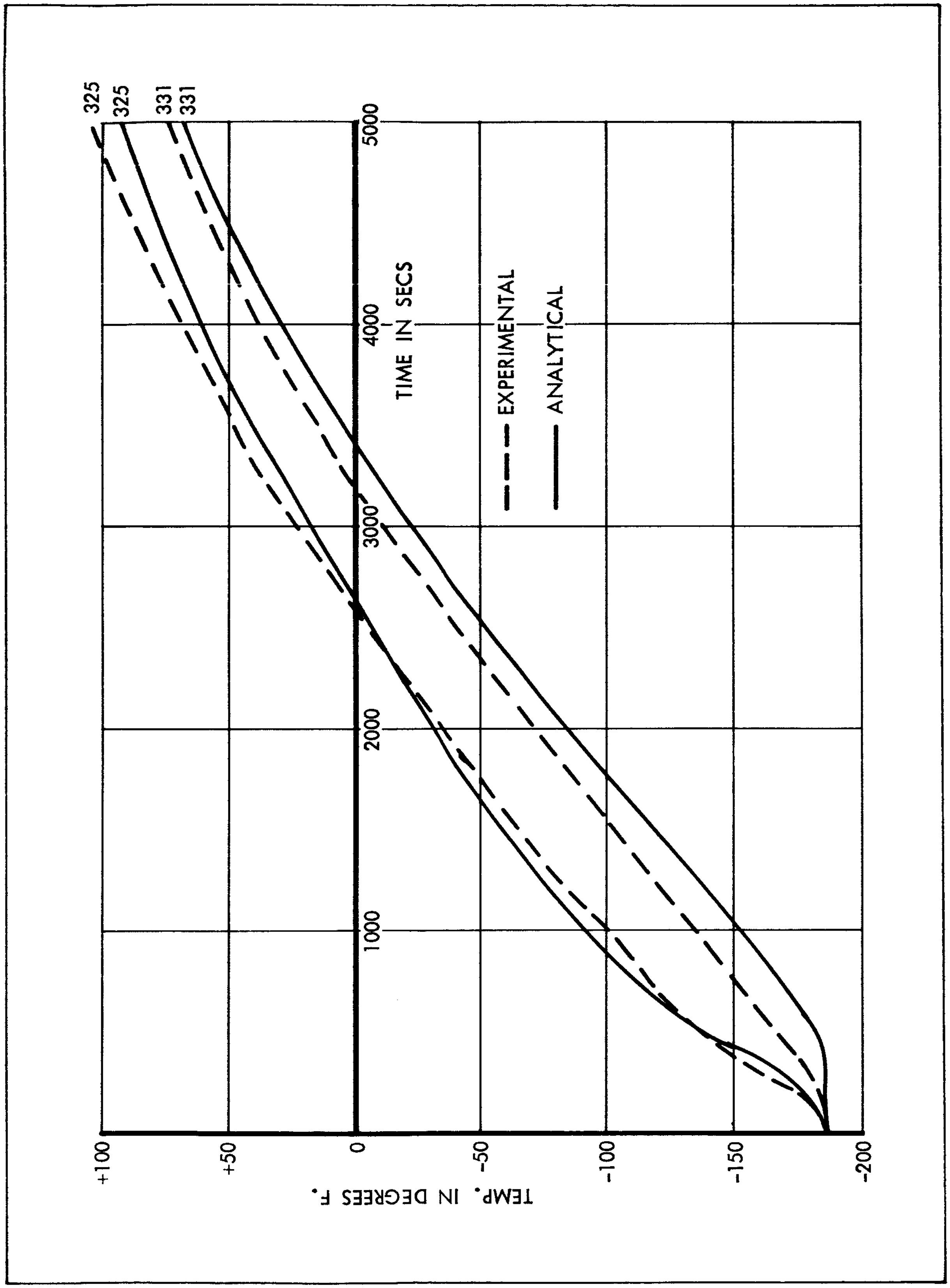

Figure 2-17 Temperature Histories of Nodes 325 and 331

Predicted temperatures for the shell node are 10 to 20°F warmer than experimental temperatures for the most part of the run. The bulkhead node 113, however, has a predicted temperature 20 to 40°F lower than the measured values. It is important to note that the experimental temperature gradient between shell node 313 and bulkhead node 113 is about 5 to 10°F, whereas the analytical temperature gradient is 40 to 80°F. Inspection of the temperatures for the shell and bulkheads indicated that predicted temperatures on the shell were typically 20°F too warm and the predicted temperatures on the bulkhead were 40°F too cool. These deviations were in great part due to the assumption that radiation from the shell to the bulkheads was negligible. This assumption is valid for the insulated models where the NRC-2 insulation is used. Figure 2-17 shows the analytical and experimental temperature histories of two representative inner cylinder nodes. In general, predicted temperatures for nodes 325 and 331 are systematically 5 to 10°F lower than experimental temperatures, except for the first half of the run for node 325, where there is excellent agreement.

The predicted Series 1 temperatures, after the modification of the radiation resistors, were generally within $\pm$ 30°F of the measured temperatures. This run pointed out the severe problems associated with radiative heat transfer in a reflective enclosure. Although the modification of the radiation resistors yielded reasonably good results, the dominance of the radiation mode of heat transfer prevented a quantitative evaluation of the conduction network. In retrospect, if the Series 1 model were highly insulated with NRC-2 to completely eliminate radiative heat transfer, this would allow a careful examination of the conduction network before the complexity of the radiation mode is added.

III - SERIES 2 MODEL

MODEL DESIGN AND FABRICATION

Six sector-partition beams were installed between the inner and outer cylinders of the Series 1 model to form the Series 2 model shown in Figure 3-1. In Figure 3-2, the Series 2 model is shown suspended from the heat-lamp fixture. The early assembly photos, Figures 3-3 and 3-4, show the Series 2 model without paint and instrumentation.

Beams

The 18-in. by 50-5/8-in. sector partition beam assemblies were fabricated from .025-in. thick 6061-O aluminum alloy. The long edge contacting the inner cylinder has a 3/4-in. channel section with a 1-in. long leg for sheet metal screw connections on 5-in. centers. The opposite long edge has two 7/16-in. angles spot-welded continuously to it to form a T-section. Platenuts are attached to the angle legs on 3-in. centers to pick up number 8-32 attachment screws inserted from the outside through the outer cylindrical panel segments. The two short edges were stiffened by being bent to form a 5/8-in. flange. Six 3/8 by 3/8 x .025 in. angles were spot-welded back-to-back across the panel at three places to provide additional stiffness. The beam cross-section was purposely kept thin to minimize conductive heat flow.

Instrumentation

Three thermocouples were attached to each sector beam before painting. These 18 thermocouples were made from Trinity Micro Corp. 30-T-EG premium-grade 30-gage Type T (Cu-Cn) wires with silicone impregnated fiberglass insulation. They were taped to the webs in the manner described in Section 2. The corresponding node numbers for these couples are shown in Appendix E. Beam No. 1 is located between Sectors I and II; beam No. 2, between Sectors II and III, etc. The total number of node thermocouples on the Series 2 model was 141. The test data were recorded on punched tape by the Mod-Sadic.

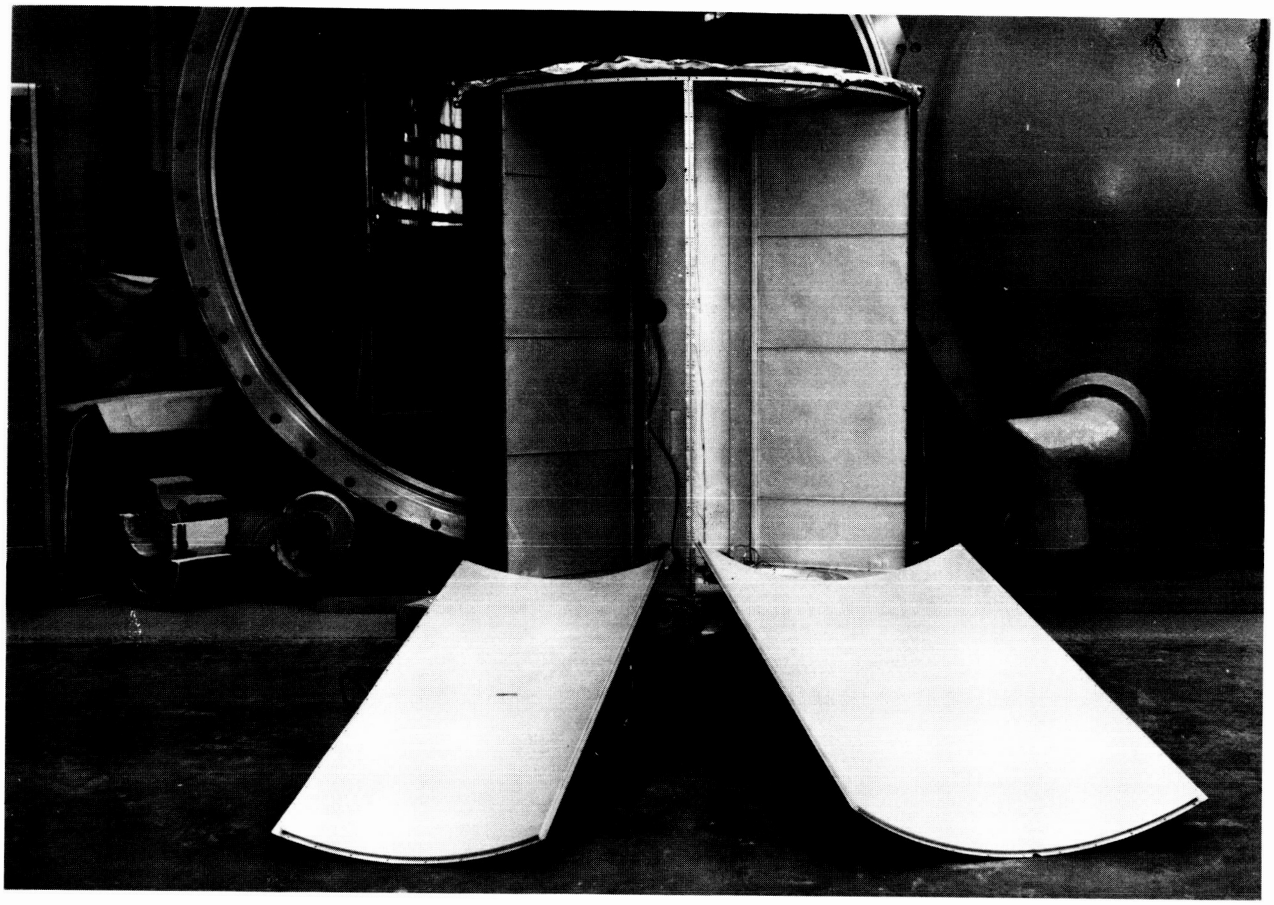

Figure 3-1 Series 2 Model With Two Side Panels Removed

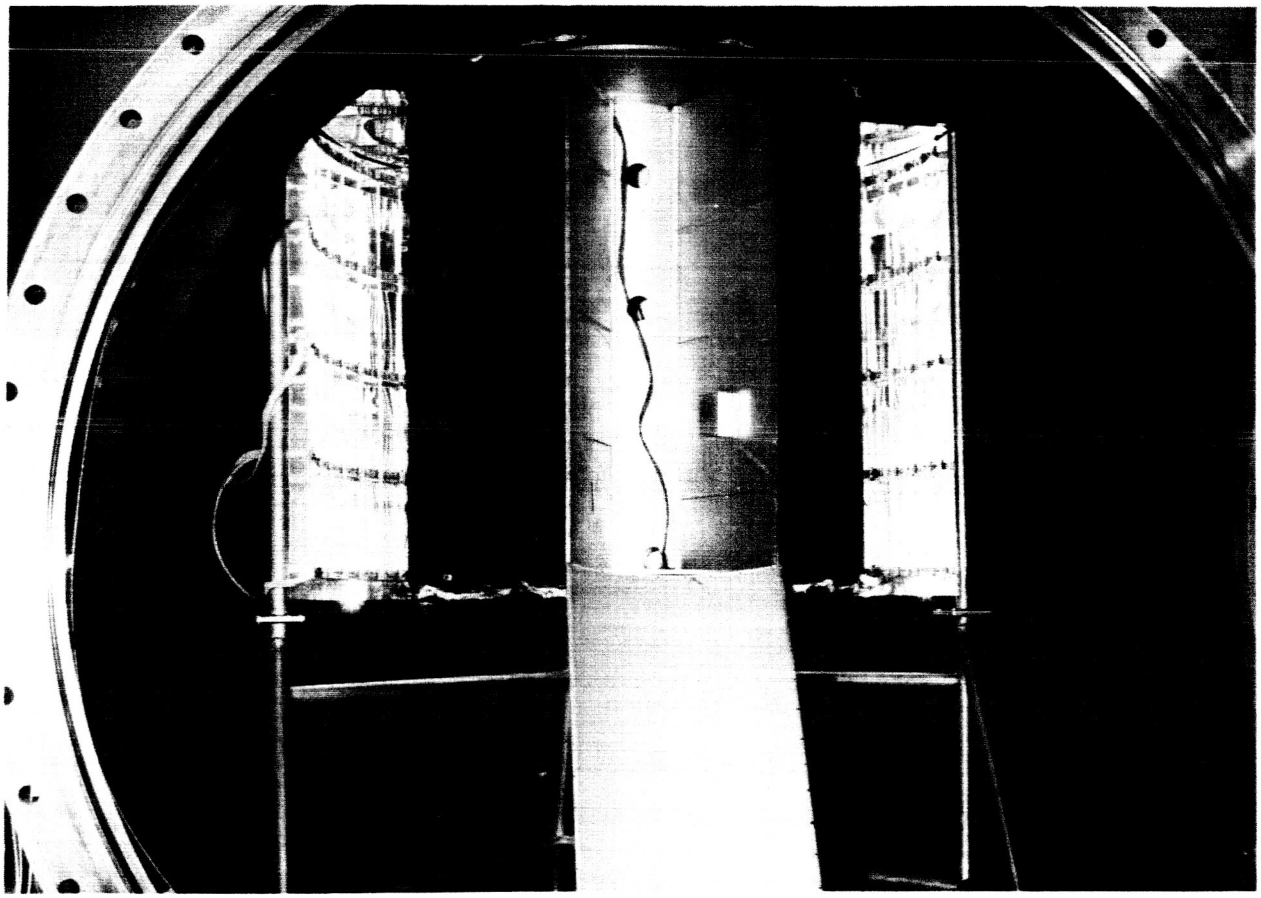

Figure 3-2 Model Mounted In Radiant Fixture One Panel Removed

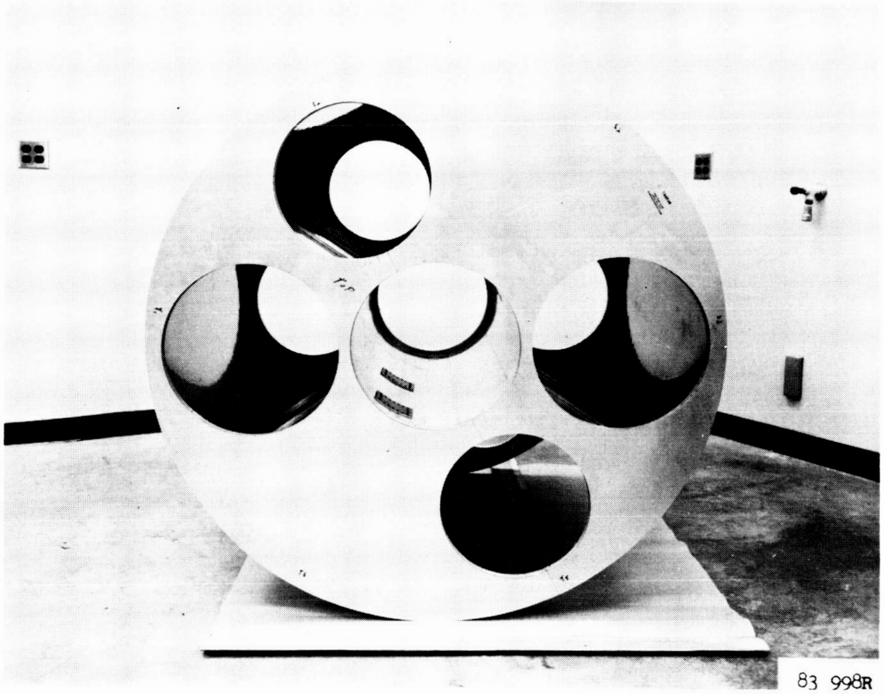

Figure 3-3 End View - Series 2 Model

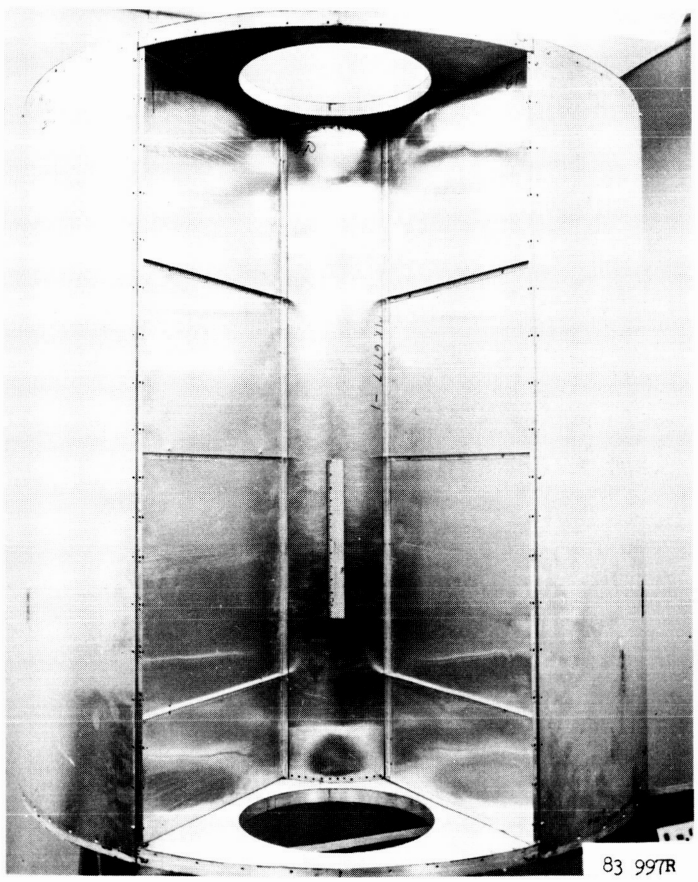

Figure 3-4 Series 2 Model Showing Sector Beams

Test Runs

Run Preparation and Checkout - After the model had been reworked to the Series 2 configuration, it was remounted in the radiant-heat fixture. The portable heater-blower was again used to check and match the beam thermocouple node location with the Mod-Sadic channels. The thermocouples previously checked on the bulkheads and inner and other cylinders were spot-checked for channel matching and inspected for damage from handling.

Series 2- Runs 1 and 2 - The Series 2 tests, each 8 hours in duration, were identical in procedure with those of Series 1. The tests were judged satisfactory, and the model was removed in preparation for conversion to the Series 3 model configuration.

Analytical Correlation

Series 2 Network - To account for the six radial beams of the Series 2 model (see Figure 3-5), a conduction network for these beams is added to the Series 1 network, Figure 3-6. The internal radiation network at station 300 is shown in Figure 3-7. Internal radiation in the diagonal direction for the Series 2 model is exactly the same as for Series 1 shown in Figure.2-12 & 2-13.

There are approximately 215 nodes in the Series 2 network. These nodes are connected by approximately 400 conduction resistors and 245 internal radiation resistors. There are 43 external radiation resistors. As in Series 1 there are also diagonal radiation resistors between the outer shell and the inner cylinder. Again, radiation in the axial direction of the model and between the shell and bulkheads is assumed negligible.

Run Correlations

The Series 2 program was run both with and without the same emissivity correction as applied to Series 1 Figures 3-8 and 3-9 show a comparison of the analytical and experimental circumferential temperature distributions on the inner and outer cylinders at 4278 seconds after run start. Here, the utilization of a modified effective emissivity has less effect than in Series 1. This is because the radial beams act as radiation barriers and thus the radiation heat transfer across the model is less important than

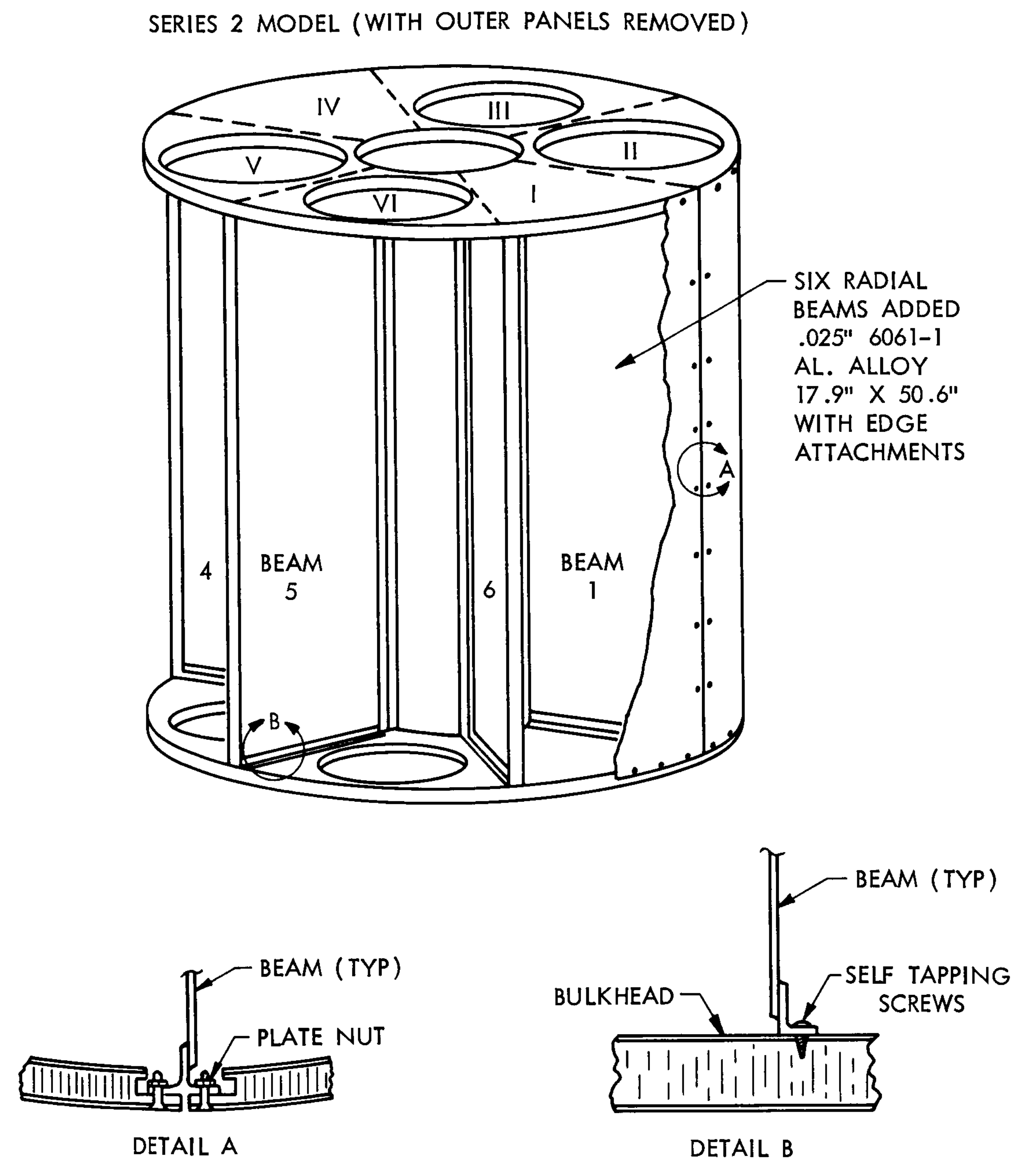

Figure 3-5 Series 2 Model

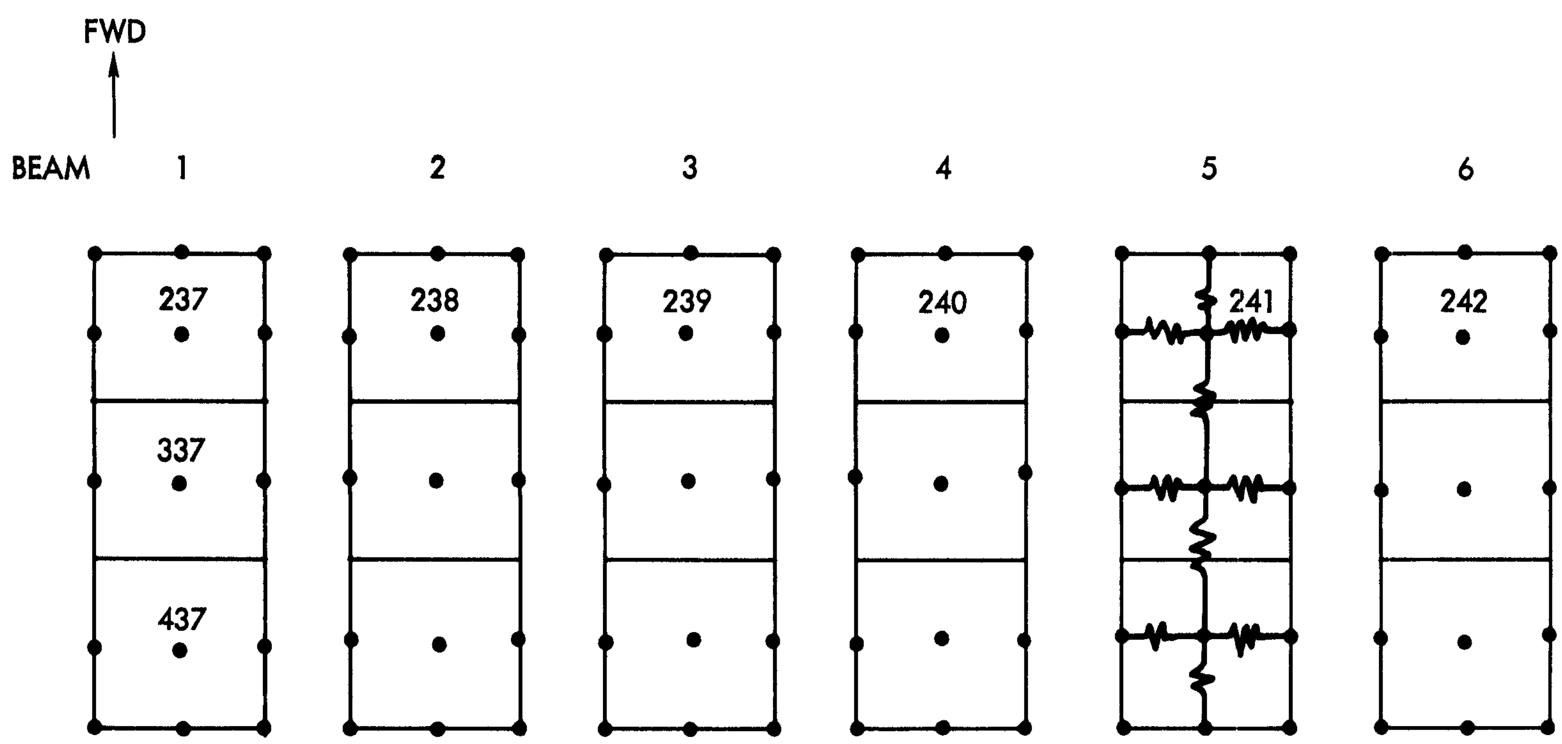

NOTES

(1) OUTSIDE EDGE TO LEFT

(2) SEE FIG E-3 FOR DETAILED DIMENSIONS AND THERMOCOUPLE LOCATIONS

Figure 3-6 Nodel Layout of Beams with Indicated Conduction Network

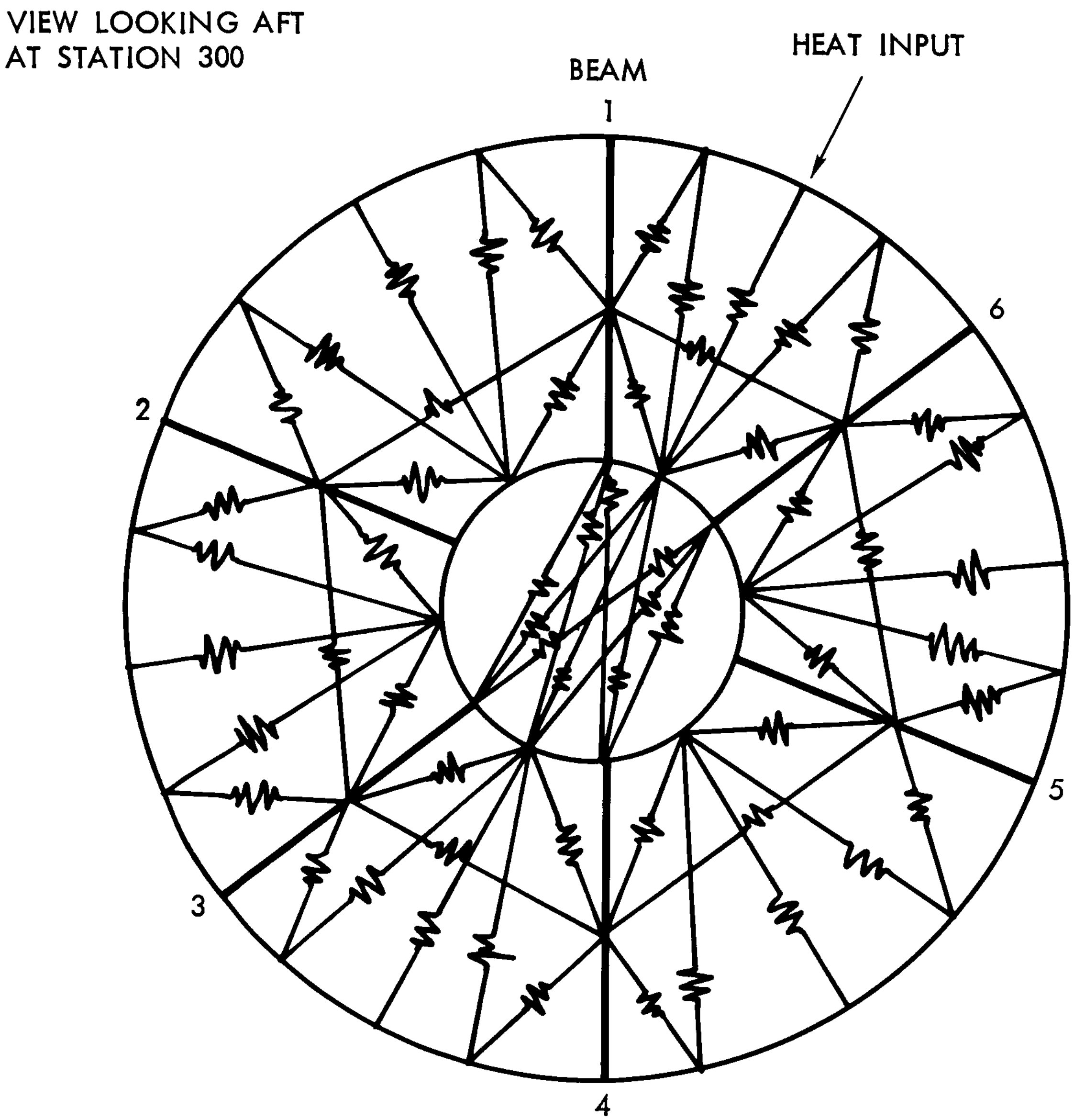

Figure 3-7 Radiation Network at Station 300

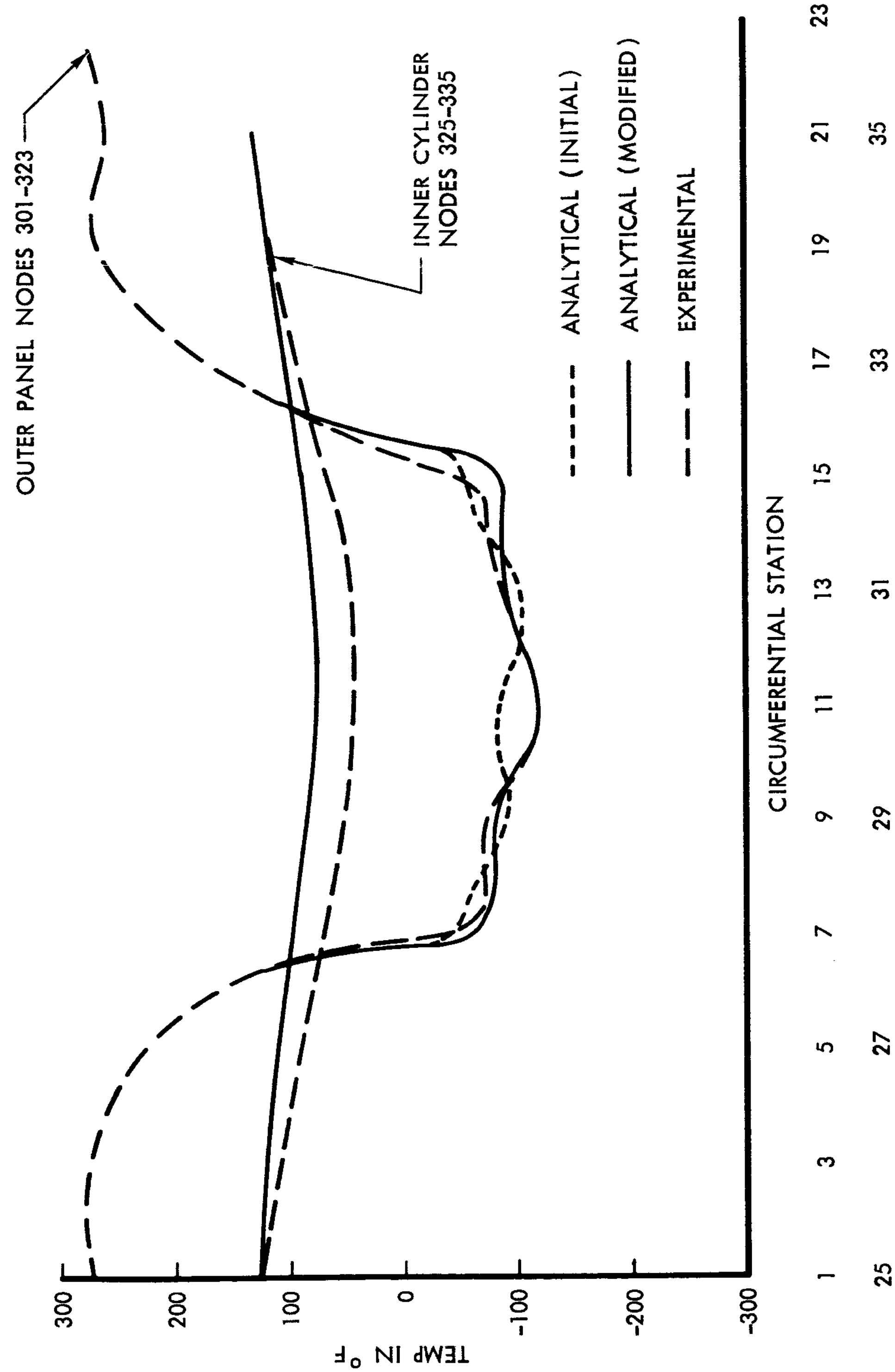

Figure 3-8 Circumferential Temperature Distribution at Station 300

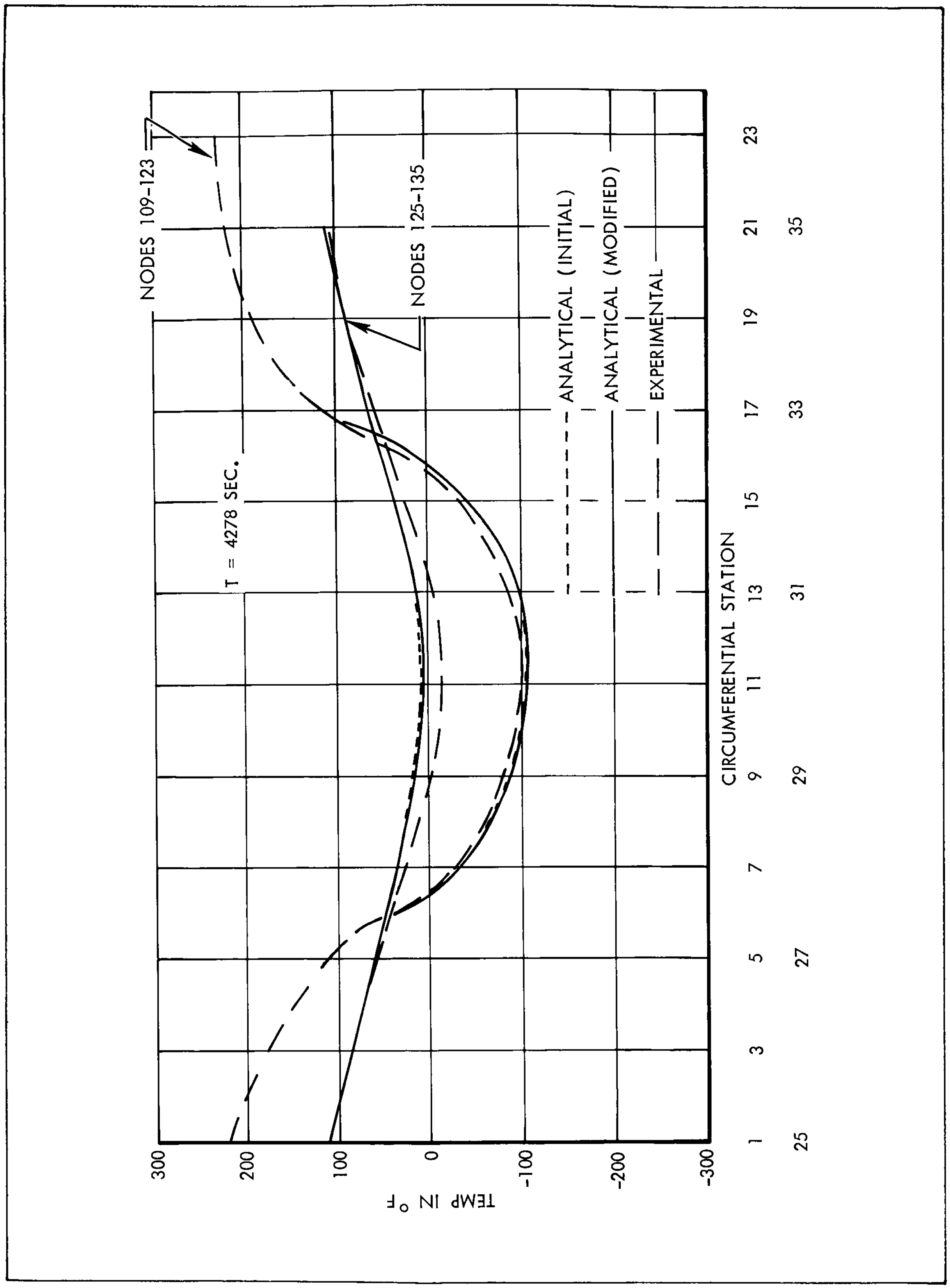

Figure 3-9 Circumferential Temperature Distribution at Station 100

in Series 1. The maximum temperature discrepancy around the outer panel is approximately 20° F at station 100 (upper bulkhead) and 30° F at station 300 (midpoint).

Around the inner cylinder, the maximum discrepancy is approximately 20° F at station 100 and 30° F at station 300. The discrepancy between predicted and experimental results is not uniform over the entire vehicle. This again is largely due to the incomplete accounting of internal radiation and indicates that the blanket emissivity correction is not a general cure-all. Figure 3-8 also shows improved correlation in the temperature distribution around the outer panels as a result of additional radiation resistors being added between the inner cylinder and outer panels. This provided a more uniform distribution of heat flux to the outer panels.

A temperature history of the shell node (313) and bulkhead node (113) is shown in Figure 3-10. For both these nodes agreement between predicted and measured temperatures is within 10°F for the temperature range of -170° F to -100° F. A comparison of these results with the same two nodes of Series 1 reveals that correlation is much better for the Series 2 run because the internal radiation heat transfer is accounted for more accurately. The beams act as a radiation barrier that reduces heat flow from the hot side of the model to the cold side shell and bulkheads. This is most graphically observed by comparing the experimental temperatures on the cold side of the model for the Series 1 and Series 2 runs.

The temperature at node 313, for comparable conditions, is -40°F for Series 1 and -95°F for Series 2. This indicates that the net heat transfer across the model is markedly reduced by the addition of the beams.

Shown in Figure 3-11 are the analytical and experimental temperature histories of two inner cylinder nodes, 325 and 331. Predicted temperatures are within 10°F of measured temperatures for node 325, while for node 331 predicted temperatures are 20°F to 30°F warmer than the measured temperatures. The temperature range for these nodes is from -150°F to 100°F. Temperature histories of beam node 337, adjacent to inner cylinder node 325, and beam node 340, adjacent to inner cylinder node 331, are shown in Figure 3-12. Beam and inner cylinder temperature predictions are similar

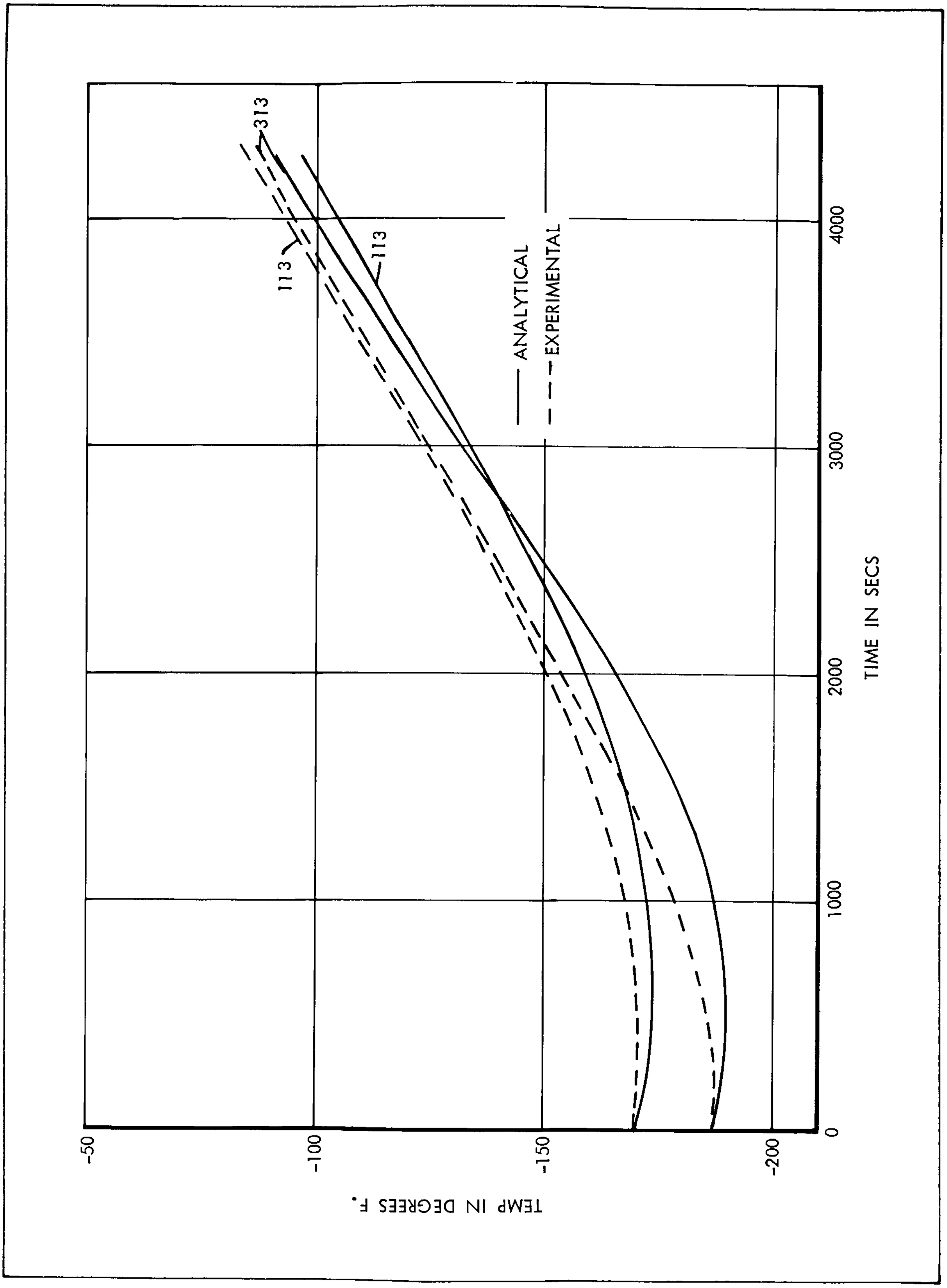

Figure 3-10 Bulkhead (Node 113) and Panel (Node 313) Temperature Histories

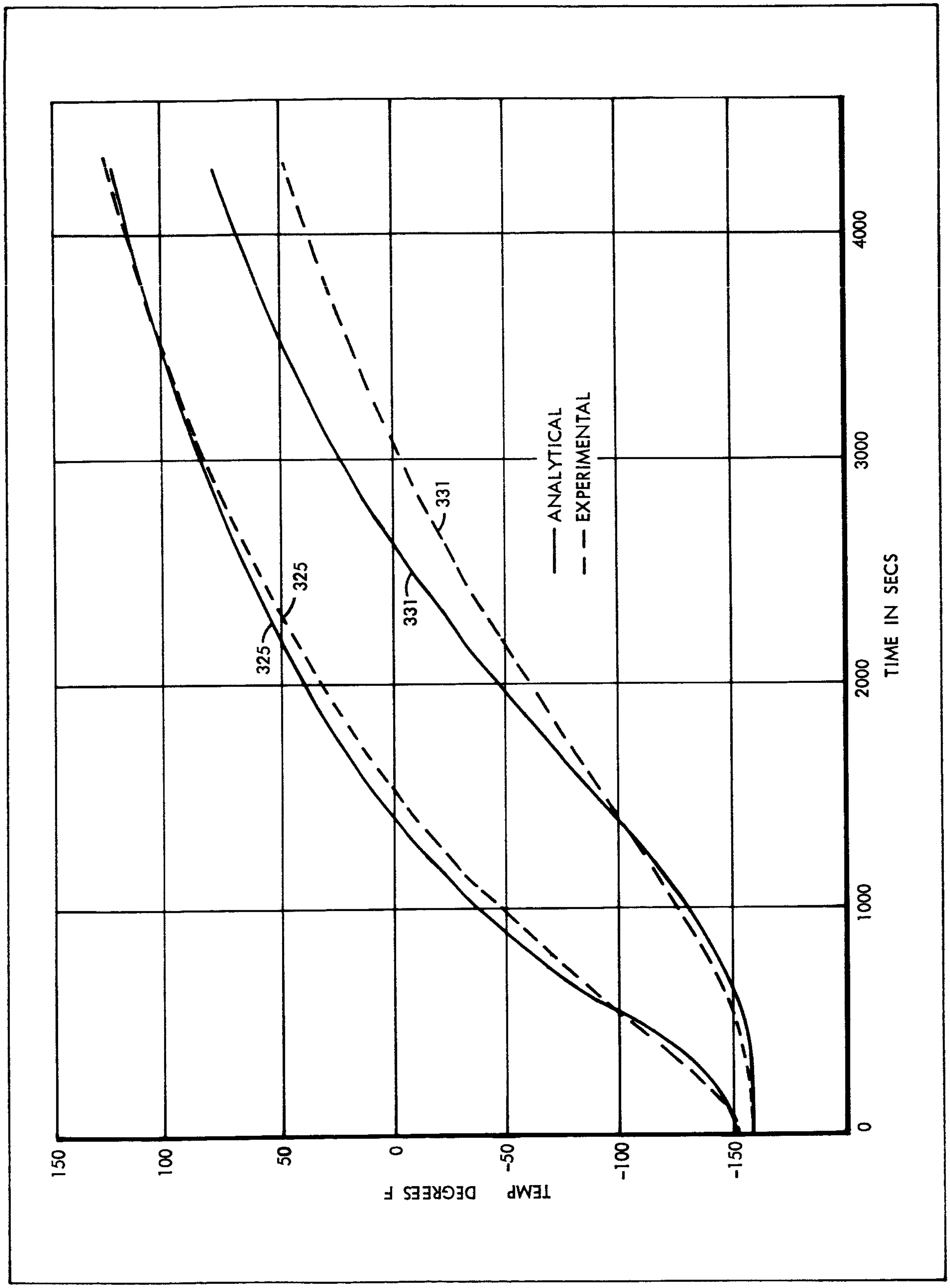

Figure 3-11 Inner Cylinder Temperature Histories (Nodes 325 and 331)

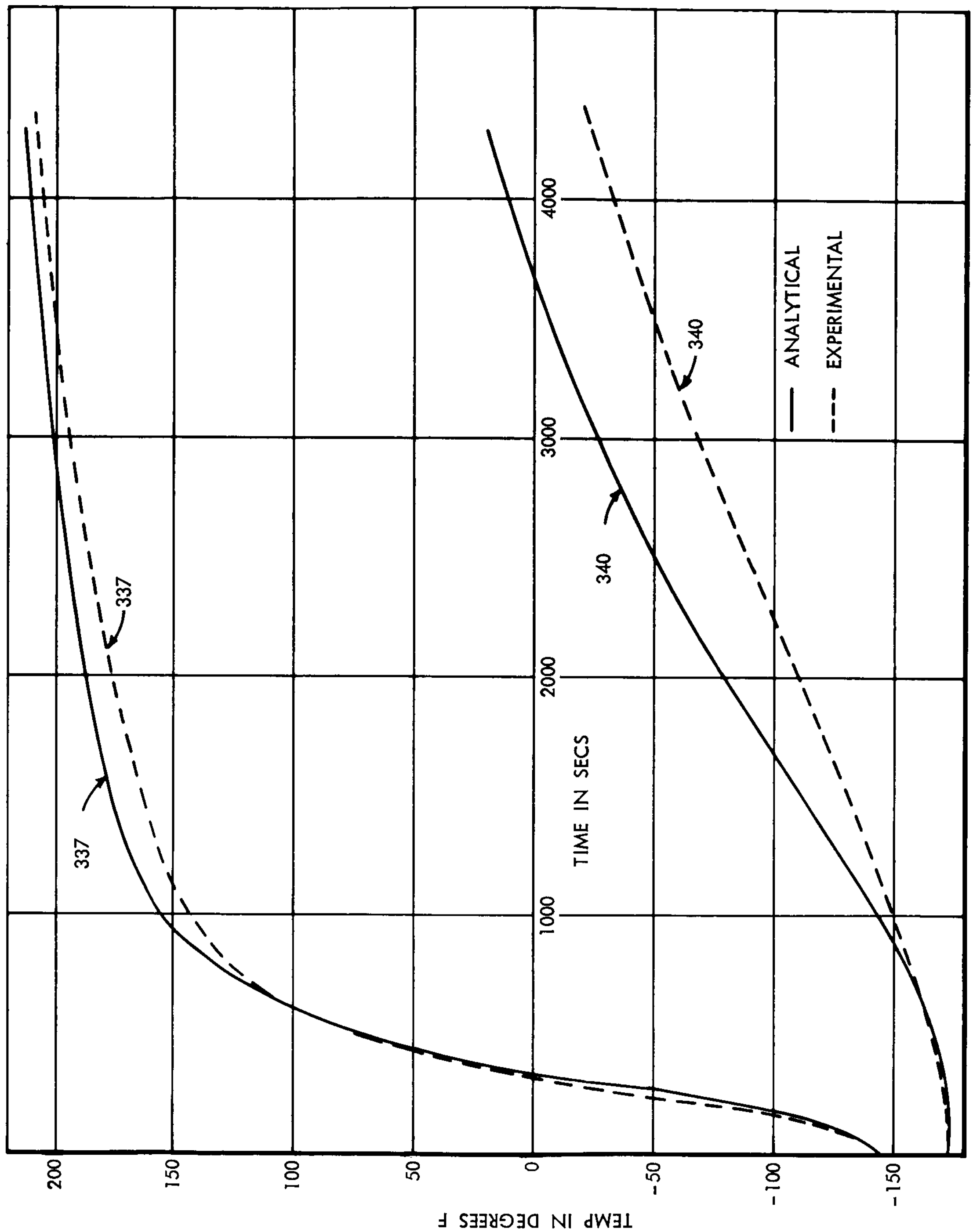

Figure 3-12 Beam Temperature Histories (Nodes 337 and 340)

in that both show differences from measured temperatures of 5°F on the warm side of the model and 20 to 30°F on the cold side of the model.

It appears that the thermal analysis is predicting a smaller temperature gradient across the model at the middle axial station (300) than the experimental results. The cause of this discrepancy cannot be isolated as to radiation or conduction problems. One possible cause of the smaller predicted temperature gradient across the model is the effect of contact resistance between the beams and inner and outer cylinders. This was assumed negligible in the analysis.

In summary the Series 2 correlation is slightly better than the Series 1. Addition of the radial beams reduced the net heat transfer across the external shell and to the bulkheads. As in Series 1, blanket modification of the effective emissivity improved overall correlation; however, because radiation heat transfer across the model was reduced by the beams, the effect of this modification was less pronounced.

IV - SERIES-3 MODEL

MODEL DESIGN AND FABRICATION

In the Series 3 model (Figure 4-1), the final level of model complexity for this program was achieved. While this model was not an exact scale model of the Apollo Service Module, the analytical problem of transient-heat transfer is comparable in all major aspects. The Series 3 model was constructed from the Series 2 model by adding:

- Two simulated fuel tanks
- Two simulated oxidizer tanks
- Two high-pressure helium bottles
- One pressure regulator, check valves, an isolation valve, relief valves, and associated plumbing.
- A heated simulated thrust nozzle
- A heated simulated thrust chamber
- A simulated fuel cell
- Simulated heat shields over the plumbing on the lower bulkhead.
- Internal thermal insulation within each compartment (on the final test only).

Propellent Tanks and Expulsion System

Two 15 in. dia. by 50-5/8 in. long cylindrical tanks with spherical ends were fabricated to simulate the Apollo Service Module fuel tanks, Figure 4-2. Stainless-steel flanged skirts, 0.06 in.-thick, were welded to the 0.06 in.-thick stainless-steel tank walls for attaching to the bulkheads. A threaded boss was provided at the upper spherical end (Figure 4-3) of each tank for instrumentation connections. An 8 in. dia. flange, with a 5-3/4 in. opening, was provided at the lower end for insertion of internal instrumentation, a

THIS MODEL INCLUDES ADDITION OF SIMULATED FUEL TANKAGE IN SECTORS III AND VI, SIMULATED OXIDIZER TANKAGE IN SECTOR IV, A HEATED NOZZLE, A SIMULATED HEATED THRUST CHAMBER, PLUMBING, AND HEAT SHIELDS.

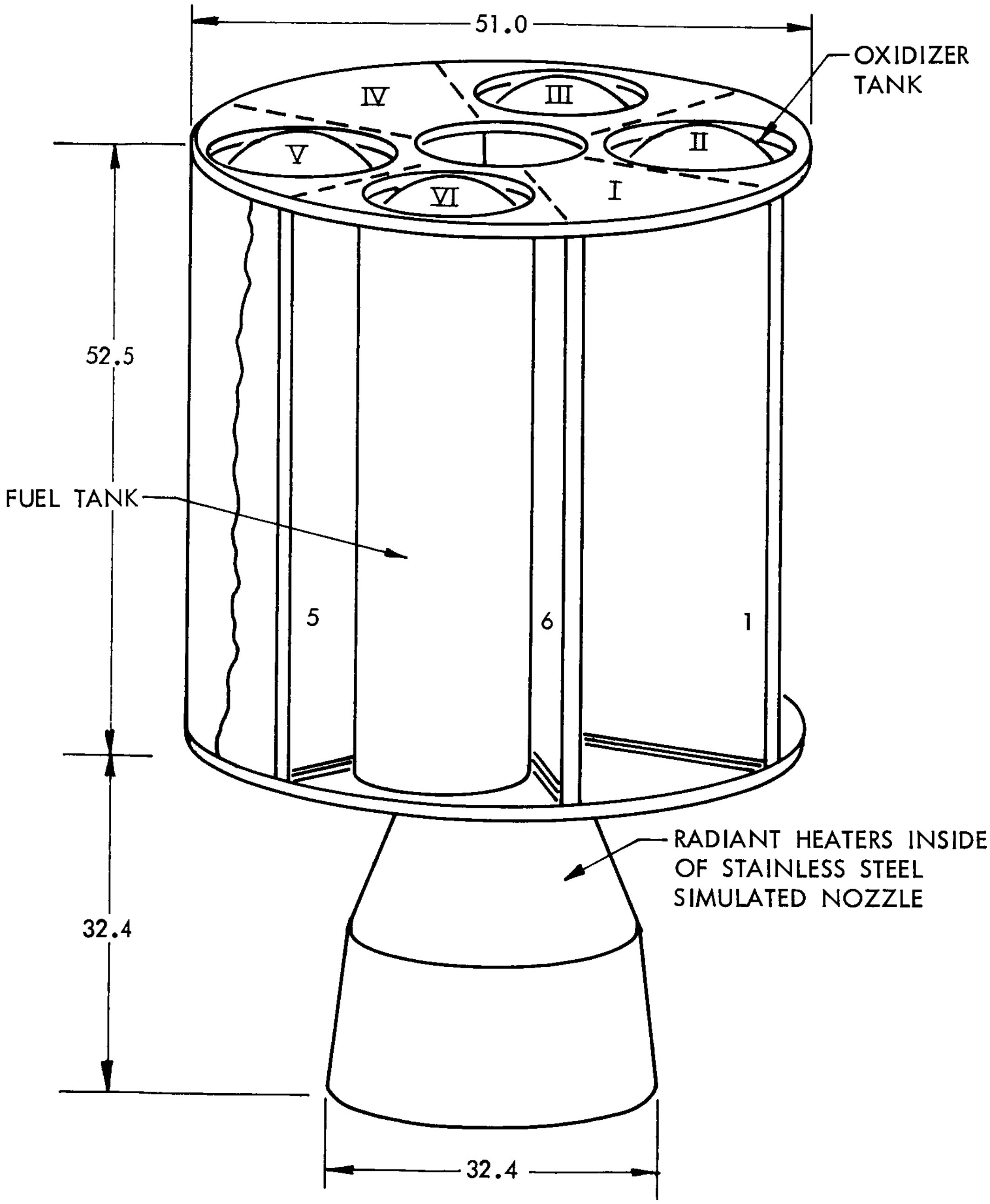

Figure 4-1 Series 3 Model

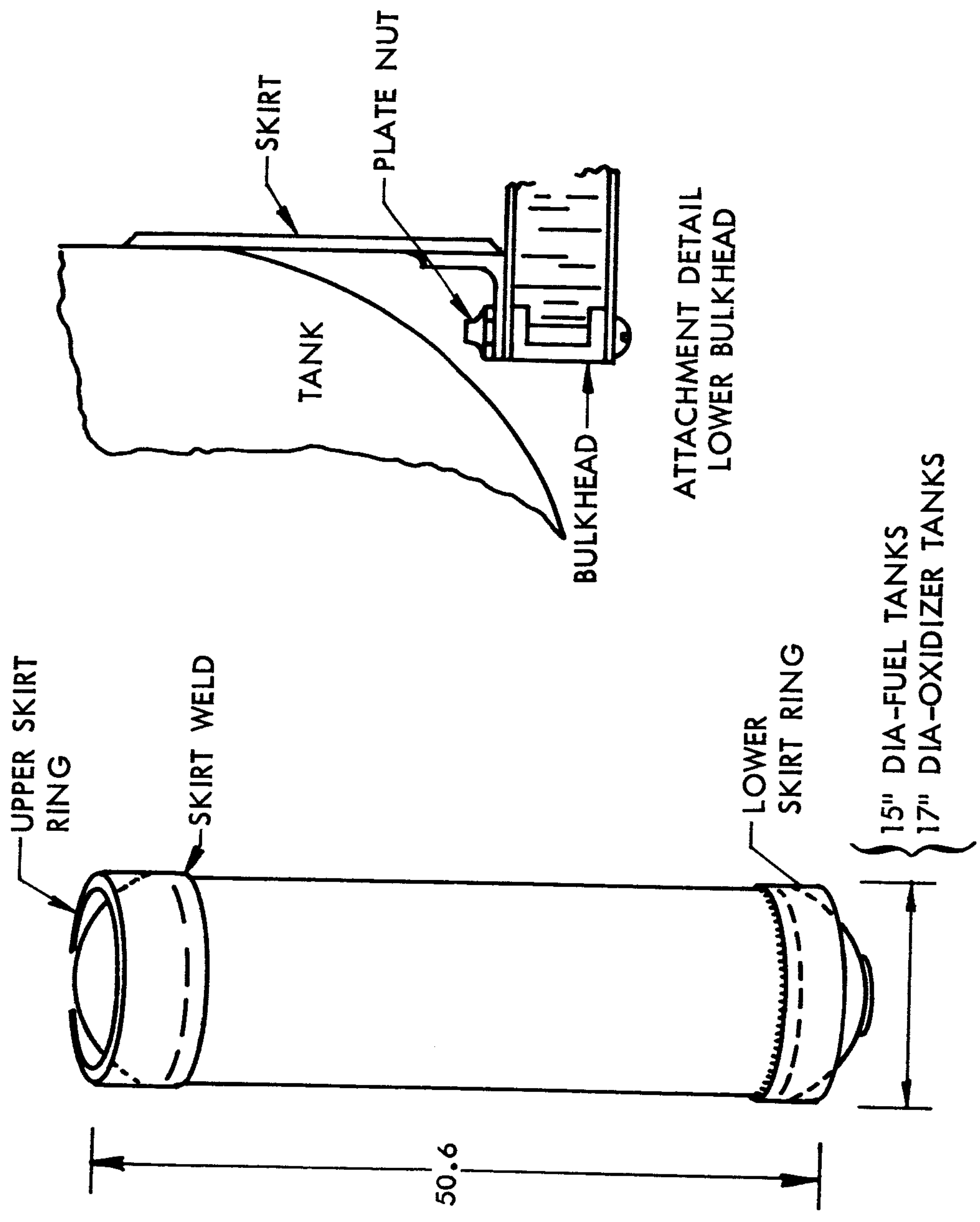

Figure 4-2 Simulated Fuel and Oxidizer Tanks

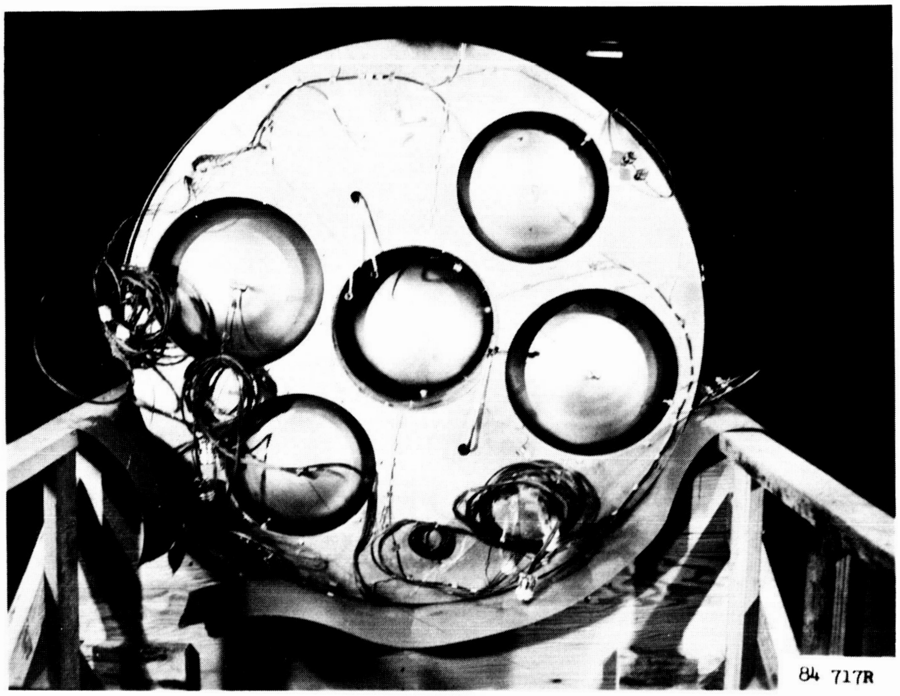

Figure 4-3. Forward End of Series 3 Model

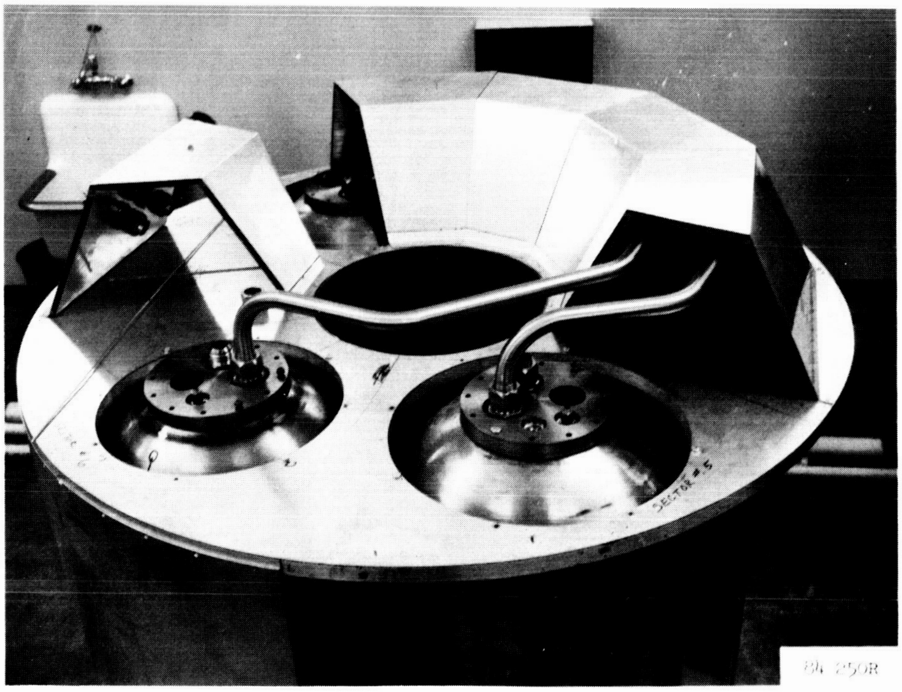

Figure 4-4 Heat Shield and Initial Plumbing

standpipe, and fluid transfer and drain fittings (Figure 4-4). The tanks were designed for 65-psig service, and were proof-pressure tested at 100 psig. Although the two simulated oxidizer tanks were larger, 17 in. dia., their design and construction features were identical to those of the 15 in. dia. simulated fuel tanks. These four tanks were given two coats of non-leafing aluminum acrylic lacquer. A design drawing (Fig.D-3) showing other tank details is reproduced in Appendix D.

The fluids in the propellant tanks were driven out by helium gas pressure. The helium gas used for this purpose was stored in two spherical bottles at 1500-psig initial pressure. These stainless-steel bottles, 13-1/2 in. O.D. with 1/2-in. thick walls, were mounted within the inner cylinder. Two diametrically opposite bosses, with 1/2-in. internal pipe threads welded to each bottle, provided the means for connecting the required plumbing. These bottles, constructed in accordance with the ASME Code for Unfired Pressure Vessels, were proof-pressure tested at 2250 psig.

The bottles were connected in parallel to the propellant tanks through a solenoid isolation valve, a pressure regulator, and check valves. The propellant tanks were connected in series as shown in the plumbing installation drawing (Fig. D-5) reproduced in Appendix D. The capacities of the simulated oxidizer and fuel tanks are 93.5 and 73.5 gallons, respectively. The 1-in. diameter discharge lines from the propellant tanks were connected to bulkhead fittings on the heat shield section located under sector one. After the model had been assembled in the chamber, line connections between the heat shield and chamber feed-through were made. Each propellant line in this section was wrapped with two 96 watt, 110 volt, "Briskeat" flexible heater strips (Briscoe Mfg. Co., Columbus, Ohio). These heaters were installed to preclude excessive test delay due to possible simulated propellant fluid freeze-up. During the test, it was found that these heaters were unnecessary for an eight hour run since the NRC-2 insulated propellant lines remained above 35°F with no heat input.

During the test runs, the expelled simulated propellants were collected in the fluid reservoirs shown in Figure 4-5. The orifice flowmeter, relief valve, throttling valve, and solenoid valve in each propellant discharge line were mounted on a board on top of these reservoirs. A pump was connected to the lower drain connection of the reservoir, to transfer the fluid into the model before the start of the test. To measure the liquid level, a level indicator was installed on each reservoir assembly.

Simulated Propellants

Two fluids to simulate nitrogen tetroxide and 50:50 UDMH:hydrazine were sought for use in the test model in order to provide experimental proofs of the applicability of the heat-transfer computer programs. It was highly desirable to have non-toxic, non-flammable, and unreactive fluids for this testing. Heat transfer fluids were considered on the basis of similarity of properties, availability, cost, and adequate available information on the fluid thermal properties. A comparison of the properties of six candidate fluids with the two liquid propellants is shown in Table 4-1. The properties of 60% ethylene glycol, 40% water, and of Freon 21, closely match those of 50:50 hydrazines and nitrogen tetroxide, respectively, and are compared at 20°F, 70°F, and 120°F. As the vapor pressure of Freon 11 is in close agreement with nitrogen tetroxide at the lower temperatures, Freon 11 properties are also included.

Since the cost of Freon 11 is considerably less than that of Freon 21, and its lower vapor pressure would allow easier handling during tests, it was selected to simulate the oxidizer. For simulation of the fuel, a 62% ethylene glycol solution was selected, following discussions with NASA personnel, as the best mixture.

The fuel reservoir was filled with a mixture of 62% inhibited ethylene glycol and 38% water by weight. The ethylene glycol used was Union Carbide and Chemical Company Ucar Thermal Fluid 17. The inhibitor in the fluid is less than 0.1% of the total weight and contains potassium borate, potassium hydrogen phosphate, and Nacap (sodium mercaptol benzol thiozole). The oxidizer reservoir was filled with Freon 11. A recirculating cooling loop was

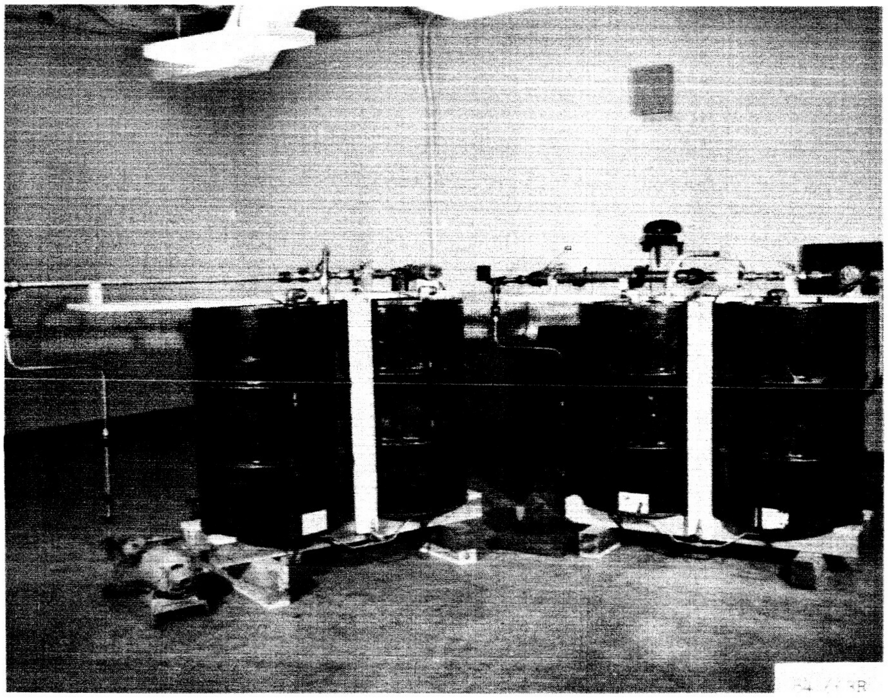

Figure 4-5 Fluid Reservoirs Used to Collect Simulated Propellants

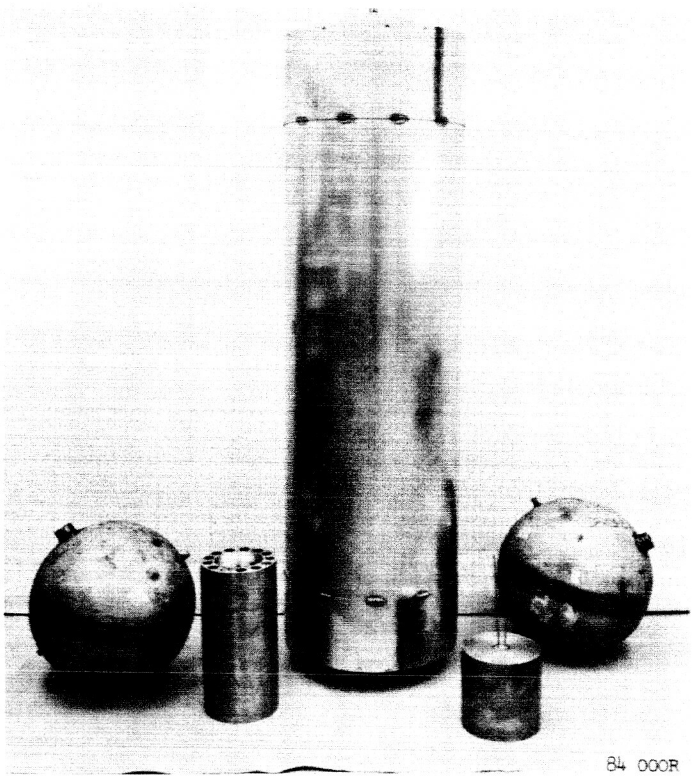

Figure 4-6 Helium Bottles, Thrust Chamber, Simulated Fuel Cell, and Propellant Tank

TABLE 4-1 COMPARISON OF HEAT TRANSFER FLUIDS

	Density	Viscosity	Specific Heat	Thermal Conductivity	Vapor Pressure	Boiling Point	Flash Point	Diffusivity	Cost
	g/cm^3	lb/sec-ft x 10^4	BTU/lb-°F	BTU/hr-ft°F	psia	°F	°F	ft^2/hr x 10^4	$/lb
20°F									
Freon 11	1.55	3.9	0.20		4.3				
60% Et. Glycol	1.08	93	0.704	0.227		232	> 200	48	
Freon 21	1.41	2.9	0.239	0.078	7.7		X	37	
Coolanol 25	0.92	93	0.419	0.080			300		
FC 75	1.84	17	0.23	0.086		214	X		
OS 45	0.91	330	0.417	0.08			430		
* 50:50 Hydrazine	0.93	10.2	0.68	0.155	0.66		5	33	
* N_2O_4	1.50	3.8	0.361	0.084	3.5		X	25	
70°F									
Freon 11	1.48	3.0	0.205	0.055	13.4		X	29	0.26
60% Et. Glycol	1.07	33	0.740	0.224			200	45	0.19
Freon 21	1.34	2.4	0.254	0.072	23.1		X	33	0.83
Coolanol 25	0.90	38	0.445	0.077					
FC 75	1.76	11	0.24	0.073					
OS 45	0.89	80	0.444	0.08					
* 50:50 Hydrazine	0.90	5.8	0.693	0.151	2.2		5	34	0.90
* N_2O_4	1.44	2.8	0.370	0.071	14.7		X	23	0.065
120°F									
Freon 11	1.42	2.3	0.21		33.0				
60% Et. Glycol	1.06	15	0.775	0.220				43	
Freon 21	1.27	2.0	0.268	0.065	55.8			30	
Coolanol 25	0.88	20	0.472	0.074					
FC 75	1.68	7	0.26	0.060					
OS 45	0.87	40	0.470	0.08					
* 50:50 Hydrazine	0.88	3.9	0.706	0.147	7.2			35	
* N_2O_4	1.35	2.0	0.418	0.068	48			19	

Ref: Garret Report STC-20-R * Denotes Apollo propellants added to the reservoir to reduce the Freon 11 evaporation loss. This loop consisted of a 5/8-in.-O.D. copper coil submerged in dry-ice-cooled water in a 10-gallon drum.

Fuel Cell Simulation

A 6-in. dia. by 6-in. long copper billet (Figure 4-6), heated by a single 1120-watt (115V) cartridge heater, was fabricated to simulate a fuel cell heat load. A manually operated 2.7KW, 135V variable transformer supplied power to the heater. After the billet had been painted with non-leafing aluminum acrylic lacquer, it was bolted in sector IV to the lower bulkhead. The billet was insulated from the bulkhead by a piece of Johns-Manville Transite, 1/2 in. thick by 6 in. dia.

Nozzle and Thrust Chamber Simulation

The simulated nozzle was made of 0.025-in. thick stainless steel; 3.42-in. dia. at the discharge end, by 34.2 in. high. A 10-in. dia. by 1/8-in. thick stainless steel disk was welded to the small, upper end of the nozzle, for attaching to the thrust chamber and for supporting the heat-lamp fixture.

The 24 heat lamps for the nozzle were attached to 1/8-in. by 1-1/4-in. ring-shaped bus bars mounted to a conical-shaped 0.025-in.-thick polished stainless steel reflector sheet with 2-in.-high ceramic stand-offs, as shown in Figure 4-7. The lamps, wired in two series-connected banks of 12 lamps, were connected to a 50KW, 480V, Research Inc. Thermac variable voltage power supply, operated manually for this test program. The entire lamp assembly was supported by the disk at the upper end of the nozzle. The nozzle, in turn, was bolted to the bottom of the simulated thrust chamber. The thrust chamber consisted of a 6-in.-dia. by 12-in.-long copper billet, heated by 13 700-watt (115/230V) cartridge heaters. Power was supplied to these heaters by a 16.2KW, 135V manually-operated 3 phase Variac variable transformer with its outputs connected in parallel. The center of the billet had been bored out to 3.7-in. diameter to reduce its mass. It was mounted on a support which was bolted to the lower bulkhead. The thrust chamber was mounted entirely within the inner cylinder.

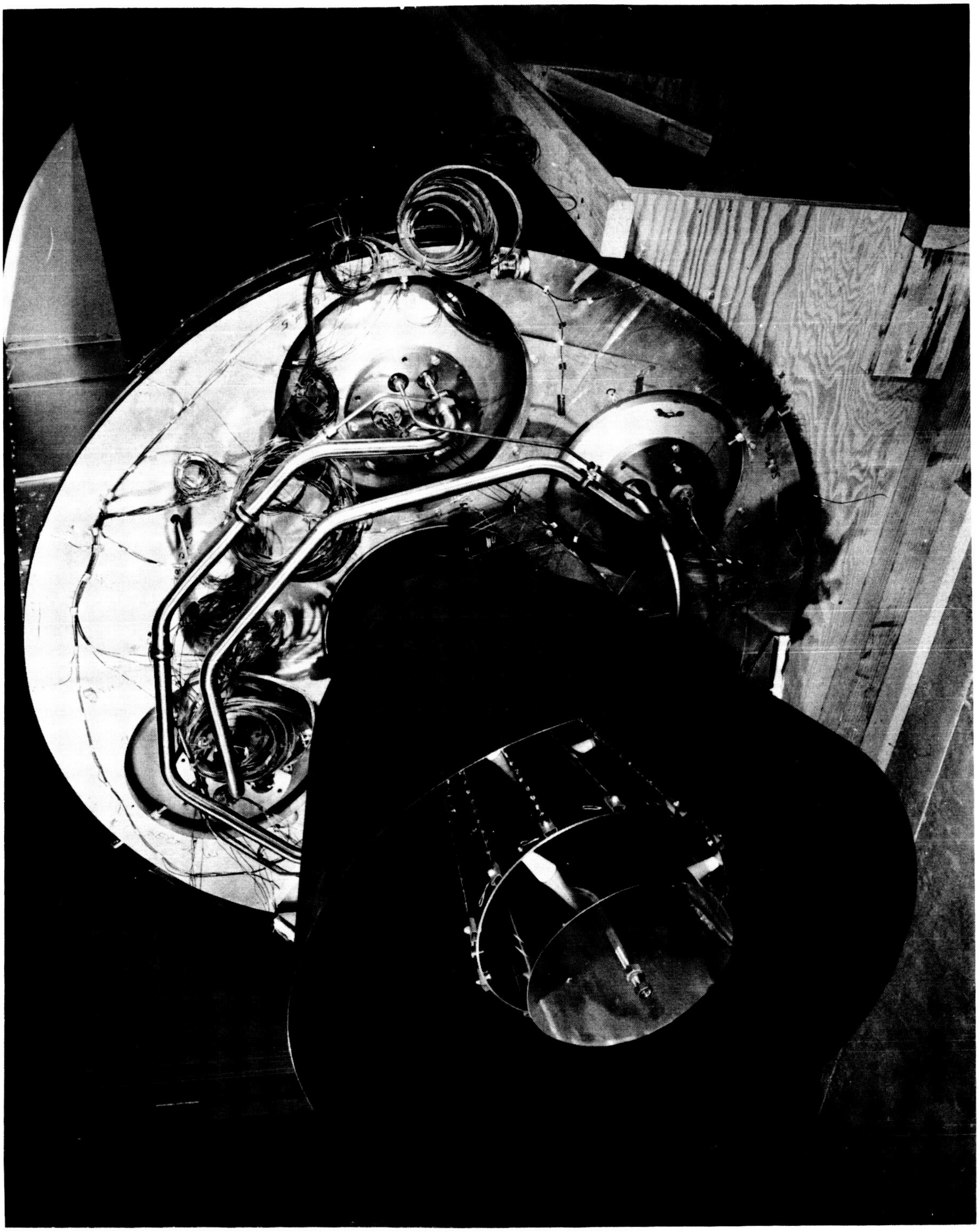

Figure 4-7 Aft End of Series 3 Model

Both the simulated thrust chamber and nozzle were given two coats of a special high-temperature Lockheed-formulated paint, designated as C144-Black. The painted nozzle (1000°F operating temperature) was subjected to a special 8-hour oven-cure, at temperatures up to 550°F. The painted thrust chamber did not require this cure because of a lower operating temperature of 600°F.

Heat Shields

Heat shields were installed to protect the plumbing lines below the lower bulkhead from the nozzle heat during firing. The simulated heat shields were made from two 0.016-in. thick 2024-T3 clad aluminum alloy sheets bonded to 3/8-in. thick Hexcel HRP3/16-GF11-4 heat-resistant phenolic hexagonal core. The bonding was performed under heat and pressure, with Bloomingdale HT 424 high-temperature adhesive. To reduce the possibility of the skin peeling off the unperforated phenolic core of the heat shield during the nozzle-heating cycle, 0.03-in. dia. holes, laid out in one-inch-square pattern, were drilled in the inner skin of the heat shield. The entire heat shield was insulated externally with a 1/2-in. thick layer of Johns-Manville Q-felt. A 0.003-in. stainless steel formed retaining foil was placed over this insulation. Ten layers of NRC-2 aluminized Mylar were fitted to the inner surfaces of the heat shield. Sections of the heat shield can be seen in Figure 4-8.

Aluminized Mylar Insulation

For the final part of the Series 3 tests, each of the six-sector compartments were insulated on three sides with 10 layers of NRC-2 aluminized Mylar. To simplify and expedite this installation, the Mylar was wrapped around a frame made of 1/4-in.-dia. aluminum tubes, as shown in Figure 4-9. The aluminized Mylar insulation is shown installed in sector 4 in Figure 4-10.

Model Assembly

In an effort to expedite the assembly of the Series 3 model, pre-test assembly and checkout of the tankage and plumbing were carried out during the Series 1 and 2 test period. For this purpose, a duplicate inner cylinder was fabricated. Helium bottles were mounted in this cylinder and a functional

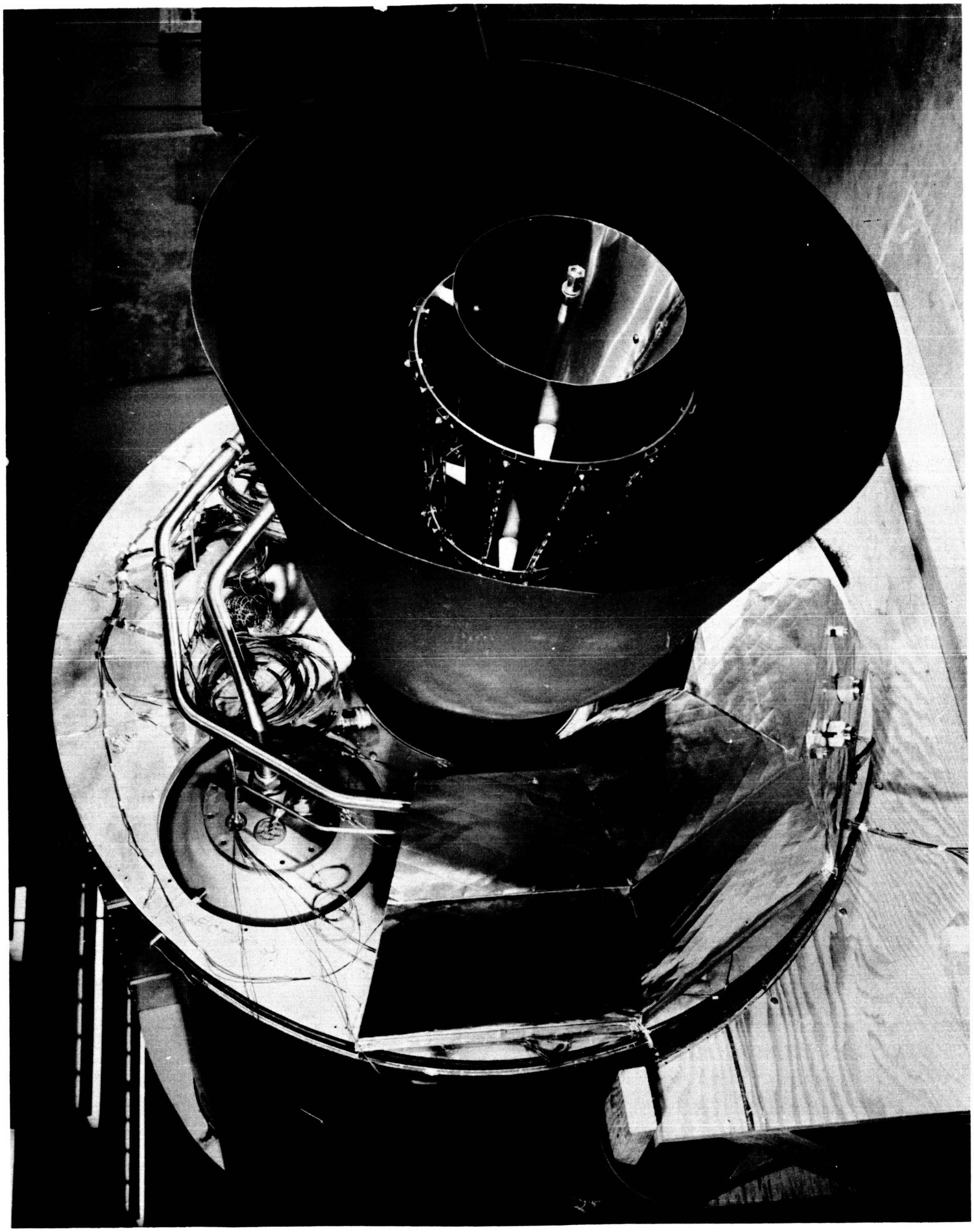

Figure 4-8 Heat Shield Installation Shown Partially Complete

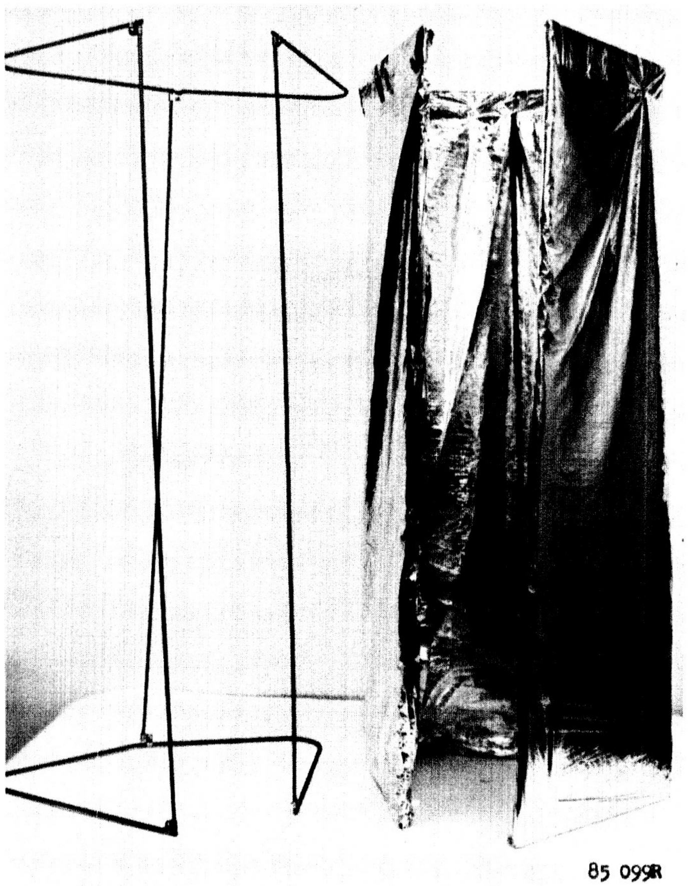

Figure 4-9. Sector Insulation, Showing Frame Only and Frame Covered with Ten Layers of NRC-2

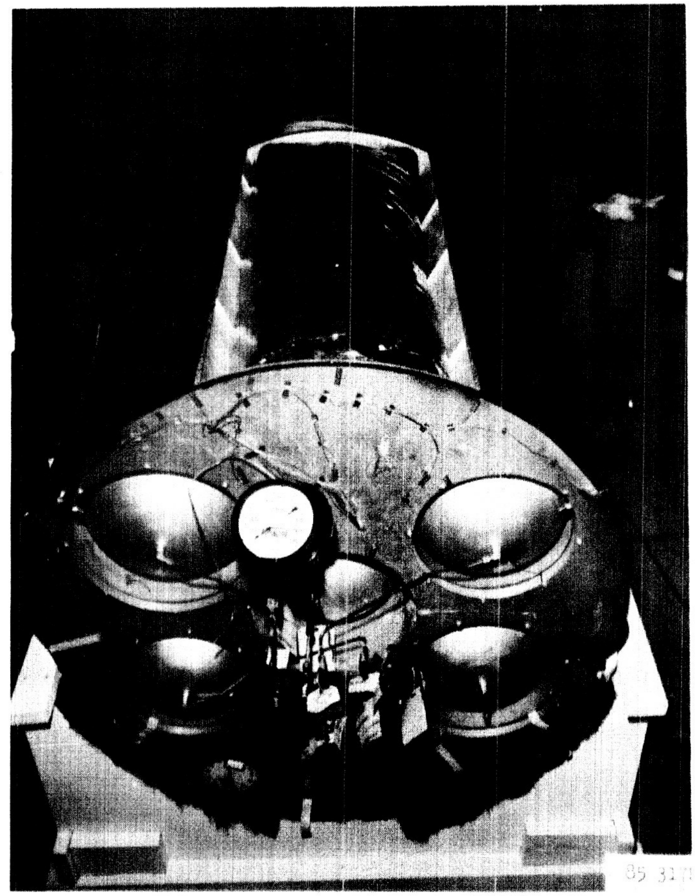

Figure 4-10. Internal Aluminized Mylar Insulation Installed in Sector 4

mockup of the tankage and plumbing, complete with the external reservoirs (Figure 4-5) was made using one inch plywood bulkheads. Sight glasses had been added to the external reservoirs to replace the weighing scale originally proposed, since the weight of the filled reservoir assemblies were beyond the capacity of the laboratory scales. The weights were estimated to be about 1400 lbs. for the Freon 11 and 900 lbs. for the water-glycol mixture. Pumps had been added to the system for transferring the fluids from the external reservoir into the tank models in the chamber. Checkout of the plumbing, pressure regulator, solenoid valve, and the external reservoir was then accomplished with water as a test fluid.

Upon completion of the Series 2 tests, the model was removed from the chamber for reworking to the Series 3 configuration (Figure 4-11). To accomplish this, the Series 2 model was completely disassembled. The inner cylinder was replaced by the duplicate inner cylinder with the helium bottles mounted inside. After the beams were attached to the inner cylinder, the four cylindrical tanks were installed. Thermocouples were attached to the inner cylinder and the cylindrical tanks before they were installed. Thermocouples were re-installed on the beams after they were placed in the model. Two coats of non-leafing aluminum acrylic lacquer were applied to these parts prior to installation. Small clip angles were attached between the skirt of the tanks and the upper bulkhead to relieve the bending moment on the bulkhead caused by the weight of the fluid in the tanks. These clip angles were positioned close to the eyebolts in the bulkhead.

Because of the model size, it was necessary to complete assembly within the C-5 chamber (Figure 4-12). After the internal plumbing and additional thermocouples had been installed, the external honeycomb panels were fastened in place. The tank bottom flanges, with the standpipes and thermocouple rake, were inserted into the tanks and bolted in place. The simulated nozzle and thrust chamber were then installed. Upon completion of the plumbing on the lower bulkhead, the heat shields were put in place. As each stage of assembly was reached, the requisite thermocouples were attached at selected locations.

Once the model assembly was completed, plumbing, power and instrumentation connections between the model and the chamber feed-through plates were

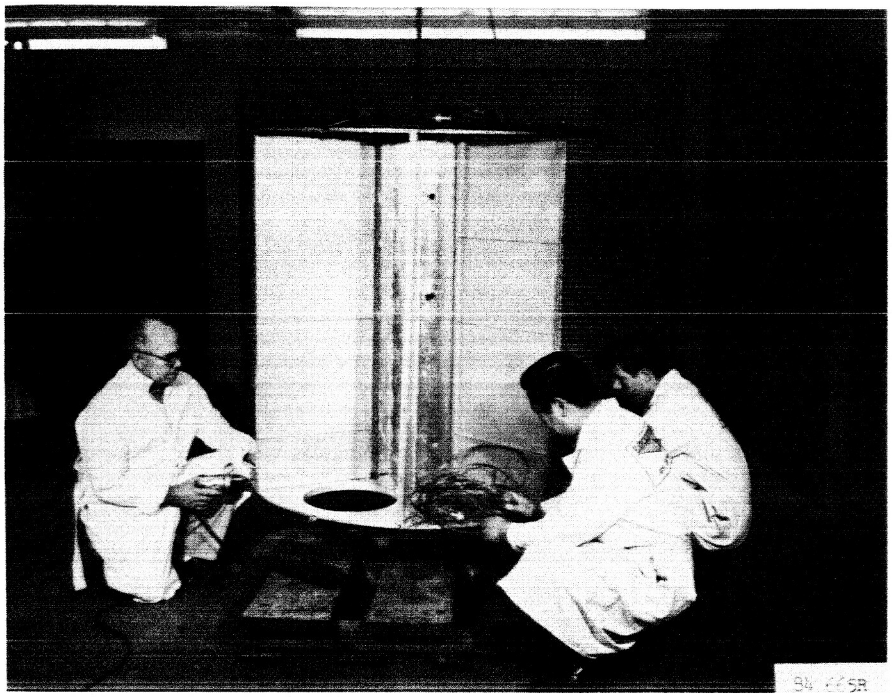

Figure 4-11 Early Stage of Series 3 Assembly

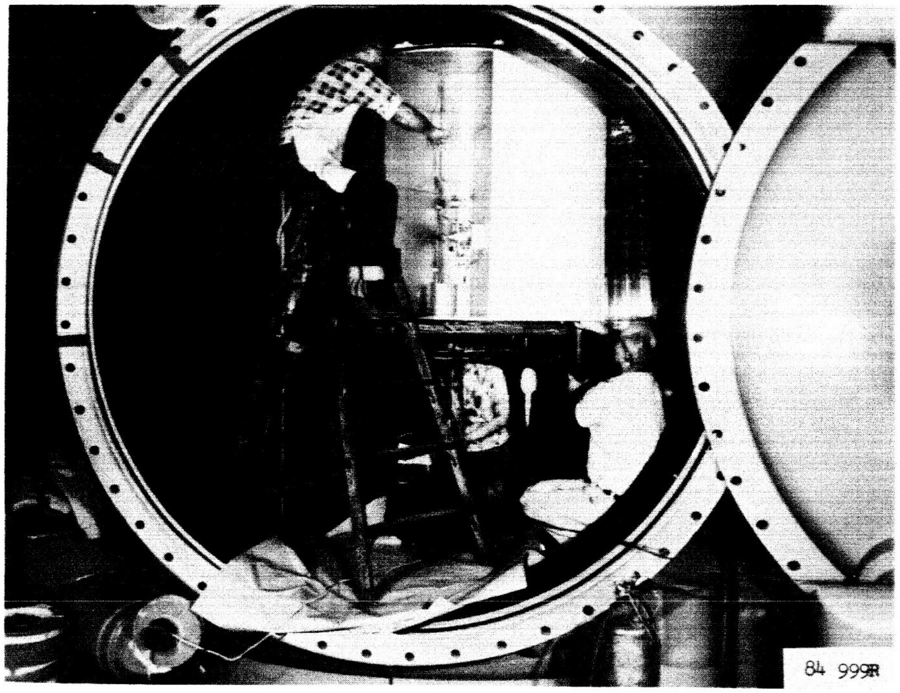

Figure 4-12 Assembly of Model in the C-5 Chamber

made. Plumbing lines were wrapped with flexible ribbon heaters to prevent freezing. A one-inch layer of unbonded fiberglass insulation was wrapped over the heaters. In addition, all lines were wrapped in five layers of NRC-2 aluminized mylar.

INSTRUMENTATION

For the Series 3 model, 83 copper-constantan thermocouples were added, resulting in a total of 224 of these thermocouples. In addition, 13 iron-constantan thermocouples were installed on the aft nozzle and thrust chamber added to the model for the Series 3 tests. A total of 11 pressure transducers were also added for this test series.

Thermocouple Calibration

An additional 144 copper-constantan couples were calibrated for use in the Series 3 tests. The calibration procedures and equipment were identical to that followed and used for the Series 1 and 2 models, as described in Section 2. The calibration points for the Series 1 through Series 3 copper-constantan couples are shown in Figure 2-4. Using the compromise curve drawn through the points in this figure, the conversion table stored in the Phase-II data reduction program was altered to match the calibration. The 16 iron-constantan couples used on the nozzle and the thrust chamber and for monitoring, were also calibrated through the range from 50 to 900°F. Up to 450°F, the calibration procedure was the same as that used for copper-constantan. Above that point, the calibration was performed using a copper thermocouple well which was heated by a muffle furnace. The standard for the upper range was a platinum resistance thermometer with NBS traceability. The calibration curve is shown in Figure 4-13. The accuracy of the iron constantan thermocouples was judged adequate without correction and the standard table (from NBS circular 561) was used for data reduction.

Thermocouple/Node Locations

The 83 additional copper-constantan couples added on the Series 3 model were installed in the following locations.

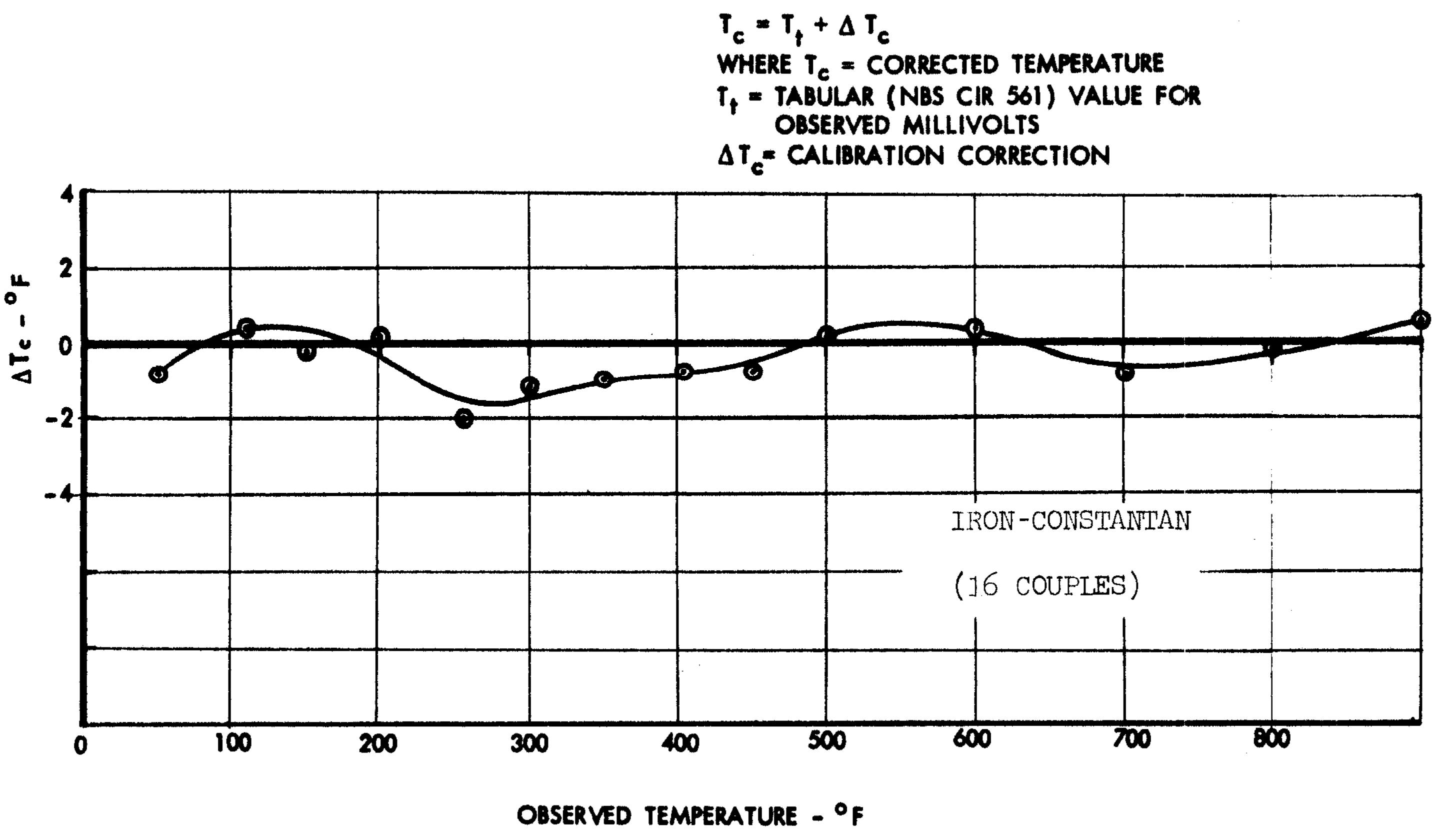

Figure 4-13 Series 3 Thermocouple Calibration

Propellant tanks	
Internal	24
External	24
Simulated fuel cell	2
Helium bottles	
Internal	2
External	2
Heat shield	15
Plumbing lines	14

These couples were attached with the aluminum-coated silicone adhesive tape described in Section 2. Of the 13 iron-constantan couples added to the Series 3 model, four were taped to the heat shield, one was staked into a small hole drilled in the thrust chamber, and eight were spot-welded to the nozzle. Stainless steel strips 0.005-in. by 1/8 in. by 3/4 in. laid over the wires and spot welded on both ends held the nozzle thermocouple wires in place. Figures showing the thermocouple/node location and a tabulation of the node number referenced to the pin and plug numbers of the thermocouples are located in Appendix E.

Pressure Transducers

Eleven Wiancko Engineering Co. (Pasadena, Calif.) pressure transducers were used in the Series 3 tests. Of the eleven transducers, three were differential pressure Type P Model 1701, and 8 were absolute pressure Type P Model 1671 transducers. Barton Instrument Corp. (Los Angeles, Calif.) differential pressure gauges, range 0 to 100 in. of water, were connected in parallel to the differential pressure transducers. Either U.S. Gauge Co. (New York, N.Y.) or Marshalltown Mfg. Co. (Marshalltown, Iowa) pressure gauges of the appropriate range were connected in parallel with the absolute pressure transducers. These gauges were used both to calibrate the transducers and to monitor the pressures during the tests. A Wiancko Engineering Co. pressure system was used to provide the means for measuring the eight absolute and three differential pressures. The sensing elements of the pressure transducers used were twisted bourdon tubes. Pressure applied to the transducers causes rotation of the sensing element, which in turn causes changes in the air gaps in the magnetic circuits of the attached magnetic armature. The result is a change in bridge inductances and an output voltage proportional to the applied pressure. This a-c output voltage from the transducers was converted to d-c by a demodulator and transferred to a range-balance unit. There it was balanced and attenuated as necessary to impart a millivolt signal to the Mod-Sadic recorder that directly matched the pressure sensed. This was possible because of the linear characteristic of the transducer and readout system in the operating pressure range.

Flow Measurement

Orifice flow meters were used in the 1.88 in. I.D. discharge line to measure the flow of the simulated fuel and oxidizer. A 0.559 in. diameter orifice was used to measure a fuel discharge rate of 9.2 gpm. A 0.934 in. diameter orifice was used for the oxidizer discharge rate of 11.7 gpm. The pressure upstream of the orifice, and the pressure drop across the orifices were measured with the Wiancko pressure system and recorded with the Mod-Sadic data acquisition system. From the data thus obtained, the flow rate could be calculated. During the tank expulsion cycle of the test, the flows were throttled to the desired flow rate with a manually operated one-inch ball valve located down-stream of the orifices. The flow rates were also monitored during expulsion by timing the rate of rise of the liquid level in the sight glasses mounted on the external reservoir with a stop watch.

TEST RUNS

Four test runs were made on the Series 3 model essentially as proposed in the test plan report, LR 18135 dated 9-4-64, and as described below. The unscheduled overheating of the model's skin at the start of this series of runs delayed the program three weeks.

Run Preparation and Checkout

While the model was being altered, test preparations outside the chamber were completed. This external work included setting up the propellant reservoir, plumbing to it, connecting transducers, pressure gauges, relief valves, and shut-off valves to the system, connecting the thermocouple extension wires to the temperature reference bath, Mod-Sadic and monitoring instruments, and connecting leads to the power supplies. After the model and the test support equipment installation had been completed, the pressure transducers were calibrated.

The helium bottles were charged with Freon 12 and dry nitrogen gas to about 1200 psig. A General Electric Co. Type H-1 Freon leak detector was then used to check for leaks in the high pressure portion of the model. Since no leak was found in this portion of the system, the solenoid isolation valve was actuated and the pressure reducer was adjusted to regulate the downstream pressure to 45 psig. After all leaks on the low pressure side had been eliminated, the pressure was dumped.

All accessible thermocouples connected to the Mod-Sadic system were checked for continuity, polarity, and channel matching by using the same procedure as described in Section 2. The heaters for the simulated fuel cell, thrust chamber, and nozzle were checked by applying power to the circuits for these items and checking the monitor thermocouples for a rise in temperature. Check out of the radiant lamp systems for heating the side of the model was accomplished by application of manually controlled power at reduced voltage. The operation was checked by visual inspection of the lamps. After vacuum cleaning the interior of the chamber, the door was closed, the LN_2 lines were connected and insulated, and the following chamber pump down procedures were initiated. After about 15 minutes of rough pumping with a 325 cfm Beach-Russ pump, the two 32-in. diameter Consolidated Vacuum Corp. diffusion pumps were turned on. After a 45-minute heat up period, the diffusion pumps reduced the chamber pressure to the 10^{-4} torr range. At this time LN_2 was introduced into the chamber walls. The chamber pressure at this point dropped to the 10^{-5} torr range. Run conditions were established upon reaching this chamber pressure and when the cold walls were stabilized near LN_2 temperature.

Model Damage

The first test run on Series 3 was attempted on March 3, 1965. The C-5 chamber was at an acceptable vacuum level of 3.5×10^{-5} torr, the cold wall was at -320°F, and checkout had been completed. The ignitron was energized to bring the heated side of the model up to 250°F. After four minutes there was a flash in the chamber and circuit breakers on the radiant lamp system kicked out. It was suspected that one or more lamps had broken or shorted out. Attempts to restart the radiant system failed. The chamber was repressurized (about four hours are required to repressurize) and the door opened. An acrid phenolic smell and bits of honeycomb on the chamber floor indicated that the failure was much more serious than was at first anticipated. Upon examination, the center heated panel, corresponding to sector I, was found to have exploded. The inner skin of this honeycomb panel had blown inward (Figures 4-14 and 4-15) deep between the beams, while the outer skin had exploded outward, smashing 15 heat lamps. The two adjacent outer panels in sectors II and VI were also partially delaminated. All three panels had to be replaced. Some damage was done to the radiant lamp fixture and side closures.

An examination of data from the Mod-Sadic indicated that panel temperatures in excess of 680°F had occurred during the heat-up. While the honeycomb core is vented, temperatures of this magnitude are sufficient to decompose and vaporize the HT 424 epoxy bonding agent, pressurizing the core and eventually blowing the faces off. A subsequent accident investigation revealed that while the control couple for the ignitron was properly located, miswiring at the feed-through caused a couple other than the control couple to be sensed by the ignitron. This control couple was properly wired during the Series 1 and 2 tests, but was apparently miswired when the thermocouples for the Series 3 test were added.

New honeycomb panels were ordered, and bent beams and broken thermocouples were replaced. The radiant lamp system was cleaned and the broken lamps replaced. Every thermocouple was rechecked for proper location and identification. A back-up temperature monitoring system using a Brown Indicating Potentiometer with three redundant thermocouples was added. Also a voltage limiting provision on the radiant lamp system was incorporated. It was impractical to attempt to thoroughly clean the chamber walls without a long down-time. However, a quick test with the chamber empty proved that a vacuum in the mid 10^{-6} torr range was easily attainable without such a cleaning.

Figure 4-14 Damaged Center Section

Figure 4-15 Outer Skin of Center Panel (right) and Arc-Burned Side Closure (left)

The new honeycomb panels arrived on March 15 and were painted and reinstrumented. All rework was completed and by March 24, twenty-one days after the accident, testing was resumed.

Series 3 Runs

The Series 3 tests consisted of four runs: (1) tanks empty and all systems passive, (2) expulsion schedule added, (3) expulsion schedule, simulated fuel cell heat load, and nozzle heating, and (4) Same as (3) except for the addition of 10 layers of aluminized mylar insulation on the interior of the sectors. The checkout and run procedure which was used in these tests is given in Appendix F. The tests were initiated by a heat-up of one-half of the model exterior skin (sectors I, II, VI) to 250°F in approximately 10 minutes. This temperature was held for 6-3/4 hours and then the heat was turned off. The tests were concluded after 7-1/2 hours. Typically, data were taken throughout the run at 10-minute intervals, except during and after expulsion events. The schedule of data acquisition during and after expulsion will be discussed under the individual runs. During all runs the vacuum was in the range from 5×10^{-6} torr to 2×10^{-5} torr.

The first test, conducted on March 24, was with all tanks empty and all systems passive.

The second test, conducted on March 25, included an expulsion schedule, shown in Figure 4-16. While the chamber was being pumped down, the bottles were charged with helium gas to 1500 psig after first having been evacuated with a portable vacuum pump. The Freon 11 was transferred into the oxidizer reservoir and the water-glycol mixture to the fuel reservoir. From the reservoir, the simulated propellants were pumped into their respective tanks within the model. For this test the data recording interval was shortened to 5 minutes for a 1/2 hour period after each expulsion event.

The third test, conducted on March 26, was the same as the second except that the local heat load in Sector 4 was held at 200°F surface temperature during the entire period, and the nozzle was heated to approximately 950°F on a coordinated schedule with the tankage utilization.

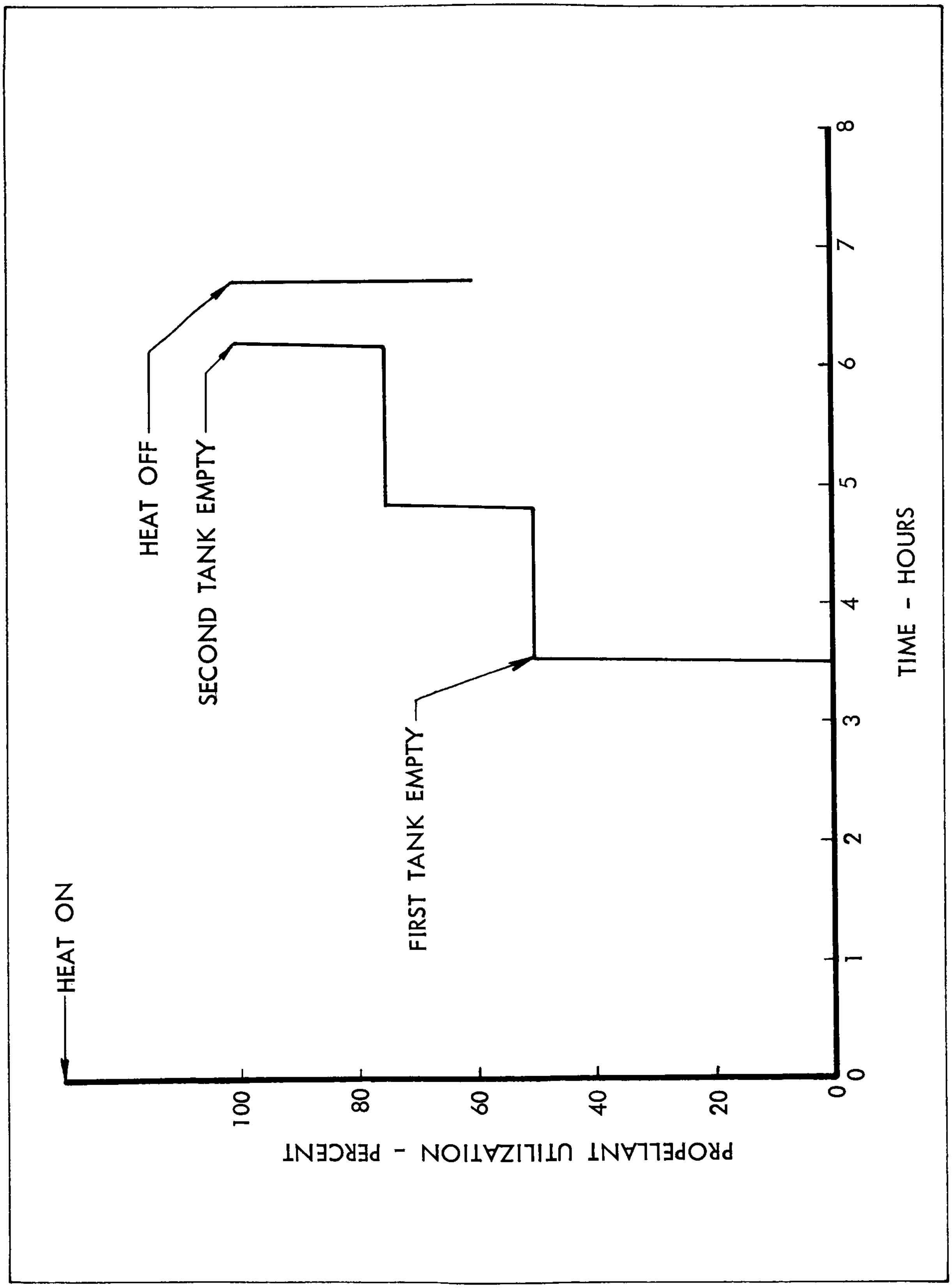

Figure 4-16 Test-Tank Expulsion Schedule

The fourth test was identical to the third except that the sectors were internally insulated with 10 layers of NRC-2 mylar insulation. Installation of the mylar took three working days, and the test was run on April 1. During this test, in order to examine phenomena during expulsion in greater detail, a special data acquisition procedure was used. A 39 point continuous loop program tape was written so that after initiation of each expulsion cycle all pressure transducers, all internal tank thermodouples, and the helium bottle temperatures were scanned continuously at the rate of 3 channels/second.

ANALYTICAL CORRELATION

Series 3 Network

The analytical model for Series 3 is similar to the Series 2 model with the following additions:

(1) Propellant tanks in bays II, III, V, and VI. These tanks are represented by a single node with a variable capacitance. The network for the tanks is indicated in Figure 4-17. Not shown in this figure are the conduction resistors in the tank skirts.

(2) Helium bottles in the inner cylinder. These bottles are also represented by a single node with a variable capacitance. Figure 4-18 shows the Series 3 inner cylinder radiation network. This figure does not show the two conduction resistors for each bottle at their point of attachment to the inner cylinder.

(3) Simulated electronic load. This is represented by a single node with a specified temperature as a boundary condition. Figure 4-19 shows the radiation network formulated for bay IV containing the simulated electronic load. There is also a conduction resistor through the transite insulation where the heated billet is bolted to the bulkhead.

(4) Heat shield on the aft bulkhead covering the propellant lines. The radiation and conduction network for the heat shield is shown in Figure 4-20.

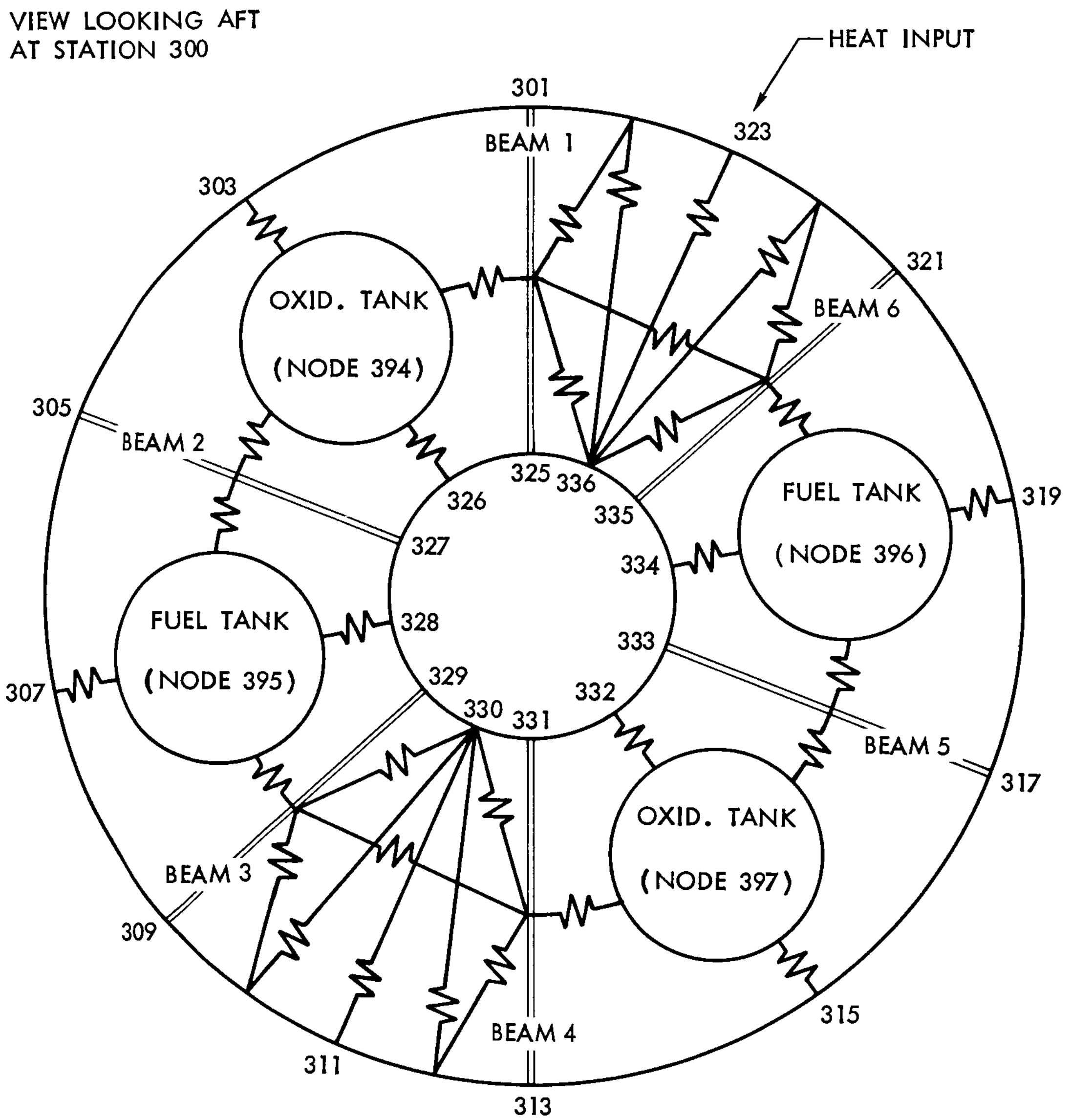

NOTE: (1) FUEL CELL AND INNER CYLINDER NETWORKS NOT SHOWN HERE (SEE FIGURES 4-18 AND 4-19)
(2) FOR DETAILED DIMENSIONS ON NODE AND THERMOCOUPLE LOCATIONS SEE FIGURE 8-9

Figure 4-17 Propellant Tank Radiation Network

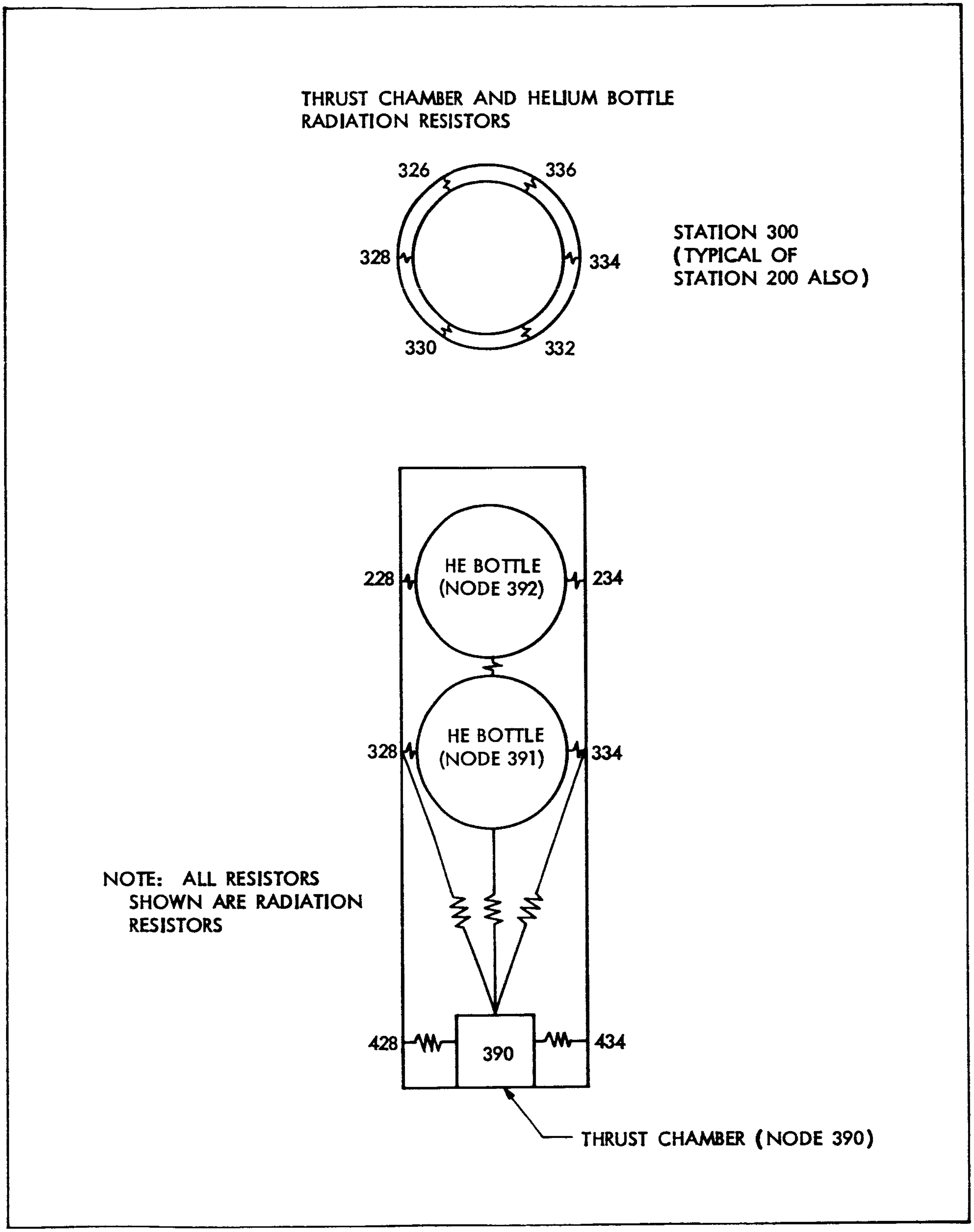

Figure 4-18 Network for the Inner Cylinder

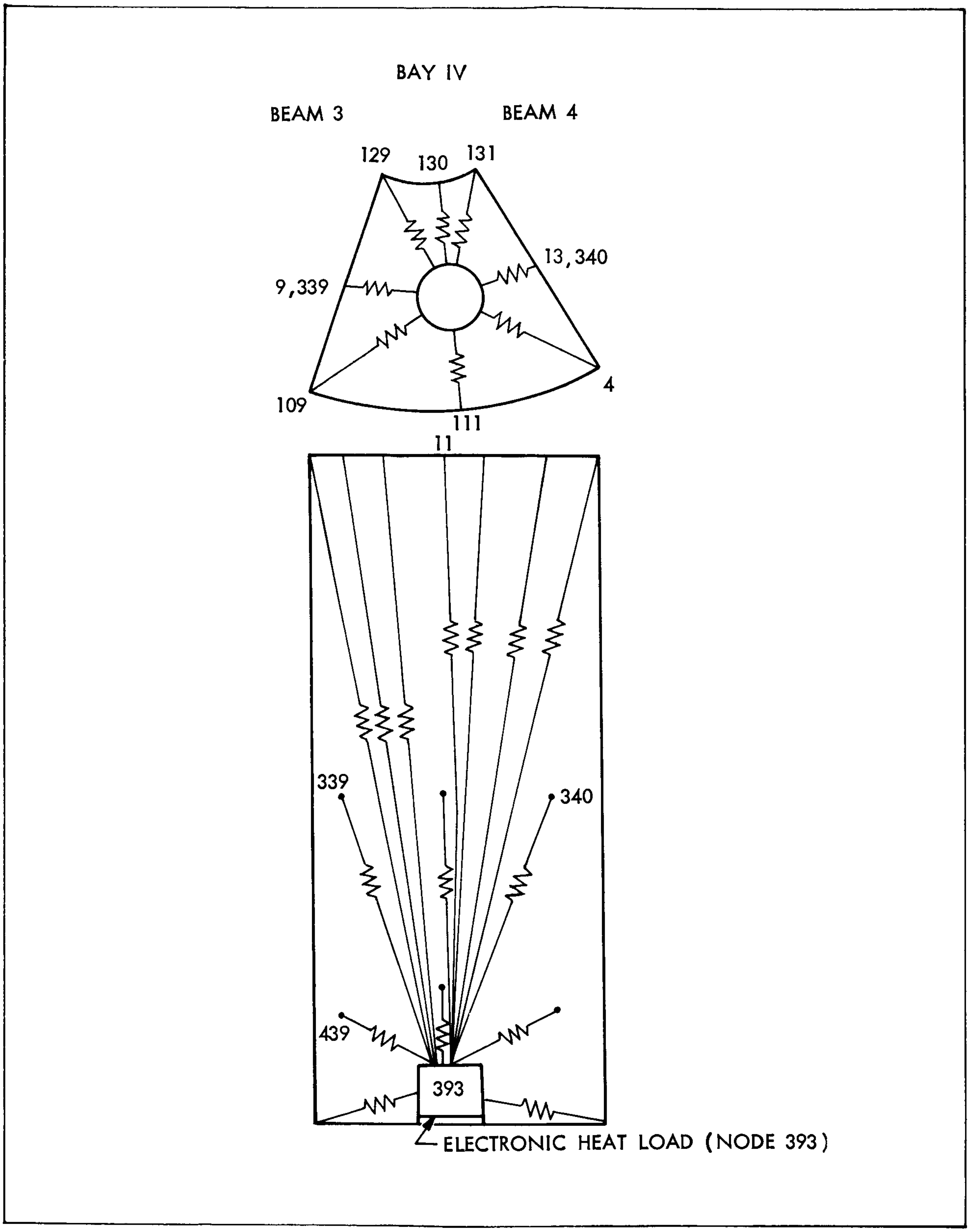

Figure 4-19 Radiation Network in Bay IV

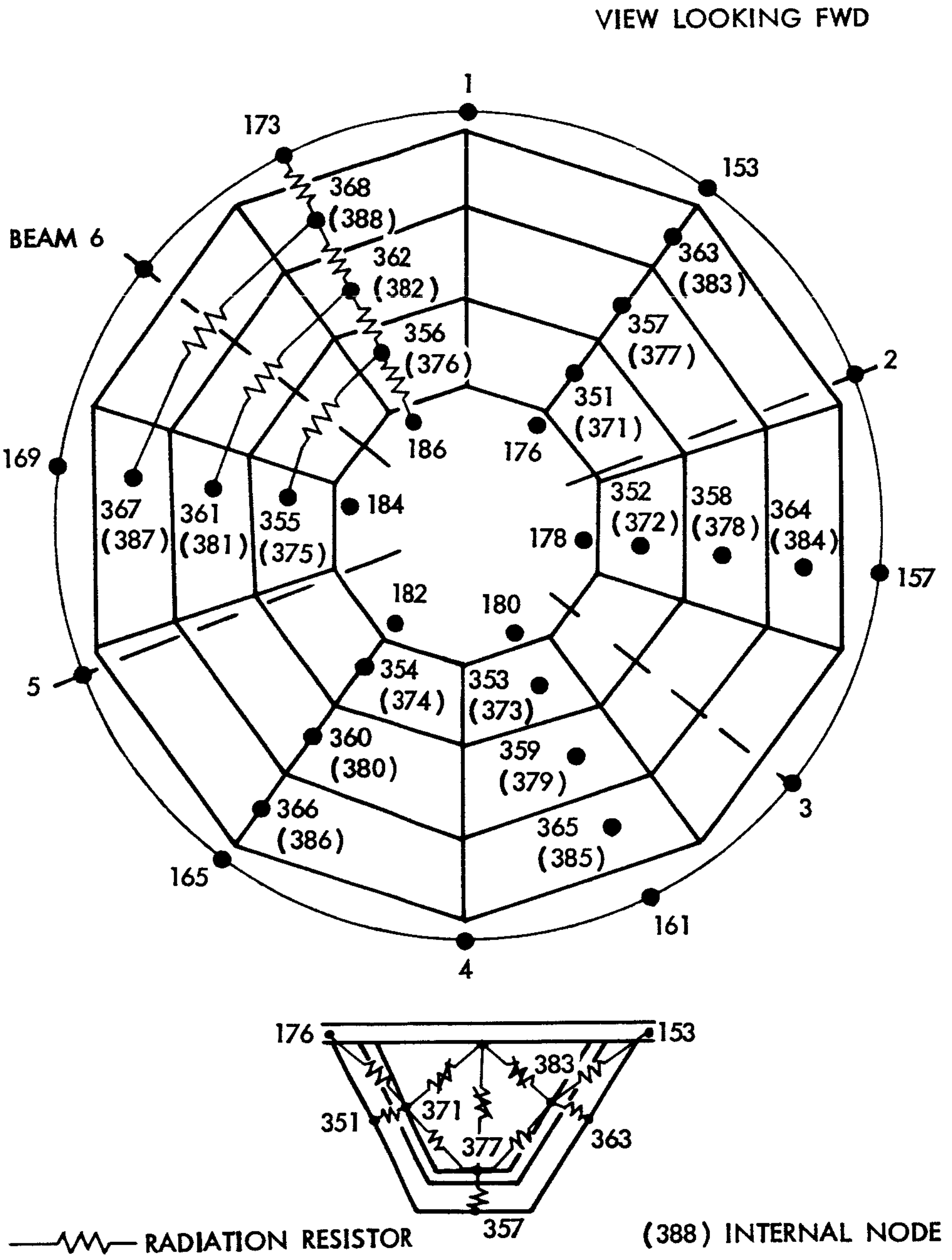

NOTE: FOR DETAILED
DIMENSIONS AND
THERMOCOUPLE LOCATION
SEE FIG. E-5

Figure 4-20 Radiation Network for Heat Shields

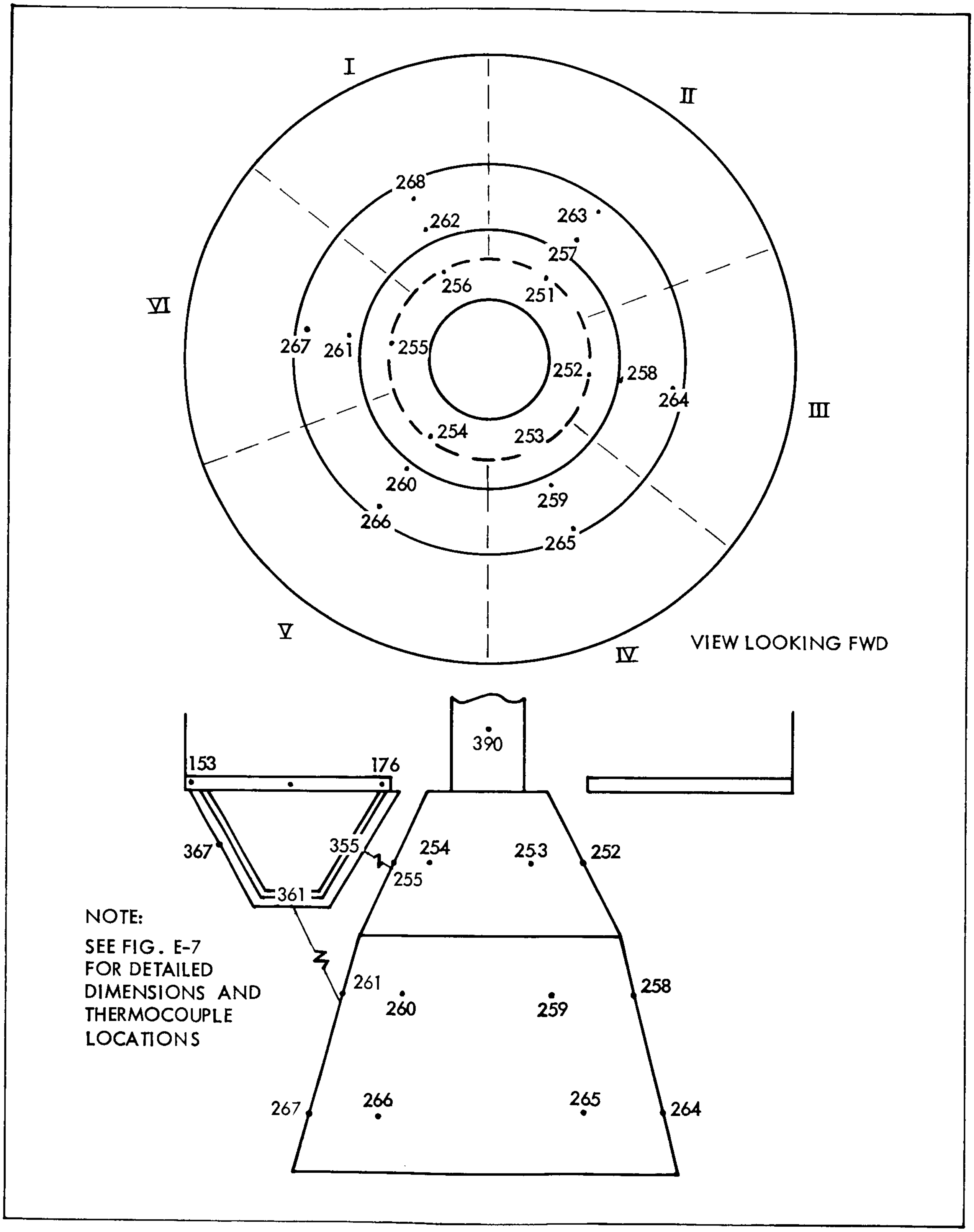

Figure 4-21 Nodal Layout for Nozzle

(5) Simulated nozzle and thrust chamber. Both the nozzle and the thrust chamber temperatures are specified as boundary conditions. As shown in Figure 4-21, the thrust chamber is represented by a single node while the nozzle is represented by 24 nodes. Also shown in this figure are the radiation resistors connecting the nozzle with the heat shield.

The Series 3 network has 260 nodes. These nodes are connected by 505 conduction resistors and 280 internal radiation resistors. There are 43 external radiation resistors connected to the chamber.

The last run in the Series 3 tests required a modification of the network to account for the addition of 10 layers of NRC-2 aluminized mylar insulation along the inside of the outer panels and to both sides of each beam. To account for this insulation, the effective emissivity of the covered surface was computed according to the semi-empirical equation derived from NRC-2 data. As in the Phase I analysis, this equation is,

$$\epsilon_{eff} = \frac{0.0018\ D^{.84}}{M + 1}$$

where

$$D = 160 \text{ layers/inch}$$
$$M = \text{number of layers}$$

The effective emissivity for 10 layers of aluminized mylar is 0.016 or approximately 1/25th of the uninsulated surface.

A preliminary analysis of the heat shield thermal network indicated that the contact resistance at the joint of the heat shield and aft bulkhead would be significant. Several values of contact resistance were assumed, and a selection was based on the correlation of predicted heat shield temperatures with Series 3 experimental temperatures. This problem is insignificant in the Phase I analysis because the contact resistance is negligible compared to the resistance of the heat shield.

Run Correlation

Three Series 3 test runs were analyzed:

- Run 3-19, uninsulated model with simulated system passive.
- Run 3-21, uninsulated model with simulated systems active.
- Run 3-22, insulated model with simulated systems active.

Run 3-20 was not analyzed because the test conditions were not significantly different than Run 3-21. The results of these runs are presented primarily in the form of analytical and experimental temperature histories of representative nodes. As a guide to the comprehension of the plotted data, a summary table for each run is presented to identify the node and its corresponding figure number. In addition, these tables show the predicted and measured temperatures at two time points during the run. One time point represents a quasi steady state condition and the other a transient condition.

Run 3-19 --- Table 4-2 summarizes the temperature histories presented in Figures 4-22 to 4-37. For all the nodes the predicted temperatures during the transient condition were lower than the measured temperatures. This indicates that the cold walls were probably warmer than the assumed -320°F temperature during the cool down period (0 to 5000 seconds). For the structural nodes, predicted temperatures were within ±20°F of the measured temperatures for the entire run. Inner cylinder node 331, which is located near the connection of the lower helium bottle and the inner cylinder, typically shows poorer temperature agreement agreement than the rest of the inner cylinder nodes because the helium bottle attachment point does not coincide with any of the existing nodes on the inner cylinder. At these attachment points, the conduction network was slightly reworked so that nodes existed where the bottles were bolted to the inner cylinder. However the thermocouples were not relocated. Predicted temperatures for node 331 ran consistently 20°F lower than the measured temperatures.

As shown in the temperature histories of the two helium bottles, Figures 4-32 and 4-33, experimental temperatures of both bottles were approximately equal, whereas, the predicted temperature for the upper bottle is 10°F higher than experimental. This poor correlation is caused by the single node

TABLE 4-2 GUIDE TO SELECTED PLOTS FOR RUN 3-19

Node Location	Ref. Figure	Temp. at 28,000 secs.		Temp. at 6,000 secs.	
		Analytical	Experimental	Analytical	Experimental
Outer Panel Nodes					
211 - Cold Side, Sector IV	4-22	-66	-67	-66	-46
315 - Cold Side, Sector V	4-23	-54	-48	-55	-42
Bulkheads					
63 - Lower, Cold Side, Between Sectors IV & V	4-24	32	30	32	42
73 - Lower, Hot Side, Sector I	4-25	185	185	116	118
11 - Upper, Cold Side, Sector IV	4-26	18	29	13	35
125 - Upper, Hot Side, Between S ctors I & II	4-27	154	156	82	86
Inner Cylinder					
225 - Hot Side, Between Sectors I & II	4-28	147	148	89	92
331 - Cold Side, Between Sectors IV & V	4-29	73	88	52	63
Radial Beams					
337 - Beam 1, Hot Side	4-30	208	217	162	173
340 - Beam 4, Cold Side	4-31	15	8	15	17
Helium Bottles					
391 - Lower Bottle	4-32	84	100	72	73
392 - Upper Bottle	4-33	111	100	72	74
Propellant Tanks					
394 - Oxidizer, Sector II	4-34	196	198	92	97
395 - Fuel, Sector III	4-35	62	84	52	72
396 - Fuel, Sector VI	4-36	181	184	87	109
397 - Oxidizer, Sector V	4-37	46	74	44	66

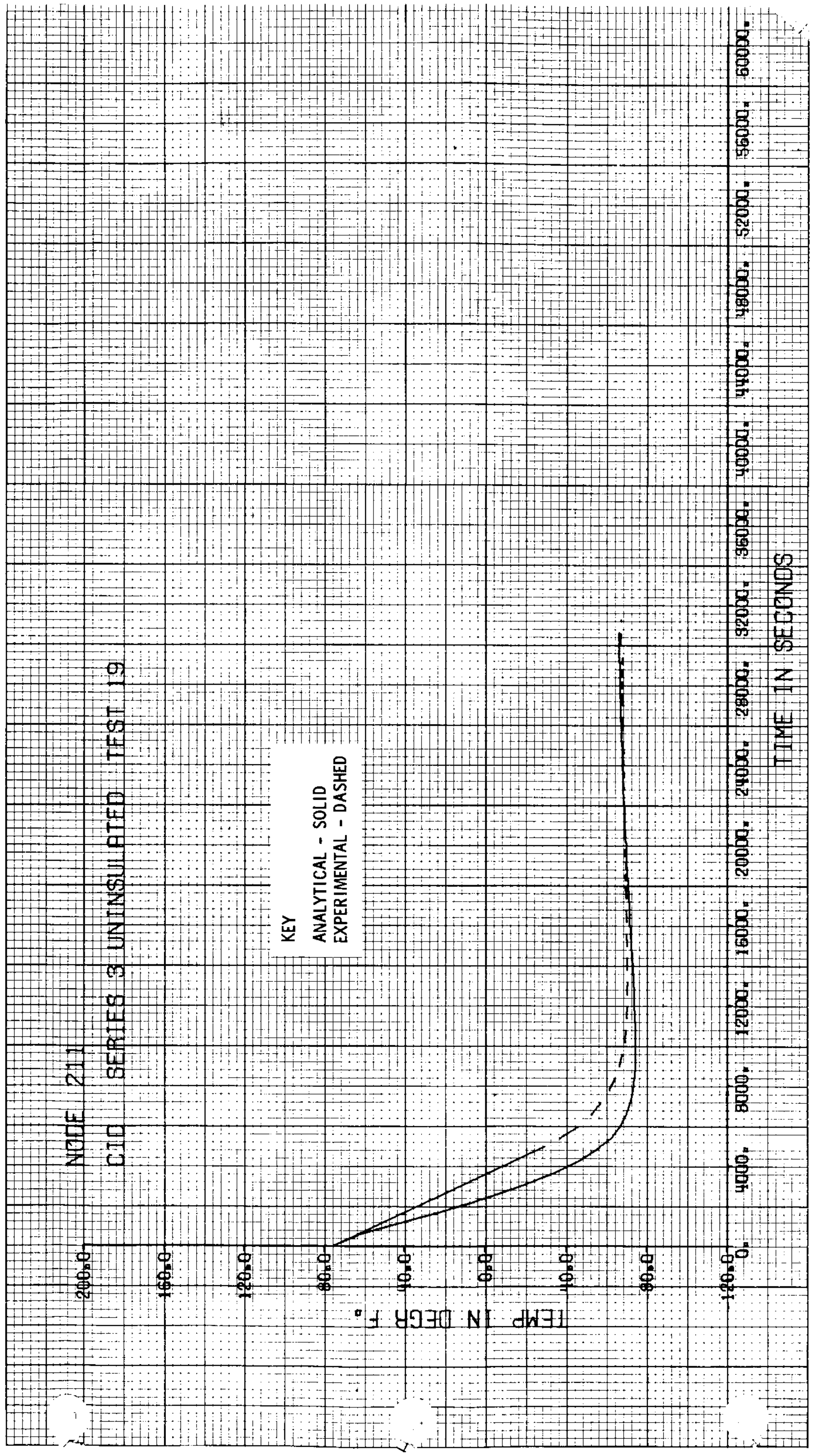

Figure 4-22 Panel Temperature History (Node 211) for Run 3-19

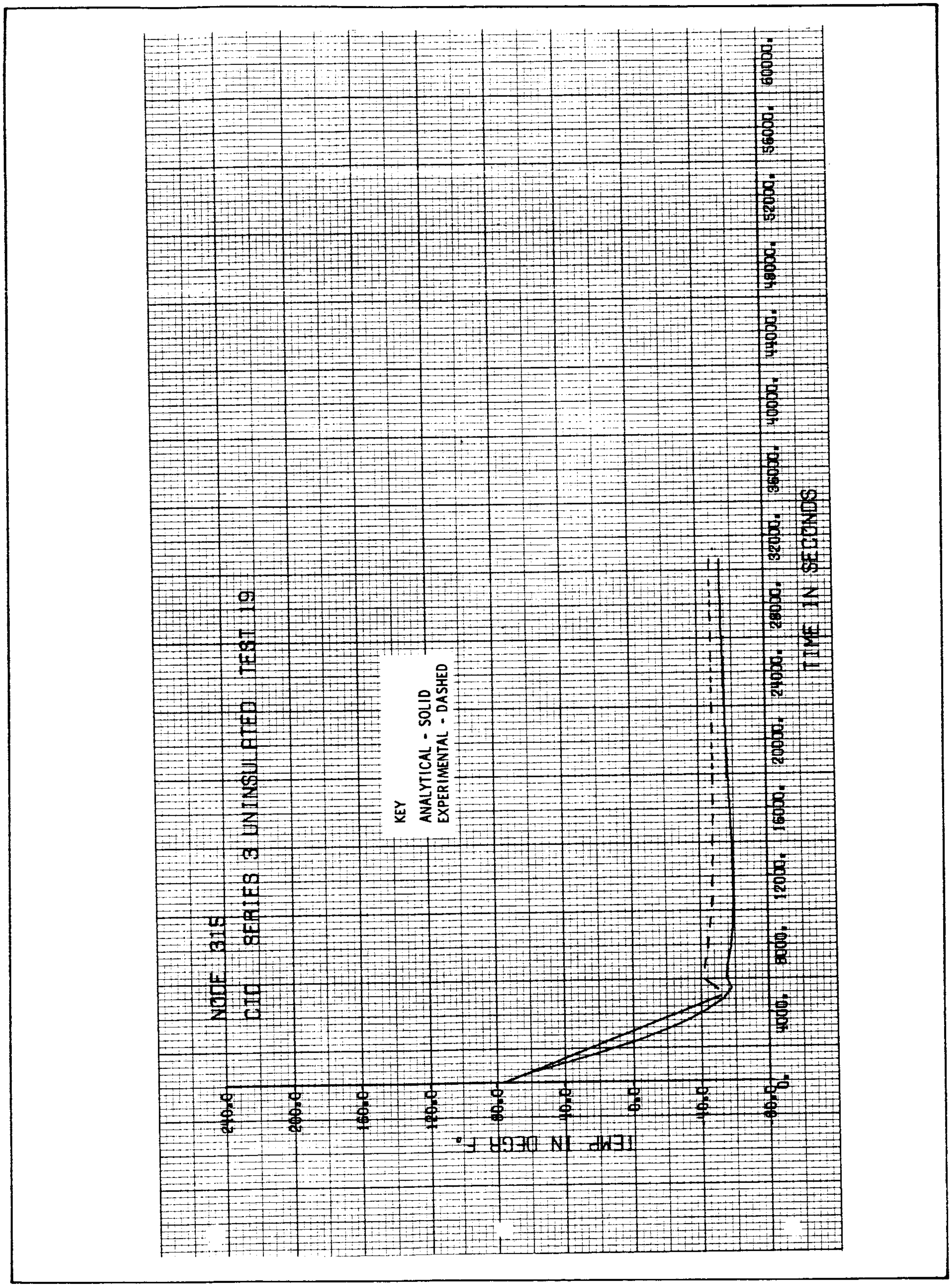

Figure 4-23 Panel Temperature History (Node 315) for Run 3-19

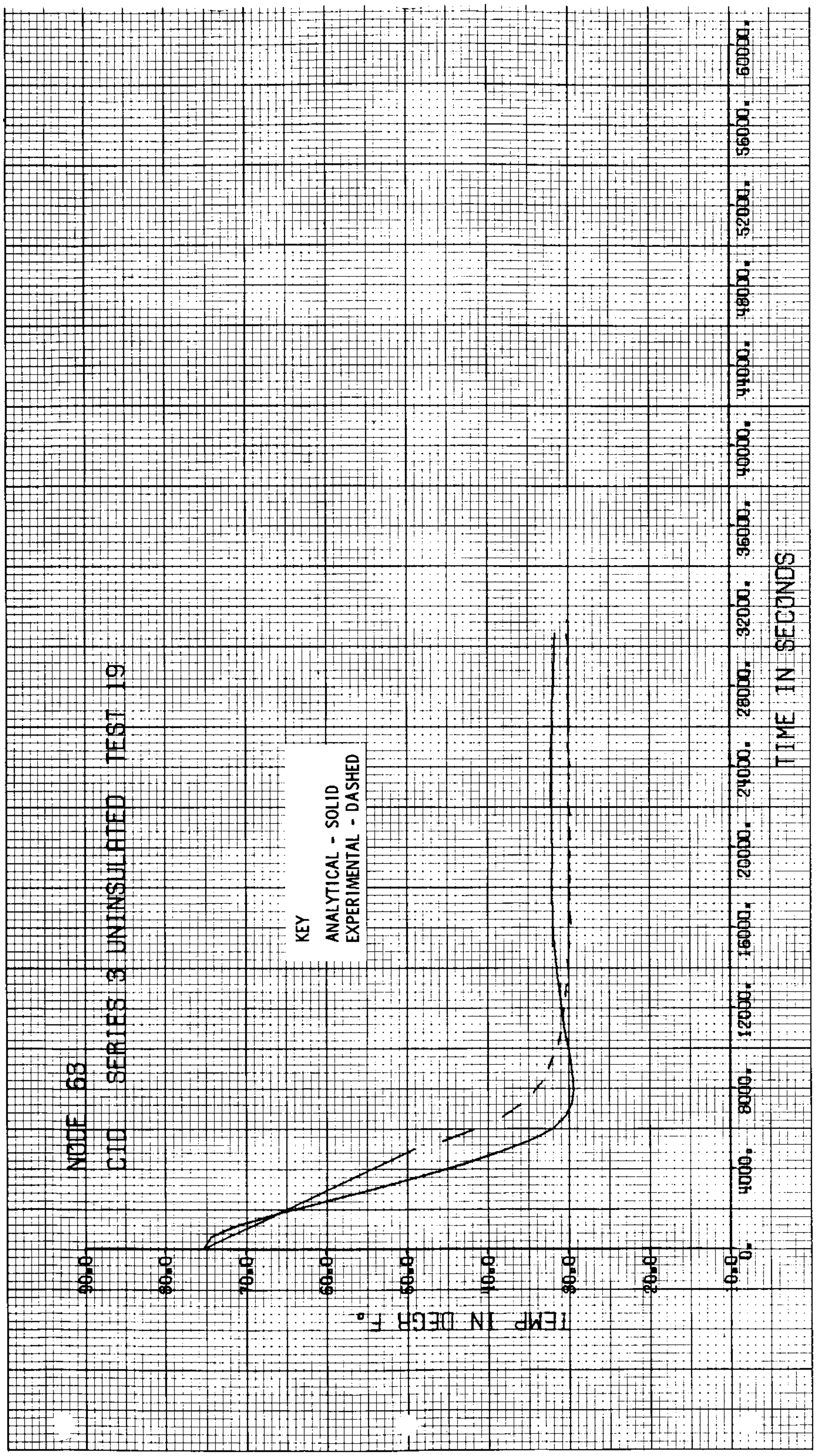

Figure 4-24 Bulkhead Temperature History (Node 63) for Run 3-19

LOCKHEED
CALIFORNIA COMPANY

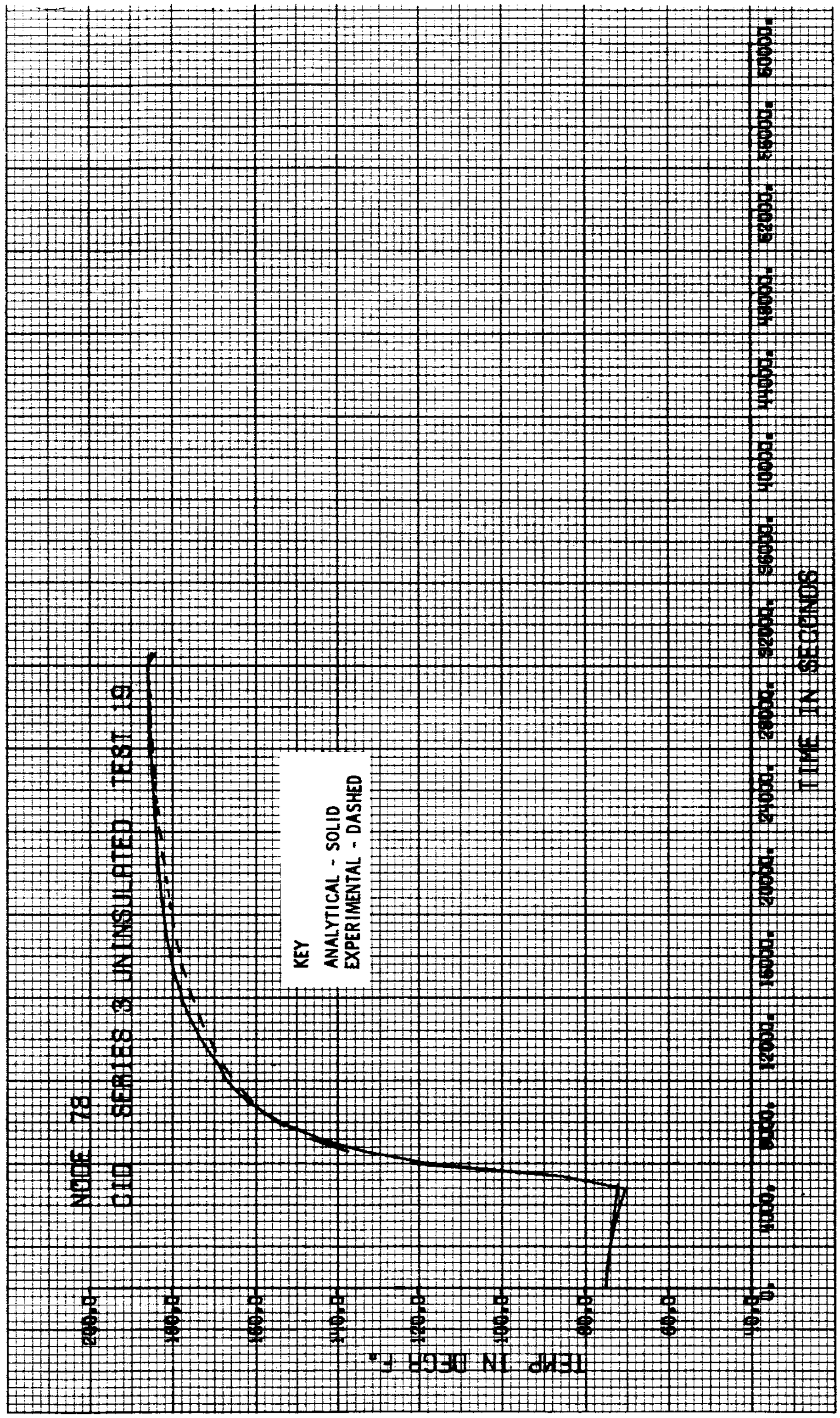

Figure 4-25 Bulkhead Temperature History (Node 73) for Run 3-19

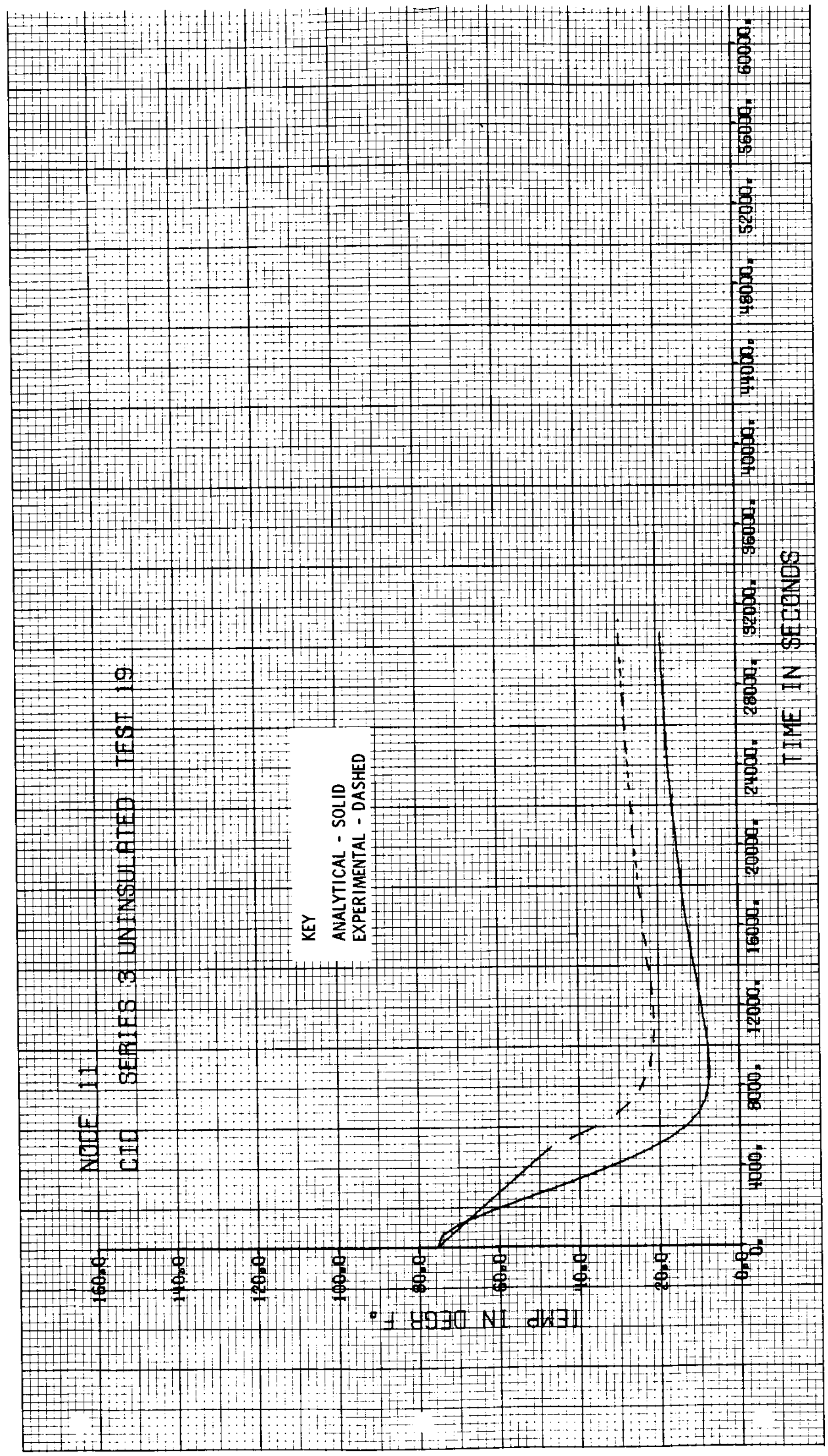

Figure 4-26 Bulkhead Temperature History (Node 11) for Run 3-19

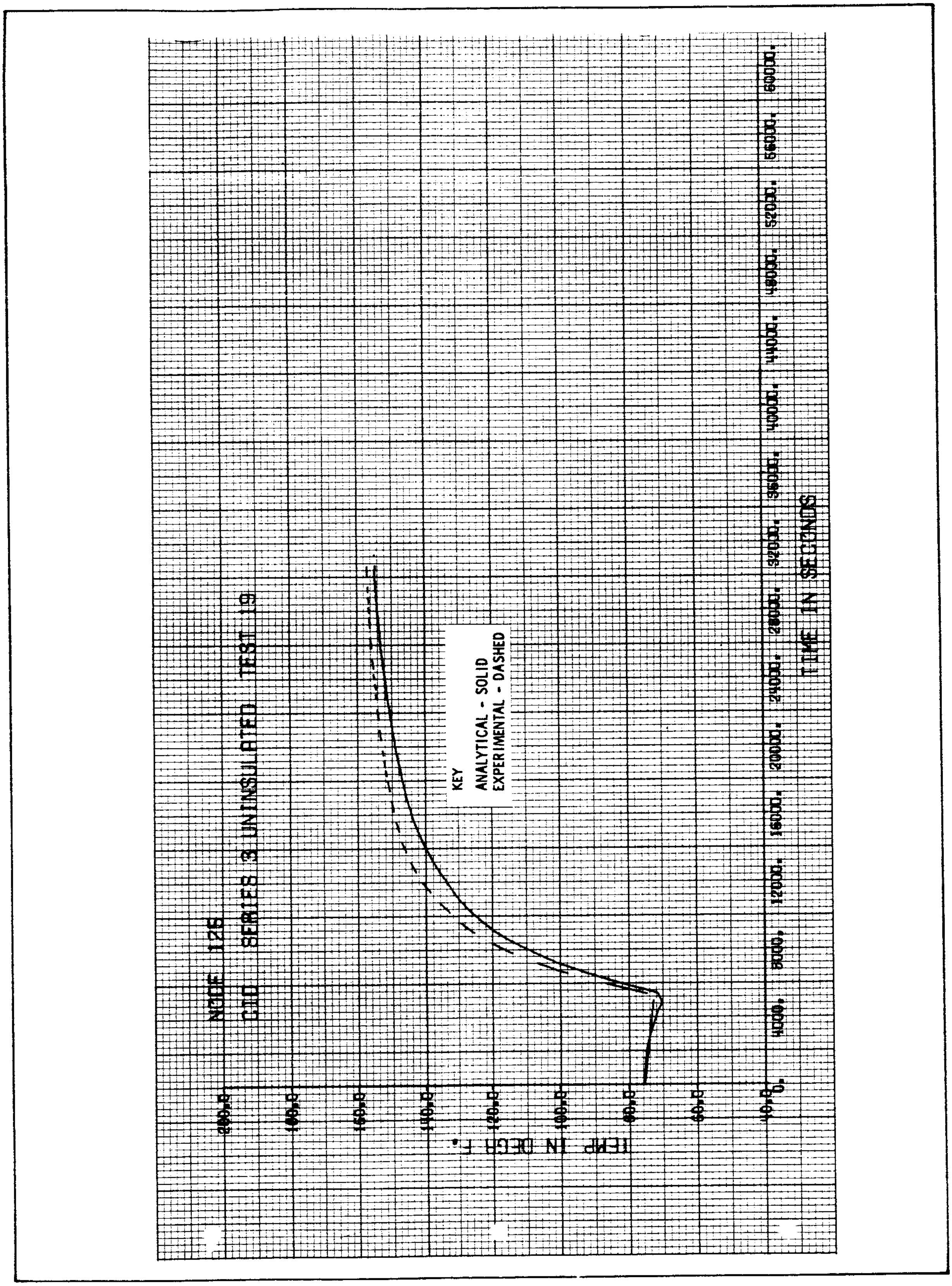

Figure 4-27 Bulkhead Temperature History (Node 125) for Run 3-19

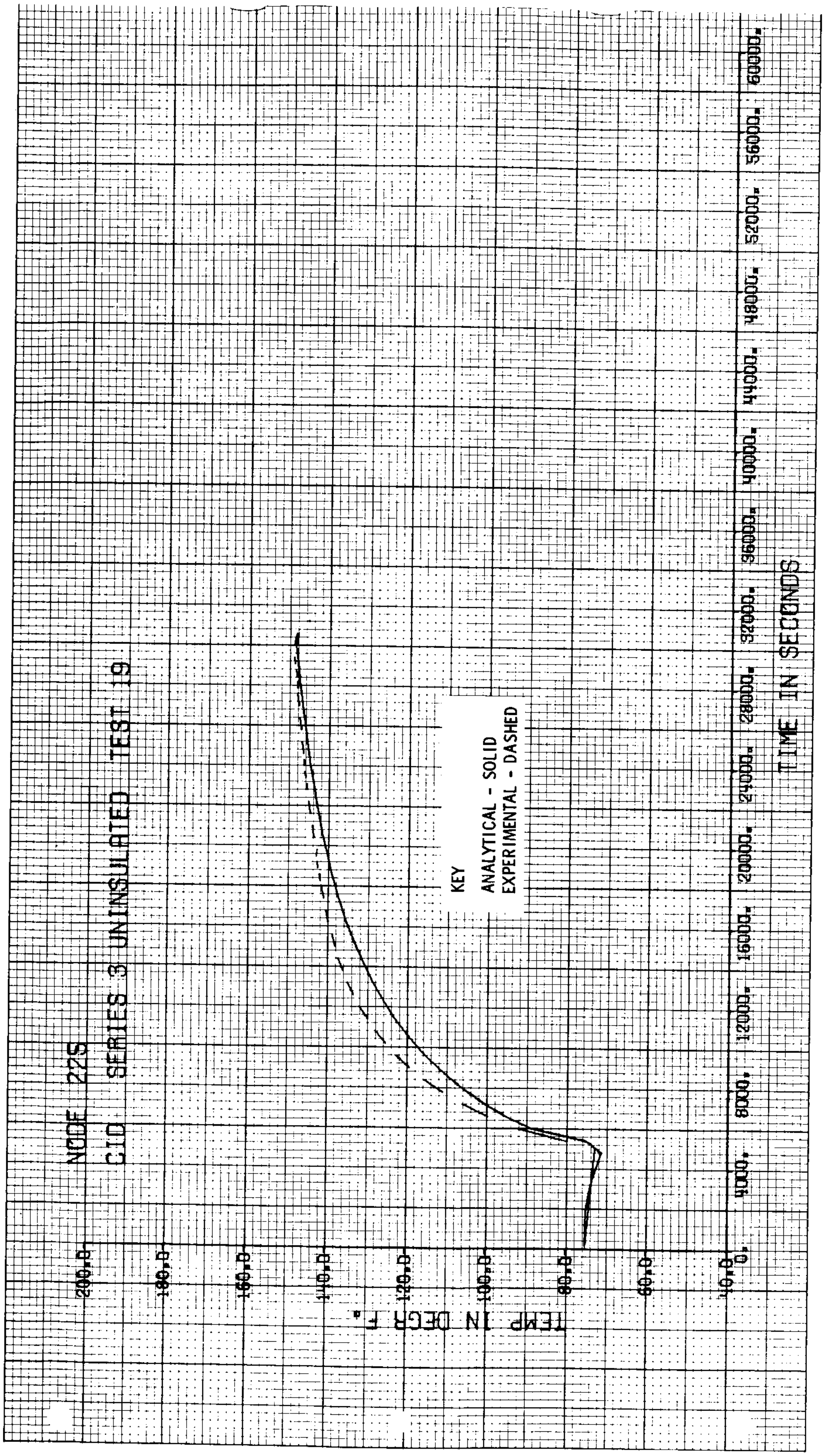

Figure 4-28 Inner Cylinder Temperature History (Node 225) for Run 3-19

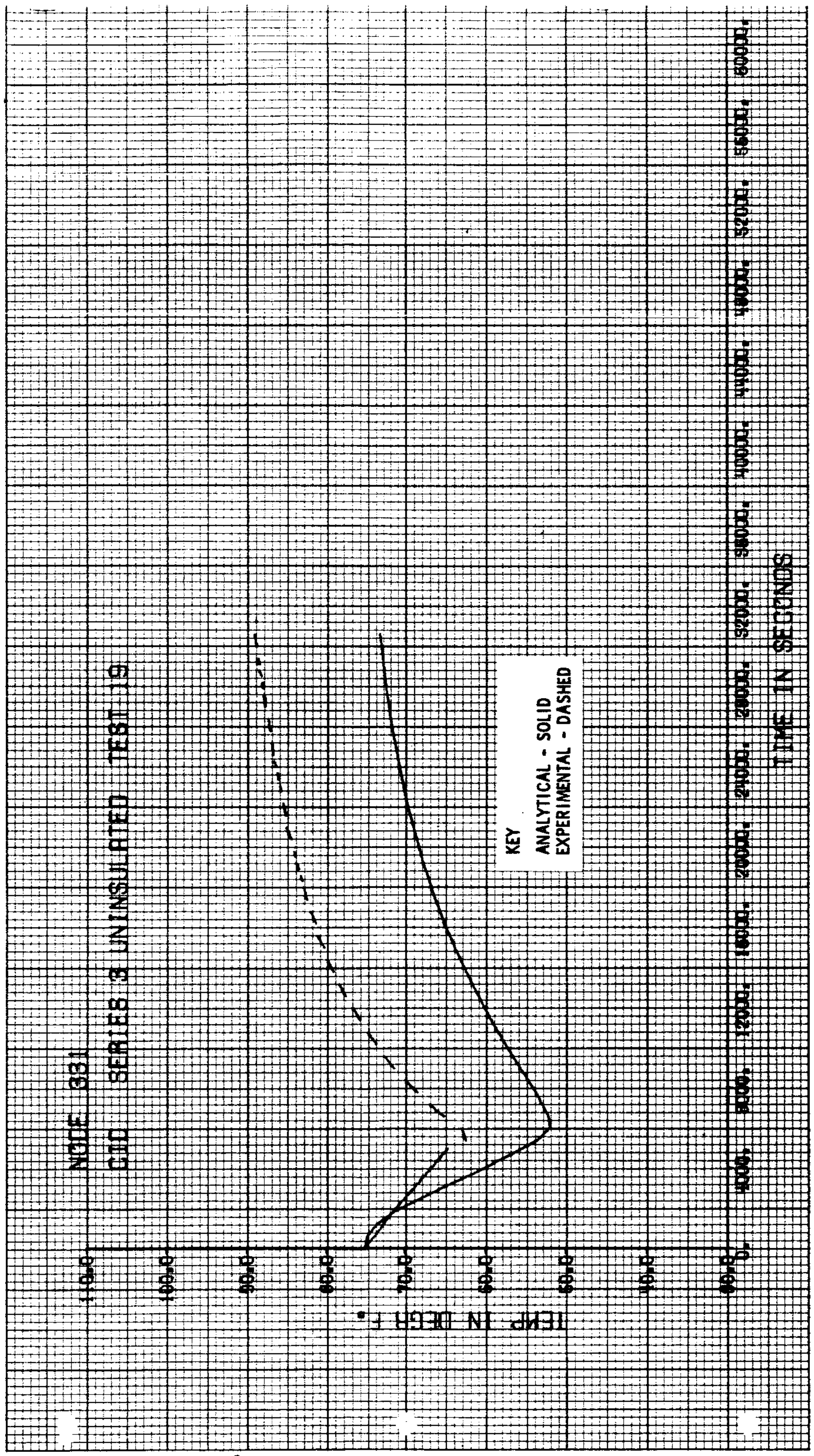

Figure 4-29 Inner Cylinder Temperature History (Node 331) for Run 3-19

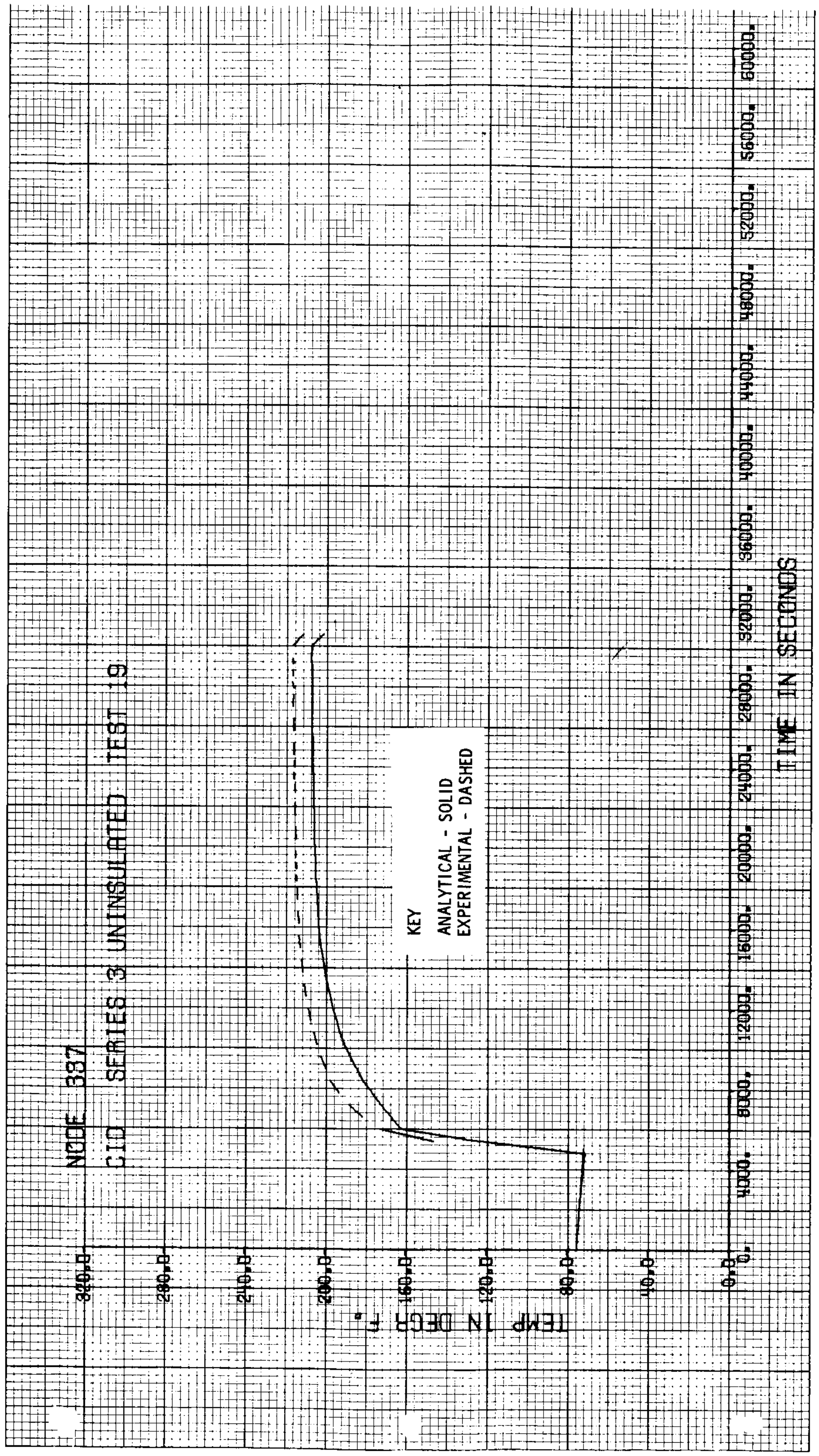

Figure 4-30 Beam Temperature History (Node 337) for Run 3-19

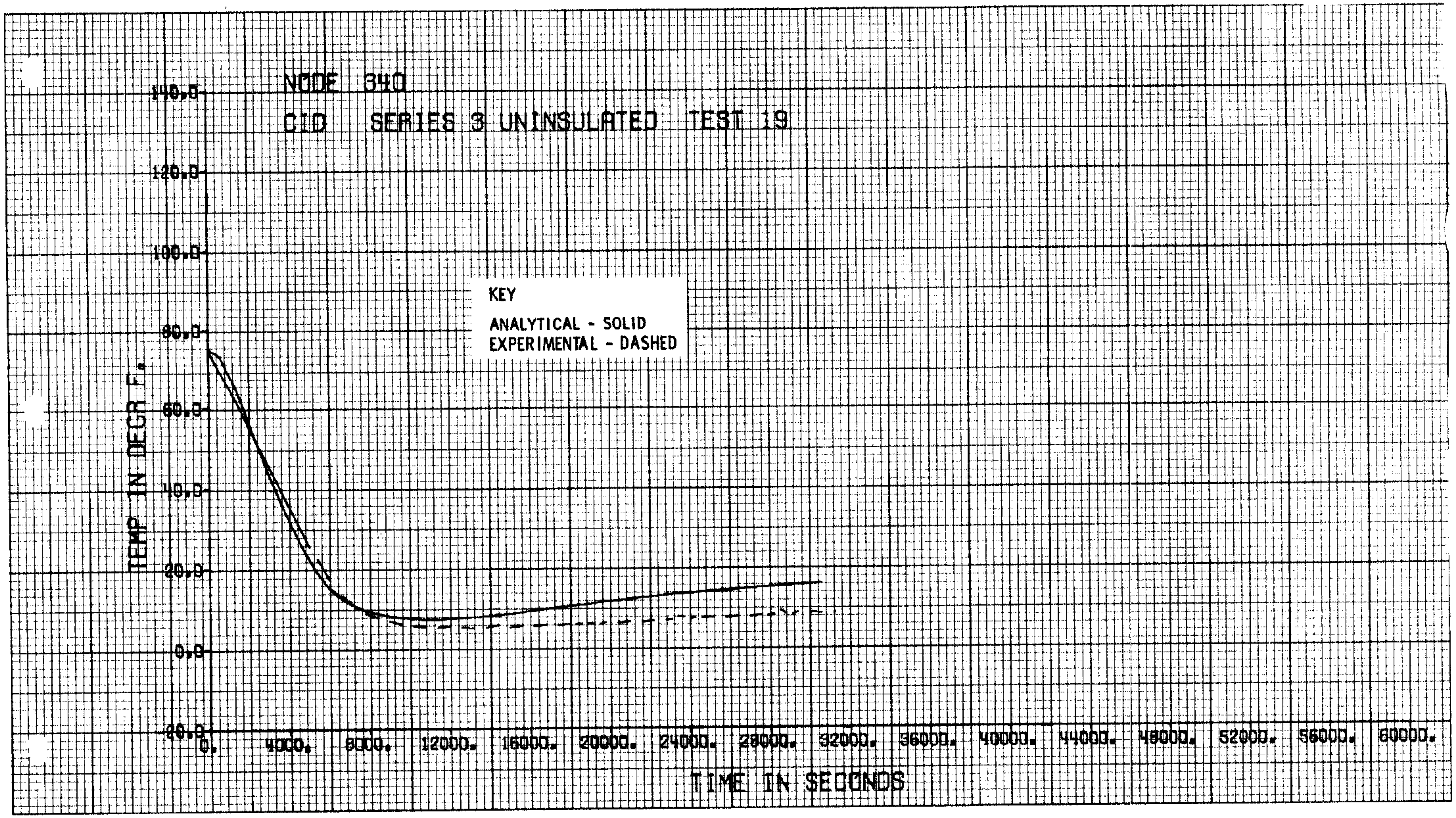

Figure 4-31 Beam Temperature History (Node 340) for Run 3-19

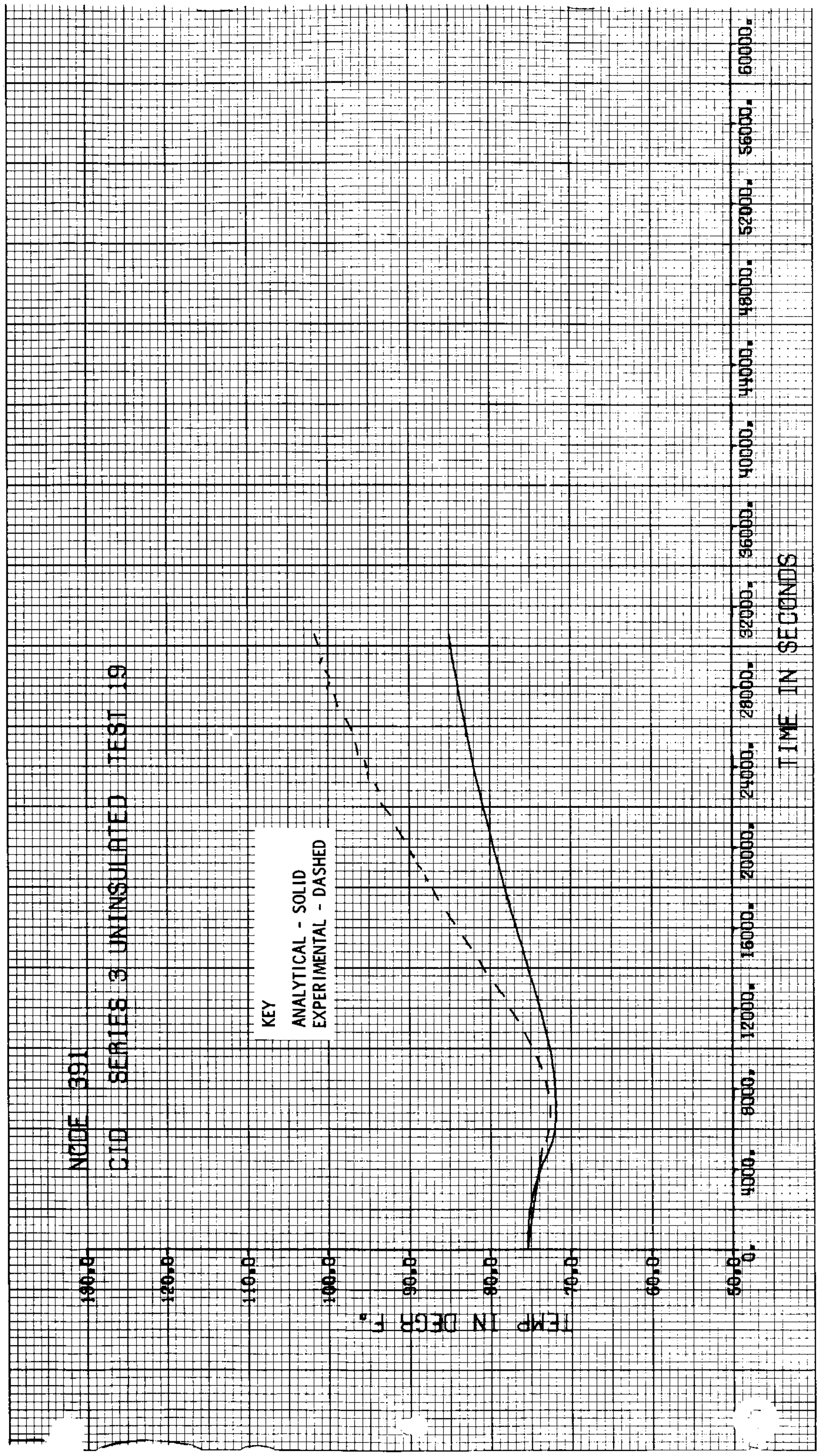

Figure 4-32 Lower Helium Bottle Temperature History (Node 391) for Run 3-19

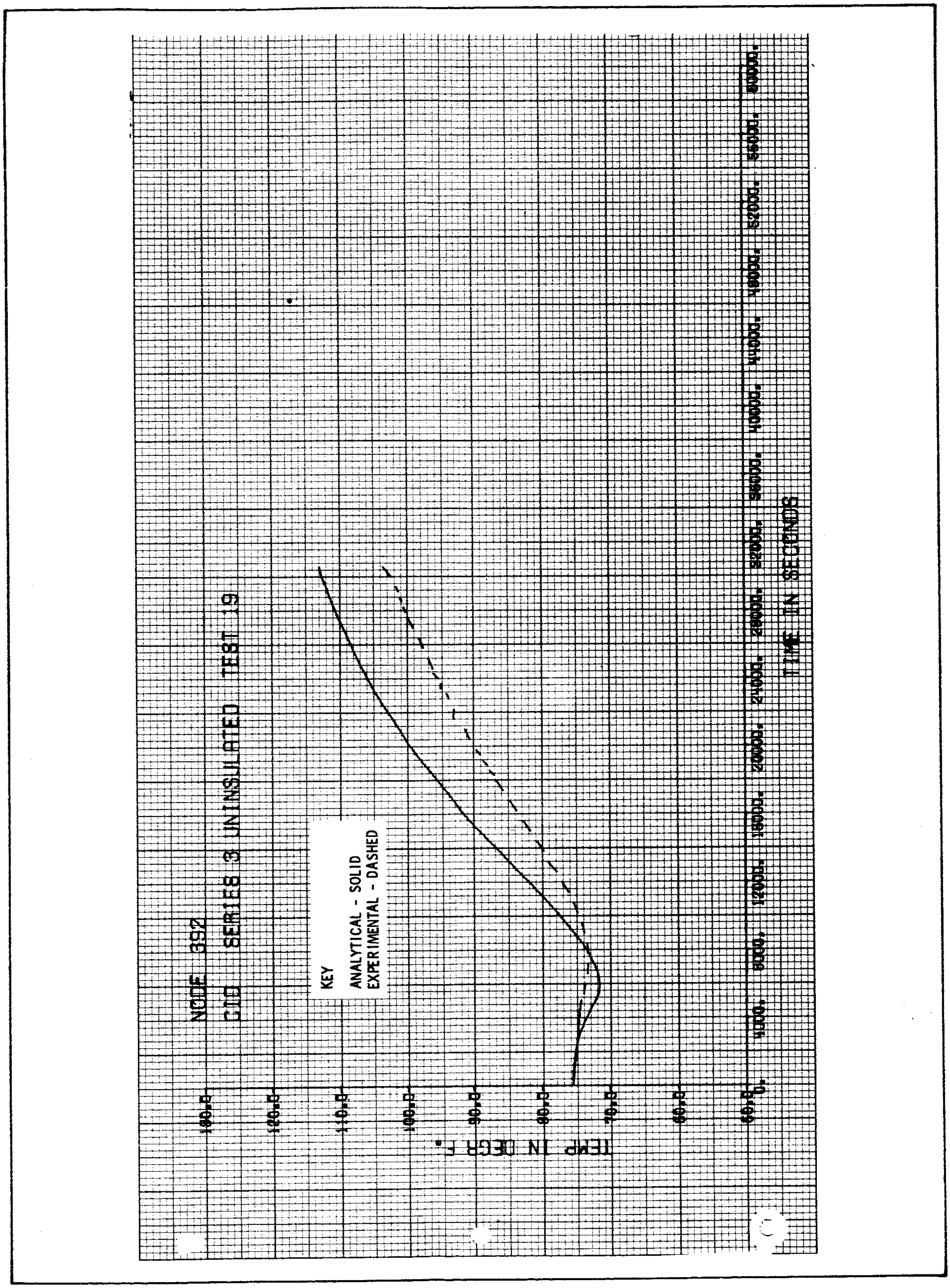

Figure 4-33 Upper Helium Bottle Temperature History (Node 392) for Run 3-19

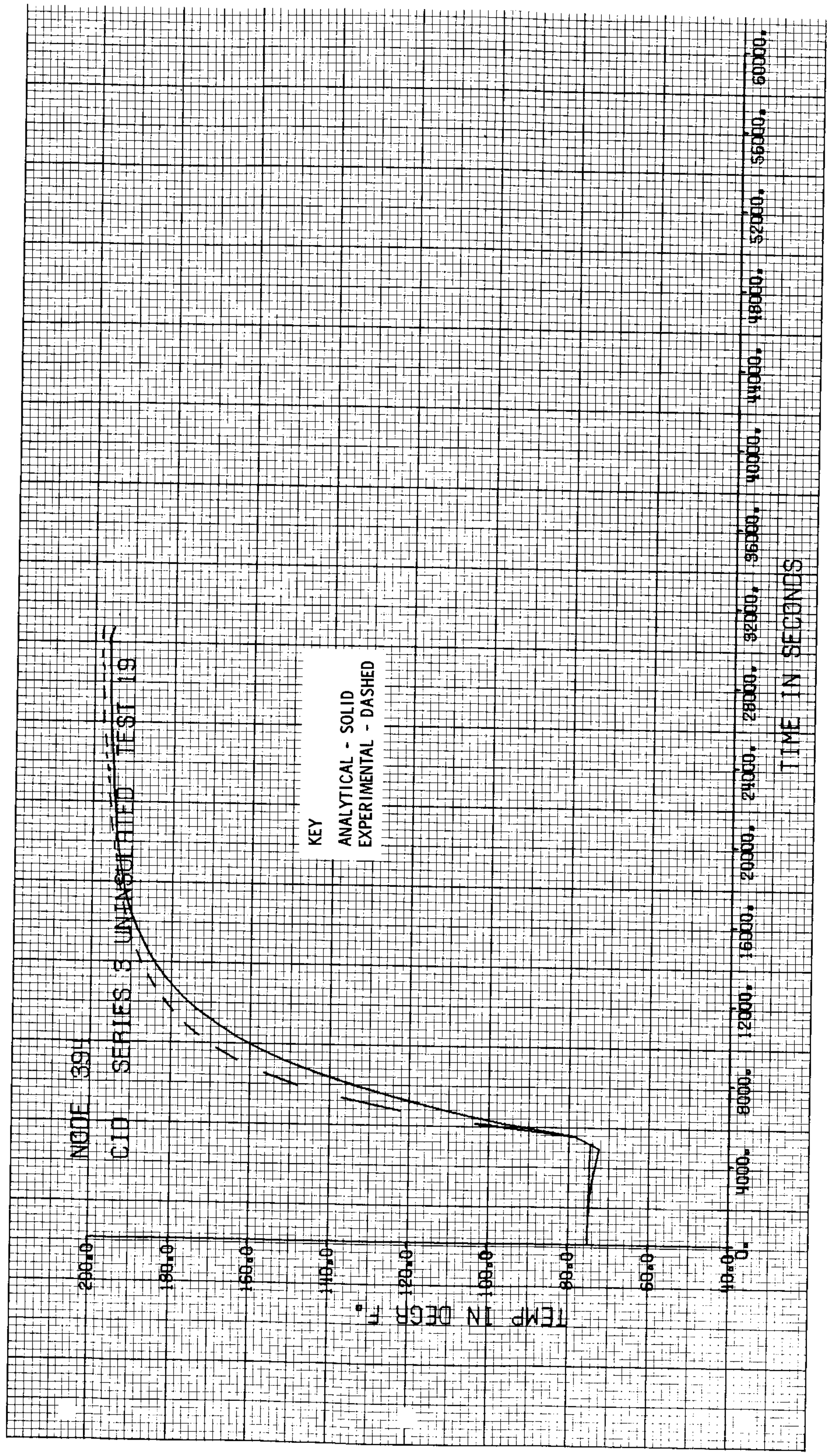

Figure 4-34 Propellant Tank Temperature History (Node 394) for Run 3-19

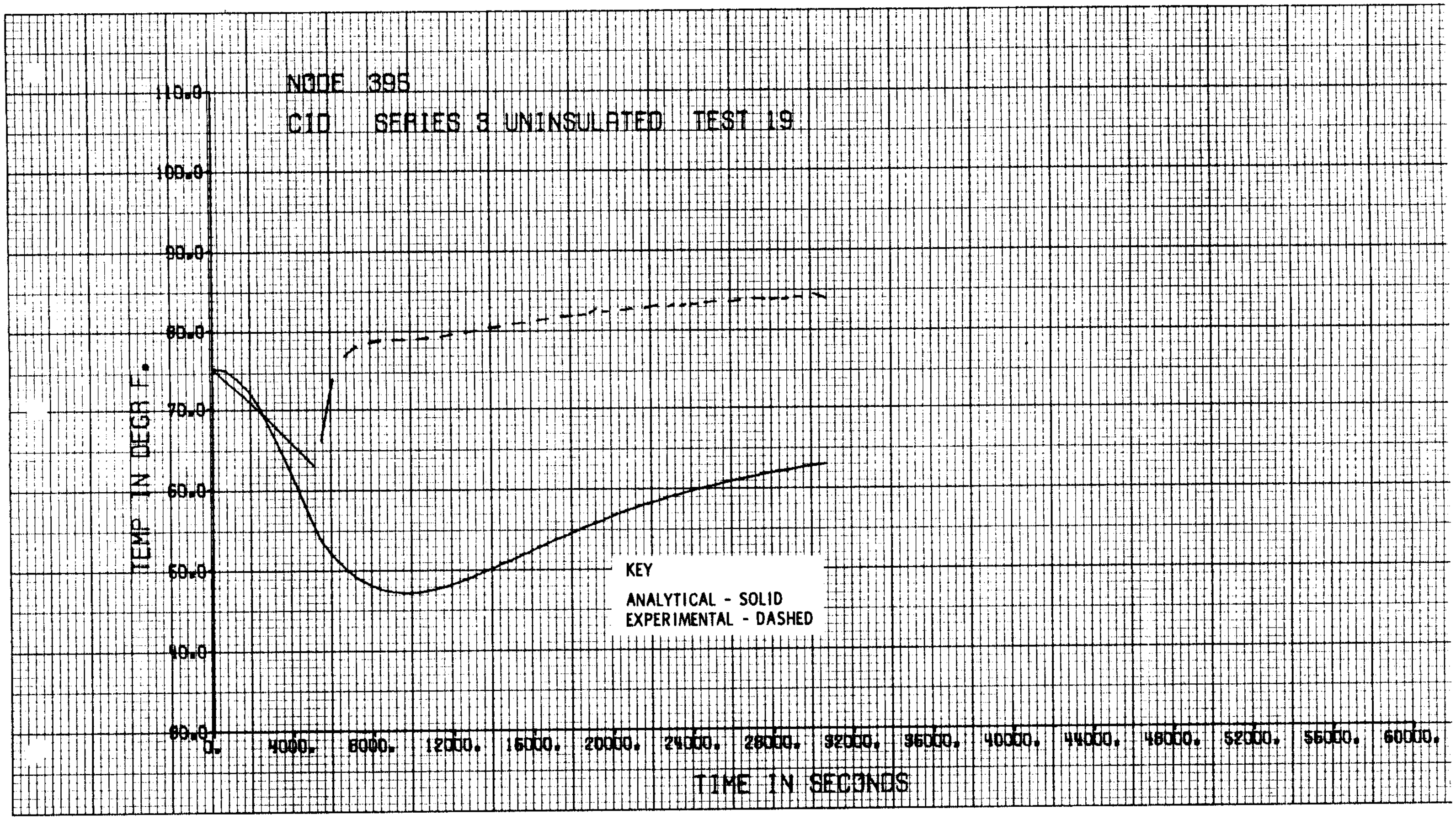

Figure 4-35 Propellant Tank Temperature History (Node 395) for Run 3-19

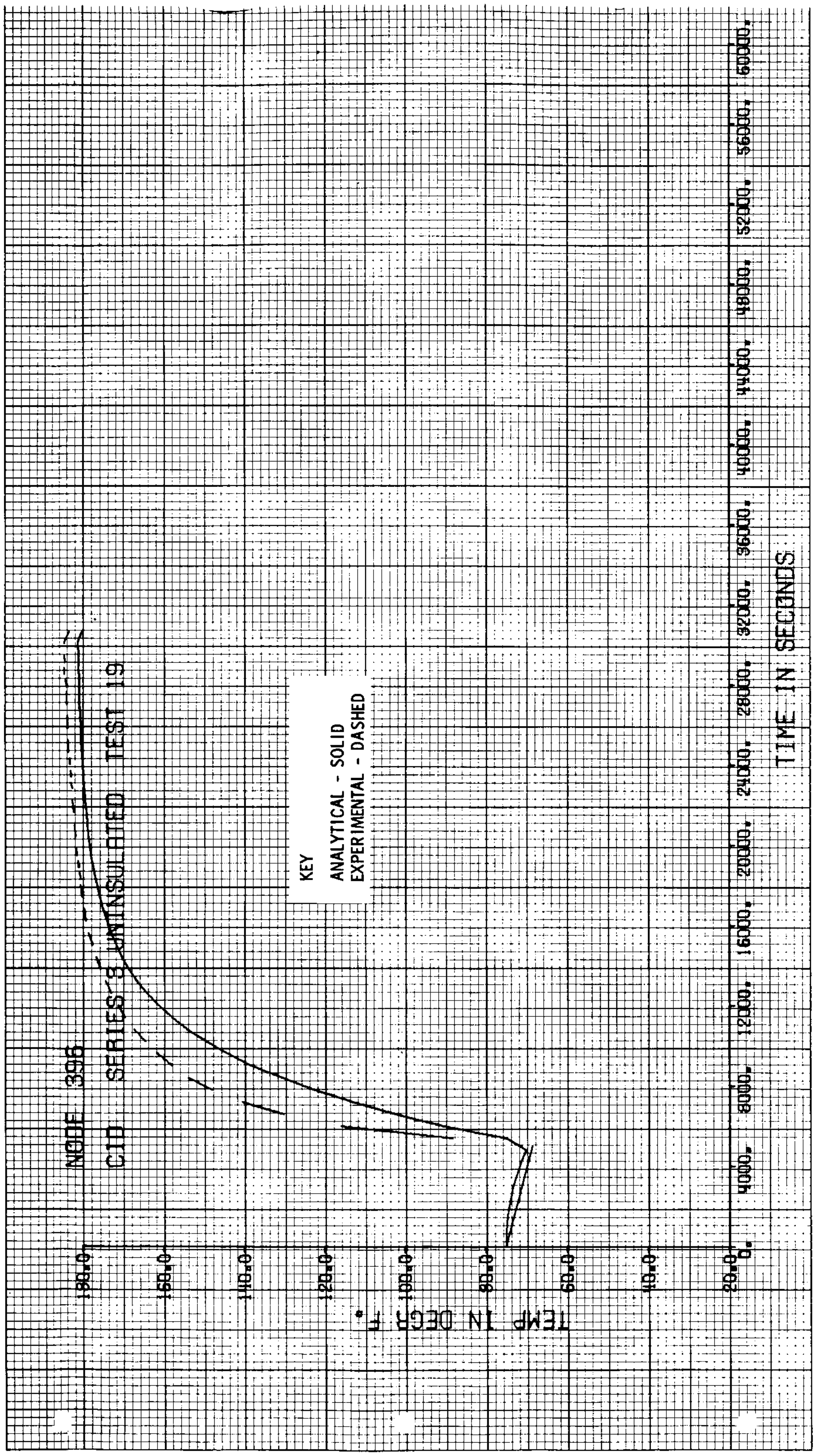

Figure 4-36 Propellant Tank Temperature History (Node 396) for Run 3-19

LOCKHEED
CALIFORNIA COMPANY

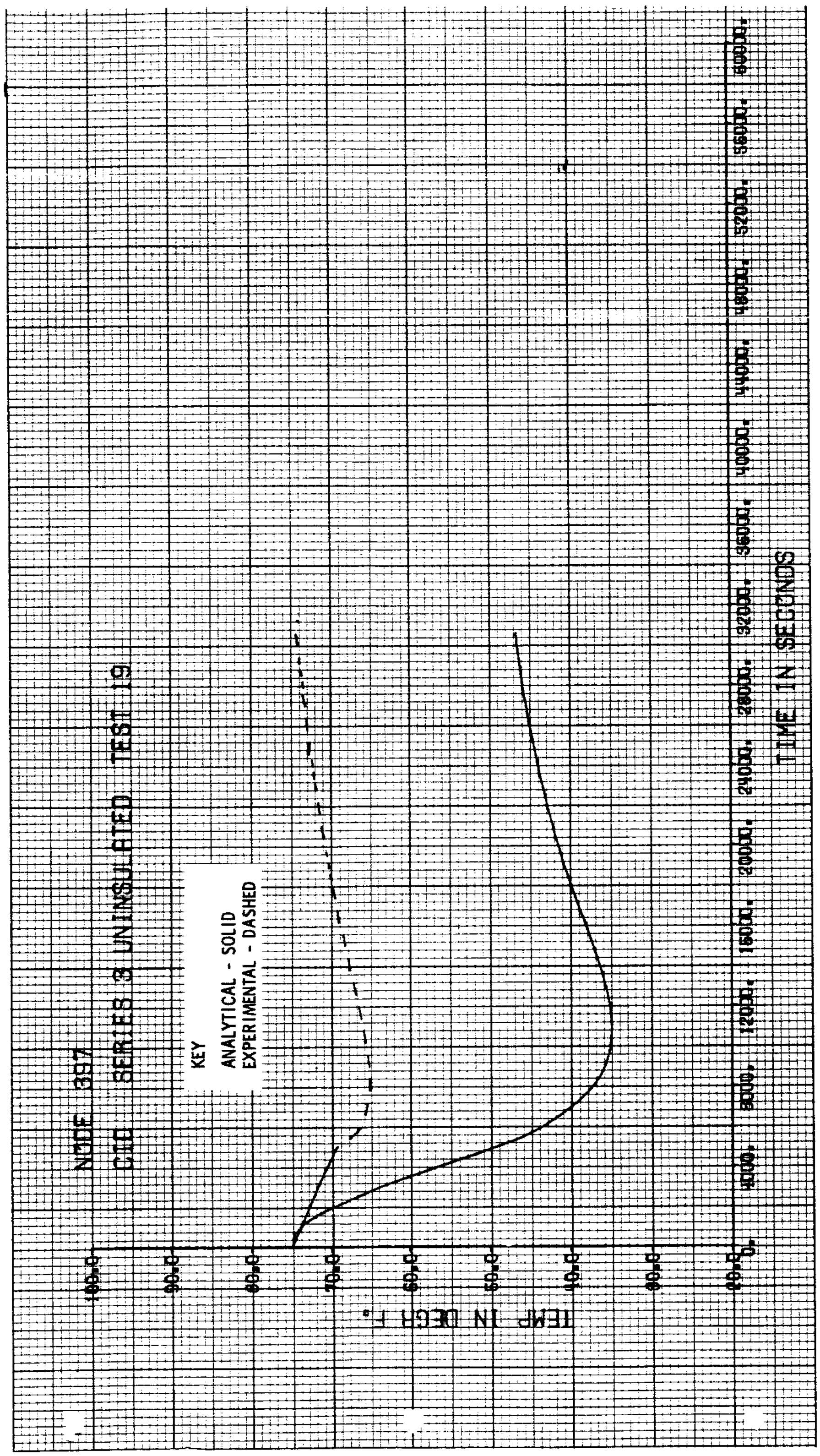

Figure 4-37 Propellant Tank Temperature History (Node 397) for Run 3-19

representation of the empty bottle, which in fact has large temperature gradients. When the bottles are filled, the temperature gradients on the bottle are greatly reduced, thus permitting single node representation. Similar problems occur on the propellant tanks in bays III and V as shown in Figures 4-35 and 4-37. From the five thermocouples on the tank in bay III, it was discovered that a 50°F temperature gradient existed on this tank during Run 3-19. Propellant tanks on the warm side of the model (Figures 4-34 and 4-36), however, show very good correlation with the measured values. This can only be attributed to the fact that thermocouples used on the warm side tank measured a more representative tank temperature than those on the tanks on the cold side of the node.

<u>Run 3-21</u> --- A comparison of analytical and experimental temperatures for Run 3-21 at 15,000 seconds is shown in Figure 4-38. This time point represents steady state conditions just prior to the simulated engine firing. Data from five regions of the model are presented in Figure 4-38. The regions are: outer panel, inner cylinder, beams, bulkheads, and tanks. As seen in Figure 4-38, the range of temperatures is from -80°F to 180°F. Eighty-five percent of the predicted temperatures are within ± 20°F of the measured temperatures. From this figure, note that about 75 percent of the analytical temperatures are below the experimental temperatures. For the most part, this is attributed to inaccurate accounting of the internal radiation heat transfer. The coarseness of the radiation network and the simplified analysis of reflections were the two major causes of inadequate prediction of internal radiation.

Table 4-3 provides a summary of the predicted and experimental temperature histores presented in Figures 4-39 to 4-55. Except for node 331, the predicted temperatures of the structural nodes are typically within ±20°F of the measured temperatures. As explained in the discussion of Run 3-19, the predicted temperature of inner cylinder node 331 is low because of faulty thermocouple location. For nodes near the simulated thrust chamber, the peak temperatures are consistently predicted too low during an engine firing, as shown in Figures 4-45 and 4-47. This is because the radiation network does not account for all the heat emitted from the thrust chamber. Once again a

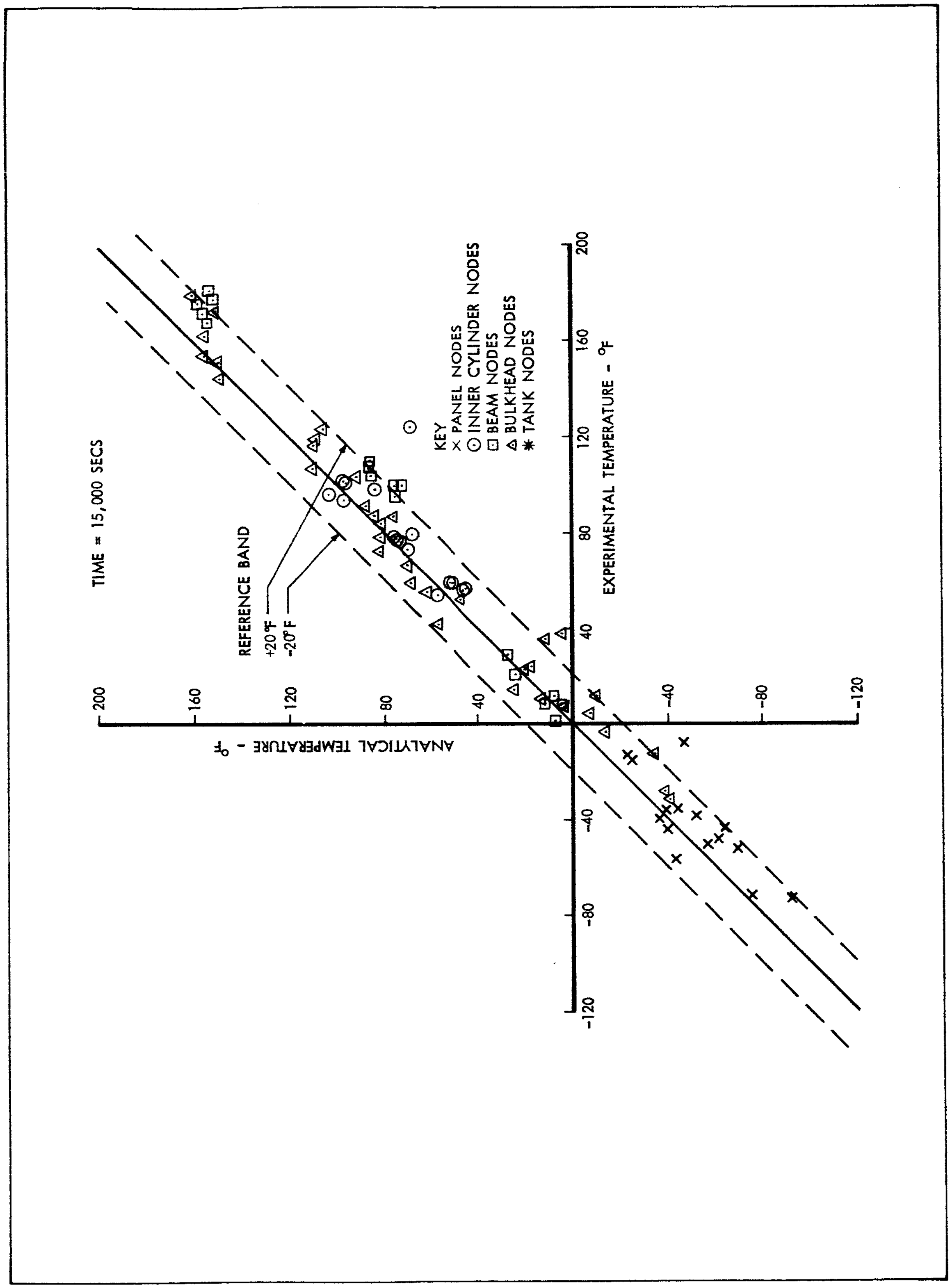

Figure 4-38 Correlation of Analytical and Experimental Data for Run 3-21

TABLE 4-3 GUIDE TO SELECTED PLOTS FOR RUN 3-21

Node Location and Number	Ref. Figure	Temp. at 15,000 secs.		Temp. at 23,000 secs.	
		Analytical	Experimental	Analytical	Experimental
Outer Panel					
211 - Cold Side, Sector IV	4-39	-75	-71	-68	-56
315 - Cold Side, Sector V	4-40	-61	-48	-56	-45
Bulkheads					
11 - Upper, Cold Side, Sector IV	4-41	25	14	35	30
125 - Upper, Hot Side, Between Sectors I & II	4-42	110	117	123	132
73 - Lower, Hot Side, Sector I	4-43	55	54	196	188
Inner Cylinder					
225 - Hot Side, Between Sectors I & II	4-44	95	101	113	129
331 - Cold Side, Between Sectors IV & V	4-45	43	56	100	145
Radial Beams					
437 - Beam 1, Hot Side	4-46	153	169	182	187
340 - Beam 4, Cold Side	4-47	5	8	29	45
Heat Shield					
376 - Hot Side	4-48	66	85	174	181
385 - Cold Side	4-49	14	4	80	80
Helium Bottles					
391 - Lower Bottle	4-50	47	57	114	127
392 - Upper Bottle	4-51	66	59	81	75
Propellant Tanks					
394 - Oxidizer, Sector II	4-52	76	81	99	140
395 - Fuel, Sector III	4-53	52	57	57	80
396 - Fuel, Sector VI	4-54	70	75	81	115
397 - Oxidizer, Sector V	4-55	38	40	44	70

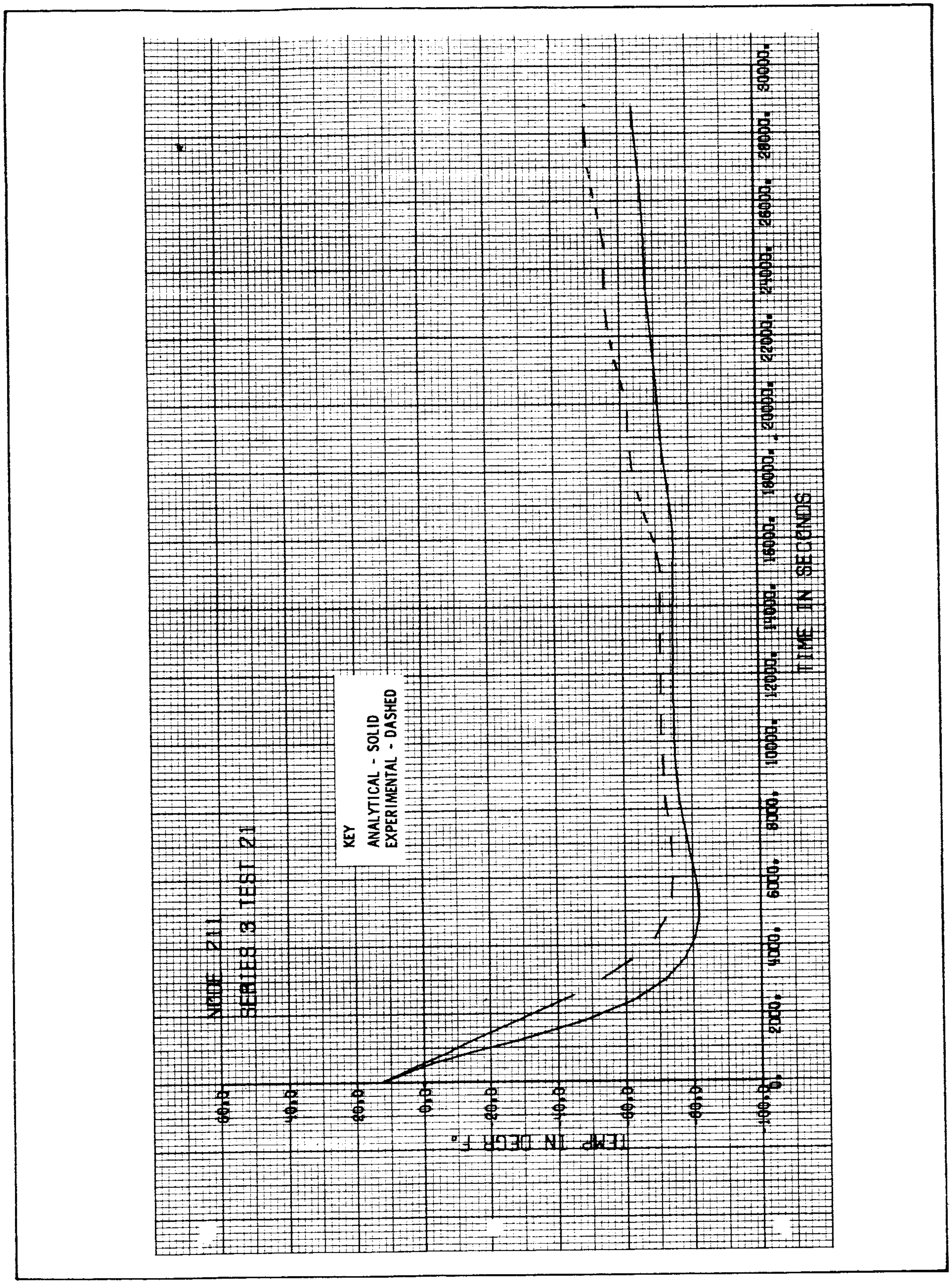

Figure 4-39 Panel Temperature History (Node 211) for Run 3-21

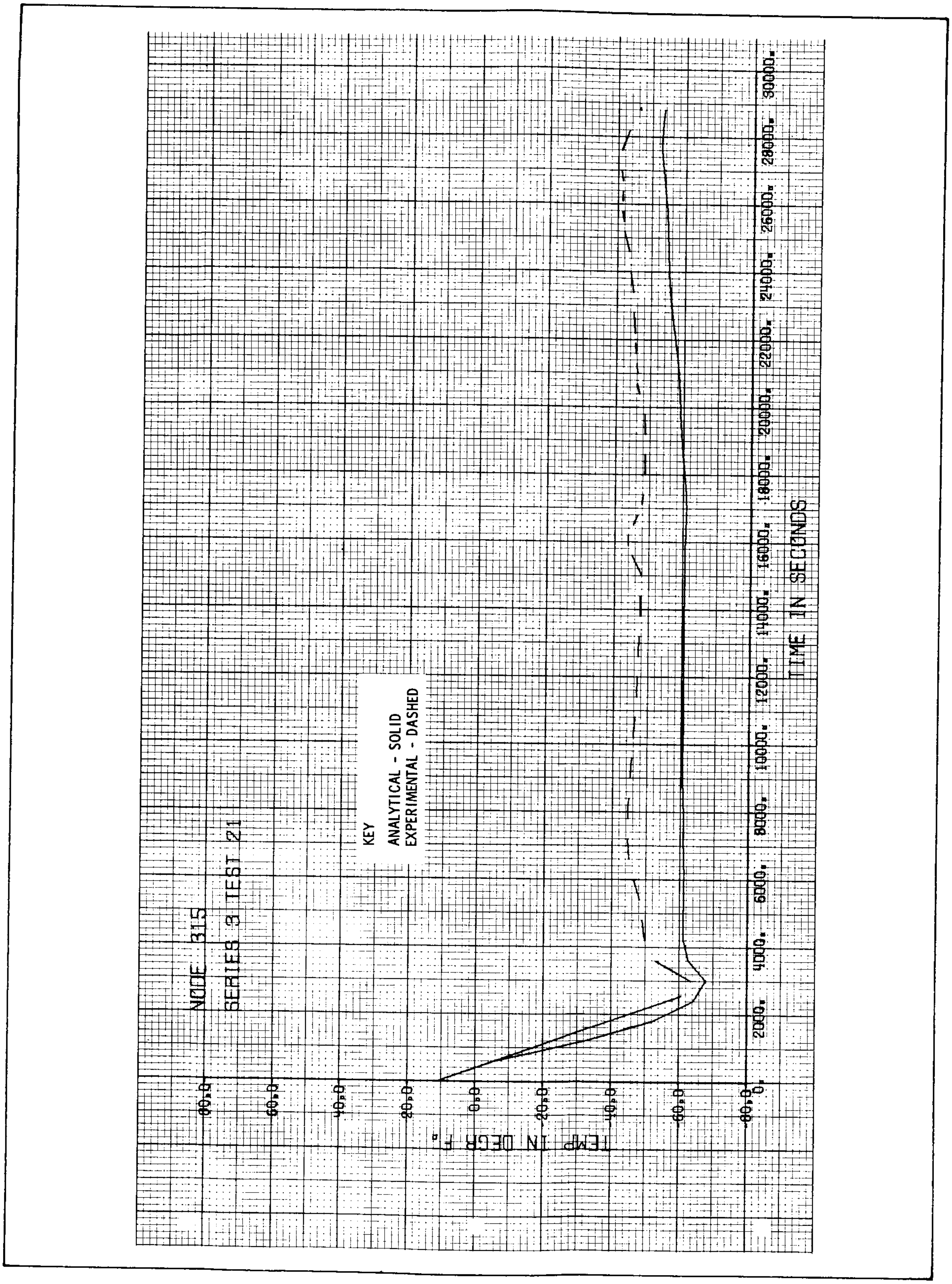

Figure 4-40 Panel Temperature History (Node 315) for Run 3-21

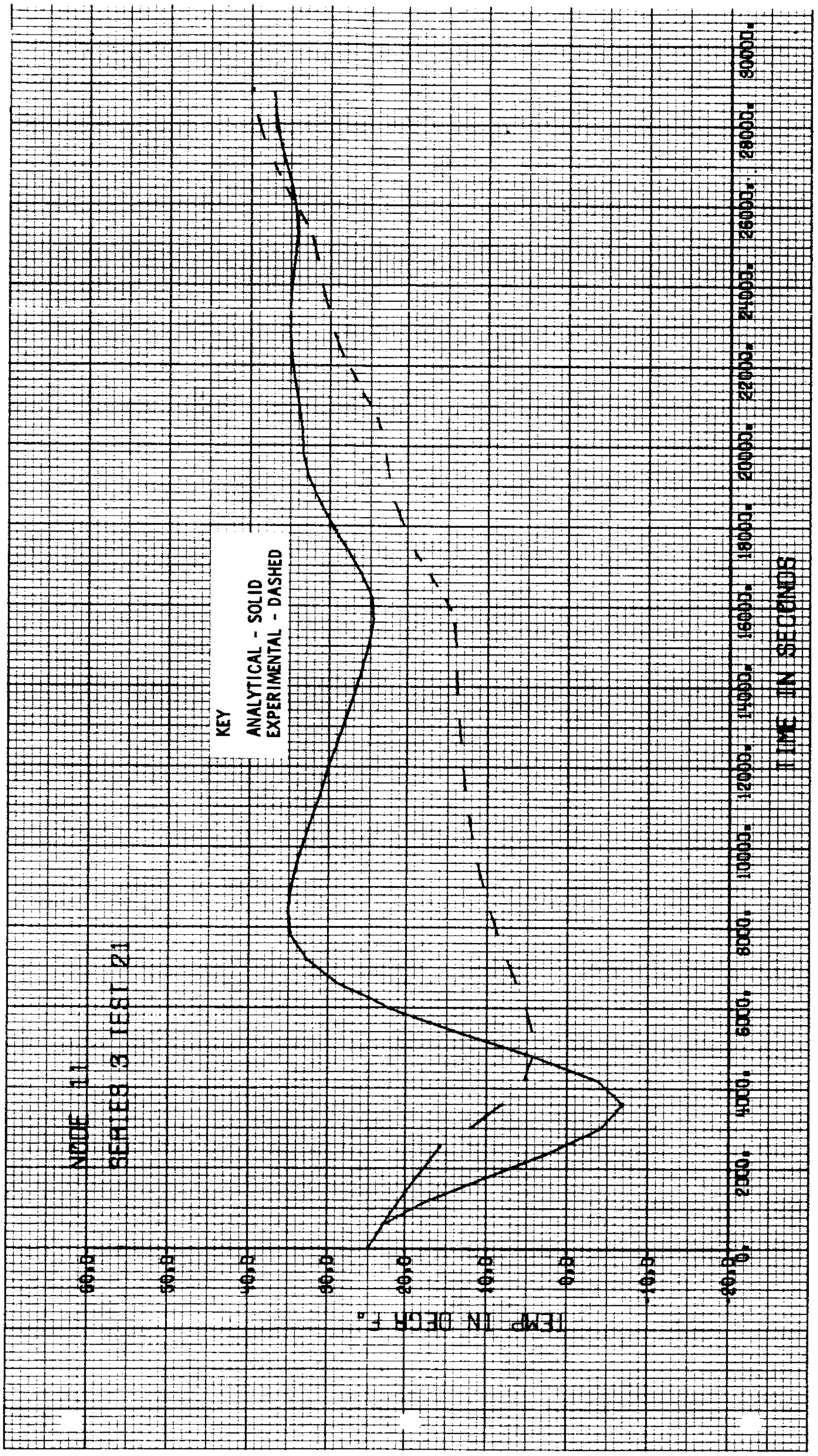

Figure 4-41 Bulkhead Temperature History (Node 11) for Run 3-21

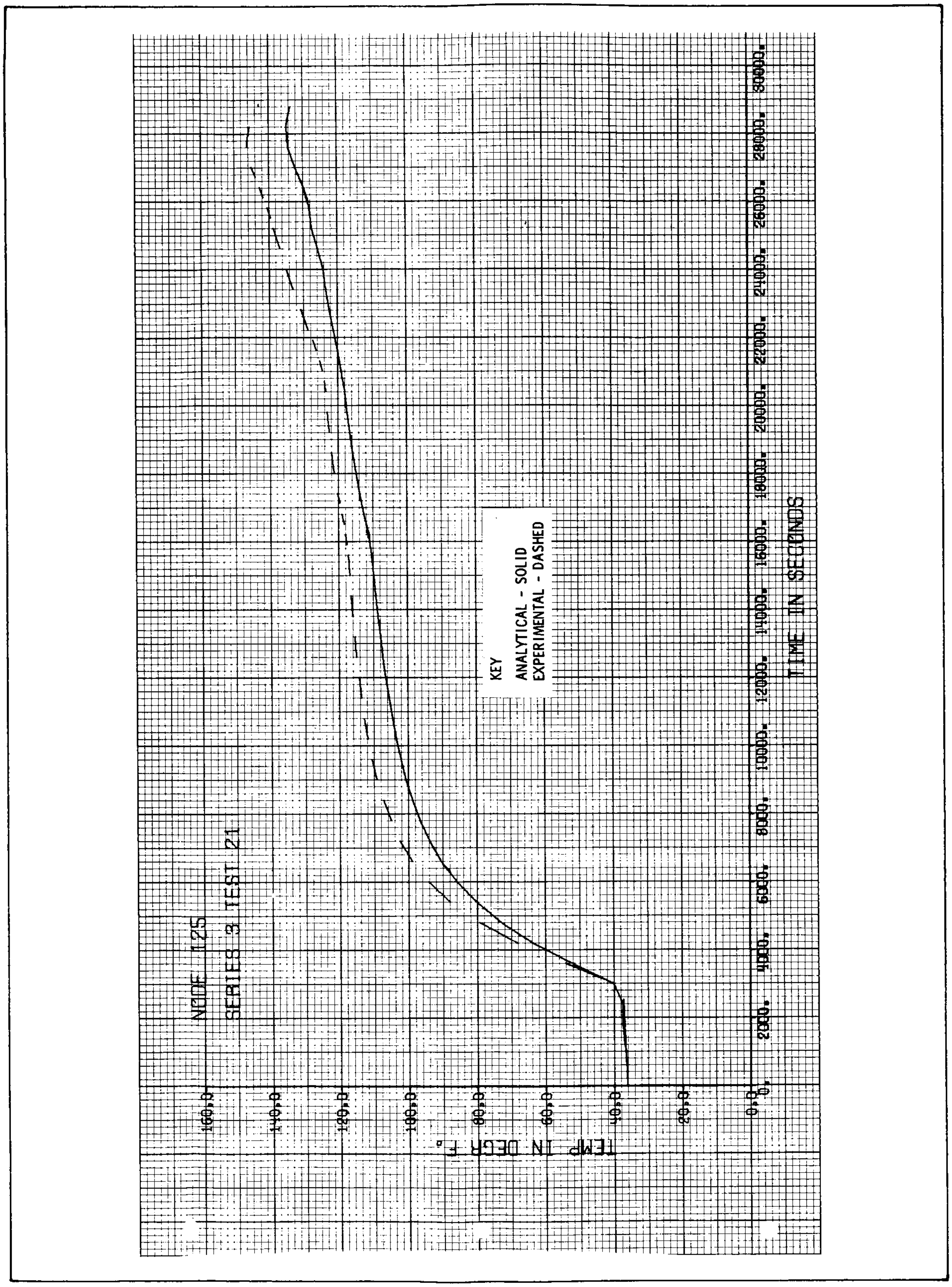

Figure 4-42 Bulkhead Temperature History (Node 125) for Run 3-21

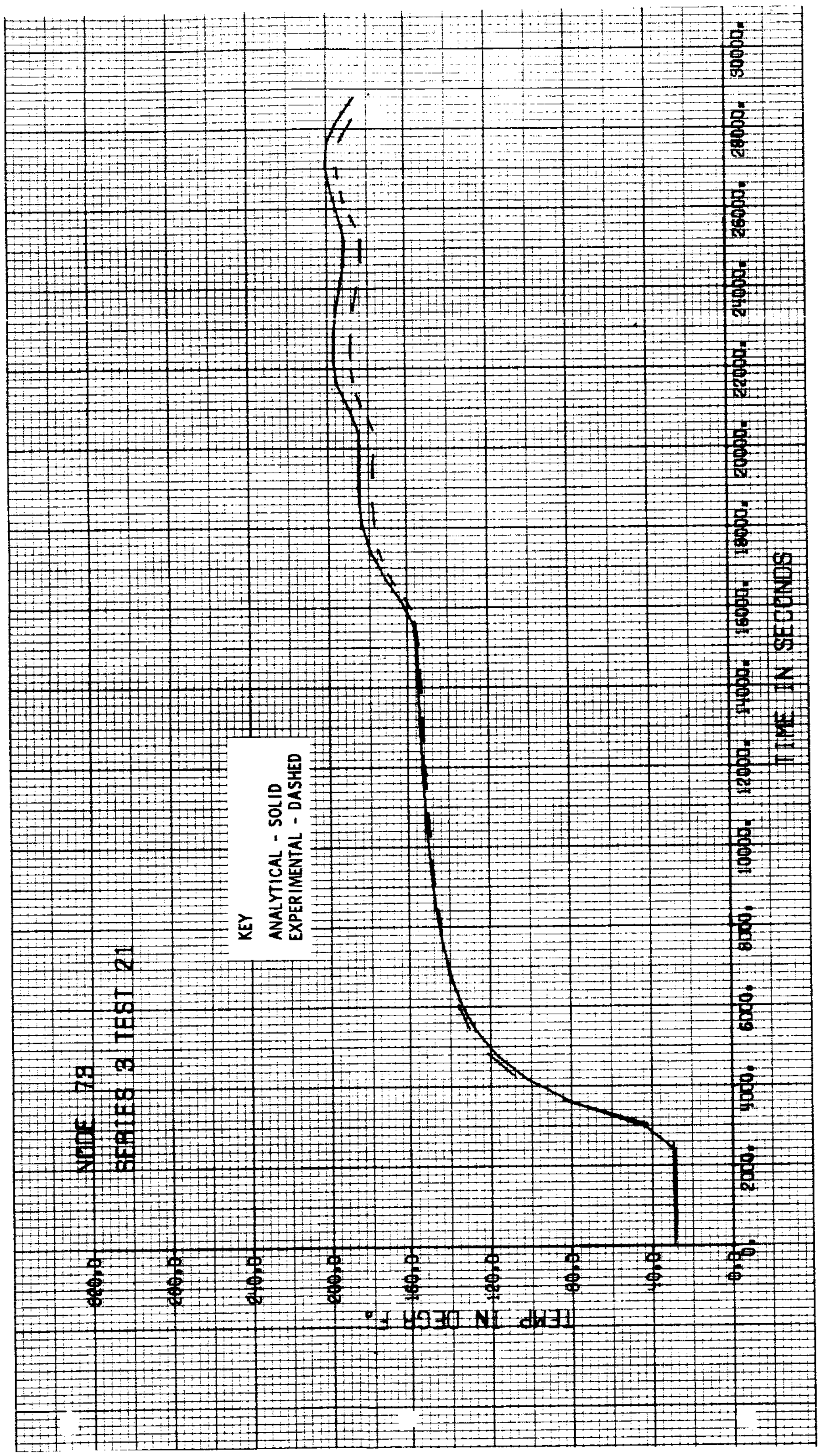

Figure 4-43 Bulkhead Temperature History (Node 73) for Run 3-21

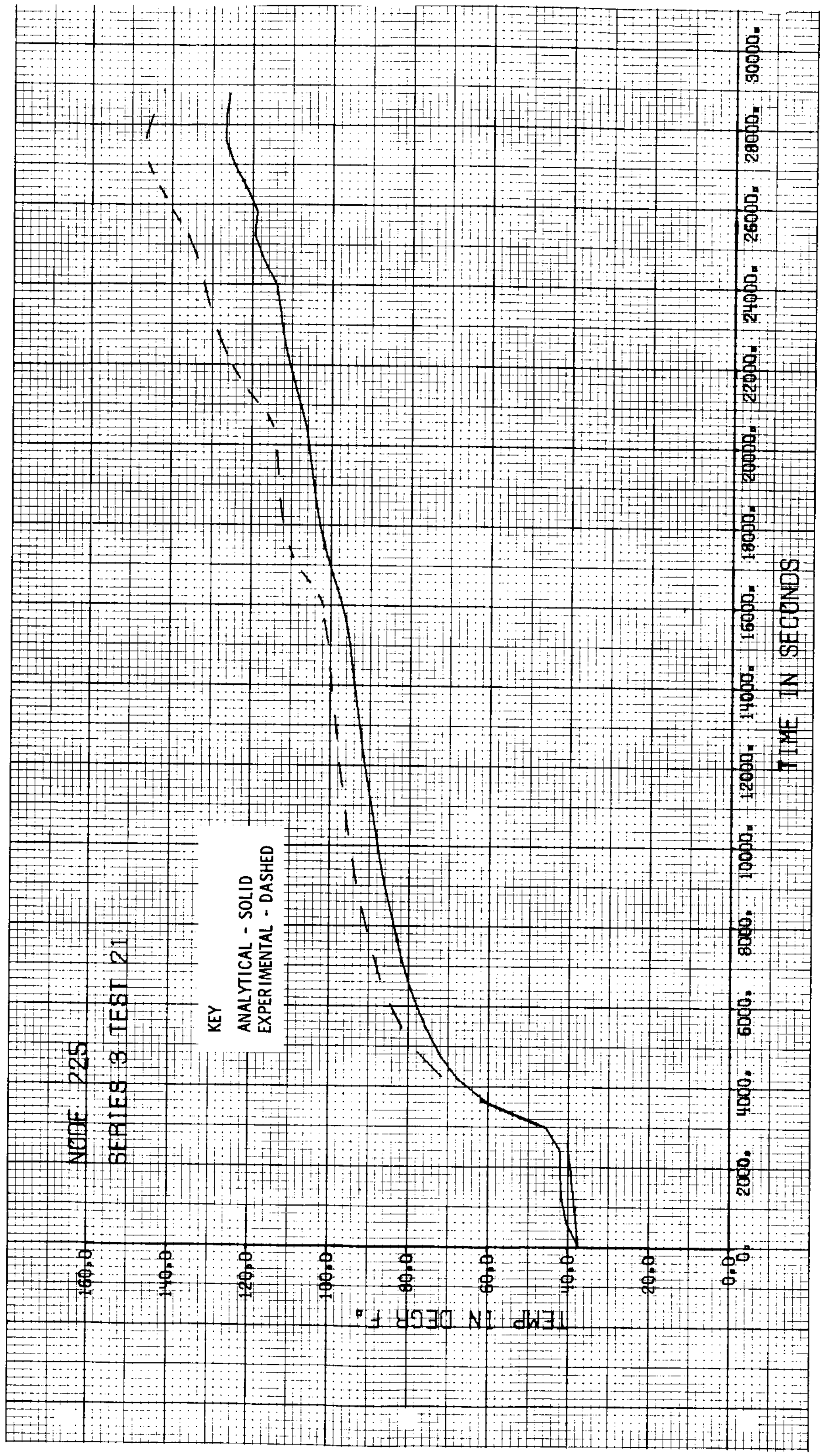

Figure 4-44 Inner Cylinder Temperature History (Node 225) for Run 3-21

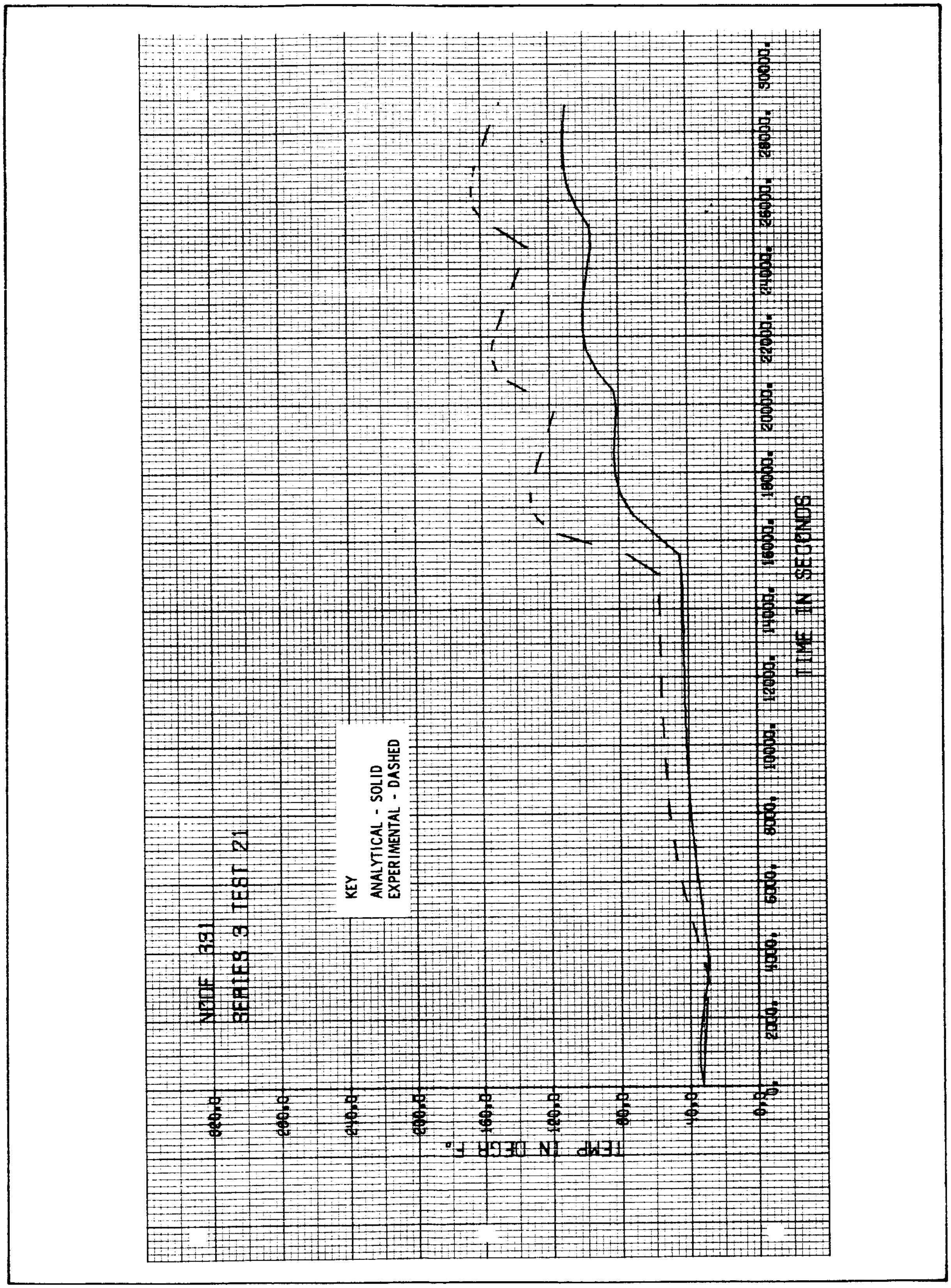

Figure 4-45 Inner Cylinder Temperature History (Node 331) for Run 3-21

LOCKHEED
CALIFORNIA COMPANY

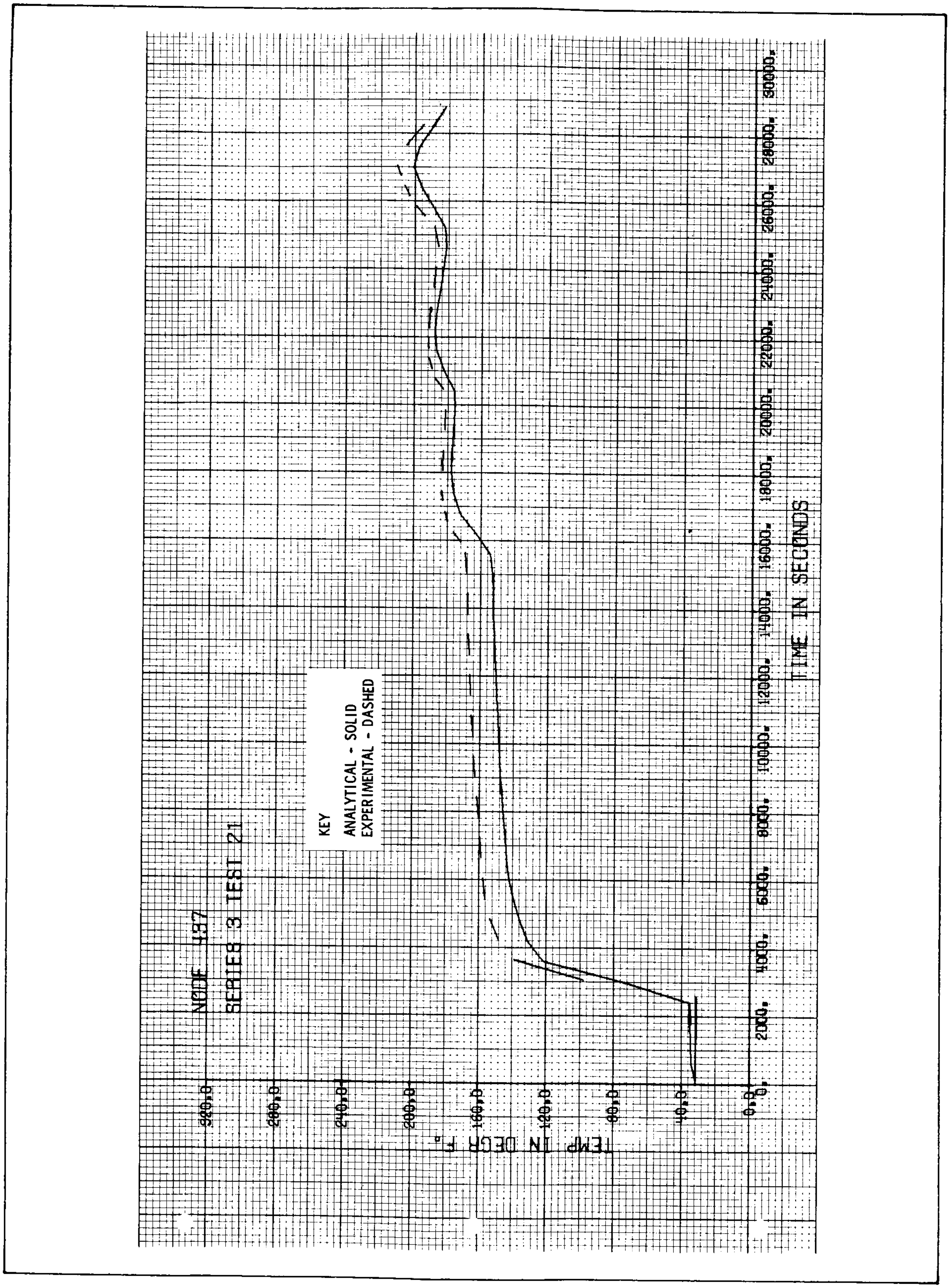

Figure 4-46 Beam Temperature History (Node 437) for Run 3-21

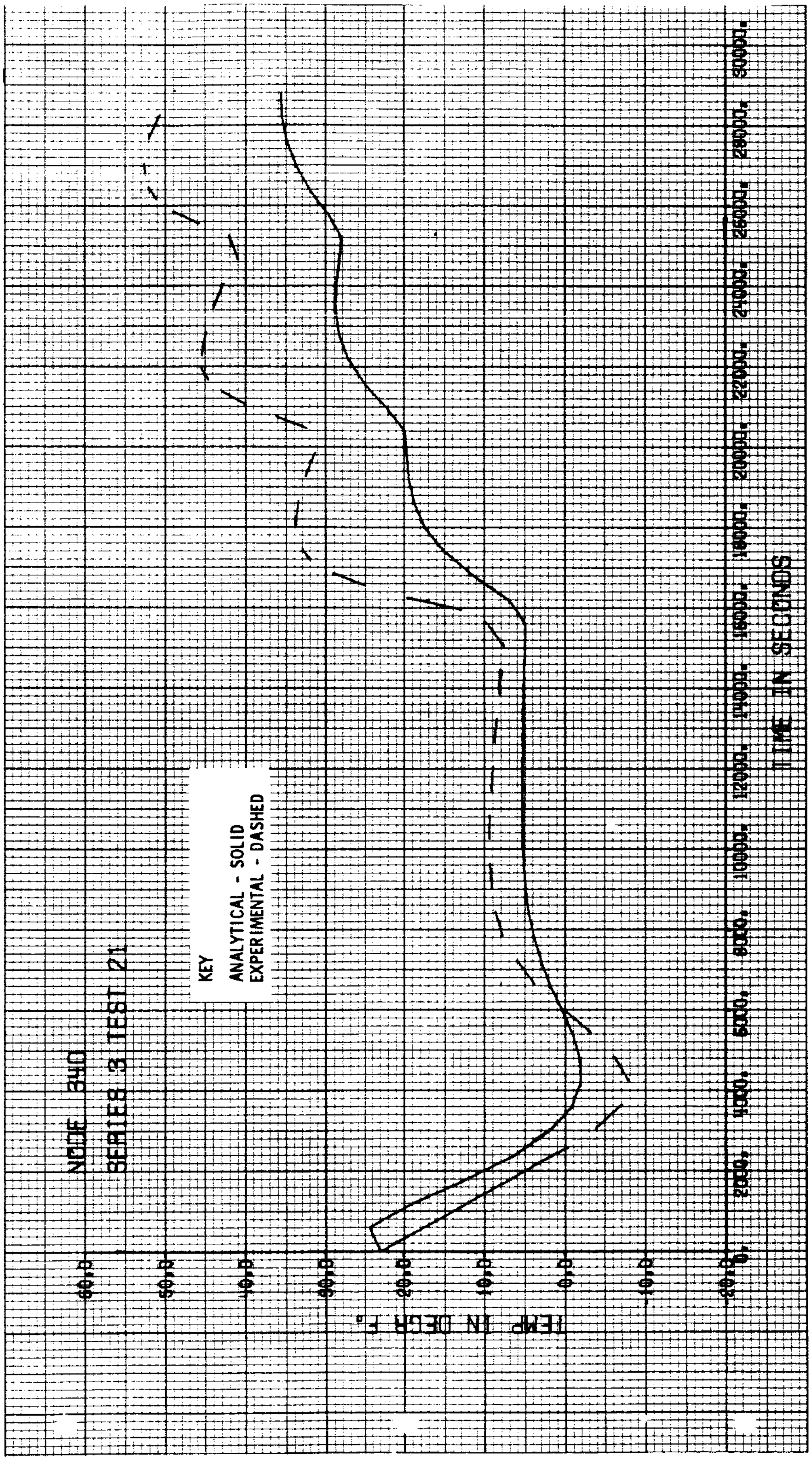

Figure 4-47 Beam Temperature History (Node 340) for Run 3-21

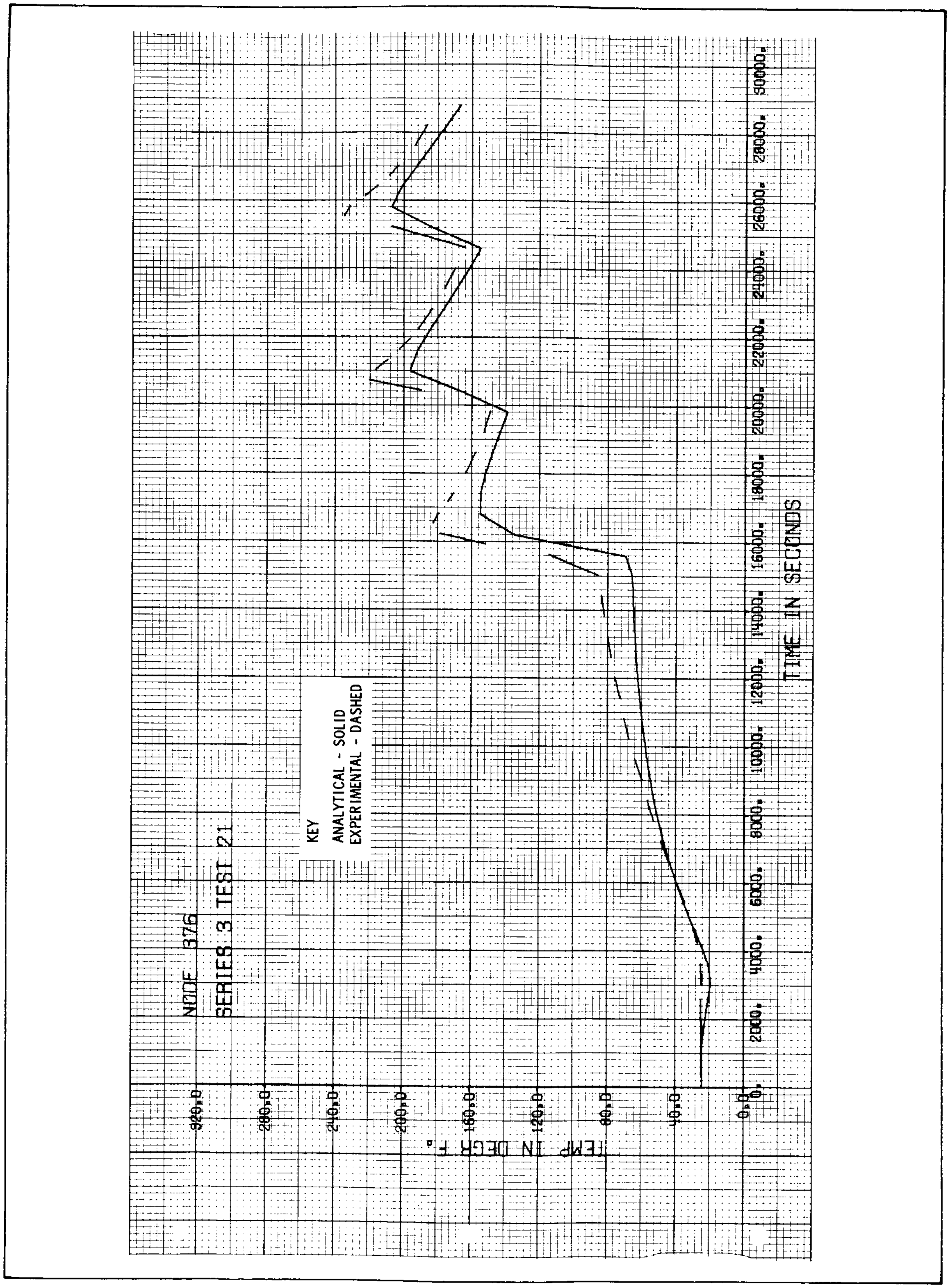

Figure 4-48 Heat Shield Temperature History (Node 376) for Run 3-21

LOCKHEED
CALIFORNIA COMPANY

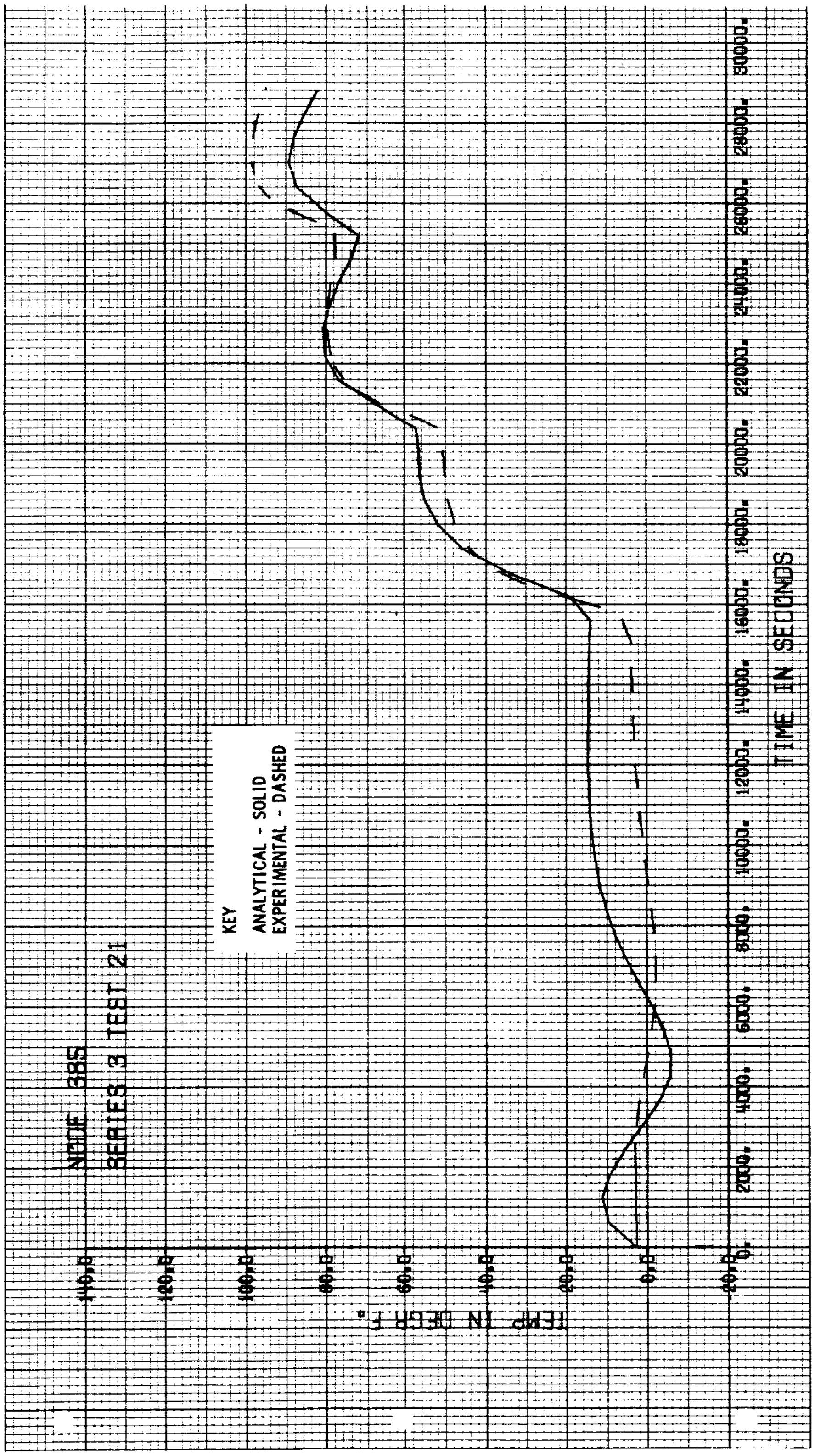

Figure 4-49 Heat Shield Temperature History (Node 385) for Run 3-21

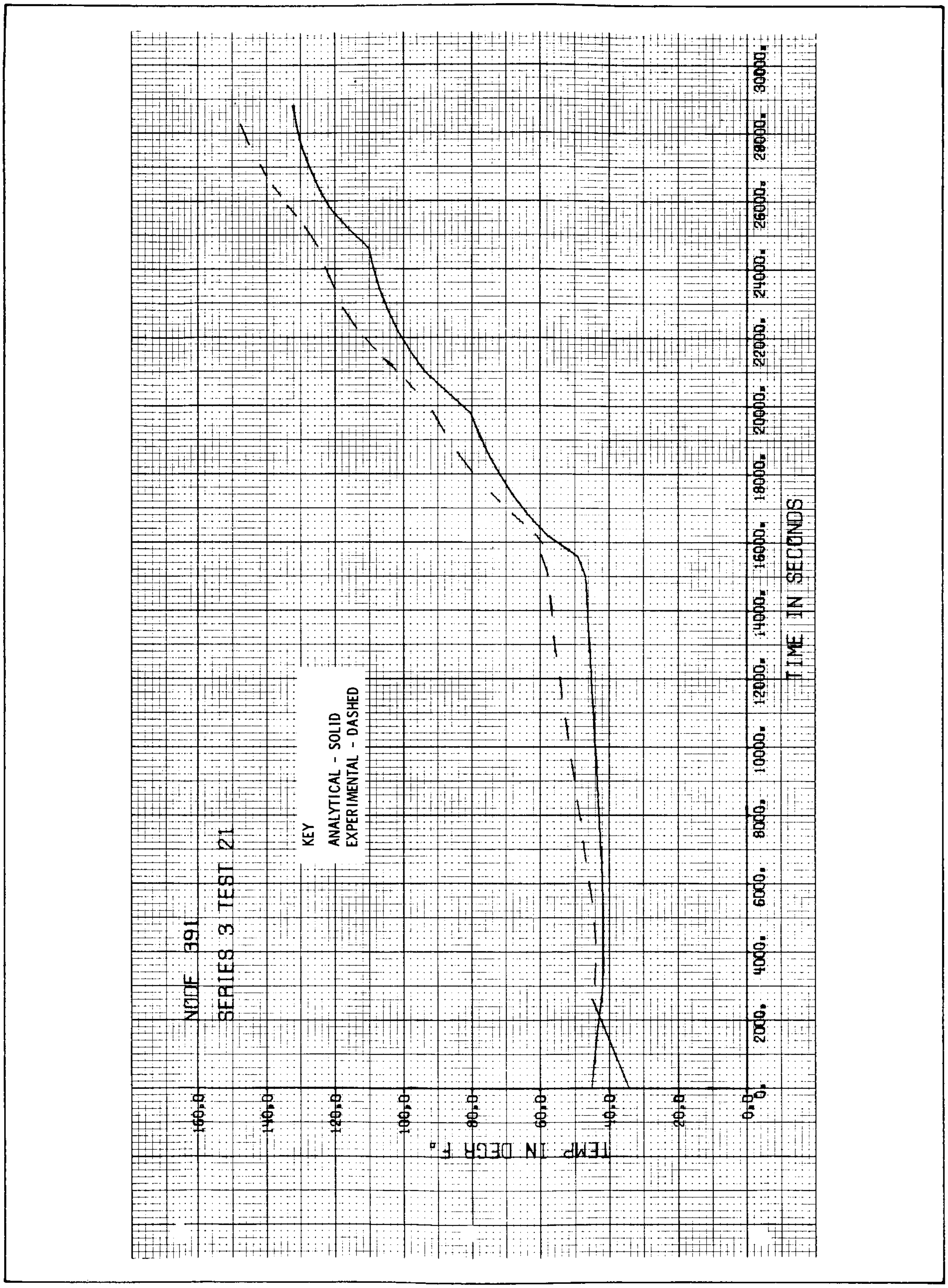

Figure 4-50 Lower Helium Bottle Temperature History (Node 391) for Run 3-21

LOCKHEED
CALIFORNIA COMPANY

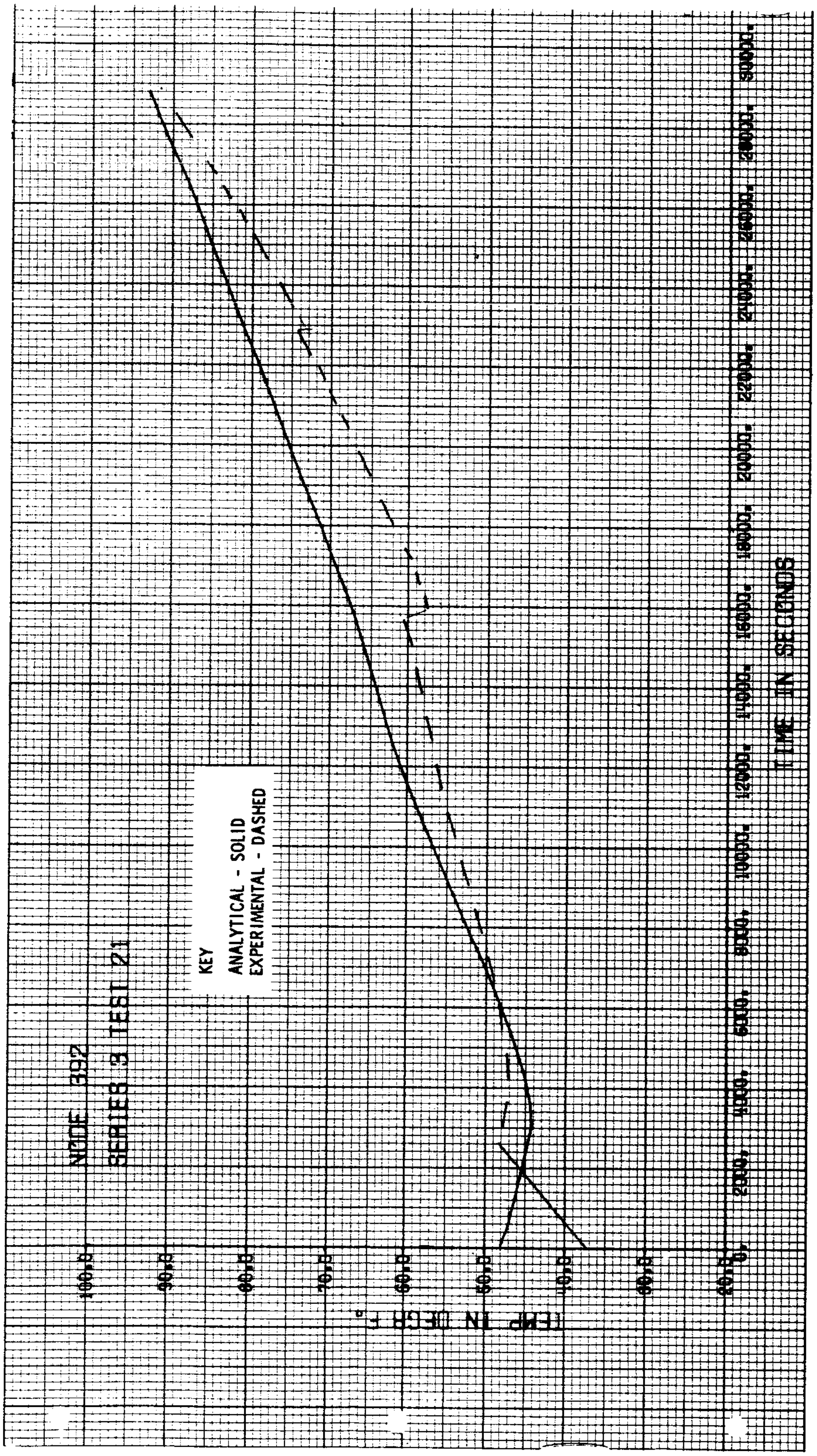

Figure 4-51 Upper Helium Bottle Temperature History (Node 392) for Run 3-21

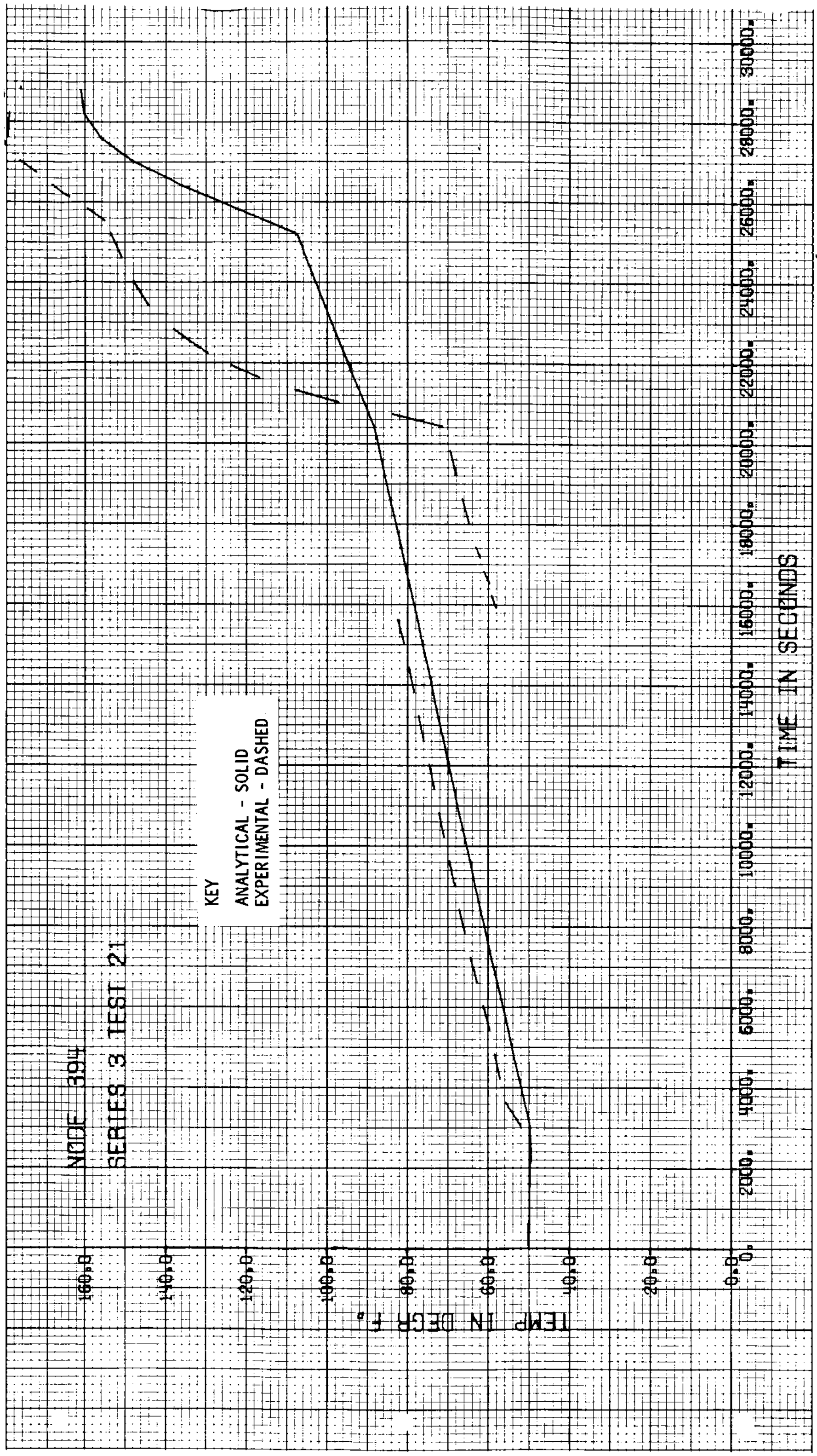

Figure 4-52 Propellant Tank Temperature History (Node 394) for Run 3-21

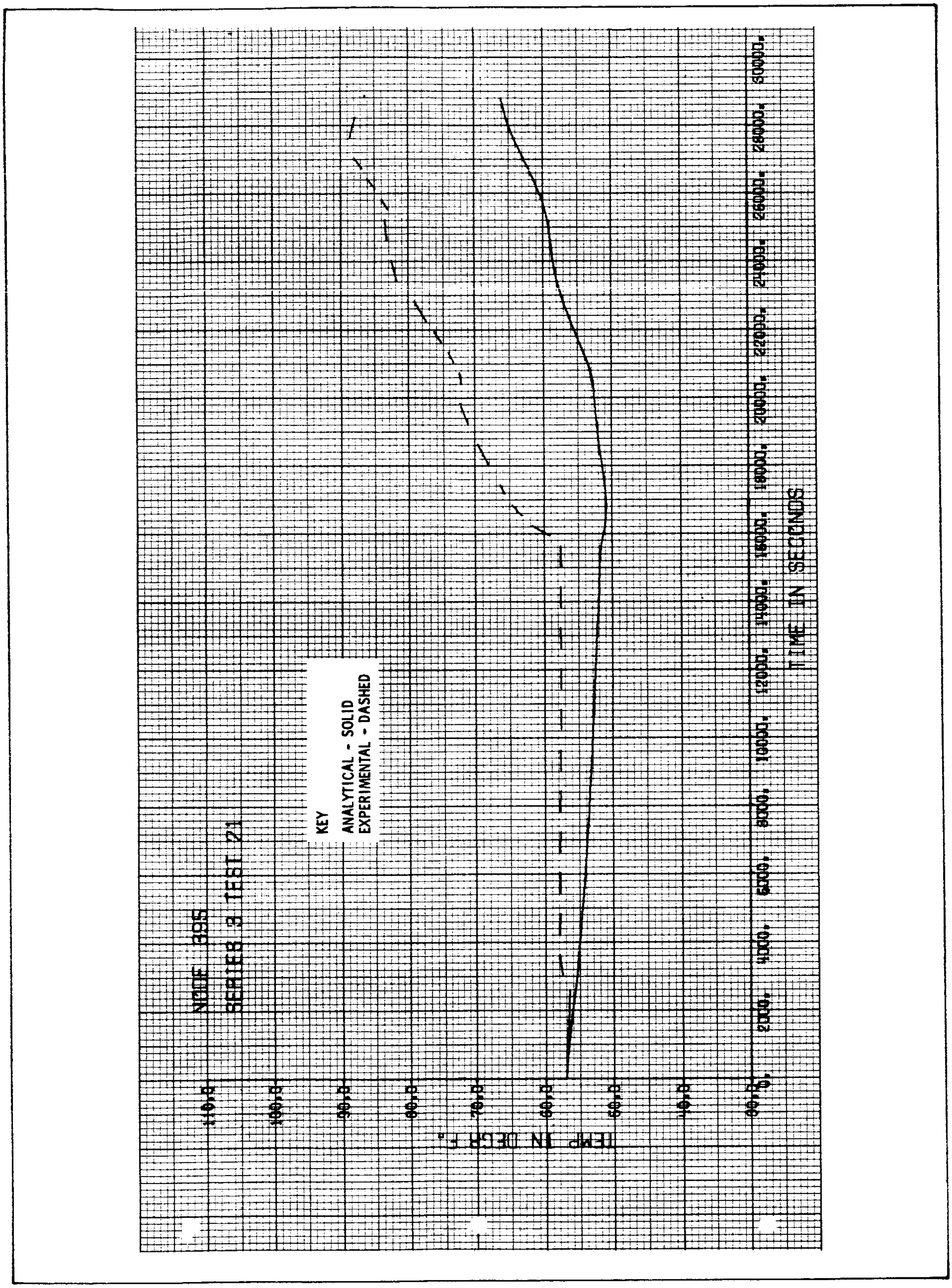

Figure 4-53 Propellant Tank Temperature History (Node 395) for Run 3-21

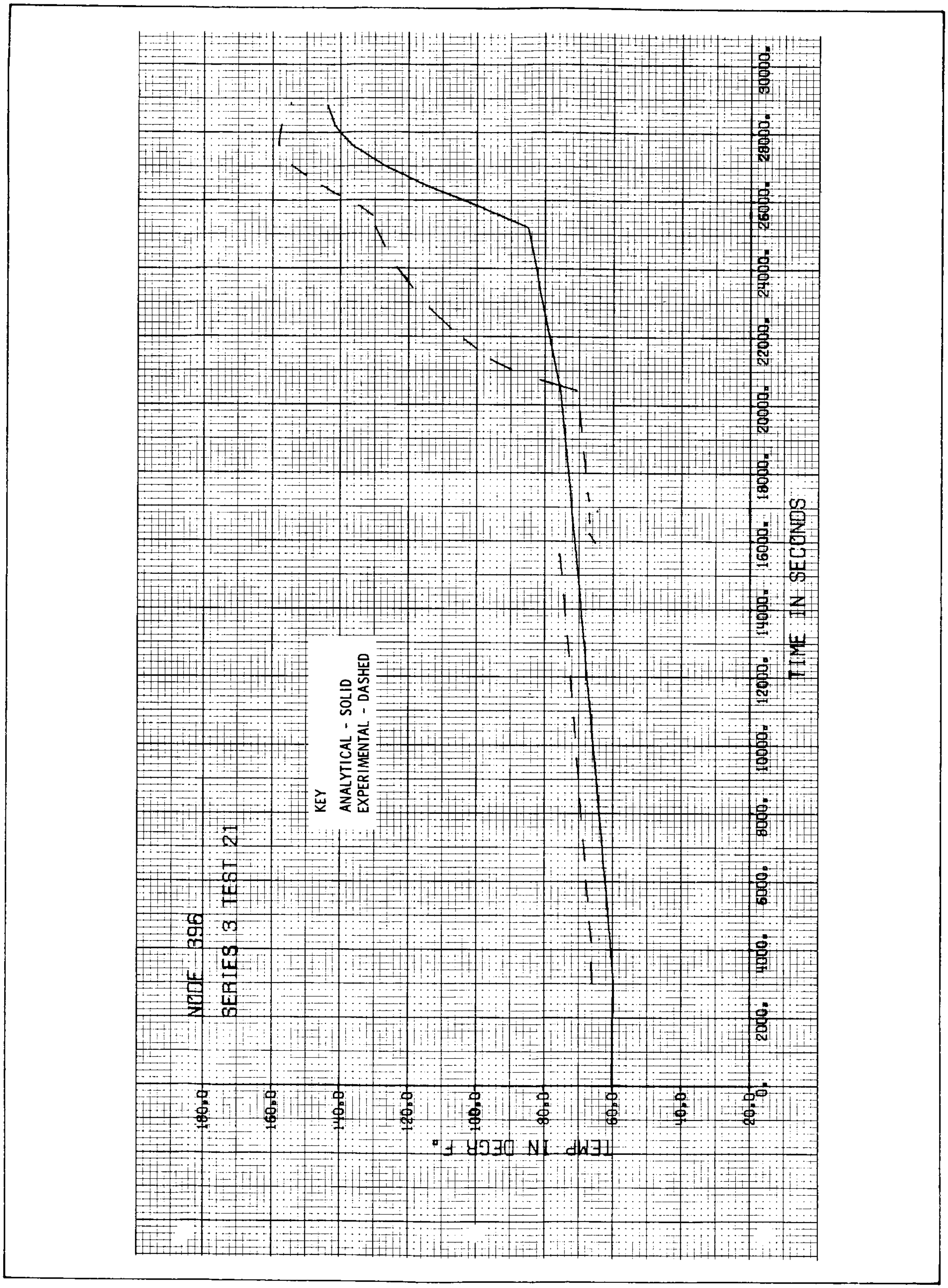

Figure 4-54 Propellant Tank Temperature History (Node 396) for Run 3-21

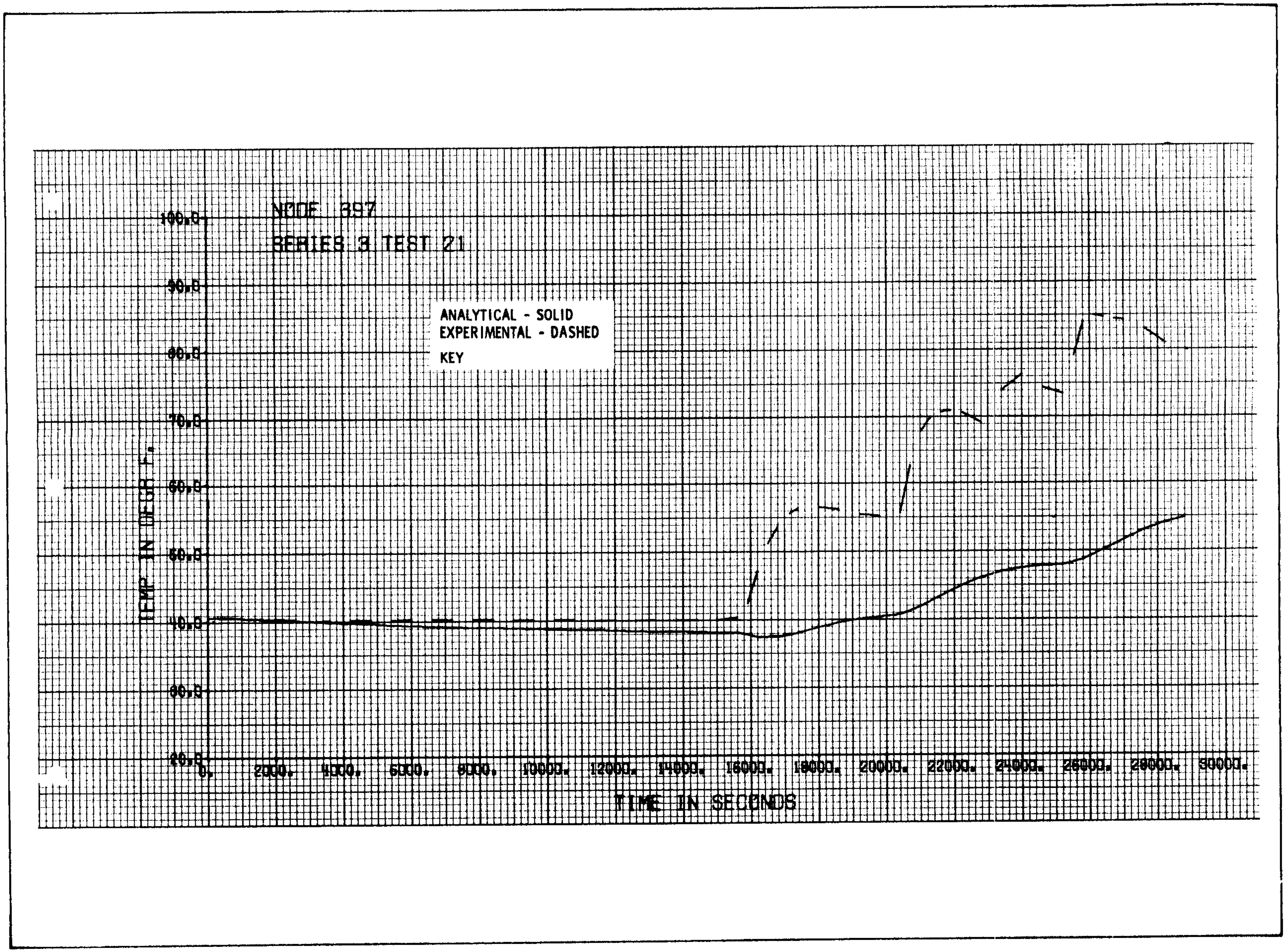

Figure 4-55 Propellant Tank Temperature History (Node 397) for Run 3-21

blanket change in effective emissivity was employed to account for the reflected radiation, but this modification, which was based on the test case of Series 1, was not of sufficient magnitude. It is judged that further study of the internal radiation would greatly improve the analysis.

Although the predicted temperatures for the heat shield nodes presented in Figures 4-48 and 4-49 show reasonably good agreement with measured values, the correlation of the analytical and experimental temperatures of the heat shield are generally poorer than the rest of the model because the thermal network in this region is too coarse for the temperature gradients encountered. Contact resistance, although partially accounted for, also contributed to the difficulty of obtaining good correlation.

Predicted temperatures for the helium bottles are within ±15°F of measured values. At the end of the test, the temperature of the lower helium bottle is 145°F or 55°F warmer than the upper helium bottle. As seen from Figure 4-51, a 3°F experimental temperature drop on the bottle occurs during the first engine firing (15,600 seconds) due to the expansion of gas. This was assumed negligible in the analysis.

In Figures 4-38 to 4-41, temperature histories are shown for the propellant tanks. The temperature history of node 394 (Figure 4-38), representing the sump tank, shows a sharp drop in temperature of 16,000 seconds because of the transfer of fluid from the tank on the cold side of the model. Inspection of the results for all propellant tanks indicates good agreement until the tanks start emptying. A single node at a single temperature cannot adequately represent the partially empty tanks, especially during a simulated engine firing, which produces large temperature gradients.

Run 3-22 --- Figure 4-56 summarizes the deviations of the analytical temperatures from the experimental temperatures for nodes on the panels, bulkheads, inner cylinder, beams, propellant tanks and helium bottles. The nodes are grouped into panel nodes and non-panel nodes. The panels area is separated because that is the region of external heat transfer and is directly affected by the chamber boundary conditions. The deviations, analytical minus experimental temperatures, are grouped into five-degree temperature intervals. These results are presented as frequency charts for two times during the test.

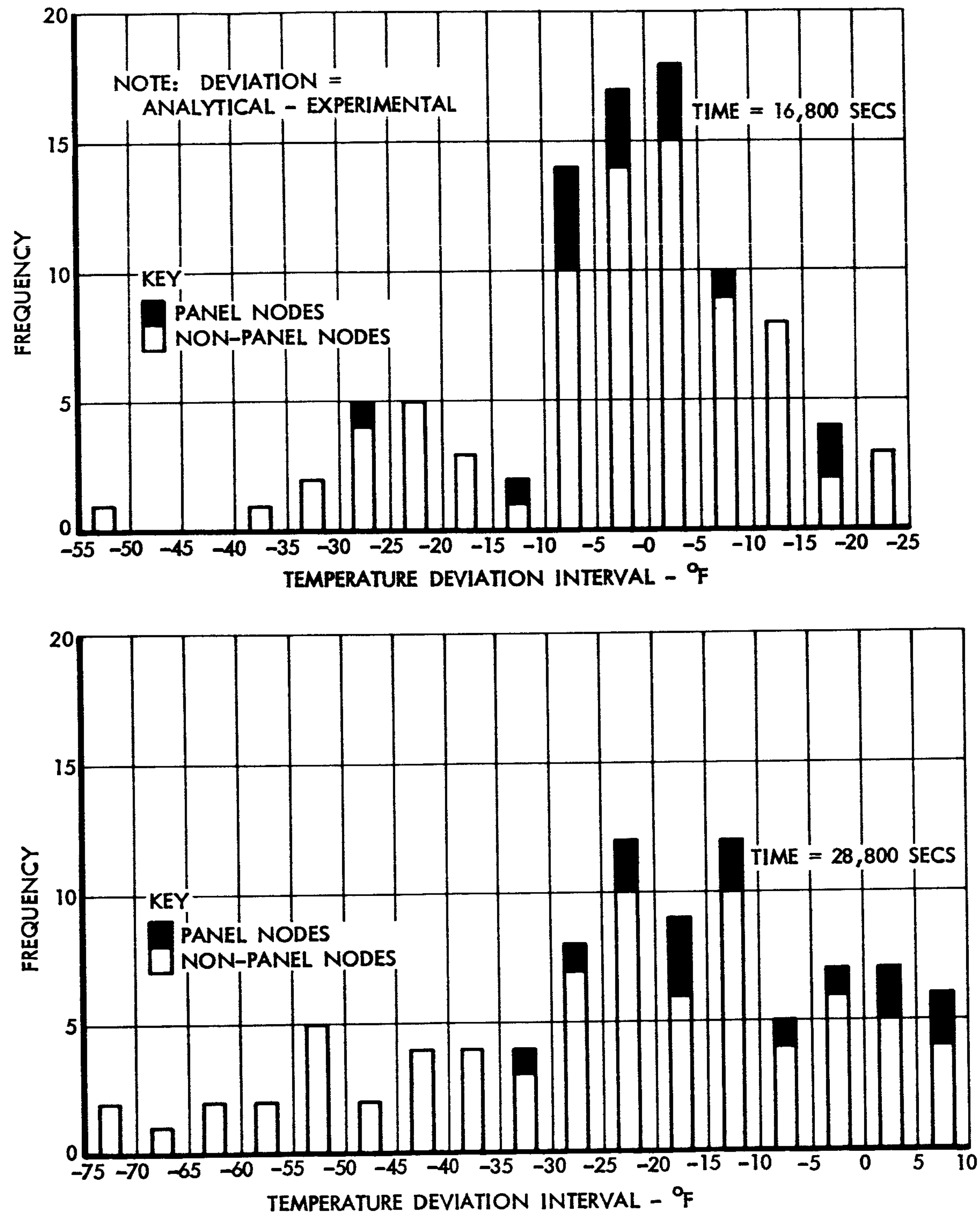

Figure 4-56 Analytical and Experimental Temperature Deviation Distribution for Run 3-22

The first time chosen was 16,800 seconds after test start. This was just before the first simulated engine firing and represents a steady state condition. The second time chosen, 28,800 seconds, was near the temperature peak of the last engine firing. This is representative of a highly transient condition. Plots of analytical temperature as a function of experimental temperature for the times discussed above are shown in Figures 4-57 and 4-58. These plots, similar to the one presented for Run 3-21, show the scatter of the data for the various regions of the model.

Both presentations illustrate the good overall correlation of the steady-state temperatures. At the time 16,800 seconds, about 85 per cent of the analytical temperature fall with ±20°F of the experimental temperatures. The data are distributed nearly uniformly about the zero error line as shown in Figure 4-57.

For the transient condition, the scatter of the data increases and there is a definite trend toward low analytical temperatures. About 60% of the data at the time 28,800 seconds falls with the 0 to -30°F error band. Figure 4-58 shows that the average deviation at this time was approximately -20°F. This is indicated by the downward shift of the data shown on this figure. This downward shift in temperatures is due to the underprediction of radiative heat transfer from the thrust chamber. This underprediction is mainly attributed to simplified methods used to account for reflections. This problem is less pronounced during the steady state portion of the run, as indicated by the better overall correlation.

The analytical and experimental temperatures summarized in Table 4-4 are taken at two time points from the temperature histories presented in Figure 4-59 to 4-74. Except for bulkhead node 109, the predicted thermal response of the outer panels and the bulkheads show reasonably close agreement with the measured temperature response as shown in Figures 4-59 to 4-65. As discussed in Series 1 and 2, nodes at the intersection of the outer panel and bulkhead, typically node 109 (Figure 4-62), show a temperature discrepancy of 40°F because of the single node network in the region of large temperature gradients.

Temperature histories of representative inner cylinder and beam nodes are within 15°F of experimental except for the period of a simulated engine

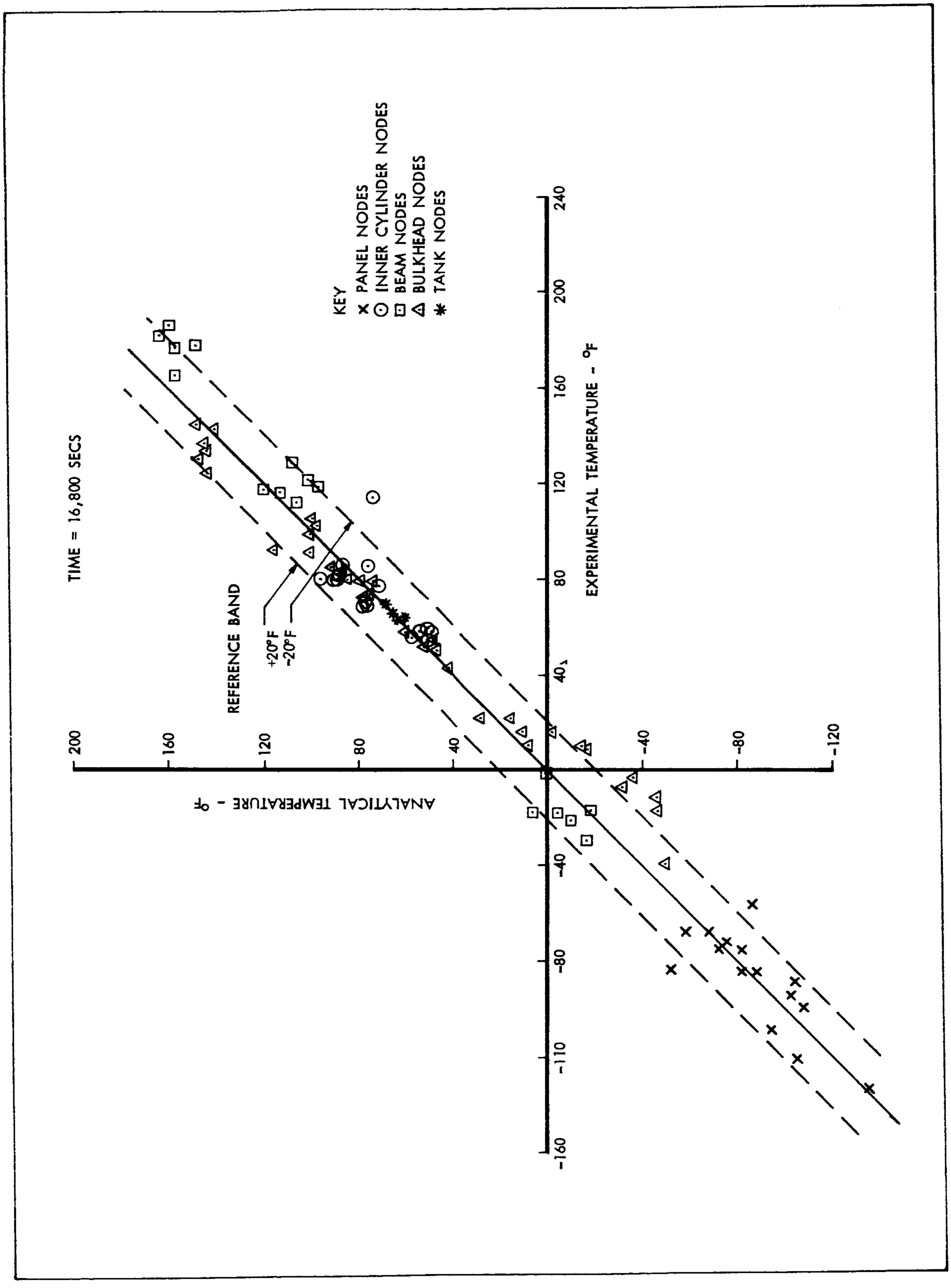

Figure 4-57 Correlation of Analytical and Experimental Data for Run 3-22

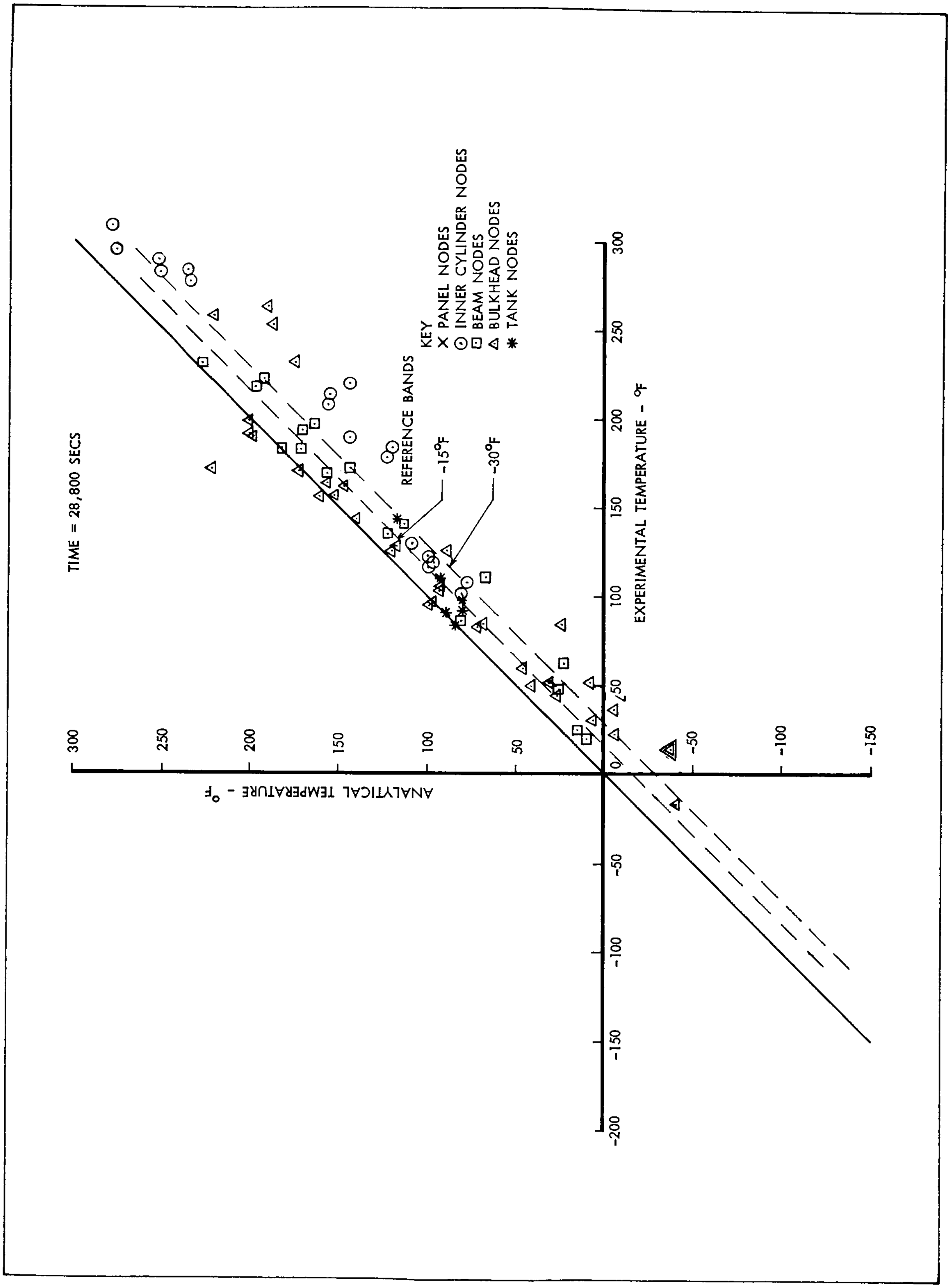

Figure 4-58 Correlation of Analytical and Experimental Data for Run 3-22

TABLE 4-4 GUIDE TO SELECTED PLOTS FOR RUN 3-22

Node Location and Number	Ref. Figure	Temp. at 17,000 secs.		Temp. at 29,000 secs.	
		Analytical	Experimental	Analytical	Experimental
Outer Panel					
215 - Cold Side, Sector V	4-59	-72	-73	-67	-67
311 - Cold Side, Sector IV	4-60	-136	-134	-124	-112
Bulkheads					
23 - Upper, Hot Side, Sector I	4-61	133	129	174	172
109 - Upper, Cold Side, Between Sectors III & IV	4-62	-46	-11	-37	16
125 - Upper, Hot Side, Between Sectors I & II	4-63	101	99	121	127
63 - Lower, Cold Side, Between Sectors IV & V	4-64	42	43	89	126
73 - Lower, Hot Side, Sector I	4-65	147	130	198	190
Inner Cylinder					
225 - Hot Side, Between Sectors I & II	4-66	86	85	110	130
325 - Hot Side, Between Sectors I & II	4-67	90	79	156	208
331 - Cold Side, Between Sectors IV & V	4-68	48	57	120	183
Radial Beam					
340 - Beam 4, Cold Side	4-69	-19	-17	23	63
437 - Beam 1, Hot Side	4-70	158	166	226	230
Heat Shield					
376 - Hot Side	4-71	59	73	210	229
382 - Hot Side	4-72	62	80	180	168
Helium Bottles					
391 - Lower Bottle	4-73	59	60	117	144
392 - Upper Bottle	4-74	63	64	85	84
Propellant Tanks					
394 - Oxidizer, Sector II	4-75	66	66	82	98
395 - Fuel, Sector III	4-76	68	69	89	92
396 - Fuel, Sector VI	4-77	70	70	81	92
397 - Oxidizer, Sector V	4-78	64	63	93	110

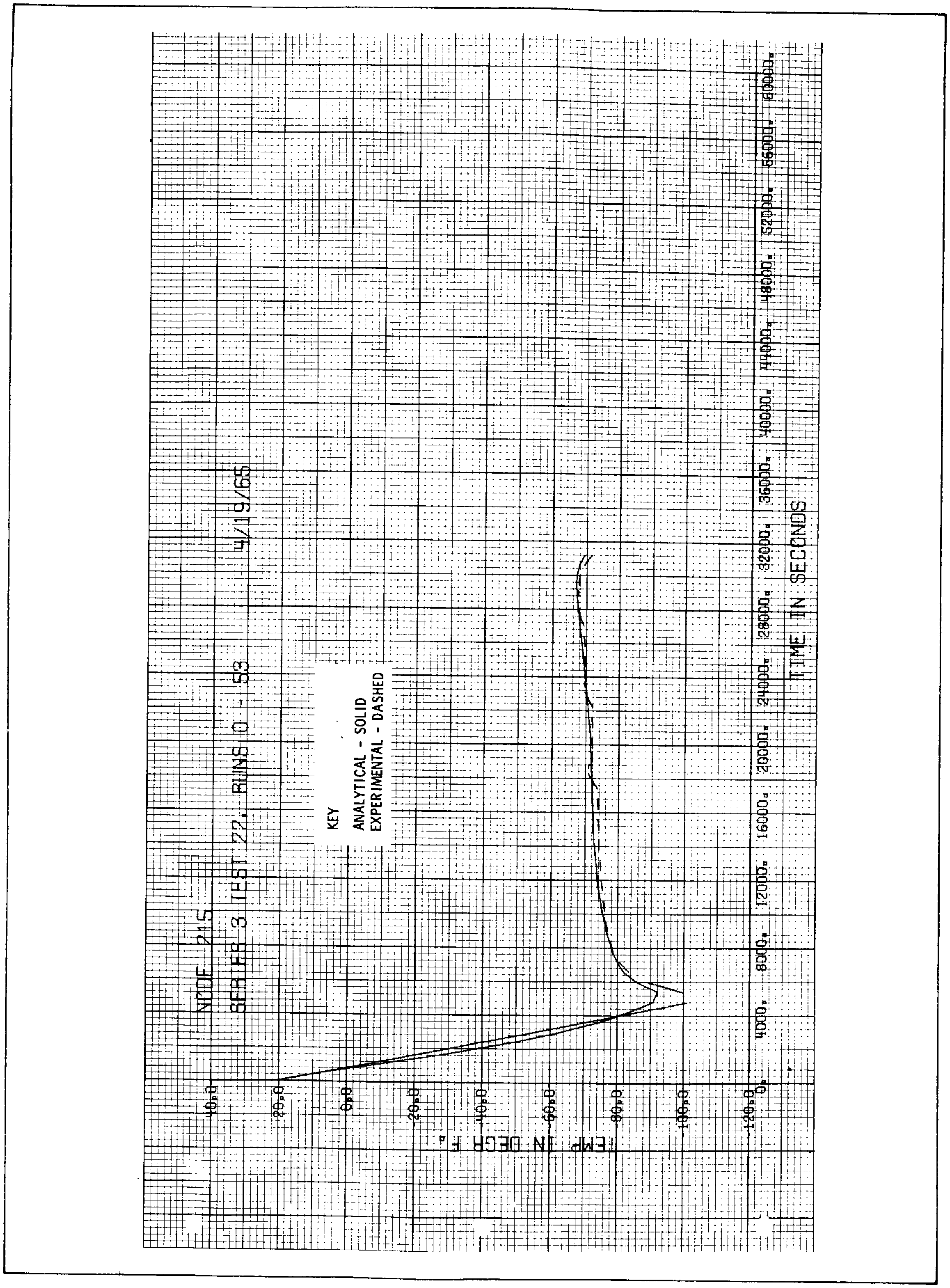

Figure 4-59 Panel Temperature History (Node 215) for Run 3-22

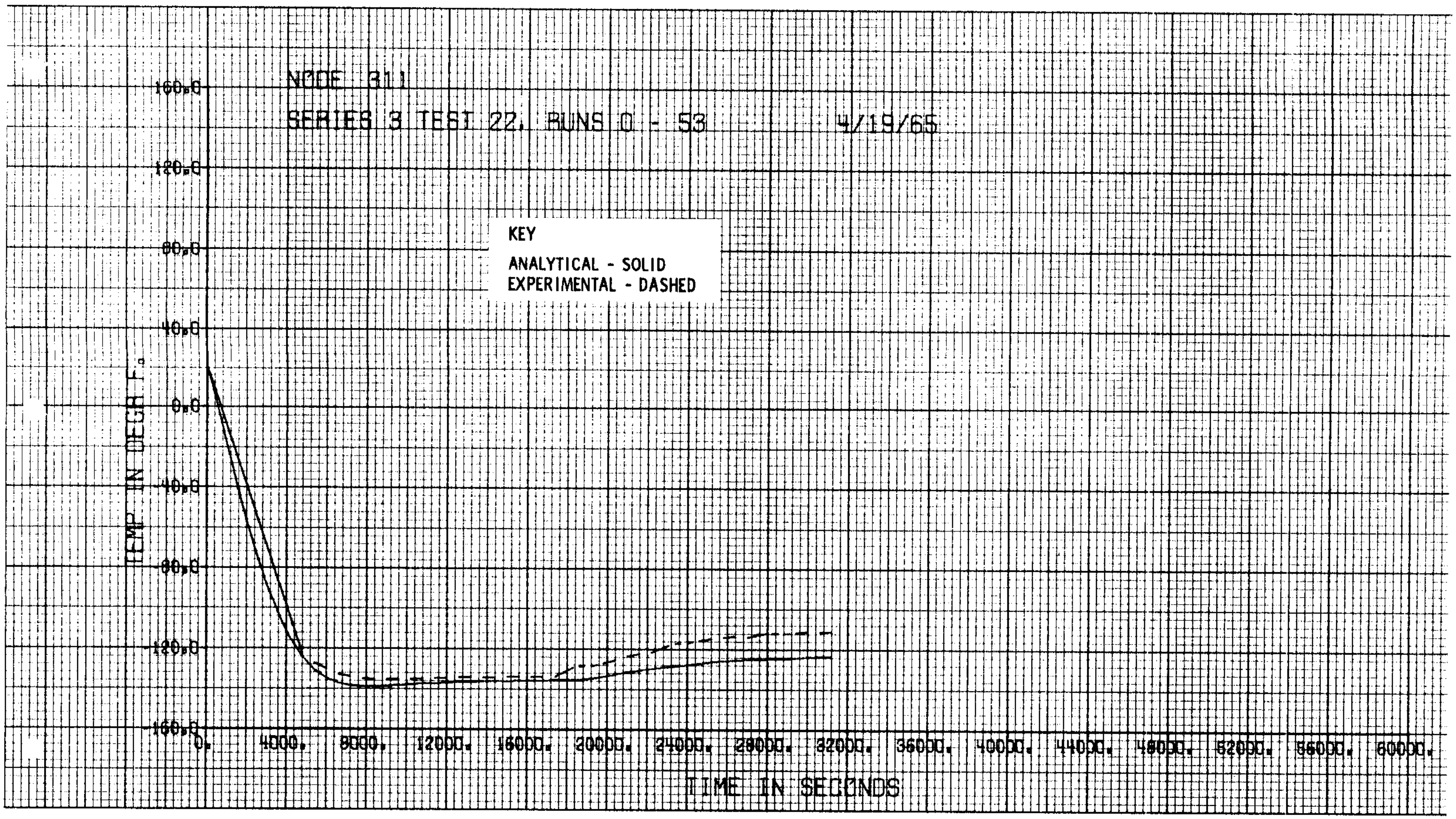

Figure 4-60 Panel Temperature History (Node 311) for Run 3-22

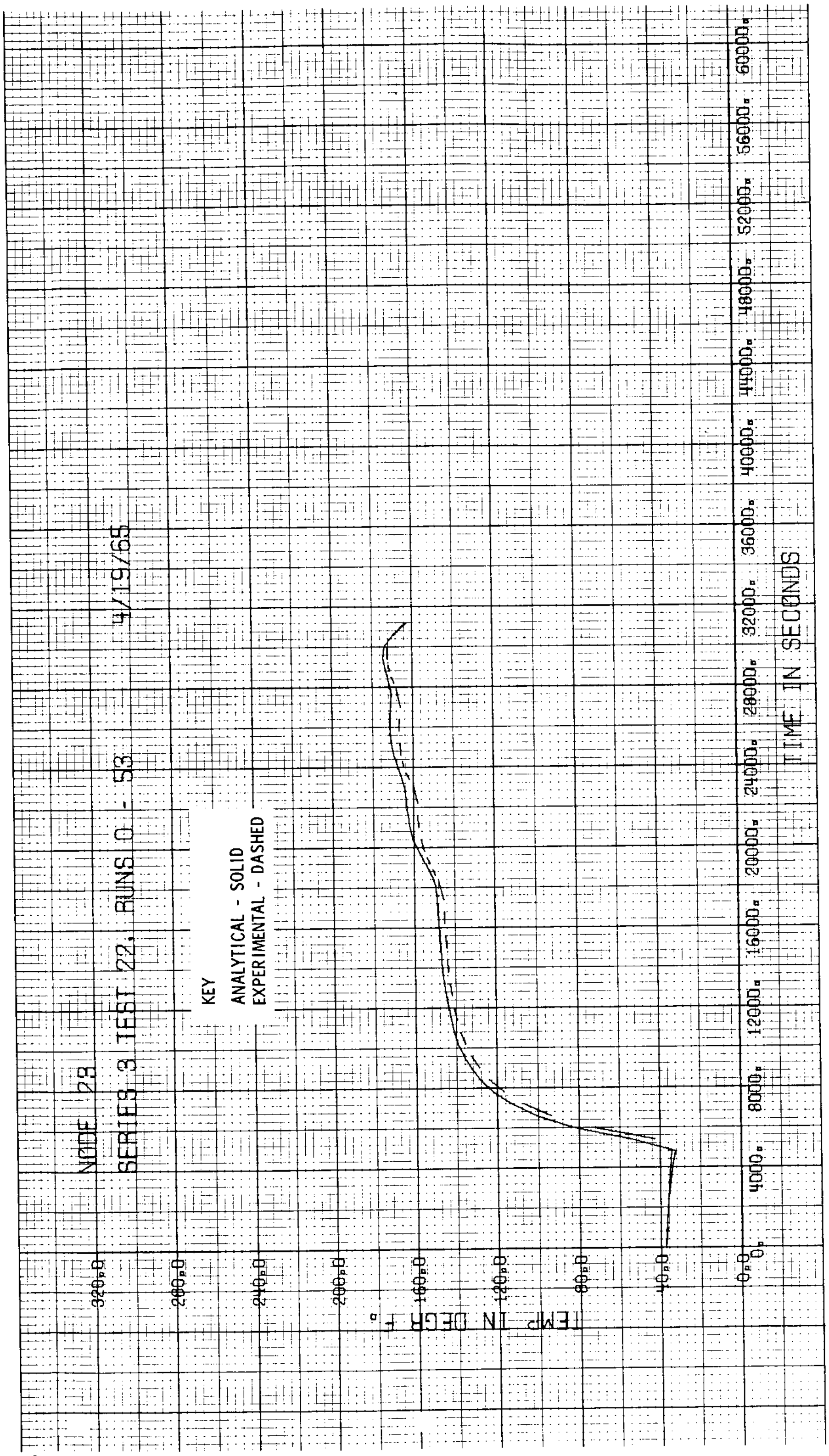

Figure 4-61 Bulkhead Temperature History (Node 23) for Run 3-22

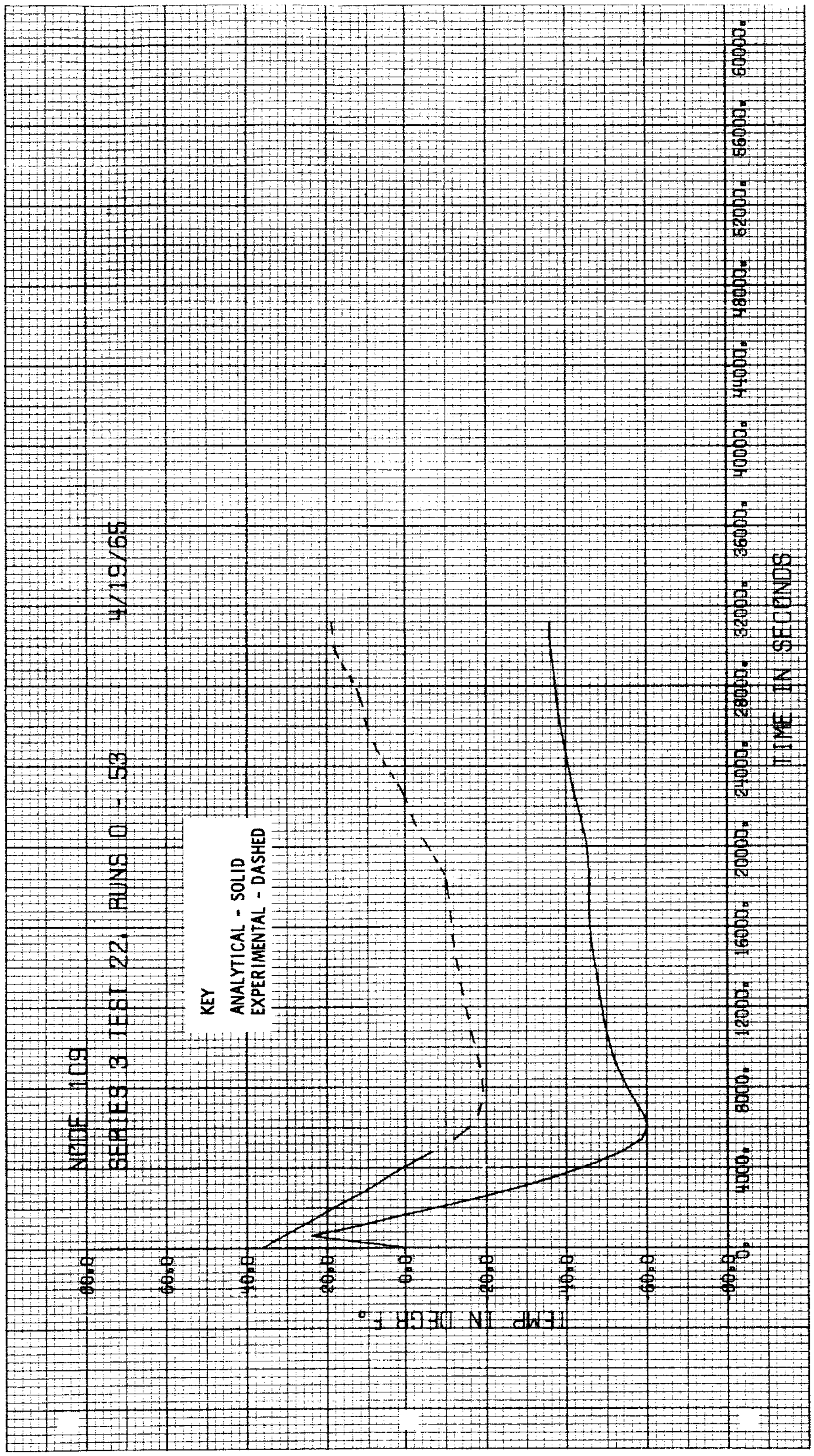

Figure 4-62 Bulkhead Temperature History (Node 109) for Run 3-22

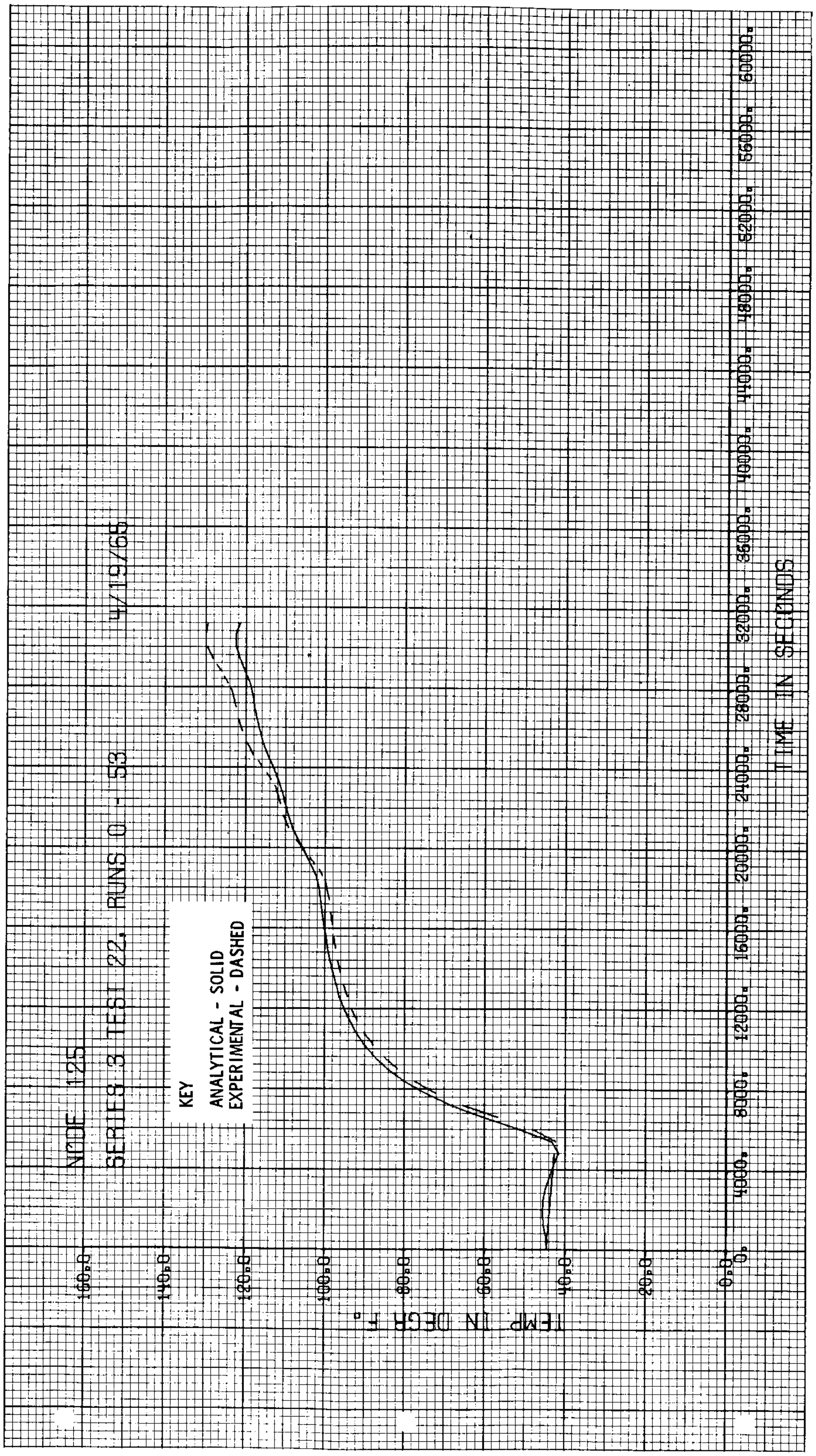

Figure 4-63 Bulkhead Temperature History (Node 125) for Run 3-22

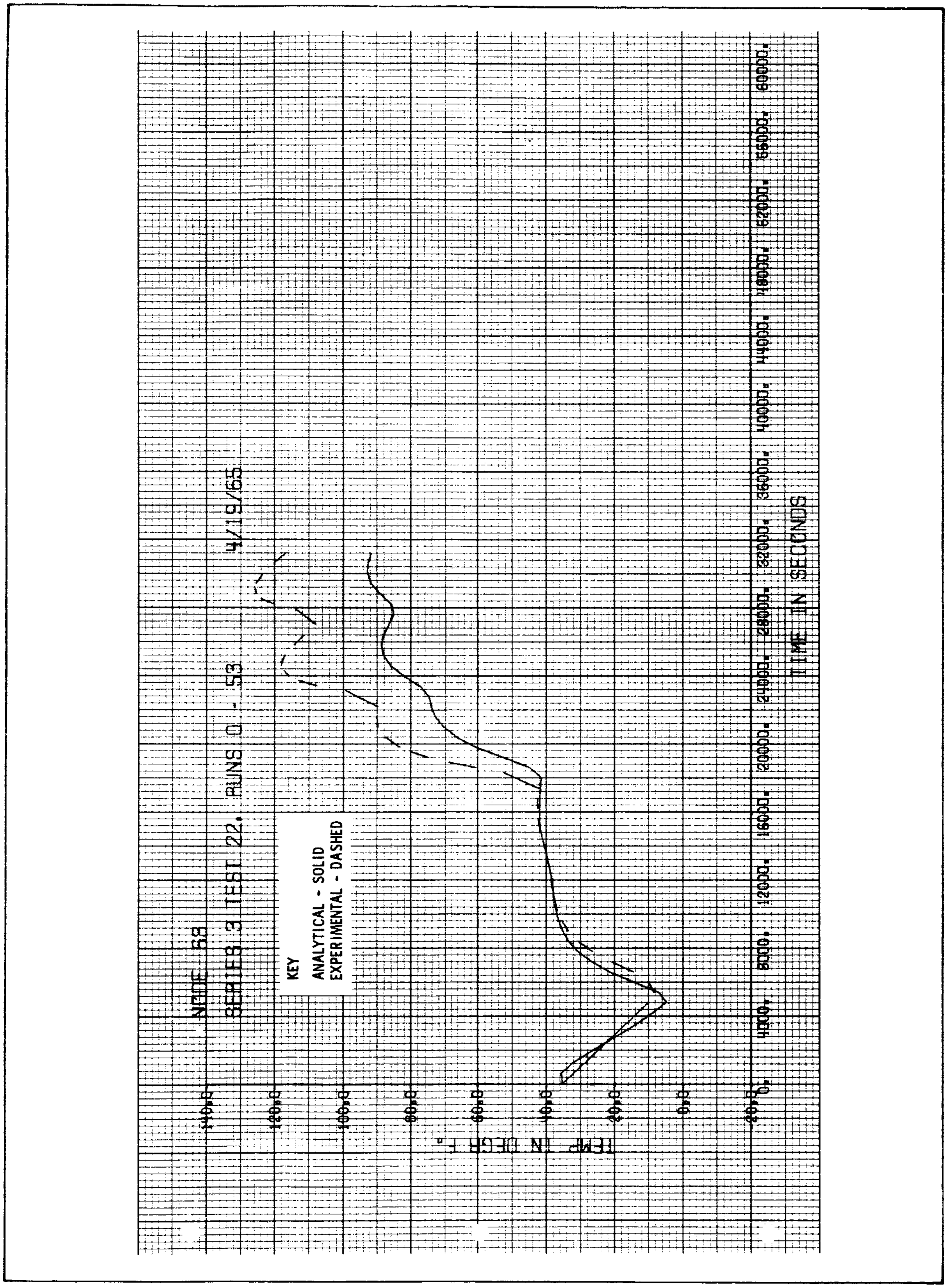

Figure 6-64 Bulkhead Temperature History (Node 63) for Run 3-22

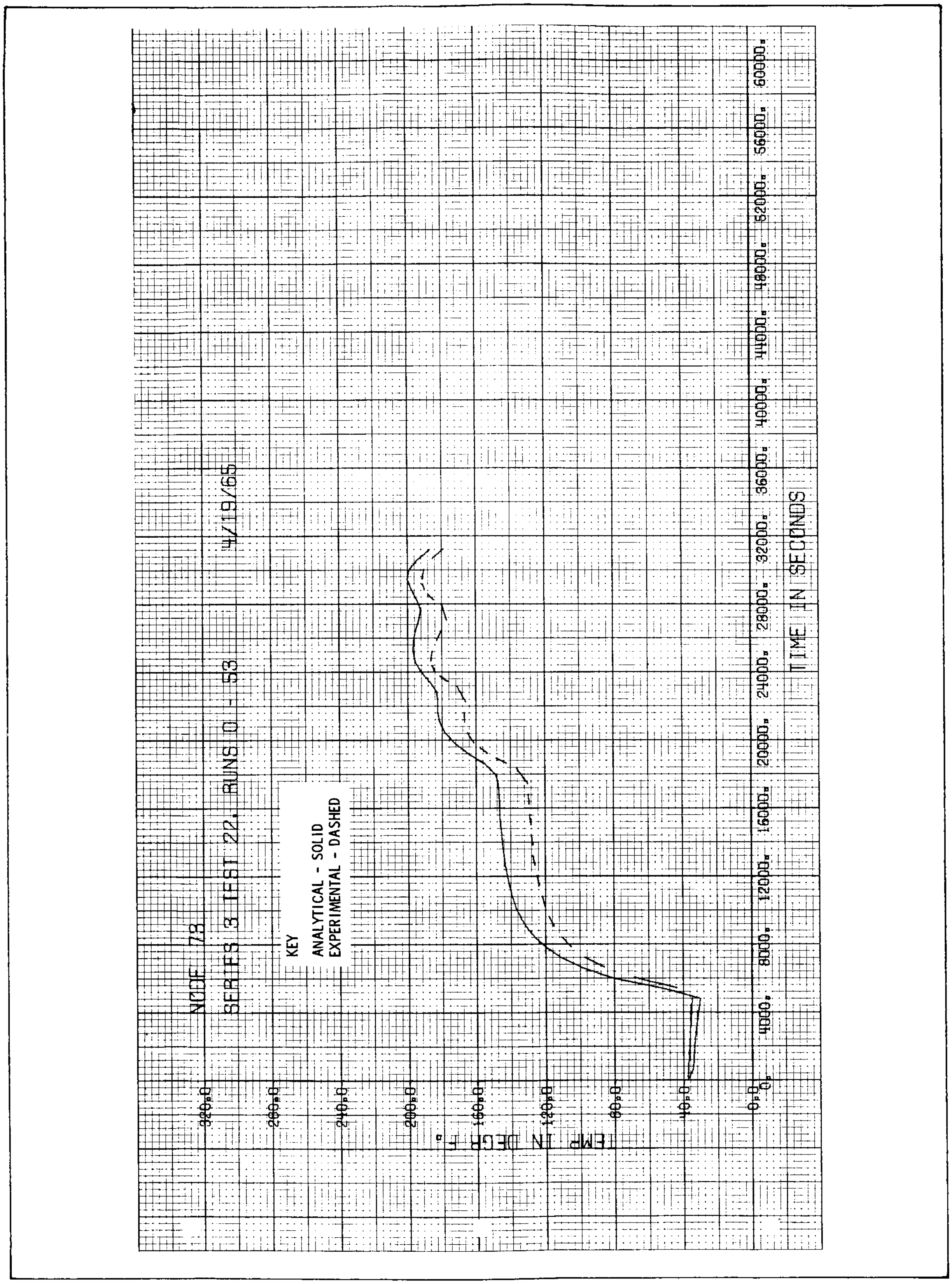

Figure 4-65 Bulkhead Temperature History (Node 73) for Run 3-22

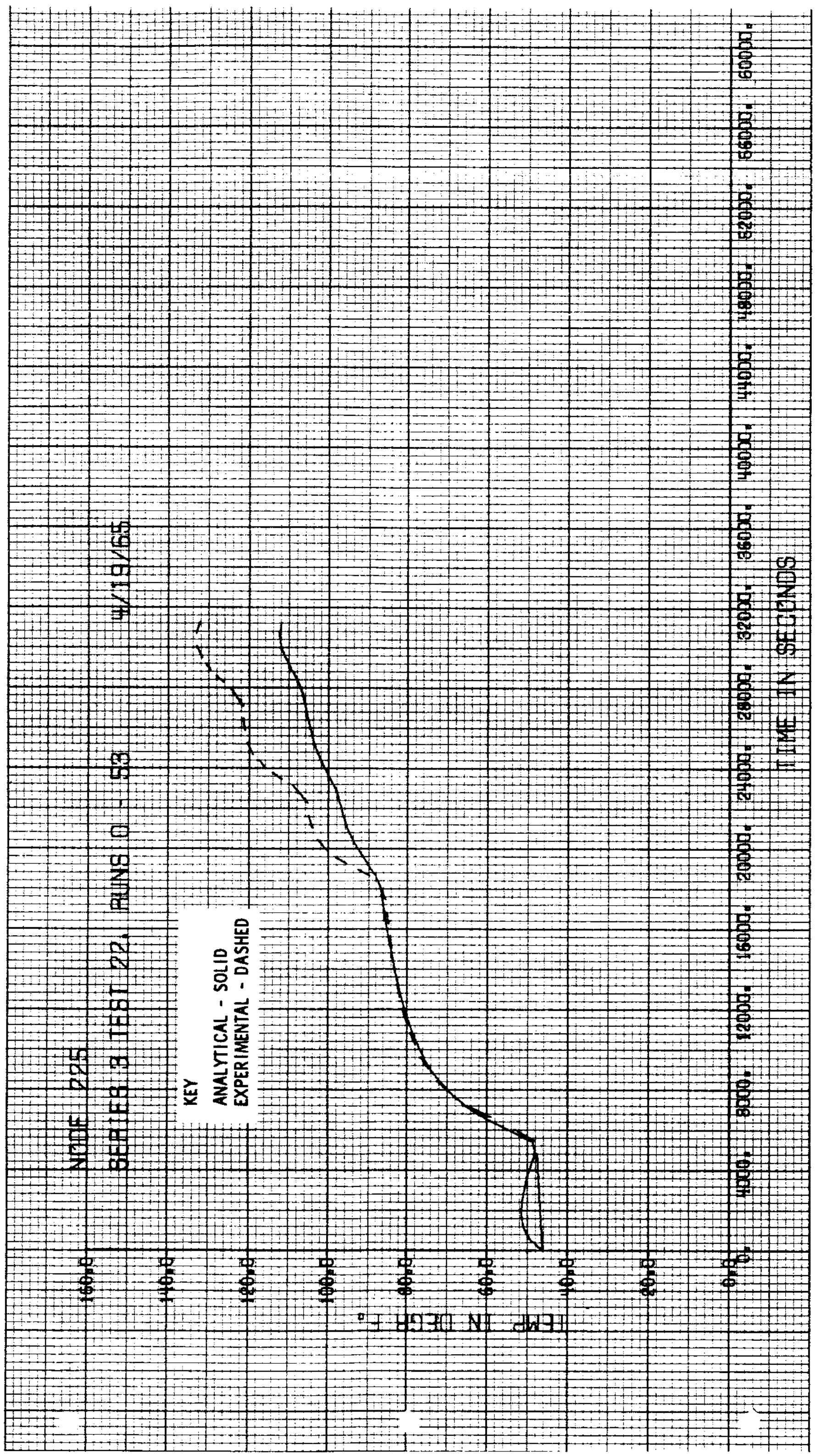

Figure 4-66 Inner Cylinder Temperature History (Node 225) for Run 3-22

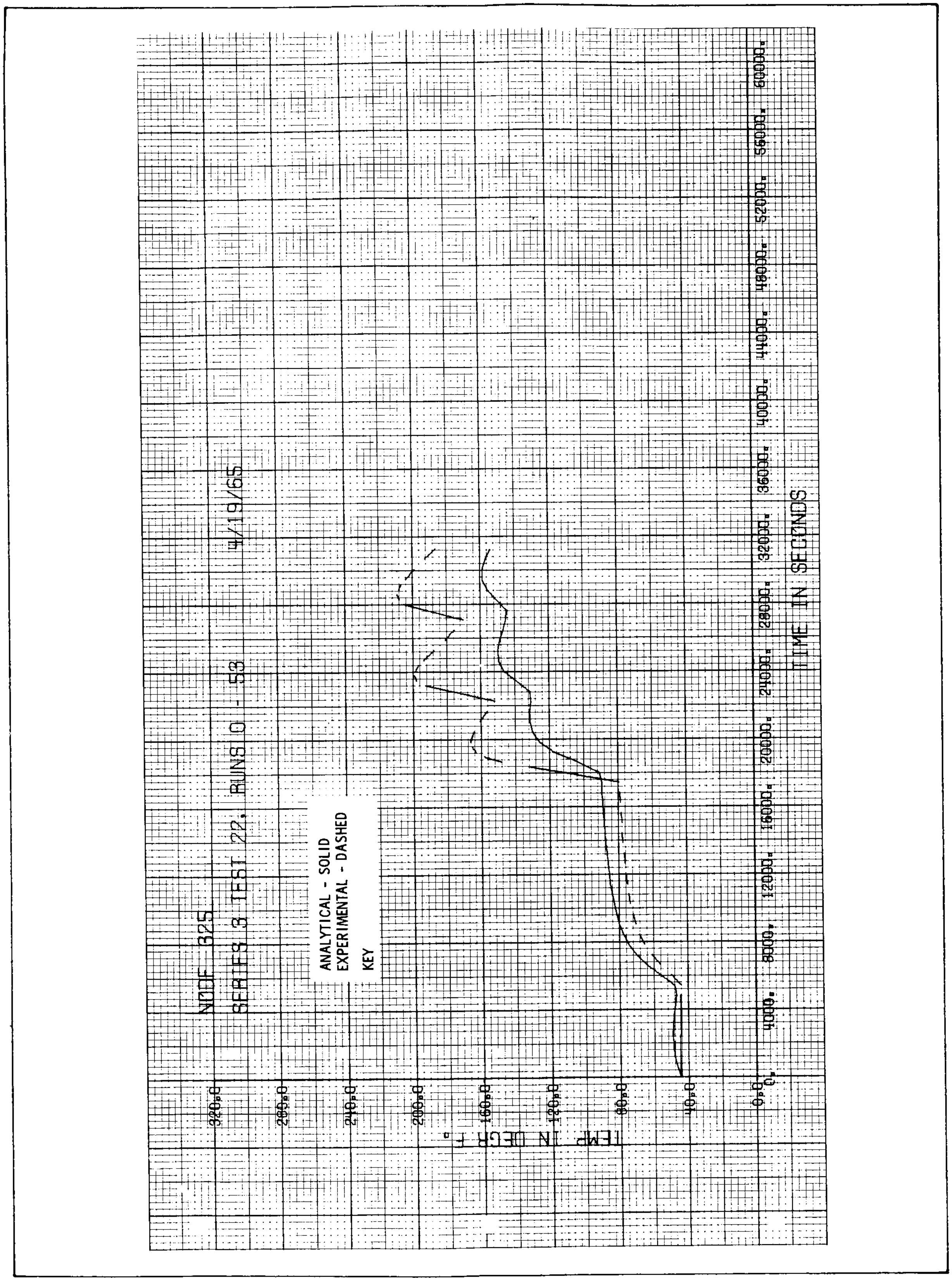

Figure 4-67 Inner Cylinder Temperature History (Node 325) for Run 3-22

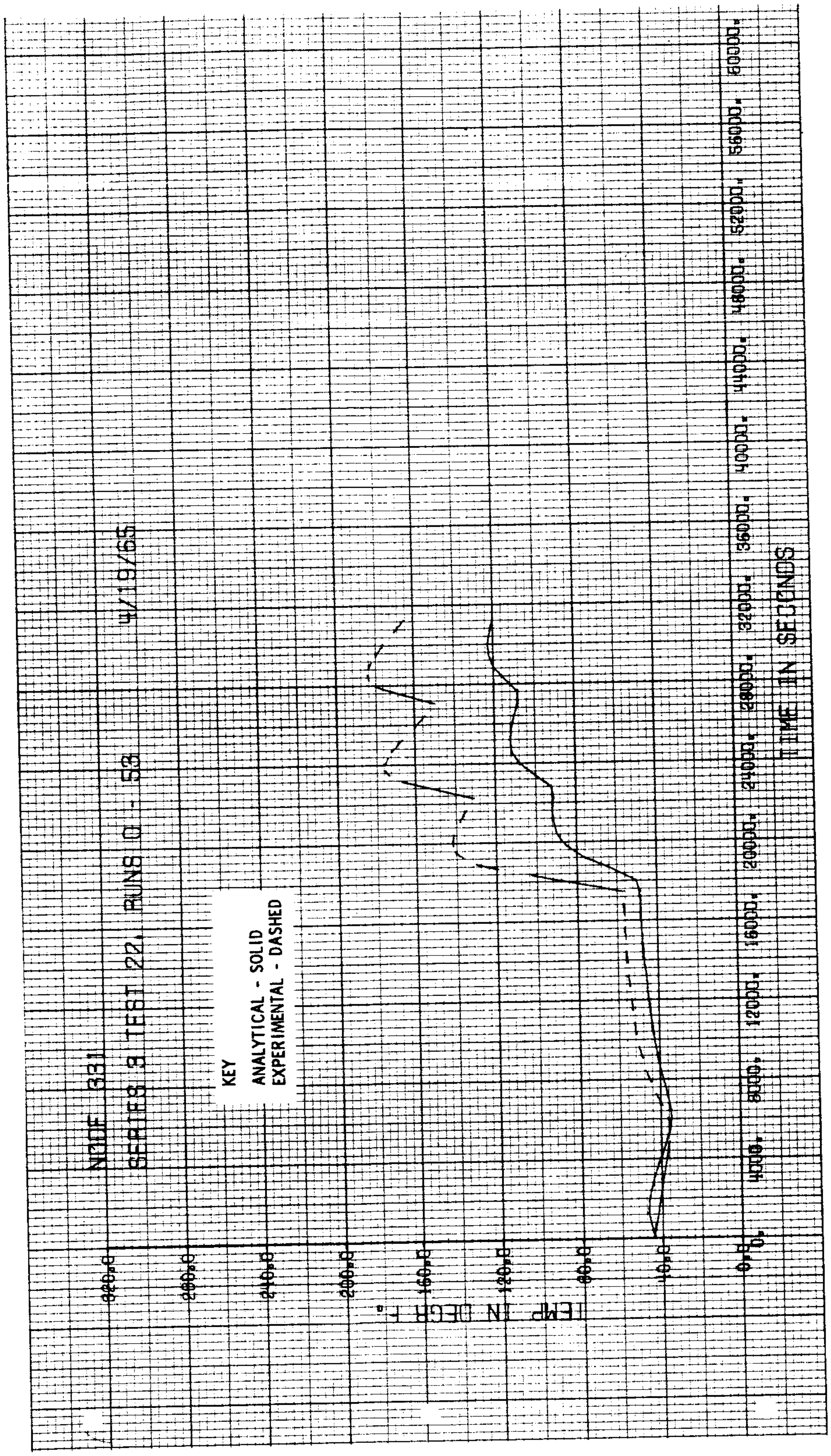

Figure 4-68 Inner Cylinder Temperature History (Node 331) for Run 3-22

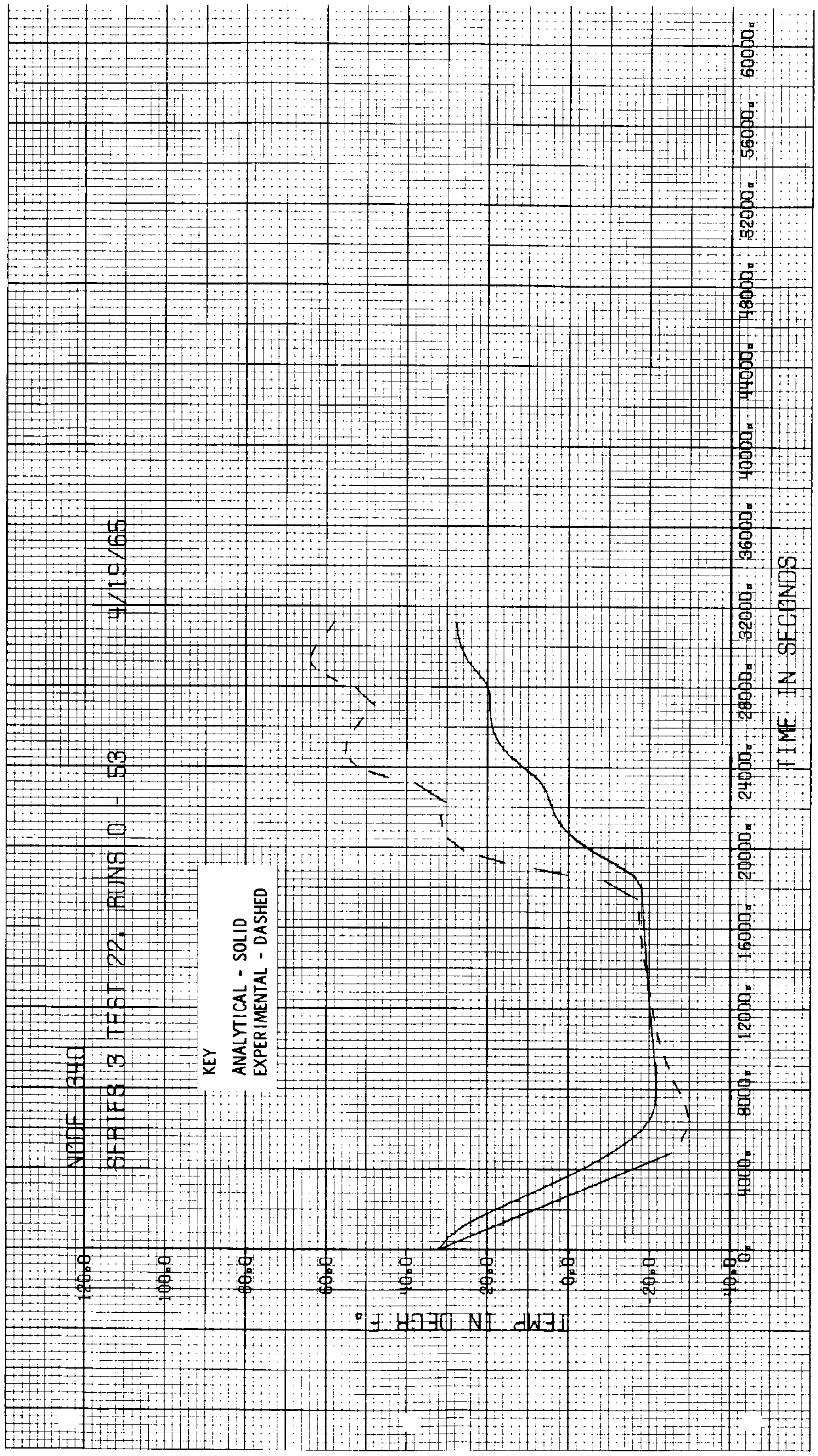

Figure 4-69 Beam Temperature History (Node 340) for Run 3-22

LOCKHEED
CALIFORNIA COMPANY

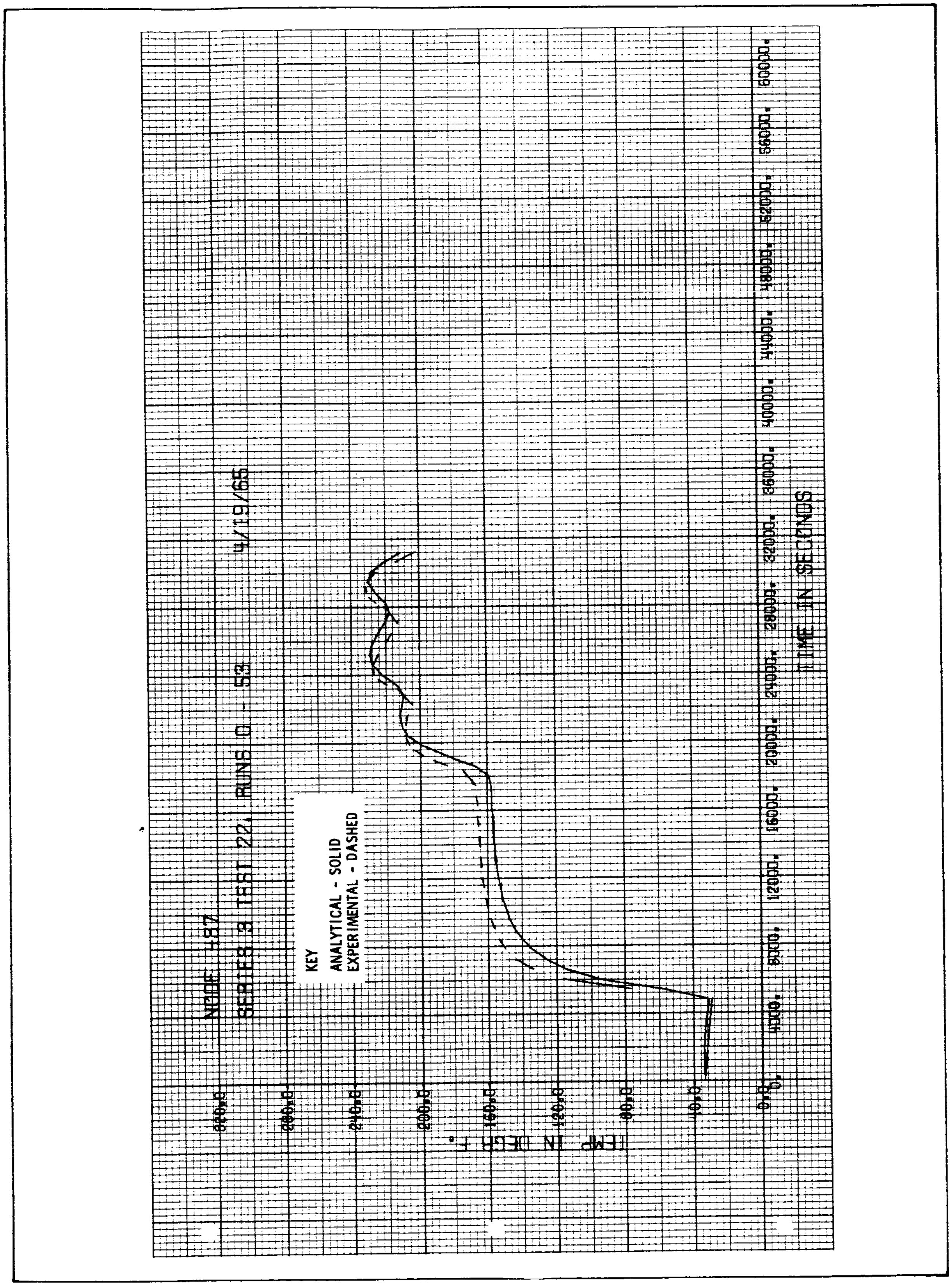

Figure 4-70 Beam Temperature History (Node 437) for Run 3-22

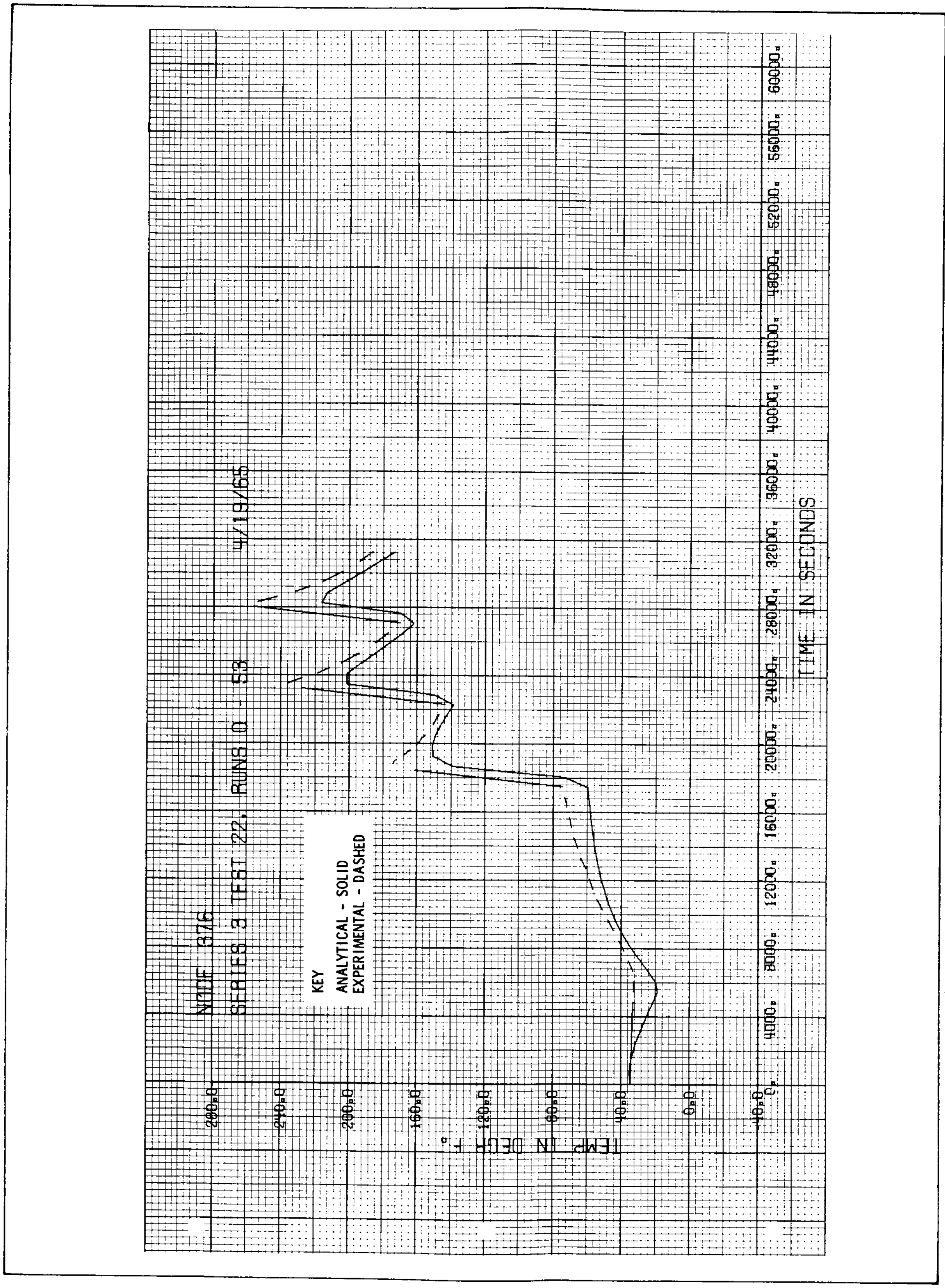

Figure 4-71 Heat Shield Temperature History (Node 376) For Run 3-22

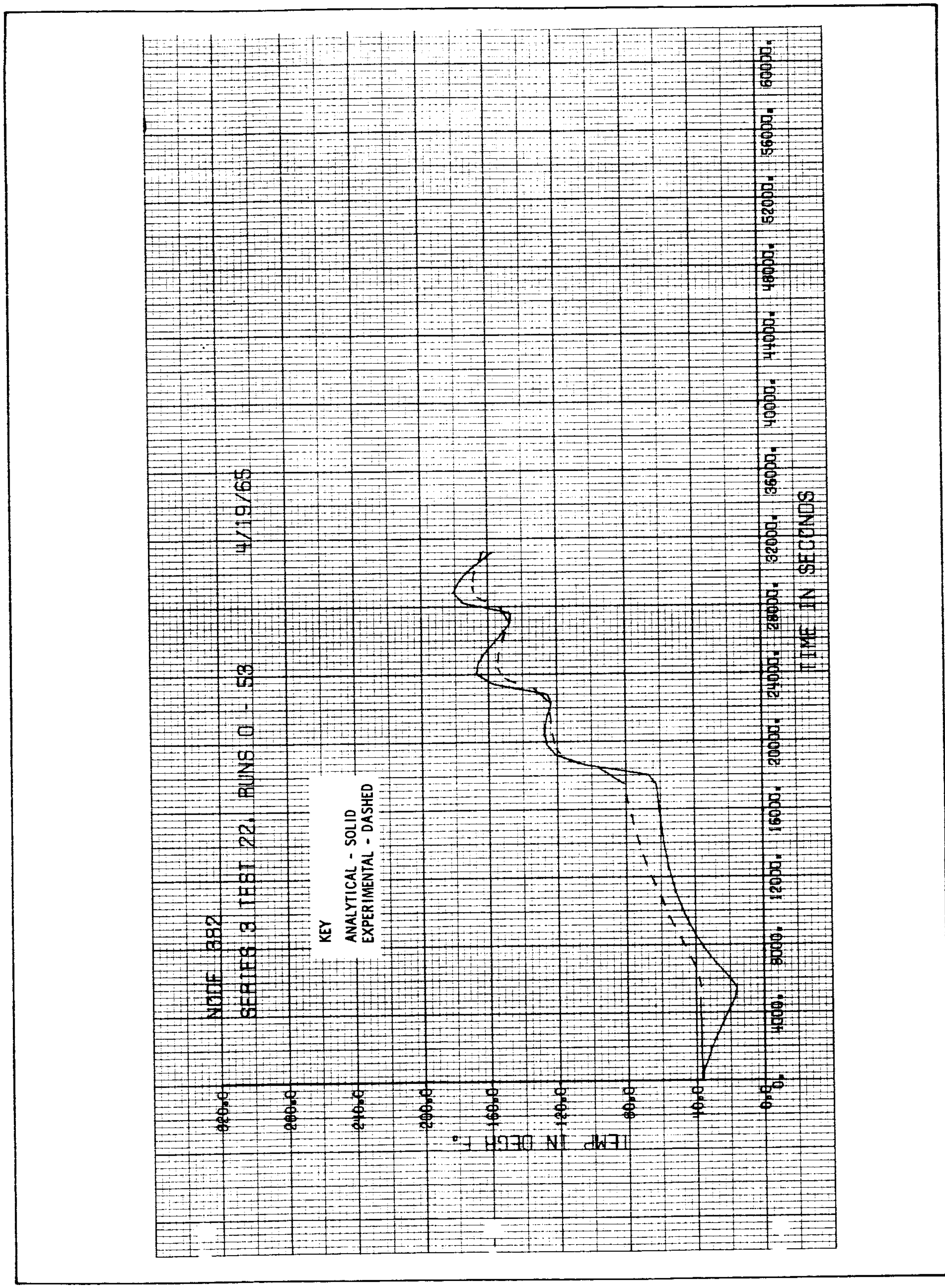

Figure 4-72 Heat Shield Temperature History (Node 382) For Run 3-22

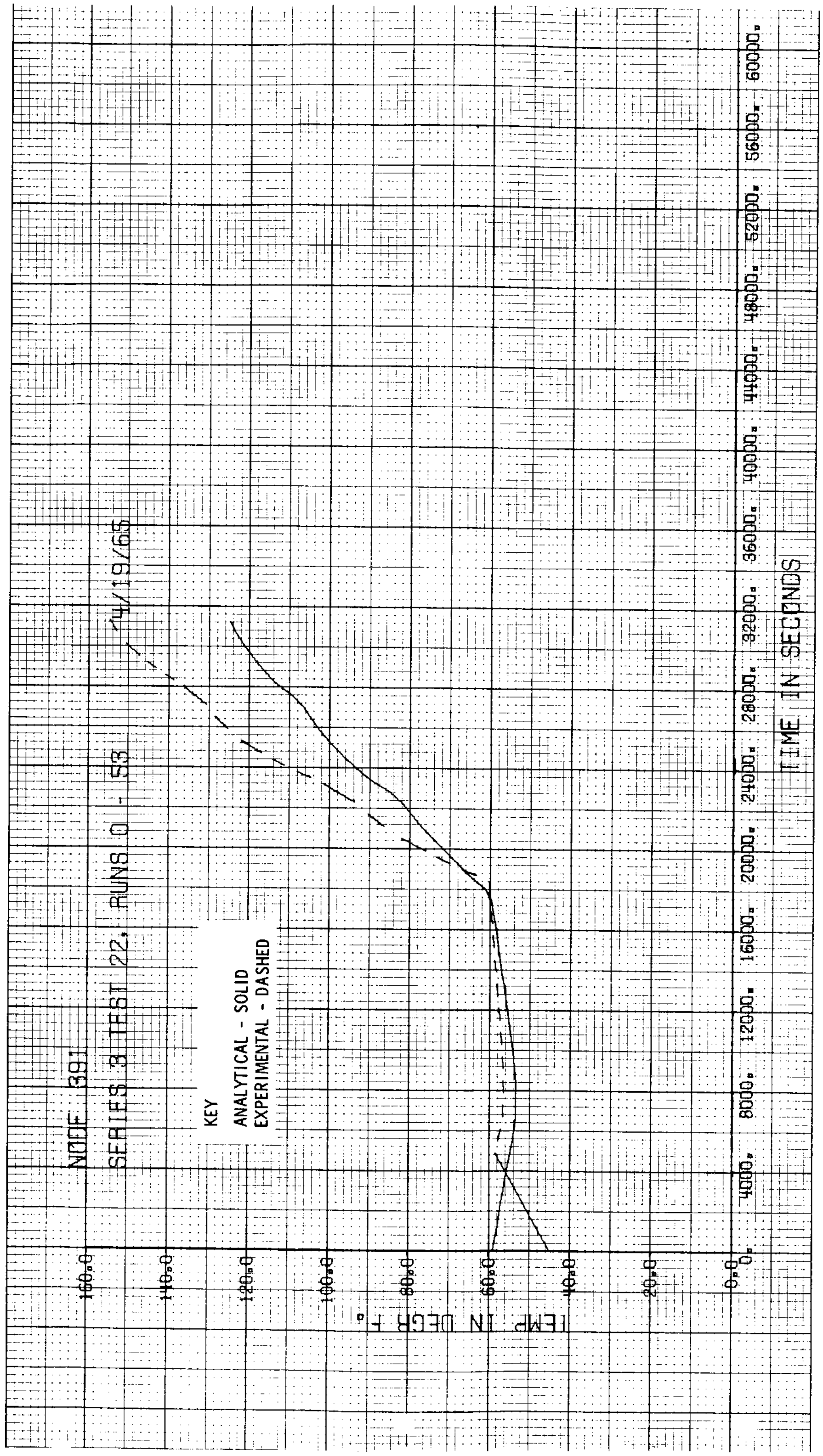

Figure 4-73 Lower Helium Bottle Temperature History (Node 391) for Run 3-22

LOCKHEED
CALIFORNIA COMPANY

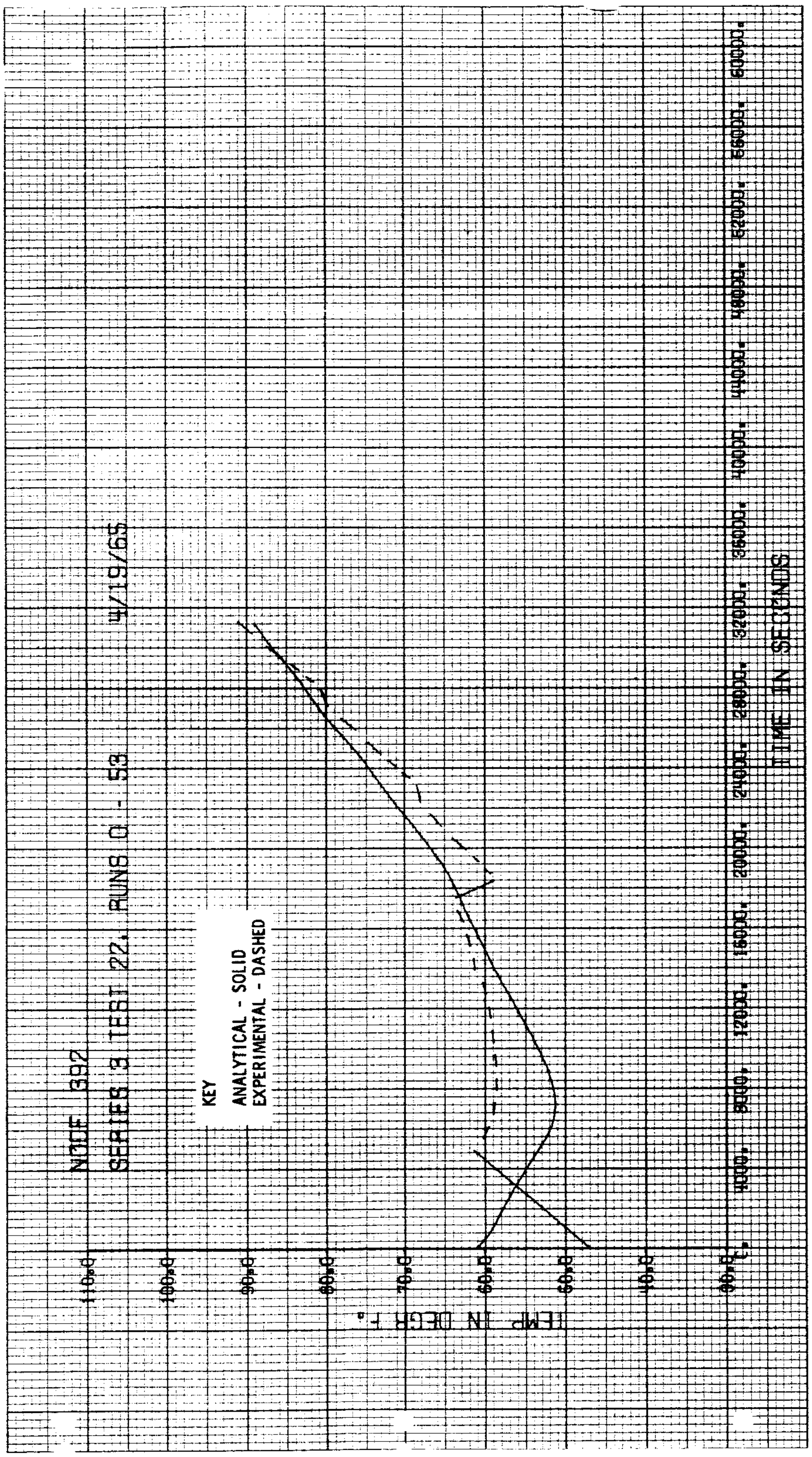

Figure 4-74 Upper Helium Bottle Temperature History (Node 392) For Run 3-22

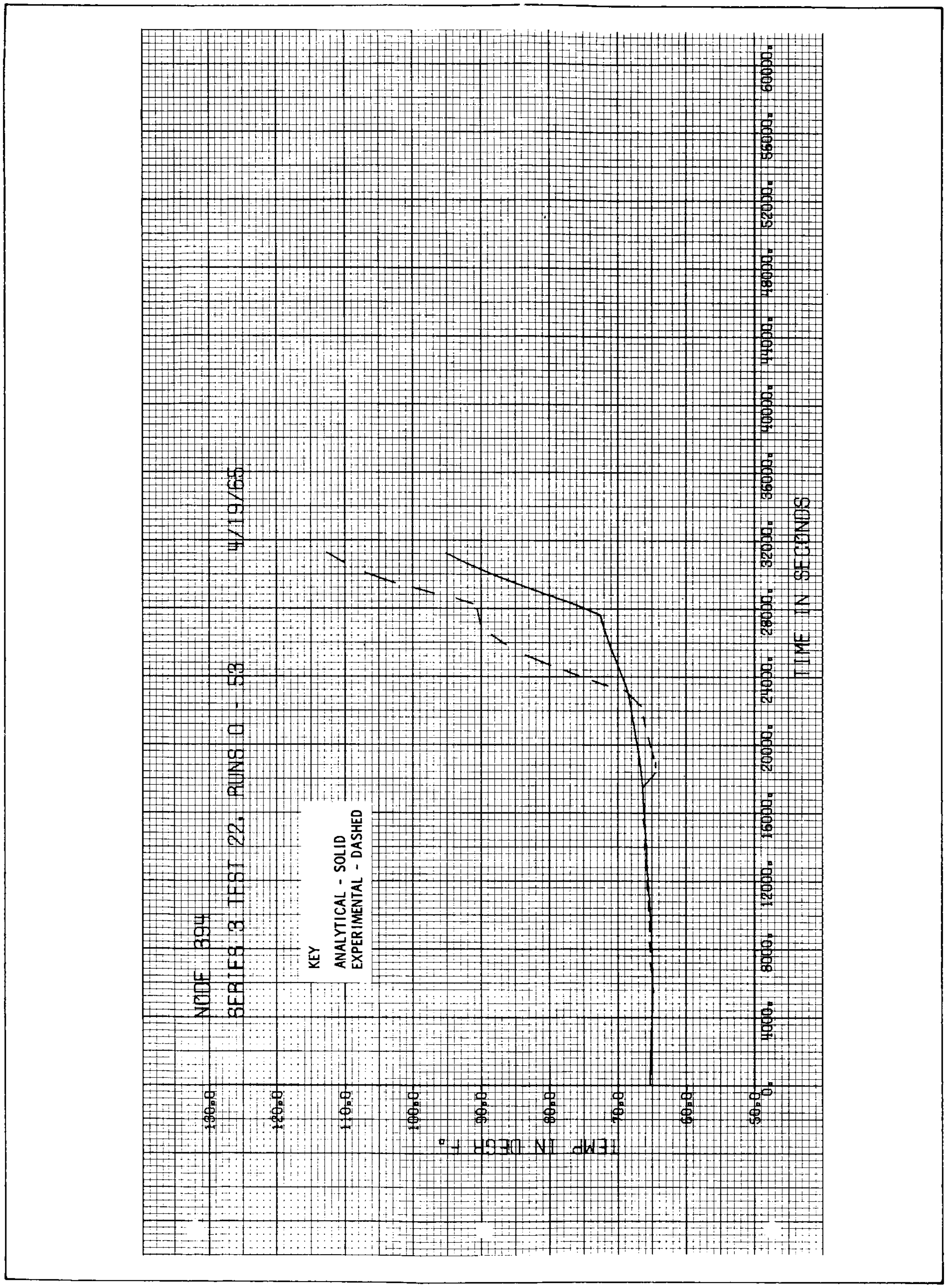

Figure 4-75 Propellant Tank Temperature History (Node 394) For Run 3-22

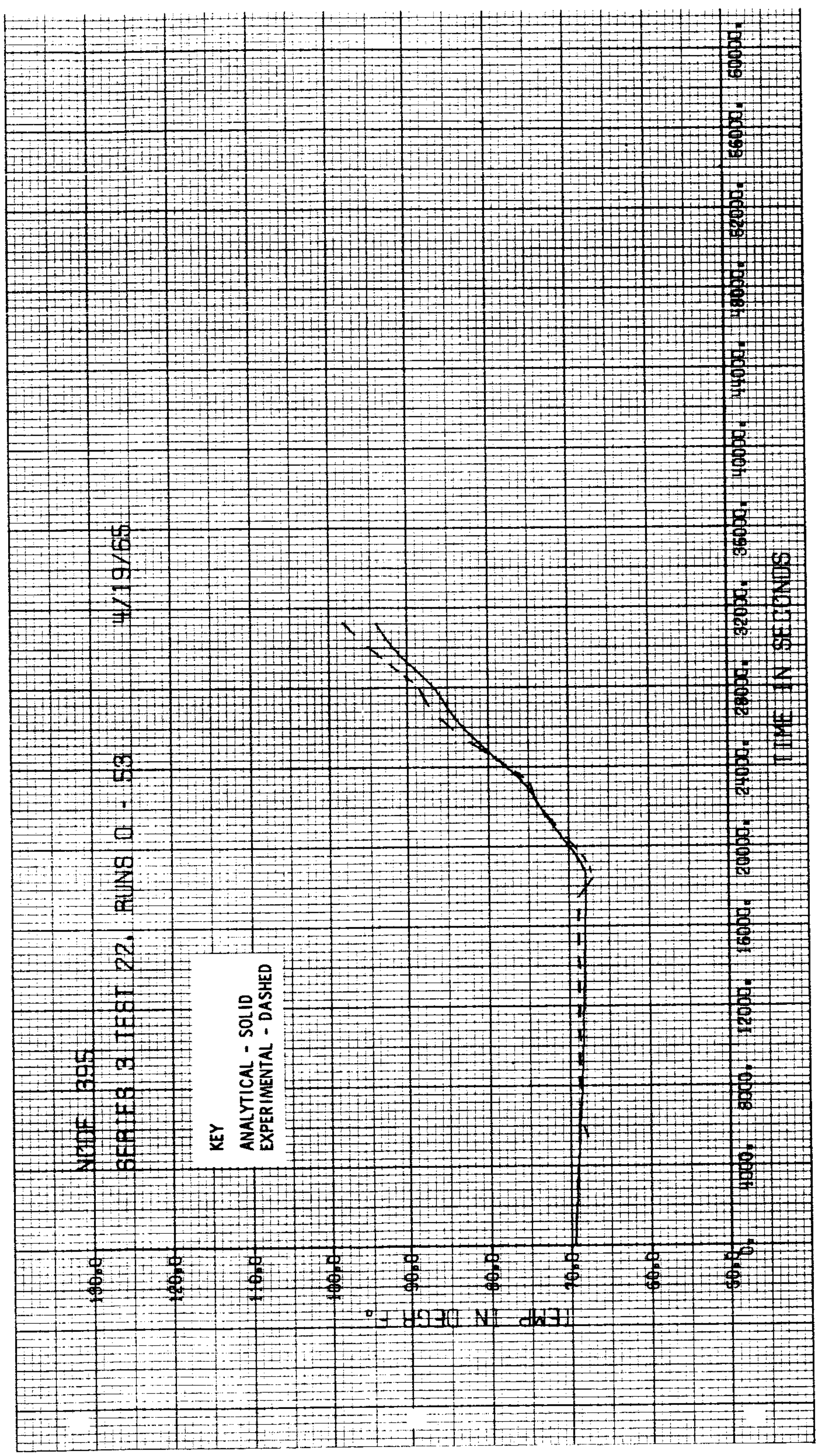

Figure 4-76 Propellant Tank Temperature History (Node 395) For Run 3-22

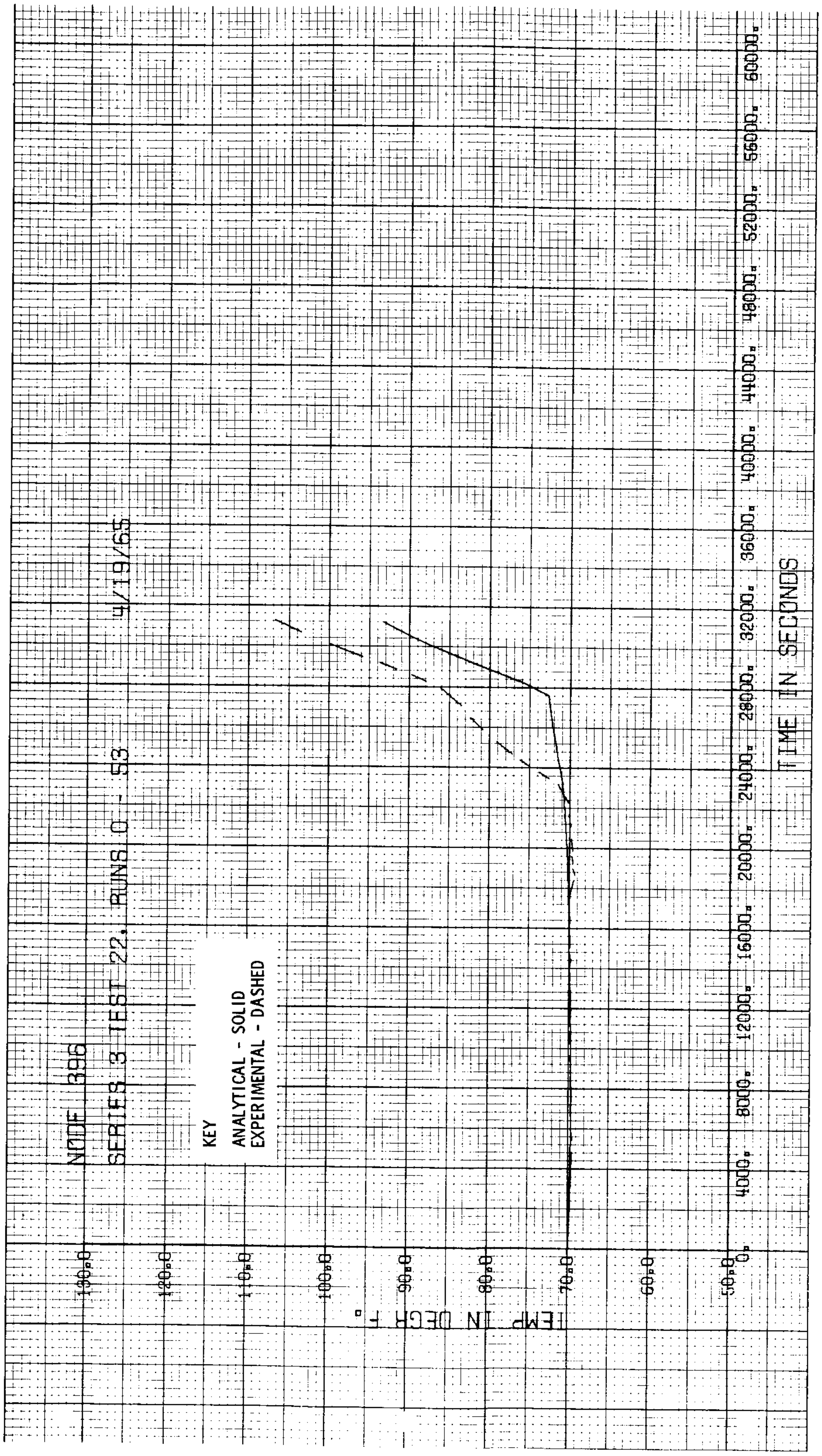

Figure 4-77 Propellant Tank Temperature History (Node 396) For Run 3-22

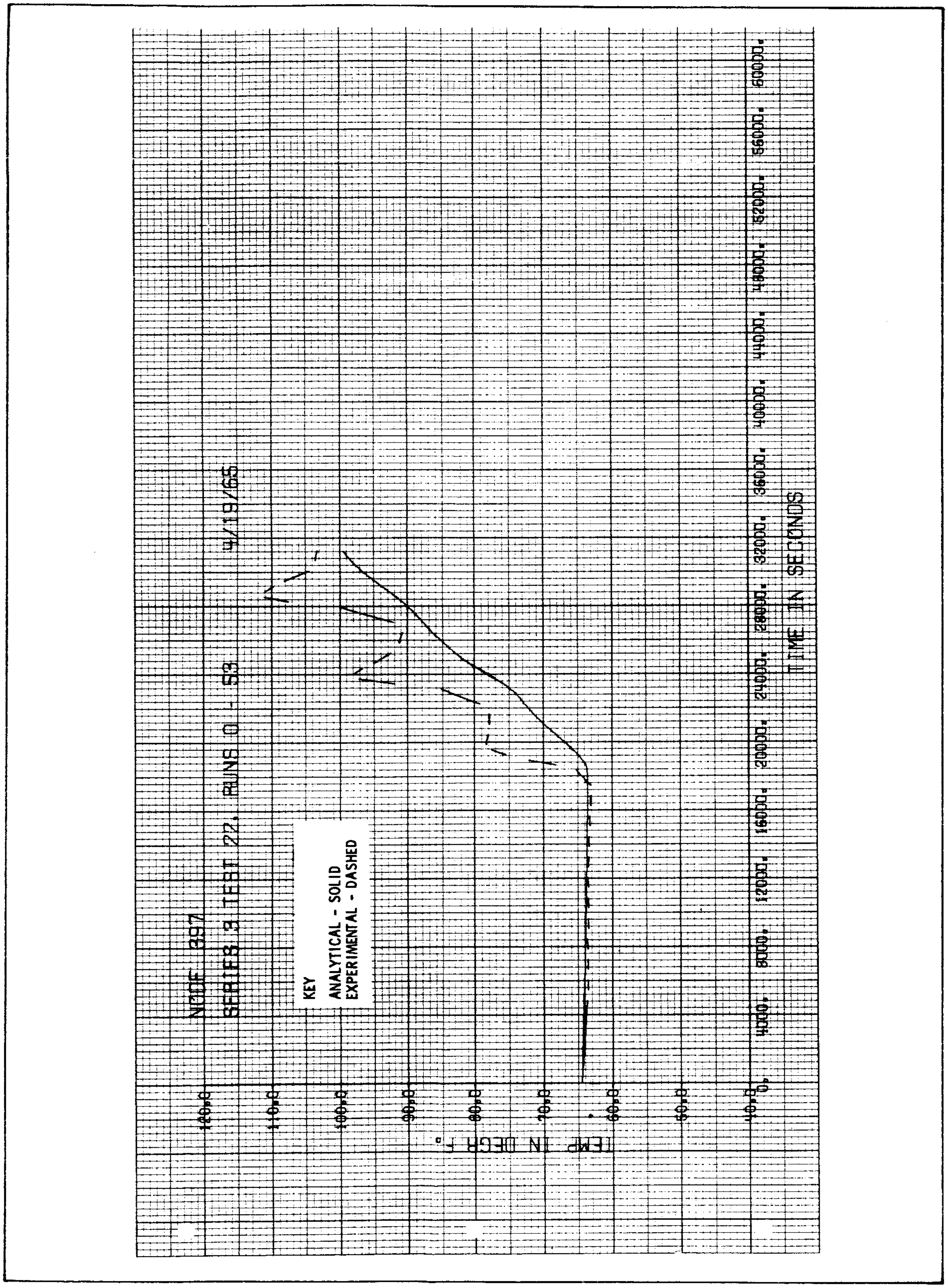

Figure 4-78 Propellant Tank Temperature History (Node 397) For Run 3-22

LOCKHEED
CALIFORNIA COMPANY

firing. During the engine firings, the predicted temperatures are as much as 50°F lower than the experimental temperatures. As discussed for Run 3-21, this is caused by the coarse radiation network from the thrust chamber and inner cylinder.

Temperature histories of representative heat shield nodes are shown in Figures 4-55 and 4-56. Agreement within ±20°F is shown for the steady-state portion of the run. During the firing time the discrepancy is as much as 35°F. The temperature range is from approximately 0°F to 250°F. Actually this is a reasonable correlation considering the temperature range and coarseness of the network in the multi-material heat shield.

Predicted and experimental temperatures for the helium bottles and propellant tanks are shown in Figures 4-73 to 4-78. As discussed for Run 3-21, predicted temperatures are in very good agreement with experimental temperatures until the tanks start emptying. In Figures 4-73 and 4-74, the discrepancy in initial temperatures is due to the fact that the helium bottles were charged 5,000 seconds after run start. To compensate for this, the bottle temperature after charging was used as the initial temperature for the analysis.

To examine the effects of the insulation on the model, a comparison of Run 3-21 and Run 3-22 is made. As might be expected, the temperatures of the outer panels for the insulated model are about 50°F cooler than the uninsulated model. Although the bulkheads are not insulated for any run, the average temperatures are about 15°F warmer during the simulated engine firings for Run 3-22. At steady state just prior to firing, the average bulkhead temperatures are 15°F cooler for Run 3-22 than for Run 3-21. Similarly, the beams and inner cylinder nodes show this same trend for the two runs. Addition of the insulation does not markedly improve overall correlation as can be seen by comparing Figures 4-38 and 4-57; however, it does improve correlation on the tank nodes. It was expected that the addition of insulation would improve correlation because it would reduce the difficulty in predicting radiative heat transfer. However, closer inspection reveals that approximately 50% of the nodes for the insulated model are uninsulated. Most of these uninsulated nodes are greatly influenced by the simulated engine firing and, consequently, transient results for the insulated model are about the same as for the uninsulated model.

In summarizing the results of the Series 3 runs, it was found that for the steady state part of the runs 85 per cent of the predicted temperatures were within $\pm 20^\circ F$ of the measured temperatures. During simulated engine firing, predicted temperatures are generally $20^\circ F$ lower than experimental because of the coarse radiation network. Improved simplified techniques are needed to properly represent the radiation heat transfer due to the simulated engine firing. Although insulation reduces the net radiation across the model, there is no marked improvement in overall correlation of the analytical and experimental temperatures for the insulated model because half of the nodes are still uninsulated for this model. From the results of these Series 3 runs, it was judged that internal heat transfer of the model is accurately represented except during simulated engine firing. Because the results of Run 3-21 and 3-22 were not available in reduced form before the Series 5 test, it was not known that the thermal network was underpredicting the heat transfer during a simulated engine firing; and consequently, the network was not modified to better represent the heat transfer in the Series 5 test.

V - SERIES 4 MODEL

MODEL DESIGN AND FABRICATION

While the first three series of tests were concerned with heat transfer internal to a complex structure, attention was directed in the Series 4 tests to heat exchange on isolated components external to a vehicle. Thus, the influences of a collimated energy source and complex shadowing effects are introduced. On the Apollo Service Module, the most interesting external heat transfer problem of this type is the nozzle protruding from the lower bulkhead. The basic Series 4 model, Figure 5-1, consisted of a disk to which a truncated cone was attached in a manner simulating a nozzle protruding from a bulkhead. A model support was fabricated to position the model in the 10-in. beam of the Aerospace Solar Simulator in the Lockheed C-5 Space Simulation chamber.

Disk and Cone

Both the disk and cone were machined from 303 stainless steel. Uniformity of thickness was essential to the test objectives. To achieve this in the cone, it was necessary first to machine the internal cone cavity. This cavity was then filled with a low-melting-point alloy and the outside machined down to establish a uniform wall thickness (± 0.0002 in.). A small 1-in. dia. by 1-in. high right cylinder and a 1-in. cube were machined from 2024 aluminum alloy for later attachment to the disk. These small masses were intended to add additional complexity by simulating bulkhead mounted equipment.

Model Orientation and Support

The disk and cone were attached to a teflon mounting with a nylon screw. The teflon mounting permitted pivoting the model to achieve various attitudes of the model relative to the solar flux. The model was insulated on the back surface with 10 layers of NRC-2 and 1 in. of Styrofoam. A stand was fabricated of aluminum pipe to support the model assembly. Adjustment of the model orientation under vacuum conditions after each run could be effected with a flexible cable utilizing a special feedthrough in the chamber wall.

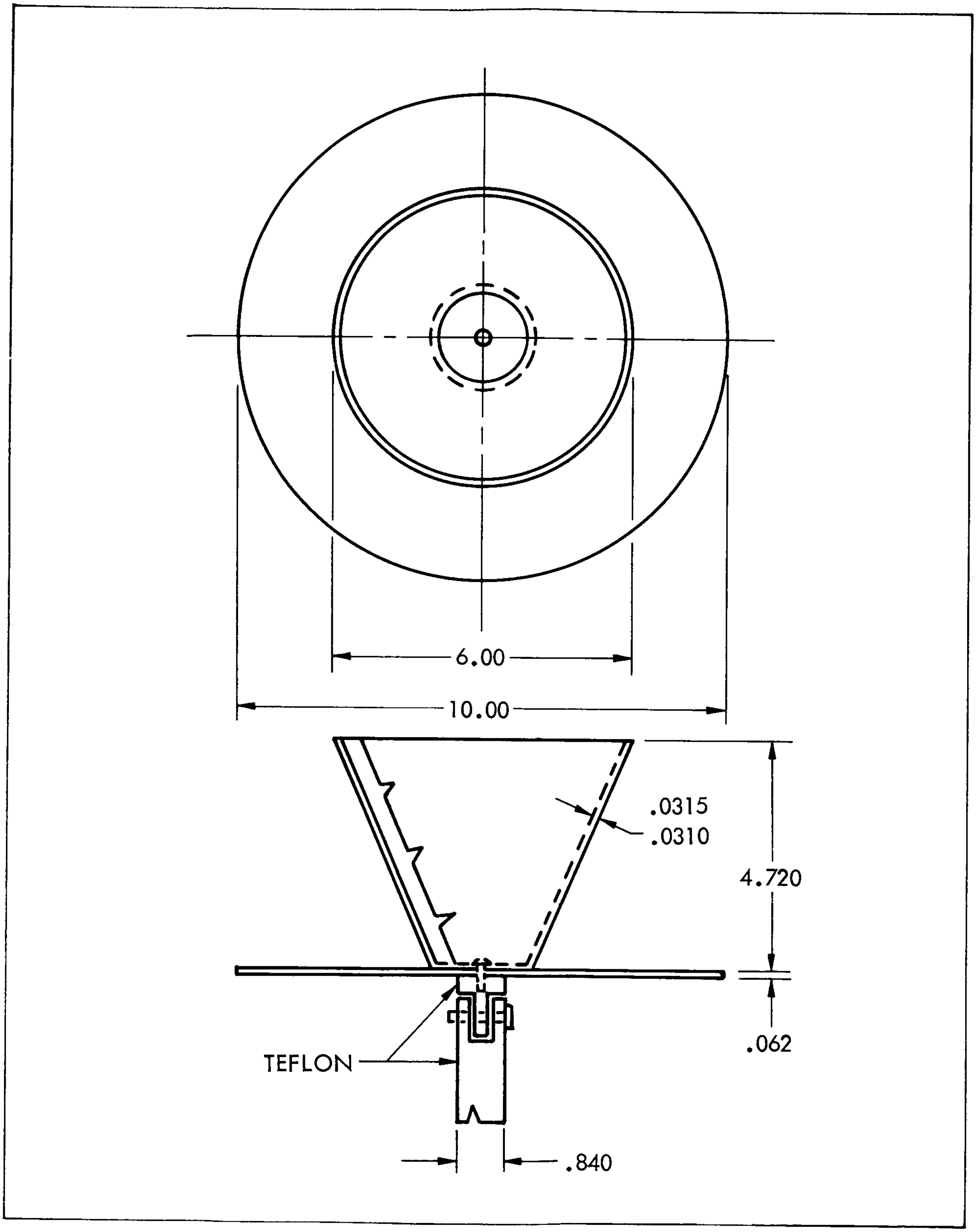

Figure 5-1 Basic Series 4 Model

The Series 4 model was installed in the C-5 chamber 3 feet from the quartz window. The model is shown in the solar simulator beam with the chamber door open in Figure 5-2. The tube curving to the left constrains the push-pull cable for changing the model's angular inclination remotely ($\pm 1^\circ$ tolerance). The inclination control cable is visible behind the disk as it exits through the tube fitting. The cable was fastened to the disk through a teflon pivot.

INSTRUMENTATION

Solar Simulator Flux Distribution

To establish the flux distribution at the Series 4 model, a simple flux mapping calorimeter was built and instrumented. This device (Figure 5-3) was a 10-in. diameter disk of 0.06-in. thick copper punched out in 9 places to accept 9 small 1-in. dia. slug-type calorimeters. The calorimeter assembly was attached to a backing of 3/4-in. Styrofoam with stainless-steel pins. Ten layers of NRC-2 were used between the calorimeter and the insulation support to reduce the flux out of the back of the calorimeters to a negligible amount. The entire assembly was supported from the Series 4 model stand. The plate and calorimeters were coated with Kemacryl flat-black lacquer having an α/ϵ of approximately 1.05. The equilibrium temperature of the calorimeters gives an indication of the flux distribution, while cool-down rates were a function of the emissivity. During the first test in C-5 under a vacuum of 10^{-6} torr with the cold walls operating, the calorimeters reached a temperature of approximately 250° F. This caused the final coat to blister, separating from the undercoat which appeared to adhere well. The device was then stripped of the Kemacryl lacquer and undercoat and was painted with CAT-A-LAC Flat Black. Information on these coatings is given in Appendix B. The CAT-A-LAC coating proved successful and was used in this application and on other models where a high emissivity coating was desired.

The flux mapping experiments indicated several problems. The flux profile over the 10" diameter was not flat as had been presumed, but varied from 0.95 solar constant at the center to about 0.65 at the edges. The profiles in two planes were not symmetrical. More disturbing, however, was

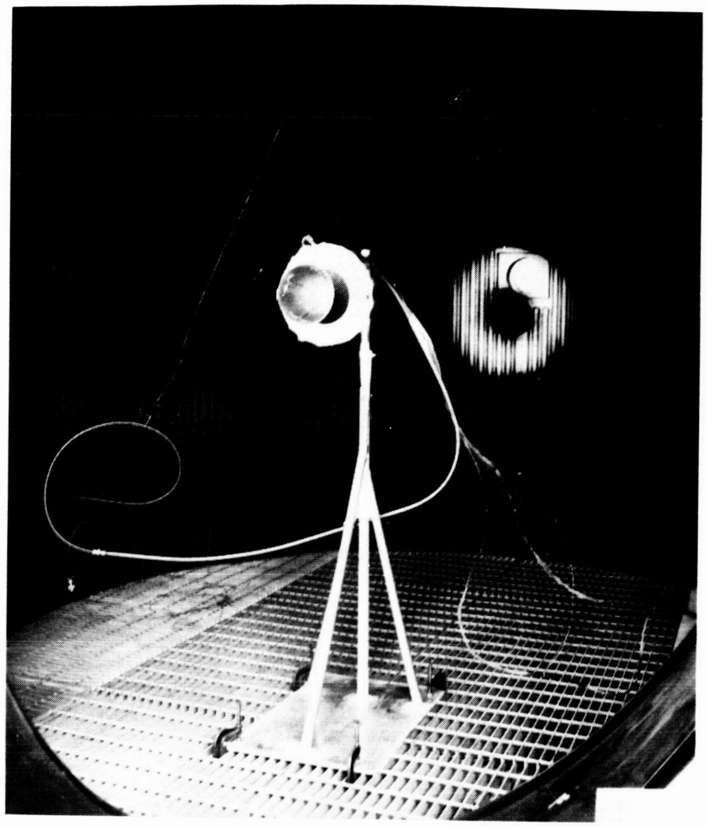

Figure 5-2 Model Test Setup in the Chamber

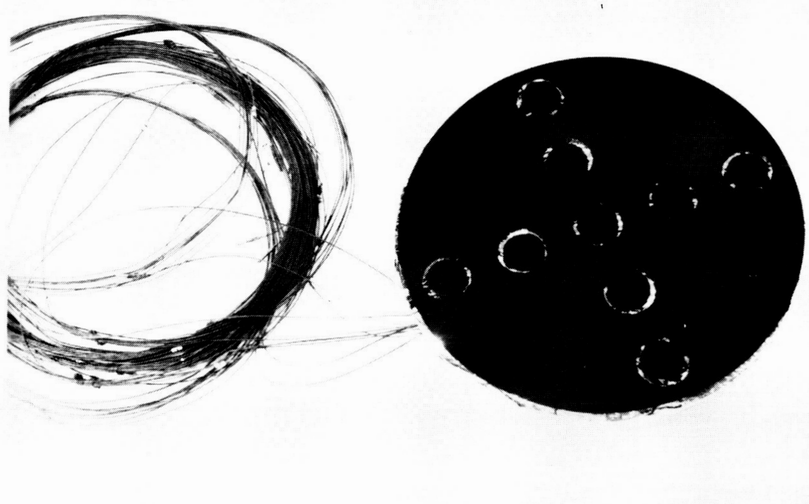

84 249R

Figure 5-3 Flux Mapping Calorimeter

the fact that each time the C-5 chamber was opened it was necessary to move the simulator. Repositioning the simulator could not be done with sufficient accuracy to obtain a reproducible flux map at the model position. Thus, the flux distribution on the model during the Series 4 tests was not well defined.

Thermocouple Calibration & Node Locations

The 36 thermocouples to be used on the Series 4 model were calibrated using the procedure already described in Section 2. A calibration curve for the Series 4 thermocouples is shown in Figure 5-4. A corrected conversion table of millivolts to degrees based on this curve was formulated for processing the Series 4 data.

The calibrated thermocouples were attached to the Series 4 model with a small amount of heat transfer cement, Thermon T-85. Installation of the thermocouples is shown in Figures 5-5 and 5-6. A detailed description of the location of each thermocouple, together with connector identification information, is given in Appendix E.

Model Coating

After installation of the thermocouples the model was coated with Kemacryl Flat Black Lacquer. Subsequent to this operation, tests with the flux calorimeter indicated the possibility of blistering with this coating. The model coating, which has been room-temperature cured for 12 days, was then given an additional overnight bakeout at 200^{o}F in the hope this would prevent blistering. However, during preliminary check-out tests with the Series 4 model severe blistering occurred. The model was then stripped down to the metal and coated with CAT-A-LAC Black.

TEST RUNS

Basic Cone and Disk

A total of 8 runs was made on the basic Series 4 model. Four positions (0^{o}, 30^{o}, 45^{o}, and 60^{o}) were made with the plain disk and cone. Each run was started at model temperatures of about-100^{o}F. The cold walls were below -300^{o}F and a vacuum of 2 x 10^{-5} torr existed. A step input of solar flux initiated the run and this was held for 1 hour and then the solar simulator was turned off and the model allowed to cool for one hour .

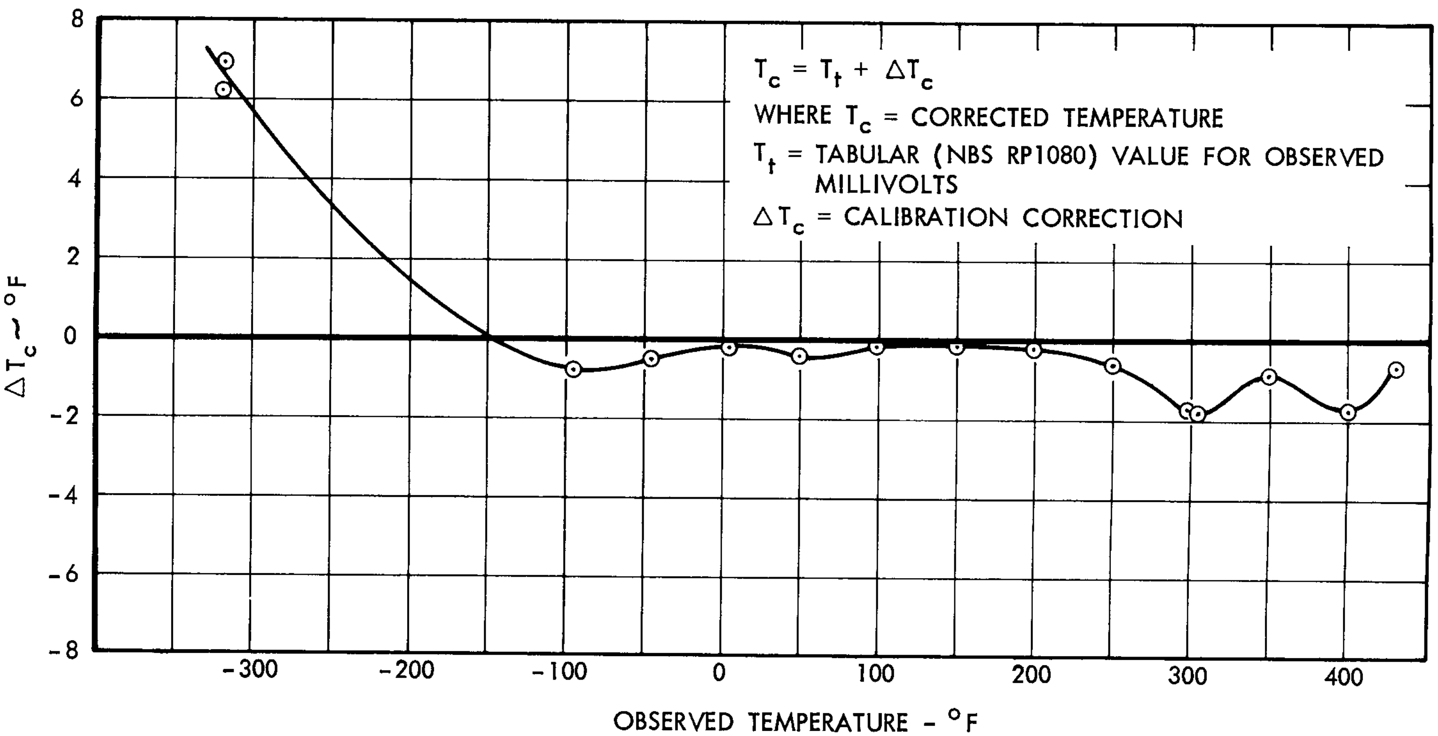

Figure 5-4 Series 4 Thermocouple Calibration

LOCKHEED CALIFORNIA COMPANY

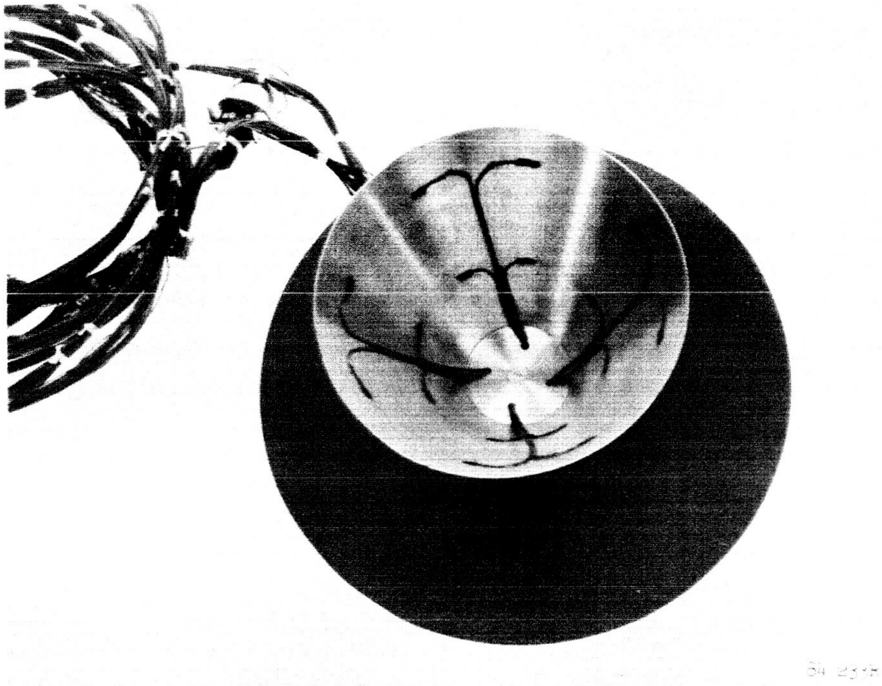

Figure 5-5 Test Model - Front

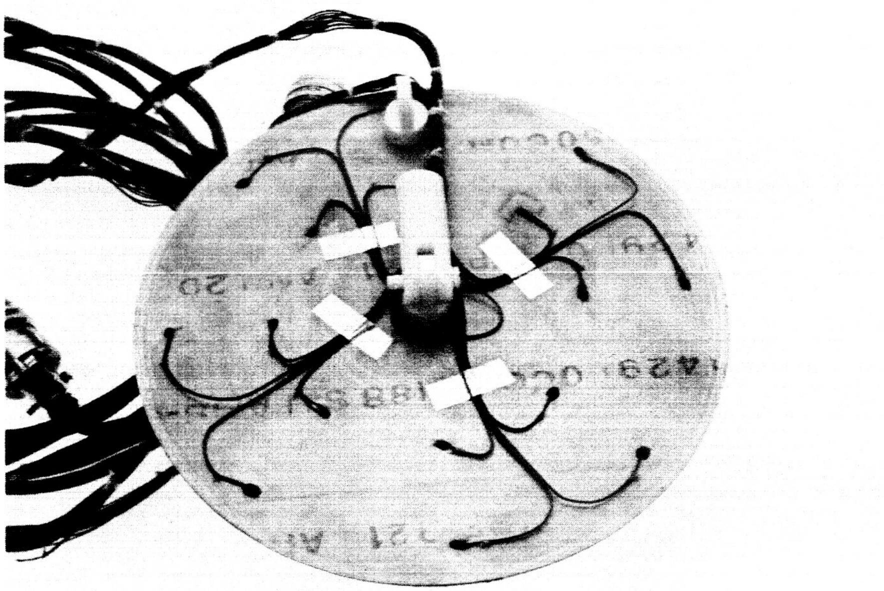

84 232R

Figure 5-6 Test Model - Rear

Data were taken during the two hour run period, the acquisition rate being every 2 minutes during rapid transients and every 5 minutes during the balance of the time. An additional run was made at 0° (this was not included in original program) to provide guidance on the flux distribution which had been assumed flat during the planning period.

Addition of Local Masses

In the second part of the Series 4 program, simulations of bulkhead mounted equipment were added to the disk and cone model. The small aluminum cylinder and cube were coated with CAT-A-LAC Black and attached with small screws to opposite edges of the disk. They were positioned so that the outermost edges were tangent to the disk edge. The coatings were not removed at the contacting surfaces. The Series 4 model in this configuration is shown illuminated by the solar simulator in Figure 5-7. This photograph also shows the degree of shadowing of the disk by the cone in the 30° position. The same run procedure was followed in tests of this model at the four angles (0°, 30°, 45°, and 60°).

At the completion of all runs an additional mapping survey was made with the calorimeter. It was observed to be significantly different than the initial distribution, pointing out the sensitivity of the flux map to exact simulator positioning. Thus, the first four Series 4 runs had a slightly different map from the second four.

ANALYTICAL CORRELATION

Series 4 Network

The nodal layout of the Series 4 model is indicated in Figure 5-8. The dimensions and thermocouple locations at these nodal points are given in Appendix E. The nodes are connected by conduction resistors running circumferentially and radially on both the disk and cone. There are 64 conduction resistors. Each node also has a radiation resistor to space, and there are radiation resistors between the disk and cone nodes and across the inside of the cone. There are 208 radiation resistors.

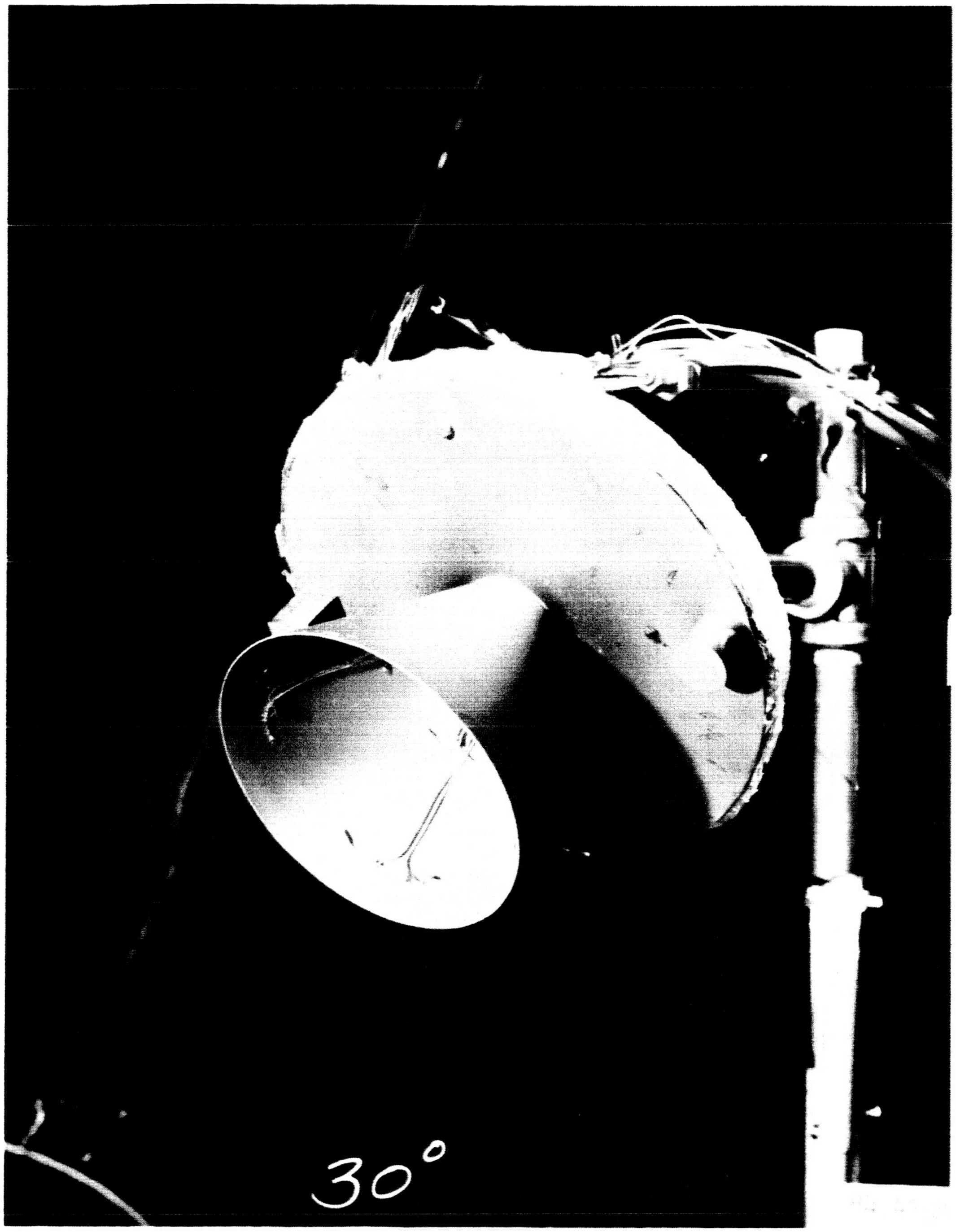

Figure 5-7 Model Inclined 30° from Vertical

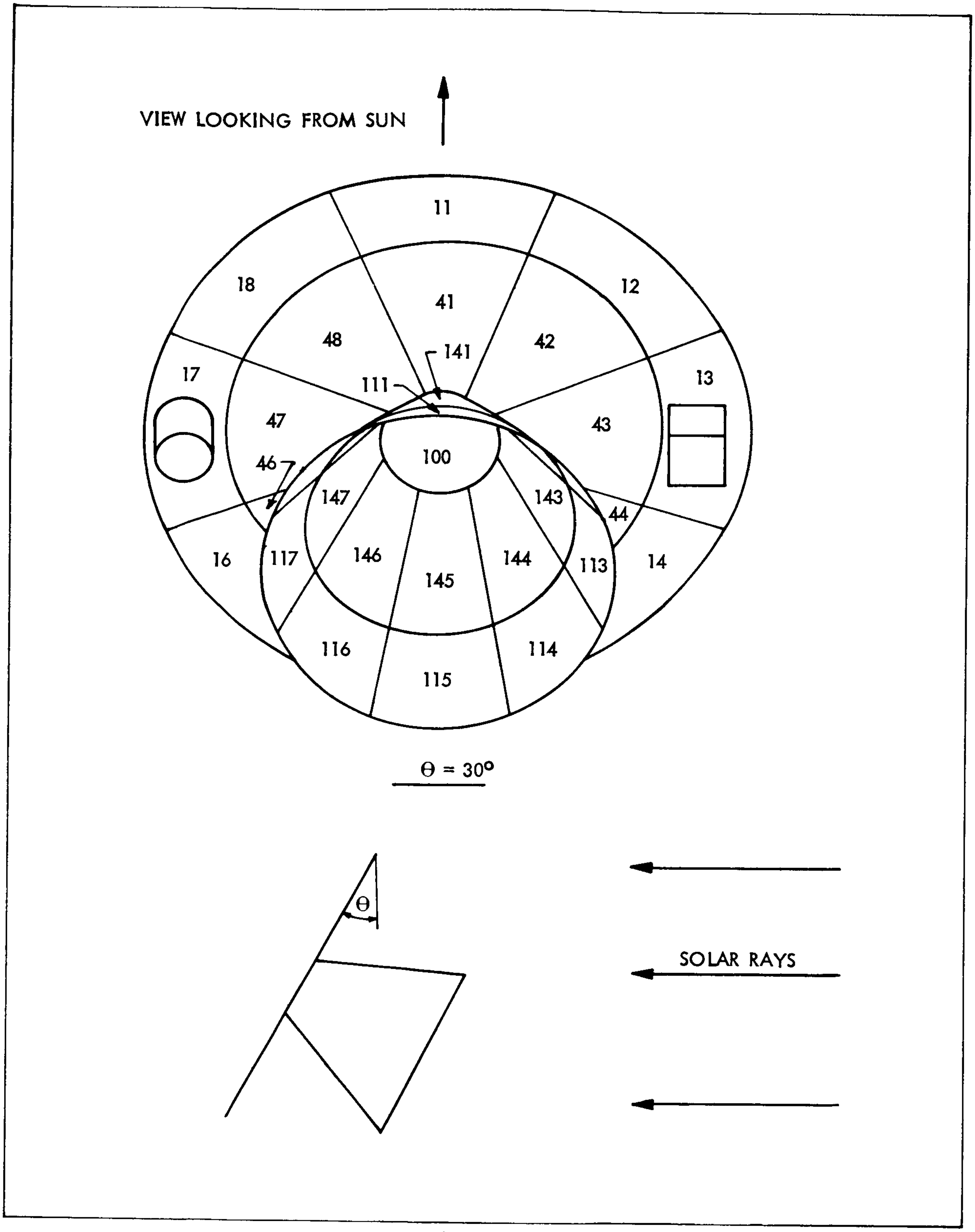

Figure 5-8 Nodal Layout

Run Correlations

The Series 4 data analysis was greatly complicated by uncertainties in the flux distribution of the Solar Simulator. A separate flux map was required for each set of four runs. The flux maps used are shown in Figures 5-9 & 5-10. These maps were developed by an iterative process from the measured equilibrium temperatures on the model when set at 0 degrees (disk perpendicular to solar rays) For a given node, a flux is assumed and the resulting analytical temperature is then compared with the experimental temperature. This process is repeated simultaneously for all the nodes until the desired degree of agreement is reached.

With the flux maps established, computer runs were then made for the model inclined at 30, 45, and 60 degrees to the solar flux, with both a plain disk and a compound disk which had masses simulating bulkhead mounted equipment. Experimental results are compared with the analytical predictions for representative nodes in Figures 5-11 to 5-20. For almost all of the nodes, experimental temperatures are within 30°F of the predicted temperatures. The correlation is about the same for all the runs. For a given angle setting, the main difference in results between the compound disk and the plain disk is that the thermal response of the two nodes (13 and 17) to which the objects are attached is slightly slower due to the added capacitance. This can be observed in comparing Figure 5-12 to Figure 5-18. The effect of these objects on non-adjacent nodes is negligible.

As detected in all the figures, there is a systematic error during the cool-down. All experimental temperatures drop more slowly than predicted temperatures and appear to be approaching an equilibrium temperature higher than the chamber temperature, -320°F. Calculations indicate that the uncooled part of the chamber door transistion (which is at a temperature of -100°F) could easily cause the experimental temperatures to be 70°F warmer than predicted.

Experimental-analytical discrepancies at the end of solar heating are mainly attributed to a poorly defined solar flux. However, another source of error is the determination of projected areas of the nodes, especially for the cone. The projected areas were determined graphically. As is shown in Figure 5-8, cone node 145 has a much larger projected area than node 141 for the 30° angular position. A small change in angular position would cause a very large percentage change in the projected area of node 141 while the percentage change in projected area of node 145 would be very small. In Figures 5-11 and 5-15 the temperature histories of nodes 141 and 145 are shown for angular positions of 30° and 60° At the end of solar heating for the 30° setting (Figure 5-11), the discrepancy between predicted and measured temperatures for node 141 is about 30° F, while for node 145 there is perfect agreement. For the 60° setting (Figure 5-15) both these nodes have the same 10°F discrepancy. These results indicate that discrepancies in predicted and measured temperatures could have been caused by errors in the graphical determination of the projected areas or errors in the angular position of the test model.

In summary, the degree of correlation indicated in Figures 5-11 to 5-20 is representative, ranging from excellent (within 5°F) to fair (within 30°) With the uncertainties that existed in the test boundary conditions, it is not possible to assign any of the observed errors to the analytical program. However, the correlation obtained is judged to substantiate the analytical techniques as applied to an external heat transfer case of the type represented by the Series 4 model.

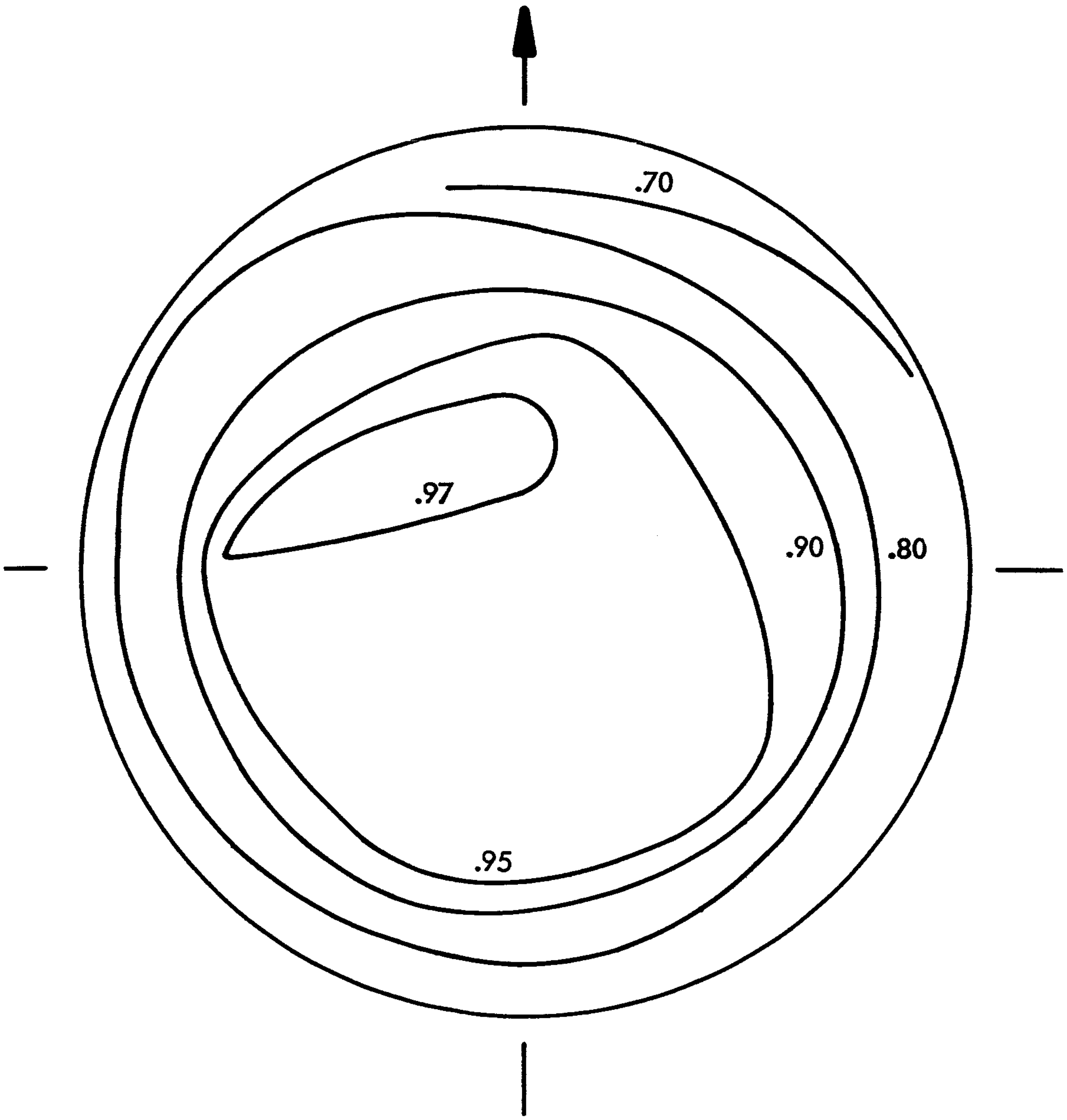

Figure 5-9 Flux Map for Basic Model

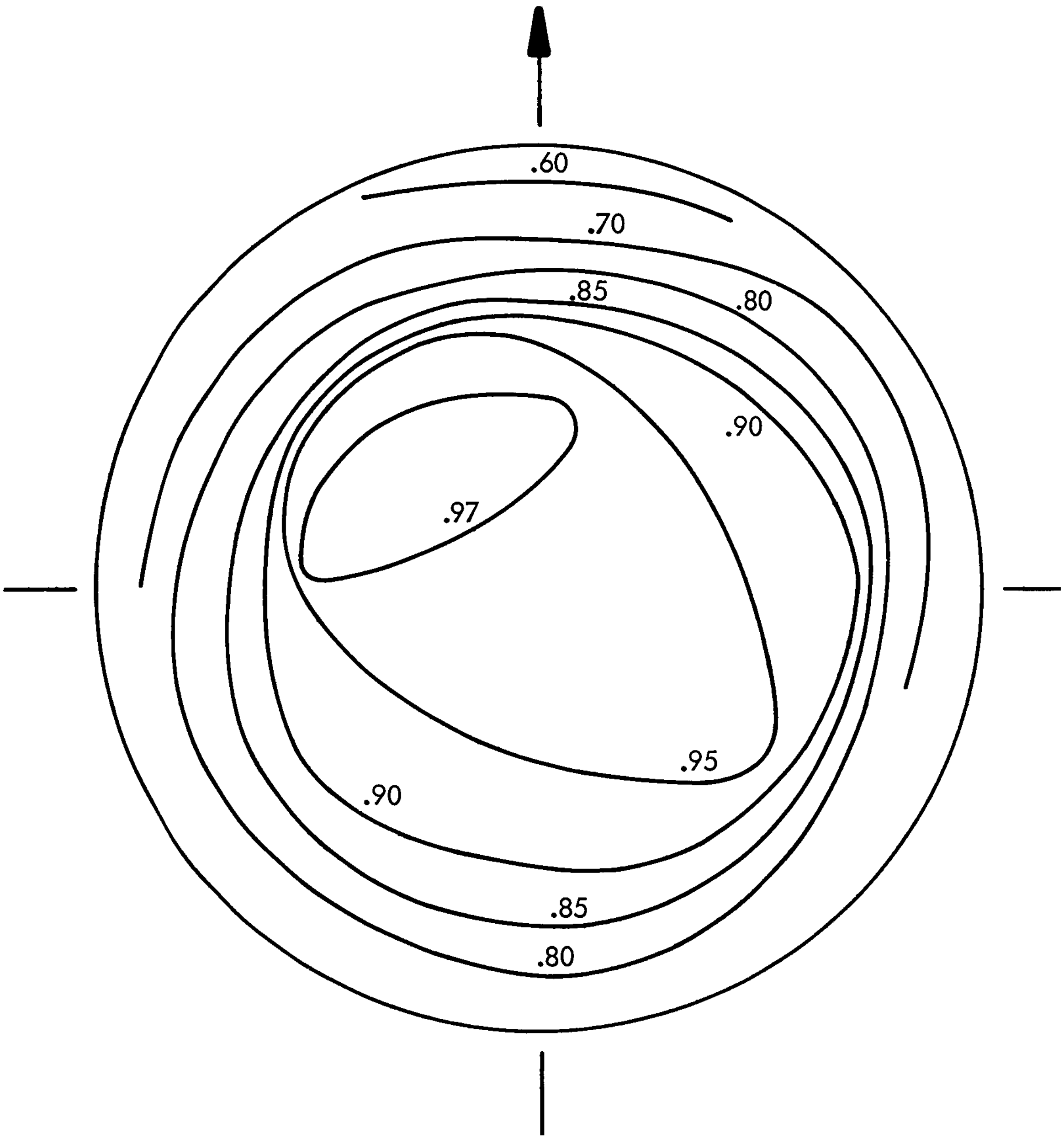

Figure 5-10 Flux Map For Model With Local Mass Added

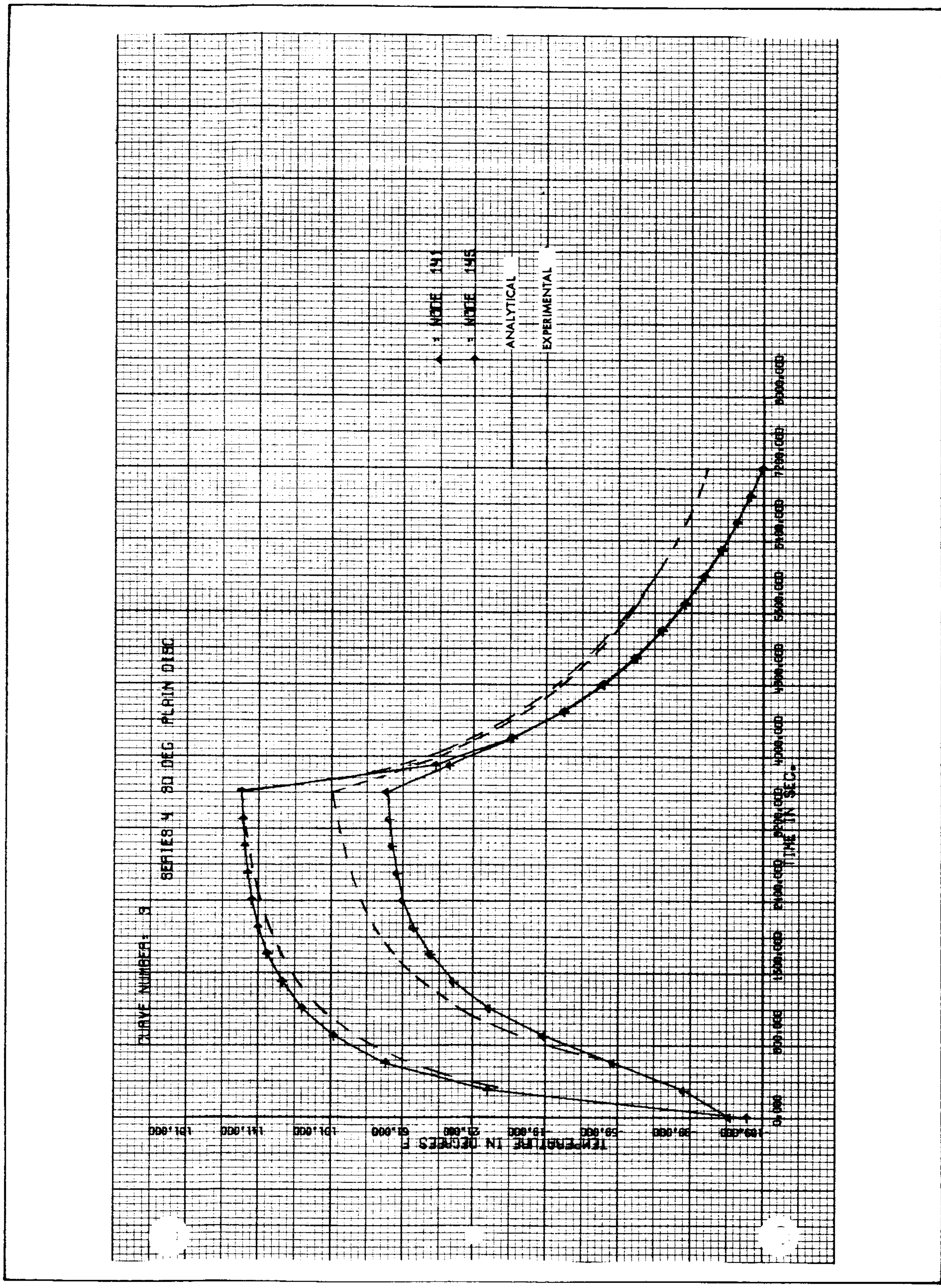

Figure 5-11 Cone Temperature Histories (Nodes 141 and 145), 30 Degree Orientation Plain Disc

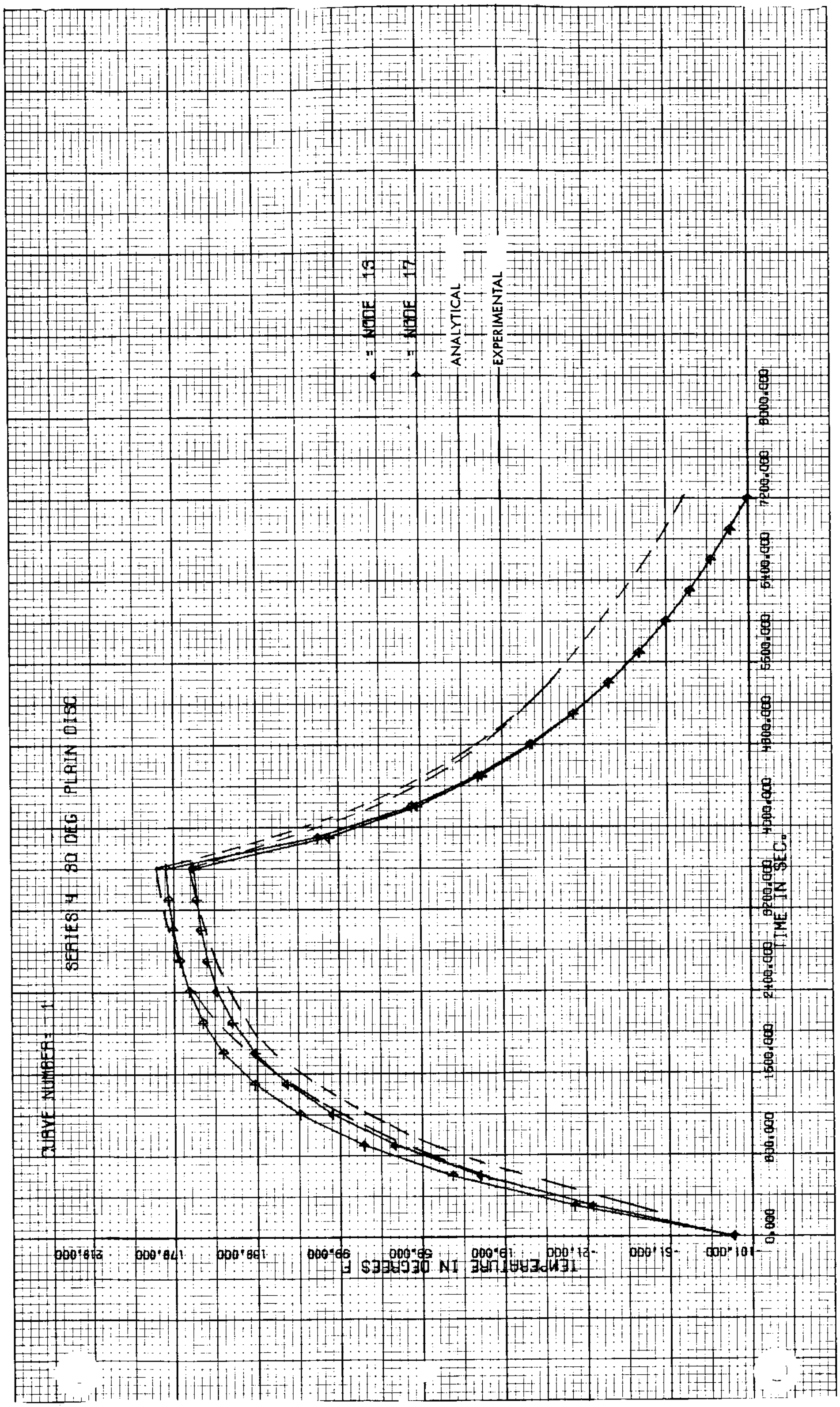

Figure 5-12 Plain Disc Temperature Histories (Nodes 13 and 17), 30 Degree Orientation

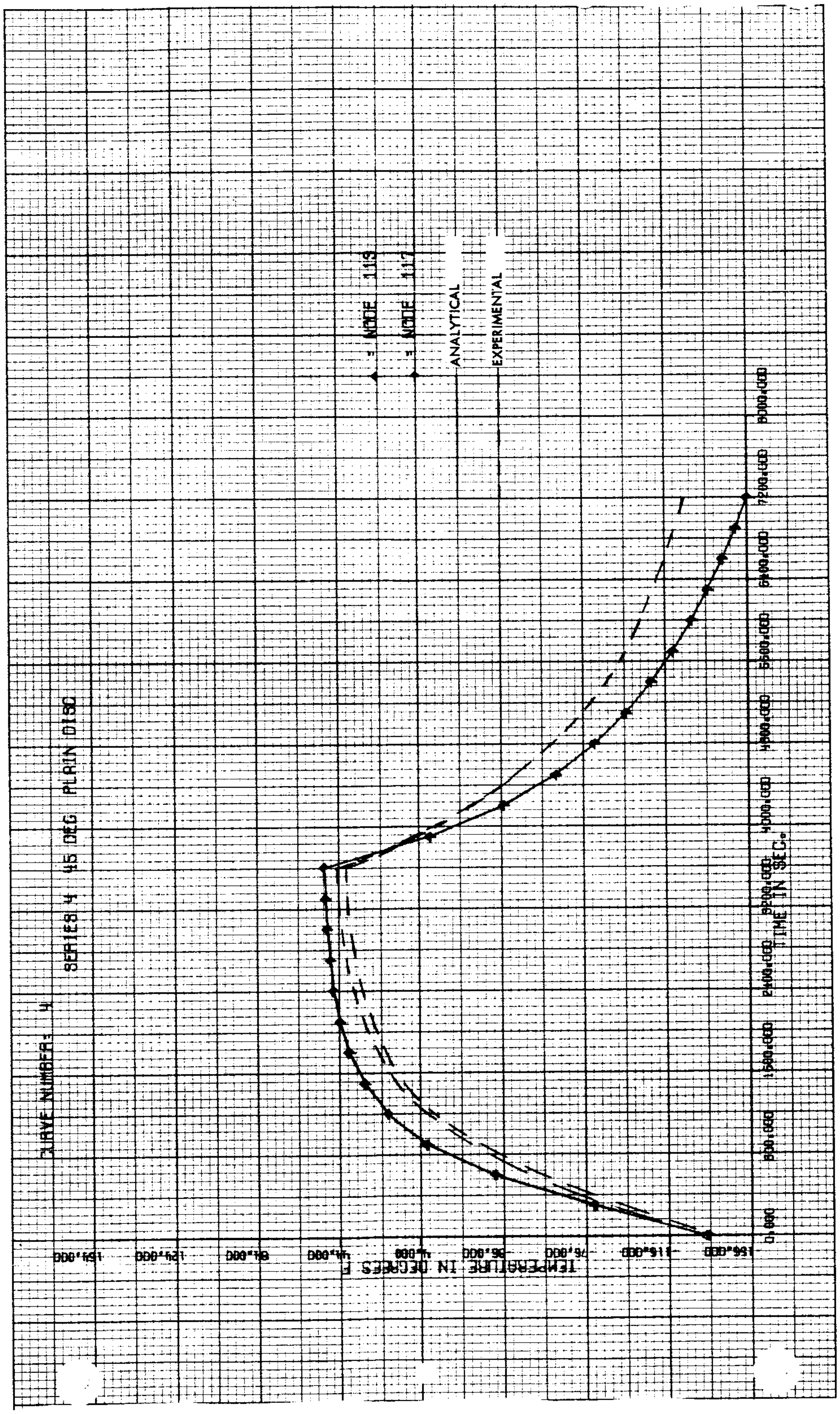

Figure 5-13 Cone Temperature Histories (Nodes 113 and 117), 45 Degree Orientation, Plain Disc

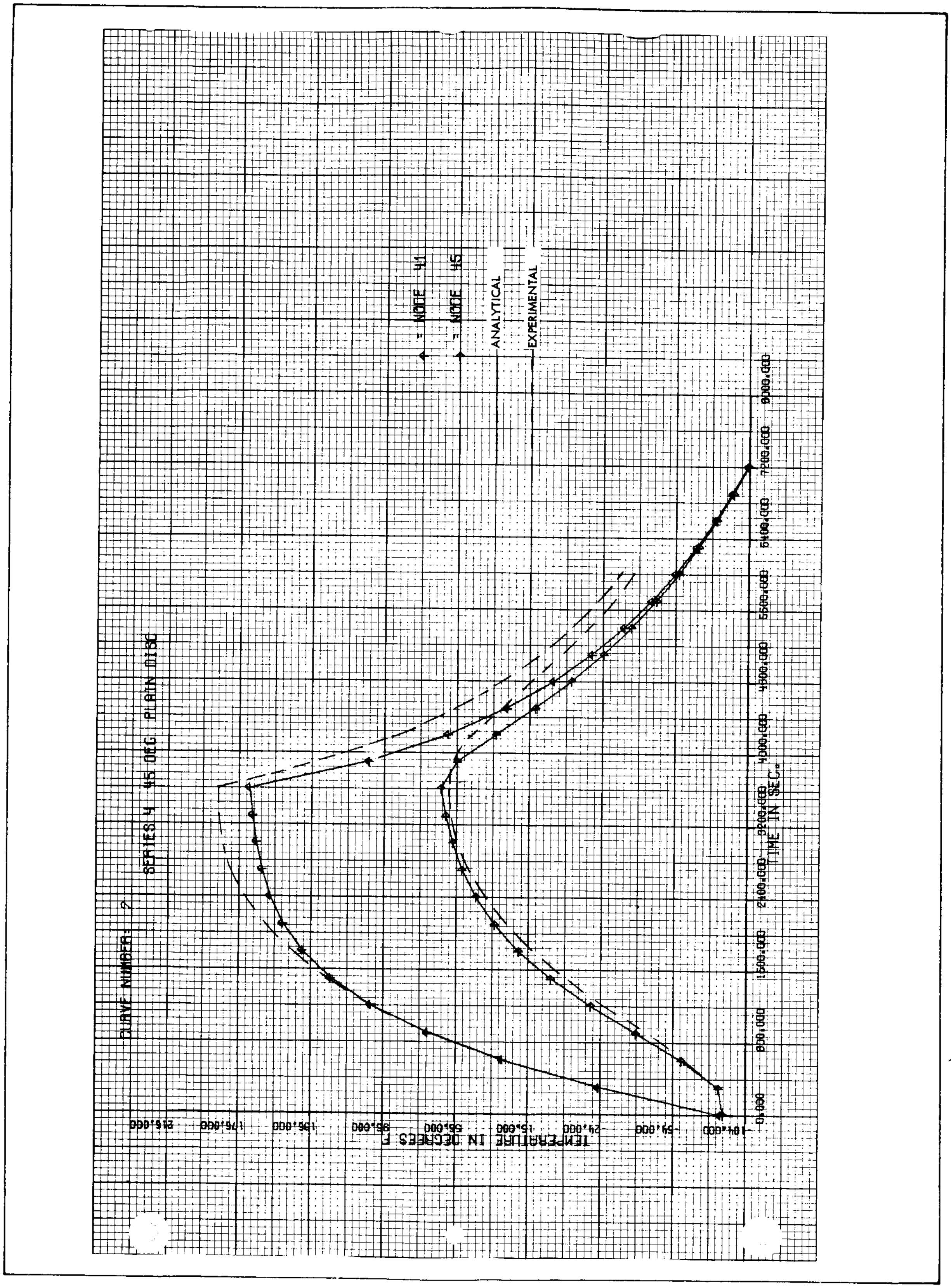

Figure 5-14 Plain Disc Temperature Histories (Nodes 41 and 45), 45 Degree Orientation

LOCKHEED
CALIFORNIA COMPANY

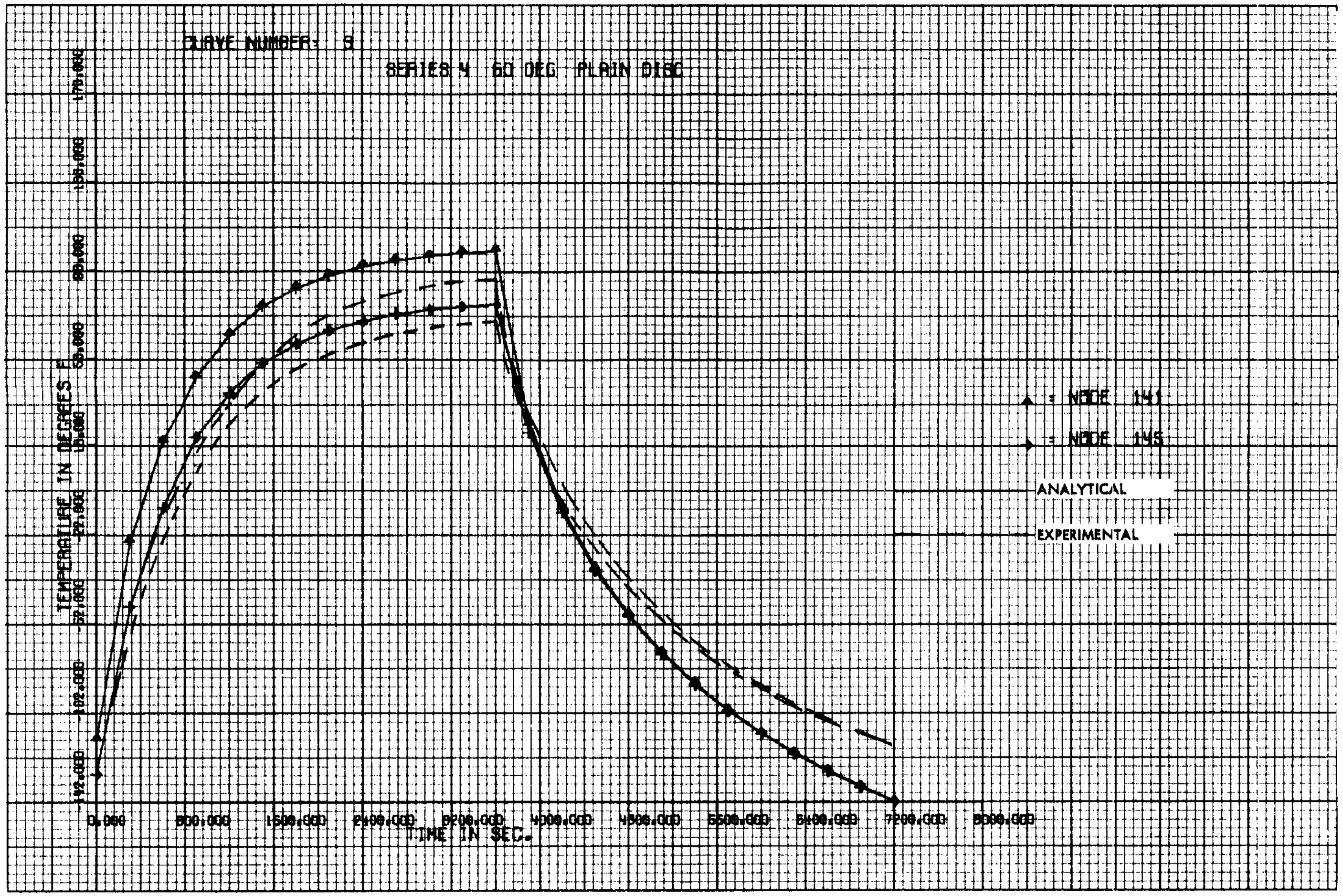

Figure 5-15 Cone Temperature Histories (Nodes 141 and 145), 60 Degree Orientation, Plain Disc

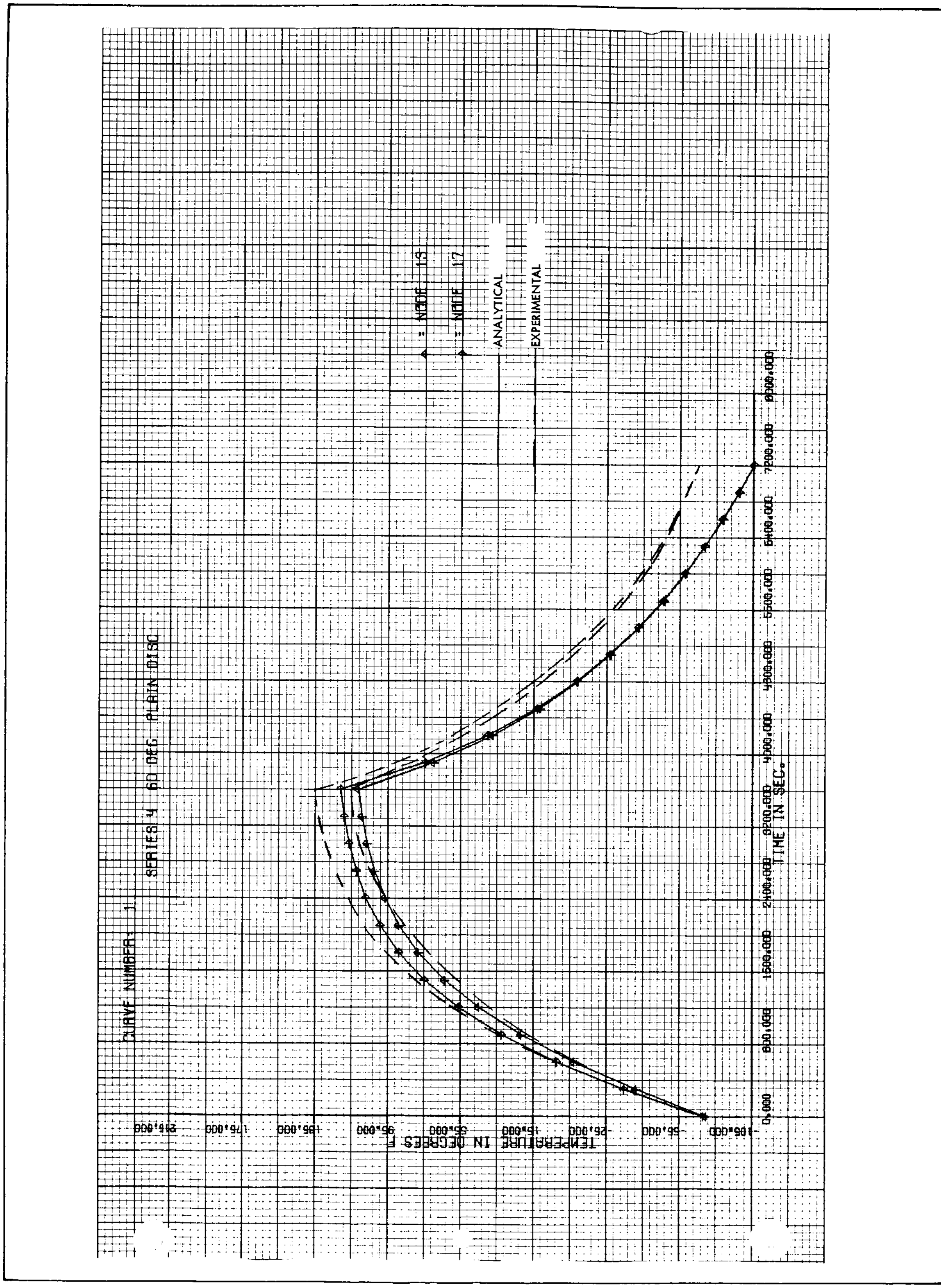

Figure 5-16 Plain Disc Temperature Histories (Nodes 13 and 17), 60 Degree Orientation

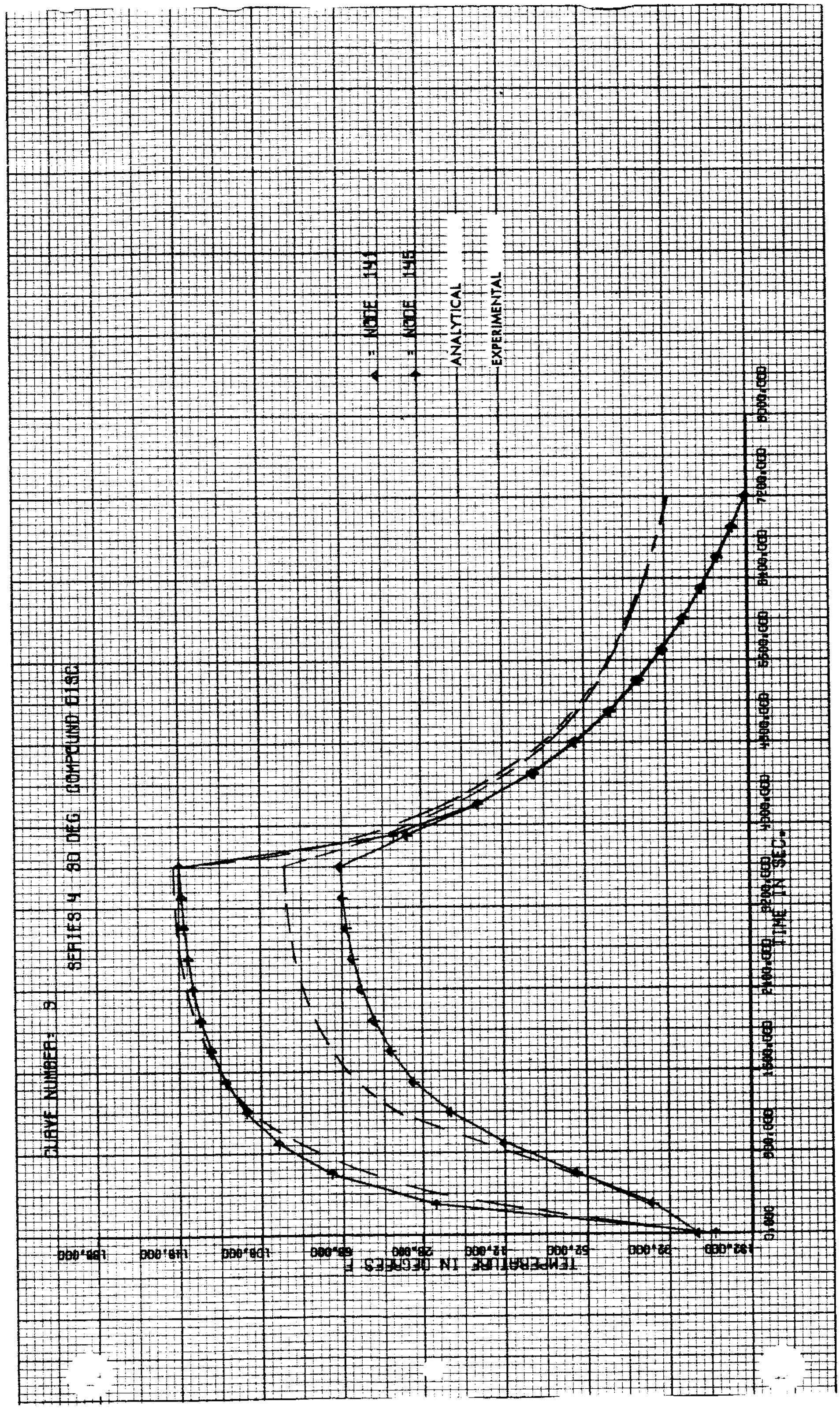

Figure 5-17 Cone Temperature Histories (Nodes 141 and 145), 30 Degree Orientation, Compound Disc

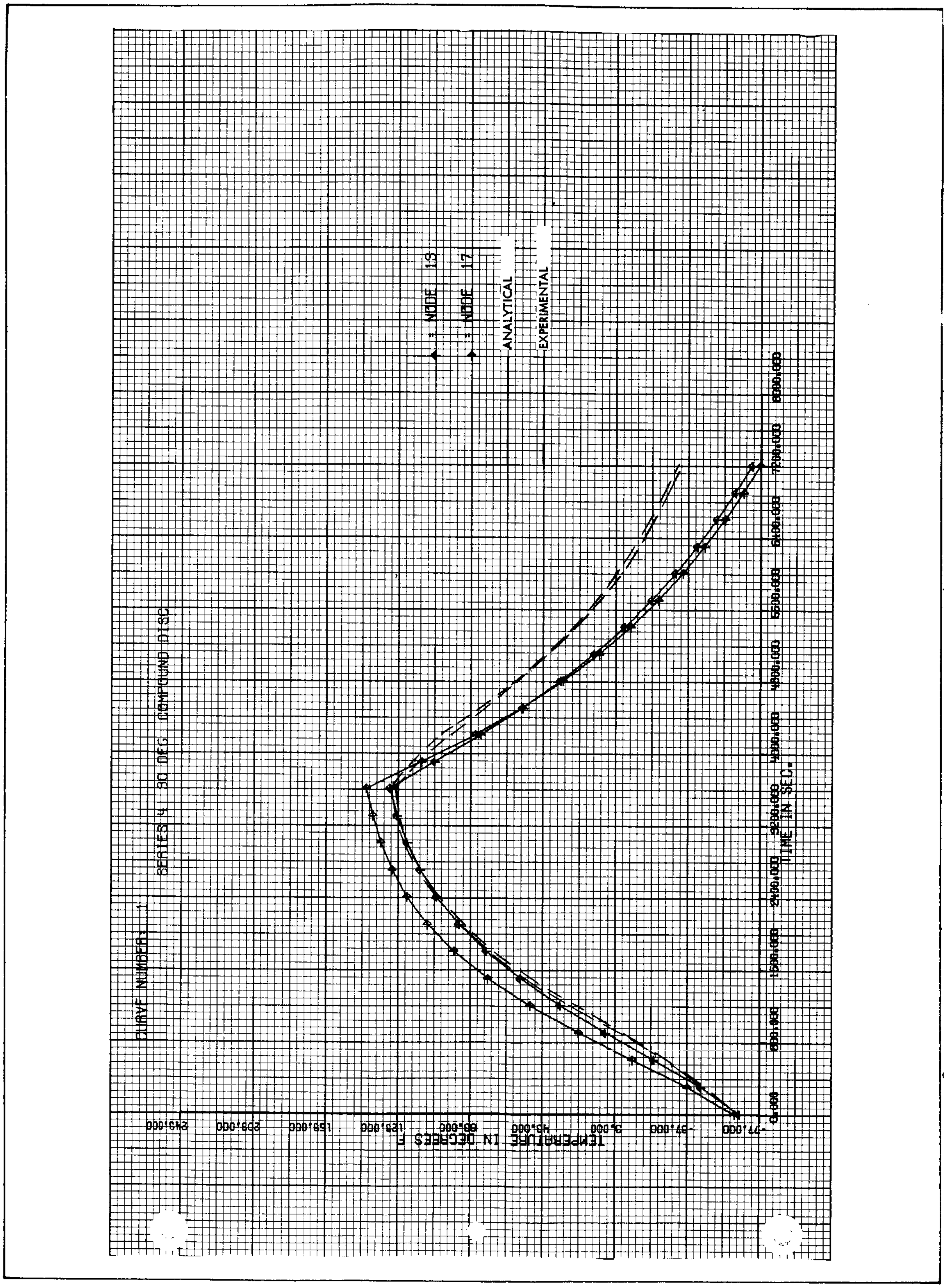

Figure 5-18 Compound Disc Temperature Histories (Nodes 13 and 17), 30 Degree Orientation

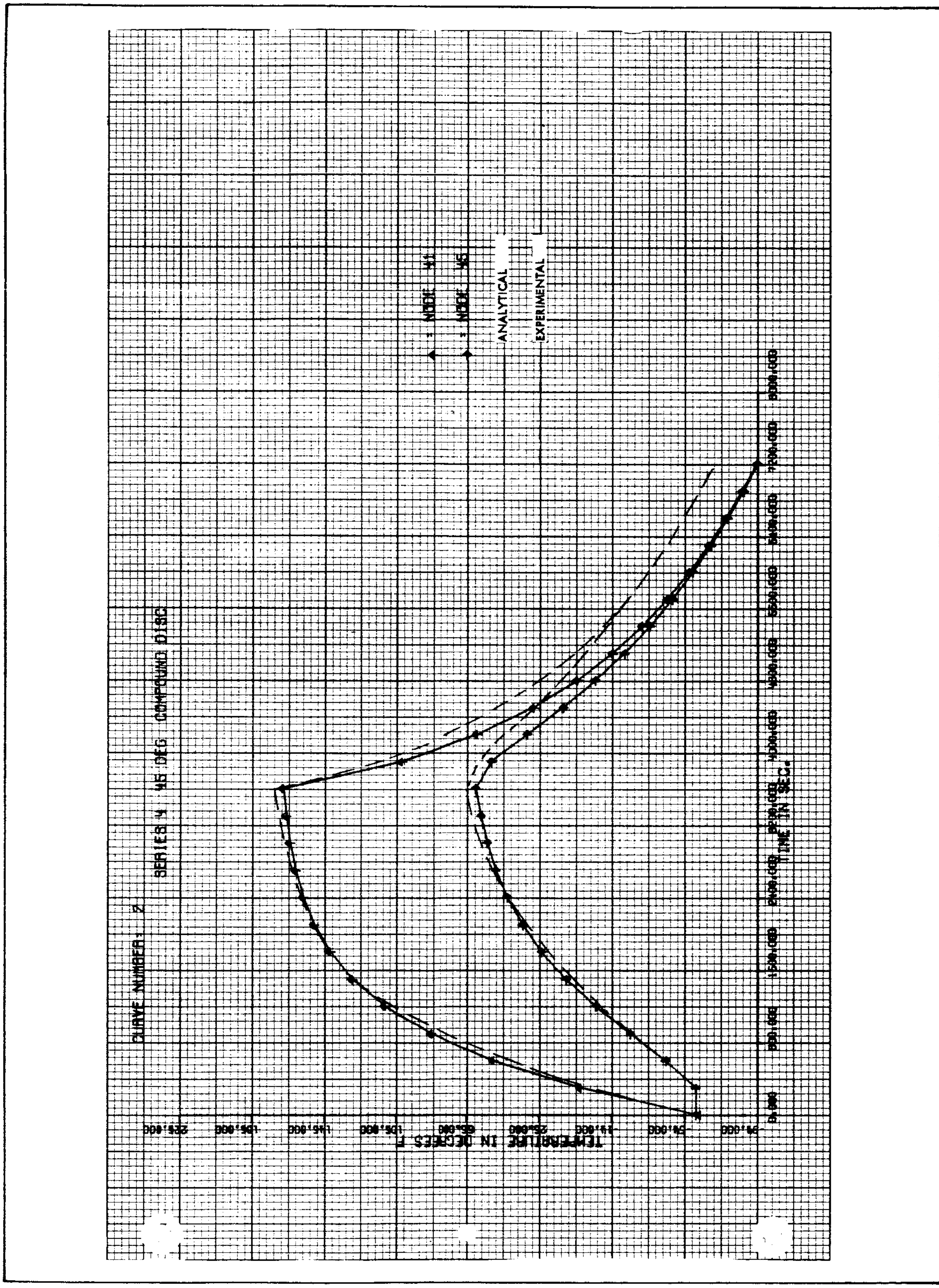

Figure 5-19 Compound Disc Temperature Histories (Nodes 41 and 45), 45 Degree Orientation

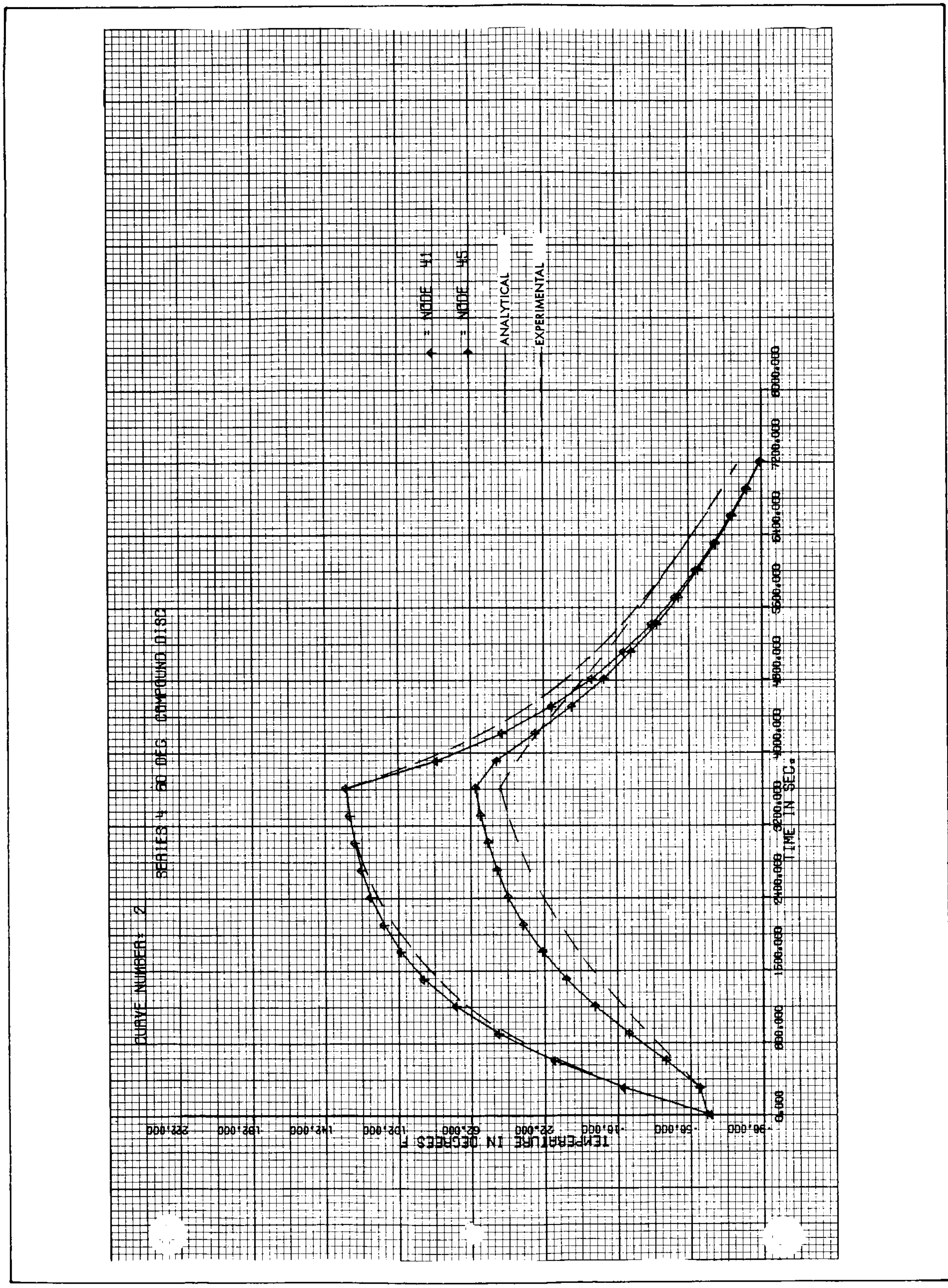

Figure 5-20 Compound Disc Temperature Histories (Nodes 41 and 45), 60 Degree Orientation

VI - SERIES 5 MODEL

MODEL DESCRIPTION

In preparation for the Series 5 tests in the Hughes chamber, it was necessary to modify the model plumbing so that the tanks would drain properly in the horizontal position. In this position (Figure 6-1) the solar flux from the simulator in the top of the Hughes chamber was normal to the model axis. Except for the modification to the plumbing, the Series 5 model was essentially the same as the Series 3 model.

Propellant System Modifications

Upon completion of the Series 3 tests, the tank flanges were removed in order to replace the standpipes and add new drain tubes. The standpipes were replaced with long tubes having a right angle bend at one end (Figure 6-2). Short tubes, bent at a right angle and positioned so that after installation the open ends would be at the lowest point within the tanks, were connected to the drain fittings on the tank flanges. The 3/8 in. diameter teflon rod (Figure 6-2) supporting the thermocouples was, in turn, supported by the stiffer 1/4 in. diameter stainless steel tube.

Support of Model in Hughes Chamber

A special supporting fixture was designed and fabricated by Hughes Aircraft Co. personnel to permit mounting the model on the end-bell of their C-4S chamber. The fixture provided for inclining the model two degrees from the horizontal, with the nozzle end down to promote drainage. It was constructed from 2 by 2 by 1/4 in. aluminum angles (6061-T6), using bolted connections (Figure 6-3). The assembled fixture was painted with 3-M Black Velvet (Minnesota Mining & Mfg. Co.), which had an emissivity of .88 to .90. The model was

Figure 6-1 The Series 5 Model on the End-Bell of the C-4 Chamber at Hughes

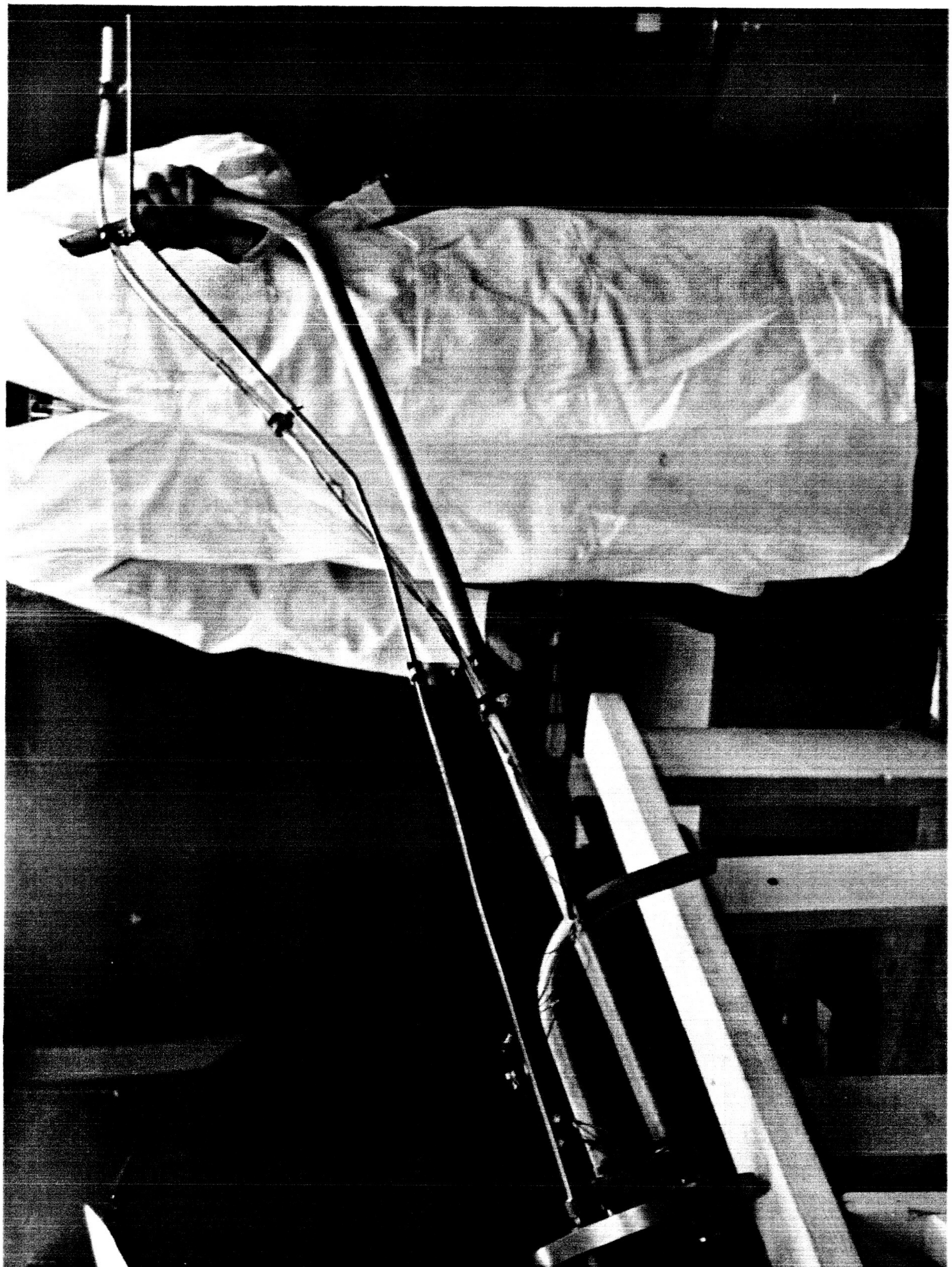

Figure 6-2 Special Standpipes for the Series 5 Tanks

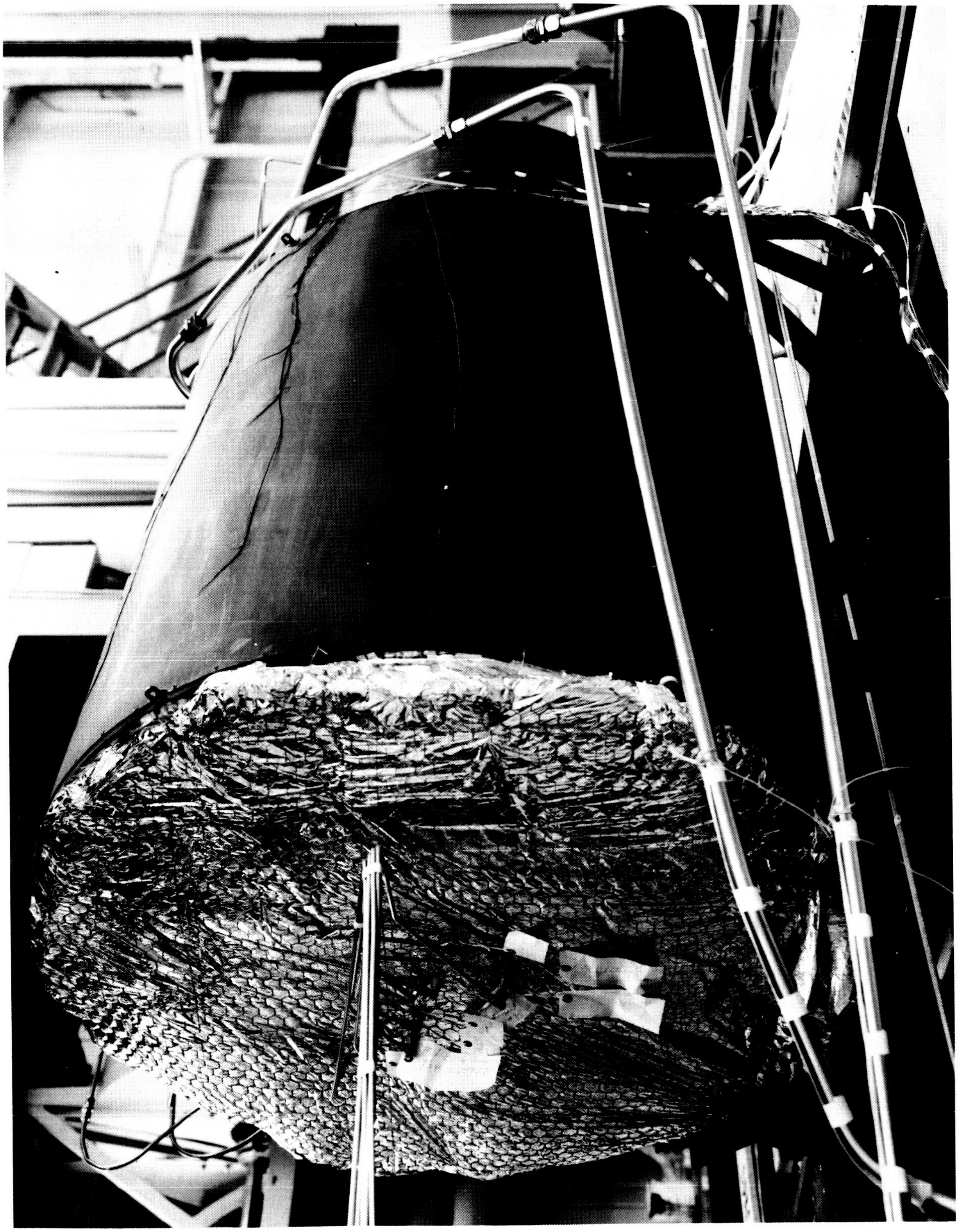

Figure 6-3 Model Support and Insulated Forward Bulkhead

attached to the support fixture with 5/16 in. diameter bolts through two eyebolts in each bulkhead. Teflon insulating spacers, 0.282 in. thick, were installed between the eyebolt and mating fixture angle, and teflon washers, 0.094 in. thick, were placed under the heads of the 5/16 in. diameter attaching bolts to minimize conductive heat transfer between the model and support fixture. In addition, 1/4 by 3 by 4 in. teflon pads were inserted under the four corners of the support fixture to insulate it from the cross-beams on the chamber end-bell.

Plumbing Penetrations

Hughes Aircraft Co. furnished a penetration flange which was modified by Lockheed to accommodate ten 1/4 in. lines, two 1 in. lines, and two Conax thermocouple wire feed-through receptacles. Of the ten 1/4 in. lines, seven were used for pressure sensing purposes, two for propellant tank venting, and one for the dual purpose of filling and venting the helium gas bottles. Of the two 1 in. lines, one was used for the fuel tank charging and expulsion, the other for charging and expulsion of the oxidizer tank. The schematic drawing (Fig. D-5) of the plumbing installation is included in Appendix D.

Power Supplies

All power supply units used on the Series 3 tests for the various heat sources within the model were transported from the Lockheed Rye Canyon facilities to the Hughes El Segundo facilities for use on the Series 5 test.

INSTRUMENTATION

No additional thermocouples were added to the Series 3 model for the Series 5 tests. The number of pressure transducers also remained unchanged.

Temperature Measurement

The copper-constantan thermocouple leads from the model were connected through existing chamber penetrations to one of two 300-channel remote stations. The feed-through connectors were identical to those used in the earlier tests in the Lockheed C-5 chamber. The remote stations contained 32°F reference junctions for the copper-constantan thermocouples, a scanner switch, and a 1000:1 solid-state amplifier which amplified the difference signal. The signal was then fed to a Kin Tel system consisting of a crossbar scanner, digital voltmeter, digital clock, control circuits, BCD translator, tape perforator, junction box, and card punch connector. This system is described in more detail in Appendix A. The iron-constantan thermocouple leads were brought out of the chamber through Conax feed-throughs. Outside the chamber, the iron leg of the couple was joined to a copper lead. The junction was placed in a 32°F reference bath outside the Hughes remote station. The thermocouple installation was then compatible with the Hughes system. The net effect of this external iron-copper reference junction, combined with the internal copper-constantan reference junction within the remote station, was to provide an iron-constantan reference bath for these couples.

Pressure Measurement

Pressure measurements were made in the same manner as described in Section 4 with the exception that one of the copper leads for each transducer from the Wiancko unit was joined to a constantan wire to make the system compatible with the Hughes data acquisition system. These junctions were placed in a 32°F reference bath external to the Hughes remote station. This external junction served to cancel the effects of the internal junction located in the 32°F reference oven within the remote station. These modifications were necessary in order to record pressure data on the Hughes data system, which has been designed for copper-constantan thermocouple output.

Flow Measurement

The flow rates were measured with sharp-edged orifices in the same manner as described in Section 4 for the Series 3 model.

Solar Flux Monitoring

The solar flux was sensed by two water-cooled Eppley Model 20 radiometers (Serial 5509A and 5510A), calibrated for vaccum application. These instruments are shown in Figures 6-1 and 6-4. The solar radiation data were recorded on Honeywell Electronik 17 strip chart recorders.

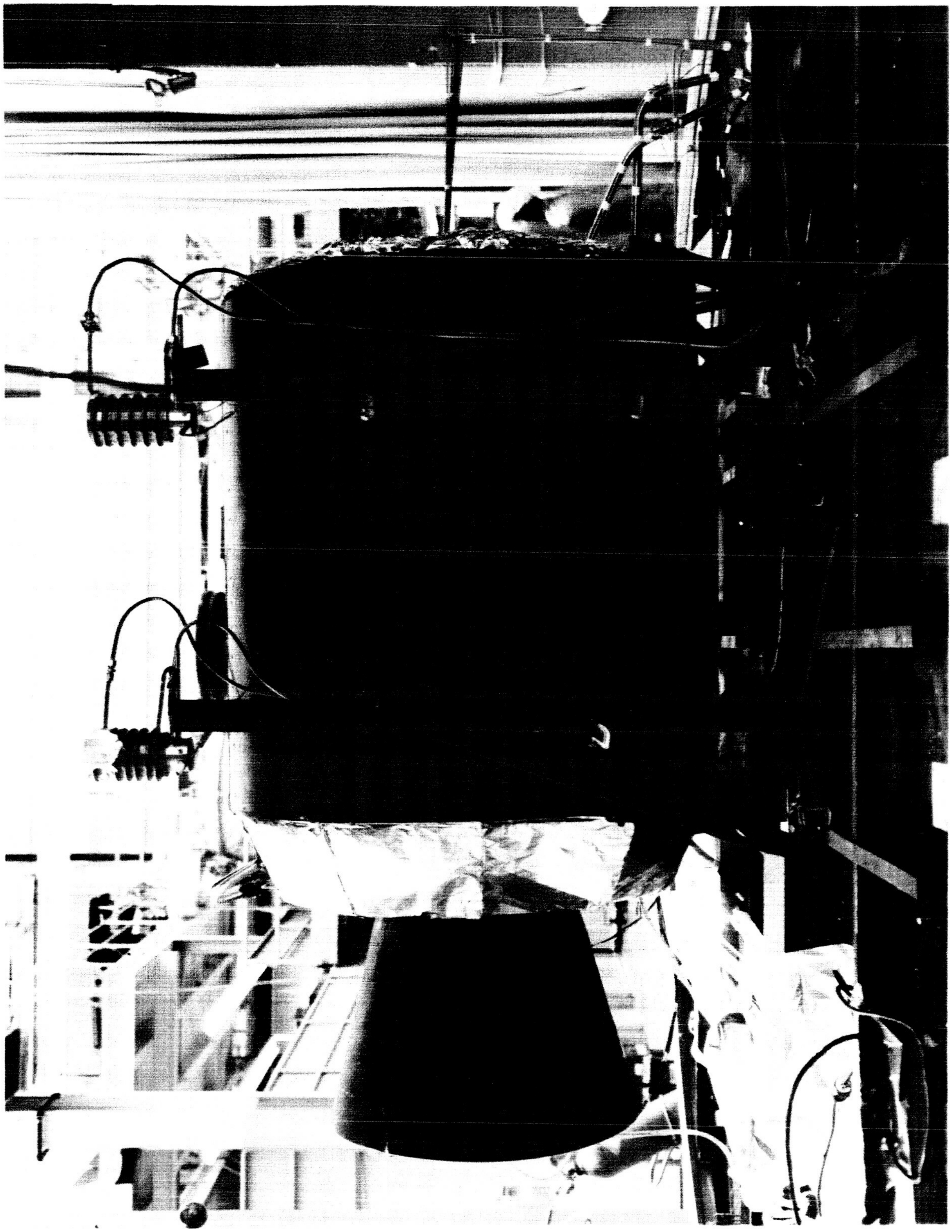

Figure 6-4 Series 5 Model Indicating Support Structure and Eppley Radiometers

TEST IN THE HUGHES CHAMBER

The Series 5 model was tested in the Hughes C-4S chamber.

Test Preparation and Checkout

The model was mounted on the special support fixture, furnished by Hughes, as described previously. After the model had been positioned on the chamber end-bell (Figure 6-1), plumbing lines were connected to a feed-through flange on the forward end of the model. After the lines had been capped off at the flange, the helium bottles were charged with Freon 12 and dry nitrogen gas to 1200 psig. A leakage check of all the lines was made in a manner similar to that described for the Series 3 test in Section 4.

All accessible thermocouples connected to the Hughes Kin Tel system were checked for continuity, polarity, and channel matching by heating each individual thermocouple with a portable heater-blower. Heaters and heat source monitor couples were checked for operation and location. Cooling water lines from the chamber feed-through flange were then connected to the Eppley radiometers. After removing the platform and tools used in setup and checkout, the end-bell was vacuum cleaned. The end-bell with the model was then raised, closing the chamber.

After the propellant reservoirs had been located below the raised end-bell (Figure 6-5), plumbing connections were made to the tanks within the model. The 11 Wiancko pressure transducers described in Section 4.2.3 were connected to the fittings on the chamber feed-through flange. Pressure gauges for monitoring were connected in parallel with the transducers. These gauges can be seen behind the hydraulic cylinder in Figure 6-5. A leakage check of these lines was then made. While the external plumbing was being installed, electrical checkout of the thermocouples and heaters continued. At this point, chamber evacuation was initiated. An electrical checkout of the nozzle heaters was still in process and corona effects burned out one of the power feed-through connections. The chamber was repressurized and access gained through a side door at the mezzanine level. Inspection showed that one of the power receptacle pins on the inside of the chamber feed-through flange had

Figure 6-5 Support Equipment Below the Raised Chamber End-Bell

grounded by welding itself to its case. This condition was corrected, the chamber resealed, and the pumps restarted after a 6-hour delay. During this time checkout of the electrical equipment and the plumbing installation had been completed. The transducer calibrations were then rechecked. The helium bottles were charged to 1500 psig with helium gas after first being evacuated with a small vacuum pump. Ninety-three gallons of Freon 11 were transferred into the oxidizer tanks, and 73 gallons of the glycol-water mixture were pumped into the fuel tanks of the model.

Liquid nitrogen was introduced into the chamber shroud after the chamber pressure had reached approximately 10 torr (one hour on the roughing pumps). Four and a half hours later the average shroud temperature reached -290°F. The shift from the roughing pumps to the diffusion pumps was made when the chamber pressure reached 3×10^{-1} torr, after about 2-3/4 hours of rough pumping. A chamber pressure of 2×10^{-6} torr was attained 4 hours after the starting of the roughing pumps. The solar simulator was turned on at 6 hours after the start of the roughing pumps. The eclipse device prevented the solar flux from impinging on the model during the warm-up period.

The 28-Hour Test

After a half-hour solar simulator warm-up period, the eclipse device was removed, initiating the start of the 28-hour test run. The eclipse device was a large water-cooled horizontal platform used to intercept the 8 ft. diameter solar simulator beam just above the quartz windows in the chamber ceiling. This device was inserted and removed with a traveling overhead crane.

The test operational sequence, listing the data-taking schedule, is shown in Table 6-1. The actual test started with the step 5 stabilization period. The 28-hour test schedule is also shown graphically in Figure 6-6, with actual temperatures recorded for the sector I outer cylinder node 94, nozzle temperature node 313, and the thrust chamber temperature node 319. The exact locations of these nodes are given in Appendix E. As shown in Figure 6-6, the 10-hour temperature stabilization period was followed by 3 cycles, each involving 90 minutes of eclipse mode, followed by 90 minutes of solar simulation. Near the end of the 10-hour temperature stabilization period, a

TABLE 6-1 TEST OPERATIONAL SEQUENCE

Step No.	Approximate Time Total	Approximate Time Step	Sequence Description	C-4S Facility	KinTel/I.B.M.	Test Article
1.	0		Pumpdown	Initiated pumpdown per standard operating procedure	Turn system on. Synchronize time with C-4S console. Scan data points as needed.	
2.	7 hr.		Prepare for Solar Simulator.	Set ductstats; turn on solar grid heaters.		
3.	8 hr.		Childown	Initiate LN_2 mode. Achieve and maintain max., cold wall & vac.		
4.	9 hr.	1/2 hr.	Solar-Thermal-Vacuum.	Turn on solar simulator blowers and power supplies. Adjust ductstats. Turn off grid heaters. With eclipse device in place, turn on lamps. When lamps are up to power, remove eclipse device. 130 watts/ft^2 required at test plane.	Begin scanning all points every 10 min.	
5.	9-1/2 hr.	10 hr.	Stabilization	Maintain 130 watts/ft^2 max. cold wall and max. vacuum	Scan all points every 10 min.	Stabilization
6.	19-1/2 hr.	9 hr.	Test Article Functional Phase. (See Lockheed Test Plan.)	Maintain above conditions. Eclipse sun for 1-1/2 hrs, followed by "sun on" for 1-1/2 hrs. Repeat for a total of 3 times.	Scan continuously 40 selected points during dumping cycles; scan all points every 10 min. between dumping cycles.	Three dumping cycles, during which liquid is discharged from tanks and nozzle is heated.
7.	28-1/2 hr.	9 hr.	Cooldown	Eclipse sun, then turn off solar simulator per standard operating procedures. Take radiometer tare readings. Maintain max. cold wall and vacuum.	Scan all points every 10 min.	Cooldown phase.
8.	37-1/2 hr.		Shutdown	Warm chamber shrouds. Dive chamber per standard operating procedures. Take final readings.	Scan all points as needed.	

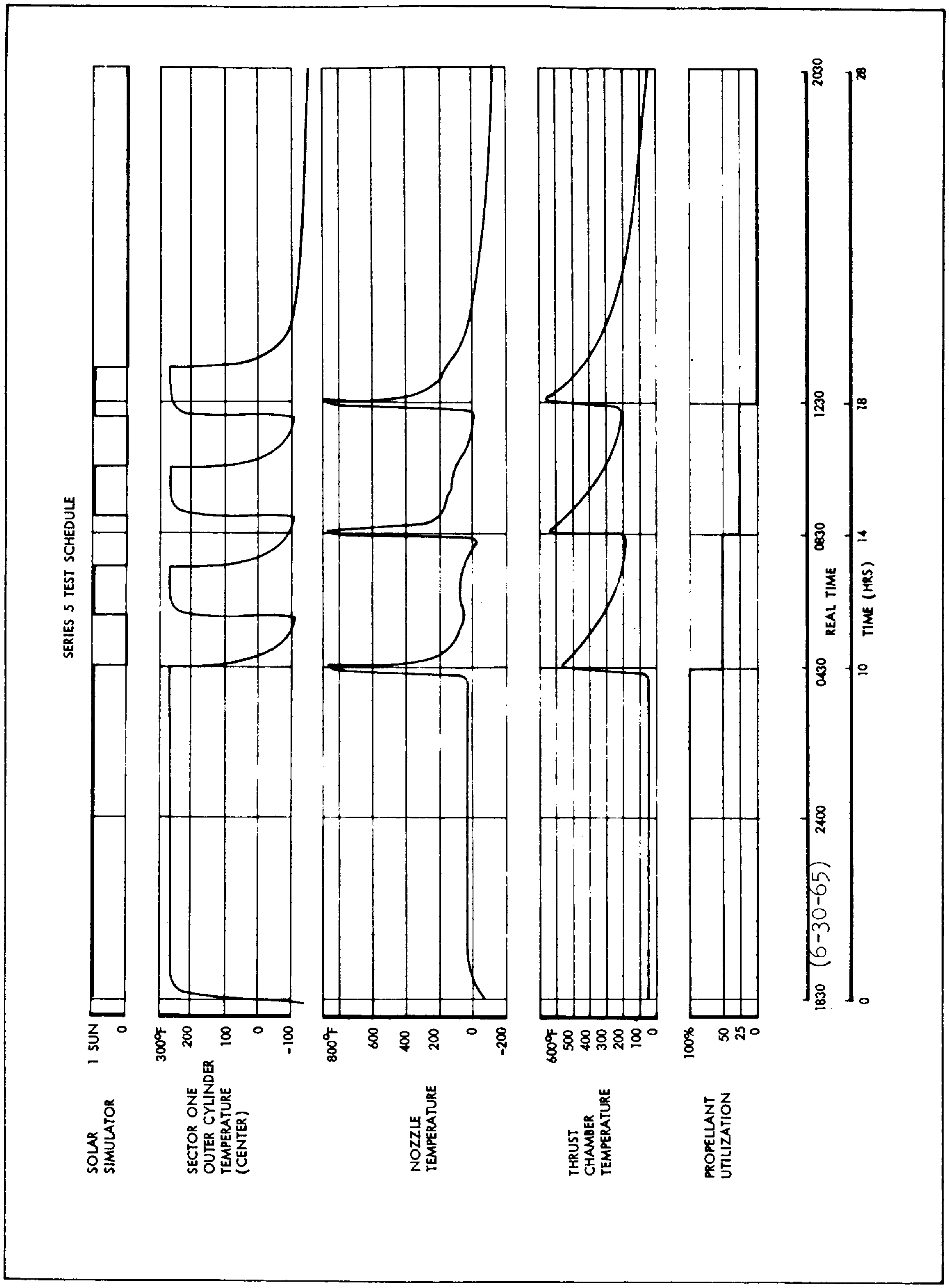

Figure 6-6 Series 5 Test Schedule

leak in the helium instrumentation line was suspected, since the bottle pressure dropped about 150 psi. However, the test was continued, since this small leakage was considered not great enough to affect fuel expulsion.

During the eclipse mode, the simulator was actually left on, but its beam was blocked by the eclipse device. A picture of the model in the chamber, taken with solar simulator lighting only, is shown in Figure 6-7.

In addition to the eclipse events, 3 simulated engine firings were performed during the test, complete with tank expulsion and nozzle and thrust chamber heating. The first simulated firing was performed on the 10th hour of the test run. At this time, half of the simulated propellants were expelled during a 4 min. period. The remainder of the simulated propellants were expelled in two additional "firings", spaced 4 hours apart. The same expulsion rate was maintained for all expulsion cycles. The nozzle and thrust chamber heaters were turned on approximately 10 minutes in advance of each expulsion cycle. This time was required to reach the 950°F desired nozzle temperature and the 600°F thrust chamber temperature at the time of expulsion. These temperatures were maintained during the expulsion and the power was turned off with the termination of expulsion. After the final solar simulator cycle, the model was permitted to cool down for a 9-hour period before terminating the test run.

During the 28-hour test period, the chamber vacuum varied between 3.0×10^{-6} and 2.1×10^{-6} torr, the temperature of the chamber wall and bottom averaged approximately -300°F, and the simulated solar radiation intensity was approximately 125 watts/sq.ft.

ANALYTICAL CORRELATION

Series 5 Network

The Series 5 network is identical to the Series 3 insulated network. Instead of imposing measured boundary temperatures on the hot side outer panels however, a programmed solar heat flux was specified for these nodes.

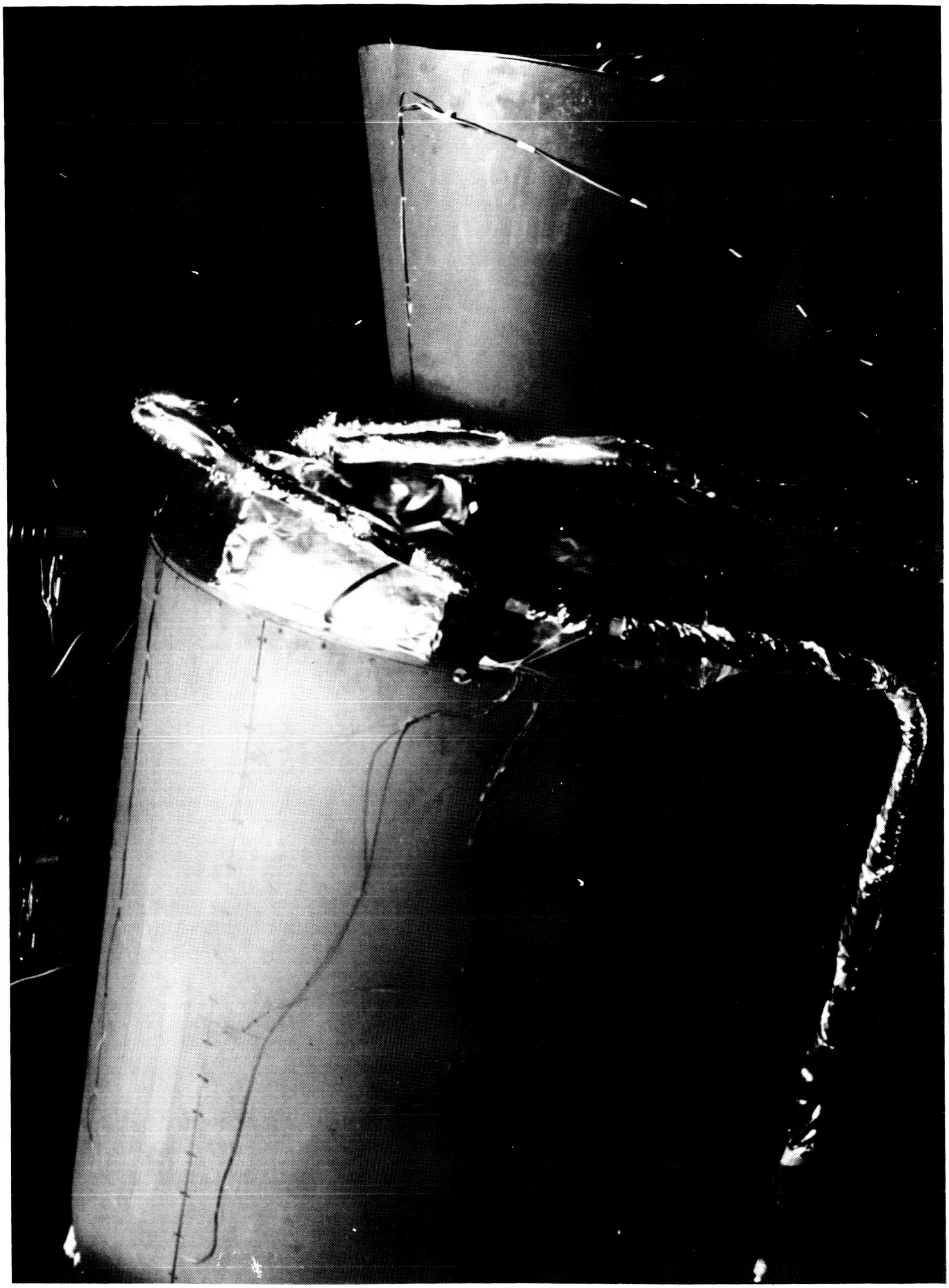

Figure 6-7 Model as Seen through Chamber Window During Series 5 Test

Radiation resistors to the chamber were added for these nodes bringing the total number of external radiation resistors to 96. The number of nodes remained at 260 and the number of resistors at 505 for conduction and 280 for internal radiation.

Run Correlation

The overall correlation of the Series 5 temperature data is presented in the same form used for Series 3. Figures 6-8 to 6-10 show these results. The times chosen to present the data are 34,800 seconds, steady state; 67,800 seconds, transients; and 100,800 seconds, cool down. For the steady state time, 85 percent of the predicted temperatures fall within ±20°F of the measured temperatures. For the transient time, there is more scatter of data and a trend of low predicted temperatures as seen from Figure 6-10. Only 65 percent of the predicted temperatures lies within ±20°F of the measured values. However, 85 percent of the predicted temperatures lies within +15°F and -30°F of the measured temperatures. The reason the downward shift for the Series 5 transient is not as pronounced as the Series 3-22 transient is that temperatures of the nodes at the intersection of the bulkhead and outer panel on the hot side of the model are overpredicted. These nodes were boundary conditions for Series 3.

As seen from Figure 6-8, predicted temperatures of the panel nodes are typically lower than measured except during the final cool down period. During cool down, the solar simulator is turned off and this causes the chamber temperature, especially on the floor, to be cooler than the assumed cold wall temperature. Analytical temperatures of the panel nodes that received solar heating are all within ±18°F of the measured temperatures.

Analytical and experimental temperatures for representative nodes in the various regions of the model are summarized in Table 6-2. These data are taken at two time points from the temperature histories presented in Figures 6-11 to 6-25. The 35,000 second time point represents steady-state conditions just prior to the first simulated engine firing, and the 68,000 second time

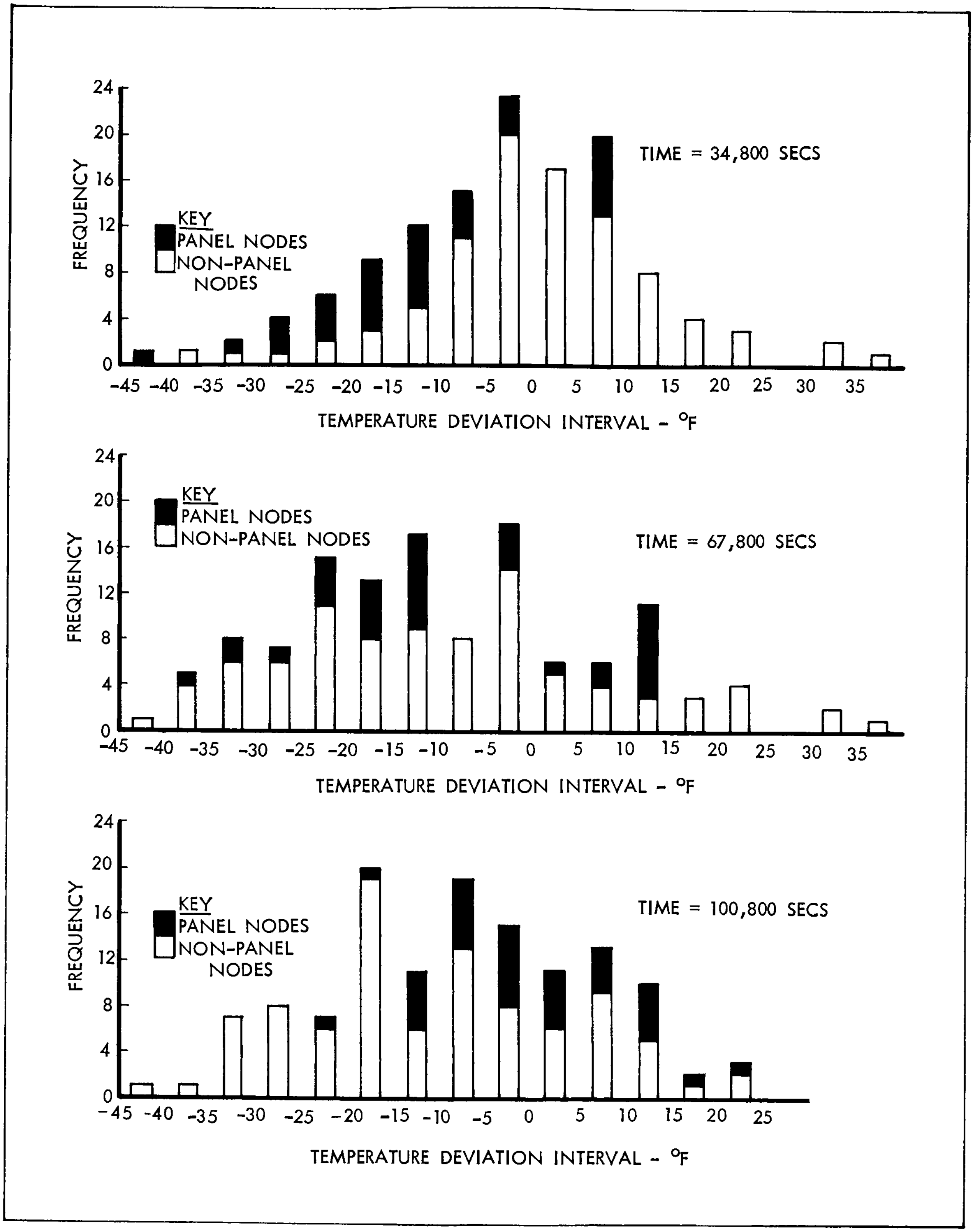

Figure 6-8 Analytical and Experimental Temperature Deviation Distribution

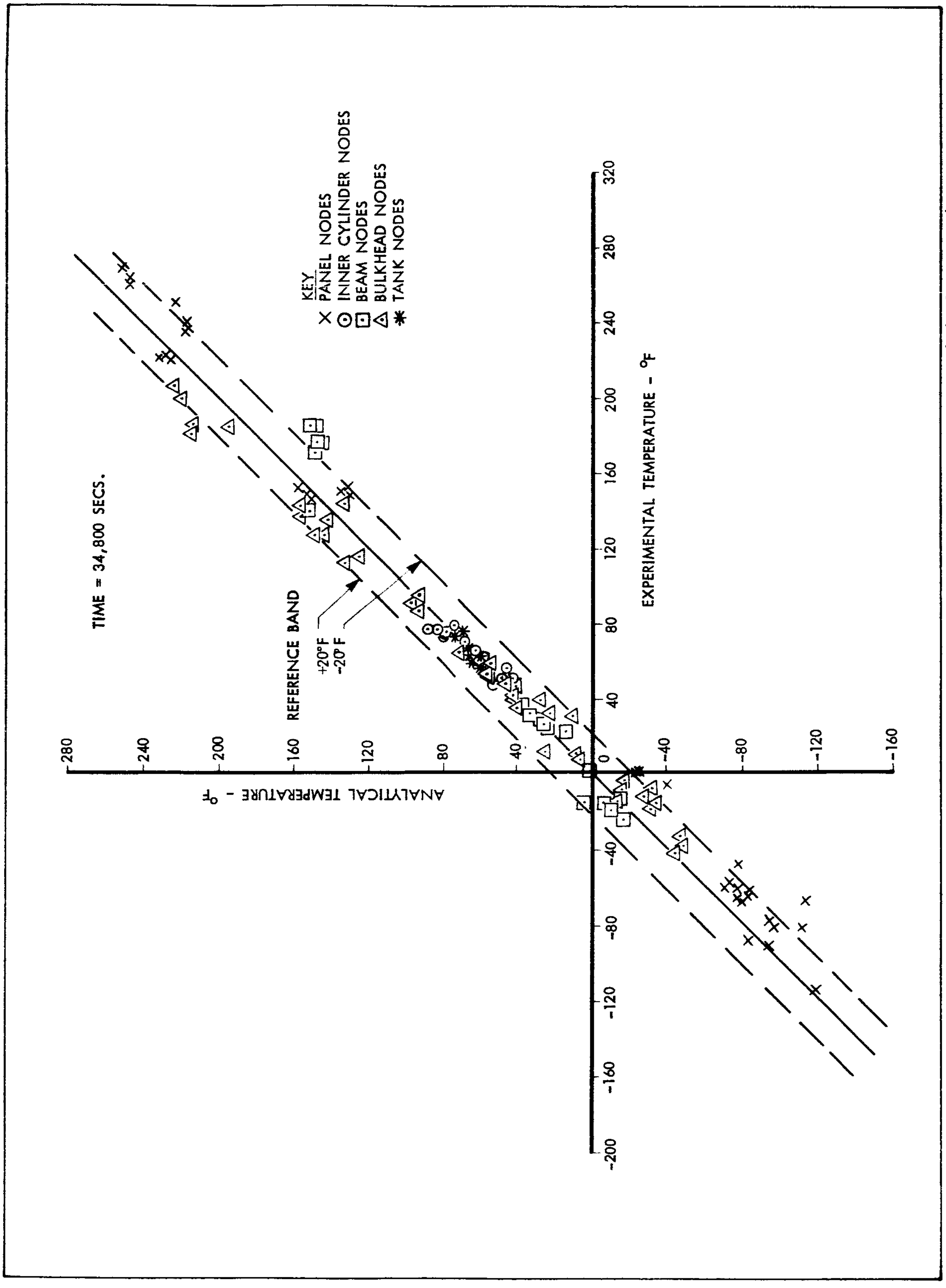

Figure 6-9 Correlation of Analytical And Experimental Data (34,800 SEC)

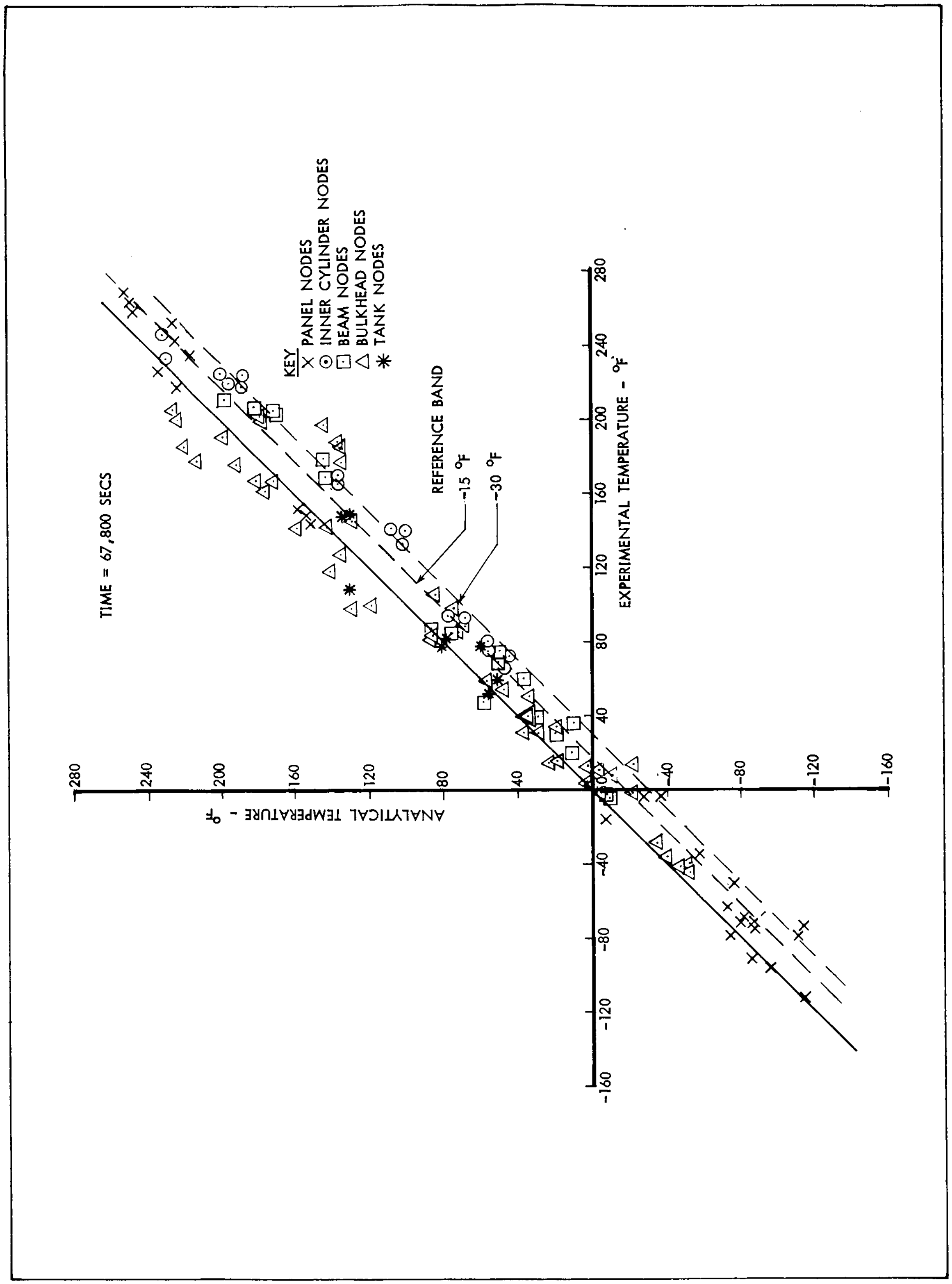

Figure 6-10 Correlation of Analytical and Experimental Data (67,800 sec)

TABLE 6-2 GUIDE TO SELECTED PLOTS FOR SERIES 5

Node Location and Number	Reference Figure	Temp. at 35,000 secs.		Temp. at 68,000 secs.	
		Analytical	Experimental	Analytical	Experimental
Outer Panel					
311-Cold Side, Sector IV	6-11	-118	-115	-113	-111
323-Hot Side	6-12	253	271	254	270
Bulkheads					
73-Lower, Hot Side, Sector I	6-13	157	138	183	169
125-Upper, Hot Side, Between Sectors I & II	6-14	94	95	86	86
Inner Cylinder					
225-Hot Side, Between Sectors I & II	6-15	80	75	78	94
331-Cold Side, Between Sectors IV & V	6-16	43	51	100	138
Radial Beam					
340-Beam 4, Cold Side	6-17	-16	-13	10	35
437-Beam 1, Hot Side	6-18	148	171	199	211
Heat Shield					
382-Hot Side	6-19	120	163	157	147
Helium Bottles					
391-Lower Bottle	6-20	59	57	132	110
392-Upper Bottle	6-21	63	58	52	60
Propellant Tanks					
394-Oxidizer, Sector II	6-22	69	72	79	84
395-Fuel, Sector III	6-23	66	67	56	53
396-Fuel, Sector VI	6-24	73	72	81	77
397-Oxidizer, Sector V	6-25	65	62	60	76

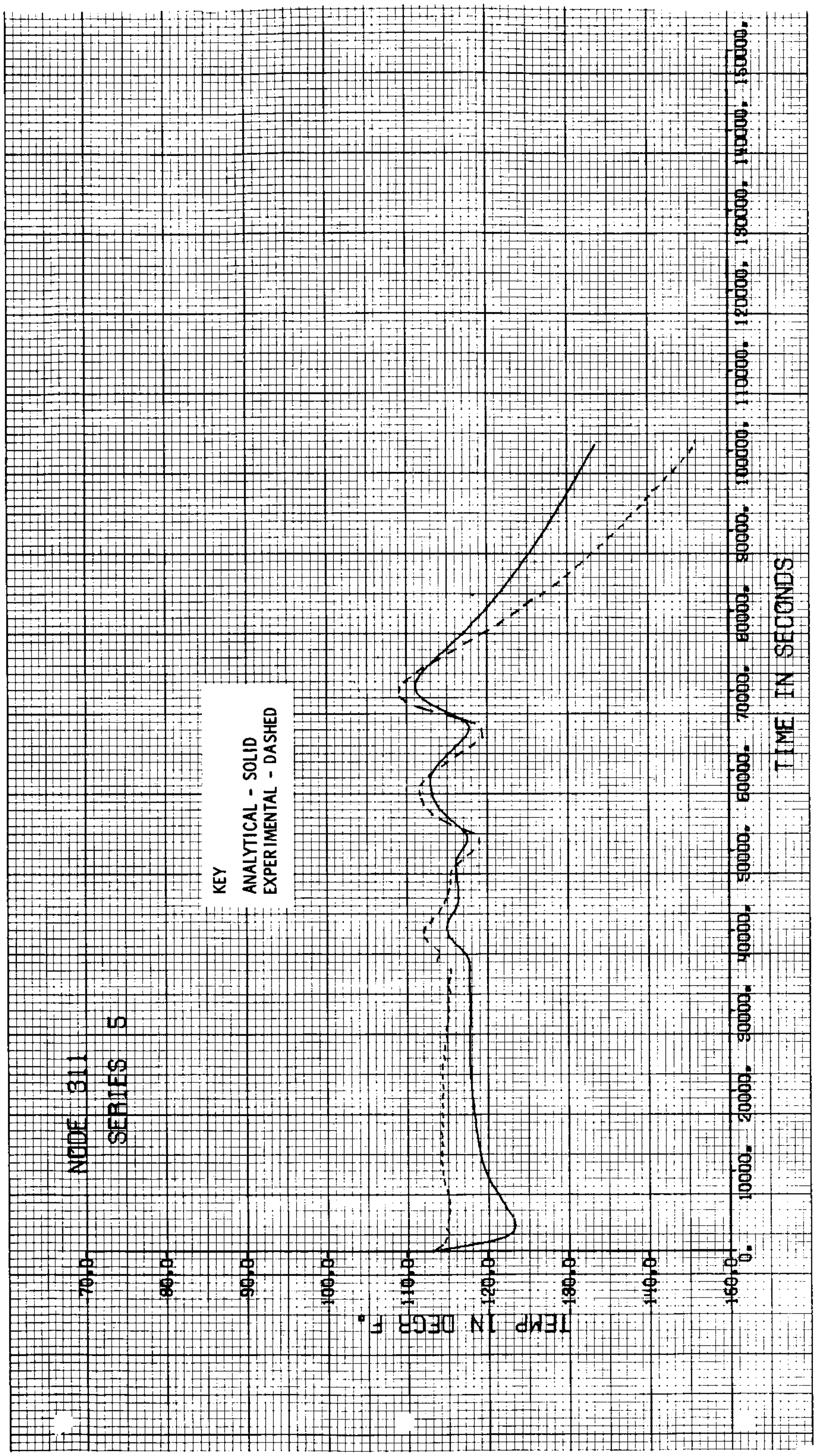

Figure 6-11 Panel Temperature History (Node 311)

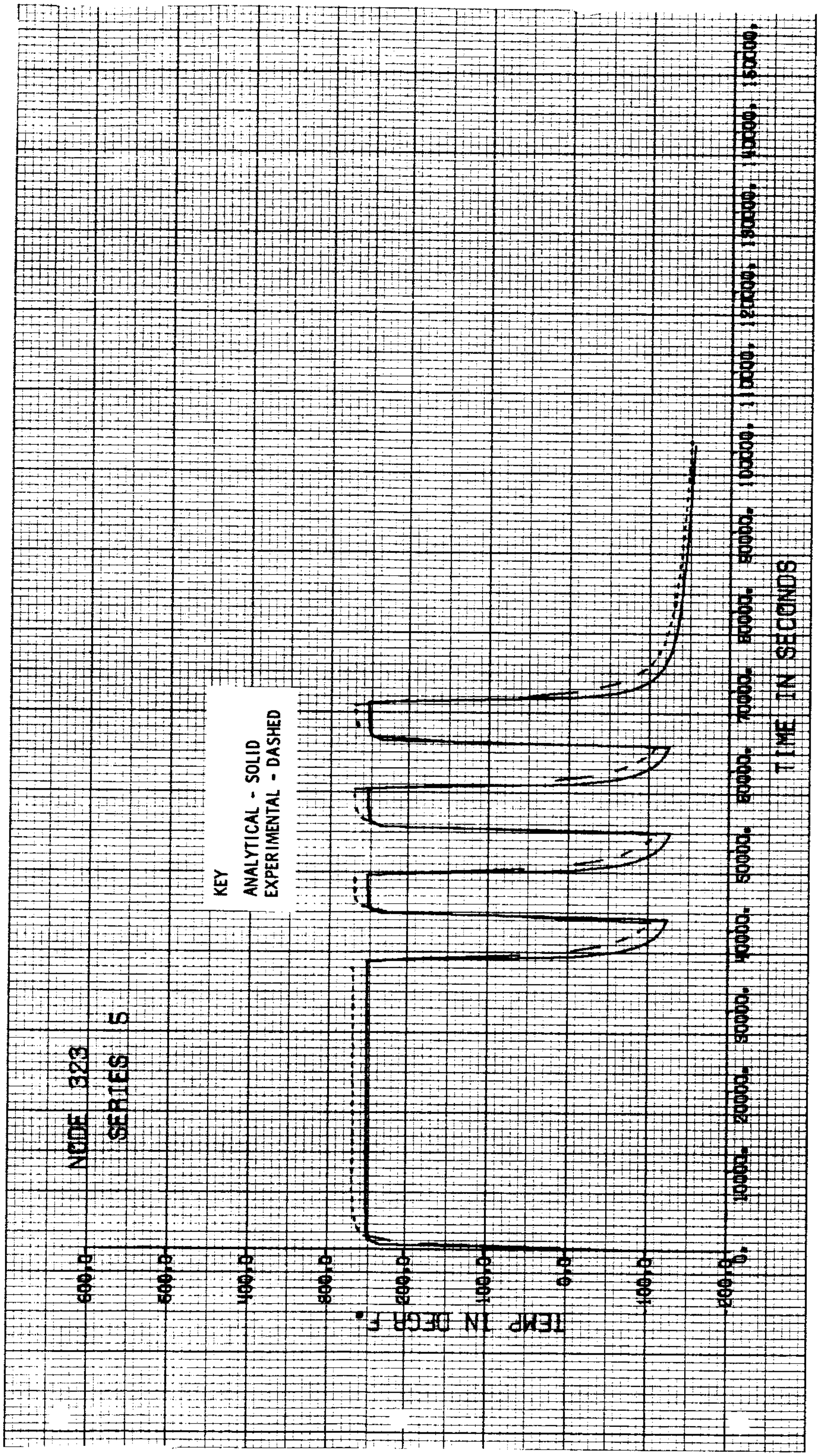

Figure 6-12 Panel Temperature History (Node 323)

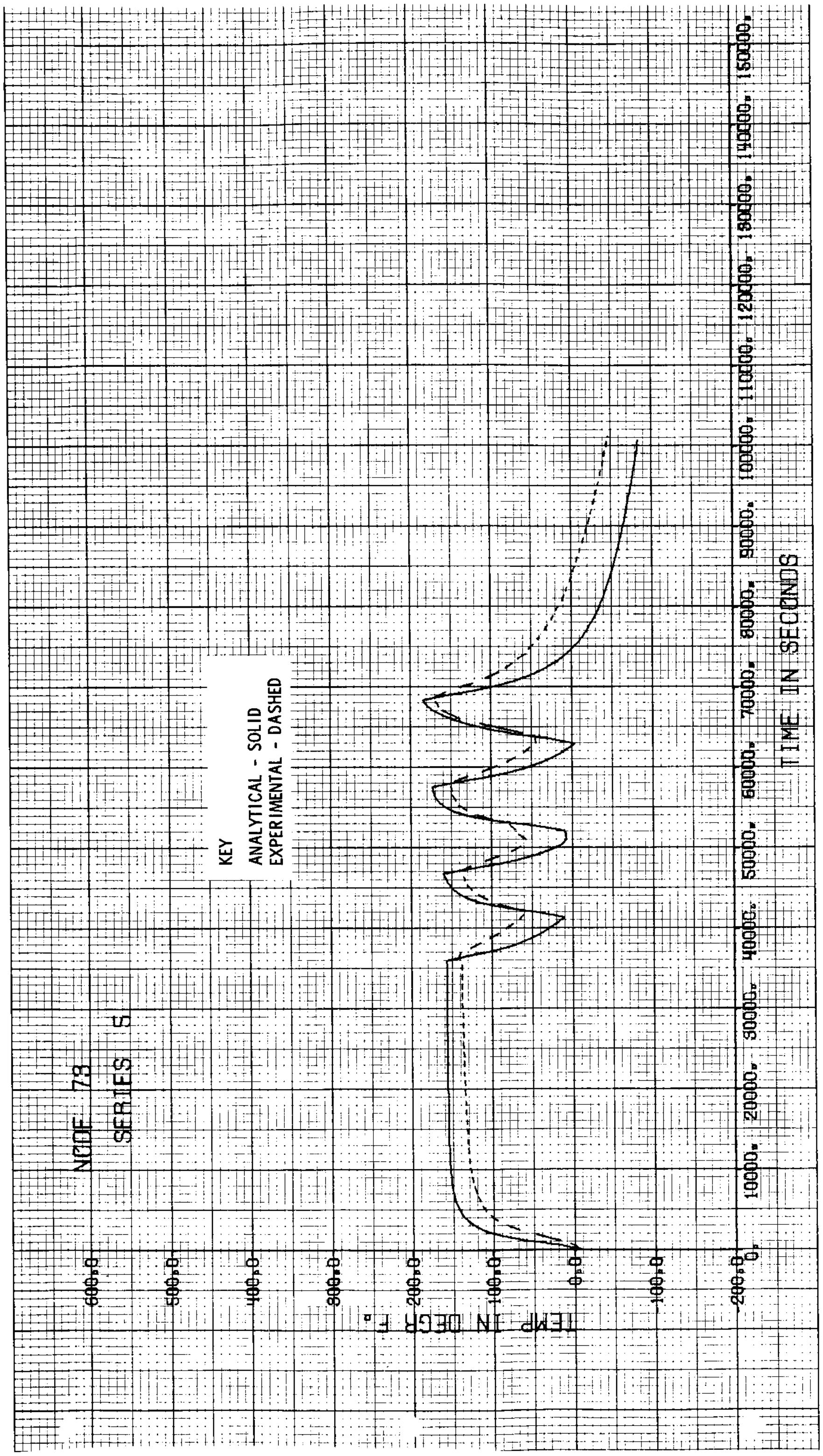

Figure 6-13 Bulkhead Temperature History (Node 73)

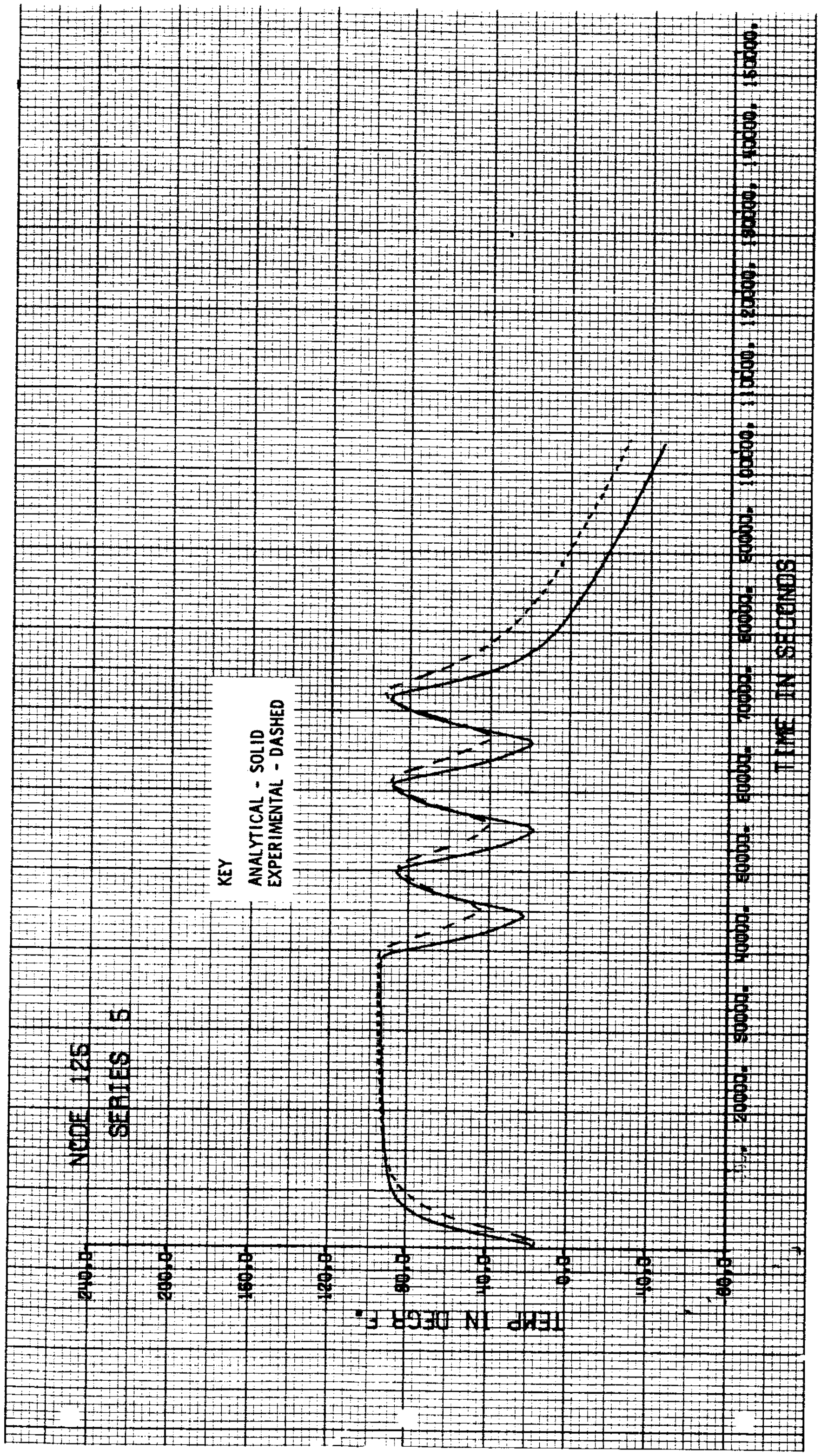

Figure 6-14 Bulkhead Temperature History (Node 125)

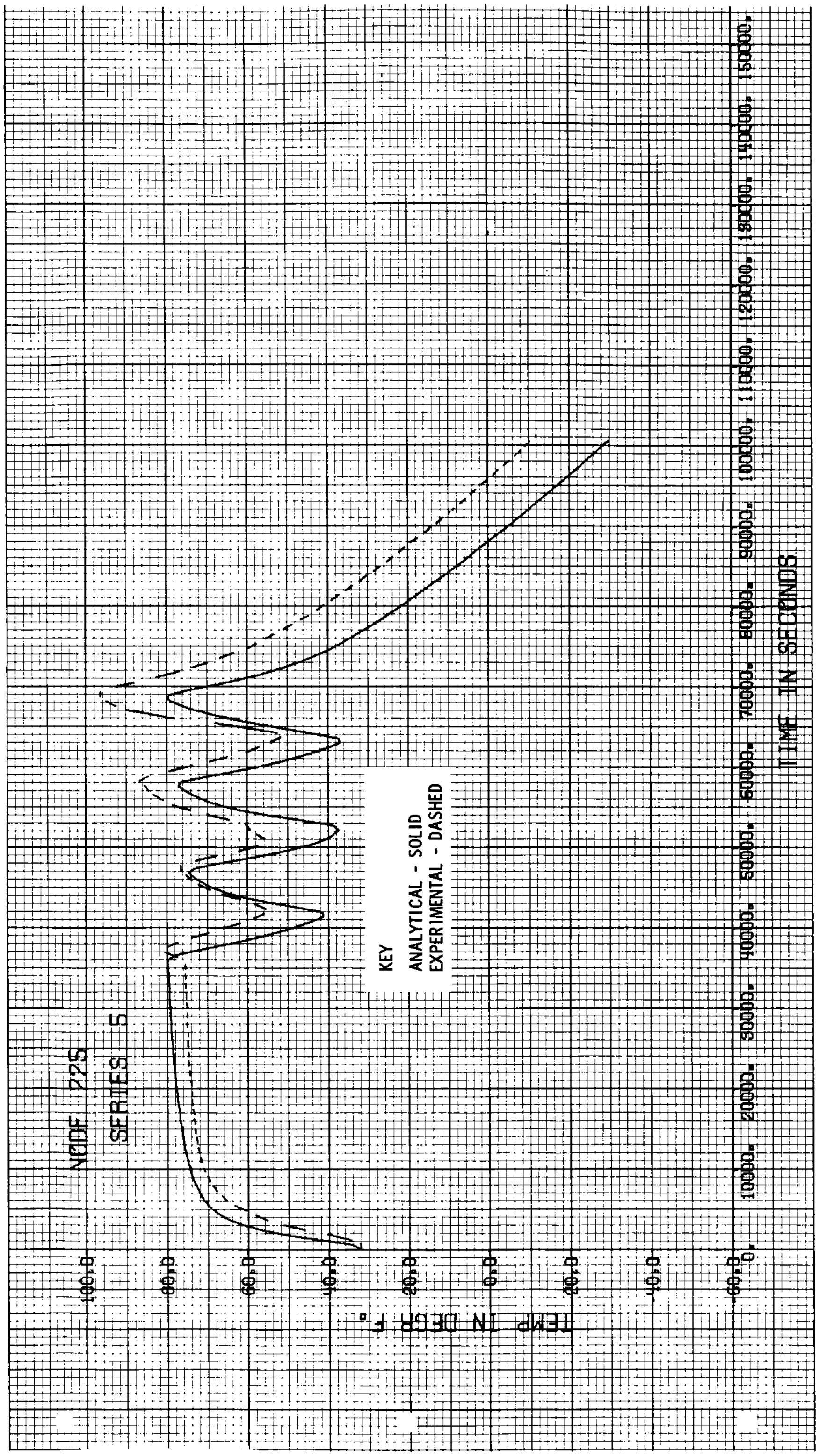

Figure 6-15 Inner Cylinder Temperature History (Node 225)

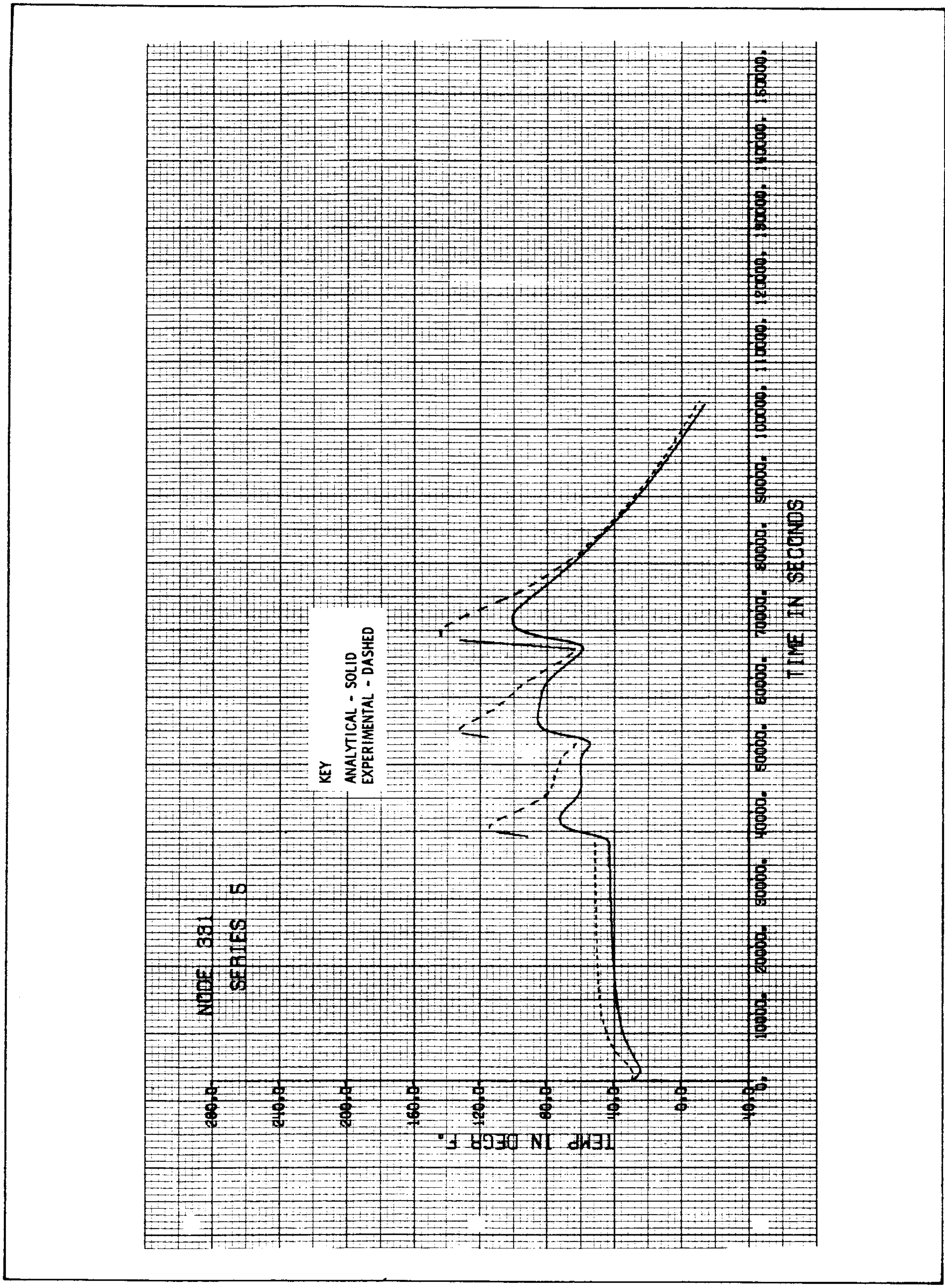

Figure 6-16 Inner Cylinder Temperature History (Node 331)

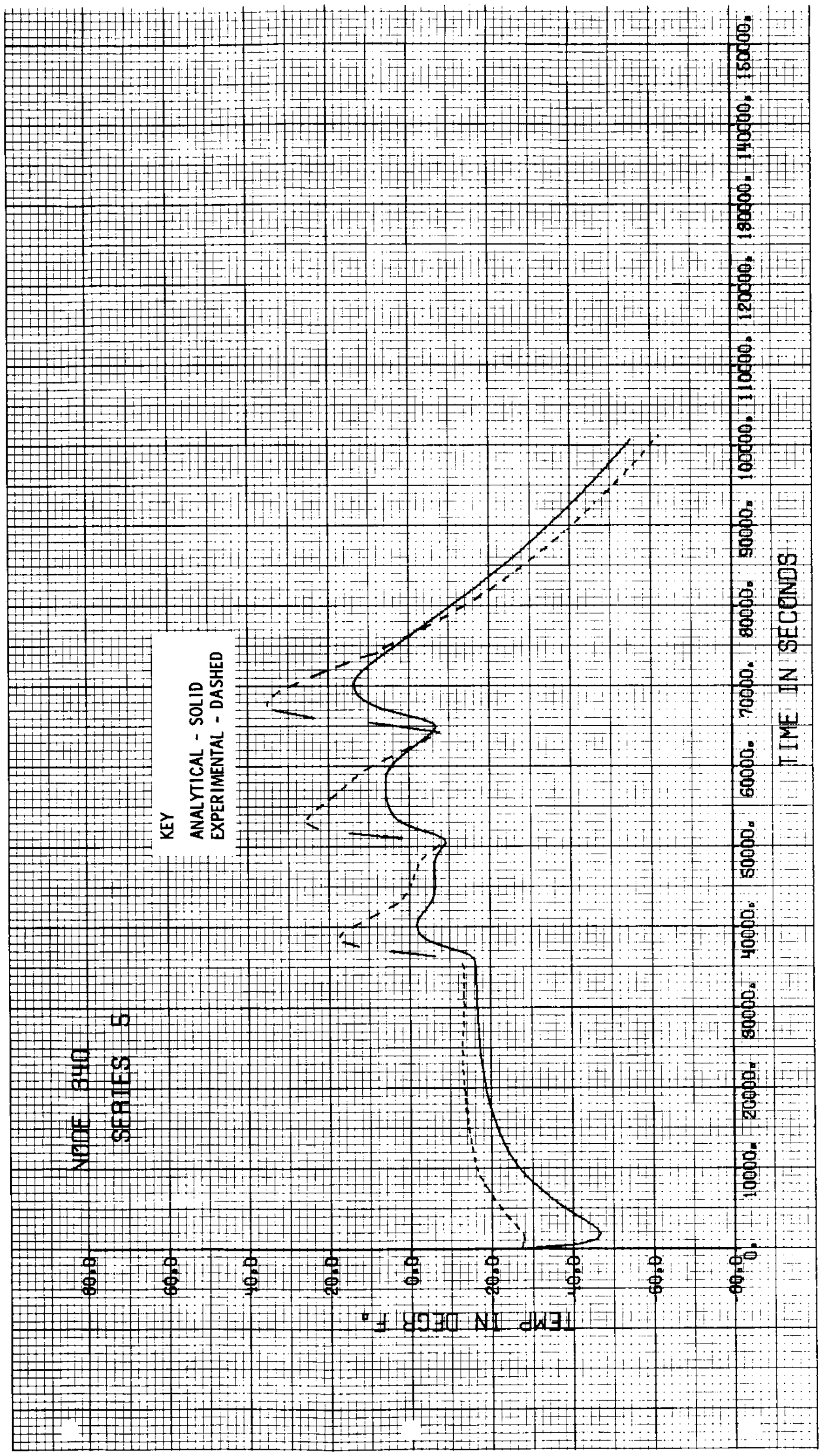

Figure 6-17 Beam Temperature History (Node 340)

LOCKHEED
CALIFORNIA COMPANY

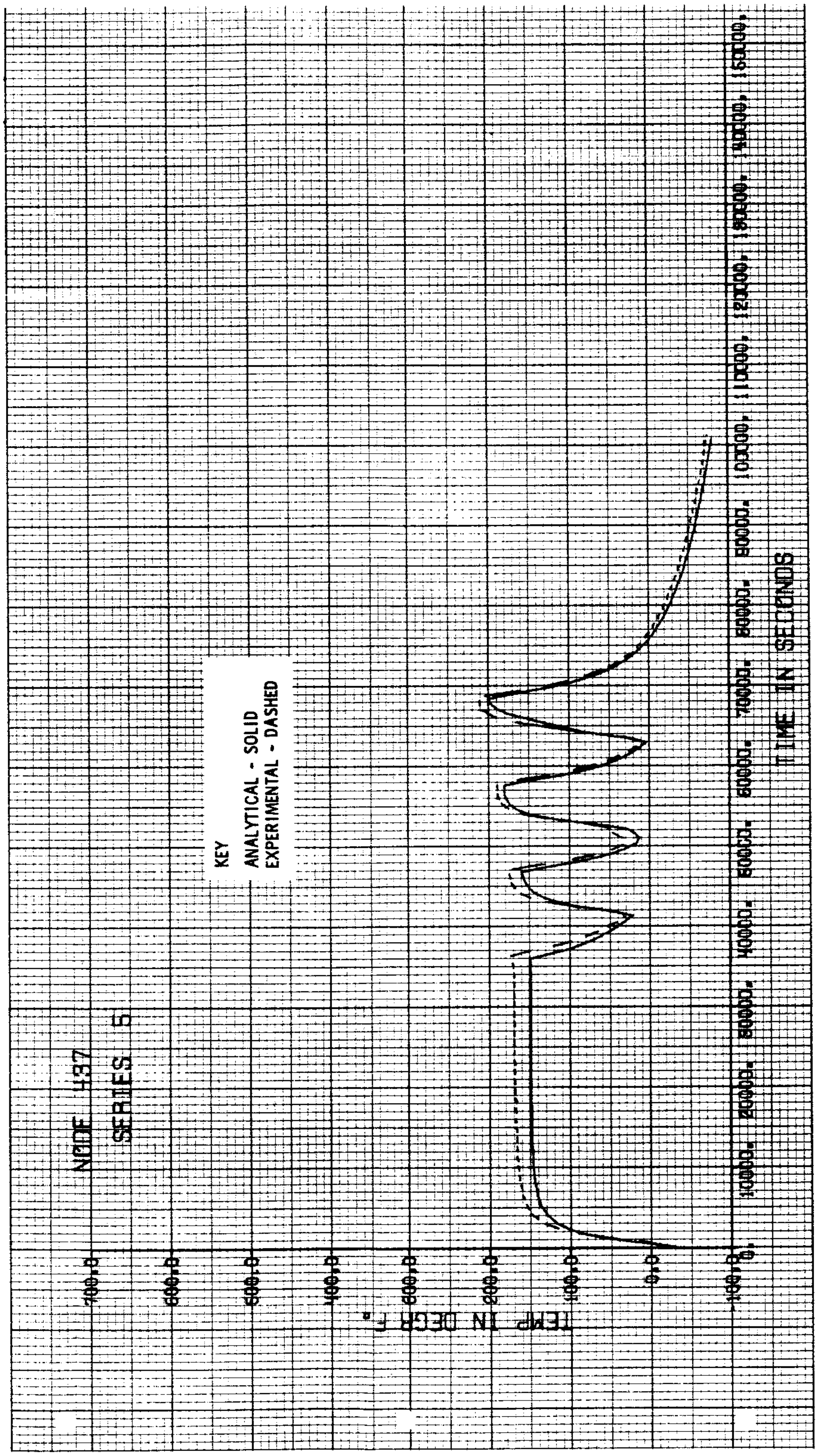

Figure 6-18 Beam Temperature History (Node 437)

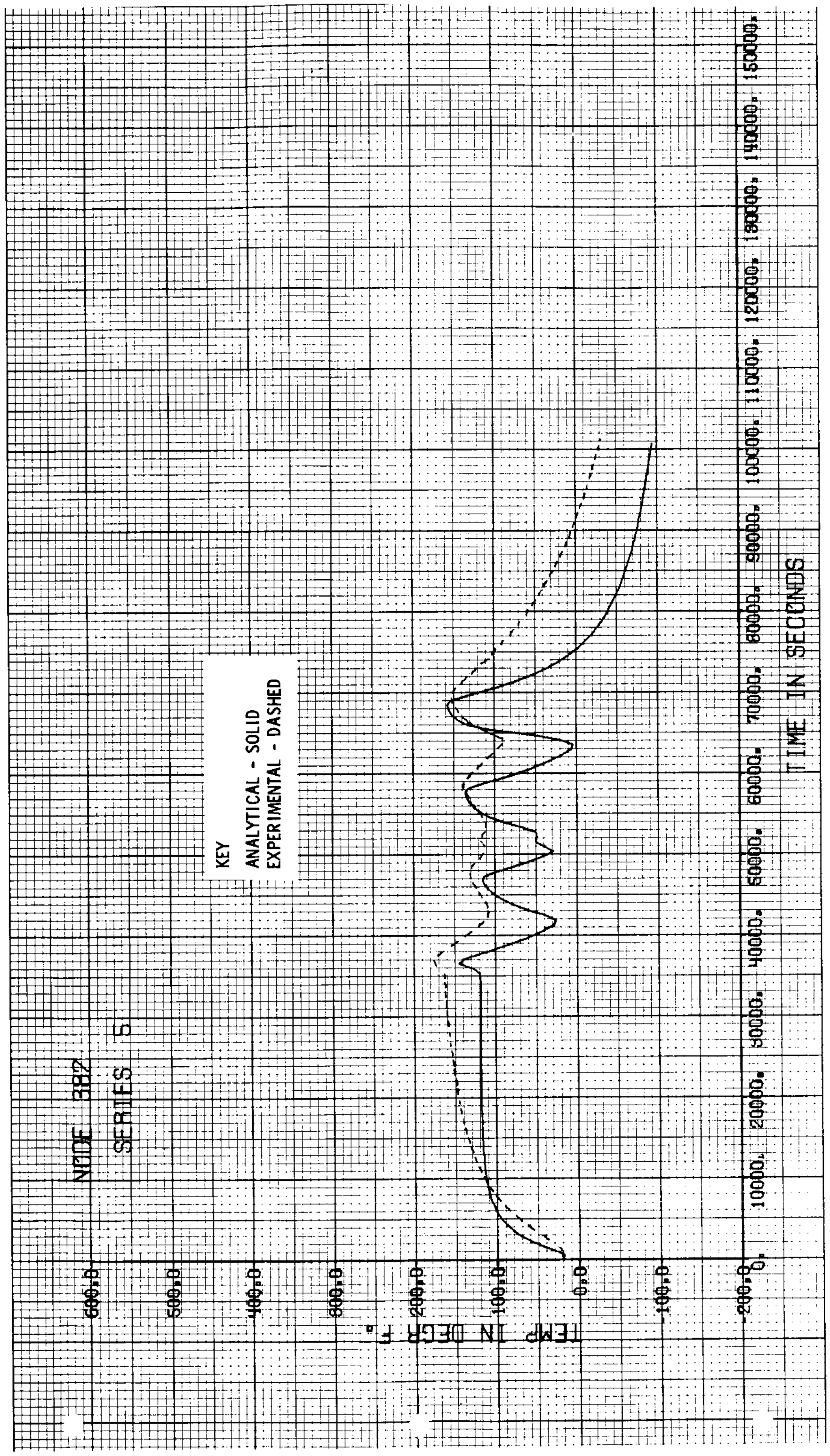

Figure 6-19 Heat Shield Temperature History (Node 382)

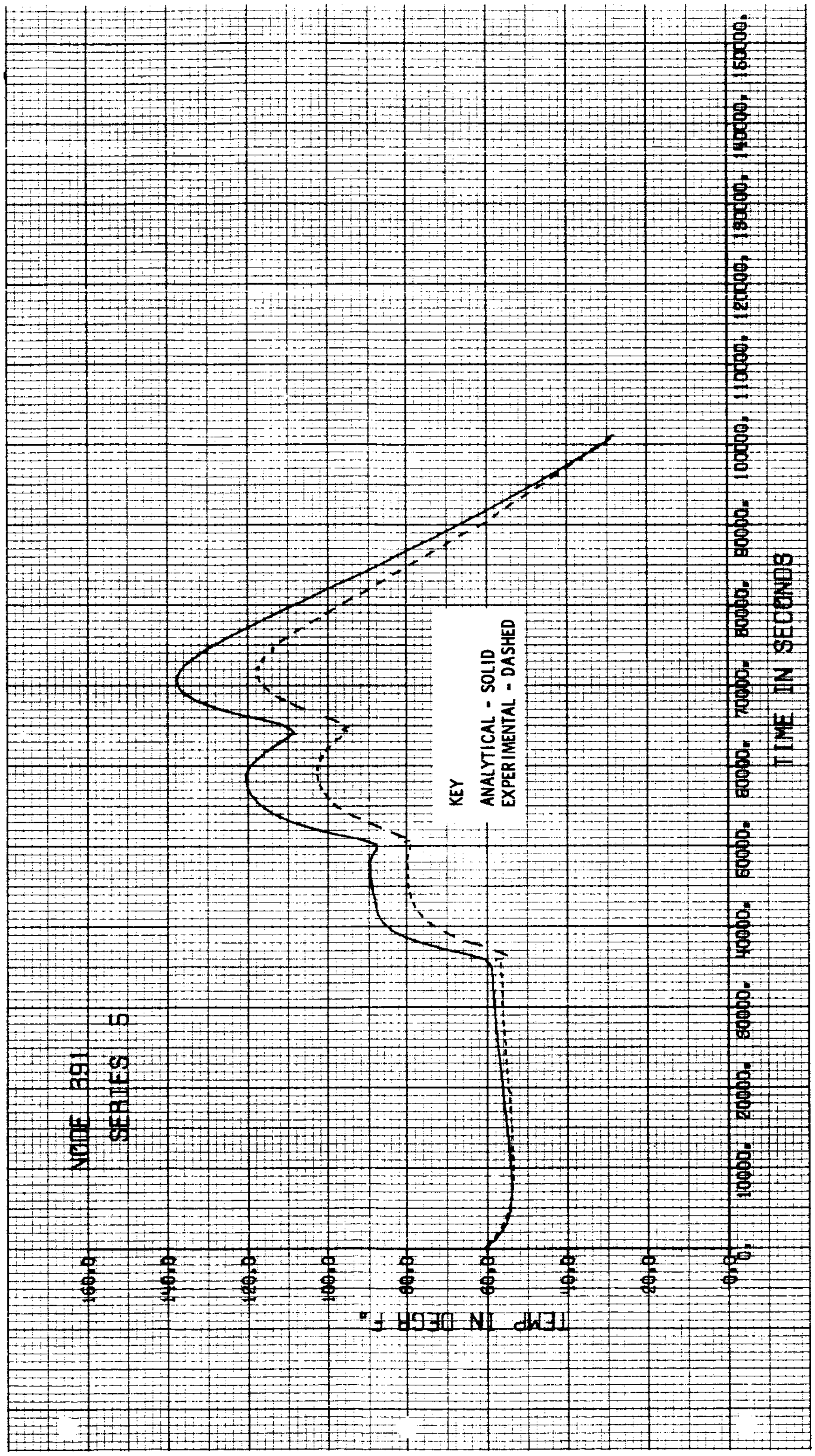

Figure 6-20 Lower Helium Bottle Temperature History (Node 391)

LOCKHEED
CALIFORNIA COMPANY

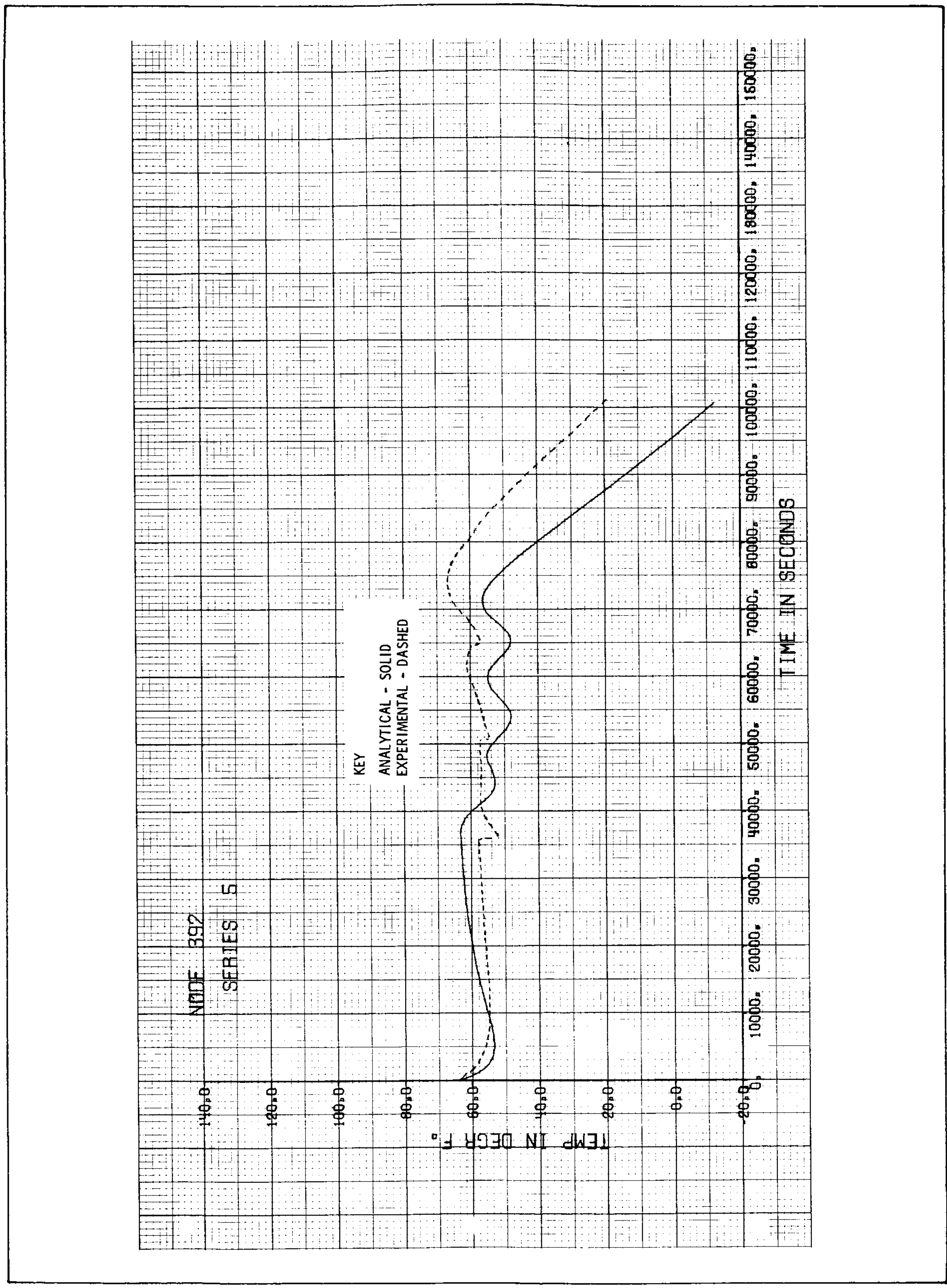

Figure 6-21 Upper Helium Bottle Temperature History (Node 392)

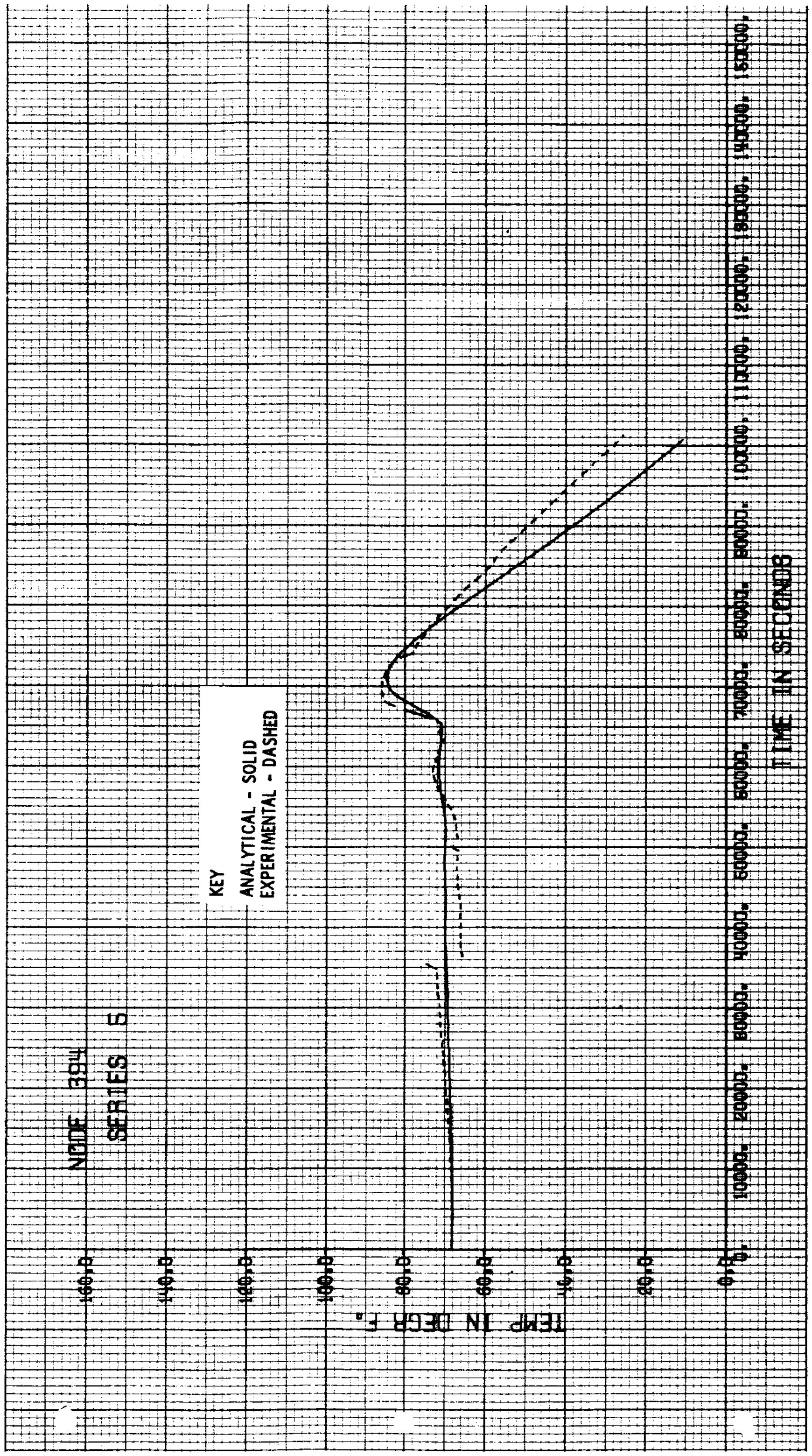

Figure 6-22 Propellant Tank Temperature History (Node 394)

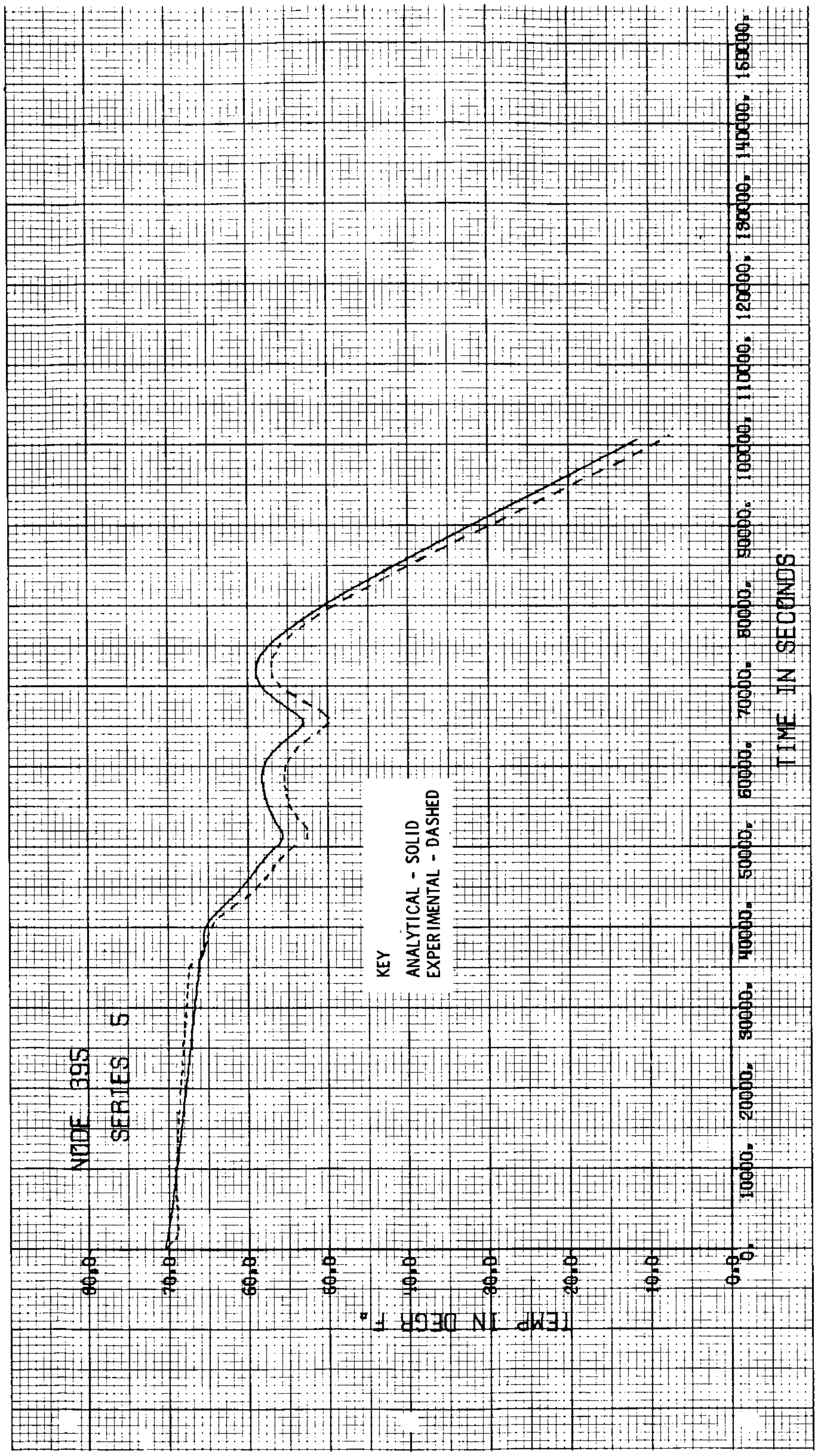

Figure 6-23 Propellant Tank Temperature History (Node 395)

LOCKHEED
CALIFORNIA COMPANY

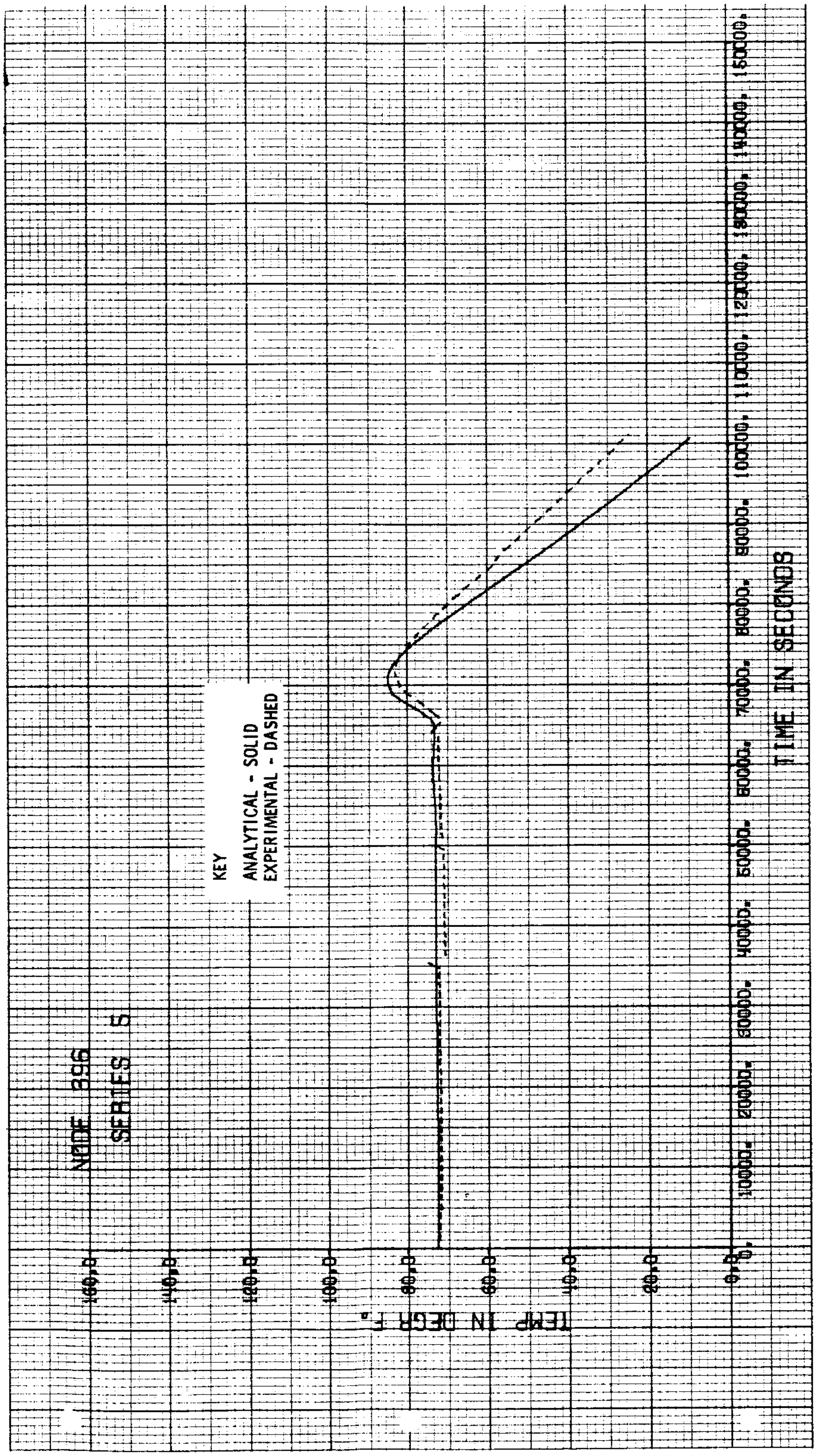

Figure 6-24 Propellant Tank Temperature History (Node 396)

LOCKHEED
CALIFORNIA COMPANY

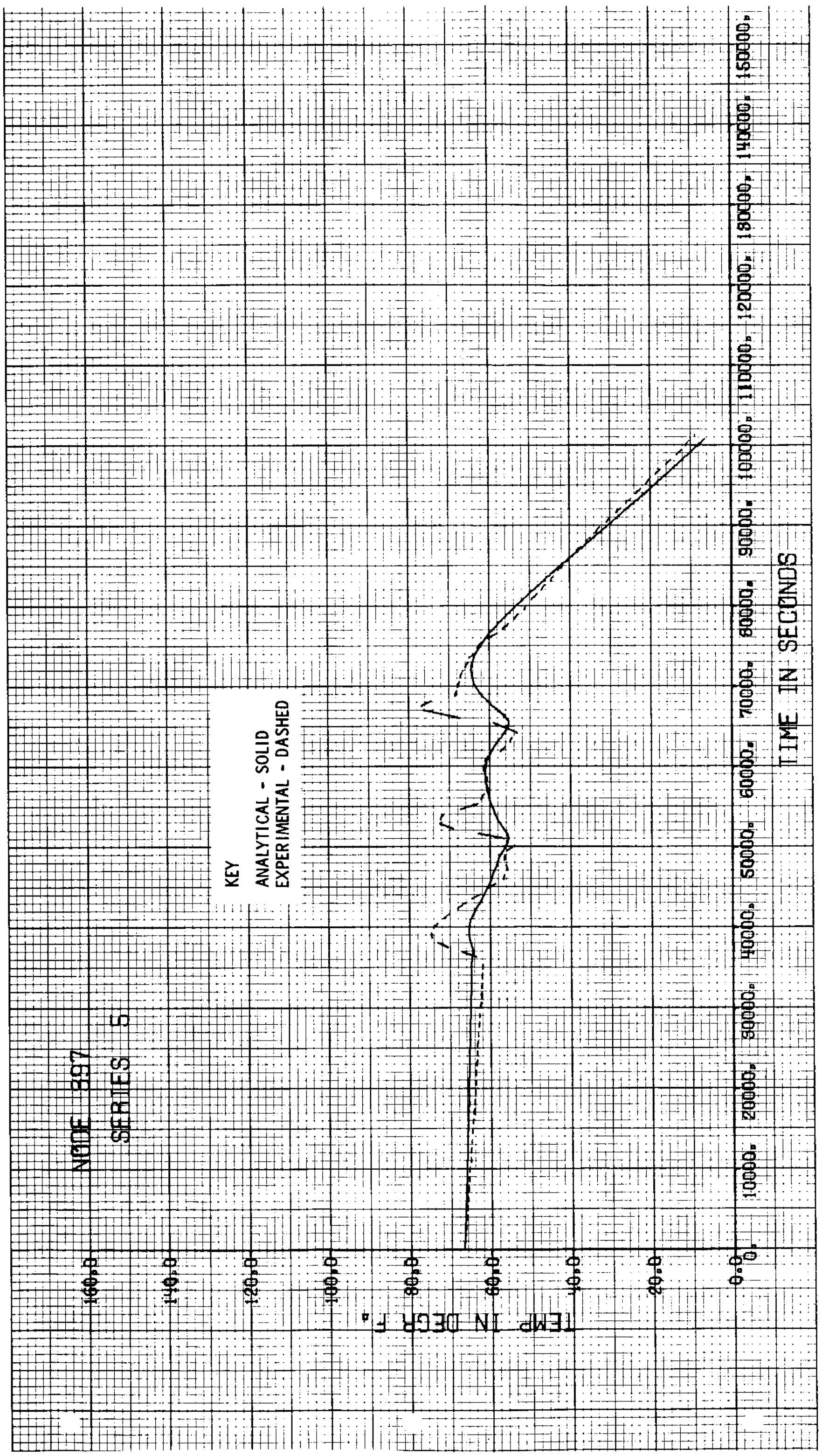

Figure 6-25 Propellant Tank Temperature History (Node 397)

point represents transient conditions during the last engine firing. In addition to summarizing the results, Table 6-2 serves as a guide to the 14 analytical and experimental temperature histories.

For node 311, located on the outer panel cold side of the model, the largest discrepancy between predicted and experimental temperatures occurs during cool down. At the final time of the run, for node 331, measured temperature is -146°F and predicted temperature is -133°F. This discrepancy is caused by a poorly defined chamber floor temperature. The model rests on metal beams on the floor of the chamber, and the tops of these beams are heated to 0°F during solar simulation. In order to account for this, a floor temperature of -200°F was assumed, while the assumed temperature of the cold wall was -230°F. When the solar simulator is turned off, -200°F is no longer a representative floor temperature. Thus, the colder than assumed floor temperature caused the measured temperatures on the cold panel to be about 15°F lower than predicted.

Predicted temperatures during simulated engine firings are lower than experimental. This is graphically shown in Figures 6-16 and 6-17. This problem is discussed for the Series 3 runs. On the hot side of the model, predicted temperatures are in reasonably good agreement with measured temperatures even during engine firing as shown in Figure 6-18. For this node, the heating effects of the thrust chamber are negligible compared to the solar heating.

A temperature history of a representative heat shield node is shown in Figure 6-19. For the heat shield nodes, correlation is only within ±50°F. In general predicted temperatures for the heat shield nodes are not as good as for the rest of the model. This is mainly due to the coarseness of the network and the uncertainty of the thermal contact resistance.

Predicted temperatures for the lower helium bottle are consistently higher than measured temperatures, especially during engine firing, as shown in Figure 6-20. Radiation from the thrust chamber to the helium bottle was over estimated. Heating effect from the thrust chamber is not as pronounced for the upper helium bottle, as observed from Figure 6-21. As discussed for

Series 3, the temperature discrepancies near the end of the run are caused by one node representation of the empty bottle. Shown in Figure 6-22 to 6-25 are the temperature histories of the propellant tanks. Predicted temperatures are within ±10°F of the measured temperatures. Correlation for the Series 5 run is much better than the Series 3 run because the tanks are in a horizontal position. One node representation of horizontal tanks is better than for vertical tanks because the temperatures on the tank are more uniform.

A comparison of the correlation for Series 3 run 22 and Series 5 indicates that the difference in boundary conditions (temperatures as opposed to heat flux) does not alter the overall results. For Series 5, chamber temperatures were more difficult to define than for Series 3 because of solar heating of the chamber floor. Also temperature correlation of the propellant tanks for Series 5 is much better in the horizontal position than the vertical position of Series 3.

The added complexity of the Series 5 model was adequately analyzed and the results obtained were as good or better than for Series 3. When the chamber temperature is well defined, external radiative heat transfer can be predicted more accurately than internal heat transfer. This integrated heat transfer analysis can predict 85 percent of the results within ±20°F of measured values. The limitation of this analysis lies only in predicting heat transfer from the thrust chamber. With a continued effort on this problem area, better results could be obtained during the simulated engine firing.

FLUID STORAGE AND PRESSURIZATION PROGRAM

Method of Analysis

The Fluid Storage and Pressurization Program is used to analyze the primary oxidizer tank and helium bottles for the Series 5 run. This program solves the analogous resistance-capacitance networks that represent the tankage and pressurization systems. Detailed information on the program assumptions and operations are contained in LR 18903 and LR 18899, Vol. I, Sec. 3.

The network for the primary oxidizer tank consists of 168 nodes and 424 resistors, while the network for the helium bottle consists of only 1 resistor and 2 nodes; one node for the gas and one node for the bottle. For boundary conditions, the experimentally obtained temperature-time histories for the tankage system ambient are input to the program. Table 6-3 lists the computer input describing the Series 5 test model, and Table 6-4 lists program output parameters.

The program, as used for this analysis, was not complete in that the subroutine accounting for fluid stratification effects due to convective processes had not yet been incorporated at the time of the analysis. Lack of this subroutine permitted analysis of heat transfer by conduction only. Use of the stratification subroutine would increase the heat transfer to the fluid by accounting for the convective component, and it would reduce the thermal gradients in the tank by accounting for fluid transport due to density gradients within the fluid. The portion of the Series 5 data being used for correlation is that obtained from the primary oxidizer tank (bay 5) and the helium bottles, up to the time at which the primary tanks are empty. System instrumentation for the tests is shown in Figure E-9. The internal tank thermocouples were located in such a manner as to give a representative tank temperature profile during either the tests of Series 3 (vertical tank) or Series 5 (horizontal tank).

The primary oxidizer tank was the only propellant tank analyzed. This tank was selected because: (1) the primary tank empties first, thus eliminating the effects of inflowing propellant, and (2) because of its higher vapor pressure the simulated oxidizer fluid provides the best opportunity to verify the assumptions of the program.

The justification for this approach is that the different tank responses are similar enough so that the program could be verified from the analysis of a single tank.

Discussion of Results

Predicted and experimental results for the oxidizer tank are presented in Figures 6-26 to 6-28. These results consist of the average tank temperature, maximum and minimum tank temperatures, and tank pressure, all as a function of time. In general, the thermal analysis of the tankage during the soak period shows good agreement with the test data. Evaluation of the test

TABLE 6-3. SERIES 5 INPUT PARAMETERS

Tank radius	0.703 ft.
Cylinder section length	3.155 ft.
Tank wall thickness	0.00517 ft.
Initial temperature	67.2°F
Initial tank pressure	50.9 psia
Ullage (gas volume)	5.69%
Minimum Operating pressure	46.5 psia
Maximum Operating pressure	63.0 psia
Molecular weight of condensible gas	137.37
Molecular weight of pressurizing gas	4.0
Initial helium temperature	65.8°F
Initial helium pressure	1270.0 psia
Volume of helium bottle	0.594 ft^3
Weight of helium bottle	74.0 lb.
Test fluid (simulated oxidizer)	Freon 11

TABLE 6-4 OUTPUT PARAMETERS

Propellant Tank

Total Pressure

Partial pressure of condensible gas

Partial pressure of non-condensible gas

Average gas temperature

Average liquid temperature

Maximum liquid nodal temperature

Volume of gas

Mass of liquid

Mass of liquid used

Liquid flow rate

Mass of condensible gas

Mass of non-condensible gas

Pressurizing system

Pressure of helium

Temperature of helium

Mass of helium

Helium flow rate

General

Time

All node temperatures

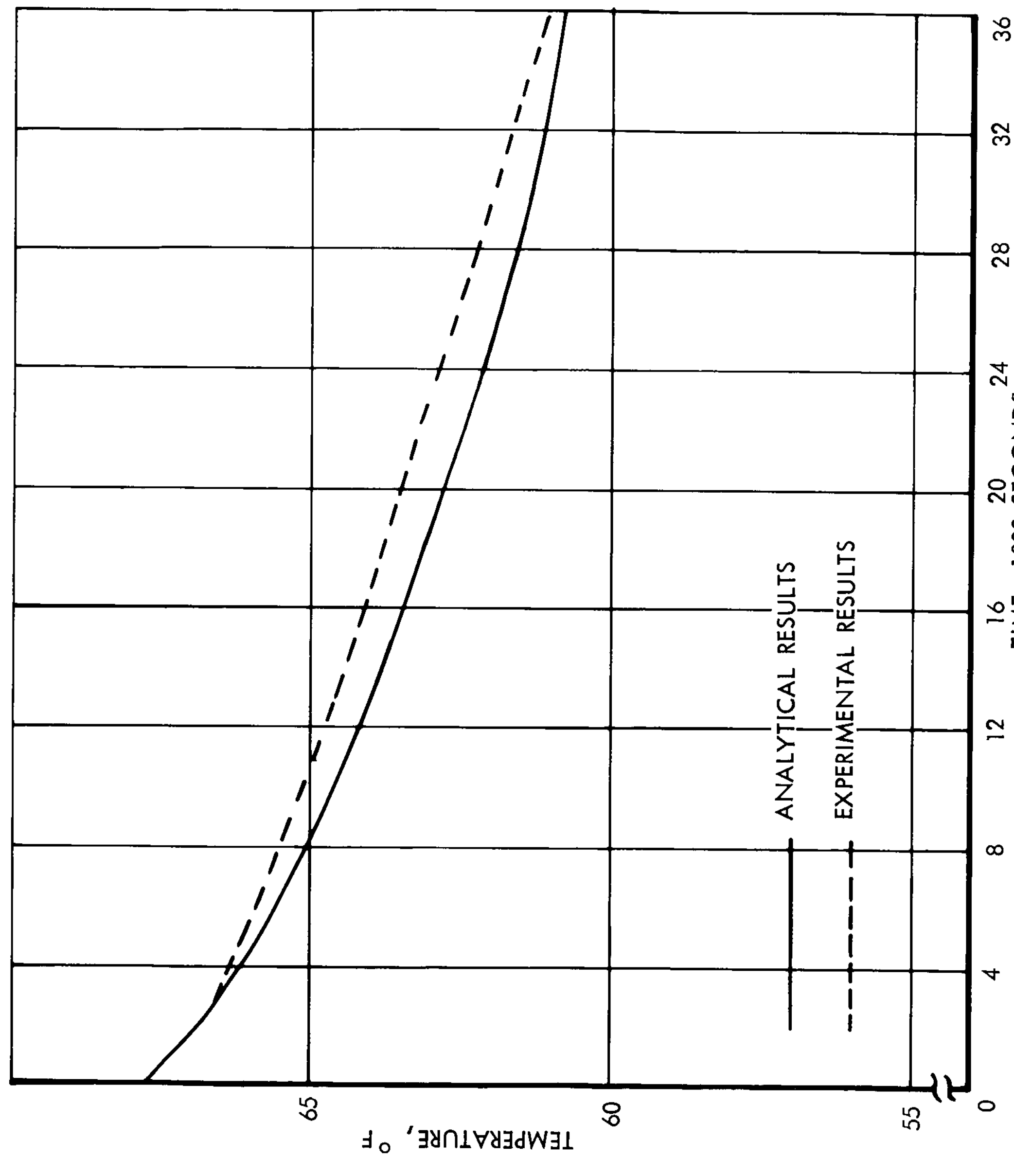

Figure 6-26 Average Temperature of Bay 5 Oxidizer

LOCKHEED
CALIFORNIA COMPANY

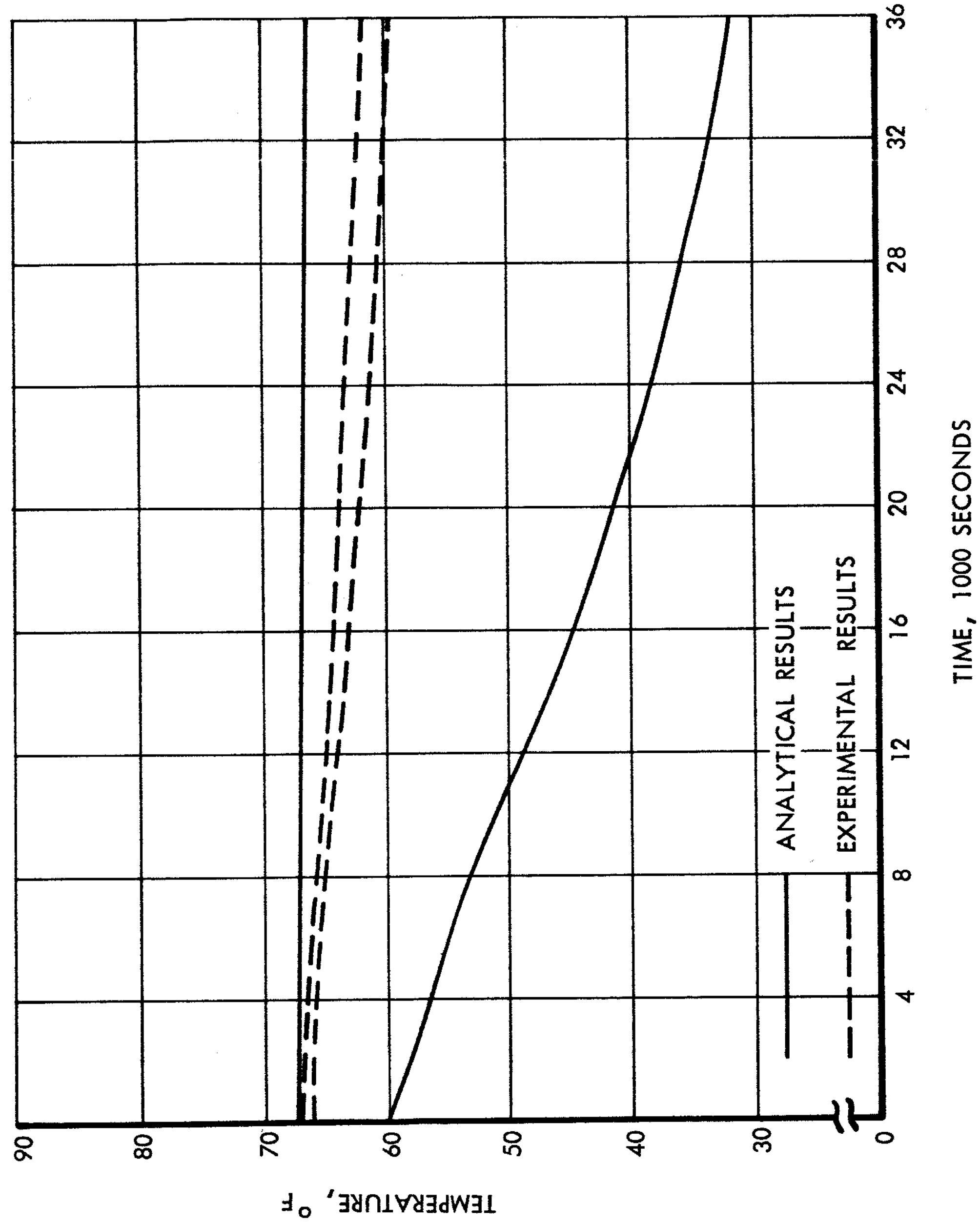

Figure 6-27 Maximum and Minimum Temperatures of Bay 5 Oxidizer

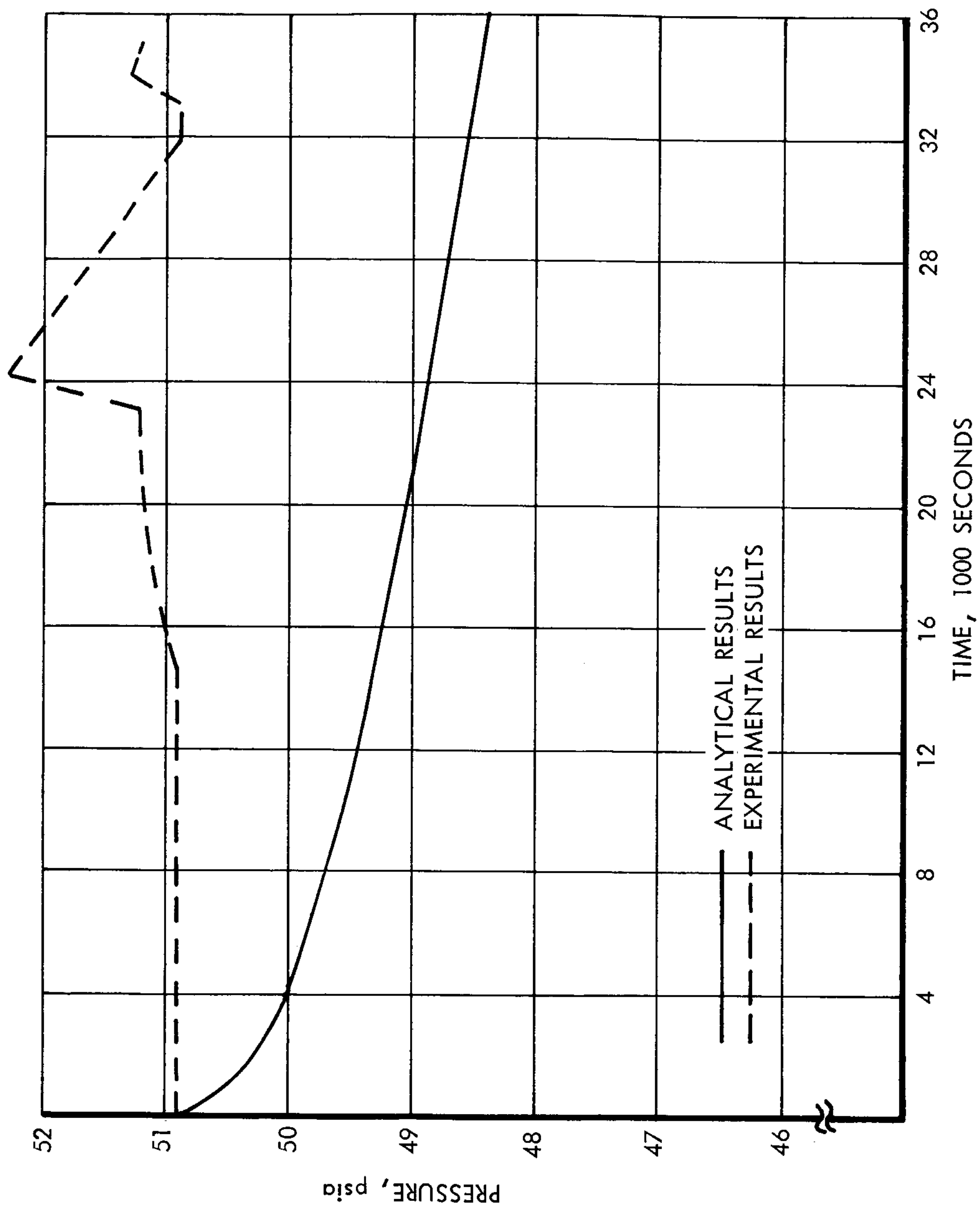

Figure 6-28 Bay 5 Oxidizer Tank Pressure

data for the pressurizing system indicates that there was some leakage of the helium during the Series 5 test.

Figure 6-26 shows a comparison of the calculated and observed average liquid temperature during the test. Good agreement is obtained with a maximum deviation of less than 1°F. The results of computer analysis show a consistently lower average temperature indicating that the inclusion of convective heat transfer in the computer study would tend to improve the correlation.

Predicted and measured maximum temperature gradients within the liquid region are shown in Figure 6-27. The 35°F analytical gradient is much larger than the 2.5°F experimental gradient. This indicates the importance of fluid stratification due to the convective process. A stratification subroutine for this program would have diminished the large analytical temperature gradient. Unfortunately this subroutine was not available at the time of the analysis.

The experimental and analytical oxidizer tank pressures are shown in Figure 6-28. Good pressure correlations in the tank and the helium bottle are difficult to achieve due to inconsistent pressure readings and the indication of a helium leak. Experimental data show a pressure decay in the helium system of about 135 psia during the ten-hour soak period before the first simulated engine firing. Just prior to the expulsion, the mass of the helium must be known to accurately predict the pressure response in the oxidizer tank.

It was observed that the pressure in the oxidizer tank rose, even though the fluid temperature fell, indicating that some of the helium leaked into the tank.

Although the calculated final conditions in the pressurant bottles are different than the observed condition, the masses of gas required to expel the liquid during the 4 minute firing are in good agreement, being 0.334 lb. and 0.320 lb. for the analytical and experimental values respectively. This good correlation verifies the assumption of liquid-vapor equilibrium during liquid outflow. However, the final temperature and pressure of the helium were higher than would be expected based upon adiabatic expansion of the gas. The predicted final conditions are -55°F and 643 psia, while the experimental final conditions are 54°F and 835 psia.

To summarize the results of the Fluid Storage and Pressurization Program, it was found that the analysis provided reasonably good predictions of the thermal responses of the system. The importance of effects of convection on stratification in the fluid was revealed by the very small experimental temperature gradients. Unfortunately, good pressure correlation was not obtained due to a leak in the helium system. However the important assumption of continuous vapor-liquid equilibrium was verified.

VII - CONCLUSIONS AND RECOMMENDATIONS

The analytical predictions were within ±20°F of the observed model temperatures for approximately 85% of the nodes during quasi-steady state conditions. For highly transient conditions, 85% of the nodes are within ±30°F. Typically, the worst nodes were in error by 20°F for the quasi-steady state conditions and 35 °F for the transient condition. The trend during the transients was for the analytical predictions to be from 10 to 20°F cooler than the observed temperatures. This is consistently observed during simulated firings and appears to be due primarily to the incomplete accounting by the analytical program of the heat transfer from the thrust chamber.

Other large discrepancies, particularly on the bulkheads and at the heat shields during both transient and steady state conditions are traceable to a lack of refinement either in the number of nodes or in the assumed radiation paths. In some cases, a single thermocouple represents a node in an area of high thermal gradients. This occurs on the propellant tanks, helium bottles, and at the intersection of the bulkheads and the outer panels. Agreement in such areas tends to be poor. Another contributory cause of observed discrepancies was the inability to precisely define the experimental boundary conditions, particularly the chamber cold wall temperature distribution and, in the case of Series 4, the small solar simulator flux area. It is impossible to allocate a portion of the observed discrepancies to boundary conditions and another portion to the lack of refinement of the analytical model.

It was demonstrated during the Series 1 and Series 2 analysis, that the representation of internal radiation heat transfer is difficult where significant reflections occur. A method of modifying the effective emissivity was found to improve correlation, but the need for further work on this problem is emphasized. Presently available techniques which are highly accurate are extremely unwieldy and consume excessive machine capacity.

The effect of the assumptions that the joint conductance was negligible and that model thermophysical properties could be considered constant could not be separately evaluated. However, the overall degree of correlation suggests that these assumptions are reasonable.

An excellent data correlation program was developed during Phase II that provided direct output plots from the computer comparing experimental results with analytical predictions on the same graph.

Improvements could be realized in the future experimental investigations of this type by blocking radiation heat transfer (with aluminized mylar) on the initial run. This step permits checking the conduction network first without the additional complexity of the radiation mode.

The importance of well established test boundary conditions was apparent throughout the program. The Series 5 tests indicated the necessity for a better definition of chamber cold wall temperatures, particularly on the shaded side of the model. The Series 4 tests pointed out the necessity of obtaining an accurately defined flux map when testing with a solar simulator.

The correlations obtained on the fluid storage and pressurization program indicated a need for continued effort. The amount of instrumentation which could be allocated to the tank and helium bottles with an already complex model was severely limited. A further experimental effort would be valuable and it should be conceived to evaluate this computer program only.

Considering the uncertainties arising in a thermal analysis of the type conducted in Phase I, a corroborative test program is valuable in establishing a confidence level for the analysis. Where the transient thermal performance of a vehicle is critical to the mission, a coordinated experimental and analytical study of the type here conducted is recommended.

APPENDIX A - FACILITIES AND EQUIPMENT

In this appendix, the important facilities and equipment utilized in the thermal test program are described in some detail.

Lockheed C-5 Space Simulation Chamber

This chamber (Figure A-1) is 9-ft. 7-in. in diameter with an 8-ft. 1-1/2-in. high clear work space and 7-ft. 8-1/2-in.-diameter door. The permissible floor loading is 750 lb/sq.ft.

The chamber temperature may be lowered from 70°F to -300°F in two hours with no live load. The -300°F temperature can be maintained with a 100-KW live load. This is accomplished by a cold wall, fabricated from single embossed stainless-steel sheets with a surface finish approaching that of a black body.

The pumping equipment, in addition to the mechanical roughing pump system, consists of two 28,000-liter/second oil diffusion pumps, a 5000-liter/second ion-gettering pump, and a 25-sq.ft. cryoplate. These pumps can decrease the pressure in the chamber to the order of 1×10^{-9} mmHg, depending on the outgassing of materials.

Six ports for television viewing of the specimen and five 12-inch instrumentation ports are provided. These ports are removable and interchangeable, or may be replaced by other types of covers to provide for the introduction of special instrumentation or other types of leads into the chamber.

Lockheed Solar Simulator

In the Series 4 tests, a spliced spectrum type of solar simulator manufactured by Aerospace Controls Corporation was used. This unit superimposed infrared, xenon-mercury, and xenon sources, to achieve a spectrum match within 10% of the Johnson curve. These three sources are blended in an optical integrating system. The beam is then directed to an off-axis parabolic

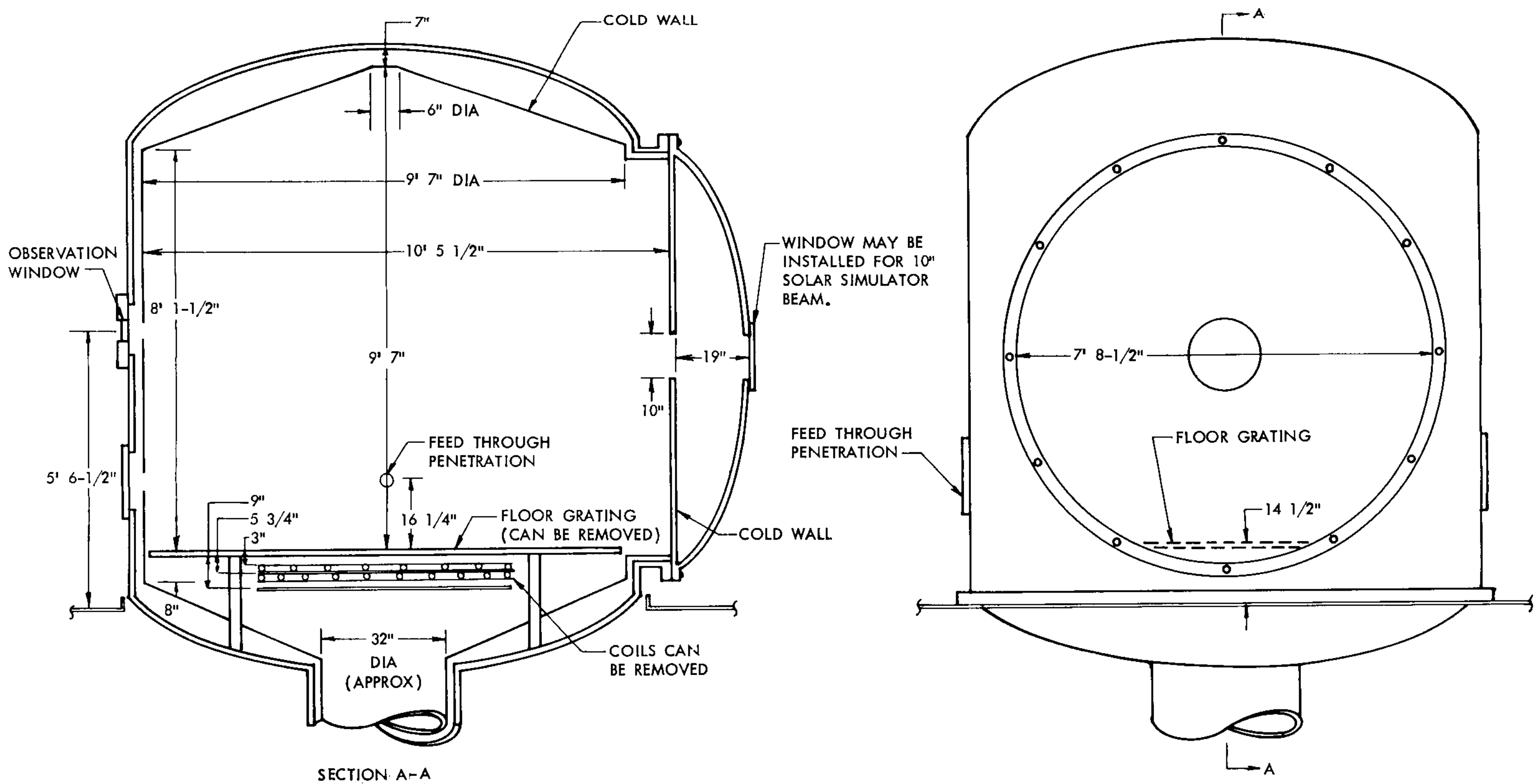

Figure A-1 Lockheed C-5 Chamber Dimensions reflector, and emerges from the simulator as a 10-in. beam, collimated to within 2 degrees. The intensity is adjustable up to 1.2 solar constants. The simulator in position for the Series 4 tests is shown in Figure A-2.

Lockheed Mod-Sadic System

The modified Sadic, Figure A-3, is a multichannel medium-speed data-acquisition system designed to convert the analog signals of either strain gages or thermocouples into digital data. The system may be programmed to read out directly in millivolts, or in any desired engineering units. A notable exception is that the inherent non-linearity of thermocouples must be linearized during the computer-oriented data-reduction phase of the program.

The Mod-Sadic input scanning system consists of five remote switching units; with four units of 50 channels each, and one unit of 99 channels, for a total of 299 possible data channels.

The system is automatically controlled with respect to channel number readout sequence by a pre-punched perforated Mylar tape. This pre-punched tape may be prepared in such a manner that various channels may be re-read any pre-selected number of times during a data readout.

System readout speed averages 300 milliseconds per channel, with five-digit resolution of ±30,000 counts and 0.03 per cent linearity. This represents an overall system accuracy of ±0.02°F with the Type-T thermocouple (limited, of course, by the thermocouple certification).

The thermocouple reference junctions are maintained at a constant known temperature. This reference junction is located between the chamber feed-through and the Mod-Sadic input scanning units.

Losses due to relatively long lead wire lengths are minimized by the system's high input impedance signal amplifier. Common mode rejection is enhanced by use of an integrating type analog-to-digital converter.

The system output consists of digital data directly proportional to the millivoltage output of the various thermocouples. This output--raw data--is permanently stored by perforating a paper tape. This tape may be processed immediately by means of a Flexowriter typewriter to provide a quick look at

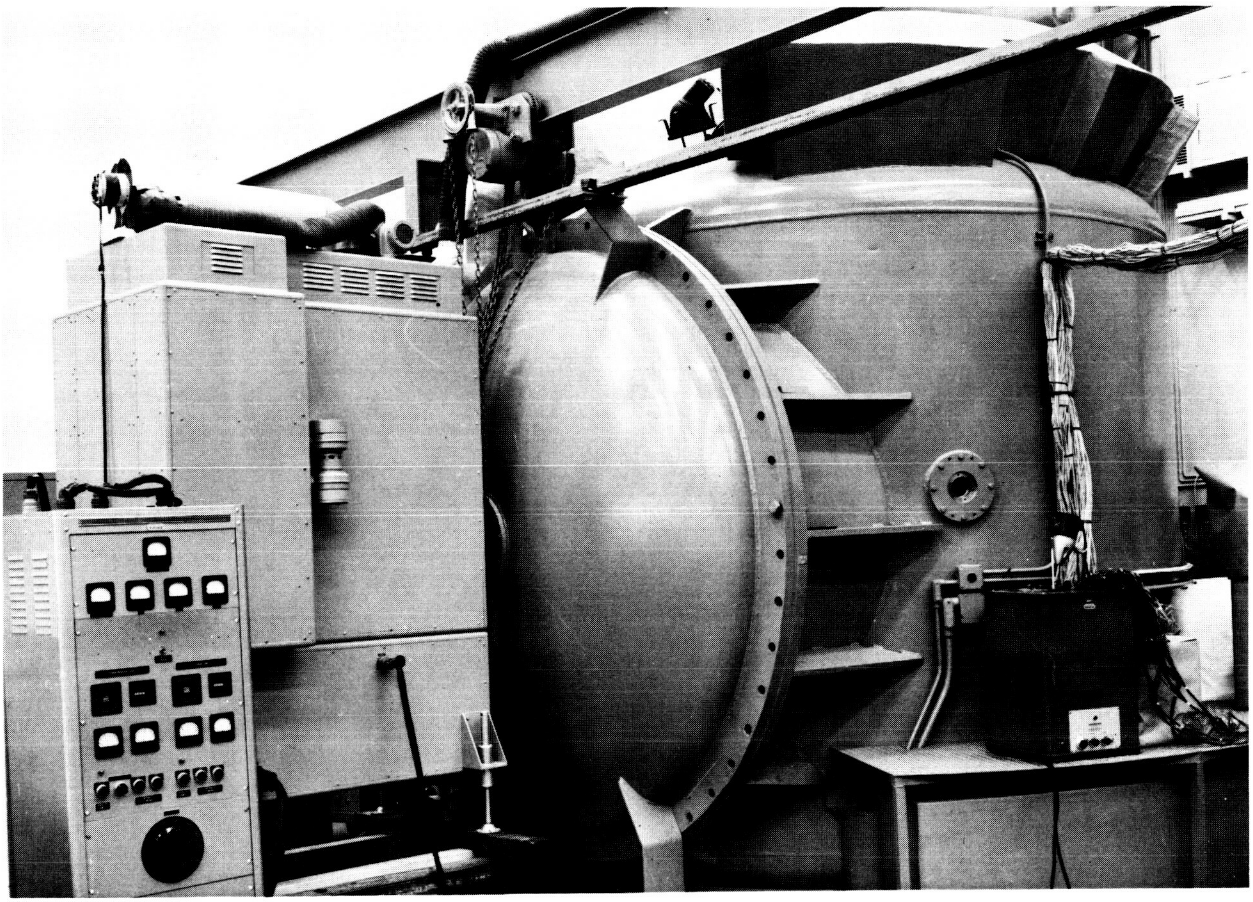

Figure A-2 Solar Simulator in Position Alongside the C-5 Chamber

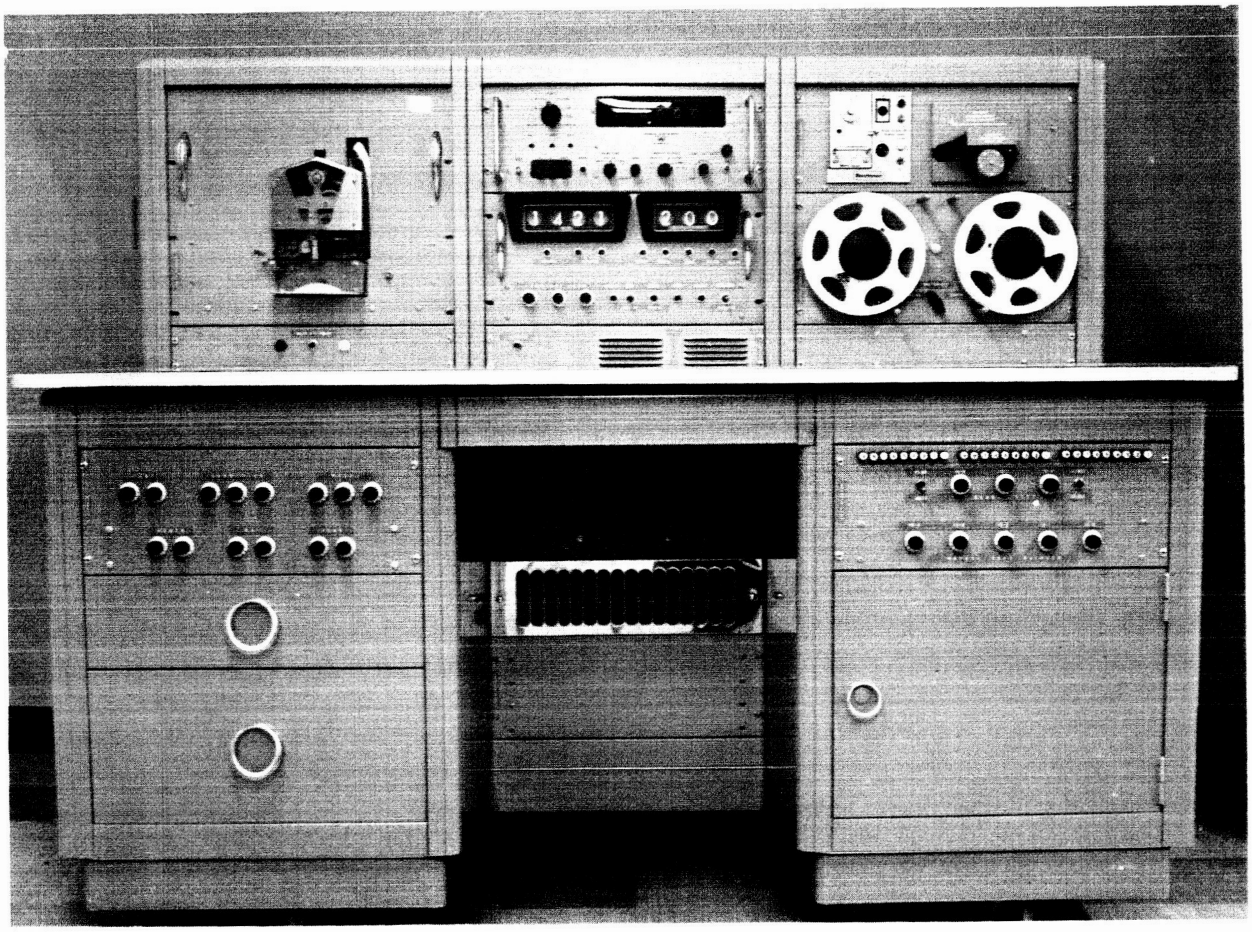

Figure A-3 Lockheed Mod-Sadic Data Acquisition System the raw data; the tape is then forwarded to the computer complex, where it is converted automatically into standard punched cards for computer processing.

Immediately prior to each full data readout, a group of constants is perforated in the output tape to indicate test conditions, real time, and date.

Hughes Serf C-4 Chamber

The Hughes Aircraft Company Space Environment Research Facilities (SERF) C-4 Chamber is 14-1/2 ft. in diameter x 36 ft. high (Figures A-4 and A-5). A bottom-loading chamber, the C-4, has an ultimate vacuum capability of 7×10^{-8} torr. All internal surfaces, except the top, are liquid-nitrogen shrouded for space thermal simulation. The shroud is coated with 3M Black Velvet.

The pumping speed is 63,000 liters/sec. at 1×10^{-5} torr, sufficient for 5-hour pump-down with a typical test model. Access ports are provided on the mezzanine level, for last-minute adjustments and connections after the end bell has been raised. The chamber has provisions for solar simulation as described in the next section.

Hughes S-4A Solar Simulator

Atop the C-4 chamber is a system of Hg-xenon lamps which can cover a target volume of 8-ft. diameter and 9-ft. high, providing solar simulation of any selected intensity from 0.1 to 1.8 solar constants. The lamps are mounted external to the chamber, and project into the chamber through a grid of quartz windows across the top of the chamber. The simulator is shown schematically in Figure A-6. A system of petals (Figure A-7) close the lamps from view during normal operation. However, these petals can be raised to permit an eclipsing plane to be inserted, obstructing the beam and providing precise on-off for orbital simulation.

The flux variation (Figure A-8) across the 8-ft.-dia. beam is ±3% at 8 ft. above the floor. Vertical variation within a 6-ft.-high target volume is ±10%. The spectral distribution can be varied somewhat by the proportion of xenon to Hg-xenon lamps. Normally, all Hg-xenon lamps are used. For tests where high UV might damage sensitive coatings, xenon lamps could be substituted. The system uses 19 5-KW lamps mounted in air-cooled interflectors.

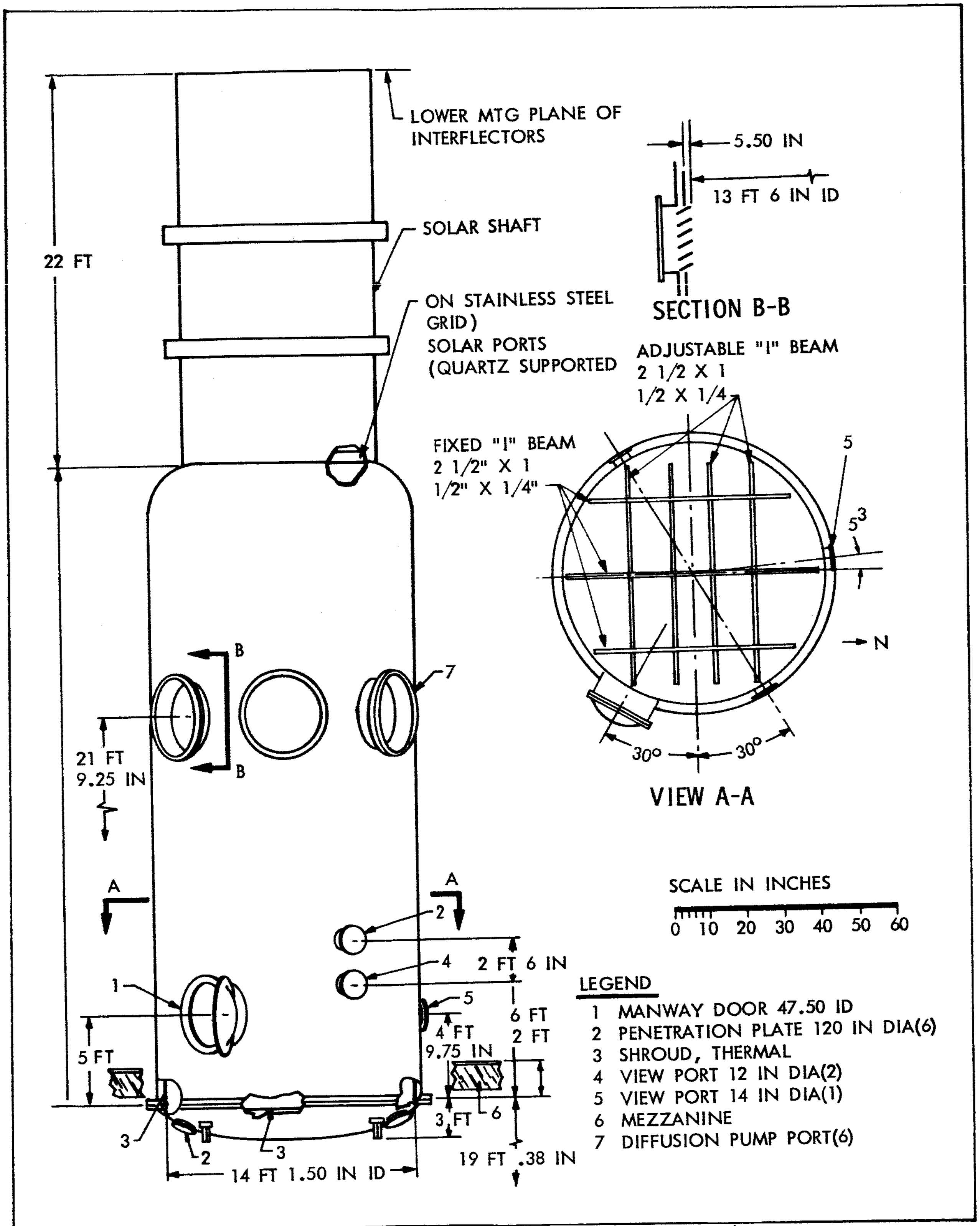

Figure A-4 The Hughes C-4 Chamber Layout

LOCKHEED
CALIFORNIA COMPANY

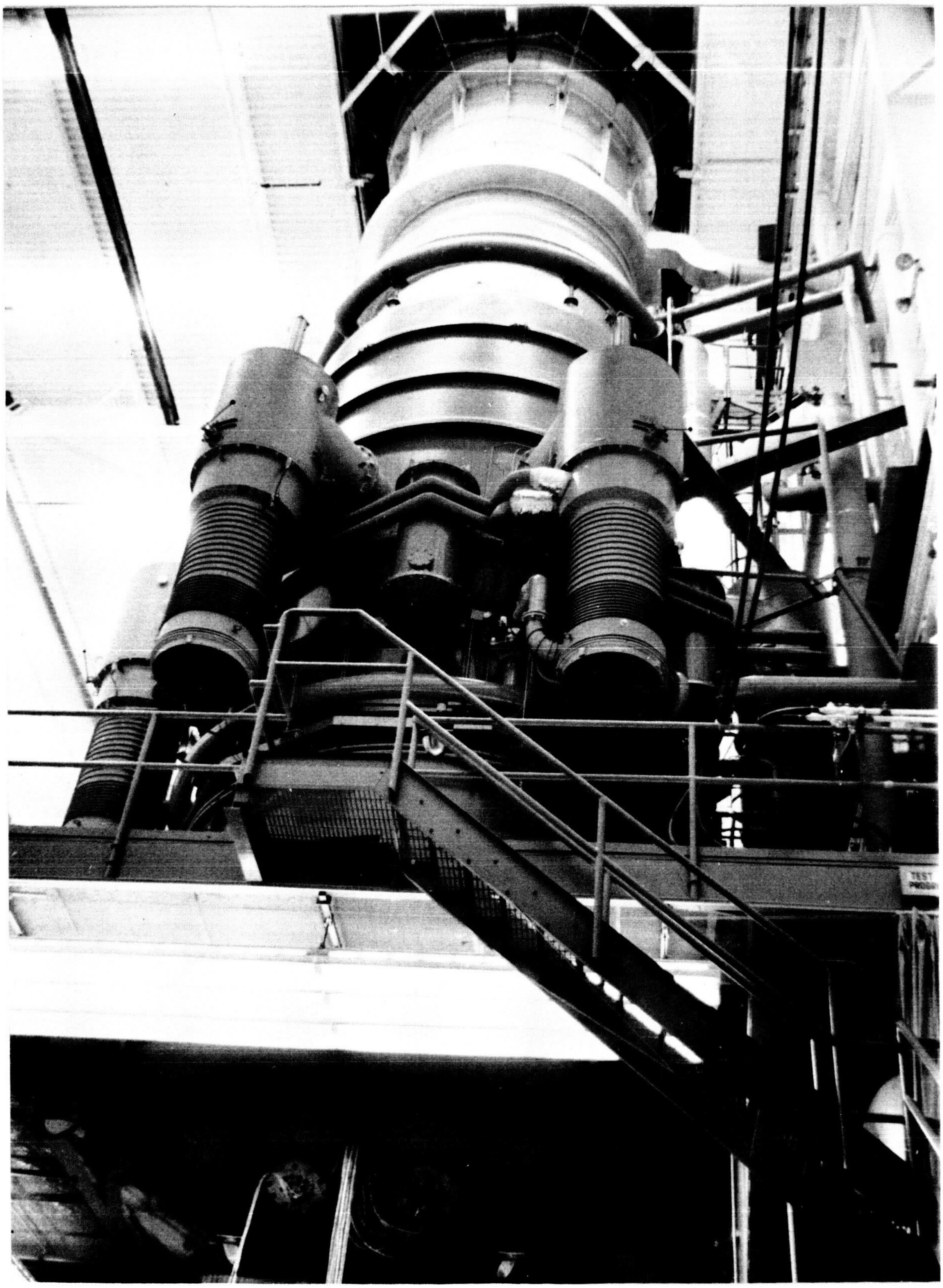

Figure A-5 The Hughes Serf C-4 Chamber

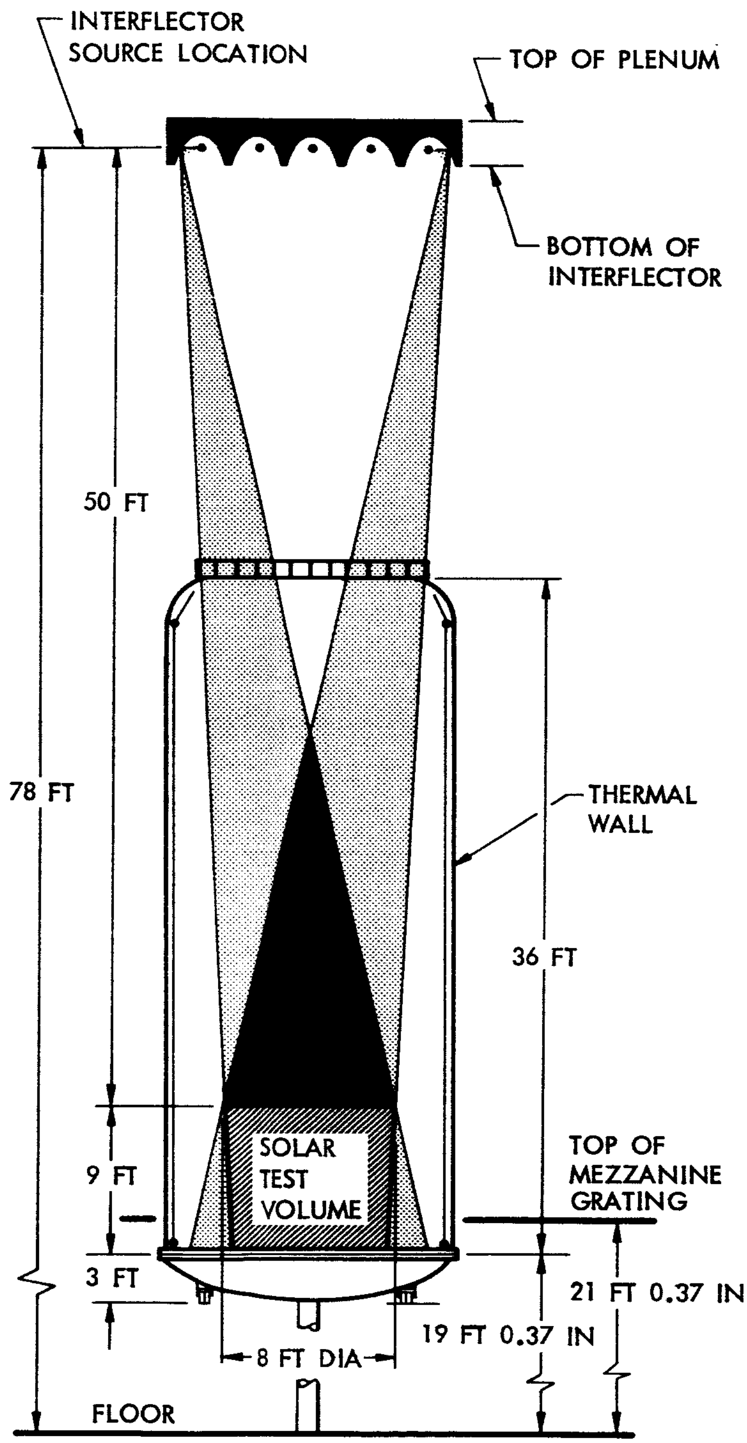

Figure A-6 S-4A Solar Simulator System

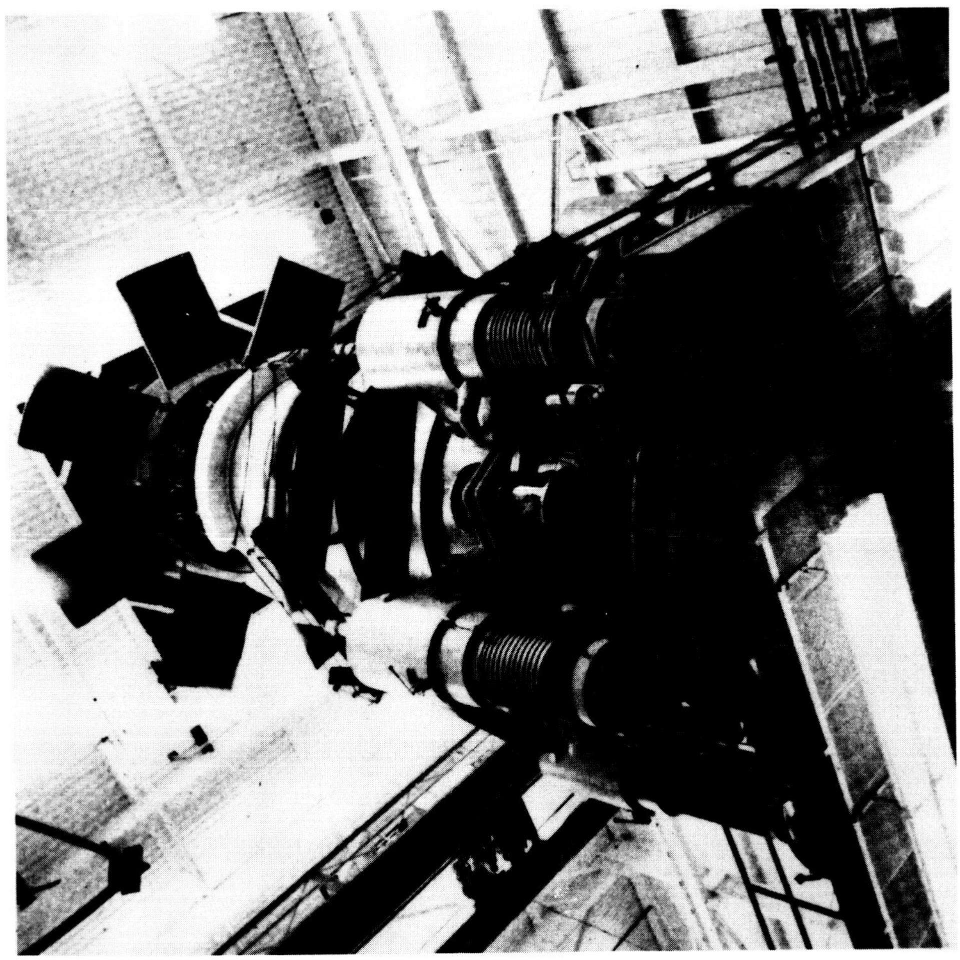

Figure A-7 Hughes S-4A Solar Simulator and Chamber

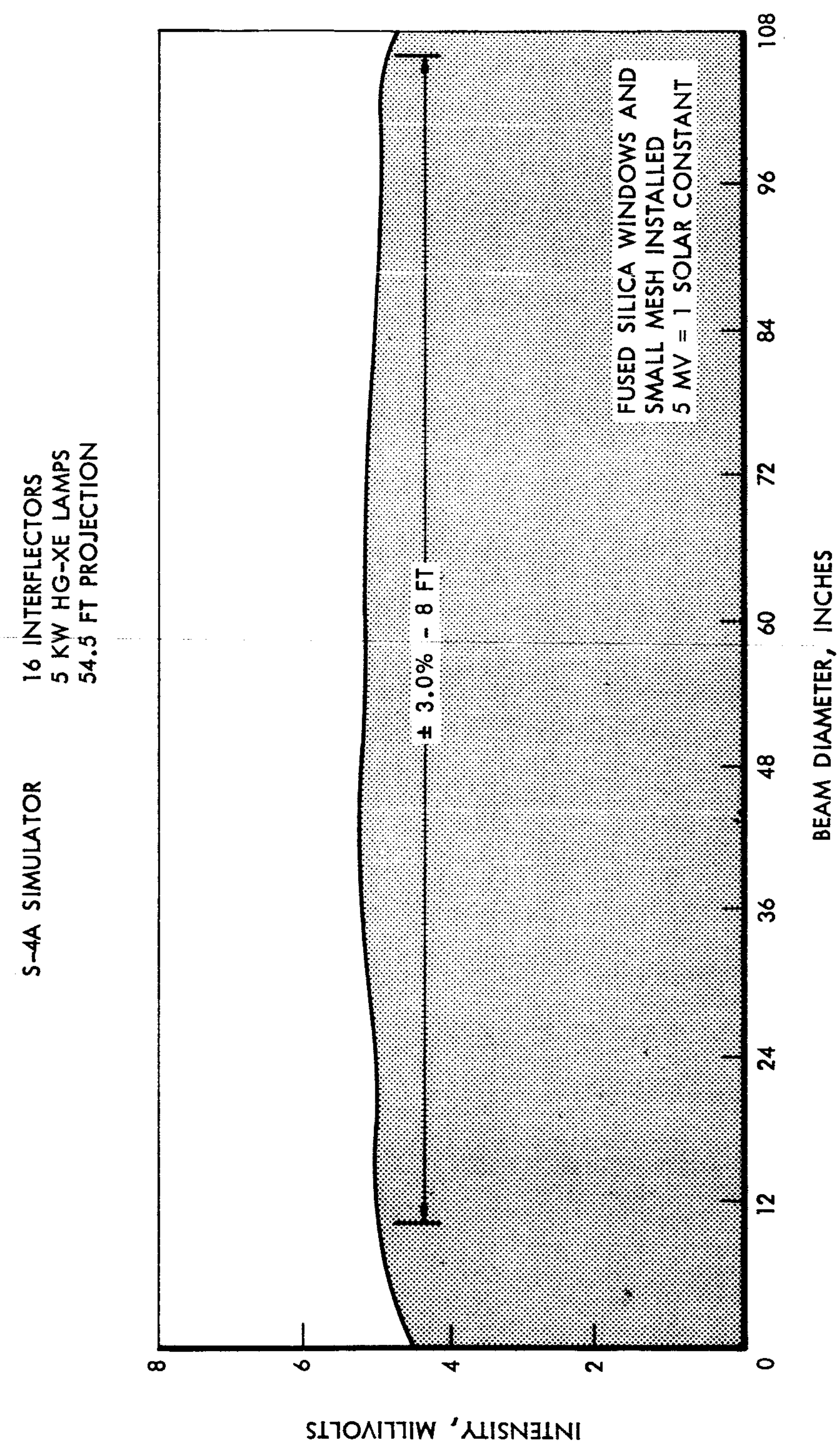

Figure A-8 Flux Distribution Across Beam Of The Hughes S-4A Simulator

Each interflector is designed to cover the target volume. Thus, a lamp failure does not affect the energy distribution. However, some side-loading results from this arrangement; 2% of solar constant on a vertical plane at the center, and 0.2 to 7.8% at the edge, depending upon orientation.

Hughes Data-Acquisition System

The automatic temperature-data-acquisition system at Hughes has a 600-data-channel capacity and an accuracy of $\pm 0.12\%$ of full-range or $\pm 1^{\circ}F$. Copper-constantan thermocouples from the test specimen are connected through the chamber penetrations to one or both of the two 300-channel remote stations. Each remote station contains a $32^{\circ}F$ oven, to which the signal is referenced, a crossbar scanning switch, and a 1000:1 solid-state amplifier which amplifies the millivolt difference signal. The crossbar scanning switch can be set to automatically scan any number from 1-600 channels. The amplified difference signal from any channel is then connected to the central-control unit which contains the logic circuitry for the system. This central-control unit contains:

a. A digital voltmeter which provides a digital display of the voltage.
b. A digital clock for temperature/time reference.
c. A junction box which allows the connection of a summary punch-to-punch cards, and provides a date reference.
d. A data translator which converts the 10-line digit-coded data to BCD digit data.
e. A tape perforator which punches the BCD data on paper tape simultaneously with the punching of cards.

The system is shown schematically in Figure A-9.

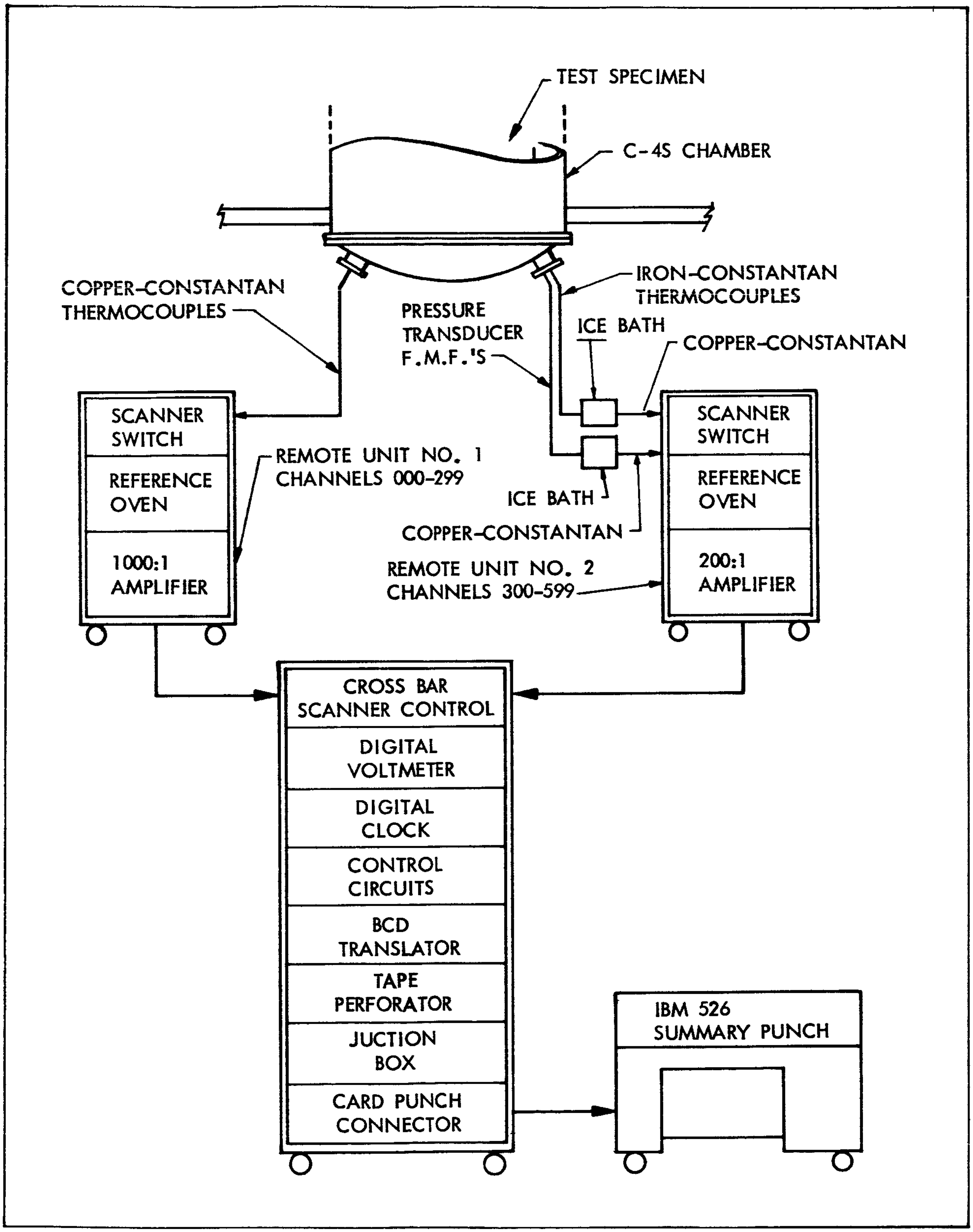

Figure A-9 Data Acquisition System At Hughes Facility

APPENDIX B - MATERIALS PROPERTIES

THERMAL CONDUCTIVITY DETERMINATIONS

Thermal conductivity determinations on the two types of honeycomb used in the model were made with a Lockheed-designed guarded hot plate, Figures B-1 and B-2. This apparatus is capable of making thermal conductivity determinations in accordance with ASTM C-177-45 to hot side temperatures of 1500°F and cold side temperatures of -100°F. At a mean temperature of 150°F and 10^{-4} torr vacuum, the aluminum-core honeycomb had a conductivity of 7 BTU/hr ft^2 - $^{\circ}$F/in, while for the same mean temperature the phenolic core had a conductivity of 0.56 BTU/hr ft^2 - $^{\circ}$F/in. The test results are shown in Figure B-3, together with those points from North American data which are roughly comparable. Table B-1 gives the actual hot side temperatures as well as details.

EMISSIVITY DETERMINATIONS

Emissivity measurements were made on the two model coatings of primary interest, CAT-A-LAC Flat Black (463-3-8), and Kemacryl non-leafing aluminum. The CAT-A-LAC coating is an epoxy base, while the Kenacryl coating is an acrylic lacquer base. Normal emissivity measurements were made with a Barnes Model R-4F1 Radiometer, using a Barnes Model 11-101 Infra-Red Radiation Source as the standard black body. The emissivity of CAT-A-LAC Flat Black was 0.975 through the temperature range of 100 to 250°F. The non-leafing aluminum acrylic lacquer had an emissivity of approximately 0.51 through the same range. A plot of the experimental data is given in Figure B-4.

PUMP-DOWN CHARACTERISTICS OF TEST MATERIALS

A brief investigation was made to determine if "virtual leaks" from the honeycomb would greatly delay pump-down time. These tests were done in the

Figure B-1 Control Console for Lockheed Guarded Hot-Plate

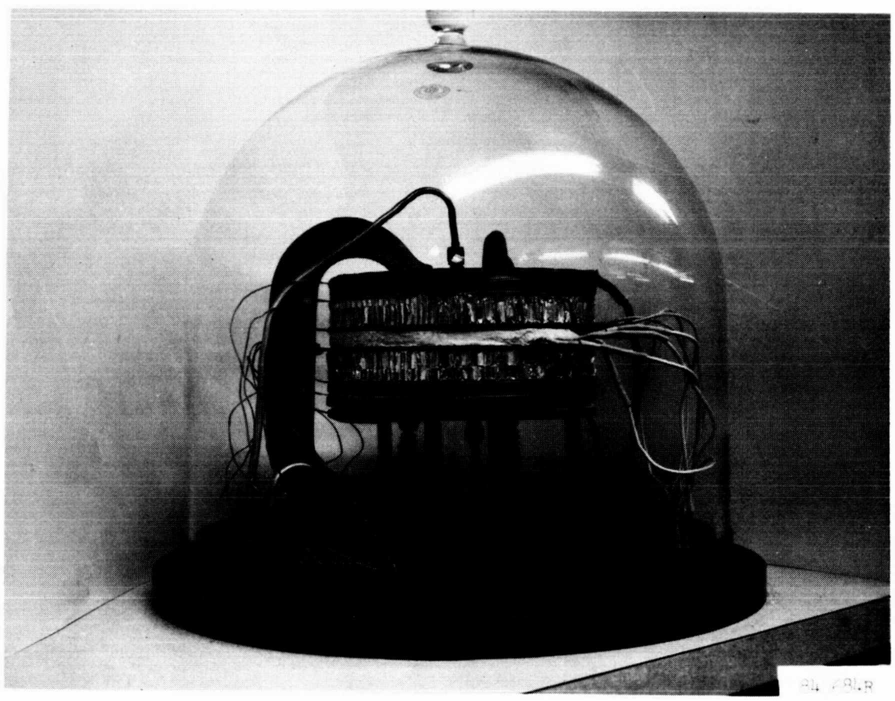

Figure B-2 Guarded Hot-Plate with Honeycomb Specimens

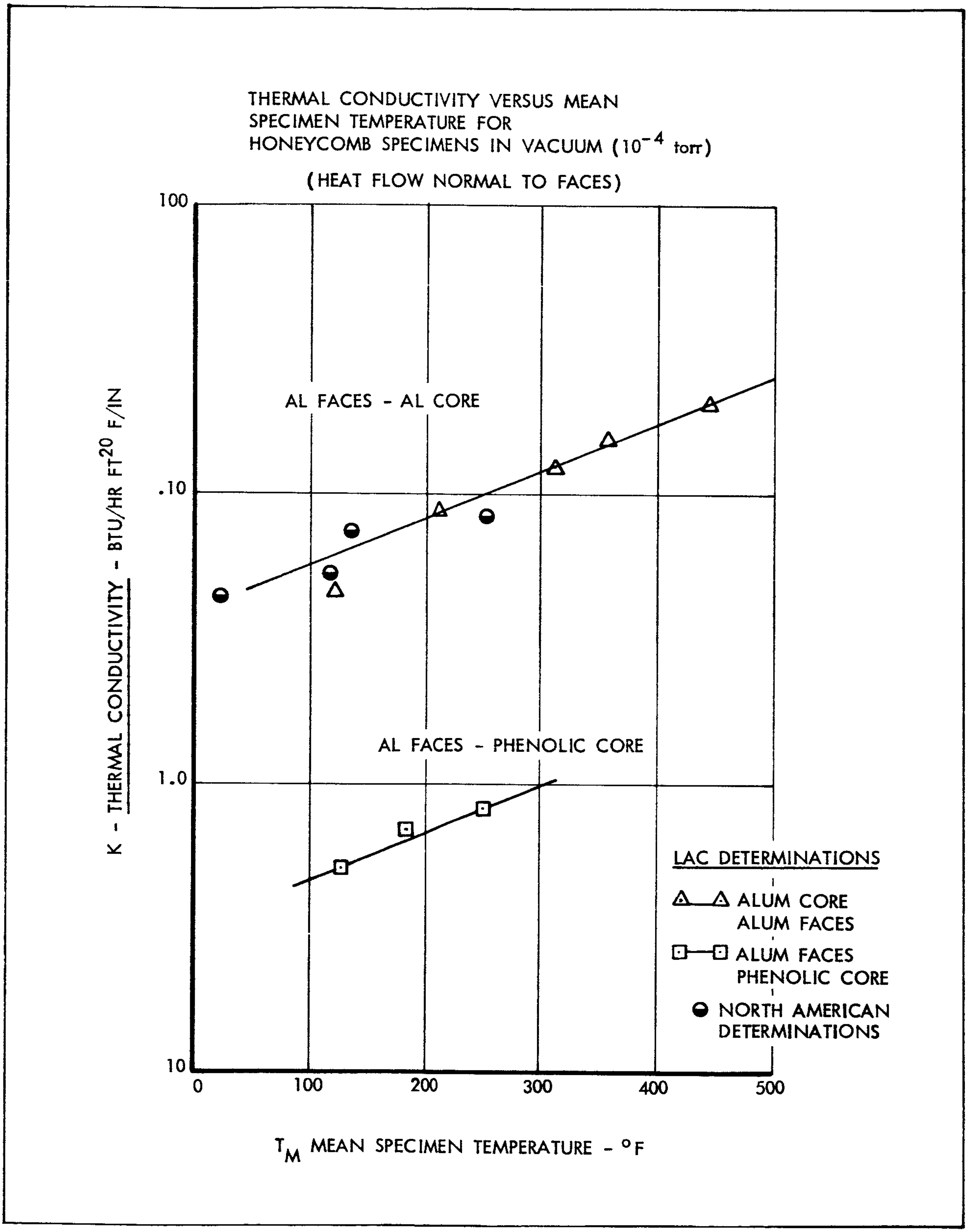

Figure B-3 Thermal Conductivity vs Mean Specimen Temperature for Honeycomb Specimens in Vacuum (10-4 torr)

Table B-1

THERMAL CONDUCTANCE OF HONEYCOMB--NORMAL TO FACES

Specimen Symbol	Temperature, °F				Thickness inches
	K*	T_{MEAN}	T_{HOT}	ΔT	
Alum. Core Alum. Faces	4.63	121.3	159.0	75.4	1.05
	8.65	211.9	221.1	18.4	"
	12.2	312.0	326.1	28.2	"
	15.1	359.3	374.0	29.4	"
(1)	20.6	443.3	460.7	34.8	"
Phenolic Core Alum. Faces	.518	125.6	156.4	61.6	.425
	.672	185.3	251.7	132.8	"
	.820	251.3	353.3	204.0	"
(2)					

*BTU-in./hr.sq.ft.°F

Note: 10^{-4} Torr Vac.

(1) Faces: 0.012" thick 2024T42 Al.Alloy
Core: 5052 Al. Alloy, 3/16" - 0.001" P
Adhesive: HT-424
Mfg: General Veneer, Los Angeles

(2) Faces: 0.016" thick 2024T3
Core: HRP 3/16" - GFH11-4 Phenolic
Adhesive: HT-424
Mfg: General Veneer, Los Angeles

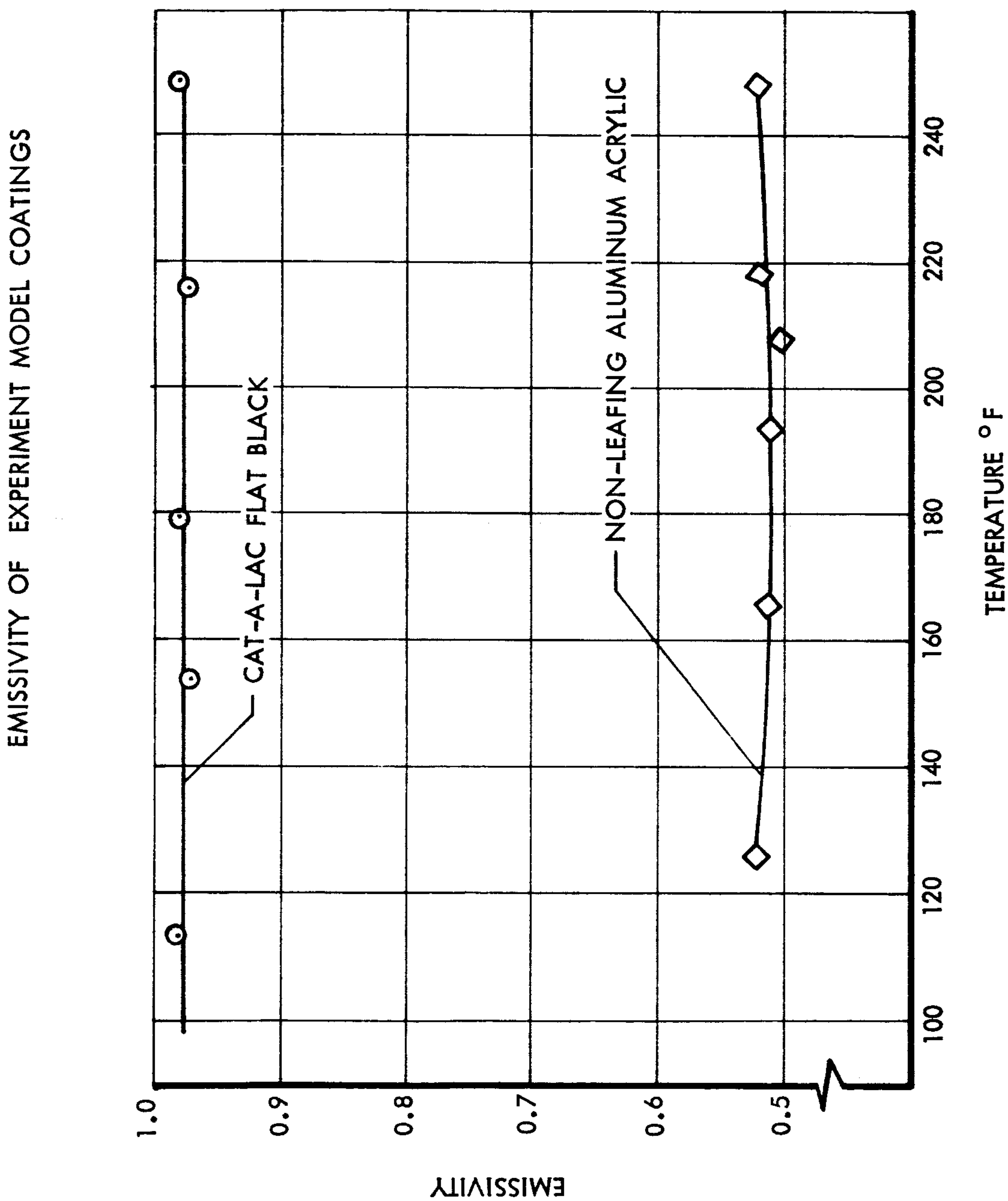

Figure B-4 Emissivity of Experimental Model Coatings small C-4 chamber. From Figure B-5 it was apparent that the honeycomb speciments did not increase the pump-down time. The fact that the chamber pumped down slightly faster with the honeycomb merely indicates the usual trend with vacuum equipment; that is, each successive pump-down de-gases the chamber walls slightly and improves the performance. This effect was apparently more significant than any out-gassing from the honeycomb. In another test, 900 feet of 30-gage copper-constantan thermocouple wire insulated with silicone impregnated fiberglas was put in the same chamber. As indicated in Figure B-6, a substantial but not serious increase in pump-down time is attributable to the thermocouple wire. The C-4 chamber in which these tests were run is 2 feet in diameter by 2-1/2 feet long. In addition to the usual mechanical forepumping equipment, it has one CVC KS-600 diffusion ejection pump and one CVC MC-28000 - 32" oil diffusion pump with cold trap.

MATERIALS AND COATINGS DATA

Various properties of materials used in the Phase II analysis are given in Table B-2. Manufacturers' data on the model or cold wall coatings used during the program are presented in Table B-3.

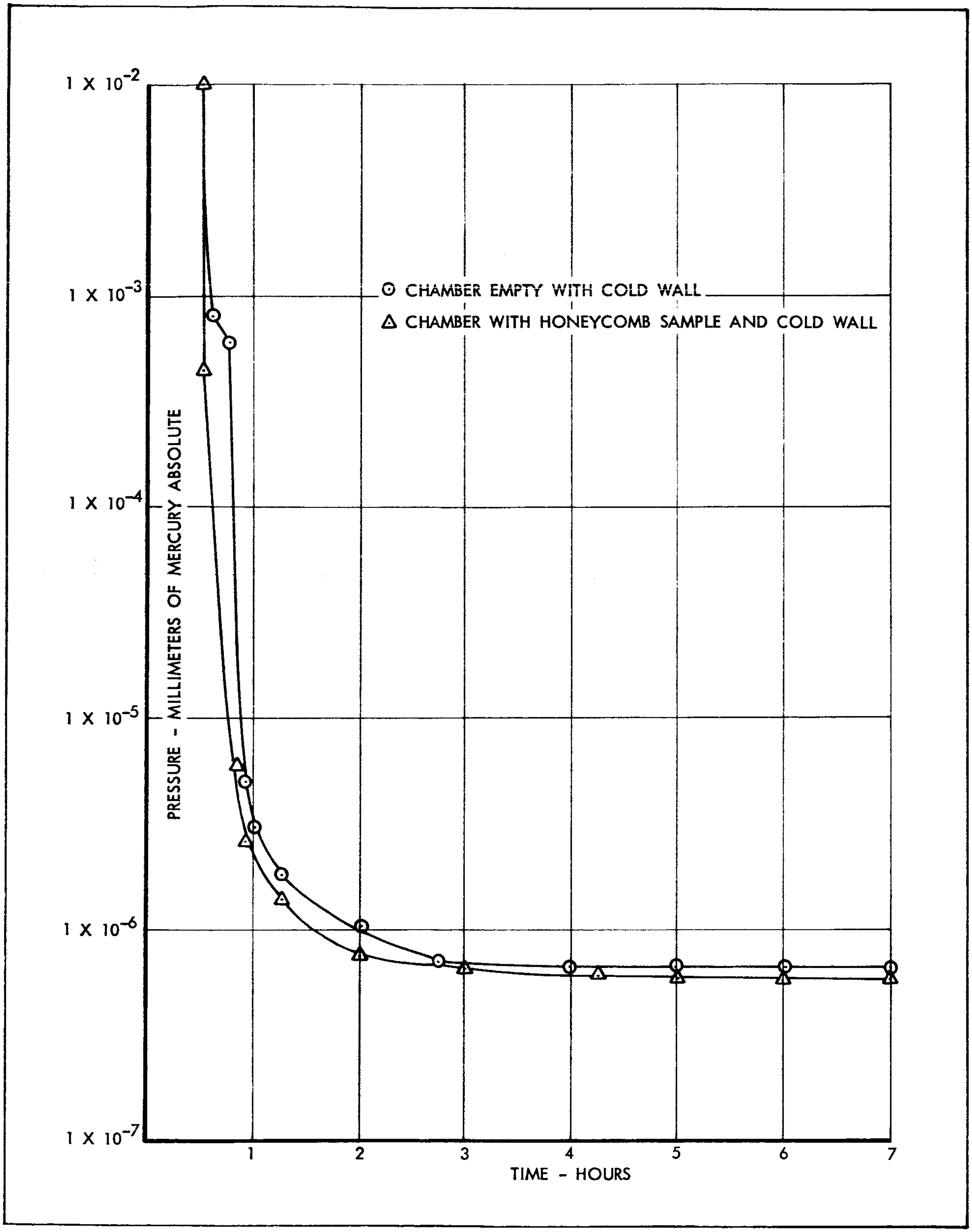

Figure B-5 Influence on Pump-Down Period of Two
9.0-in.-dia. x 1.0-in.-thick Cored Specimens

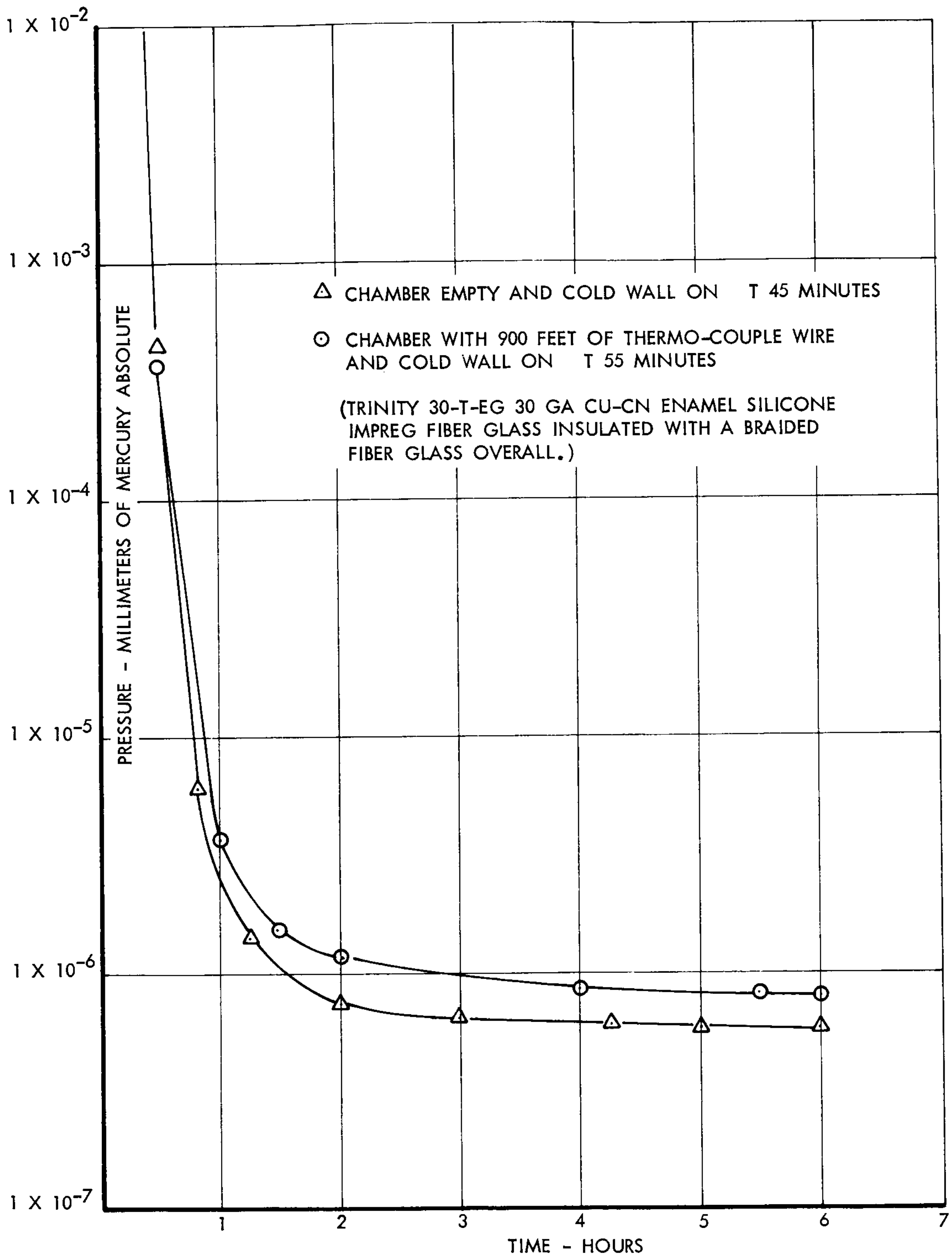

Figure B-6 Influence on Pump-Down Period of 900 ft of Thermocouple Wire

TABLE B-2 MATERIAL PROPERTIES

Material	Type	Thermal Conductivity BTU/hr. ft.°F	Density lb/in.^{3}	Specific Heat BTU/lb °F
Aluminum	5052	80.	0.0968	0.206
	2024	73.	0.100	0.206
	7075	73.	0.101	0.206
	6061	67.	0.098	0.206
	6063	84.	0.098	0.206
Stainless steel	304	9.4	0.282	0.282
Transite		0.375	0.058	--
Quartz fiber		2.7×10^{-3}	0.00347	0.187

Honeycomb	Dimensions	R $\frac{\text{Sec °F}}{\text{BTU}}$	C $\frac{\text{BTU}}{\text{°F}}$
Bulkhead (Al core)	1/8 x 0015 x 1.0	$15,400\ (\frac{L}{W})$	11.4×10^{-4} (A)
Panel (Al core)	3/16 x 0.001 x 3/8	$22,800\ (\frac{L}{W})$	6.07×10^{-4} (A)
Heat shield (Phenolic core)		$43,000\ (\frac{L}{A})$	8.9×10^{-4} (A)

Note: L = inches W = inches A = inches^2

TABLE B-3 MANUFACTURER'S INFORMATION ON MODEL COATINGS

Description	Characteristics and Composition	Commercial Product	Absorptance (α)	Emittance (ϵ)	Cure Requirements
Acrylic Primer	Primer for Acrylic Lacquer	P40GC1 Primer V66VC48 Catalyst			Room temperature cure primer one (1) hour before top coating
Black Acrylic Lacquer	Black No. 37038 (flat) per Fed. Std. 595	Kemacryl M49BC12 Reducer R7KC234 (Sherwin Williams Co.)	0.93 ± .03	$0.90\,^{+.03}_{-.06}$	Room temperature cure ½ hr. minimum between coats and 24 hrs. (min.) after final coat
Aluminum Acrylic Lacquer (Non-Leafing)	Composition as follows:		.41 ± .03	.48 ± .05	Room temperature cure 1 hr. (min.) before top coating
	(1) Clear Acrylic 96.0 ± 0.5 fluid ounces	Kemacryl T40CC6 (Sherwin Williams Co.)			Room temperature cure ½ hr. between coats and 48 hrs. (min.) after final coat
	(2) Aluminum Paste 18.0 ± 0.1 ounces	MD 787 (Metals Disintegrating Co.)			
	(3) Ethylene Glycol Monobutyl Ether 13 ± 0.5 fluid ounces	---			
	(4) Toluol 13 ± 0.5 fluid ounces	---			
Black Epoxy		CAT-A-LAC Flat Black 463-3-8 Catalyst 463-3-8 Reducer TL-29 (Finch Paint & Chemical Co. Torrance, Calif.)		.9 @ 530°R	Room temperature cure 1 hr. before top coating Room temperature cure 24 hrs. after final coat
Black Lacquer	C144 Black Special (Z6020 Catalyst -- not used) Lockheed formulated Thin with lacquer thinner (150% by volume) before use.			.93	Air dry overnight. Then step cure from 150°F through 550°F in 100° increments and one hour hold, except at 550°F, hold for four hours.
Alkyd Enamel Oil Base	101C10 Black Velvet	101C10 Black Velvet (Minn. Mining & Mfg. Co.)	0.95 - 0.98	0.933 @ 100°K 0.942 @ 300°K	

LOCKHEED
CALIFORNIA COMPANY

APPENDIX C - SELECTED TEST DATA

The data presented in Figures C-1 through C-3 consist of the pressure, temperature, and solar radiation values which were maintained during the Series 5 tests.

RESISTOR AND CAPACITOR VALUES

The values of resistors and capacitors used during the analysis of the Series 5 model are listed in Table C-1. In Table C-1, the terms DEC01, DEC02, etc., refer to the number of resistor or capacitor values listed on that line. Each resistor entry consists of the resistor number, the node numbers connected by the resistor, and the value of the resistor in sec-$^{\circ}$F/Btu. A value of 0. is a dummy value, indicating a radiation resistor. Radiation resistors are listed again separately, giving the radiation K values. Capacitor entries consist of node number followed by the capacity of the node in Btu/$^{\circ}$F.

SAMPLE COMPUTER OUTPUT

Sample pages of the computer output for the Series 4 and Series 5 runs are shown in Tables C-2 and C-3. The output format consists of node numbers and temperatures grouped according to their regional location on the model. The time, computation interval, R-C minimum, and the computation cycle are printed on the top of each output page.

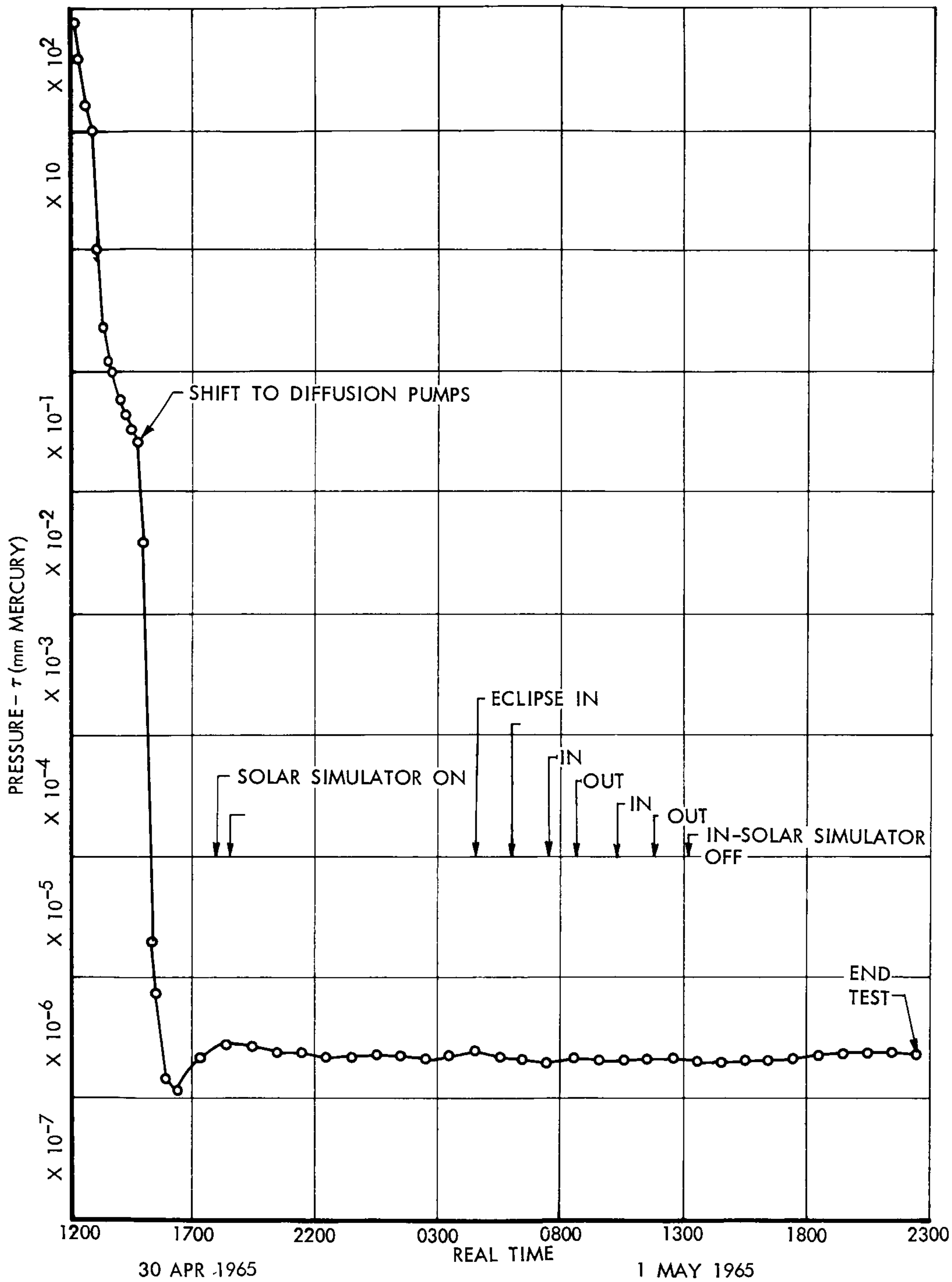

Figure C-1 Hughes C-4 Chamber Pressure During Series 5 Tests

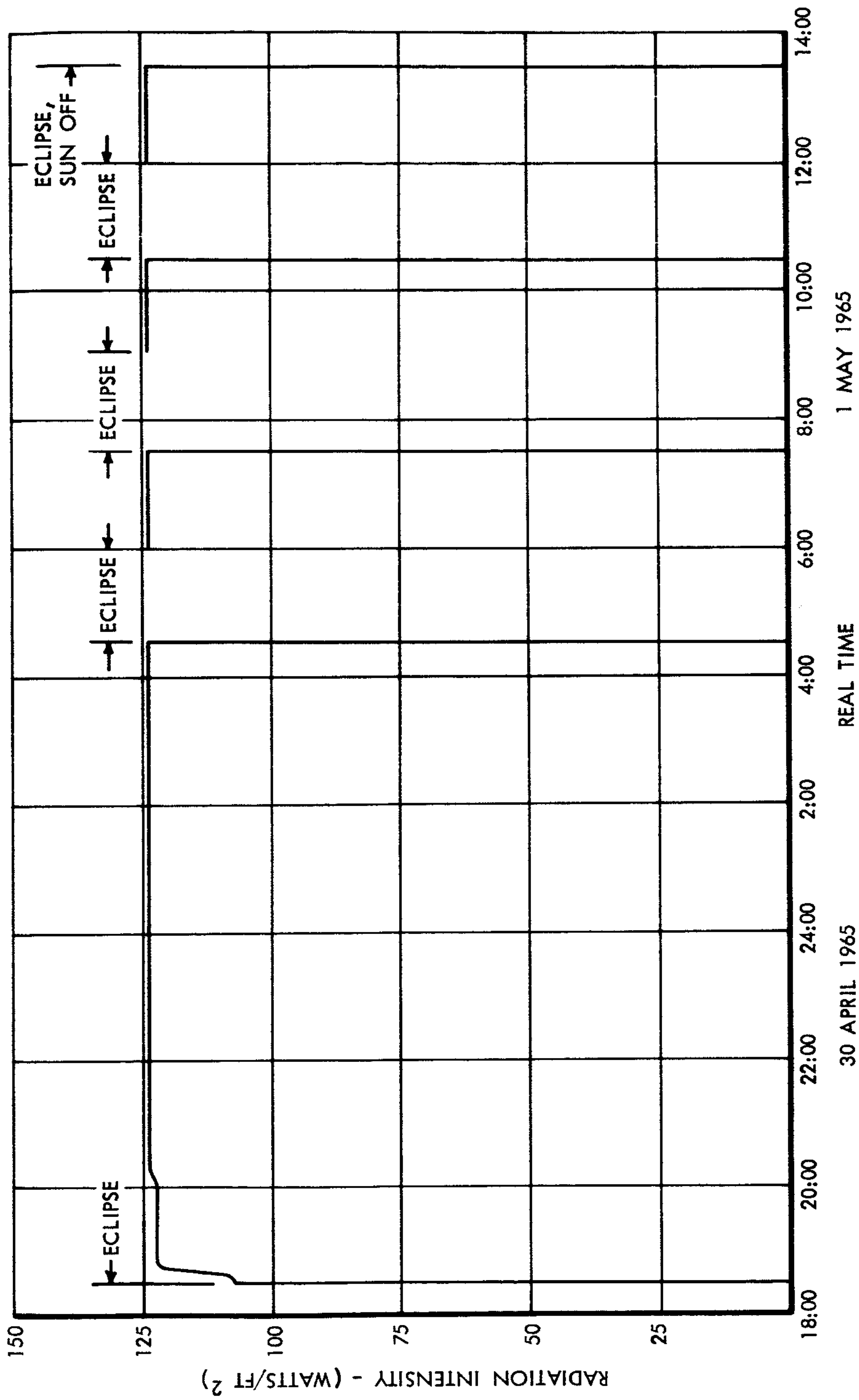

Figure C-2 Solar Radiation Intensity During Series 5 Test

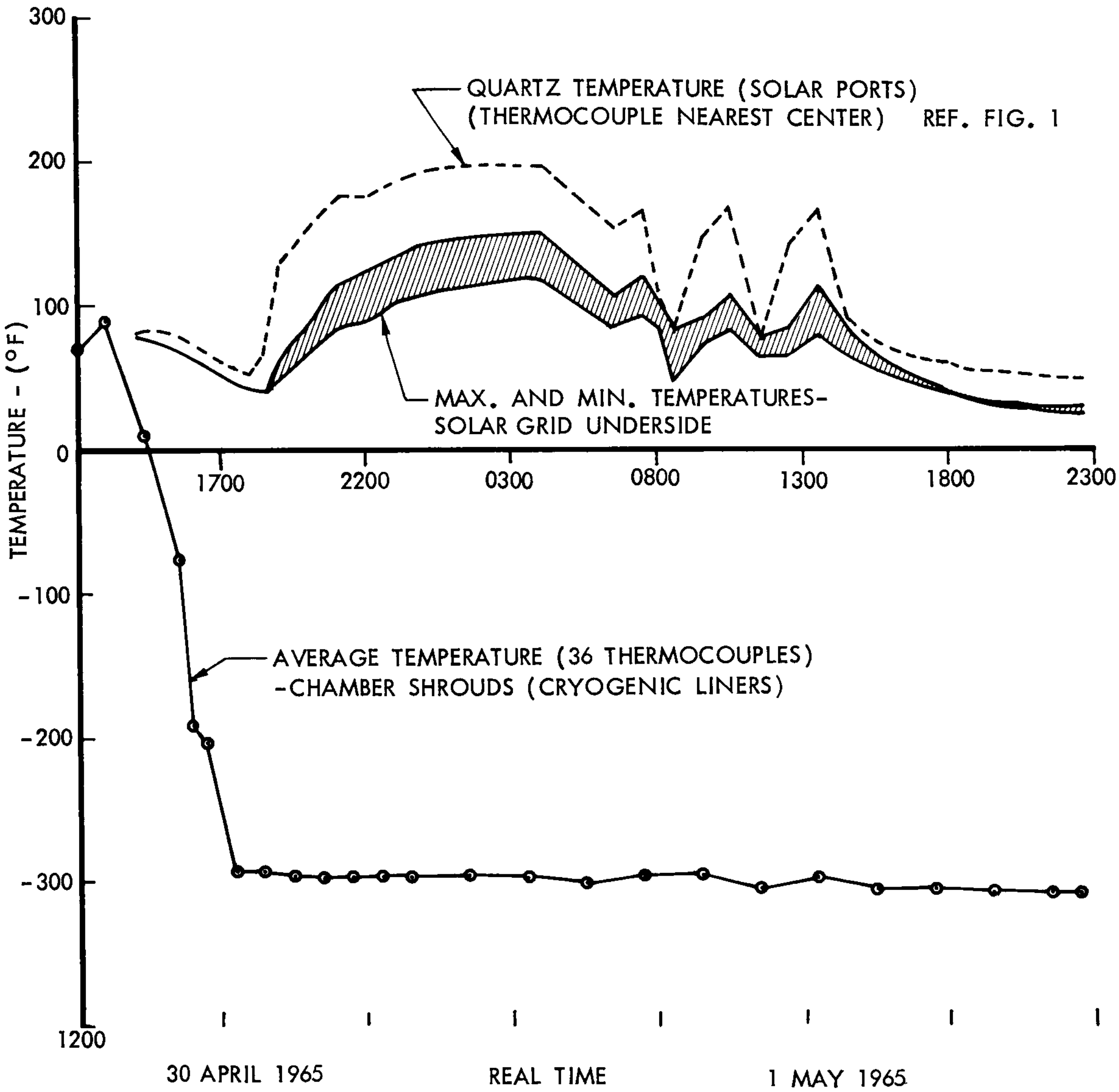

Figure C-3 Temperature of Critical C-4 Chamber Elements During the Series 5 Test

TABLE C-1 INPUT LISTING

```
                        THRUST CHAMBER
      R(490)=RAD(426,390,3.28E-5)
      R(491)=RAD(428,390,2.77E-5)
      R(492)=RAD(430,390,2.33E-5)
      R(493)=RAD(432,390,3.28E-5)
      R(494)=RAD(434,390,2.77E-5)
      R(495)=RAD(436,390,2.33E-5)
      R(390)=RAD(326,390,3.13E-6)
      R(391)=RAD(328,390,2.63E-6)
      R(392)=RAD(330,390,2.23E-6)
      R(393)=RAD(332,390,3.13E-6)
      R(394)=RAD(334,390,2.63E-6)
      R(395)=RAD(336,390,2.23E-6)
      R(396)=RAD(391,390,4.15E-5)
                        NOZZLE-H.S.
      R(551)=RAD(251,351,2.74E-5)
      R(552)=RAD(252,352,2.34E-5)
      R(553)=RAD(253,353,1.95E-5)
      R(554)=RAD(254,354,2.74E-5)
      R(555)=RAD(255,355,2.34E-5)
      R(556)=RAD(256,356,1.95E-5)
      R(557)=RAD(257,357,1.04E-5)

      R(558)=RAD(258,358,.885E-5)
      R(559)=RAD(259,359,.740E-5)
      R(560)=RAD(260,360,1.04E-5)
      R(561)=RAD(261,361,.885E-5)
      R(562)=RAD(262,362,.740E-5)
                        HEAT SHIELD EXT RAD
      R(657)=RAD(357,100,2.27E-4)/E3
      R(658)=RAD(358,100,1.95E-4)/E3
      R(659)=RAD(359,100,1.62E-4)/E3
      R(660)=RAD(360,100,2.27E-4)/E3
      R(661)=RAD(361,100,1.95E-4)/E3
      R(662)=RAD(362,100,1.62E-4)/E3
      R(663)=RAD(363,100,5.65E-4)/E3
      R(664)=RAD(364,200,4.84E-4)/E3
      R(665)=RAD(365,200,4.05E-4)/E3
      R(666)=RAD(366,200,5.65E-4)/E3
      R(667)=RAD(367,100,4.85E-4)/E3
      R(668)=RAD(368,100,4.05E-4)/E3
                        HEAT SHIELD INT. RAD
      R(750)=RAD(371,394,1.68E-6)
      R(751)=RAD(372,395,1.43E-6)
      R(752)=RAD(373,61,1.20E-6)
      R(753)=RAD(374,397,1.68E-6)
      R(754)=RAD(375,396,1.43E-6)
      R(755)=RAD(376,73,1.20E-6)
      R(756)=RAD(377,394,1.02E-6)
      R(757)=RAD(378,395,0.88E-6)
      R(758)=RAD(379,61,0.74E-6)
      R(759)=RAD(380,397,1.02E-6)
      R(760)=RAD(381,396,0.88E-6)
      R(761)=RAD(382,73,0.74E-6)
      R(762)=RAD(383,394,1.68E-6)
      R(763)=RAD(384,395,1.43E-6)
      R(764)=RAD(385,61,1.20E-6)
      R(765)=RAD(386,397,1.68E-6)
      R(766)=RAD(387,396,1.43E-6)
      R(767)=RAD(388,73,1.20E-6)
```

```
                        FUEL CELL            SERIES 3
      R(701)=RAD(59,393,12.0E-6)
      R(702)=RAD(159,393,5.0E-6)
      R(703)=RAD(161,393,7.0E-6)
      R(704)=RAD(163,393,5.0E-6)
      R(705)=RAD(63,393,12.0E-6)
      R(706)=RAD(181,393,4.0E-6)
      R(707)=RAD(180,393,3.0E-6)
      R(708)=RAD(179,393,4.0E-6)
      R(709)=RAD(339,393,2.30E-6)
      R(710)=RAD(330,393,.820E-6) /27.2
      R(711)=RAD(340,393,2.30E-6)
      R(712)=RAD(311,323,2.88E-6)
      R(713)=RAD(439,393,20.8E-6)
      R(714)=RAD(430,393,6.75E-6) /27.2
      R(715)=RAD(440,393,20.8E-6)
      R(716)=RAD(411,393,25.3E-6)
                        EMISSIVITY CORRECTION
      DO 107 I=1,16
      R(I+700)=R(I+700)*39.4
  107 CONTINUE
                        EXT RAD  OUTER PANEL
      E1=.92
      DO 108 I=100,150,50

      R(I+ 1)=RAD(100,I+ 1,1.11E-4)/E1
      R(I+ 3)=RAD(100,I+ 3,1.30E-4)/E1
      R(I+ 5)=RAD(100,I+ 5,1.21E-4)/E1
      R(I+ 7)=RAD(200,I+ 7,1.11E-4)/E2
      R(I+ 9)=RAD(200,I+ 9,1.02E-4)/E2
      R(I+11)=RAD(200,I+11,.933E-4)/E2
      R(I+13)=RAD(200,I+13,1.11E-4)/E2
      R(I+15)=RAD(200,I+15,1.30E-4)/E2
      R(I+17)=RAD(100,I+17,1.21E-4)/E1
      R(I+19)=RAD(100,I+19,1.11E-4)/E1
      R(I+21)=RAD(100,I+21,1.02E-4)/E1
      R(I+23)=RAD(100,I+23,.933E-4)/E1
  108 CONTINUE
      DO 109 I=200,400,200
      R(I+ 1)=RAD(100,I+ 1,1.49E-4)/E1
      R(I+ 2)=RAD(100,I+ 2,1.73E-4)/E1
      R(I+ 3)=RAD(100,I+ 3,2.59E-4)/E1
      R(I+ 4)=RAD(100,I+ 4,1.73E-4)/E1
      R(I+ 5)=RAD(100,I+ 5,1.75E-4)/E1
      R(I+ 6)=RAD(100,I+ 6,1.49E-4)/E1
      R(I+ 7)=RAD(200,I+ 7,2.22E-4)/E2
      R(I+ 8)=RAD(200,I+ 8,1.48E-4)/E2
      R(I+ 9)=RAD(200,I+ 9,1.36E-4)/E2
      R(I+10)=RAD(200,I+10,1.24E-4)/E2
      R(I+11)=RAD(200,I+11,1.86E-4)/E2
      R(I+12)=RAD(200,I+12,1.24E-4)/E2
      R(I+13)=RAD(200,I+13,1.49E-4)/E2
      R(I+14)=RAD(200,I+14,1.73E-4)/E2
      R(I+15)=RAD(200,I+15,2.59E-4)/E2
      R(I+16)=RAD(100,I+16,1.73E-4)/E1
      R(I+17)=RAD(100,I+17,1.75E-4)/E1
      R(I+18)=RAD(100,I+18,1.48E-4)/E1
      R(I+19)=RAD(100,I+19,2.22E-4)/E1
      R(I+20)=RAD(100,I+20,1.48E-4)/E1
      R(I+21)=RAD(100,I+21,1.36E-4)/E1
      R(I+22)=RAD(100,I+22,1.24E-4)/E1
      R(I+23)=RAD(100,I+23,1.86E-4)/E1
      R(I+24)=RAD(100,I+24,1.24E-4)/E1
```

TABLE C-1 (CONTINUED)

```
109   CONTINUE                                                    392
      R(301)=RAD(100,301,1.99E-4)/E1                              393
      R(302)=RAD(100,302,2.32E-4)/E1                              394
      R(303)=RAD(100,303,3.45E-4)/E1                              395
      R(304)=RAD(100,304,2.32E-4)/E1                              396
      R(305)=RAD(100,305,2.33E-4)/E1                              397
      R(306)=RAD(100,306,1.98E-4)/E1                              398
      R(307)=RAD(200,307,2.98E-4)/E2                              399
      R(308)=RAD(200,308,1.98E-4)/E2                              401
      R(309)=RAD(200,309,1.82E-4)/E2                              402
      R(310)=RAD(200,310,1.65E-4)/E2                              403
      R(311)=RAD(200,311,2.48E-4)/E2                              404
      R(312)=RAD(200,312,1.65E-4)/E2                              405
      R(313)=RAD(200,313,1.99E-4)/E2                              406
      R(314)=RAD(200,314,2.32E-4)/E2                              407
      R(315)=RAD(200,315,3.45E-4)/E2                              408
      R(316)=RAD(100,316,2.32E-4)/E1                              409
      R(317)=RAD(100,317,2.33E-4)/E1                              410
      R(318)=RAD(100,318,1.98E-4)/E1                              411
      R(319)=RAD(100,319,2.98E-4)/E1                              412
      R(320)=RAD(100,320,1.98E-4)/E1                              413
      R(321)=RAD(100,321,1.82E-4)/E1                              414
      R(322)=RAD(100,322,1.65E-4)/E1                              415
      R(323)=RAD(100,323,2.48E-4)/E1                              416
      R(324)=RAD(100,324,1.65E-4)/E1                              417
C                         EMISSIVITY CORRECTIONS   SERIES 3        420
      F1=.96                                                      421
      DO 110 I=1,6                                                422
      R(I+389)=R(I+389)*F1*.7                                     423
      R(I+489)=R(I+489)*F1                                        424
110   CONTINUE                                                    425
C     TO PREVENT UNDERFLOW AT OR BEFORE STATEMENT 121...          430
      DO 111 I=11,49                                              431
      R(I+1250)=1.                                                432
      R(I+1350)=1.                                                433
      R(I+1450)=1.                                                434
111   CONTINUE                                                    435
C                         10 LAYERS NRC                           448
      G1=.333                                                     449
C                         INT RAD  PANEL-I.C. STRAIGHT            450
      DO 112 I=1,3                                                451
      K=I*100                                                     452
      R(K+1164)=RAD(K+130,K+110,.829E-5) *G1                      459
      R(K+1165)=RAD(K+130,K+111,.829E-5) *G1                      460
      R(K+1166)=RAD(K+130,K+112,.829E-5) *G1                      461
      R(K+1173)=RAD(K+136,K+122,.829E-5) *G1                      468
      R(K+1174)=RAD(K+136,K+123,.829E-5) *G1                      469
      R(K+1175)=RAD(K+136,K+124,.829E-5) *G1                      470
112   CONTINUE                                                    471
C                         INT RAD PANEL-I.C.   DIAGONAL           472
      DO 113 I=1,3                                                473
      K=I*100                                                     474
      R(K+1180)=RAD(I+309,230,.237E-5)     *G1                    479
      R(K+1181)=RAD(I+209,330,.237E-5)     *G1                    480
      R(K+1186)=RAD(I+321,236,.237E-5)     *G1                    485
      R(K+1187)=RAD(I+221,336,.237E-5)     *G1                    486
      R(K+1192)=RAD(I+409,330,.237E-5)     *G1                    491
      R(K+1193)=RAD(I+309,430,.237E-5)     *G1                    492
      R(K+1198)=RAD(I+421,336,.237E-5)     *G1                    497
      R(K+1199)=RAD(I+321,436,.237E-5)     *G1                    498
113   CONTINUE                                                    499
C                         PROPELLANT TANKS      SERIES 3          500
      R(226)=RAD(203,394,9.54E-5)                                 501
      R(241)=RAD(202,394,6.63E-5)                                 502
      R(265)=RAD(237,394,13.1E-5)                                 503
      R(242)=RAD(204,394,6.63E-5)                                 504
      R(266)=RAD(238,394,13.1E-5)                                 505
      R(277)=RAD(226,394,7.29E-5)                                 506
      R(267)=RAD(238,395,12.8E-5)                                 507
      R(243)=RAD(206,395,5.45E-5)                                 508
      R(228)=RAD(207,395,7.28E-5)                                 509
      R(244)=RAD(208,395,5.45E-5)                                 510
      R(268)=RAD(239,395,12.8E-5)                                 511
      R(278)=RAD(228,395,5.80E-5)                                 512
      R(274)=RAD(242,396,12.8E-5)                                 513
      R(281)=RAD(234,396,5.80E-5)                                 514
      R(273)=RAD(241,396,12.8E-5)                                 515
      R(249)=RAD(218,396,5.45E-5)                                 516
      R(234)=RAD(219,396,7.28E-5)                                 517
      R(250)=RAD(220,396,5.45E-5)                                 518
      R(280)=RAD(232,397,7.29E-5)                                 519
      R(271)=RAD(240,397,13.1E-5)                                 520
      R(247)=RAD(214,397,6.63E-5)                                 521
      R(232)=RAD(215,397,9.54E-5)                                 522
      R(248)=RAD(216,397,6.63E-5)                                 523
      R(272)=RAD(241,397,13.1E-5)                                 524
      R(341)=RAD(302,394,6.63E-5)                                 525
      R(326)=RAD(303,394,9.54E-5)                                 526
      R(342)=RAD(304,394,6.63E-5)                                 527
      R(366)=RAD(338,394,13.1E-5)                                 528
      R(377)=RAD(326,394,7.29E-5)                                 529
      R(365)=RAD(337,394,13.1E-5)                                 530
      R(367)=RAD(338,395,12.8E-5)                                 531
      R(343)=RAD(306,395,5.45E-5)                                 532
      R(328)=RAD(307,395,7.28E-5)                                 533
      R(344)=RAD(308,395,5.45E-5)                                 534
      R(368)=RAD(339,395,12.8E-5)                                 535
      R(378)=RAD(328,395,5.80E-5)                                 536
      R(374)=RAD(342,396,12.8E-5)                                 537
      R(381)=RAD(334,396,5.80E-5)                                 538
      R(373)=RAD(341,396,12.8E-5)                                 539
      R(349)=RAD(318,396,5.45E-5)                                 540
      R(334)=RAD(319,396,7.28E-5)                                 541
      R(350)=RAD(320,396,5.45E-5)                                 542
      R(380)=RAD(332,397,7.29E-5)                                 543
      R(371)=RAD(340,397,13.1E-5)                                 544
      R(347)=RAD(314,397,6.63E-5)                                 545
      R(332)=RAD(315,397,9.54E-5)                                 546
      R(348)=RAD(316,397,6.63E-5)                                 547
      R(372)=RAD(341,397,13.1E-5)                                 548
      R(441)=RAD(402,394,6.63E-5)                                 549
      R(426)=RAD(403,394,9.54E-5)                                 550
      R(442)=RAD(404,394,6.63E-5)                                 551
      R(466)=RAD(438,394,13.1E-5)                                 552
      R(477)=RAD(426,394,7.29E-5)                                 553
      R(465)=RAD(437,394,13.1E-5)                                 554
      R(467)=RAD(438,395,12.8E-5)                                 555
      R(443)=RAD(406,395,5.45E-5)                                 556
      R(428)=RAD(407,395,7.28E-5)                                 557
      R(444)=RAD(408,395,5.45E-5)                                 558
      R(468)=RAD(439,395,12.8E-5)                                 559
      R(478)=RAD(428,395,5.80E-5)                                 560
      R(474)=RAD(442,396,12.8E-5)                                 561
      R(481)=RAD(434,396,5.80E-5)                                 562
      R(473)=RAD(441,396,12.8E-5)                                 563
      R(449)=RAD(418,396,5.45E-5)                                 564
      R(434)=RAD(419,396,7.28E-5)                                 565
      R(450)=RAD(420,396,5.45E-5)                                 566
```

TABLE C-1 (CONTINUED)

```
      R(480)=RAD(432,397,7.29E-5)                                       567
      R(471)=RAD(440,397,13.1E-5)                                       568
      R(447)=RAD(414,397,6.63E-5)                                       569
      R(432)=RAD(415,397,9.54E-5)                                       570
      R(448)=RAD(416,397,6.63E-5)                                       571
      R(472)=RAD(441,397,13.1E-5)                                       572
C                           INTERNAL RADIATION  PANEL-BEAM              600
C                            20 LAYERS NRC                              601
      G1=2.                                                             602
      R(245)=RAD(210,239,7.90E-5)       *G1                             605
      R(246)=RAD(212,240,7.90E-5)       *G1                             606
      R(251)=RAD(222,242,7.90E-5)       *G1                             611
      R(252)=RAD(224,237,7.90E-5)       *G1                             612
      R(345)=RAD(310,339,7.90E-5)       *G1                             617
      R(346)=RAD(312,340,7.90E-5)       *G1                             618
      R(351)=RAD(322,342,7.90E-5)       *G1                             623
      R(352)=RAD(324,337,7.90E-5)       *G1                             624
      R(445)=RAD(310,439,7.90E-5)       *G1                             629
      R(446)=RAD(412,440,7.90E-5)       *G1                             630
      R(451)=RAD(422,442,7.90E-5)       *G1                             635
      R(452)=RAD(424,437,7.90E-5)       *G1                             636
C                           INTERNAL RADIATION  BEAM-I.C.               637
C                            10 LAYERS NRC                              638
      G1=1.                                                             639
      R(269)=RAD(239,230,1.71E-5)       *G1                             642
      R(270)=RAD(240,230,1.71E-5)       *G1                             643
      R(275)=RAD(242,236,1.71E-5)       *G1                             648
      R(276)=RAD(237,236,1.71E-5)       *G1                             649
      R(369)=RAD(339,330,1.71E-5)       *G1                             654
      R(370)=RAD(340,330,1.71E-5)       *G1                             655
      R(375)=RAD(342,336,1.71E-5)       *G1                             660
      R(376)=RAD(337,336,1.71E-5)       *G1                             661
      R(469)=RAD(439,430,1.71E-5)       *G1                             666
      R(470)=RAD(440,430,1.71E-5)       *G1                             667
      R(475)=RAD(442,436,1.71E-5)       *G1                             672
      R(476)=RAD(437,436,1.71E-5)       *G1                             673
C                           INTERNAL RADIATION  BEAM-BEAM               674
      G1=2.                                                             675
      R(279)=RAD(239,240,1.64E-4)       *G1                             677
      R(282)=RAD(242,237,1.64E-4)       *G1                             680
      R(379)=RAD(339,340,1.64E-4)       *G1                             683
      R(382)=RAD(342,337,1.64E-4)       *G1                             686
      R(479)=RAD(439,440,1.64E-4)       *G1                             689
      R(482)=RAD(442,437,1.64E-4)       *G1                             690
      DO 116 I=2,12,2                                                   691
      R(I+800)=RAD(392,I+223,3.53E-5)                                   692
      R(I+820)=RAD(391,I+323,3.53E-5)                                   693
  116 CONTINUE                                                          694
C                           REMOVE INS FROM I.C.                        700
      DO 117 I=100,300,100                                              701
      F1=.0276                                                          702
      R(I+177)=R(I+177)*F1                                              703
      R(I+178)=R(I+178)*F1                                              704
      R(I+180)=R(I+180)*F1                                              705
      R(I+181)=R(I+181)*F1                                              706
  117 CONTINUE                                                          707
C                           F.C.-UPPER BLKHD                            800
      S1=1.                                                             801
      R(720)=RAD(393,  9,3.76E-6)*S1                                    802
      R(721)=RAD(393, 13,3.76E-6)*S1                                    803
      R(722)=RAD(393,129,1.88E-6)*S1                                    804
      R(723)=RAD(393,131,1.88E-6)*S1                                    805
      R(724)=RAD(393,109,3.76E-6)*S1                                    806
      R(725)=RAD(393,113,3.76E-6)*S1                                    807
      R(726)=RAD(393,111,3.76E-6)*S1                                    808
      R(727)=RAD(393, 11,15.0E-6)*S1                                    809
      R(728)=RAD(73,23,8.65E-5)                                         810
      R(729)=RAD(253,391,7.23E-6)                                       811
      R(730)=RAD(11,61,7.39E-5)                                         812
      R(731)=RAD(391,392,1.50E-5)                                       813
C                           EMISSIVITY CORRECTIONS  INT RAD             850
      F1=27.2                                                           851
      DO 120 I=6,62                                                     852
      R(I+220)=R(I+220)*F1                                              853
      R(I+320)=R(I+320)*F1                                              854
      R(I+420)=R(I+420)*F1                                              855
  120 CONTINUE                                                          856
      DO 121 I=11,49                                                    857

      R(I+1250)=R(I+1250)*F1                                            858
      R(I+1350)=R(I+1350)*F1                                            859
      R(I+1450)=R(I+1450)*F1                                            860
  121 CONTINUE                                                          861
C                           CORRECT FOR H.S. CONTACT RESISTANCE         862
      IF (M(1).GT.M(2)) GO TO 123                                       863
      DO 122 I=1,6                                                      864
      R(I+2270)=R(I+2270)+T(30)                                         865
      R(I+2288)=R(I+2288)+T(30)                                         866
  122 CONTINUE                                                          867
  123 CONTINUE                                                          868
```

```
DEC01 2202  201  202   6900.            PANEL CONDUCTION       2001
DEC01 2203  202  203  13800.                                   2002
DEC01 2204  203  204  13800.                                   2003
DEC01 2205  204  205   6900.                                   2004
DEC01 2206  205  206   6250.                                   2005
DEC01 2207  206  207  11800.                                   2006
DEC01 2208  207  208  11800.                                   2007
DEC01 2209  208  209   6250.                                   2008
DEC01 2210  209  210   4950.                                   2009
DEC01 2211  210  211   9900.                                   2010
DEC01 2212  211  212   9900.                                   2011
DEC01 2213  212  213   4950.                                   2012
DEC01 2214  213  214   6900.                                   2013
DEC01 2215  214  215  13800.                                   2014
DEC01 2216  215  215  13800.                                   2015
DEC01 2217  216  217   6900.                                   2016
DEC01 2218  217  218   6250.                                   2017
DEC01 2219  218  219  11800.                                   2018
DEC01 2220  219  220  11800.                                   2019
DEC01 2221  220  221   6250.                                   2020
DEC01 2222  221  222   4950.                                   2021
DEC01 2223  222  223   9900.                                   2022
DEC01 2224  223  224   9900.                                   2023
DEC01 2201  224  201   4950.                                   2024
DEC01 2302  301  302   6900.                                   2025
DEC01 2303  302  303  13800.                                   2026
DEC01 2304  303  304  13800.                                   2027
DEC01 2305  304  305   6900.                                   2028
DEC01 2306  305  306   6250.                                   2029
DEC01 2307  306  307  11800.                                   2030
DEC01 2308  307  308  11800.                                   2031
DEC01 2309  308  309   6250.                                   2032
DEC01 2310  309  310   4950.                                   2033
DEC01 2311  310  311   9900.                                   2034
DEC01 2312  311  312   9900.                                   2035
DEC01 2313  312  313   4950.                                   2036
```

TABLE C-1 (CONTINUED)

DEC01	2314	313	314	6900.		2037
DEC01	2315	314	315	13800.		2038
DEC01	2316	315	316	13800.		2039
DEC01	2317	316	317	6900.		2040
DEC01	2318	317	318	6250.		2041
DEC01	2319	318	319	11800.		2042
DEC01	2320	319	320	11800.		2043
DEC01	2321	320	321	6250.		2044
DEC01	2322	321	322	4950.		2045
DEC01	2323	322	323	9900.		2046
DEC01	2324	323	324	9900.		2047
DEC01	2301	324	301	4950.		2048
DEC01	2402	401	402	6900.		2049
DEC01	2403	402	403	13800.		2050
DEC01	2404	403	404	13800.		2051
DEC01	2405	404	405	6900.		2052
DEC01	2406	405	406	6250.		2053
DEC01	2407	406	407	11800.		2054
DEC01	2408	407	408	11800.		2055
DEC01	2409	408	409	6250.		2056
DEC01	2410	409	410	4950.		2057
DEC01	2411	410	411	9900.		2058
DEC01	2412	411	412	9900.		2059
DEC01	2413	412	413	4950.		2060
DEC01	2414	413	414	6900.		2061
DEC01	2415	414	415	13800.		2062
DEC01	2416	415	416	13800.		2063
DEC01	2417	416	417	6900.		2064
DEC01	2418	417	418	6250.		2065
DEC01	2419	418	419	11800.		2066
DEC01	2420	419	420	11800.		2067
DEC01	2421	420	421	6250.		2068
DEC01	2422	421	422	4950.		2069
DEC01	2423	422	423	9900.		2070
DEC01	2424	423	424	9900.		2071
DEC01	2401	424	401	4950.		2072
DEC01	1201	101	201	11600.	SERIES 2-5	2073
DEC01	1203	103	203	9400.		2074
DEC01	1205	105	205	11600.	SERIES 2-5	2075
DEC01	1207	107	207	11000.		2076
DEC01	1209	109	209	11600.	SERIES 2-5	2077
DEC01	1211	111	211	13200.		2078
DEC01	1213	113	213	11600.	SERIES 2-5	2079
DEC01	1215	115	215	9400.		2080
DEC01	1217	117	217	11600.	SERIES 2-5	2081
DEC01	1219	119	219	11000.		2082
DEC01	1221	121	221	11600.	SERIES 2-5	2083
DEC01	1223	123	223	13200.		2084
DEC01	1301	201	301	29600.	SERIES 2-5	2085
DEC01	1302	202	302	37600.		2086
DEC01	1303	203	303	37600.		2087
DEC01	1304	204	304	37600.		2088
DEC01	1305	205	305	29600.	SERIES 2-5	2089
DEC01	1306	206	306	44000.		2090
DEC01	1307	207	307	44000.		2091
DEC01	1308	208	308	44000.		2092
DEC01	1309	209	309	29600.	SERIES 2-5	2093
DEC01	1310	210	310	52400.		2094
DEC01	1311	211	311	52400.		2095
DEC01	1312	212	312	52400.		2096
DEC01	1313	213	313	29600.	SERIES 2-5	2097
DEC01	1314	214	314	37600.		2098
DEC01	1315	215	315	37600.		2099
DEC01	1316	216	316	37600.		2100

DEC01	1317	217	317	29600.	SERIES 2-5	2101
DEC01	1318	218	318	44000.		2102
DEC01	1319	219	319	44000.		2103
DEC01	1320	220	320	44000.		2104
DEC01	1321	221	321	29600.	SERIES 2-5	2105
DEC01	1322	222	322	52400.		2106
DEC01	1323	223	323	52400.		2107
DEC01	1324	224	324	52400.		2108
DEC01	1401	301	401	29600.	SERIES 2-5	2109
DEC01	1402	302	402	37600.		2110
DEC01	1403	303	403	37600.		2111
DEC01	1404	304	404	37600.		2112
DEC01	1405	305	405	29600.	SERIES 2-5	2113
DEC01	1406	306	406	44000.		2114
DEC01	1407	307	407	44000.		2115
DEC01	1408	308	408	44000.		2116
DEC01	1409	309	409	29600.	SERIES 2-5	2117
DEC01	1410	310	410	52400.		2118
DEC01	1411	311	411	52400.		2119
DEC01	1412	312	412	52400.		2120
DEC01	1413	313	413	29600.	SERIES 2-5	2121
DEC01	1414	314	414	37600.		2122
DEC01	1415	315	415	37600.		2123
DEC01	1416	316	416	37600.		2124
DEC01	1417	317	417	29600.	SERIES 2-5	2125
DEC01	1418	318	418	44000.		2126
DEC01	1419	319	419	44000.		2127
DEC01	1420	320	420	44000.		2128
DEC01	1421	321	421	29600.	SERIES 2-5	2129
DEC01	1422	322	422	52400.		2130
DEC01	1423	323	423	52400.		2131
DEC01	1424	324	424	52400.		2132
DEC01	1501	401	151	11600.	SERIES 2-5	2133
DEC01	1503	403	153	9400.		2134
DEC01	1505	405	155	11600.	SERIES 2-5	2135
DEC01	1507	407	157	11000.		2136
DEC01	1509	409	159	11600.	SERIES 2-5	2137
DEC01	1511	411	161	13200.		2138
DEC01	1513	413	163	11600.	SERIES 2-5	2139
DEC01	1515	415	165	9400.		2140
DEC01	1517	417	167	11600.	SERIES 2-5	2141
DEC01	1519	419	169	11000.		2142
DEC01	1521	421	171	11600.	SERIES 2-5	2143
DEC01	1523	423	173	13200.		2144
DEC01	2002	101	103	14800.	BULKHEAD CONDUCTION	2145
DEC01	2004	103	105	14800.		2146
DEC01	2006	105	107	12700.	(UPPER)	2147
DEC01	2008	107	109	12700.		2148
DEC01	2010	109	111	10500.		2149
DEC01	2012	111	113	10500.		2150
DEC01	2014	113	115	14800.		2151
DEC01	2016	115	117	14800.		2152
DEC01	2018	117	119	12700.		2153
DEC01	2020	119	121	12700.		2154
DEC01	2022	121	123	10500.		2155
DEC01	2024	123	101	10500.		2156
DEC01	2025	125	126	7300.		2157
DEC01	2026	126	127	7300.		2158
DEC01	2027	127	128	6150.		2159
DEC01	2028	128	129	6150.		2160
DEC01	2029	129	130	5200.		2161
DEC01	2030	130	131	5200.		2162
DEC01	2031	131	132	7300.		2163
DEC01	2032	132	133	7300.		2164
DEC01	2033	133	134	6150.		2165
DEC01	2034	134	135	6150.		2166
DEC01	2035	135	136	5200.		2167

TABLE C-1 (CONTINUED)

DEC01	2036	136	125	5200.			2168
DEC01	2051	1	2	3750.			2169
DEC01	2052	2	103	15500.	TANK SKIRTS	SERIES 3-5	2170
DEC01	2053	103	4	15500.		SERIES 3-5	2171
DEC01	2054	4	5	3750.			2172
DEC01	2055	5	6	3750.			2173
DEC01	2056	6	107	14000.		SERIES 3-5	2174
DEC01	2057	107	8	14000.		SERIES 3-5	2175
DEC01	2058	8	9	3750.			2176
DEC01	2059	9	11	8220.			2177
DEC01	2061	11	13	8220.			2178
DEC01	2063	13	14	3750.			2179
DEC01	2064	14	115	15500.		SERIES 3-5	2180
DEC01	2065	115	16	15500.		SERIES 3-5	2181
DEC01	2066	16	17	3750.			2182
DEC01	2067	17	18	3750.			2183
DEC01	2068	18	119	14000.		SERIES 3-5	2184
DEC01	2069	119	20	14000.		SERIES 3-5	2185
DEC01	2070	20	21	3750.			2186
DEC01	2071	21	23	8220.			2187
DEC01	2073	23	1	8220.			2188
DEC01	1025	1	125	27800.			2189
DEC01	1026	2	126	15500.		SERIES 3-5	2190
DEC01	1027	4	126	15500.		SERIES 3-5	2191
DEC01	1028	5	127	30800.			2192
DEC01	1029	6	128	14000.		SERIES 3-5	2193
DEC01	1030	8	128	14000.		SERIES 3-5	2194
DEC01	1031	9	129	34500.			2195
DEC01	1032	11	130	15400.			2196
DEC01	1033	13	131	27800.			2197
DEC01	1034	14	132	15500.		SERIES 3-5	2198
DEC01	1035	16	132	15500.		SERIES 3-5	2199
DEC01	1037	18	134	14000.		SERIES 3-5	2201
DEC01	1038	20	134	14000.		SERIES 3-5	2202
DEC01	1039	21	135	34500.			2203
DEC01	1040	23	136	15400.			2204
DEC01	1001	101	1	13900.			2205
DEC01	1005	105	5	15400.			2206
DEC01	1009	109	9	17400.			2207
DEC01	1011	111	11	9700.			2208
DEC01	1013	113	13	13900.			2209
DEC01	1017	117	17	15400.			2210
DEC01	1021	121	21	17400.			2211
DEC01	2233	232	233	2880.			2312
DEC01	1023	123	23	9700.			2212
DEC01	2234	233	234	2480.			2313
DEC01	2102	151	153	14800.	BULKHEAD CONDUCTION		2213
DEC01	2235	234	235	2480.			2314
DEC01	2104	153	155	14800.			2214
DEC01	2236	235	236	2070.			2315
DEC01	2106	155	157	12700.	(LOWER)		2215
DEC01	2225	236	225	2070.			2316
DEC01	2108	157	159	12700.			2216
DEC01	2326	325	326	2890.			2317
DEC01	2110	159	161	10500.			2217
DEC01	2327	326	327	2880.			2318
DEC01	2112	161	163	10500.			2218
DEC01	2328	327	328	2480.			2319
DEC01	2114	163	165	14800.			2219
DEC01	2329	328	329	2480.			2320
DEC01	2116	165	167	14800.			2220
DEC01	2330	329	330	1035.		SERIES 3-5	2321
DEC01	2118	167	169	12700.			2221
DEC01	2120	169	171	12700.			2222
DEC01	2122	171	173	10500.			2223
DEC01	2124	173	151	10500.			2224
DEC01	2125	175	176	6600.	THRUST CHAMBER-	SERIES 3-5	2225
DEC01	2126	176	177	6600.		SERIES 3-5	2226
DEC01	2127	177	178	5600.	I.C. TIE-IN	SERIES 3-5	2227
DEC01	2128	178	179	5600.		SERIES 3-5	2228
DEC01	2129	179	180	4700.		SERIES 3-5	2229
DEC01	2130	180	181	4700.		SERIES 3-5	2230
DEC01	2131	181	182	6600.		SERIES 3-5	2231
DEC01	2132	182	183	6600.		SERIES 3-5	2232
DEC01	2133	183	184	5600.		SERIES 3-5	2233
DEC01	2134	184	185	5600.		SERIES 3-5	2234
DEC01	2135	185	186	4700.		SERIES 3-5	2235
DEC01	2136	186	175	4700.		SERIES 3-5	2236
DEC01	2151	51	52	3750.			2237
DEC01	2152	52	153	15500.		SERIES 3-5	2238
DEC01	2153	153	54	15500.		SERIES 3-5	2239
DEC01	2154	54	55	3750.			2240
DEC01	2155	55	56	3750.			2241
DEC01	2156	56	157	14000.		SERIES 3-5	2242
DEC01	2157	157	58	14000.		SERIES 3-5	2243
DEC01	2158	58	59	3750.			2244
DEC01	2159	59	61	8220.			2245
DEC01	2161	61	63	8220.			2246
DEC01	2163	63	64	3750.			2247
DEC01	2164	64	165	15500.		SERIES 3-5	2248
DEC01	2165	165	66	15500.		SERIES 3-5	2249
DEC01	2166	66	67	3750.			2250
DEC01	2167	67	68	3750.			2251
DEC01	2168	68	169	14000.		SERIES 3-5	2252
DEC01	2169	169	70	14000.		SERIES 3-5	2253
DEC01	2170	70	71	3750.			2254
DEC01	2171	71	73	8220.			2255
DEC01	2173	73	51	8220.			2256
DEC01	1125	51	175	27800.			2257
DEC01	1126	52	176	15500.		SERIES 3-5	2258
DEC01	1127	54	176	15500.		SERIES 3-5	2259
DEC01	1128	55	177	30800.			2260
DEC01	1129	56	178	14000.		SERIES 3-5	2261
DEC01	1130	58	178	14000.		SERIES 3-5	2262
DEC01	1131	59	179	34500.			2263
DEC01	1132	61	180	17400.			2264
DEC01	1133	63	181	27800.			2265
DEC01	1134	64	182	15500.		SERIES 3-5	2266
DEC01	1135	66	182	15500.		SERIES 3-5	2267
DEC01	1136	67	183	30800.			2268
DEC01	1137	68	184	14000.		SERIES 3-5	2269
DEC01	1138	70	184	14000.		SERIES 3-5	2270
DEC01	1139	71	185	34500.			2271
DEC01	1140	73	186	15400.			2272
DEC01	1101	151	51	13900.			2273
DEC01	1105	155	55	15400.			2274
DEC01	1109	159	59	17400.			2275
DEC01	1111	161	61	9700.			2276
DEC01	1113	163	63	13900.			2277
DEC01	1117	167	67	15400.			2278
DEC01	1121	171	71	17400.			2279
DEC01	1123	173	73	9700.			2280
DEC01	1226	126	226	8050.	INNER CYL COND.	SERIES 2-5	2281
DEC01	1228	128	228	9100.		SERIES 2-5	2282
DEC01	1230	130	230	6000.		SERIES 2-5	2283
DEC01	1232	132	232	8050.		SERIES 2-5	2284
DEC01	1234	134	234	9100.		SERIES 2-5	2285
DEC01	1236	136	236	6000.		SERIES 2-5	2286
DEC01	1326	226	326	16100.		SERIES 2-5	2287
DEC01	1328	228	328	18200.		SERIES 2-5	2288
DEC01	1330	230	330	9180.		SERIES 3-5	2289
DEC01	1332	232	332	16100.		SERIES 2-5	2290
DEC01	1334	234	334	18200.		SERIES 2-5	2291
DEC01	1336	236	336	9180.		SERIES 3-5	2292

TABLE C-1 (CONTINUED)

DEC01	1426	326	426	16100.		SERIES 2-5	2293
DEC01	1428	328	428	18200.		SERIES 2-5	2294
DEC01	1430	330	430	14820.		SERIES 3-5	2295
DEC01	1432	332	432	16100.		SERIES 2-5	2296
DEC01	1434	334	434	14100.		SERIES 2-5	2297
DEC01	1436	336	436	14820.		SERIES 3-5	2298
DEC01	1526	426	176	8050.		SERIES 2-5	2299
DEC01	1528	428	178	9100.		SERIES 2-5	2300
DEC01	1530	430	180	6000.		SERIES 2-5	2301
DEC01	1532	432	182	8050.		SERIES 2-5	2302
DEC01	1534	434	184	9100.		SERIES 2-5	2303
DEC01	1536	436	186	6000.		SERIES 2-5	2304
DEC01	2226	225	226	2880.			2305
DEC01	2227	226	227	2880.			2306
DEC01	2228	227	228	2480.			2307
DEC01	2229	228	229	2480.			2308
DEC01	2230	229	230	2070.			2309
DEC01	2231	230	231	2070.			2310
DEC01	2232	231	232	2880.			2311
DEC01	2331	330	331	2000.		SERIES 3-5	2322
DEC01	2332	331	332	2880.			2323
DEC01	2333	332	333	2880.			2324
DEC01	2334	333	334	2480.			2325
DEC01	2335	334	335	2480.			2326
DEC01	2336	335	336	1035.		SERIES 3-5	2327
DEC01	2325	336	325	2000.		SERIES 3-5	2328
DEC01	2426	425	426	2880.			2329
DEC01	2427	426	427	2880.			2330
DEC01	2428	427	428	2450.			2331
DEC01	2429	428	429	2430.			2332
DEC01	2430	429	430	2070.			2333
DEC01	2431	430	431	2070.			2334
DEC01	2432	431	432	2880.			2335
DEC01	2433	432	433	2880.			2336
DEC01	2434	433	434	2480.			2337
DEC01	2435	434	435	2490.			2338
DEC01	2436	435	436	2070.			2339
DEC01	2425	436	425	2070.			2340
DEC01	2237	201	237	10800.	BEAM CONDUCTION	SERIES 2-5	2341
DEC01	2238	237	225	10800.		SERIES 2-5	2342
DEC01	2239	205	238	10800.		SERIES 2-5	2343
DEC01	2240	238	227	10800.		SERIES 2-5	2344
DEC01	2241	209	239	10800.		SERIES 2-5	2345
DEC01	2242	239	229	10800.		SERIES 2-5	2346
DEC01	2243	213	240	10800.		SERIES 2-5	2347
DEC01	2244	240	231	10800.		SERIES 2-5	2348
DEC01	2245	217	241	10800.		SERIES 2-5	2349
DEC01	2246	241	233	10800.		SERIES 2-5	2350
DEC01	2247	221	242	10800.		SERIES 2-5	2351
DEC01	2248	242	235	10800.		SERIES 2-5	2352
DEC01	2249	301	337	10800.		SERIES 2-5	2353
DEC01	2250	337	325	10800.		SERIES 2-5	2354
DEC01	2251	305	338	10800.		SERIES 2-5	2355
DEC01	2252	338	327	10800.		SERIES 2-5	2356
DEC01	2253	309	339	10800.		SERIES 2-5	2357
DEC01	2254	339	329	10800.		SERIES 2-5	2358
DEC01	2255	313	340	10800.		SERIES 2-5	2359
DEC01	2256	340	331	10800.		SERIES 2-5	2360
DEC01	2257	317	341	10800.		SERIES 2-5	2361
DEC01	2258	341	333	10800.		SERIES 2-5	2362
DEC01	2259	321	342	10800.		SERIES 2-5	2363
DEC01	2260	342	335	10800.		SERIES 2-5	2364
DEC01	2261	401	437	10800.		SERIES 2-5	2365
DEC01	2262	437	425	10800.		SERIES 2-5	2366
DEC01	2263	405	438	10800.		SERIES 2-5	2367
DEC01	2264	438	427	10800.		SERIES 2-5	2368
DEC01	2265	409	439	10800.		SERIES 2-5	2369
DEC01	2266	439	429	10800.		SERIES 2-5	2370
DEC01	2267	413	440	10800.		SERIES 2-5	2371
DEC01	2268	440	431	10800.		SERIES 2-5	2372
DEC01	2269	417	441	10800.		SERIES 2-5	2373
DEC01	2270	441	433	10800.		SERIES 2-5	2374
DEC01	2271	421	442	10800.		SERIES 2-5	2375
DEC01	2272	442	435	10800.		SERIES 2-5	2376
DEC01	1237	1	237	11200.		SERIES 2-5	2377
DEC01	1238	5	238	11200.		SERIES 2-5	2378
DEC01	1239	9	239	11200.		SERIES 2-5	2379
DEC01	1240	13	240	11200.		SERIES 2-5	2380
DEC01	1241	17	241	11200.		SERIES 2-5	2381
DEC01	1242	21	242	11200.		SERIES 2-5	2382
DEC01	1243	51	437	11200.		SERIES 2-5	2383
DEC01	1244	55	438	11200.		SERIES 2-5	2384
DEC01	1245	59	439	11200.		SERIES 2-5	2385
DEC01	1246	63	440	11200.		SERIES 2-5	2386
DEC01	1247	67	441	11200.		SERIES 2-5	2387
DEC01	1248	71	442	11200.		SERIES 2-5	2388
DEC01	1249	237	337	22400.		SERIES 2-5	2389
DEC01	1250	238	338	22400.		SERIES 2-5	2390
DEC01	1251	239	339	22400.		SERIES 2-5	2391
DEC01	1252	240	340	22400.		SERIES 2-5	2392
DEC01	1253	241	341	22400.		SERIES 2-5	2393
DEC01	1254	242	342	22400.		SERIES 2-5	2394
DEC01	1255	337	437	22400.		SERIES 2-5	2395
DEC01	1256	338	438	22400.		SERIES 2-5	2396
DEC01	1257	339	439	22400.		SERIES 2-5	2397
DEC01	1258	340	440	22400.		SERIES 2-5	2398
DEC01	1259	341	441	22400.		SERIES 2-5	2399
DEC01	1260	342	442	22400.		SERIES 2-5	2400
DEC01	2371	371	372	22900.	HEAT SHIELD COND	SERIES 3-5	2400
DEC01	2372	372	373	19430.		SERIES 3-5	2401
DEC01	2373	373	374	21250.		SERIES 3-5	2402
DEC01	2374	374	375	22900.		SERIES 3-5	2403
DEC01	2375	375	376	19430.		SERIES 3-5	2404
DEC01	2376	376	371	21250.		SERIES 3-5	2405
DEC01	2377	377	378	52900.		SERIES 3-5	2406
DEC01	2378	378	379	45400.		SERIES 3-5	2407
DEC01	2379	379	380	49200.		SERIES 3-5	2408
DEC01	2380	380	381	52900.		SERIES 3-5	2409
DEC01	2381	381	382	45400.		SERIES 3-5	2410
DEC01	2382	382	377	49200.		SERIES 3-5	2411
DEC01	2383	383	384	43250.		SERIES 3-5	2412
DEC01	2384	384	385	36700.		SERIES 3-5	2413
DEC01	2385	385	386	40000.		SERIES 3-5	2414
DEC01	2386	386	387	43250.		SERIES 3-5	2415
DEC01	2387	387	388	36700.		SERIES 3-5	2416
DEC01	2388	388	383	40000.		SERIES 3-5	2417
DEC01	2351	351	371	5.67E4		SERIES 3-5	2418
DEC01	2352	352	372	6.78E4		SERIES 3-5	2419
DEC01	2353	353	373	8.00E4		SERIES 3-5	2420
DEC01	2354	354	374	5.67E4		SERIES 3-5	2421
DEC01	2355	355	375	6.78E4		SERIES 3-5	2422
DEC01	2356	356	376	8.00E4		SERIES 3-5	2423
DEC01	2357	357	377	6.10E4		SERIES 3-5	2424
DEC01	2358	358	378	7.21E4		SERIES 3-5	2425
DEC01	2359	359	379	8.60E4		SERIES 3-5	2426
DEC01	2360	360	380	6.10E4		SERIES 3-5	2427

TABLE C-1 (CONTINUED)

DEC01	2361	361	381	7.21E4		SERIES 3-5	2428
DEC01	2362	362	382	8.60E4		SERIES 3-5	2429
DEC01	2363	363	383	2.81E4		SERIES 3-5	2430
DEC01	2364	364	384	3.29E4		SERIES 3-5	2431
DEC01	2365	365	385	3.96E4		SERIES 3-5	2432
DEC01	2366	366	386	2.81E4		SERIES 3-5	2433
DEC01	2367	367	387	3.29E4		SERIES 3-5	2434
DEC01	2368	368	388	3.96E4		SERIES 3-5	2435
DEC01	2271	176	371	8340.		SERIES 3-5	2436
DEC01	2272	178	372	9840.		SERIES 3-5	2437
DEC01	2273	180	373	11960.		SERIES 3-5	2438
DEC01	2274	182	374	8340.		SERIES 3-5	2439
DEC01	2275	184	375	9840.		SERIES 3-5	2440
DEC01	2276	186	376	11960.		SERIES 3-5	2441
DEC01	2277	371	377	9030.		SERIES 3-5	2442
DEC01	2278	372	378	10780.		SERIES 3-5	2443
DEC01	2279	373	379	12830.		SERIES 3-5	2444
DEC01	2280	374	380	9030.		SERIES 3-5	2445
DEC01	2281	375	381	10780.		SERIES 3-5	2446
DEC01	2282	376	382	12830.		SERIES 3-5	2447
DEC01	2283	377	383	6660.		SERIES 3-5	2448
DEC01	2284	378	384	7900.		SERIES 3-5	2449
DEC01	2285	379	385	9430.		SERIES 3-5	2450
DEC01	2286	380	386	6660.		SERIES 3-5	2451
DEC01	2287	381	387	7900.		SERIES 3-5	2452
DEC01	2288	382	388	9430.		SERIES 3-5	2453
DEC01	2289	383	153	3630.		SERIES 3-5	2454
DEC01	2290	384	157	4130.		SERIES 3-5	2455
DEC01	2291	385	161	5150.		SERIES 3-5	2456
DEC01	2292	386	165	3630.		SERIES 3-5	2457
DEC01	2293	387	169	4330.		SERIES 3-5	2458
DEC01	2294	388	173	5150.		SERIES 3-5	2459
DEC01	2390	177	390	257000.	T.C. SUPPORT	SERIES 3-5	2460
DEC01	2391	180	390	257000.		SERIES 3-5	2461
DEC01	2392	183	390	257000.		SERIES 3-5	2462
DEC01	2393	186	390	257000.		SERIES 3-5	2463
DEC01	1050	2	394	56200.	TANK SKIRT-BLKHD	SERIES 3-5	2464
DEC01	1051	103	394	56200.		SERIES 3-5	2465
DEC01	1052	4	394	56200.	UPPER	SERIES 3-5	2466
DEC01	1053	126	394	56200.		SERIES 3-5	2467
DEC01	1054	14	397	56200.		SERIES 3-5	2468
DEC01	1055	115	397	56200.		SERIES 3-5	2469
DEC01	1056	16	397	56200.		SERIES 3-5	2470
DEC01	1057	132	397	56200.		SERIES 3-5	2471
DEC01	1058	6	395	50500.		SERIES 3-5	2472
DEC01	1059	107	395	50500.		SERIES 3-5	2473
DEC01	1060	3	395	50500.		SERIES 3-5	2474
DEC01	1061	128	395	50500.		SERIES 3-5	2475
DEC01	1062	18	395	50500.		SERIES 3-5	2476
DEC01	1063	119	396	50500.		SERIES 3-5	2477
DEC01	1064	20	396	50500.		SERIES 3-5	2478
DEC01	1065	134	396	50500.		SERIES 3-5	2479
DEC01	1150	52	394	44900.	TANK SKIRT-BLKHD	SERIES 3-5	2480
DEC01	1151	153	394	44900.		SERIES 3-5	2481
DEC01	1152	54	394	44900.	LOWER	SERIES 3-5	2482
DEC01	1153	176	394	44900.		SERIES 3-5	2483
DEC01	1154	64	397	44900.		SERIES 3-5	2484
DEC01	1155	165	397	44900.		SERIES 3-5	2485
DEC01	1156	66	397	44900.		SERIES 3-5	2486
DEC01	1157	182	397	44900.		SERIES 3-5	2487
DEC01	1158	56	395	44250.		SERIES 3-5	2488

DEC01	1159	157	395	44250.		SERIES 3-5	2489
DEC01	1160	58	395	44250.		SERIES 3-5	2490
DEC01	1161	178	395	44250.		SERIES 3-5	2491
DEC01	1162	64	396	44250.		SERIES 3-5	2492
DEC01	1163	169	396	44250.		SERIES 3-5	2493
DEC01	1164	66	396	44250.		SERIES 3-5	2494
DEC01	1165	182	396	44250.		SERIES 3-5	2495
DEC01	2296	392	229	2070.	HELIUM BOTTLE SUPPORT		2496
DEC01	2297	392	230	2070.			2497
DEC01	2298	392	235	2070.			2498
DEC01	2299	392	236	2070.			2499
DEC01	2396	391	333	4140.			2500
DEC01	2397	391	336	4140.			2501
DEC01	2398	393	61	2040.	FUEL CELL BASE		2502
DEC01	1901	400	340	13100.	REGULATOR		A2503
DEC01	1902	400	440	13100.			B2503
DEC01	242	204	394	1.		SERIES 3-5	2504
DEC01	266	238	394	1.		SERIES 3-5	2505
DEC01	277	226	394	1.		SERIES 3-5	2506
DEC01	267	238	395	1.		SERIES 3-5	2507
DEC01	243	206	395	1.		SERIES 3-5	2508
DEC01	228	207	395	1.		SERIES 3-5	2509
DEC01	244	208	395	1.		SERIES 3-5	2510
DEC01	268	239	395	1.		SERIES 3-5	2511
DEC01	278	228	395	1.		SERIES 3-5	2512
DEC01	274	242	396	1.		SERIES 3-5	2513
DEC01	281	234	396	1.		SERIES 3-5	2514
DEC01	273	241	396	1.		SERIES 3-5	2515
DEC01	249	218	396	1.		SERIES 3-5	2516
DEC01	234	219	396	1.		SERIES 3-5	2517
DEC01	250	220	396	1.		SERIES 3-5	2518
DEC01	290	232	397	1.		SERIES 3-5	2519
DEC01	271	240	397	1.		SERIES 3-5	2520
DEC01	247	214	397	1.		SERIES 3-5	2521
DEC01	232	215	397	1.		SERIES 3-5	2522
DEC01	248	216	397	1.		SERIES 3-5	2523
DEC01	272	241	397	1.		SERIES 3-5	2524
DEC01	341	302	394	1.		SERIES 3-5	2525
DEC01	326	303	394	1.		SERIES 3-5	2526
DEC01	342	304	394	1.		SERIES 3-5	2527
DEC01	366	338	394	1.		SERIES 3-5	2528
DEC01	377	326	394	1.		SERIES 3-5	2529
DEC01	365	337	394	1.		SERIES 3-5	2530
DEC01	367	339	395	1.		SERIES 3-5	2531
DEC01	343	306	395	1.		SERIES 3-5	2532
DEC01	328	307	395	1.		SERIES 3-5	2533
DEC01	344	308	395	1.		SERIES 3-5	2534
DEC01	368	337	395	1.		SERIES 3-5	2535
DEC01	378	323	395	1.		SERIES 3-5	2536
DEC01	374	342	396	1.		SERIES 3-5	2537
DEC01	381	334	396	1.		SERIES 3-5	2538
DEC01	373	341	396	1.		SERIES 3-5	2539
DEC01	349	318	396	1.		SERIES 3-5	2540
DEC01	324	319	396	1.		SERIES 3-5	2541
DEC01	350	320	396	1.		SERIES 3-5	2542
DEC01	330	332	397	1.		SERIES 3-5	2543
DEC01	371	340	397	1.		SERIES 3-5	2544
DEC01	347	314	397	1.		SERIES 3-5	2545
DEC01	332	315	397	1.		SERIES 3-5	2546
DEC01	348	316	397	1.		SERIES 3-5	2547
DEC01	372	341	397	1.		SERIES 3-5	2548

TABLE C-1 (CONTINUED)

DEC01	441	402	394	1.			SERIES 3-5	2549
DEC01	426	403	.394	1.			SERIES 3-5	2550
DEC01	442	404	394	1.			SERIES 3-5	2551
DEC01	466	438	394	1.			SERIES 3-5	2552
DEC01	477	426	394	1.			SERIES 3-5	2553
DEC01	465	437	394	1.			SERIES 3-5	2554
DEC01	467	438	395	1.			SERIES 3-5	2555
DEC01	443	406	395	1.			SERIES 3-5	2556
DEC01	428	407	395	1.			SERIES 3-5	2557
DEC01	444	408	395	1.			SERIES 3-5	2558
DEC01	468	439	395	1.			SERIES 3-5	2559
DEC01	478	428	395	1.			SERIES 3-5	2560
DEC01	474	442	396	1.			SERIES 3-5	2561
DEC01	481	434	396	1.			SERIES 3-5	2562
DEC01	473	441	396	1.			SERIES 3-5	2563
DEC01	449	418	396	1.			SERIES 3-5	2564
DEC01	434	419	396	1.			SERIES 3-5	2565
DEC01	450	420	396	1.			SERIES 3-5	2566
DEC01	480	432	397	1.			SERIES 3-5	2567
DEC01	471	440	397	1.			SERIES 3-5	2568
DEC01	447	414	397	1.			SERIES 3-5	2569
DEC01	432	415	397	1.			SERIES 3-5	2570
DEC01	448	416	397	1.			SERIES 3-5	2571
DEC01	472	441	397	1.			SERIES 3-5	2572
DEC01	226	203	394	1.			SERIES 3-5	2573
DEC01	241	202	394	1.			SERIES 3-5	2574
DEC01	265	237	394	1.			SERIES 3-5	2575
DEC01	101	101	100	1.		EXT RAD	SERIES 5	2601
INC	2	2	0	0.	2		SERIES 5	2602
DEC01	107	107	200	1.			SERIES 5	2603
INC	2	2	0	0.	4		SERIES 5	2604
DEC01	117	117	200	1.			SERIES 5	2605
INC	2	2	0	0.	3		SERIES 5	2606
DEC01	151	151	100	1.			SERIES 5	2607
INC	2	2	0	0.	2		SERIES 5	2608
DEC01	157	157	200	1.			SERIES 5	2609
INC	2	2	0	0.	4		SERIES 5	2610
DEC01	167	167	200	1.			SERIES 5	2611
INC	2	2	0	0.	3		SERIES 5	2612
DEC01	201	201	100	1.			SERIES 5	2613
INC	1	1	0	0.	5		SERIES 5	2614
DEC01	207	207	200	1.			SERIES 5	2615
INC	1	1	0	0.	8		SERIES 5	2616
DEC01	216	216	100	1.			SERIES 5	2617
INC	1	1	0	0.	8		SERIES 5	2618
DEC01	301	301	100	1.			SERIES 5	2619
INC	1	1	0	0.	5		SERIES 5	2620
DEC01	307	307	200	1.			SERIES 5	2621
INC	1	1	0	0.	8		SERIES 5	2622
DEC01	316	316	100	1.			SERIES 5	2623
INC	1	1	0	0.	8		SERIES 5	2624
DEC01	401	401	100	1.			SERIES 5	2625
INC	1	1	0	0.	5		SERIES 5	2626
DEC01	407	407	200	1.			SERIES 5	2627
INC	1	1	0	0.	8		SERIES 5	2628
DEC01	416	416	100	1.			SERIES 5	2629
INC	1	1	0	0.	8		SERIES 5	2630
DEC01	1264	230	210	1.		INT RAD PANEL-I.C. STRAIGHT		2640
INC	100	100	100	0.	2			2641
DEC01	1265	230	211	1.				2642
INC	100	100	100	0.	2			2643

DEC01	1266	230	213	1.				2644
INC	100	100	100	0.	2			2645
DEC01	1273	236	222	1.				2646
INC	100	100	100	0.	2			2647
DEC01	1274	236	223	1.				2648
INC	100	100	100	0.	2			2649
DEC01	1275	236	224	1.				2650
INC	100	100	100	0.	2			2651
DEC01	1280	310	230	1.		INT RAD PANEL-I.C. DIAGONAL		2660
INC	100	1	0	0.	2			2661
DEC01	1281	210	330	1.				2662
INC	100	1	0	0.	2			2663
DEC01	1286	322	236	1.				2672
INC	100	1	0	0.	2			2673
DEC01	1287	222	336	1.				2674
INC	100	1	0	0.	2			2675
DEC01	1292	410	330	1.				2684
INC	100	1	0	0.	2			2685
DEC01	1293	310	430	1.				2686
INC	100	1	0	0.	2			2687
DEC01	1298	422	336	1.				2696
INC	100	1	0	0.	2			2697
DEC01	1299	322	436	1.				2698
INC	100	1	0	0.	2			2699
DEC01	245	210	239	1.		PANEL-BEAM	SERIES 2,3	2705
DEC01	246	212	240	1.			SERIES 2,3	2706
DEC01	251	222	242	1.			SERIES 2,3	2711
DEC01	252	224	237	1.			SERIES 2,3	2712
DEC01	345	310	339	1.			SERIES 2,3	2717
DEC01	346	312	340	1.			SERIES 2,3	2718
DEC01	351	322	342	1.			SERIES 2,3	2723
DEC01	352	324	337	1.			SERIES 2,3	2724
DEC01	445	410	439	1.			SERIES 2,3	2729
DEC01	446	412	440	1.			SERIES 2,3	2730
DEC01	451	422	442	1.			SERIES 2,3	2735
DEC01	452	424	437	1.			SERIES 2,3	2736
DEC01	269	239	230	1.		BEAM-I.C.	SERIES 2,3	2805
DEC01	270	240	230	1.			SERIES 2,3	2806
DEC01	275	242	236	1.			SERIES 2,3	2811
DEC01	276	237	236	1.			SERIES 2,3	2812
DEC01	369	339	330	1.			SERIES 2,3	2817
DEC01	370	340	330	1.			SERIES 2,3	2818
DEC01	375	342	336	1.			SERIES 2,3	2823
DEC01	376	337	336	1.			SERIES 2,3	2824
DEC01	469	439	430	1.			SERIES 2,3	2829
DEC01	470	440	430	1.			SERIES 2,3	2830
DEC01	475	442	436	1.			SERIES 2,3	2835
DEC01	476	437	436	1.			SERIES 2,3	2836
DEC01	279	239	240	1.			SERIES 2,3	2839
DEC01	282	242	237	1.			SERIES 2,3	2842
DEC01	379	339	340	1.			SERIES 2,3	2845
DEC01	382	342	337	1.			SERIES 2,3	2848
DEC01	479	439	440	1.			SERIES 2,3	2851
DEC01	482	442	437	1.			SERIES 2,3	2854
DEC01	490	426	390	1.		T.C. RAD	SERIES 3-5	2900
DEC01	491	428	390	1.			SERIES 3-5	2901
DEC01	492	430	390	1.			SERIES 3-5	2902
DEC01	493	432	390	1.			SERIES 3-5	2903
DEC01	494	434	390	1.			SERIES 3-5	2904
DEC01	495	436	390	1.			SERIES 3-5	2905
DEC01	390	326	390	1.			SERIES 3-5	2906

LOCKHEED
CALIFORNIA COMPANY

TABLE C-1 (CONTINUED)

DEC01	391	328	390	1.		SERIES 3-5	2907
DEC01	392	330	390	1.		SERIES 3-5	2908
DEC01	393	332	390	1.		SERIES 3-5	2909
DEC01	394	334	390	1.		SERIES 3-5	2910
DEC01	395	336	390	1.		SERIES 3-5	2911
DEC01	396	391	390	1.		SERIES 3-5	2912
DEC01	551	251	351	1.	NOZZLE-H.S. RAD	SERIES 3-5	2913
DEC01	552	252	352	1.		SERIES 3-5	2914
DEC01	553	253	353	1.		SERIES 3-5	2915
DEC01	554	254	354	1.		SERIES 3-5	2916
DEC01	555	255	355	1.		SERIES 3-5	2917
DEC01	556	256	356	1.		SERIES 3-5	2918
DEC01	557	257	357	1.		SERIES 3-5	2919
DEC01	558	258	358	1.		SERIES 3-5	2920
DEC01	559	259	359	1.		SERIES 3-5	2921
DEC01	560	260	360	1.		SERIES 3-5	2922
DEC01	561	261	361	1.		SERIES 3-5	2923
DEC01	562	262	362	1.		SERIES 3-5	2924
DEC01	657	357	100	1.	HEAT SHIELD EXT RAD	SERIES 3-5	2931
DEC01	658	358	100	1.		SERIES 3-5	2932
DEC01	659	359	100	1.		SERIES 3-5	2933
DEC01	660	360	100	1.		SERIES 3-5	2934
DEC01	661	361	100	1.		SERIES 3-5	2935
DEC01	662	362	100	1.		SERIES 3-5	2936
DEC01	663	363	100	1.		SERIES 3-5	2937
DEC01	664	364	200	1.		SERIES 3-5	2938
DEC01	665	365	200	1.		SERIES 3-5	2939
DEC01	666	366	200	1.		SERIES 3-5	2940
DEC01	667	367	100	1.		SERIES 3-5	2941
DEC01	668	368	100	1.		SERIES 3-5	2942
DEC01	701	59	393	1.	FUEL CELL RAD	SERIES 3-5	2943
DEC01	702	159	393	1.		SERIES 3-5	2944
DEC01	703	161	393	1.		SERIES 3-5	2945
DEC01	704	163	393	1.		SERIES 3-5	2946
DEC01	705	63	393	1.		SERIES 3-5	2947
DEC01	706	181	393	1.		SERIES 3-5	2948
DEC01	707	180	393	1.		SERIES 3-5	2949
DEC01	708	179	393	1.		SERIES 3-5	2950
DEC01	709	339	393	1.		SERIES 3-5	2951
DEC01	710	330	393	1.		SERIES 3-5	2952
DEC01	711	340	393	1.		SERIES 3-5	2953
DEC01	712	311	393	1.		SERIES 3-5	2954
DEC01	713	439	393	1.		SERIES 3-5	2955
DEC01	714	430	393	1.		SERIES 3-5	2956
DEC01	715	440	393	1.		SERIES 3-5	2957
DEC01	716	411	393	1.		SERIES 3-5	2958
DEC01	750	371	394	1.	HEAT SHIELD INT.RAD.	SERIES 3-5	2959
DEC01	751	372	395	1.		SERIES 3-5	2960
DEC01	752	373	61	1.		SERIES 3-5	2961
DEC01	753	374	397	1.		SERIES 3-5	2962
DEC01	754	375	396	1.		SERIES 3-5	2963
DEC01	755	376	73	1.		SERIES 3-5	2964
DEC01	756	377	394	1.		SERIES 2-5	2965
DEC01	757	378	395	1.		SERIES 3-5	2966
DEC01	758	379	61	1.		SERIES 3-5	2967
DEC01	759	380	397	1.		SERIES 3-5	2968
DEC01	760	381	396	1.		SERIES 3-5	2969
DEC01	761	332	73	1.		SERIES 3-5	2970
DEC01	762	383	394	1.		SERIES 3-5	2971
DEC01	763	384	395	1.		SERIES 3-5	2972
DEC01	764	385	61	1.		SERIES 3-5	2973

DEC01	765	386	397	1.			SERIES 3-5	2974
DEC01	766	387	396	1.			SERIES 3-5	2975
DEC01	767	388	73	1.			SERIES 3-5	2976
DEC01	802	392	225	1.			SERIES 3'5	2977
INC	2	0	2	0.	5		SERIES 3'5	2978
DEC01	822	391	325	1.			SERIES 3'5	2979
INC	2	0	2	0.	5		SERIES 3'5	2980
DEC01	720	393	9	1.				2981
DEC01	721	393	13	1.				2982
DEC01	722	393	129	1.				2983
DEC01	723	393	131	1.				2984
DEC01	724	393	109	1.				2985
DEC01	725	393	113	1.				2986
DEC01	726	393	111	1.				2987
DEC01	727	323	11	1.				2988
DEC01	728	73	23	1.				2989
DEC01	729	253	391	1.				2990
DEC01	730	11	61	1.				2991
DEC01	731	391	392	1.				2992
NBK								2999
DEC02	201	.098	202	.054		OUTER PANEL		3001
DEC02	203	.082	204	.054				3002
DEC02	205	.098	206	.047				3003
DEC02	207	.070	208	.047				3004
DEC02	209	.098	210	.039				3005
DEC02	211	.058	212	.039				3006
DEC02	213	.078	214	.054				3007
DEC02	215	.082	216	.054				3008
DEC02	217	.078	218	.047				3009
DEC02	219	.070	220	.047				3010
DEC02	221	.098	222	.039				3011
DEC02	223	.058	224	.039				3012
DEC02	301	.130	302	.073				3013
DEC02	303	.109	304	.073				3014
DEC02	305	.130	306	.062				3015
DEC02	307	.094	308	.062				3016
DEC02	309	.130	310	.052				3017
DEC02	311	.078	312	.052				3018
DEC02	313	.130	314	.073				3019
DEC02	315	.109	316	.073				3020
DEC02	317	.130	318	.062				3021
DEC02	319	.094	320	.062				3022
DEC02	321	.130	322	.052				3023
DEC02	323	.078	324	.052				3024
DEC02	401	.098	402	.054				3025
DEC02	403	.082	404	.054				3026
DEC02	405	.098	406	.047				3027
DEC02	407	.070	408	.047				3028
DEC02	409	.098	410	.039				3029
DEC02	411	.058	412	.039				3030
DEC02	413	.098	414	.054				3031
DEC02	415	.082	416	.054				3032
DEC02	417	.098	418	.047				3033
DEC02	419	.070	420	.047				3034
DEC02	421	.098	422	.039				3035
DEC02	423	.058	424	.039				3036
DEC02	225	.1360	226	.0820		INNER CYL	SERIES 2-5	3043
DEC02	227	.1405	228	.0706			SERIES 2-5	3044
DEC02	229	.1305	230	.0590			SERIES 2-5	3045
DEC02	231	.1360	232	.0820			SERIES 2-5	3046
DEC02	233	.1405	234	.0706			SERIES 2-5	3047
DEC02	235	.1305	236	.0590			SERIES 2-5	3048

TABLE C-1 (CONTINUED)

DEC02	325	.1360	326	.0820		SERIES 2-5	3049
DEC02	327	.1405	328	.0706		SERIES 2-5	3050
DEC02	329	.1305	330	.0590		SERIES 2-5	3051
DEC02	331	.1360	332	.0820		SERIES 2-5	3052
DEC02	333	.1405	334	.0706		SERIES 2-5	3053
DEC02	335	.1305	336	.0590		SERIES 2-5	3054
DEC02	425	.1360	426	.0820		SERIES 2-5	3055
DEC02	427	.1405	428	.0706		SERIES 2-5	3056
DEC02	429	.1305	430	.0590		SERIES 2-5	3057
DEC02	431	.1360	432	.0820		SERIES 2-5	3058
DEC02	433	.1405	434	.0706		SERIES 2-5	3059
DEC02	435	.1305	436	.0590		SERIES 2-5	3060
DEC02	101	.152	103	.326	UPPER BLKHD		3061
DEC02	105	.184	107	.169			3062
DEC02	109	.149	111	.162			3063
DEC02	113	.152	115	.326			3064
DEC02	117	.184	119	.169			3065
DEC02	121	.149	123	.162			3066
DEC02	1	.0385	2	.1975		SERIES 3-5	3072

DEC02	4	.1975	5	.0310		SERIES 3-5	3073
DEC02	6	.151	8	.151		SERIES 3-5	3074
DEC02	9	.0310	11	.0550			3075
DEC02	13	.0385	14	.1975		SERIES 3-5	3076
DEC02	16	.1975	17	.0310		SERIES 3-5	3077
DEC02	18	.151	20	.151		SERIES 3-5	3078
DEC02	21	.0310	23	.0550			3079
DEC02	125	.0312	126	.228		SERIES 3-5	3080
DEC02	127	.0338	128	.1772		SERIES 3-5	3081
DEC02	129	.0290	130	.0310			3082
DEC02	131	.0312	132	.228		SERIES 3-5	3083
DEC02	133	.0338	134	.1772		SERIES 3-5	3084
DEC02	135	.0290	136	.0310			3085
DEC02	151	.152	153	.343	LOWER BLKHD		3086
DEC02	155	.184	157	.169			3087
DEC02	159	.149	161	.192			3088
DEC02	163	.152	165	.343			3089
DEC02	167	.184	169	.169			3090
DEC02	171	.149	173	.192			3091
DEC02	51	.0385	52	.1679		SERIES 3-5	3092
DEC02	54	.1679	55	.0310		SERIES 3-5	3093
DEC02	56	.140	58	.140		SERIES 3-5	3094
DEC02	59	.0310	61	.0550			3095
DEC02	63	.0385	64	.1679		SERIES 3-5	3096
DEC02	66	.1679	67	.0310		SERIES 3-5	3097
DEC02	68	.140	70	.140		SERIES 3-5	3098
DEC02	71	.0310	73	.0550			3099
DEC02	175	.0312	176	.2195		SERIES 3-5	3100
DEC02	177	.0338	178	.1838		SERIES 3-5	3101
DEC02	179	.0290	180	.0468		SERIES 3-5	3102
DEC02	181	.0312	182	.2195		SERIES 3-5	3103
DEC02	183	.0338	184	.1838		SERIES 3-5	3104
DEC02	185	.0290	186	.0468		SERIES 3-5	3105
DEC01	237	.162			BEAM CAP.	SERIES 2-5	3151
INC	1	0.	5			SERIES 2-5	3152
DEC01	337	.162				SERIES 2-5	3153
INC	1	0.	5			SERIES 2-5	3154
DEC01	437	.162				SERIES 2-5	3155
INC	1	0.	5			SERIES 2-5	3156

DEC02	351	.0633	352	.0528	H.S. CAP	SERIES 3-5	3200
DEC02	353	.0450	354	.0633		SERIES 3-5	3201
DEC02	355	.0528	356	.0450		SERIES 3-5	3202
DEC02	357	.0784	358	.0665		SERIES 3-5	3203
DEC02	359	.0557	360	.0784		SERIES 3-5	3204
DEC02	361	.0665	362	.0557		SERIES 3-5	3205
DEC02	363	.1281	364	.1089		SERIES 3-5	3206
DEC02	365	.0906	366	.1281		SERIES 3-5	3207
DEC02	367	.1089	368	.0906		SERIES 3-5	3208
DEC02	371	.0633	372	.0528		SERIES 3-5	3209
DEC02	373	.0450	374	.0633		SERIES 3-5	3210
DEC02	375	.0528	376	.0450		SERIES 3-5	3211
DEC02	377	.0784	378	.0665		SERIES 3-5	3212
DEC02	379	.0557	380	.0784		SERIES 3-5	3213
DEC02	381	.0665	382	.0557		SERIES 3-5	3214
DEC02	383	.1281	384	.1089		SERIES 3-5	3215
DEC02	385	.0906	386	.1281		SERIES 3-5	3216
DEC02	387	.1089	388	.0906		SERIES 3-5	3217
DEC02	391	8.3	392	8.3			3995
DEC02	394	9.7	395	9.7	OXID TANKS		3996
DEC02	396	8.2	397	8.2	FUEL TANKS		3997
DEC01	400	.7			REGULATOR		3998

LOCKHEED
CALIFORNIA COMPANY

TABLE C-2 SAMPLE OUTPUT FOR SERIES 4

SERIES 4 45 DEG PLAIN DISC

TIME= 4800. SECONDS COMP. INTERVAL= 60.000 SECONDS (RC)MIN= 120.000 SECONDS AT NODE 0.

TEMPERATURE OF OUTER DISC NODES (DEG F)

11	12	13	14	15	16	17	18
-2.	-4.	-9.	-16.	-19.	-14.	-7.	-3.

TEMPERATURE OF INNER DISC NODES (DEG F)

41	42	43	44	45	46	47	48	100
-5.	-6.	-10.	-14.	-16.	-13.	-8.	-5.	-19.

TEMPERATURE OF UPPER CONE NODES (DEG F)

111	112	113	114	115	116	117	118
-96.	-97.	-97.	-98.	-98.	-97.	-96.	-96.

TEMPERATURE OF LOWER CONE NODES (DEG F)

141	142	143	144	145	146	147	148
-75.	-75.	-76.	-76.	-76.	-76.	-76.	-75.

TABLE C-3 SAMPLE OUTPUT FOR SERIES 5

SERIES 5

TIME=99600. SECONDS COMP. INTERVAL= 29.7 SECONDS (RC)MIN= 31.2 SECONDS AT NODE 330. CYCLE= 3487.

TEMPERATURE OF PANEL NODES (DEG F)

201	203	205	207	209	211	213	215	217	219	221	223
-128.	-138.	-124.	-124.	-106.	-116.	-108.	-126.	-124.	-135.	-125.	-138.
301	303	305	307	309	311	313	315	317	319	321	323
-138.	-160.	-135.	-144.	-117.	-133.	-117.	-147.	-135.	-157.	-137.	-155.
401	403	405	407	409	411	413	415	417	419	421	423
-129.	-137.	-121.	-119.	-97.	-102.	-97.	-120.	-122.	-137.	-137.	-141.

TEMPERATURE OF INNER CYLINDER NODES (DEG F)

225	227	229	231	233	235
-27.	-28.	-18.	-23.	-28.	-21.
325	327	329	331	333	335
-17.	-19.	-9.	-11.	-19.	-15.
425	427	429	431	433	435
-34.	-27.	-18.	-18.	-28.	-32.

TEMPERATURE OF PROPELLANT TANKS (DEG F)

394	395	396	397
14.	14.	12.	9.

TEMPERATURE OF HELIUM TANKS (DEG F)

391	392
33.	-10.

TEMPERATURE OF BEAM NODES (DEG F)

237	238	239	240	241	242
-75.	-70.	-55.	-57.	-71.	-72.
337	338	339	340	341	342
-75.	-71.	-56.	-53.	-72.	-74.
437	438	439	440	441	442
-78.	-68.	-41.	-40.	-69.	-79.

TEMPERATURE OF T.C., F.C. NODES (DEG F)

390	393	61
48.	181.	84.

TABLE C-3 (Continued)

TEMPERATURE OF UPPER BULKHEAD NODES (DEG F)

101	103	105	107	109	111	113	115	117	119	121	123
-112.	-103.	-105.	-87.	-86.	-79.	-86.	-92.	-103.	-97.	-109.	-110.
125	127	129	131	133	135						
-45.	-41.	-30.	-30.	-38.	-44.						
1	5	9	11	13	15	17	21	23			
-76.	-66.	-46.	-27.	-48.	-6.	-68.	-73.	-79.			

TEMPERATURE OF LOWER BULKHEAD NODES (DEG F)

151	153	155	157	159	161	163	165	167	169	171	173
-112.	-100.	-100.	-76.	-68.	-44.	-66.	-79.	-100.	-99.	-114.	-112.
175	176	177	178	179	180	181	182	183	184	185	186
-50.	-43.	-35.	-27.	-15	-6.	-13.	-25.	-39.	-49.	-52.	-50.
51	55	59	61	63	67	71	73				
-78.	-61.	-5.	84.	-5.	-63.	-82.	-83.				

TEMPERATURE OF HEAT SHIELD NODES (DEG F)

373	376	379	382	385	388
-59.	-78.	-71.	-93.	-74.	-102.

TEMPERATURE OF NOZZLE NODES (DEG F)

253	256	259	262	265	268
108.	-111.	-185.	-177.	-200.	-191.

APPENDIX D - MODEL DESIGN DETAILS

The following list covers all design drawing used in the fabrication of the models.

Dwg. No.	Title	Latest Revision	
*MR 6778	Panel Assy - Cored	B	(Fig. D-1)
*MR 6779	Blkhd Assy - Cored	B	(Fig. D-2)
*MR 6791	TankAssy - Welded Propellant	A	(Fig. D-3)
MR 6792	Shield Assy - Cored	-	
MR 6793	Disk Assy - Series 4 Test	-	
MR 6794	Equipment - Series 4 Test	A	
MR 6795	Support Assy - Series 4 Test	-	
MR 6796	Web Assy - Series 2	B	
MR 6797	Cylinder Assy - Series 1	A	
MR 6798	Spt for IR Heating Panel	-	
MR 6799	IR Heating Panel	-	
MR 6800	Thrust Chamber Model	-	
MR 6801	Simulated Electronic Billet - Heated	-	
MR 6802	Nozzle Assy	-	
MR 6803	Heater Assy - Nozzle	-	
MR 6804	Reflector Cone Support	-	
MR 6805	Reflector Sheet	-	
MR 6806	Bus Bar - Apollow S.M Nozzle	-	
MR 6807	Stiffener - Nozzle	-	
MR 6808	Tank Flange - Propellant	A	
*MR 6809	C-5 Chamber Installation	-	(Fig. D-4)
MR 6810	I/R Heating Closures	-	
*MR 6811	Plumbing Schematic - Series 3		(Fig. D-5)
MR 6812	Spherical Bottle Assembly		
MR 6813	Cradle Assembly - Shipping		

*These selected key drawings are reproduced in this appendix.

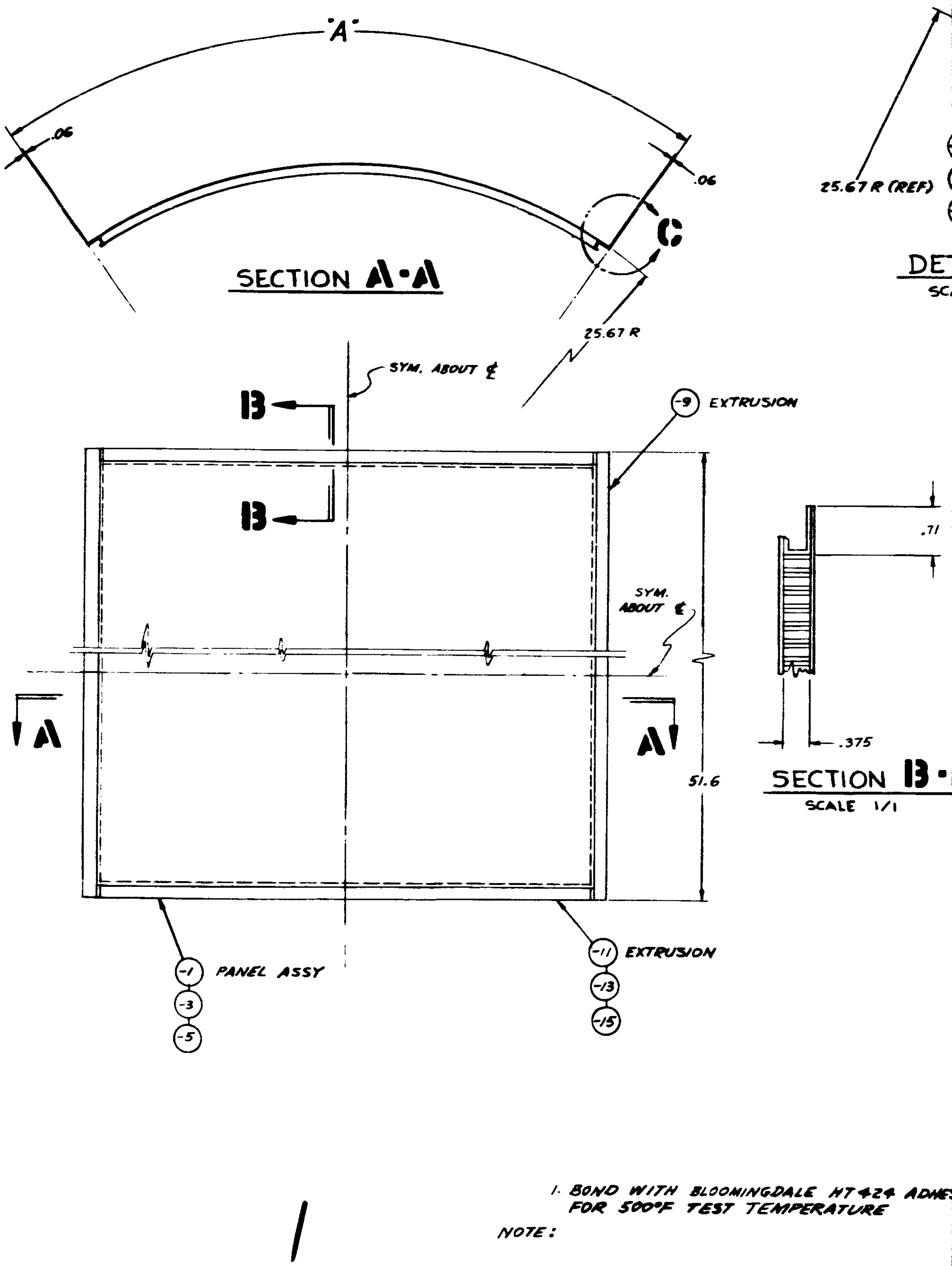

"A"
.06
.06
C
SECTION A-A
25.67 R
25.67 R (REF)
DET
SC
SYM. ABOUT ℄
B
B
-9 EXTRUSION
.71
SYM. ABOUT ℄
A
A
.375
51.6
SECTION B
SCALE 1/1
-1 PANEL ASSY
-3
-5
-11 EXTRUSION
-13
-15
1. BOND WITH BLOOMINGDALE HT424 ADHE
FOR 500°F TEST TEMPERATURE
NOTE:

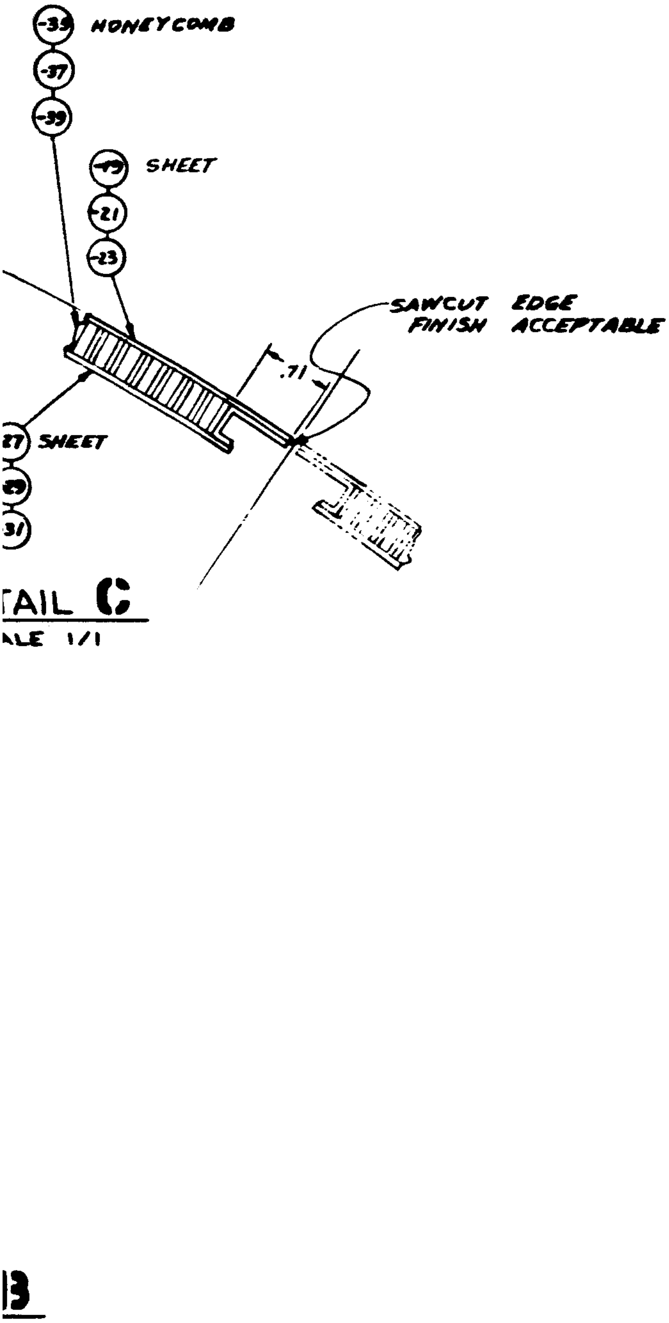

Figure D-1 Panel Assembly - Honeycomb

LOCKHEED CALIFORNIA COMPANY

2

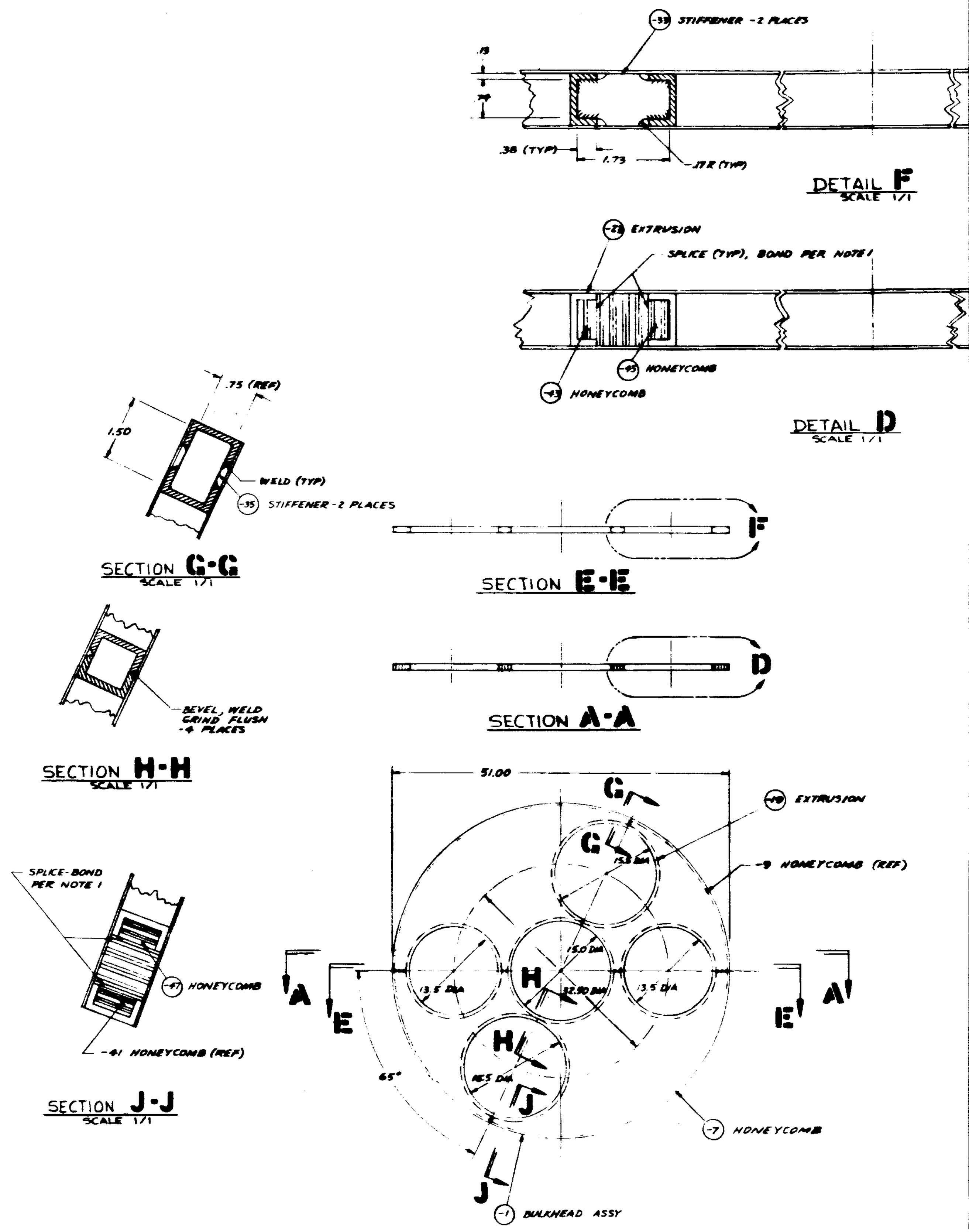

1. BOND WITH BLOOMINGDALE HT4...
FOR 500°F TEST TEMPERATU...

NOTE:

1

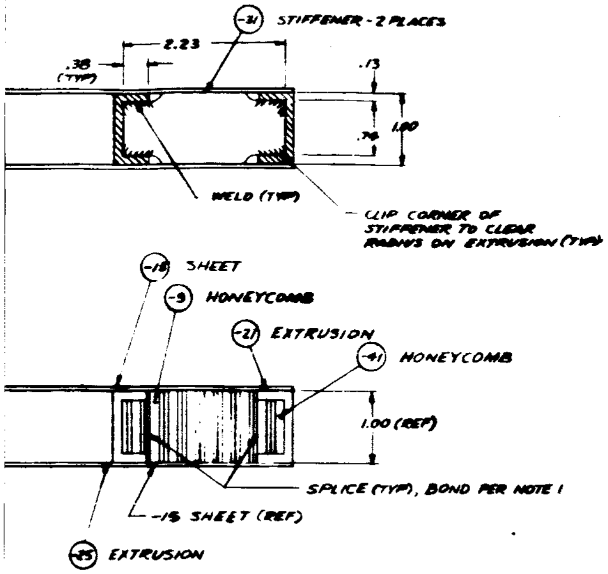

Figure D-2 Bulkhead Assembly - Honeycomb

ADHESIVE

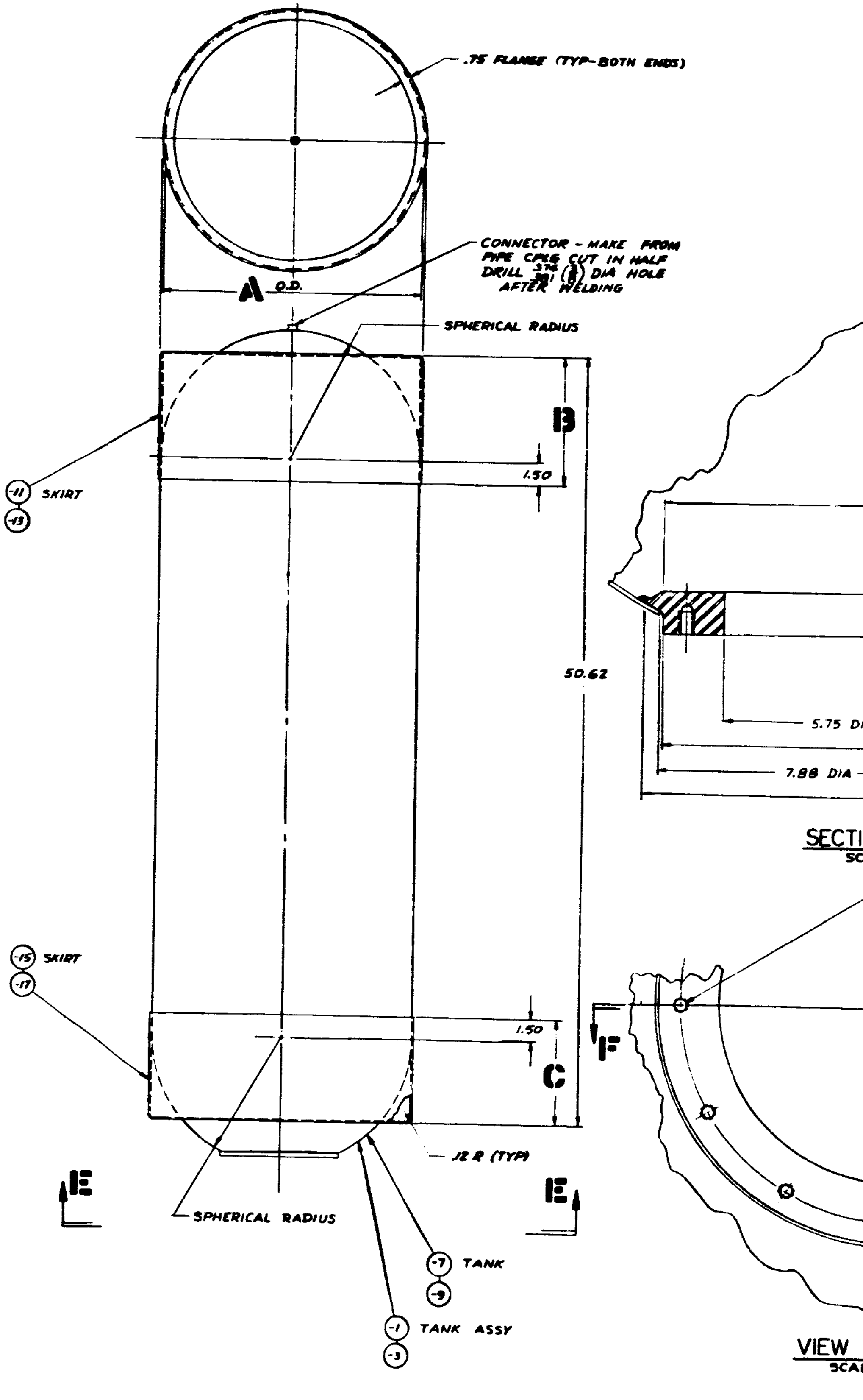

2. TEMPERATURE RANGE +200°F MAX., PROOF PRESSURE TEST 100 PSIG

⚠1 MACHINE AFTER WELDING

NOTE:

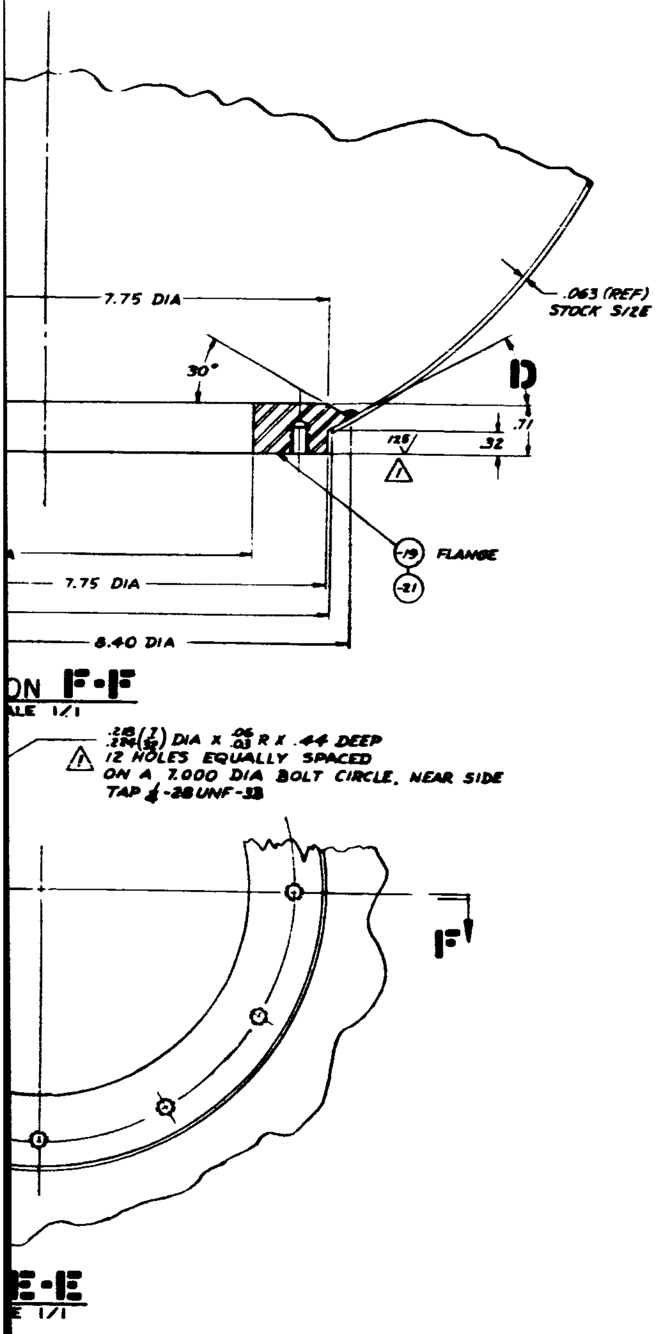

Figure D-3 Tank Assembly - Propellant Welded

00°F MIN.

LOCKHEED
CALIFORNIA COMPANY

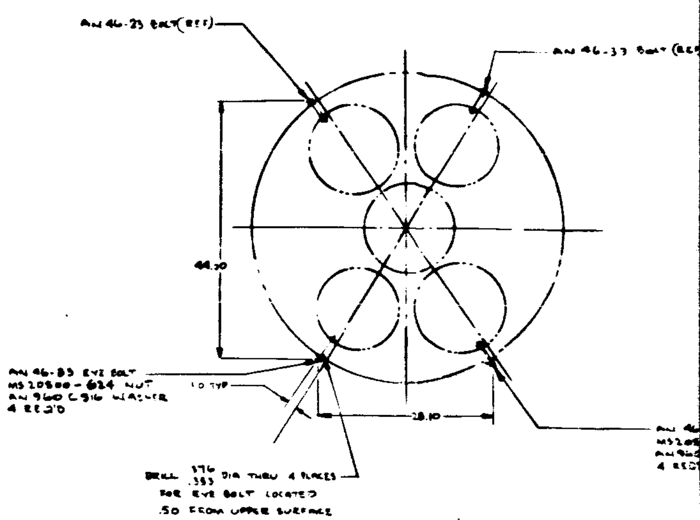

DETAILS OF ATTACHMENT
TO MR6779 BULKHEAD

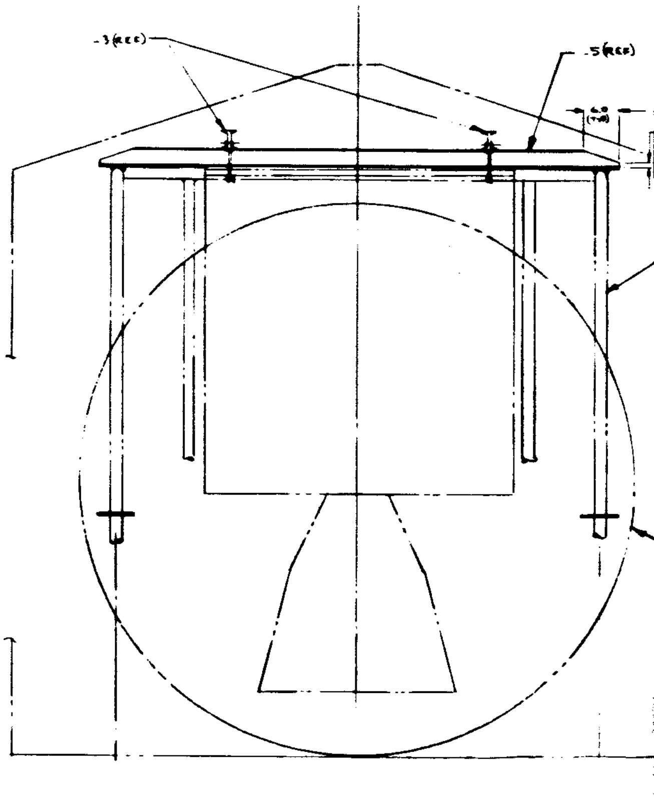

FRONT VIEW

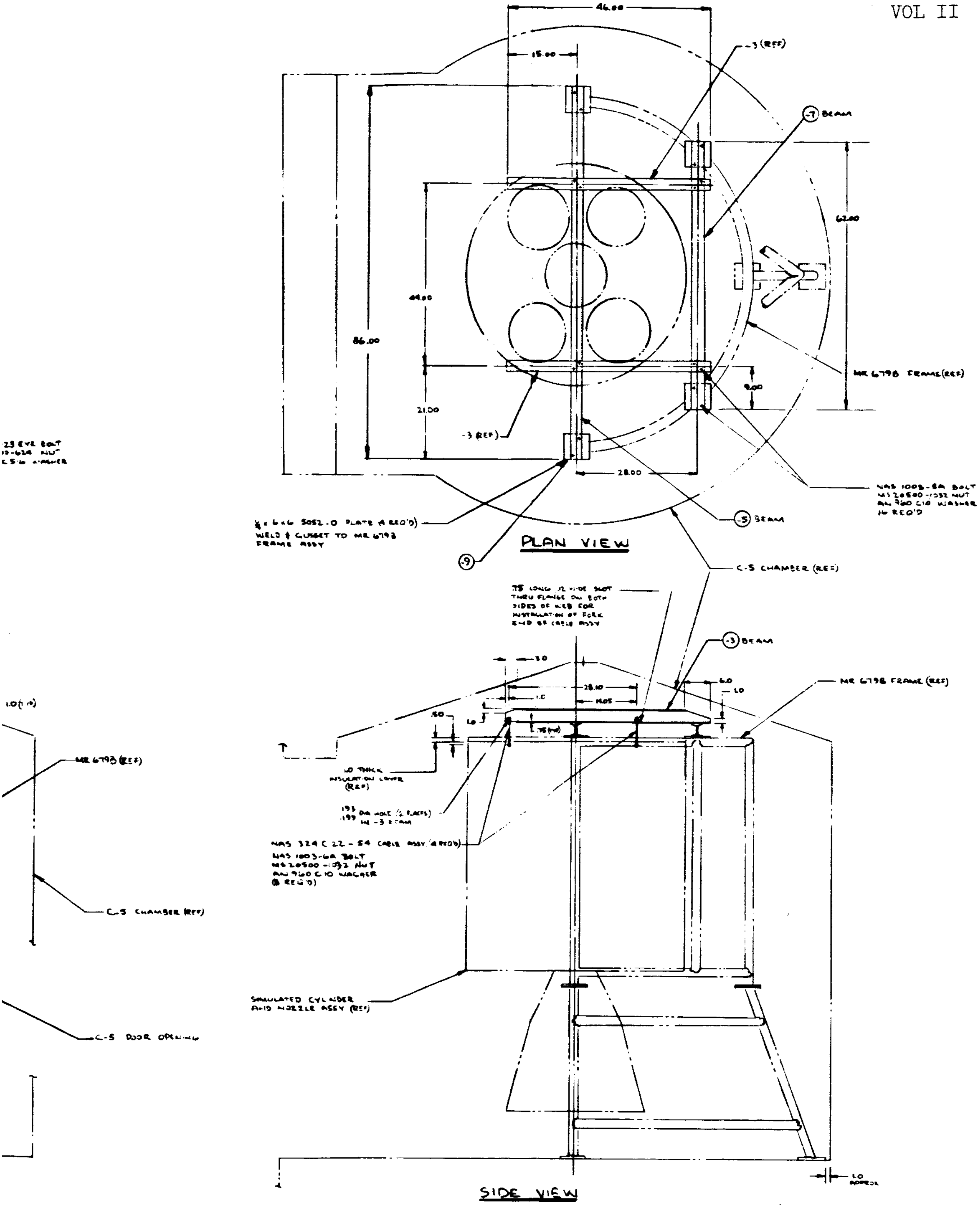

Figure D-4 C-5 Chamber Installation - Apollo Service Module

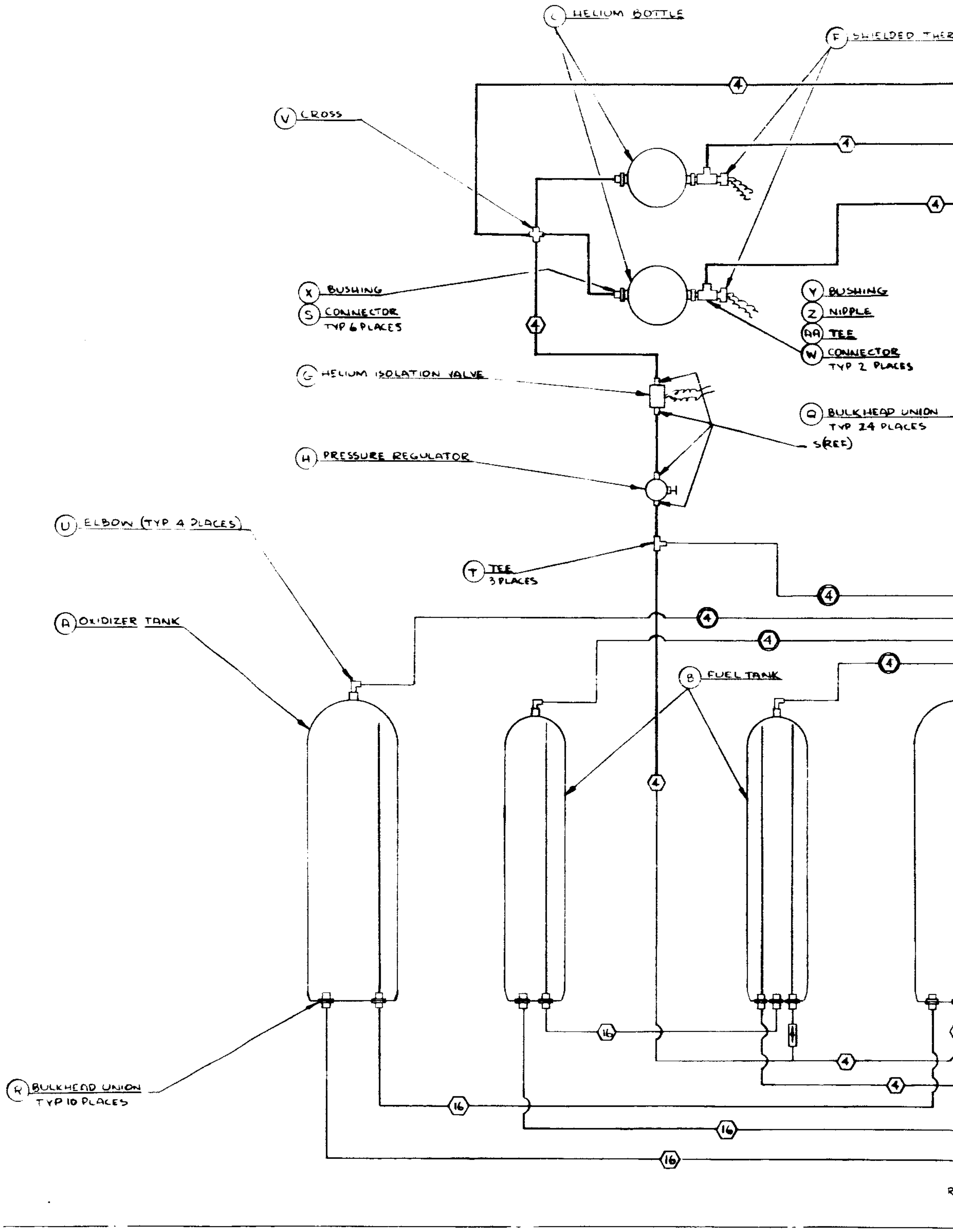

6 NUMBERS IN HEXAGONAL SYMBOL INDICATES TUBE DIAMETER IN SIXTEENTHS OF AN INCH

5 LINES BETWEEN TEST MODEL BLKH'D FITTINGS AND LOCKHEED C-5 CHAMBER FEED THRU TO BE CHANGED FOR SERIES 5 TEST IN HUGHES CHAMBER

4 (4) 5052-O ALUMINUM TUBING .25 O.D x .028 WALL, ABOUT 100 FT TOTAL REQ'D

3 LOCKHEED LABORATORY EQUIPMENT ITEMS

2 (4) 304 1/8 HARD STAINLESS STEEL TUBING, .25 O.D. x .028 WALL ABOUT 100 FT TOTAL REQ'D

1 (16) 304 1/8 HARD STAINLESS STEEL TUBING, 1.00 O.D. x .035 WALL ABOUT 60 FT TOTAL REQ'D

LEGEND:

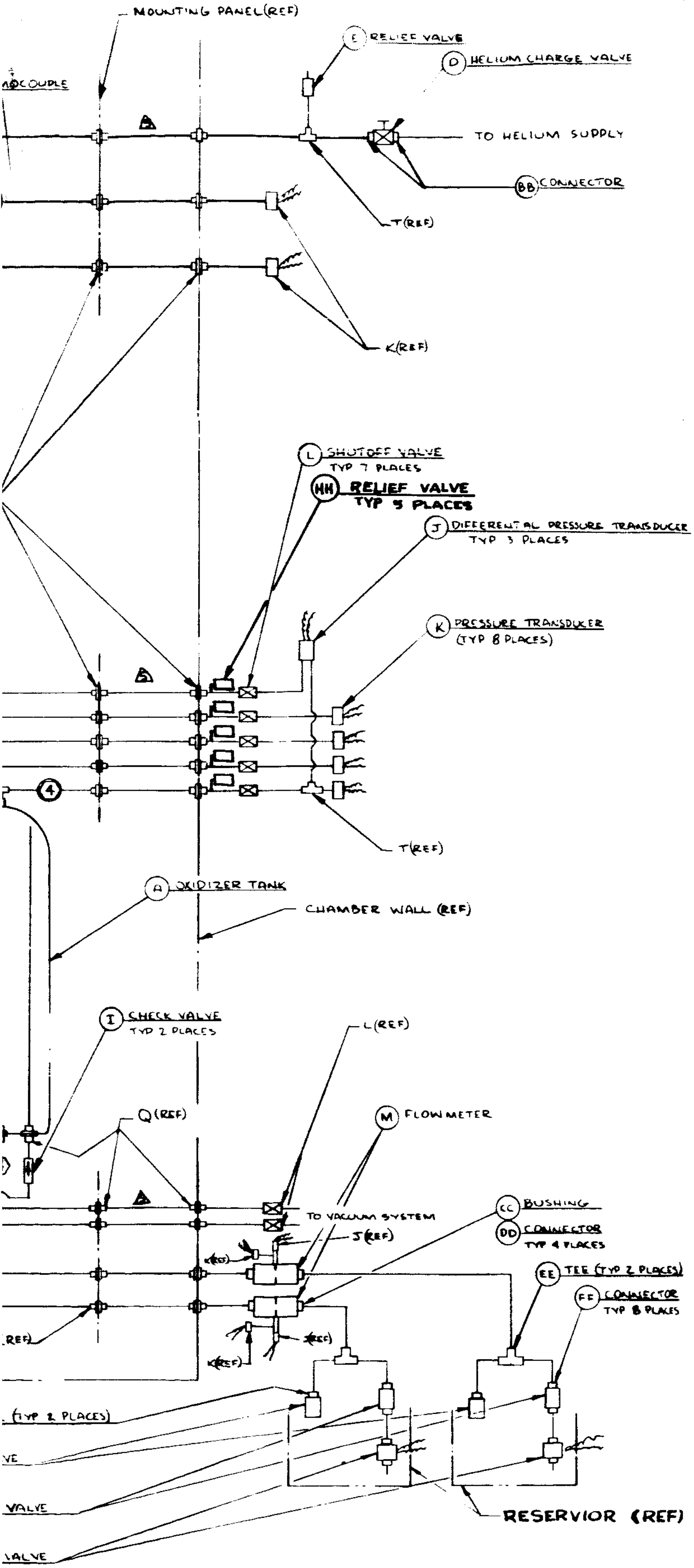

Figure D-5 Plumbing Installation Propellant System - Apollo Service Module

APPENDIX E - THERMOCOUPLE/NODE LOCATIONS

In this appendix, drawings are included (Figure E-1 to E-9) which indicate thermocouple/node locations for the Series 1, 2, 3, and 5. Table E-1 lists the node numbers for these models as well as the Deutsch connector pin numbers. In any future runs of the Series 3/5 model, these pin numbers will provide the required information for connection to the data acquisition system. Similar drawings, Figure E-10 and E-11, as well as the tabular listing (Table E-2, are given for the Series 4 model.

TABLE E -1 APOLLO SERIES 3/5 INSTRUMENTATION IDENTIFICATION

NODE	NODE LOCATION	PLUG NO.	PIN NOS.
	OUTER SHELL (Fig. E-1)		
201	EC1-T-E *	6	1, 2
301	EC1-M-E	6	3, 4
401	EC1-B-E	6	5, 6
223	EC1-T-C	6	7, 8
323	EC1-M-C	6	9, 10
423	EC1-B-C	6	11, 12
221	EC6-T-E	6	13, 14
321	EC6-M-E	6	15, 16
421	EC6-B-E	6	17, 18
219	EC6-T-C	6	19, 20
319	EC6-M-C	6	21, 22
419	EC6-B-C	6	23, 24
217	EC5-T-E	6	25, 26
317	EC5-M-E	6	27, 28
417	EC5-B-E	6	29, 30
215	EC5-T-C	6	31, 32
315	EC5-M-C	6	33, 34
415	EC5-B-C	6	35, 36

NOTE: 1. All plug and pin numbers listed are Deutsch.

a. Odd numbers - copper
b. Even numbers - constantan

2. IC = iron-constantan

* Explanation of this identification code is given at the conclusion of this table.

LOCKHEED
CALIFORNIA COMPANY

TABLE E-1 (cont'd)

NODE	NODE LOCATION		PLUG NO.	PIN NOS.
	OUTER SHELL - CONT'D.			
213	EC4-T-E		7	1, 2
313	EC4-M-E		7	3, 4
413	EC4-B-E		7	5, 6
211	EC4-T-C		7	7, 8
311	EC4-M-C		7	9, 10
411	EC4-B-C		7	11, 12
209	EC3-T-E		7	13, 14
309	EC3-M-E		7	15, 16
409	EC3-B-E		7	17, 18
207	EC3-M-C		7	21, 22
307	EC3-T-C		7	19, 20
407	EC3-B-C		7	23, 24
·205	EC2-T-E		7	25, 26
305	EC2-M-E		7	27, 28
405	EC2-B-E		7	29, 30
203	EC2-T-C		7	31, 32
303	EC2-M-C		7	33, 34
403	EC2-B-C		7	35, 36
398	EC3-M-C	Inside	10	31, 32
399	EC4-M-C	Inside	10	33, 34
1102	EC1-M-E	Inside on sector beam web angle	5	21, 22
1101	EC1-M-C	Inside	5	5, 6

NOTE: 1. All plug and pin numbers listed are Deutsch.

a. Odd numbers - copper
b. Even numbers - constantan

2. IC = iron-constantan

TABLE E-1 (cont'd)

NODE	NODE LOCATION	PLUG NO.	PIN NOS.
	INNER CYLINDER (Fig. E-2)		
233	IC56-T	11	1, 2
333	IC56-M	11	3, 4
433	IC56-B	11	5, 6
231	IC45-T	11	7, 8
331	IC45-M	11	9, 10
431	IC45-B	11	11, 12
229	IC34-T	11	13, 14
329	IC34-M	11	15, 16
429	IC34-B	11	17, 18
227	IC23-T	11	19, 20
327	IC23-M	11	21, 22
427	IC23-B	11	23, 24
226	IC2-T	11	25, 26
326	IC2-M	11	27, 28
426	IC2-B	11	29, 30
225	IC12-T	11	33, 34
325	IC12-M	11	31, 32
425	IC12-B	12	35, 36
235	IC61-T	12	29, 30
335	IC61-M	12	31, 32
435	IC61-B	12	33, 34

NOTE: 1. All plug and pin numbers listed are Deutsch.
a. Odd numbers - copper
b. Even numbers - constantan

2. IC = iron-constantan

TABLE E-1 (cont'd)

NODE	NODE LOCATION	PLUG NO.	PIN NOS.
	RADIAL BEAMS (Fig. E-3)		
437	B1-B	13	19, 20
337	B1-M Inner	13	21, 22
237	B1-T	13	23, 24
438	B2-B	13	25, 26
338	B2-M	13	27, 28
238	B2-T	13	29, 30
439	B3-B	13	31, 32
339	B3-M	13	33, 34
239	B3-T	13	35, 36
440	B4-B	13	1, 2
340	B4-M	13	3, 4
240	B4-T	13	5, 6
441	B5-B	13	7, 8
341	B5-M	13	9, 10
241	B5-T	13	11, 12
442	B6-B	13	13, 14
342	B6-M	13	15, 16
242	B6-T	13	17, 18
	LOWER BULKHEAD (Fig. E-4)		
51	LB12-M	12	21, 22
52	LB2-M Tank Opening	12	9, 10
54	LB2-M Tank Opening	12	27, 28
55	LB23-M	8	35, 36
56	LB3-M Tank Opening	8	1, 2

NOTE: 1. All plug and pin numbers listed are Deutsch.

a. Odd numbers - copper
b. Even numbers - constantan

2. IC = iron-constantan

TABLE E-1 (cont'd)

NODE	NODE LOCATION		PLUG NO.	PIN NOS.
	LOWER BULKHEAD - CONT'T			
58	LB3-M	Tank Opening	8	7, 8
59	LB34-M		8	9, 10
61	LB4-M		8	15, 16
63	LB45-M		8	21, 22
67	LB56-M		8	29, 30
71	LB61-M		12	19, 20
73	LB1-M		12	13, 14
90	LB1-M	Upper Side	12	5, 6
91	LB4-M	Upper Side	8	17, 18
151	LB12-O		12	11, 12
153	LB2-O		12	23, 24
155	LB23-O		8	33, 34
157	LB3-O		8	3, 4
159	LB34-O		8	5, 6
161	LB4-O		8	13, 14
163	LB45-O		8	23, 24
165	LB5-O		8	25, 26
167	LB56-O		8	31, 32
169	LB6-O		12	3, 4
171	LB61-O		12	15, 16
173	LB1-O		12	25, 26
175	LB12-I		12	1, 2
177	LB23-I		12	7, 8
179	LB34-I		8	11, 12
181	LB45-I		8	19, 20
183	LB56-I		8	27, 28
185	LB61-I		12	17, 18

NOTE: 1. All plug and pin numbers listed are Deutsch.
a. Odd numbers - copper
b. Even numbers - constantan

2. IC = iron-constantan

TABLE E-1 (cont'd)

NODE	NODE LOCATION	PLUG NO.	PIN NOS.
	HEAT SHIELD (Fig. E-5)		
356	HS1-I-S	IC	# 1
362	HS1-M-S	14	7, 8
368	HS1-O-S	14	5, 6
372	HS8-I	IC	# 2
373	HS6-I	IC	# 4
374	HS45-I	IC	# 12
376	HS1-I	14	11, 12
377	HS910-M	14	19, 20
379	HS6-M	5	29, 30
381	HS3-M	14	9, 10
382	HS1-M	14	15, 16
384	HS8-O	5	23, 24
385	HS6-O	5	31, 32
386	HS45-O	5	15, 16
388	HS1-O	14	13, 14
	UPPER BULKHEAD (Fig. E-6)		
1	UB12-M	9	3, 4
2	UB2-M Tank Opening	9	19, 20
4	UB2-M Tank Opening	9	23, 24
5	UB23-M	9	27, 28
6	UB3-M Tank Opening	9	31, 32
8	UB3-M Tank Opening	10	3, 4
9	UB34-M	10	7, 8
11	UB4-M	10	13, 14

NOTE: 1. All plug and pin numbers listed are Deutsch.
   a. Odd numbers - copper
   b. Even numbers - constantan

2. IC = iron-constantan

TABLE E-1 (cont'd)

NODE	NODE LOCATION	PLUG NO.	PIN NOS.
	UPPER BULKHEAD - CONT'D		
13	UB45-M	10	21, 22
17	UB56-M	10	29, 30
21	UB61-M	9	15, 16
23	UB1-M	9	9, 10
40	UB1-M Underside	9	11, 12
41	UB4-M Underside	10	17, 18
101	UB12-O	9	1, 2
103	UB2-O	9	21, 22
105	UB23-O	9	25, 26
107	UB3-O	10	1, 2
109	UB34-O	10	5, 6
111	UB4-O	10	11, 12
113	UB45-O	10	19, 20
115	UB5-O	10	25, 26
117	UB56-O	10	27, 28
119	UB6-O	9	35, 36
121	UB61-O	9	13, 14
123	UB1-O	9	7, 8
125	UB12-I	9	5, 6
127	UB23-I	9	29, 30
129	UB34-I	10	9, 10
131	UB45-I	10	23, 24
133	UB56-I	9	33, 34
135	UB61-I	9	17, 18
Cold Wall	Cold Wall	11	35, 36

NOTE: 1. All plug and pin numbers listed are Deutsch.
   a. Odd numbers - copper
   b. Even numbers - constantan

2. IC = iron-constantan

TABLE E-1 (cont'd)

NODE	NODE LOCATION	PLUG NO.	PIN NOS.
	NOZZLE (Fig. E-7)		
253	N4-T	IC	# 14
254	N5-T	IC	# 9
256	N1-T	IC	# 10
257	N2-M	IC	# 13
259	N4-M	IC	# 5
262	N1-M	IC	# 11
265	N4-B	IC	# 16
268	N1-B	IC	# 15
	THRUST CHAMBER		
390	Middle	IC	# 6
	BILLET		
393	Top of Local Heat Source	5	11, 12
1176	Side of Local Heat Source	5	17, 18
	HELIUM BOTTLE PROBES (Fig. E-8)		
1181	Inside Upper HE Bottle	16	29, 30
1182	Inside Lower HE Bottle	16	31, 32

NOTE: 1. All plug and pin numbers listed are Deutsch.
   a. Odd numbers - copper
   b. Even numbers - constantan

2. IC - iron-constantan

TABLE E-1 (cont'd)

NODE	NODE LOCATION	PLUG NO.	PIN NOS.
	MISCELLANEOUS (Fig. E-8)		
392	HE Bottle, Lower, Outside	16	35, 36
391	HE Bottle, Upper, Outside	16	33, 34
603	Pressure Regulator	14	17, 18
604	Pressure Reg. Discharge	5	25, 26
605	PO1-L Discharge	5	33, 34
606	PO1-L Transfer In	5	19, 20
607	PF1-L Transfer In	14	31, 32
608	PF1-L Discharge	14	25, 26
609	PF2-L Transfer Out	5	27, 28
610	PF2-G In	5	35, 36
611	PO2-L Transfer Out	14	29, 30
612	PO2-G In	14	27, 28
613	PO1-L Inside Heat Shield	14	35, 36
614	PO1-L Inside Heat Shield	14	21, 22
615	PF1-L Line Heater	5	9, 10
616	PO1-L Line Heater	5	7, 8
	INSIDE AND ON TANKS (Fig. E-9)		
1262	Inside Oxid. Tank 1	16	1, 2
1263	Side of Oxid. Tank 2	16	3, 4
1264	Inside Oxid. Tank 1	16	5, 6
1265	Inside Oxid. Tank 1	16	7, 8
1266	Inside Oxid. Tank 1	16	9, 10
1267	Inside Oxid. Tank 1	16	11, 12

NOTE: 1. All plug and pin numbers listed are Deutsch.
a. Odd numbers - copper
b. Even numbers - constantan

2. IC = iron-constantan

TABLE E-1 (cont'd)

NODE	NODE LOCATION	PLUG NO.	PIN NOS.
	INSIDE AND ON TANKS - CONT'D.		
1151	Inside Oxid. Tank 1	16	13, 14
1152	Inside Oxid. Tank 1	16	15, 16
1153	Inside Oxid. Tank 2	16	17, 18
1154	Inside Oxid. Tank 2	16	19, 20
1155	Inside Oxid. Tank 2	16	21, 22
1156	Inside Oxid. Tank 2	16	23, 24
1157	Inside Oxid. Tank 2	16	25, 26
1158	Side of Oxid. Tank 2	16	27, 28
1159	Side of Oxid. Tank 2	14	1, 2
1160	Side of Oxid. Tank 2	14	3, 4
1161(397)	Side of Oxid. Tank 2	14	23, 24
1162	Side of Oxid. Tank 2	14	33, 34
1163	Inside Fuel Tank 1	17	1, 2
1164	Inside Fuel Tank 1	17	3, 4
1165	Inside Fuel Tank 1	17	5, 6
1166	Inside Fuel Tank 1	17	7, 8
1167	Inside Fuel Tank 1	17	9, 10
1168	Inside Fuel Tank 1	17	11, 12
1169	Inside Fuel Tank 1	17	13, 14
1170	Inside Fuel Tank 2	17	15, 16
1171	Inside Fuel Tank 2	17	17, 18
1172	Inside Fuel Tank 2	17	19, 20
1173	Inside Fuel Tank 2	17	21, 22
1174	Inside Fuel Tank 2	17	23, 24

NOTE: 1. All plug and pin numbers listed are Deutsch.

a. Odd numbers - copper
b. Even numbers - constantan

2. IC = iron-constantan

TABLE E-1 (cont'd)

NODE	NODE LOCATION	PLUG NO.	PIN NOS.
	INSIDE AND ON TANKS - CONT'D		
1279	Lower Side of Oxid. Tank 1	15	1, 2
1100	Lower Side of Fuel Tank 2	15	3, 4
1201	Side of Oxid. Tank 1	15	5, 6
1202(394)	Side of Oxid. Tank 1	15	7, 8
1203	Side of Oxid.Tank 1	15	9, 10
1204	Side of Oxid. Tank 1	15	11, 12
1205	Side of Fuel Tank 1	15	13, 14
1206	Side of Fuel Tank 1	15	15, 16
1207(396)	Side of Fuel Tank 1	15	17, 18
1208	Side of Fuel Tank 1	15	19, 20
1209	Side of Fuel Tank 1	15	21, 22
1210	Side of Fuel Tank 2	15	23, 24
1211	Side of Fuel Tank 2	15	25, 26
1212(395)	Side of Fuel Tank 2	15	27, 28
1213	Side of Fuel Tank 2	15	29, 30
1214	Side of Fuel Tank 2	15	31, 32
1215	Side of Oxid. Tank 1	15	33, 34
1216	Side of Fuel Tank 1	15	35, 36
	PRESSURES (Fig. E-8)		
10188	PSIG, HE Bottle 1, Upper		
10189	PSIG, HE Bottle 2, Lower		
10190	PSIG, Top Oxid. Tank 1		
10191	PSIG, Top Fuel Tank 1		
10192	PSIG, Top Oxid. Tank 2		
10193	PSIG, Top Fuel Tank 2		

NOTE: 1. All plug and pin numbers listed are Deutsch.

a. Odd numbers - copper
b. Even numbers - constantan

2. IC = iron-constantan

TABLE E-1 (cont'd)

NODE	NODE LOCATION	PLUG NO.	PIN NOS.
	PRESSURES - CONT'D		
10194	PSIG, Oxidizer Meter		
10195	PSIG, Fuel Meter		
10196	Δ P, Inches H_2O, Oxid. Meter		
10197	Δ P, Inches H_2O, Fuel Meter		
10198	Δ P, Inches H_2O, Reg. to Top, Oxid. 2		
	MONITORS		
253	N4-T	IC	# 3
390	Middle of Thrust Chamber	IC	# 7
1176	Side of Local Heat Source	IC	# 8
321	EC6-M-E	20	1, 2
301	EC1-M-E	20	3, 4
305	EC2-M-E	20	5, 6
617	Line Monitor	20	7, 8
618	Line Monitor	20	9, 10
301	EC1-M-E	10	35, 36

NOTE: 1. All plug and pin numbers listed are Deutsch.
- a. Odd numbers - copper
- b. Even numbers - constantan

2. IC = iron-constantan

TABLE E-1 (cont'd)

CODE FOR NODE LOCATIONS

EC	External cylinder & sector no.	-	T, top M, middle B, bottom	-	C, center of panel E, edge of panel
B	Beam no. (1 between sector 1 & 2 2 between sector 2 & 3 etc.)	-	T, top M, middle B, bottom	-	All centered between inner & outer cylinder
LB UB	Upper or lower bulkhead sector or intersect 12 = sector 1 & 2 intersect 23 = sector 2 & 3 intersect, etc. Outside unless noted otherwise	-	O, radially outside M, radially middle I, radially inside		
IC	Internal cylinder, sector or sector intersect	-	T, top M, middle B, bottom		
N	Nozzle & area under sector no.	-	T, top M, middle B, bottom		
HS	Heat shield no. or intersect	-	I, radially inside M, radially middle O, radially outside	-	S - sandwiched between outer skin & Q-felt "S" omitted, inside heat shield
PF	Plumbing - fuel tank & tank no.	-	L - liquid line G - gas line		
PO	Plumbing - oxid. tank & tank no.	-	L - liquid line G - gas line		

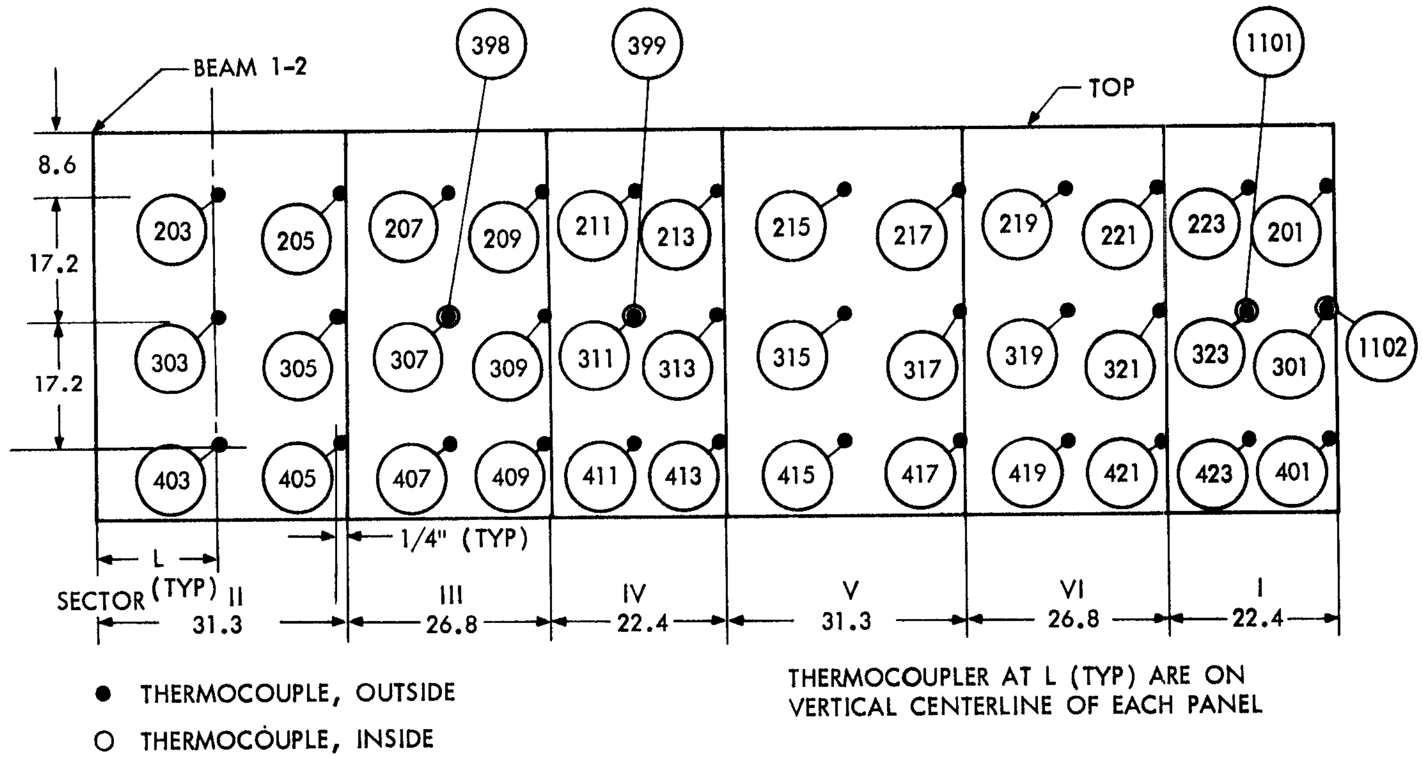

FIGURE E-1. NODE LOCATION ON EXTERNAL CYLINDER

Figure E-1 Node Location on External Cylinder

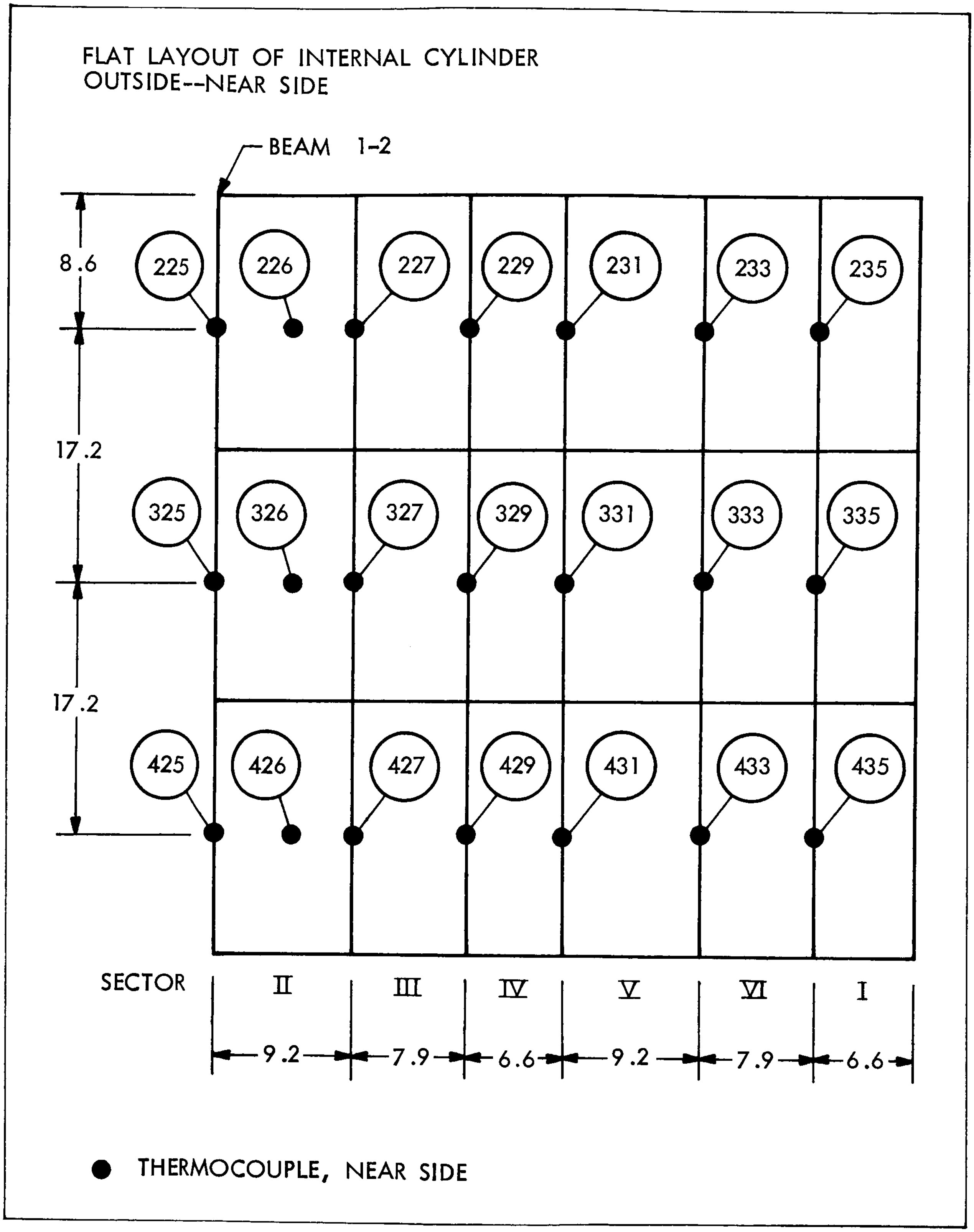

Figure E-2 Node Location on Inner Cylinder

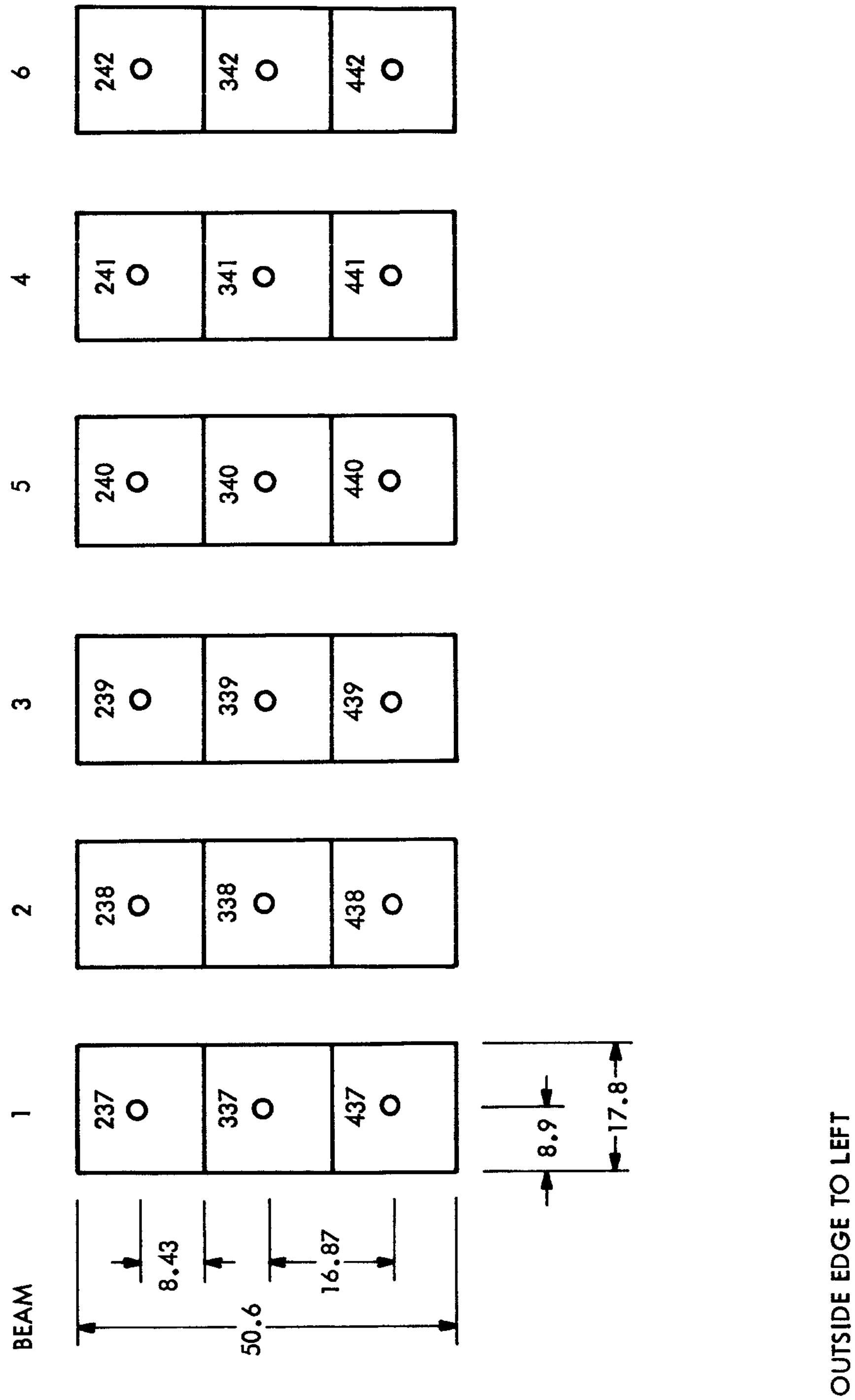

Figure E-3 Node Location Sector Beam

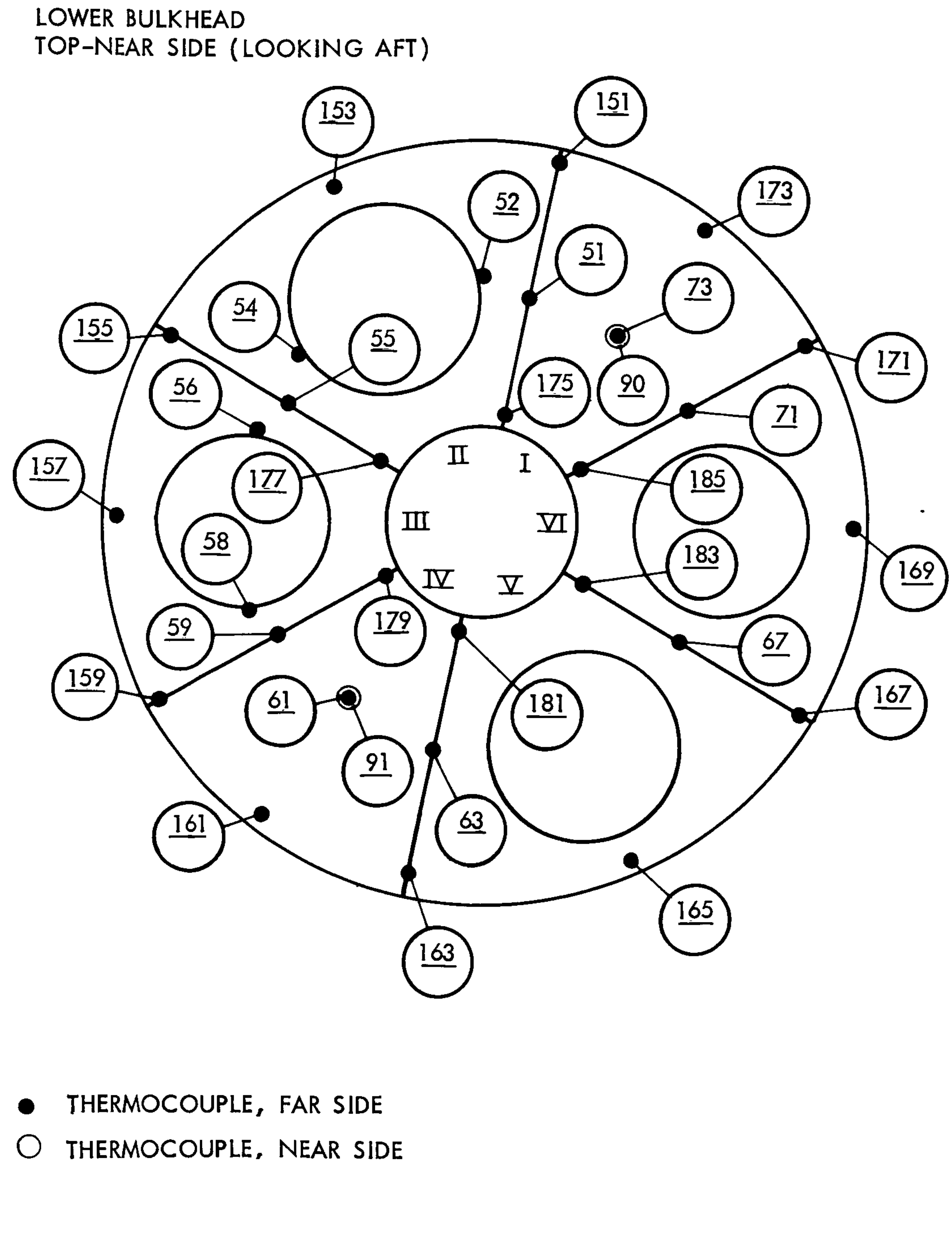

Figure E-4 Node Location on Lower Bulkhead

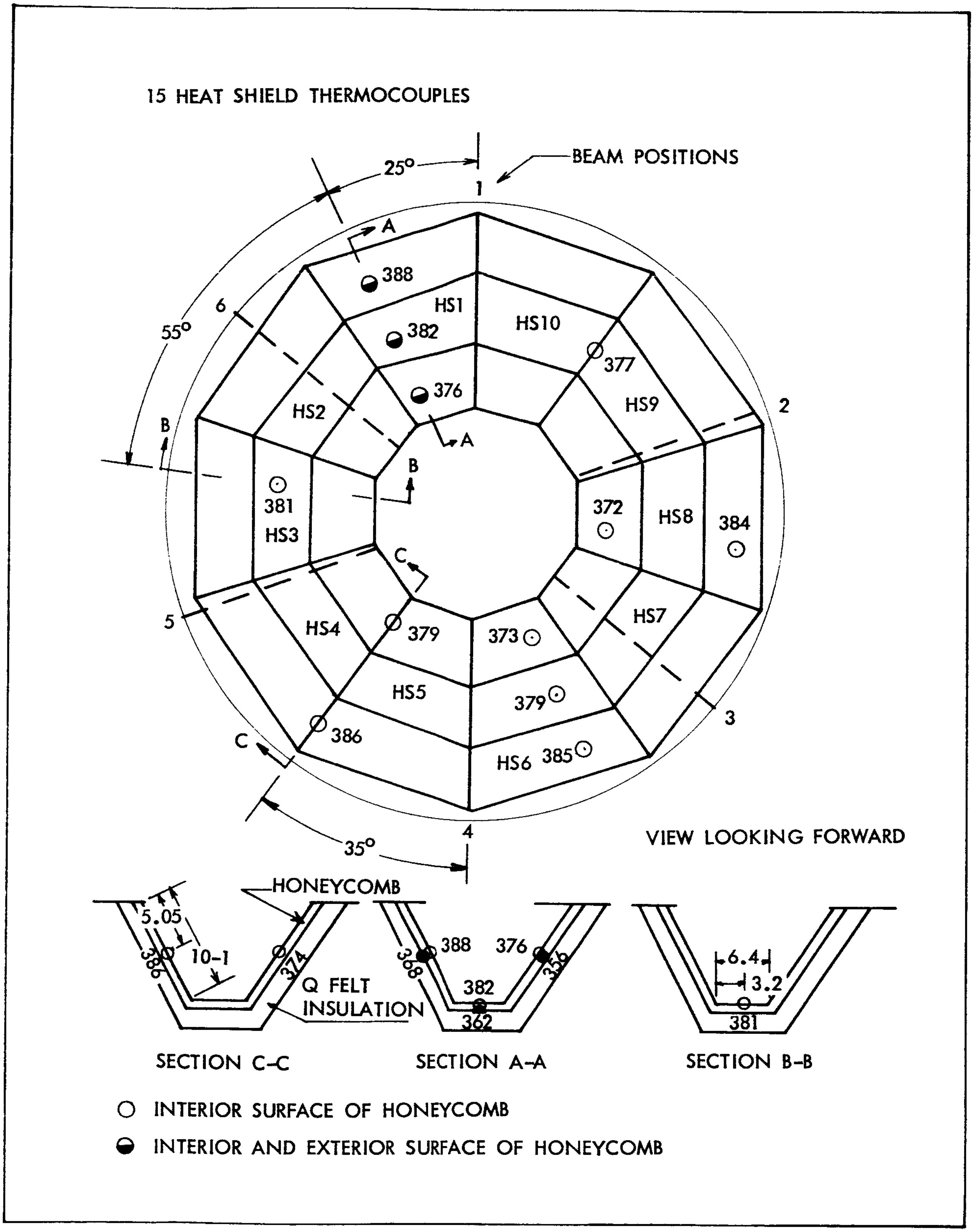

Figure E-5 Heat Shield Node Locations

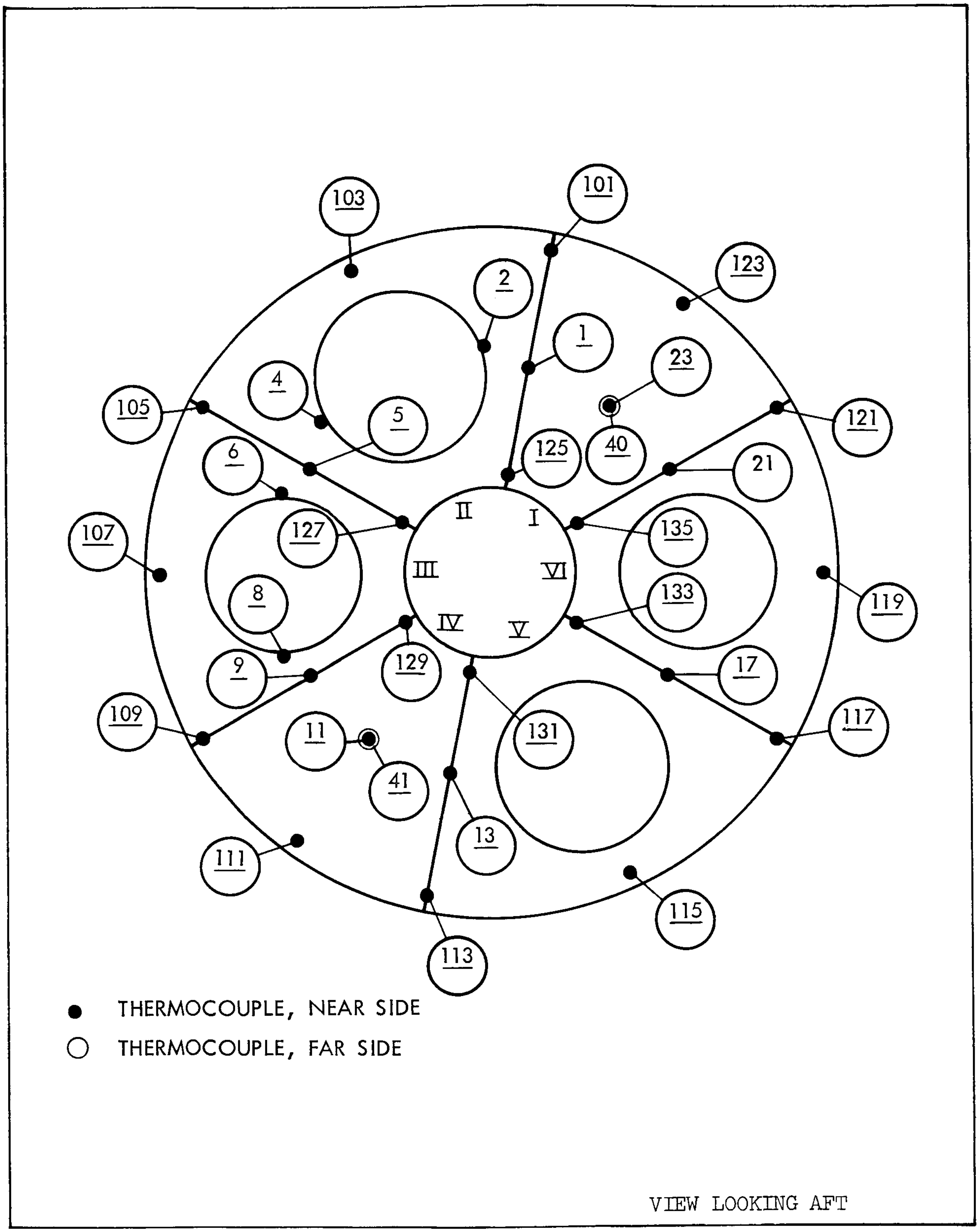

Figure E-6 Node Location on Upper Bulkhead

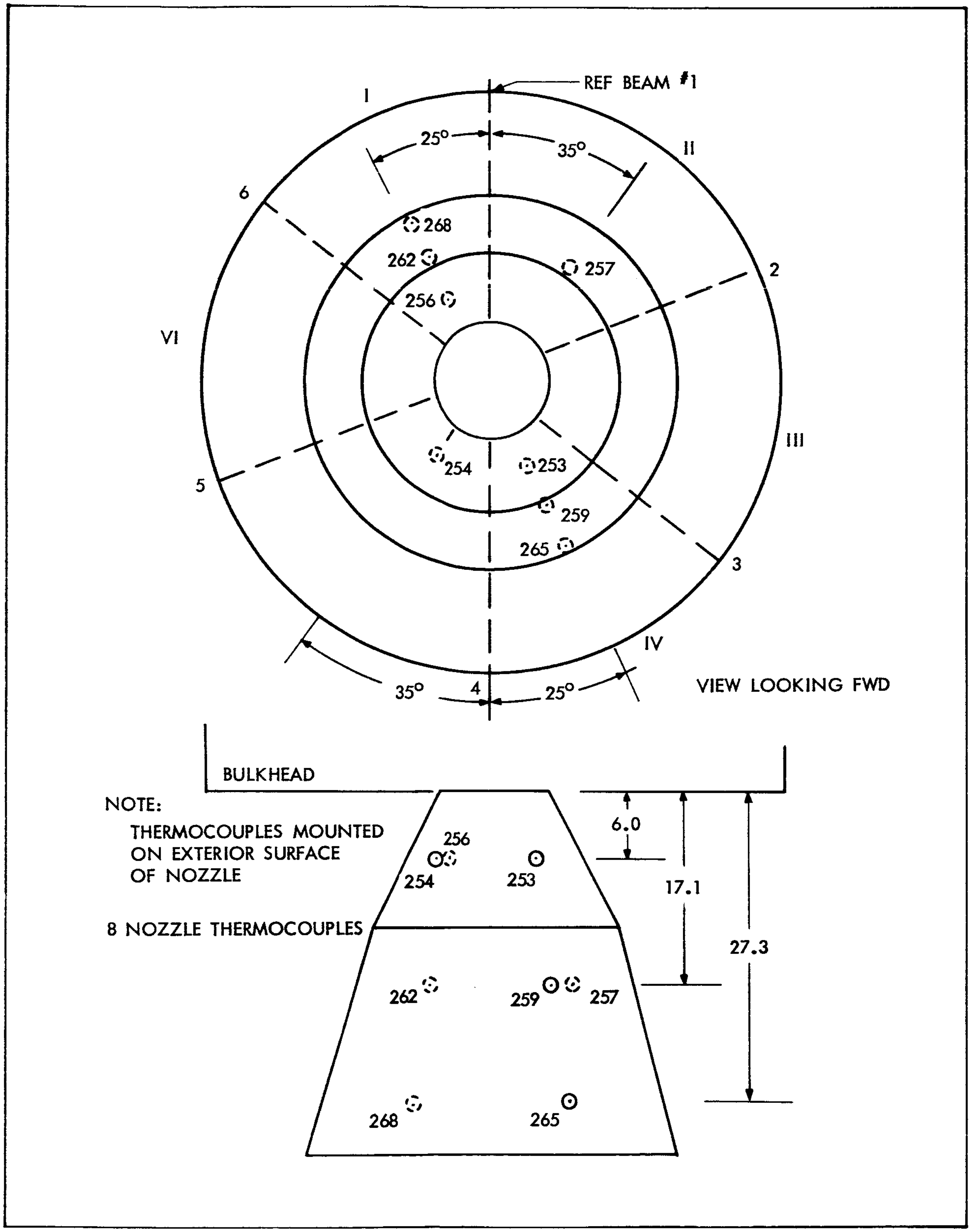

Figure E-7 Nozzle Node Locations

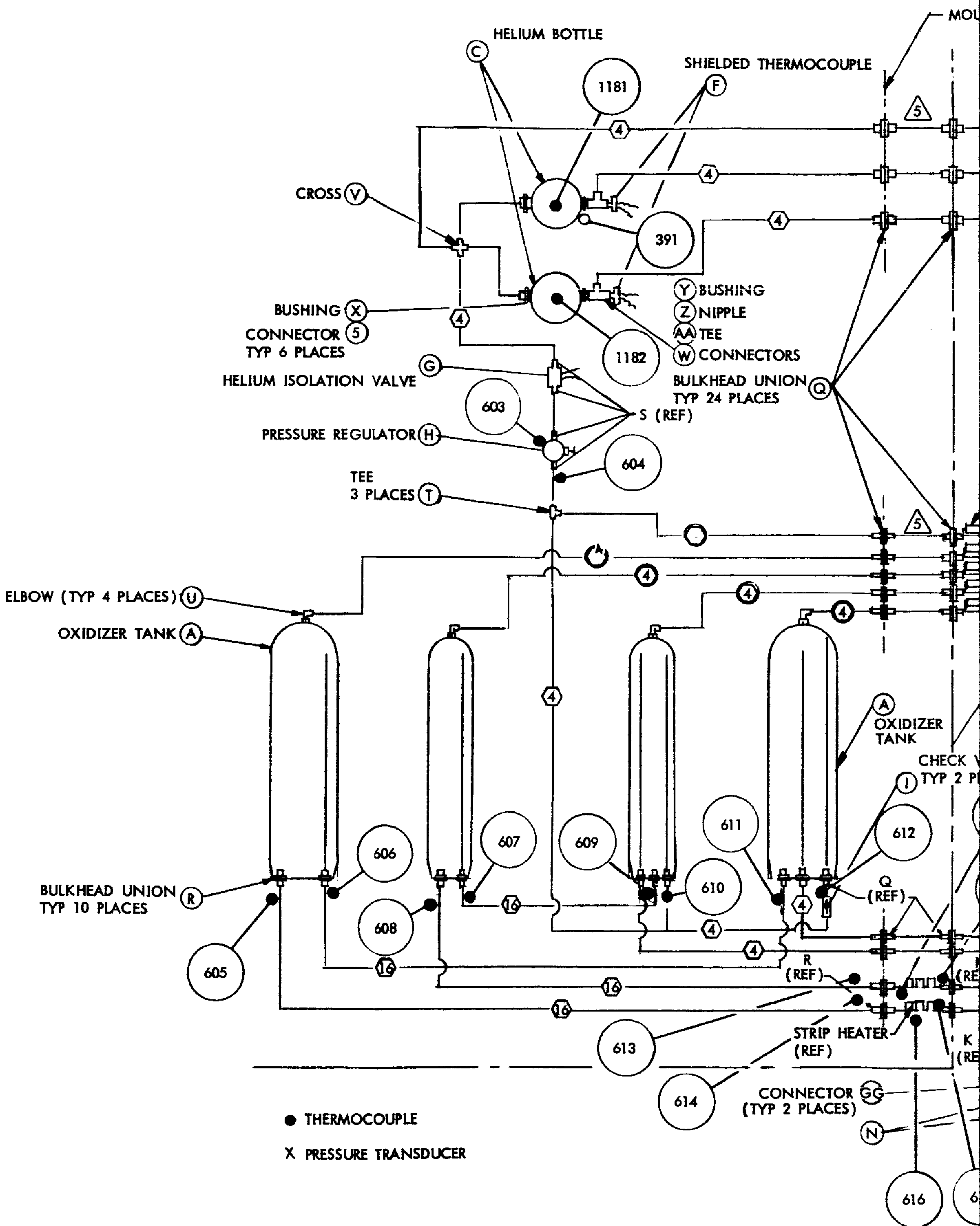

LOCKHEED
CALIFORNIA COMPANY

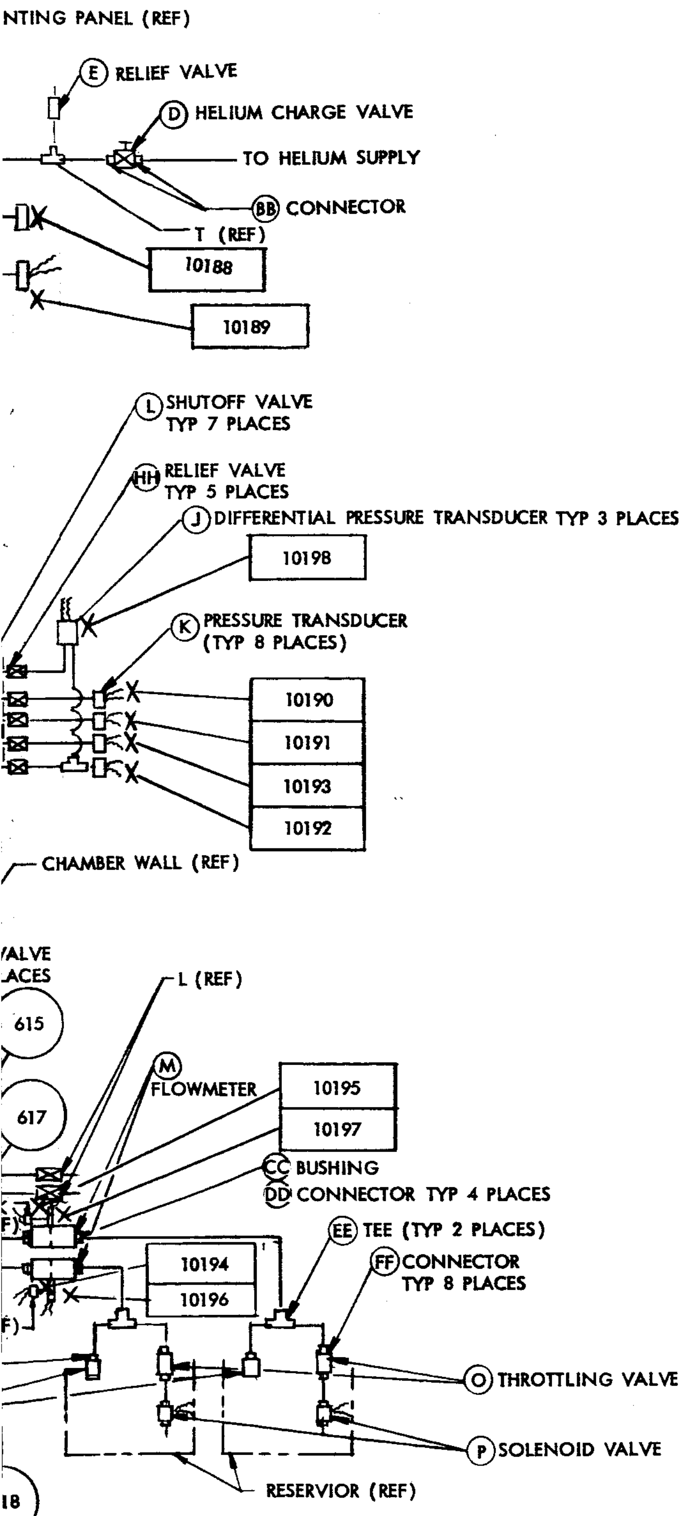

Figure E-8 Location of Plumbing Line Nodes and Pressure Transducers

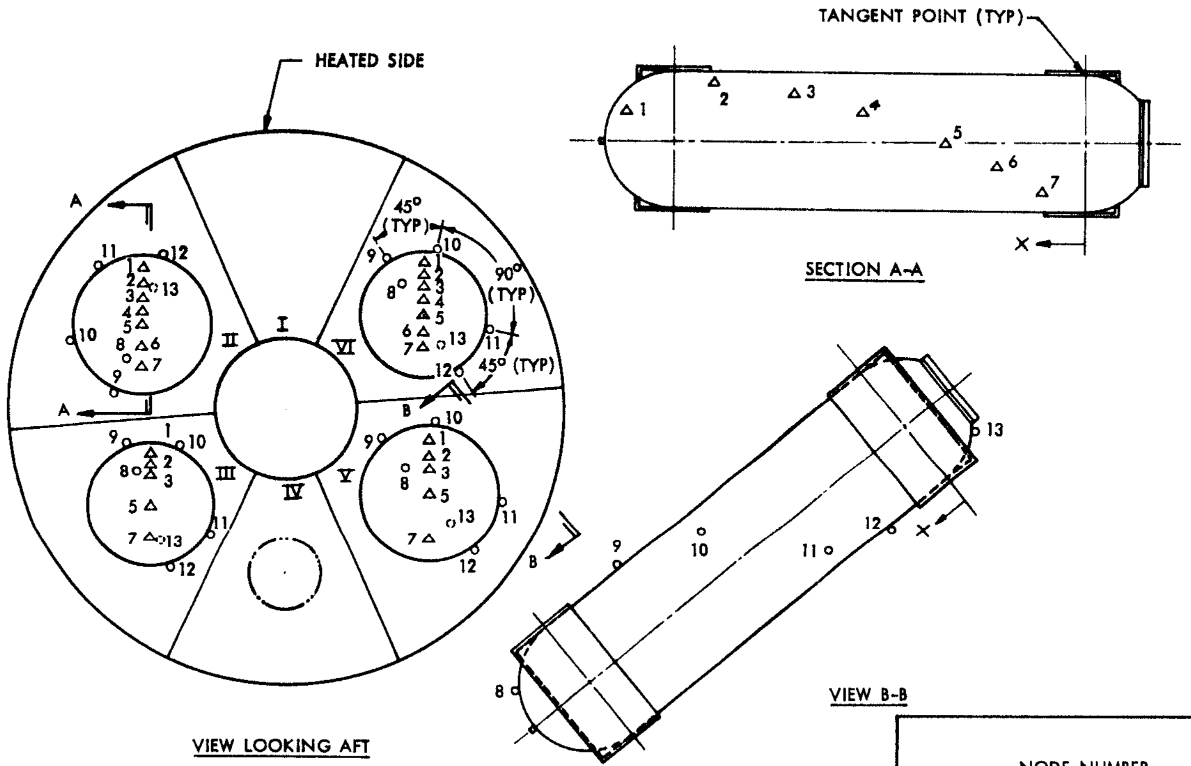

NOTE:
o - OUTSIDE TANK
Δ - INSIDE TANK

THERMOCOUPLE IDENTIFICATION	NODE NUMBER				THERMOCOUPLER LOCATION X (IN.)	
	OXIDIZER TANK 1	OXIDIZER TANK 2	FUEL TANK 1	FUEL TANK 2	OXIDIZER TANK	FUEL TANK
1	1262	1153	1168	1170	43.03	44.92
2	1264	1154	1163	1171	34.72	37.02
3	1265	1155	1164	1172	28.41	30.29
4	1266		1165		22.10	23.56
5	1267	1156	1166	1173	15.78	16.83
6	1151		1167		9.47	10.10
7	1152	1157	1169	1174	3.16	3.37
8	1215	1159	1216	1210	43.88	45.68
9	1201	1160	1206	1211	28.41	30.29
10	394	397	396	395	22.10	23.56
11	1203	1162	1208	1213	15.78	16.83
12	1204	1263	1209	1214	9.47	10.10
13	1279	1158	1205	1100	- 6.00	- 5.30

Figure E-9 Tank Node Locations

TABLE E-2 APOLLO SERIES 4 INSTRUMENTATION IDENTIFICATION

CODE NODE	PLUG #2 PIN NOS.	PLATE NODE	PLUG #1 PIN NOS.
111	1-2	11	1-2
112	5-6	12	5-6
113	9-10	13	9-10
114	13-14	14	13-14
115	17-18	15	17-18
116	21-22	16	21-22
117	25-26	17	25-26
118	29-30	18	29-30
141	3-4	41	3-4
142	7-8	42	7-8
143	11-12	43	11-12
144	15-16	44	15-16
145	19-20	45	19-20
146	23-24	46	23-24
147	27-28	47	27-28
148	31-32	48	31-32
		100	33-34

(See Figs. E-10 and E-11)

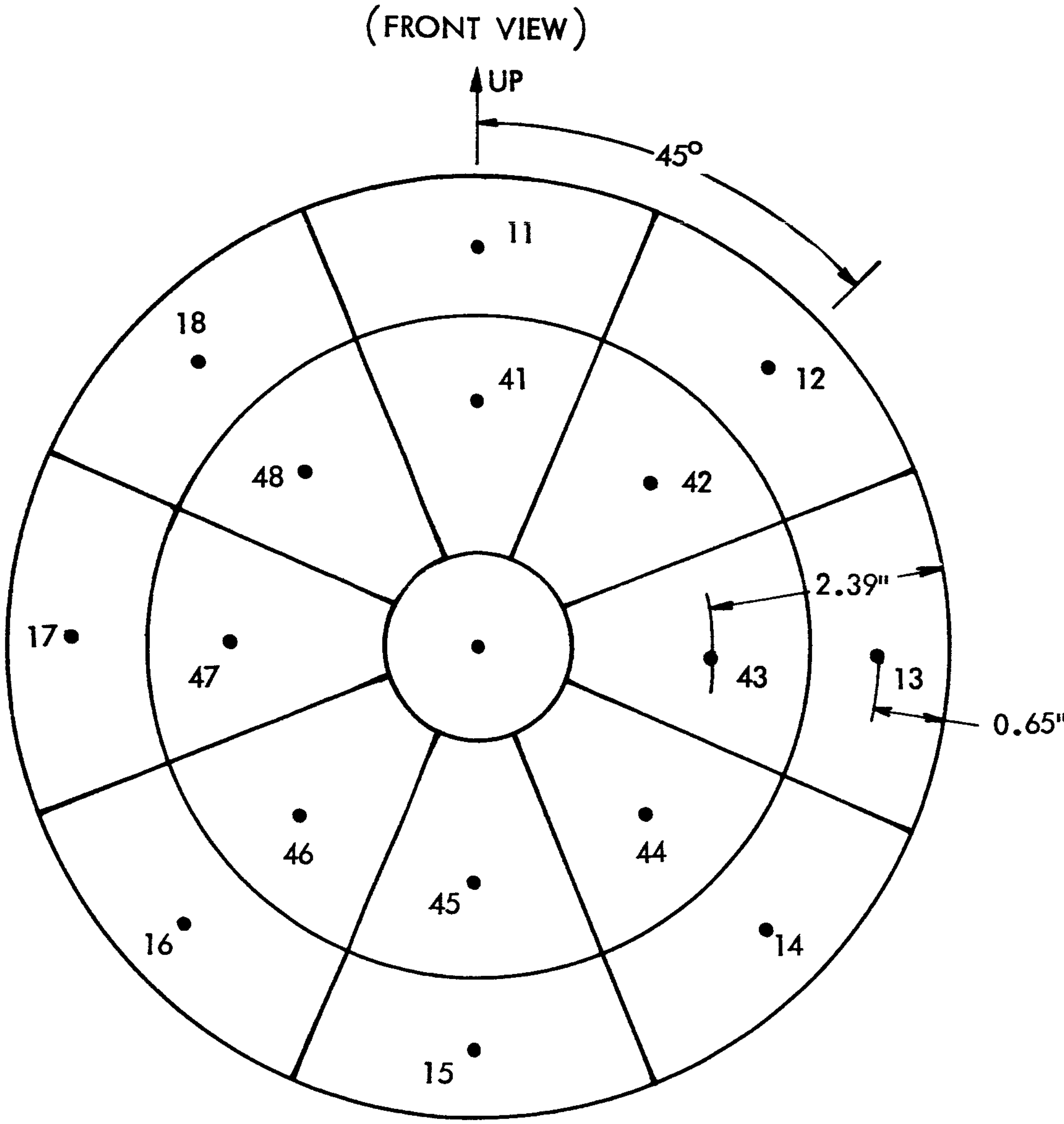

FIGURE E-10. THERMOCOUPLE LOCATIONS AT NODES ON DISK OF SERIES 4 MODEL

Figure E-10 Thermocouple Locations at Nodes on Disk of Series 4 Model

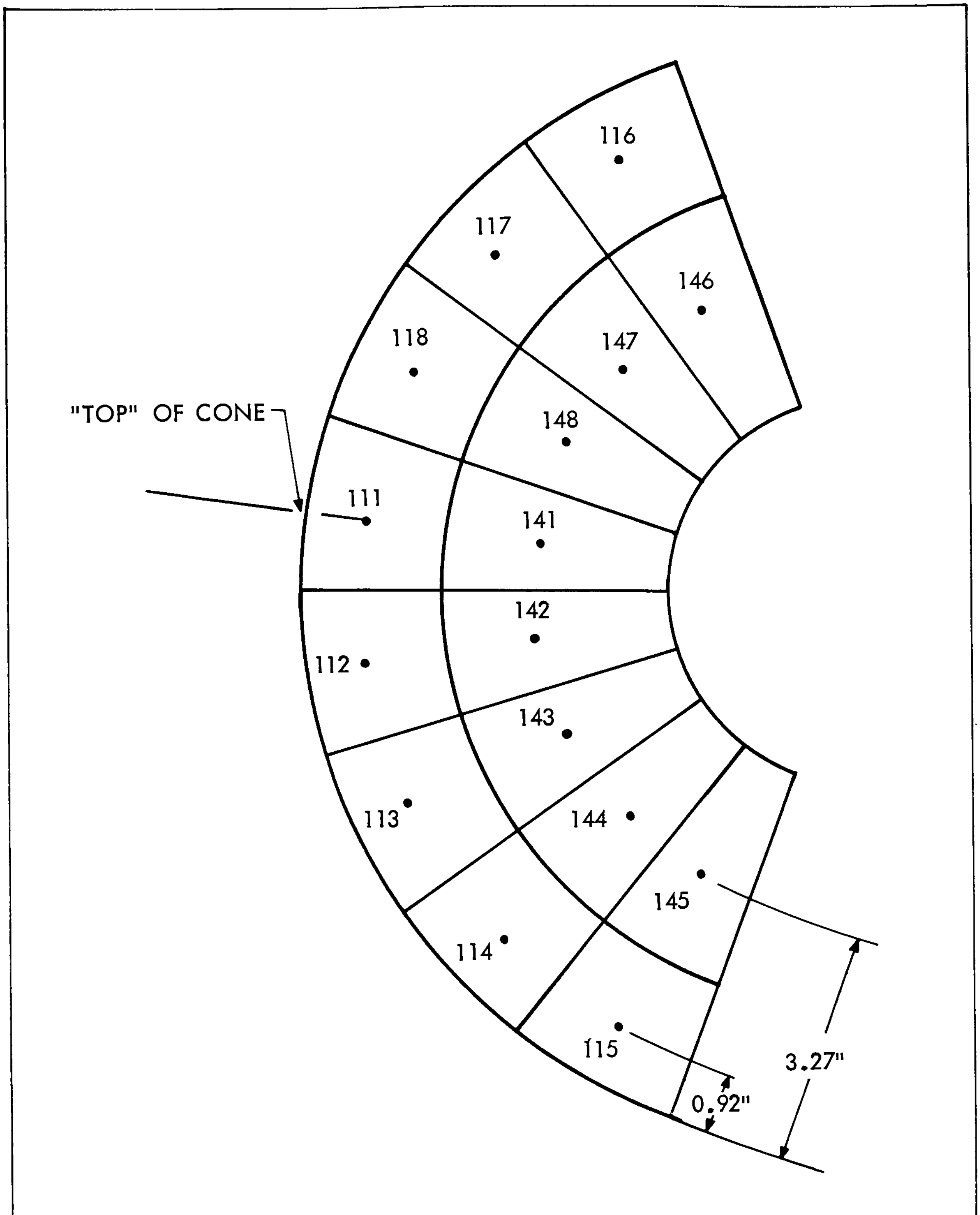

Figure E-11 Thermocouple Locations at Nodes on Cone of Series 4 Model

APPENDIX F - TEST PROCEDURE

Tests of this level of complexity require detail coordination between the test personnel for smooth operation. The following procedure for the Series 3 and 5 tests describe the sequence followed in performing these tests.

TEST PROCEDURE: APOLLO THERMAL TEST SERIES 5

1. System Checkout (end bell under chamber at ground level)
   - A. Mechanical
     - 1) Line heater and insulation installation
     - 2) Solenoid valve operation
     - 3) Plumbing leakage
   - B. Electrical
     - 1) Match thermocouple location with Hughes channel
     - 2) Connect heater power supplies and check heater operation
       - a) Line heaters (0 to 50°F)
       - b) Thrust chamber (600°F)
       - c) Nozzle (1000°F)
       - d) Copper billet (200°F)
2. Pre-Test Operation
   - A. Charge liquid tanks
   - B. Close chamber
   - C. Connect external plumbing lines
   - D. Evacuate air from liquid tanks
   - E. Evacuate helium bottles, then charge
   - F. Record a set of temperature and pressure data and inspect for open circuits.
   - G. Recheck heater operation step 1-B-2, and check temperature monitor systems.

3. Test
   A. Pre-data-taking period
      1) Chamber pump-down accomplished
      2) Cold walls stabilized
   B. Data-taking period
      1) Warm up solar simulator
      2) Take zero reading
      3) Remove eclipse device and adjust simulator to one sun
      4) Test events and data acquisition intervals as shown in Figure F-1
4. Post Test
   A. Shut-down procedure
      1) Turn off cold walls
      2) Turn off copper billet and line heaters
      3) Turn off pumps
      4) Turn on nozzle heaters, control to 300°F for 2 hours to warm up cold walls
      5) Start repressurization
      6) Unplug all electrical power cords
      7) Make sure all tanks are depressurized
   B. Disassemble test setup and prepare for return to Lockheed

TEST PROCEDURE: APOLLO THERMAL TEST SERIES 3

1. System Checkout (Chamber open)
   A. Mechanical
      1) Plumbing leakage
      2) Plumbing insulation
      3) Solenoid valve operation
      4) Tank charging
         a) External
         b) Internal
   B. Electrical
      1) Thermocouple location matched with Sadic channel
      2) Control and monitor thermocouples locations and operations

3) Heaters

a) Nozzle 1000°F

b) Thrust chamber 600°F

c) Plumbing line heaters 75°F ± 50°F

d) Copper billet 200°F

4) Mod-Sadic operation

5) Solenoid valve operation

6) Ignitron operation

7) Reference temperature bath operations

C. Ignitron

1) Voltage 230 V. max. (hold skin rise rate to 20°F/min.)

2) Monitor thermocouple

3) Temperature recorder

2. Pre-Test Operations (Chamber closed)

A. Take chamber to altitude (3×10^{-5} torr or higher). Turn on cold walls. Check temperature.

B. Manually set Sadic on channel 2 (Ignitron) and copper billet and monitor during initial heat up.

C. Turn on Ignitron (230 V. max.). Hold skin rise rate to 20°F/min. Level off Ignitron.

3. Test

A. Watch for start signal from H. Ogimachi.

B. Turn on copper billet heater control to 200°F. Monitor on Brown and Sadic.

C. Turn on Ignitron. Hold skin rise rate to 20°F/min. Level off at 250°F (Max. voltage 230 V.). Monitor at Ignitron and Sadic.

D. Watch chamber pressure gauge during initial heat up. If rapid altitude loss is indicated, turn off the heat sources.

E. Change Sadic over to automatic operation after steady state skin temperature has been established.

F. Take zero percent load reading on the Sadic.

G. Follow the tank expulsion schedule (Figure F-1).

4. Post Test
   - A. Prepare for next test run or
   - B. Shut down procedure
     1) Turn off cold walls
     2) Turn off Ignitron
     3) Turn off copper billet and line heaters
     4) Turn on nozzle heater, control to 300°F for 45 min. to warm up cold walls.
     5) Turn off pumps
     6) Start repressurization
     7) Turn of Sadic
     8) Turn off temperature reference bath
     9) Unplug all electrical power cords
     10) Make sure all tanks are depressurized

Series 3 Test Conditions

Run 1 Test 19 Cond 050 Model 003 Tanks empty, nozzle passive, half shell heated to 250°F, copper billet cold.

Run 2 Test 20 Cond 060 Model 003 as above with tank expulsion schedule added, copper billet 200°F.

Run 3 Test 21 Cond 070 Model 003 as above with nozzle heating cycle coordinated with tank expulsion schedule.

Run 4 Test 22 Cond 080 Model 003 as above with NRC-2 mylar insulation added inside sectors.

Sadic Data Acquisition Schedule

Run 1	Test 19	Cond 050	Model 003
Run 2	Test 20	Cond 060	Model 003
Run 3	Test 21	Cond 070	Model 003
Run 4	Test 22	Cond 080	Model 003

% load	Time between readings (min.)
Monitor	Ignitron on
	Change to automatic when operating skin temperature is stabilized
0	Initial reading (05)
1-27	10 min. (1% load, zero + 5 min.)
28-33	5 min., dump 1/2 tank
34-39	10 min.
40-45	5 min, dump 1/4 tank
46-51	10 min.
52-57	5 min., dump tanks completely

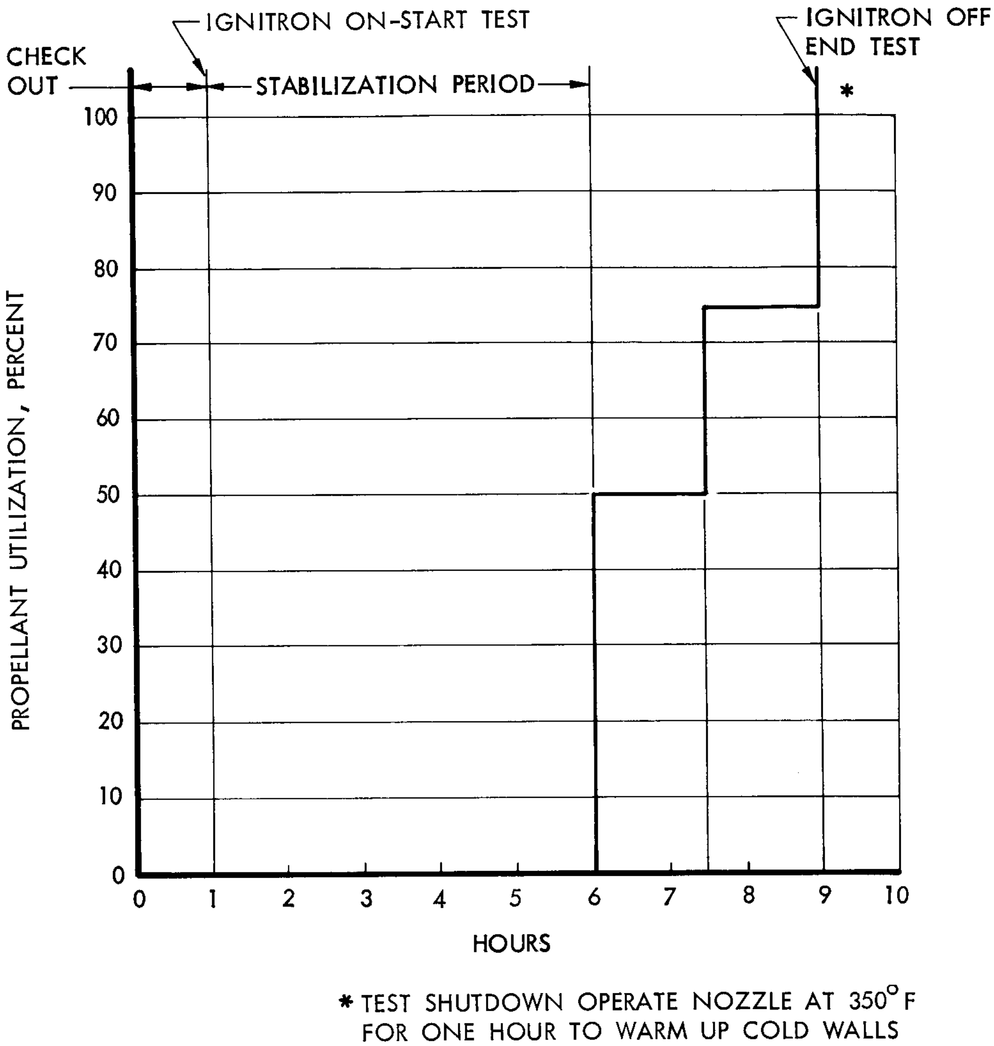

NOTE:

1. THE IGNITRON WILL BE TURNED ON THROUGHOUT EACH TEST RUN.
2. THE COPPER BILLET WILL BE HEATED TO 200 °F FOR RUNS 2, 3, AND 4.
3. THE NOZZLE AND THRUST CHAMBER WILL BE HEATED DURING TANK EXPULSION ONLY.
4. THE LINE HEATERS WILL BE TURNED ON AND THE TEMPERATURES MONITORED DURING THE TIME THE COLD WALLS ARE ON.

Figure F-1 Tank Expulsion Schedule - Series 3

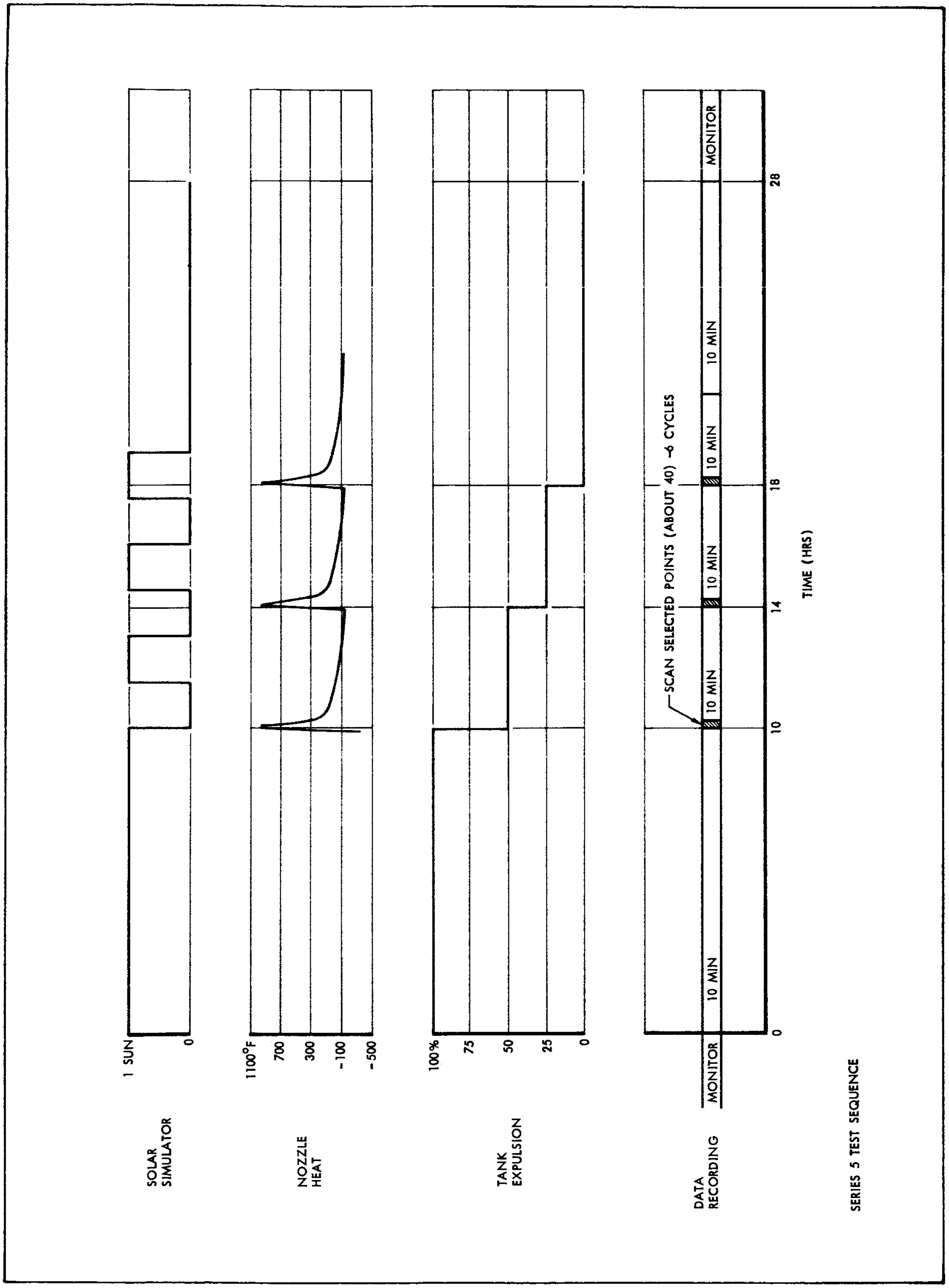

Figure F-2 Series 5 Test Sequence

LOCKHEED
CALIFORNIA COMPANY